Progress on LDAR Innovation

Report on Research Under CRADA #914-16

EPA Publication Number EPA/600/R-20/422
Revision Number: 0.8
January 28, 2021

Prepared by:
The LDAR Innovation CRADA Team

Published by:
U.S. Environmental Protection Agency
Office of Research and Development
Center for Environmental Measurement and Modeling
Research Triangle Park, NC 27709

Table of Contents

Figures....3
Tables....4
List of Appendices....5
Acknowledgments and Disclaimer....5
Executive Summary....6
1.0 Introduction....6
1.1 LDAR Innovation CRADA - Background and Status....6
1.2 Report Organization....7
1.3 CRADA Research Objectives....8
1.4 Executive View of LDSN/DRF....9
1.4.1 The LDSN - Current Sensor Used....10
1.4.2 The LDSN/DRF Process....11
2.0 Refinery LDAR Innovation....12
2.1 Current Work Practice - Comprehensive M21....12
2.1.1 Overview of M21....12
2.1.2 Strengths of M21-based CWP....13
2.1.3 Weaknesses of M21-based CWP....14
2.2 Comparing the CWP to Proposed Alternatives....15
2.2.1 Comparison of CWP and LDSN/DRF....15
2.2.2 Alternate Work Practice – OGI....16
2.3 CRADA Scientific Approach....17
3.0 LDSN/DRF Development and Testing....19
3.1 Exploratory Research....20
3.2 LDSN/DRF Development 1....24
3.3 FHR SLOF Pilot Test....31
3.4 LDSN/DRF Development 2....35
3.5 FHR CC Pilot Test....38
4.0 LDSN/DRF to CWP Equivalency....43
4.1 Historical LDAR Monitoring Data m-Xylene and Mid-Crude....44
4.2 Emissions Equivalency Analysis Approach....47
4.2.1 LeakDAS Data Processing....47
4.2.2 Emissions Calculations Methods....49
4.2.3 Monte Carlo Simulation....53
4.3 Simulation Results....56
4.4 Additional LDSN/DRF Benefits....60
4.5 Conclusions....61
5.0 LDSN/DRF Methods and Quality Assurance....61

5.1 LDSN/DRF Monitoring Plan Design....62
5.2 LDSN Node Pre-deployment and In-field QA Testing....64
5.3 The DRF Procedure....66
5.4 Ongoing QA of LDSN....69
5.4 Independent QA Audits of LDSN/DRF....71
6.0 Summary and Future Work....73
6.1 Major Accomplishments and Findings to Date....73
6.2 Development of an LDSN/DRF OTM....74
6.3 System Design Criteria and Method Standardization....75
6.4 Emission Reporting and Permit Representations....76
6.5 The Power of LDSN/DRF - Forward Research....77
7.0 Acronyms and Acknowledgments....78
8.0 References and Endnotes....81

Figures

Figure 1-1. Overview of the LDSN/DRF infrastructure....9
Figure 1-2. Overview of the LDSN/DRF system....10
Figure 1-3. Overview of LDSN based on fixed-place 10.6 eV PIDs....11
Figure 1-4. Overview of the LDSN/DRF process and DRF equipment....11
Figure 2-1. (a) and (b) M21 gear weighing 39.5 lbs, (c) donned gear with thermal sleeves....14
Figure 2-2. Examples of commercial OGI cameras....17
Figure 2-3. Example of 10.6 eV PID relative response....18
Figure 3-1. Sequence of LDSN/DRF development and testing....19
Figure 3-2. Exploratory trials at EPA ORD test range....20
Figure 3-3. Example of early collocated sensor node test....21
Figure 3-4. Example of a network detection....23
Figure 3-5. Evolution of LDSN prototypes....24
Figure 3-6. Illustration of distance effects of detection....25
Figure 3-7. Controlled release ERs, M21 values and DT band....26
Figure 3-8. DT bands for FHR CC m-Xylene and Mid-Crude....29
Figure 3-9. Leak clusters in historical CWP data....29
Figure 3-10. Overview of the FHR SLOF pilot test....32
Figure 3-11. Fin-fan leak behavior over night....34
Figure 3-12. An early mSyte™ detection in complex background....34
Figure 3-13. Molex's pre-production sensor - 2019....35
Figure 3-14. Molex's mSyte™ data platform....36
Figure 3-15. Leak detection on mSyte™ (a) sensor signal, and (b) PSL box....36

Figure 3-16. LDAR technician demonstrating the mSyte™ mobile device 37
Figure 3-17. mSyte™ leak investigation dashboard 38
Figure 3-18. View of Mid-Crude and m-Xylene process units 39
Figure 3-19. Examples of DRF leak quantification 39
Figure 3-20. FHR CC pilot test summary 41
Figure 4-1. Historical LDAR leak apportionment by component category, SVs, and emissions 45
Figure 4-2. FHR CC historical leak profiles (a) SV distribution, (b) cumulative emissions 46
Figure 4-3. Historical AVO leak identification: a) Mid-Crude and (b) m-Xylene 47
Figure 4-4. LeakDAS data processing methods 48
Figure 4-5. EPA ORD Monte Carlo emissions model 54
Figure 4-6. Molex Monte Carlo emissions model 54
Figure 4-7. Example EPA ORD Simulation of daily emissions: (a) Mid-Crude, (b) m-Xylene 55
Figure 4-8. Example EPA ORD simulation of cumulative emissions: (a) Mid-Crude, (b) m-Xylene 56
Figure 4-9. LDSN/DRF simulated net emissions compared to M21 LDAR (a) Mid-Crude and (b) m-Xylene 58
Figure 4-10. Emissions scenario leak repairs (a) Mid-Crude, (b) m-Xylene 59
Figure 4-11. Pegged leak relation to LDSN/DRF equivalency (a) Mid-Crude, (b) m-Xylene 60
Figure 5-1. Key elements of a fugitive emission management plan 63
Figure 5-2. Example of LDSN node placement in FHR CC Mid-Crude 64
Figure 5-3. LDSN fabrication and implementation procedures 64
Figure 5-4. LDSN node bump test QA check 65
Figure 5-5. Basic DRF procedures and mobile interface 67
Figure 5-6. DRF in action on a leak found under insulation 69
Figure 5-7. Example of LDSN data review: (a) meteorological data, (b) LDSN data 70
Figure 5-8. Assessment of Molex LDSN data with an open-source approach 72
Figure 6-1. Typical sensor layout plan 76
Figure 6-2. Example of a TE detection 78

Tables

Table 2-1. Comparison of CWP and LDSN/DRF attributes 16
Table 2-2. Select 10.6eV PID RFs 19
Table 3-1. Summary of LDSN/DRF detection sensitivity terms 31
Table 3-2. Comparison of M21 SVs leaks detected by CWP and LDSN/DRF 42
Table 4-1. Description of EPA ORD modeling terms 50
Table 4-2. Description of Molex modeling terms 50
Table 4-3. Equivalency simulation results 57
Table 5-1. Summary of LDSN data review for Figure 5-6 71

Table 7-1. Acronyms and abbreviations 78
Table 7-2. Acknowledgment of contributions 81

List of Appendices

Appendix A: Exploratory Tests A1-A51
A1: RTP Test 1 Summary..... A2-A16
A2: RTP Test 2 Summary..... A17-A51

Appendix B: FHR SLOF Tests B1-B55
B1: SLOF Test 3.1 Summary..... B2-B26
B2: SLOF Test 3.2 Summary. B27-B55

Appendix C: FHR CC Tests C1-C59
C1: LDSN Node Layouts for FHR CC Tests..... C2-C13
C2: Summary of LDSN PSLs and DRF SVs..... C14-C48
C3: Revised LDSN Node Layouts for FHR CC..... C49-C59

Appendix D: Test Methods and Procedures..... D1-D68
D1: EPA Method 21 Procedures D2-D8
D2: FHR TVA 1000-B FID Calibration Procedure D9-D18
D3: Phx42™ FID Use and Calibration Procedures..... D19-D35
D4: MiniRAE 3000 and Cub PID Information and Procedures..... D36-D44
D5: Optical Gas Imaging Procedures..... D45-D58
D6: Node Field Test Procedures (Sensor Bump Test and Cal.)..... D59-D62
D7: Simulated Leak Test Gas Release Procedures..... D63-D68

Appendix E: EPA ORD Equivalency Simulations..... E1-E41
E1: EPA ORD Simulation Approach E2-28
E2: EPA ORD Software Code..... E29-E40
E3: Simulation Files..... E41-E41

Appendix F: Molex Equivalency Simulations..... F1-F43
F1: Molex Simulation Approach..... F2-F32
F2: FHR CC Test Unit Leak Cluster Simulation and Analysis..... F33-F43

Acknowledgments and Disclaimer

As detailed in Acronyms and Acknowledgments section, this work has many contributors. Funding and in-kind support for this project was provided by the U.S. Environmental Protection Agency (EPA), Office of Research and Development (ORD), Flint Hills Resources (FHR), and Molex under cooperative research and development agreement 914-16. This document has been reviewed in accordance with EPA policy and approved for publication. Approval does not signify that the contents reflect the views of the Agency, nor does mention of trade names or commercial products constitute endorsement or recommendation for use. Any mention of trade names, products, services, or enterprises does not imply an endorsement by EPA, FHR, or Molex.

Executive Summary

Under a collaborative research agreement, FHR, Molex, and EPA ORD developed and tested a fugitive leak detection approach that provides environmental, safety, and cost saving advantages over the current manual EPA Method 21 inspection procedure. The automated and continuous Leak Detection Sensor Network system, along with optimized facility response protocols, enables leaks to be detected and repaired faster and more efficiently than with quarterly or annually executed Method 21. This report reviews the strengths and weaknesses of sensor-based leak detection approaches and describes the development and testing process that culminated in long-term trials in working FHR refinery process units. The real-time analytics of Molex's mSyte™ sensor information system helped the facility repair team discover and assess a range of leak sizes, many with emission levels well below that routinely detectable with other next-gen survey approaches, such as optical gas imaging. In addition to leaks associated with routinely monitored components, unexpected emission sources not detectable by other approaches were also found, illustrating the value of the 24/7 area-monitoring concept. Multiyear simulated emission modeling based on real-world leak detection data showed that the new sensor-based approach can provide equivalent or better emissions control to Method 21 for cost-realizable sensor network node densities. In addition to development, testing, and emission modeling results, this report describes quality assurance advantages of the developed approach and outlines areas for potential future research.

1.0 Introduction

This introductory section provides an executive view of this research program and this report.

1.1 LDAR Innovation CRADA - Background and Status

In the United States (U. S.), volatile organic compound (VOCs) and hazardous air pollutant (HAPs) industrial fugitive emissions (leaks) from process components have traditionally been managed using scheduled manual inspection of individual components with U.S. Environmental Protection Agency EPA Method 21 (M21) as part of leak detection and repair (LDAR).[1-3] Although sensitive and flexible, M21 is resource intensive, requiring equipment-laden operators to physically inspect and document a vast number of components, searching for the approximate 1-2% that are leaking (FHR data believed typical of refineries). Due to the implementation burden of M21-based LDAR, it is conducted infrequently (quarterly to annually), creating the potential for emissions to go undetected for extended periods of time. Additionally, M21 LDAR programs are not designed to comprehensively monitor all potential fugitive emission points in a facility. This likely increases the risk that unintended emissions can go undiscovered indefinitely, or until worsening to the point of human detection by audio-visual-olfactory (AVO) procedures or safety monitors in more serious cases.

Emerging leak detection assessment approaches, such as optical gas imaging (OGI)[4-8] and remote sensor systems,[9-14] may form the basis for more efficacious fugitive emission management strategies in a range of industrial applications. As a driving motivation for facilities such as refineries and chemical plants, faster and more cost-effective detection and repair of

fugitive leaks and other unintended emissions directly reduces air pollution and associated impacts.[15-19] Better LDAR can save companies money through improved operational performance, reduced and better maintenance, and promotion of safer working environments. Regulators benefit from development of new LDAR systems that further understanding, identification, and documentation of overall emissions and emissions sources, enabling optimal control strategies. Future congruent stakeholder benefits, such as enhanced transparency and community relations, can also be envisioned.

Under its next generation emission measurement (NGEM) program, EPA ORD's Center for Environmental Measurement and Modeling (CEMM) works collaboratively with industry, regulators, academic groups, and innovative companies to explore new air pollutant source management strategies made possible by advancing technologies. In 2015, representatives from FHR, a refinery operator, approached EPA ORD regarding potential collaboration on cutting-edge fugitive emission detection research. In 2017, EPA ORD CEMM[20], FHR, and Molex (a sensor/connector company) initiated work under a cooperative research and development agreement (CRADA)[21] to explore new NGEM-based emission detection techniques for petrochemical and other facilities.

As of December 2019, the "LDAR Innovation CRADA" (EPA #914-16) has successfully developed and tested a first-of-its-kind refinery leak detection sensor network (LDSN) that operates with specialized facility procedures defined in a detection response framework (DRF) to produce an integrated emission monitoring and documentation system. The LDSN/DRF prototype system has demonstrated the potential for improved fugitive emission detection and mitigation capability for select applications in pilot deployments in working petrochemical facilities. This report summarizes work under the CRADA and presents the scientific and business cases for LDSN/DRF as an alternative for M21-based LDAR. The report outlines what is known and the work that remains to understand regarding this novel fugitive emissions detection approach.

1.2 Report Organization

The primary purpose of this report is to describe research and development activities and results since project inception, covering an approximate 2.5-year period that represents the midway point for a typical five-year CRADA. This report is organized into the following sections that sequentially discuss progress against the CRADA objectives outlined in Section 1.3.

Sections 1 and 2 of this report outline technical milestones and provide an overview of the innovative LDAR technology developed under the CRADA. The advantages and disadvantages of M21 and other forms of leak detection are described to provide context for the developed approach. These sections briefly discuss the necessary components of the LDSN/DRF system, including sensor hardware, informatics, data management, and procedures for assessing and documenting emissions and quality assured operation.

Section 3 of this report summarizes technology development and testing performed to date. With support from Appendices A and B, Section 3 discusses test methods and LDSN/DRF development steps in the context of key findings from field trials. The concept of a detection threshold (DT) performance band for the LDSN/DRF approach in the context of refinery process unit applications is presented and discussed.

Section 4 and Appendices E-G explore the environmental performance of the LDSN/DRF system compared to the current work practice (CWP) for the FHR process units studied. Section 5 outlines the method quality assurance/quality control (QA/QC) procedures needed to assure positive environmental and business benefits for the process units studied. Section 6 briefly summarizes major accomplishments to date and discusses additional attributes and challenges of the concept and the work needed to further develop a transferable performance-based method. Project acknowledgments and a list of acronyms are provided in Section 7 with cited references and endnotes contained in Section 8.

1.3 CRADA Research Objectives

This CRADA has both near-term objectives (NTOs) and longer-term objectives (LTOs), listed below. The former focuses on determination of the basic feasibility of an innovative LDAR approach, whereas the latter evaluates standardization, transferability, and the ultimate use cases of the same. This report focuses on progress against key NTOs and outlines potential for continued work against LTOs.

- NTO 1: Investigate candidate approaches for the LDAR Innovation CRADA and select one for development and testing. This objective was met in the selection of a fixed-placed multi-node sensor network approach, called LDSN/DRF [progress ●●●●●].
- NTO 2: Through progressive design iterations and testing, develop one embodiment (one sensor type) of the LDSN/DRF system and evaluate implementation feasibility in multi-month pilot testing in working FHR process units [progress ●●●●○].
- NTO 3: Establish LDSN/DRF emission control performance in comparison to M21 [the CWP] in the FHR pilot test process units [progress ●●●●○].
- NTO 4: Establish the ongoing method, QA, and documentation requirements necessary to ensure ongoing validated performance of the specific embodiment of the LDSN/DRF in the FHR pilot test process units [progress ●●●○○].
- LTO 1: Understand the method requirements and regulatory hurdles for creation of a standardized, performance-based LDSN/DRF approach for possible consideration as an alternative work practice (AWP) to the M21-based CWP [progress ●●●○○].
- LTO 2: If feasible, deliver a standardized performance-based method for LDSN/DRF[22] [progress ●●○○○].
- LTO 3: Understand the potential range of applications and additional benefits (e.g. improved emission inventory knowledge) that may be realized from this NGEM approach. [progress ●●○○○].
- LTO 4: Disseminate non-proprietary technical learning established in this CRADA by publishing aspects of this research as part of scientific conferences and in peer reviewed journal articles and reports [progress ●●○○○].

1.4 Executive View of LDSN/DRF

Figures 1-1 and 1-2 provide conceptual overviews of the LDSN/DRF infrastructure and systems, the primary product of this CRADA. In brief, sensitive leak detection *sensor nodes* are deployed at strategically selected positions inside a facility process unit to form the *LDSN* system. A web-based analytics platform (called *mSyte*™) automatically acquires and analyzes real-time data from the network of wireless sensors, along with wind information and facility metadata, to identify, locate, and categorize emissions of interest (Figure 1-1). Together, this hardware and cloud-based software is called the LDSN.

An equally important part of this innovative LDAR approach is the *DRF* (lower right of Figure 1-2). The DRF represents the procedures facility personnel use both to respond to information delivered by the LDSN and to provide important metadata and QA inputs to the LDSN to ensure ongoing performance. The interaction of the machine (the LDSN) and the human (the DRF) is facilitated by mobile device technologies (cell phones and tablet interfaces) that are viewable by personnel while working in the unit. The DRF and the LDSN work together to locate, assess, and produce auditable records of discovered leaks and associated repairs under the innovative LDAR program. Tools like M21 and OGI are part of the DRF and assist in identifying and assessing emissions. The LDSN/DRF focuses on timely detection of larger emissions sources, facilitating more rapid mitigation and leading to emissions reductions.

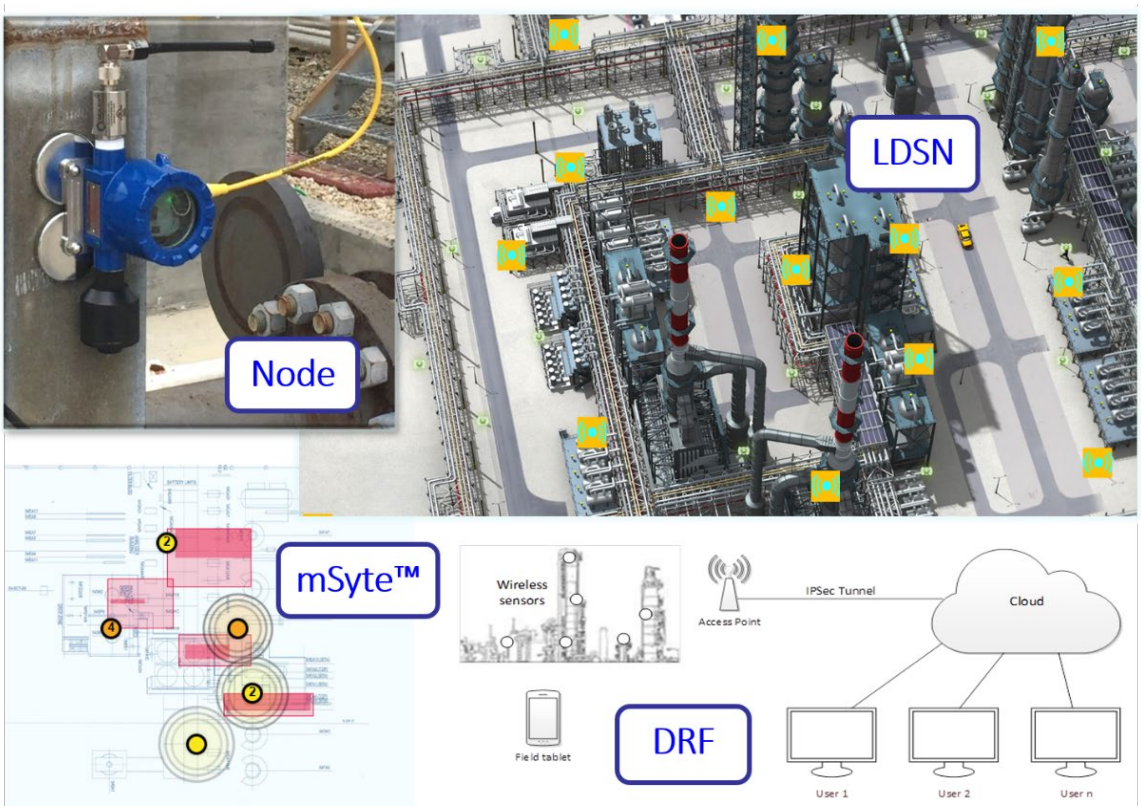

Figure 1-1. Overview of the LDSN/DRF infrastructure

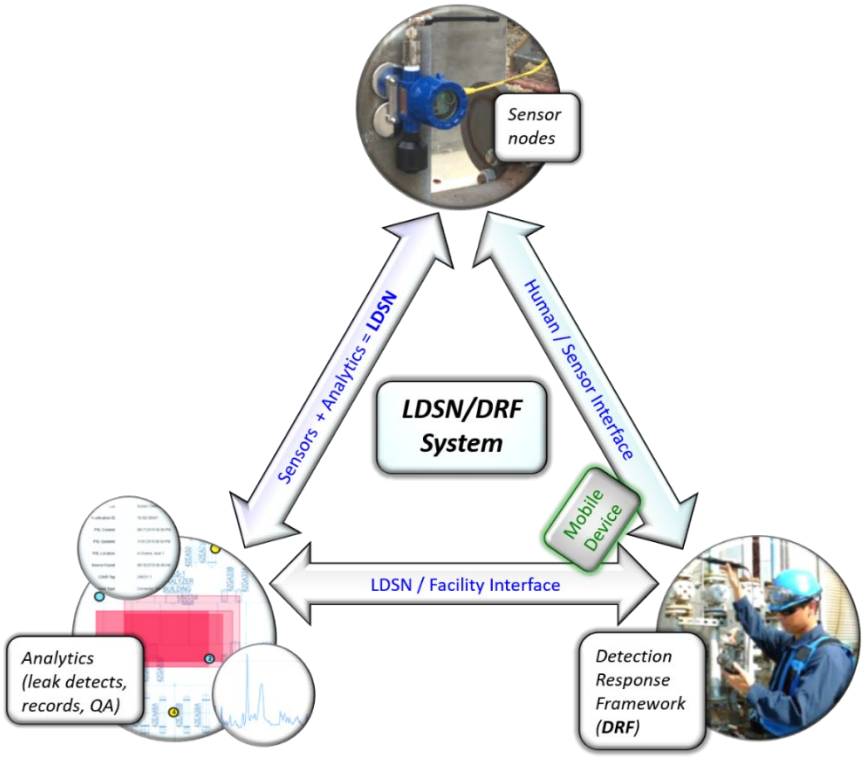

Figure 1-2. Overview of the LDSN/DRF system

1.4.1 The LDSN - Current Sensor Used

Leveraging advancements in information technology and innovative manufacturing, the performance of gas sensors is improving over time, while the cost for integration into business operations is steadily decreasing. Current and future LDSNs can utilize different types of sensors to optimally monitor for leaks and malfunctions in specific applications (e.g. a methane sensor for natural gas). The mode of sensor deployment may include fixed networks or mobile systems (e.g. airborne drone, work truck, or next-gen personal safety monitors), and systems may be point sensors or utilize extended open-path optical beams.

For this project, an LDSN approach consisting of a fixed-place network of 10.6 eV photoionization detectors (PIDs) was selected for development and testing. This specific embodiment of an LDSN (Figure 1-3) was chosen based on an analysis of the current state of VOC sensor technology (near-term ready), the expected performance of the envisioned system, and projected development and implementation cost factors. In this project a new high sensitivity wireless sensor node suitable for deployment in hazardous environments was developed [Figure1-3(a)]. The pumpless PID sensor node passively samples air in the process unit, producing a concentration measurement once every second. The PID ionizes certain air pollutant molecules [Figure 1-3(b)] that are emitted from leaks and malfunctions, producing a time-resolved measure with detected excursions above baseline indicating proximate emission events [Figure 1-3(c)]. The automated LDSN system collaboratively analyzes sensor and wind data, reporting detection and location estimates through the DRF communication process.

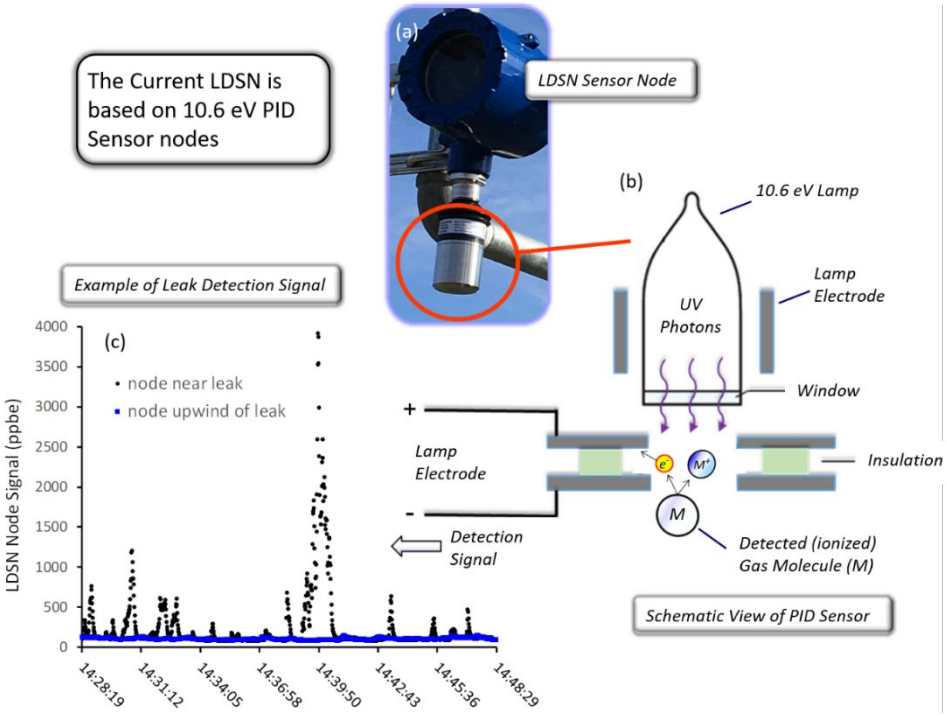

Figure 1-3. Overview of LDSN based on fixed-place 10.6 eV PIDs

1.4.2 The LDSN/DRF Process

An effective LDSN/DRF system must meet technical performance requirements including robust automated LDSN operation and requisite leak detection capability at cost-realizable node densities. Additionally, there are other requirements related to the intelligence of the system, such as the way it communicates with and is utilized by the facility, that are equally important. As detailed in this report, the LDSN/DRF is part of an overall operational process that brings in necessary metadata, personnel interactions, record keeping, supporting measurements, and site-specific factors. In this manner, both business processes and environmental objectives can be optimized. A schematic representation of the LDSN/DRF is shown in Figure 1-4.

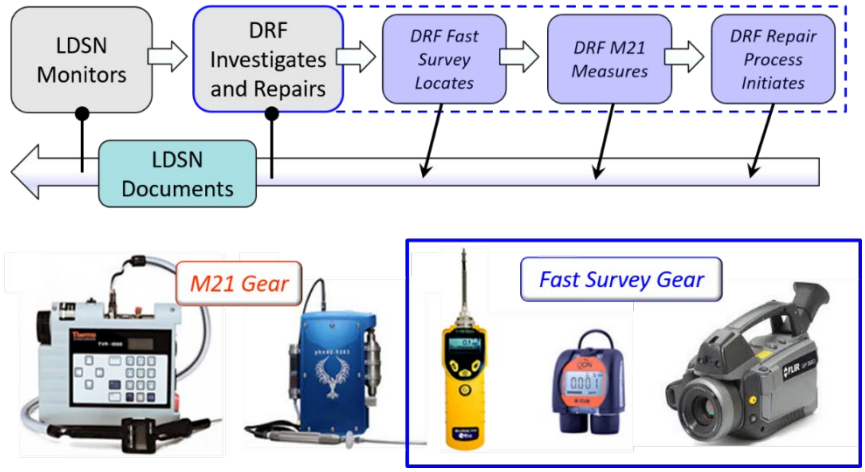

Figure 1-4. Overview of the LDSN/DRF process and DRF equipment

The LDSN system automatically detects, categorizes, and approximates the location of emissions in the monitored process unit based on VOC and meteorological measurements. The LDSN notifies the facility LDAR team of detected emissions, who then take appropriate action under the DRF. A detected emission that may represent a potential safety concern is communicated quickly through an alert and/or alarm and requires immediate attention (an augmentation to existing safety systems). Other more routine emissions are detected and communicated over time (hours to days), with repeating detected concentration peaks [Figure 1-3(c)] under varying wind directions building confidence in the assignment of an emission event. Once a notification threshold is reached, a potential source location (PSL) window is assigned. With information from a mobile device, the LDAR personnel respond, per the DRF, to investigate the PSL and identify (pinpoint) the source(s), first with "fast survey gear" that is easily deployed. The identified source is then measured with calibrated M21-gear to document the leak's peak concentration value and initiate repair procedures. Information is efficiently entered into the mobile device and recorded for regulatory, operational, and QA purposes. Other metadata, such as maintenance activities, are entered into the system to facilitate intelligent LDSN operation.

2.0 Refinery LDAR Innovation

This section describes the strengths and weakness of the CWP (Section 2.1), compares CWP and LDSN/DRF attributes (Section 2.2), and outlines the scientific approach used in this CRADA to investigate this innovative LDAR monitoring approach (Section 2.3).

2.1 Current Work Practice - Comprehensive M21

The first step to improve LDAR monitoring is to understand the strengths and weaknesses of the CWP. Comprehensive manual M21 is used in multiple industrial sectors and is a required work practice in over 45 U.S. federal and numerous state regulations. Since one of the NTOs of this CRADA centered on FHR operations, this report focuses on petrochemical refining facilities. Alternative monitoring to Manual M21 under a CWP for other source categories (e.g. chemical facilities that process/store high toxicity compounds) may vary in implications and applicability.

2.1.1 Overview of M21

Methane, VOCs, and organic HAPs can be emitted from a variety of sources in refineries. Known and/or permitted emissions can originate from stacks, tanks, vents, and other sources as part of normal operations. Unintended emissions from various sources can also occur and remain unknown until detected and assessed. This source category includes fugitive emissions from potential sources that are typically part of facility LDAR programs under the CWP, with emissions originating from potential leak interfaces on process equipment and components. Valve packing, pump seals, compressor seals, and flange gaskets are examples of common potential leak interfaces that are periodically monitored with M21. Other unintended sources include potential emissions from components or equipment that are not routinely monitored as part of LDAR programs or from process malfunctions. Although this latter category of sources may be considered fugitive in nature, they are typically not considered to be fugitive emissions under LDAR program definitions and are accounted for in other ways for regulatory, permitting and inventory purposes.

A U.S. refinery may be subject to a combination of federal, state, and local regulations that require LDAR programs for fugitive emissions control. The work practices are designed to identify leaking equipment so that emissions of VOCs and HAPs can be reduced through effective repairs. Although site-specific compliance requirements can be complex, each LDAR regulation/work practice essentially consists of periodic direct (manual) inspection of LDAR program components in light liquid or gas vapor VOC service [as per 40 CFR Part 60 Appendix A-7 (M21)[1-4]] to find fugitive leaks, followed by repair and re-inspection within a specified time frame. Maintaining records necessary to demonstrate compliance and reporting is a key part of every LDAR program.

The primary tool used in M21 is an extractive hand-held probe, a portable instrument that determines the effective concentration of the emitted gas stream at the leak interface. The M21 probe is calibrated daily and must be sufficiently sensitive to the potentially emitted compounds and meet other method requirements, such as response time, linearity, and flow rate. To execute M21, an LDAR technician carries the M21 instrument to the inspection point and places the extractive probe in direct contact with the component under test and slowly traces its circumference to check the potential leak surface (or leak interface). The technician must dwell an appropriate amount of time (seconds) to register a reading of leak concentration. The M21 peak leak concentration, also called screening value (SV), is the measured air mixing ratio of combustible fraction [for a flame ionization detector (FID)-based unit] or ionizable fraction [for a 10.6 eV PID-based unit] of the emitted stream as determined by the M21 hand-held probe and can be affected by several factors.[15] If the highest M21 concentration reading (its SV) for the inspected component is found to be above an action control limit set by regulation or permit [typically 500 to 10,000 parts per million by volume (ppmv) on a specific calibration compound basis], the component is defined as "leaking" and is tagged for repair. Typically, an FID-based hand-held probe is calibrated to methane whereas a PID-based unit is calibrated to isobutylene. The instrument response for a given compound is expressed in in relation to the calibration gas used.

2.1.2 Strengths of M21-based CWP

There are several inherent method strengths to the use of M21 in refineries (listed below). The final benefit cited is derived from the prescription for use of M21 under the CWP.

- M21 is a manually implemented physical contact inspection procedure that provides rapid feedback to the LDAR technician as the probe is moved around the leak surface. In this manner, the origin (the cause) of the component's emission can usually be determined, providing valuable information for the repair (if required).
- Because M21 uses a sensitive and calibrated hand-held probe, the method can deliver relatively reproduceable SV assessments against a specific leak definition (when executed by well-trained and diligent operators) over a wide range of leak interface concentration values.
- The SV at the leak interface recorded by M21 can be used to estimate the mass emission rate (ER) of the leak through established correlation equations for use in fugitive emissions inventories and other regulatory reporting purposes.[2]

- Since M21 is required by many federal and state regulations, the business ecosystem supporting the vast record keeping associated with its execution is well-developed.
- M21 is an established technique used by different industries providing common points of comparison and useful historical performance data to facility operators and regulators.
- Under the CWP, M21 is comprehensively applied to all the LDAR program components in a facility on at least an annual basis. The primary purpose for this is to attempt to ensure that leaking components are found and fixed within (at least) a one-year time horizon (components such as valves are typically inspected quarterly). As an additional benefit, this indiscriminate application of M21 to the complete set of LDAR program components provides population data for emissions inventory purposes.

2.1.3 Weaknesses of M21-based CWP

The M21-based CWP for refineries has several technical and business-related weaknesses that should be understood in the context of an improved LDAR monitoring approach.

- Due in part to the implementation burden of the M21-based CWP, it is executed periodically (e.g. quarterly or annually), depending on component type. Because of this high temporal latency, it is possible for large leaks to emerge between M21 inspection cycles and go undetected for weeks to years
- There is potential for unintended emissions to occur which originate from components, equipment, or malfunctioning processes that are not part of the CWP LDAR monitoring program and, therefore, can go undiscovered for extended periods of time.
- The accuracy of fugitive leak mass ER estimates based on M21concentration measurements at the leak interface is relatively modest.
- M21 is physically demanding, requiring equipment laden LDAR technicians (Figure 2-1) to frequently work in challenging environmental conditions and access hard to reach locations. This creates safety concerns for LDAR Technicians and additional expenses for companies.

Figure 2-1. (a) and (b) M21 gear weighing 39.5 lbs, (c) donned gear with thermal sleeves

- The daily M21 inspector's job is difficult, and turnover rates are among the highest in a facility. Variation in M21 application can be a concern, leading to high oversight and training costs.

- The calibration and record keeping aspects of the CWP are significant, creating thousands of opportunities for defects and associated monetary and reputational impacts.
- The M21-based CWP represents an inefficient business practice. For FHR for example, overall LDAR program monitoring expenditures for facilities are measured in the millions of dollars per year with fully accounted costs ranging up to $8 per component per monitoring event in some cases. A weakness of the CWP is the unnecessary expenditure of resources on non-leaking components. Since typically over 98% of individual M21 inspections result in "no leak" findings requiring no action (other than record keeping), the strategy of progressive inspection through the complete set of LDAR program components in the uninformed search for the few requiring attention is inefficient (produces no environmental benefit and yet has significant cost) and produces personnel safety risk.
- The M21-based CWP emissions control strategy is not optimized due to its systematic assessment of all components. The vast majority of emissions from LDAR program components originate from a small population of high emitters.[23] Monitoring techniques that focus on more timely identification and repair of high emitters should support more effective control strategies.
- The M21-based CWP creates difficulty to interface with data management and reporting software resulting in multiple touchpoints and opportunities for data loss.

2.2 Comparing the CWP to Proposed Alternatives

Any successful AWP must compare favorably with the CWP in two respects. The AWP must be equivalently protective of the environment. In this case, an alternative NGEM-based LDAR monitoring approach and associated facility response must control fugitive air pollutant emissions at least as well as the CWP. Equally important, a successful AWP must also make sense from a business perspective, for if the proposed alternative is more expensive or burdensome to execute, facilities will choose the CWP. In Section 2.2.1, these factors are discussed by comparing select attributes of the CWP previously described to the envisioned LDSN/DRF approach. Section 2.2.2 provides further context on the comparison by briefly examining the current OGI-based AWP and why that LDAR alternative has not been widely adopted by industry.

2.2.1 Comparison of CWP and LDSN/DRF

For the purposes of the following comparison (Table 2-1), it is assumed that the specific LDSN/DRF implementation has been shown to produce equivalent (or better) mass emissions reductions compared to the CWP (discussed in Section 4). In addition to fugitive control, several other technical benefits and cost factor attributes are discussed.

Table 2-1. Comparison of CWP and LDSN/DRF attributes

CWP Attribute	LDSN/DRF Attribute
A CWP *technical strength* is the use of well-established M21 procedures to produce actionable SVs against leak definitions, to derive mass emission estimates for leaks, and to inform leak repairs.	This is also a *technical strength* for LDSN/DRF since M21 procedures are used to characterize the emissions from leaks discovered by the system.
A CWP *technical strength* lies in the use of the sensitive M21 physical contact inspection procedure to examine LDAR program components in order to identify and document both actionable leaks and small to moderate emissions that are ubiquitously present.	This is a *technical weakness* for LDSN/DRF (and other NGEM approaches like OGI). Since LDSN is not a physical contact inspection procedure, it is less sensitive to lower-level emission rate leaks and cannot directly identify the leak source.
A *secondary benefit* of the CWP is derived from the comprehensive (100%) manual inspection of all LDAR program components. The large dataset thus produced is useful for fugitive emission inventory estimation.	Because LDSN/DRF does not require 100% manual inspection of all LDAR program components, other emission inventory approaches are required. One such approach is discussed in later sections of this report.
A *technical weakness* of the CWP is the delayed discovery and repair of actionable leaks for LDAR program components due to the periodic nature of the inspection procedure (increasing emissions).	A *technical strength* of LDSN/DRF lies in the continuous discovery and timely mitigation of significant emissions from LDAR program components (reducing emissions).
A *technical weakness* of the CWP is it typically results in identification and control of emissions only from LDAR program components.	As an added benefit to an LDAR program, a *technical strength* of LDSN/DRF lies in the continuous discovery and timely mitigation of significant emissions from non-LDAR program components (reducing emissions).
A *business weakness* of the CWP is the requirement for comprehensive (100%) documentation and inspection of a vast number of LDAR program components using a resource-intensive manual inspection method in an uninformed search for a typically small number (<2%) of leaking components.	A *business strength* of LDSN/DRF is that resources are focused on timely discovery and mitigation of significant emissions using continuous information gathering and optimized response, providing both operational and safety benefit.

2.2.2 Alternate Work Practice – OGI

For the past decade, OGI has played an important role in LDAR innovation.[4-8] In this CRADA, OGI is used as a supporting tool under the DRF to help facility technicians locate and assess emissions that are detected by the LDSN. OGI systems work in a sub-region of the infrared (IR) spectrum where molecules that comprise hydrocarbon emission plumes absorb and emit energy in the form of IR photons. The most widely used OGI camera, the model FLIR® GF320 (FLIR Systems, Billerica, MA), which operates in the 3.2 to 3.4 µm region (Figure 2-2, far left). The OGI camera operator looks at a scene containing the LDAR component(s) under inspection and observes the IR photons emitted from objects in the background, the component(s), and by the gas itself (if emitted). If a fugitive or vented gas emission is present above detection limit, the molecules in the plume can net absorb IR radiation (or net emit if the gas is hotter than the scene), producing a discernable contrast in the image that makes the normally invisible plume visible. The emitted gas must have IR spectral features detectable by the OGI camera utilized to be observed.

Figure 2-2. Examples of commercial OGI cameras

In 2008, EPA promulgated an LDAR AWP[4-8] that allows use of OGI on a bimonthly inspection schedule in lieu of M21 for certain applications. Although facilities that choose to adopt the current OGI AWP can reduce the amount of M21 executed, full application of the CWP's M21 manual inspection approach is still required under the AWP once per year.

From the regulatory development perspective, there were likely several reasons why annual M21 remained a requirement under the OGI AWP. Some of these reasons may have been related to the risk tolerance of EPA, showing caution with full adoption of a new technology where methods and performance assessments were not fully mature. Other reasons may have been related to perceived weaknesses in the mass emission reduction equivalency calculations and hesitancy to abandon established procedures with clear secondary benefits associated with emission inventory determination, discussed in Table 2-1. Regardless of the underlying reasons, a decade later it is now clear that annual M21 and associated documentation requirements significantly reduced the business case for OGI-AWP adoption. As a consequence, the OGI-AWP is little used by the refinery sector. Some lessons learned from the OGI-AWP process are considered in the discussion and formulation of a the proposed LDSN/DRF alternative.

2.3 CRADA Scientific Approach

To achieve CRADA NTOs 1-4 (Section 1.3), significant sensor and system engineering advancement was required. Early engineering development was complicated by the lack of established knowledge regarding remote detection of emissions in complex industrial environments (e.g. refinery process units). For this reason, an observational research approach was adopted whereby progressively more complex field testing using steadily advancing LDSN prototypes allowed the parameter space to be efficiently explored, sensor design decisions to be evaluated, and QA methods to be developed and refined (Section 3).

One of the key scientific and engineering questions for the LDSN/DRF approach centered on the ability of the developed system to robustly detect leaks of various sizes in process units, with acceptably low false positive rates. Due to its remote observation nature, factors affecting detection sensitivity for LDSN/DRF (and other NGEM systems) differ from a physical contact inspection approach, such as M21. The time-resolved "leak signal" recorded by a sensor node [Figure 1-3(c)] depends on leak ER, integrated sensor response to emitted compounds, source to sensor node separation distance, atmospheric plume transport and dispersion, and wind field obstructions, with the first two factors shared by M21. As detailed in Section 3, initial testing was performed using rudimentary prototypes and simulated leak scenarios where release of a known amount of a test gas allowed certain factors to be explored. As the LDSN/DRF system advanced, testing progressed into full process unit deployments where simulated-leak information was replaced with real-world emission data.

As sensor science develops over time, new systems that can provide more sensitive and/or speciated measurement of VOCs and HAPs will emerge. For example, a sensor that mimics the broad VOC detection capability and sensitivity of a gas-powered FID may one day be available in a miniaturized package suitable for automated and long-term sensor network deployment. These new sensors can be used in LDSN/DRF approaches in the future. For this project, the best available sensor technology for LDSN development and testing was determined to be a 10.6 eV PID (Figure 1-3). For this reason, the detection capability of this sensor type to the compounds comprising the refinery emissions of interest was a focus of the research. Figure 2-3 presents the relative response of this sensor type for some common industrial gases, noting that compounds with an ionization potential (IP) greater than 10.6 eV are not detectable. The primary gas used for simulated-leak controlled-release testing was isobutylene, a standard calibration gas choice for PIDs with a universally defined response factor of 1.0. As described in Sections 3 and 4, testing in FHR process units was conducted across a spectrum of compounds possessing a range of PID responses to assist in understanding LDSN/DRF detection capability in a variety of real-world scenarios.

Figure 2-3 illustrates relative strength of the response of a 10.6 eV PID to select gas species. For example, a concentration of 1 ppmv benzene produces approximately 1.89 times the PID signal compared to 1 ppmv of isobutylene (the calibration standard). To express a PID-measured benzene reading in terms of isobutylene, the signal is multiplied by a calibration correction factor, also called the response factor (RF), that for benzene is expressed as:

$$RF_{benzene} = 1/1.89 \text{ (relative response)} = 0.53 \qquad \text{eq. 1}$$

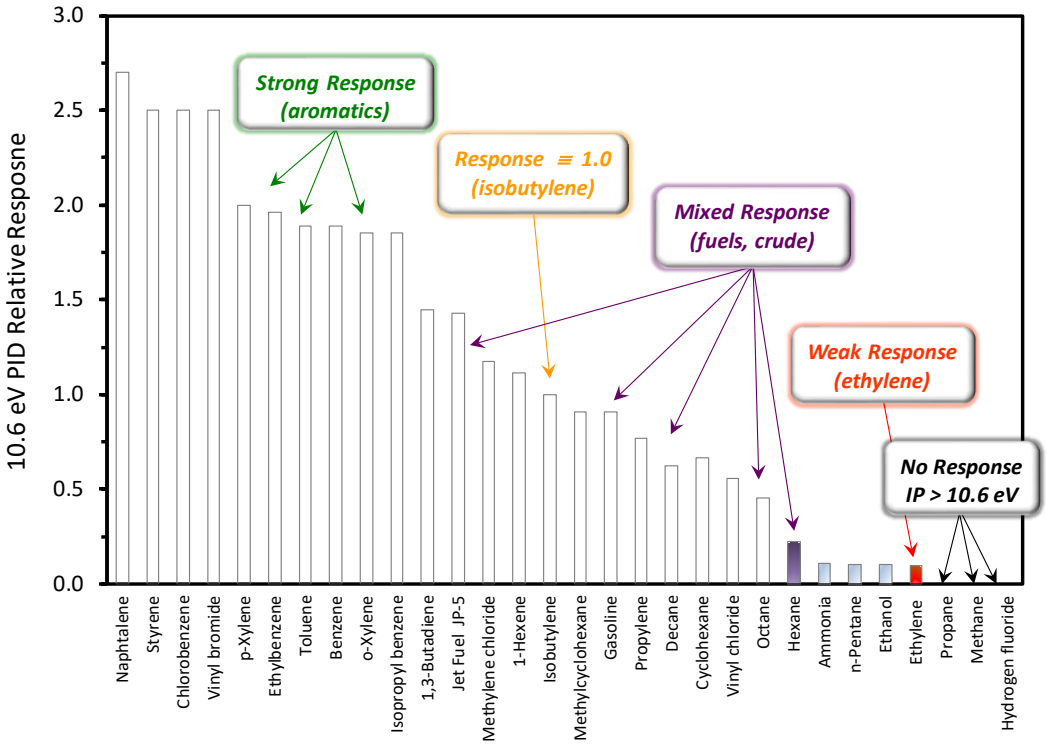

Figure 2-3. Example of 10.6 eV PID relative response

Compounds with RFs > 1.0 produce less PID signal than isobutylene and are therefore more difficult to detect. A sample of PID RFs for compounds relevant to initial CRADA testing is found in Table 2-2.[24] Compounds such as methane and propane possess ionization energies above 10.6 eV, so are not detectable. Instruments like FIDs and OGI also have compound-specific RFs and perform well on saturated alkanes not suitable for PIDs. As part of the scientific approach design, CRADA testing included controlled releases of isobutylene with real-world testing in process units with emitted gas steams that spanned the range of PID RFs. The use of LDSN/DRF in process units possessing multiple gas streams is discussed in Section 3.

The time-resolved signal produced on an LDSN sensor node from a leak located some distance away is a function of atmospheric conditions and local wind flow obstructions. As part of the scientific approach, tests were conducted at multiple locations that possessed a variety of wind flow complexity and base meteorological conditions. These tests are described in Sections 3.1, 3.3, and 3.5 and associated appendices.

Compound	RF
Benzene	0.5
m-Xylene	0.5
Toluene	0.6
Jet Fuel JP-8	0.7
Diesel	0.7
Gasoline	0.9
Isobutylene	1.0
Cyclohexane	1.3
Propylene	1.4
Heptane	1.7
n-Hexane	3.0
n-Pentane	7.0
n-Butane	40
Propane	non detect
Methane	non detect

Table 2-2. Select 10.6eV PID RFs

3.0 LDSN/DRF Development and Testing

This section summarizes research and engineering progress accomplished under the CRADA in pursuit of the NTOs discussed in Section 1.3. As outlined in Figure 3-1, the incremental design advancements in hardware, software, and procedures that now form the LDSN/DRF methodology were developed and tested over time, starting in the fall of 2017. As the LDSN/DRF approach matured, it was deployed in progressively more complex testing scenarios. Field trials culminated in a long-term pilot test at FHR's Sour Lake Olefins Facility (FHR SLOF) in 2018 and a full-scale pilot test in two process units at the FHR's Corpus Christi West Refinery (FHR CC) in 2019. Sections 3.1 through 3.5 provide an overview of the LDSN/DRF development and testing, with supporting information found in appendices. These sections introduce important technical concepts that are necessary for system performance assessment in comparison to the CWP (Section 4), and in the discussion of methods required to maintain and document the performance of LDSN/DRF as an alternative LDAR approach (Section 5).

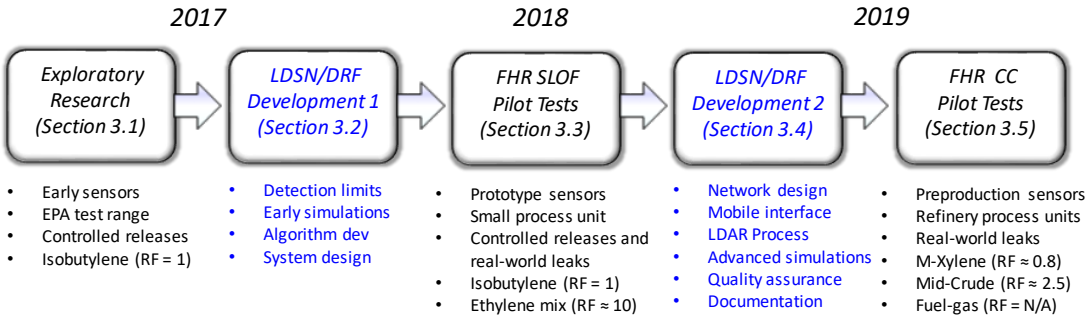

Figure 3-1. Sequence of LDSN/DRF development and testing

3.1 Exploratory Research

Work to identify candidate sensor technologies was executed by EPA ORD and Molex in separate laboratory and field trials during the initial phases of research. EPA ORD performed field test comparisons of its PID-based SPod fenceline sensor as part of near-source research studies,[17, 25] and Molex conducted environmental chamber tests to carefully examine the effects of temperature and relative humidity on various PID sensor designs. Collaborative field testing of early prototypes using controlled releases of simulated-leak test gases (primarily isobutylene) was executed at the EPA ORD test range in Durham, NC, from 11/27/2017 to 12/07/2017 and 2/26/2018 to 3/07/2018 (Figure 3-2). The objectives of these exploratory tests were to establish the basic feasibility of a 10.6 eV PID-based LDSN approach and to develop detection sensitivity and engineering data to facilitate the development of progressively more advanced prototype LDSN systems. These tests also explored early aspects of DRF development as each of the controlled-release experiments was characterized using M21, OGI, and other leak assessment approaches. These trials examined early aspects of source location approaches, building off the fenceline approaches developed by EPA ORD. Additionally, these tests helped develop sensor QA procedures, such as node-specific functional tests, described in Section 5.

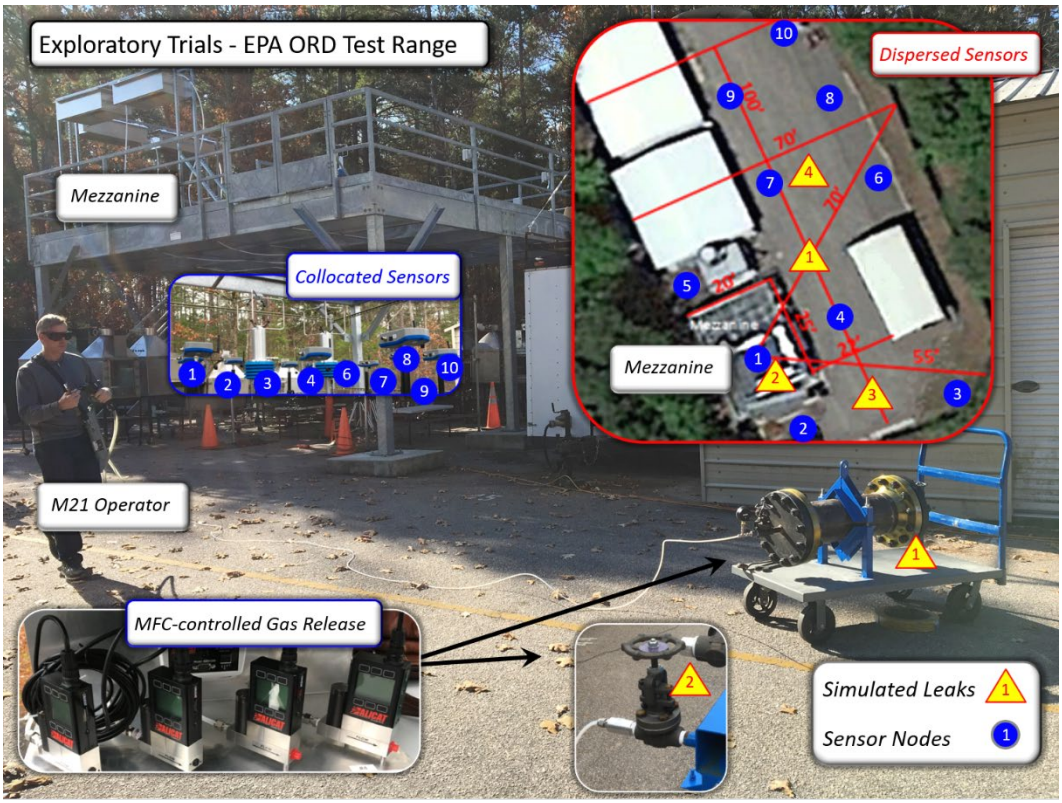

Figure 3-2. Exploratory trials at EPA ORD test range

Controlled-release testing used the early prototype sensors, described in Section 3.2, in both collocated and dispersed (network) scenarios, with the simulated leak and sensor positions systematically varied. The specifics of the exploratory tests are summarized in Appendix A with details of the mass flow controller (MFC)-based controlled releases and supporting M21 and OGI methods discussed in Appendix D. In these exploratory tests, a total of 40 controlled-release

trials were conducted using instrument grade isobutylene (>99.5% pure). The isobutylene tests utilized controlled-release mass ERs ranging from 0.26 g/hr to 14.2 g/hr, with 75% of the tests (30 of 40) conducted on the low end of the release range at ERs ≤ 1.42 g/hr. The shortest and longest duration trials for this subset were 11 minutes and 100 minutes, respectively, with an average duration of 41 minutes. The separation distance between the simulated leak points and the sensor nodes ranged from 5 ft to 72 ft and is further discussed in Section 3.2 in context of LDSN detection performance evaluation. Experiments involving vertical offset of the simulated leak points and sensors were also conducted in preparation for multilevel process unit field trials subsequently discussed. A total of three pure ethylene and two pure methane (both instrument grade gas) releases were also conducted for M21 and OGI comparison purposes, and to explore the atypically large range in RF values (10 to 40) for ethylene found in PID manufacturers' RF tables. Understanding the ethylene RF was important since this was the main compound of interest in the FHR SLOF pilot test (Section 3.3) and represents the low range of RF parameter space potentially observable with 10.6 eV PID (with dense node deployments).

Figure 3.3 shows an example of an early controlled-release test with five collocated prototype sensors (several PID types), placed 38 ft from a simulated leak that was continuously emitting isobutylene test gas at 0.71 g/hr (5 sccm). The abscissa (x-axis) indicates the time of the sensor reading at a data acquisition rate of 1 Hz, while the primary ordinate (y-axis) shows the raw output voltage from the sensors. The secondary y-axis shows the approximate sensor reading in units of parts per billion by volume "equivalent" (ppbe). As discussed in Section 2, a leak detection in a process unit represents a mixture of compounds with different PID response factors, so the reading is reported in units of ppbe, with reference to isobutylene as a calibration standard gas.

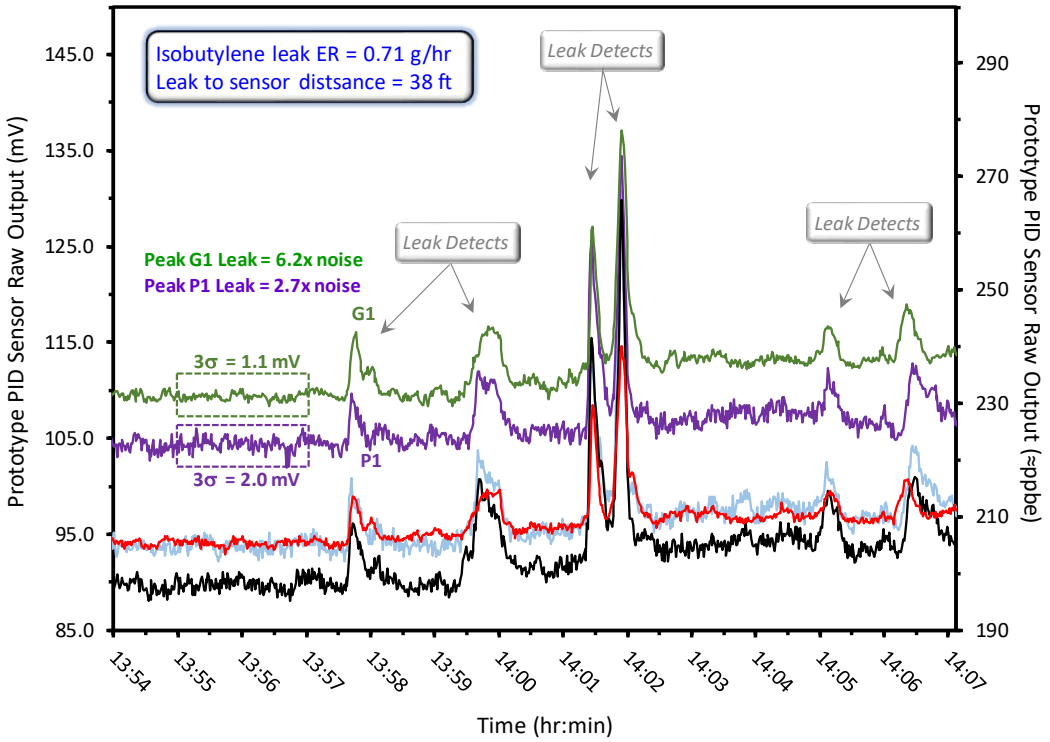

Figure 3-3. Example of early collocated sensor node test

As is typically observed in collocated studies, the 10.6 eV PID sensors exhibited very similar time-resolved signals, with offsets in raw voltage baselines that could be corrected (if desired) through calibration and analytical adjustment in software (called baseline-correction in SPod fenceline sensor applications). In general, the short-term excursion in a sensor's output voltage above its respective baseline level (called a peak) represents a potential emission detection (typically called a leak detection). The peak signal excursion must be above the sensor's noise floor to be considered a detection. The definition of an LDSN sensor signal peak detection is typical of other analytical approaches. The LDSN peak must be greater than 3-times the local standard deviation (3σ) in time-resolved data defining the noise floor. Examples of the 3σ noise calculation are shown in the green (G) and purple (P) traces of Figure 3-3. Here the 3σ noise floors of the G and P signals inside the indicated windows (dashed-line boxes) are 1.1 mV and 2.0 mV respectively. Detectable *signals* (peaks) must exceed these *noise* levels [i.e. signal to noise (S/N) ratio >1] to counted. In these cases, peaks G1 and P1 exhibit S/N ratios of 6.2 and 2.7, respectively, indicating detections. Complexity arises in real-time tracking of a sensor node's noise floor in cases where low level leak signal is persistent in the time series data (convolution of noise and leak signal). This factor can be encountered in process units, and the 3σ noise floor is typically higher than the example of Figure 3-3. Some aspects of automated peak detection from LDSN time series data are discussed in the methods section (Section 5).

The signal registered by a high time-resolution leak detection sensor is always temporally intermittent. The potential for a leak detection "event" in the sensor's time series data occurs when a part of an emitted gas plume (an air parcel carrying some number density of target molecules) physically overlaps (touches) a sensor node. The air parcels carrying the leaked target molecules are transported from the emission point to the sensor location by constantly changing wind directions and eddies, creating temporally intermittent plume to sensor overlap. The instantaneous signal level and temporal duration during a detection event also depends on the leak's mass ER, physical properties of the emitted gas, the sensor's RF to the emitted gas, the sensor's time-resolution, and the leak to sensor node separation distance. However, factors affecting emission plume transport (wind speed and direction, atmospheric dispersion, and physical structures in the process unit creating eddies and channeling of flow) determine a sensor's response to a large extent. With other variables fixed, the signal of Figure 3-3 is completely determined by emission plume transport factors that can affect the observed instantaneous peak heights and integrated widths by over an order of magnitude.

Shorter-term lulls in windspeed and longer-term low wind speed and compressed atmospheric boundary layer states (e.g. overnight stagnation/calms) can feature prominently in LDSN signal analysis. These instantaneous or prolonged low-flow atmospheric conditions can first accumulate, and then puff-transport gas emitted from leak(s), increasing target molecule concentrations in the air parcels delivered to the sensor. This temporal integration of emitted mass assists in LDSN detection of emission issues and has no analog in M21 or OGI LDAR monitoring. In addition to the potential for detection enhancement due to temporal mass ER integration (under certain conditions), a single LDSN node spatially integrates mass ER information transported to it from the upwind areas under observation. A *cluster* of small leaks that individually may be below LDSN detection can combine to produce a detectable signal, with the specific components ultimately identified, assessed, and repaired through DRF procedures.

This feature of LDSN/DRF also has no analog in M21 or OGI monitoring. These factors are further discussed in later sections.

Whereas Figure 3-3 illustrates collocated prototype sensor detections during a controlled-release experiment, Figure 3-4 provides an example of a release trial conducted with spatially separated nodes to form a detection network. Here the sensor data has been baseline-corrected through simple subtraction of an offset value for ease of viewing. The sensor nodes (black, blue, and red circles and corresponding timeseries) were positioned with respect to the simulated leak point (yellow triangle) as indicated in the inset of Figure 3-4. The mass ER in this case was 1.42 g/hr of isobutylene. With multiple sensor locations around the emission point, the probability of achieving spatial overlap of the plume and a sensor node increases. In this example, under light and variable winds, the detection moved frequently between the sensor node positions, producing a signal that could be triangulated by the LDSN algorithm, which factors-in general wind conditions.

The excursions in the red sensor's time series at 58 ft distance are generally weak, except for the peak around 10:14 AM. This is likely an example of temporal mass integration caused by a lull in wind speed coupled with eddy/channeling effects, resulting in a higher concentration air parcel delivered to the location of the red sensor node. This detection enhancement around 10:14 AM is also evident in the black sensor signal that lies closer to the simulated leak and along the same plume transport line of action as the red sensor. This type of multi-node corroborated detection is typical in LDSN sensor network applications and provides opportunity for both detection level and source location performance enhancement and inter-node QA assessment for sensor health and false positive protection.

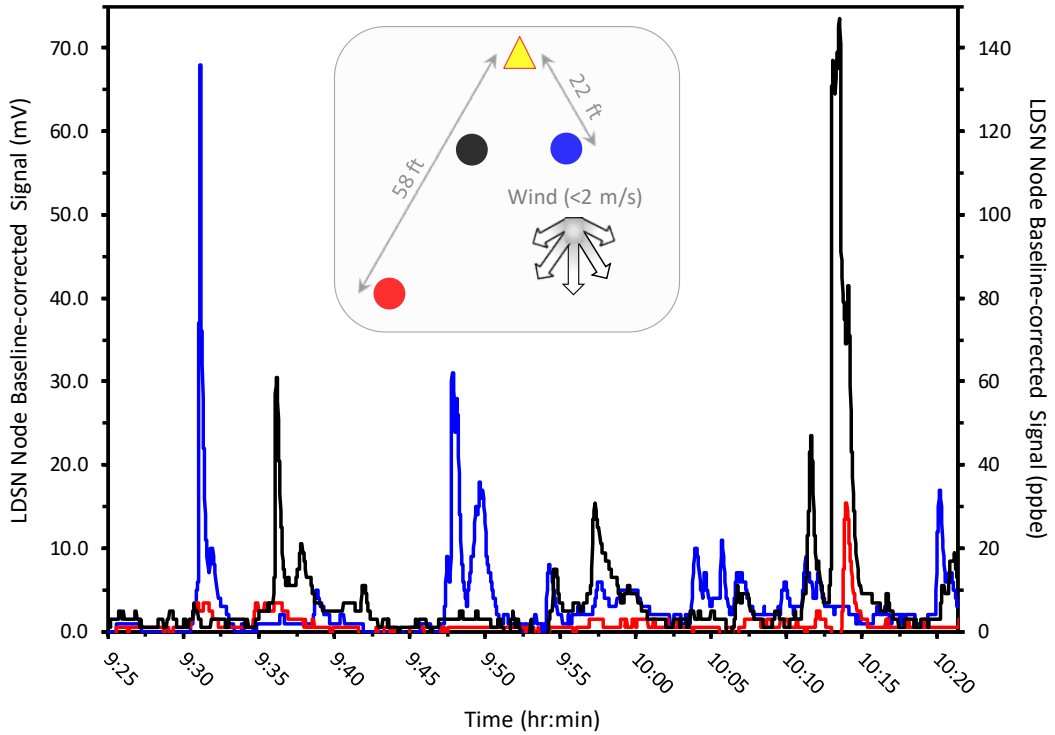

Figure 3-4. Example of a network detection

Although many scientific questions remained and much engineering development work was yet to be done, the exploratory tests conducted at EPA ORD convinced the team that a 10.6 eV PID-based LDSN system could be viable from both business and regulatory perspectives. The decision was made to pursue this embodiment of the LDSN approach, effectively meeting CRADA NTO 1 (Section 1.3).

3.2 LDSN/DRF Development 1

Starting with exploratory tests and continuing through the 2018 FHR SLOF pilot, initial LDSN/DRF design concepts and systems engineering were steadily advanced by the CRADA team. Early LDSN development included progression of both sensor hardware and leak detection software. In parallel, the team considered the practical use and QA of LDSN by the facility operations as part of the DRF. Figure 3-5 provides an overview of wireless sensor engineering advancement. In initial tests at the EPA ORD test range, the LDSN sensors were "breadboard prototypes", suitable for basic comparisons between different variations and preparations of several 10.6 eV PIDs. These tests were further informed by collocated EPA SPod fenceline sensors in controlled-release trials. By early 2018, the LDSN Prototype 1 wireless sensor node was developed and used for the early sensor network trials at EPA ORD (Section 3.1). With learning from early trials, an improved wireless senor node (LDSN Prototype 2) was developed and deployed for the long-term testing at FHR SLOF (Section 3.2), producing important real-world use data in hot and humid conditions. As discussed in Section 3.4, the LDSN sensor node design was advanced once again to pre-production form, obtaining a certification milestone in preparation for the long-term, full-scale process unit implementation as part of FHR CC pilot tests (Section 3.5). The LDSN control and data management software platform called "mSyte™", along with its facility interface and relation to the DRF are discussed in Sections 3.4 and 3.5. The methodization of the approach is the subject of Section 5.

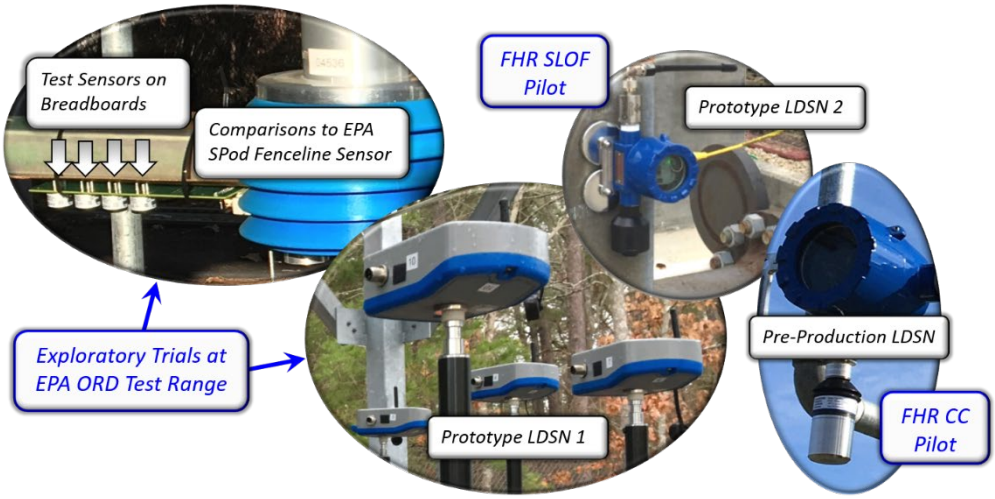

Figure 3-5. Evolution of LDSN prototypes

For LDAR monitoring applications, sensor network and other NGEM techniques differ significantly in operational approach from the M21-based CWP. As part of the LDSN/DRF development process it was important to understand these differences in a context relevant to LDAR programs. It was also important to define the expected performance of the LDSN/DRF

approach in relation to the CWP, using both simulated and real-world testing. The controlled-release simulated leak testing conducted at EPA RTP and FHR SLOF, along with the full-scale pilot testing at FHR CC, provided an information foundation for the LDSN/DRF design and development process.

As discussed in Section 2, M21 is a sensitive physical contact leak interface inspection method that assigns an SV in ppm for the assessed emission point (leak interface). M21 is a point concentration measurement that is correlated with (a proxy for) the mass ER of the leak. When considering different leak types (e.g. pressure, leak surface, size, shape), an M21 SV determination for a given ER can vary significantly. As described in Section 3.1, the LDSN leak detection signal registered by a sensor node is fundamentally determined by the instantaneous local concentration of the emitted plume at the sensor position (some distance from the leak). The local plume concentration at a moment in time is a function of atmospheric conditions, stochastic eddy flow, separation distance, and other factors but is directly related to the ER of the leak (total number of molecules emitted by the leak per unit time).

Whereas the direct-contact inspection instruments used in M21 feature easily determined method detection limits (MDLs), the analog for LDSN/DRF is more complex as it is a remote observation affected by several external factors. The leak detection capability of a sensor node is not expressed as a single value but forms a range called the detection threshold (DT) band (Figures 3-6 through 3-8). As illustrated in Section 3.1, an instantaneous leak detection occurs when the time-resolved signal produced by the leak on the LDSN node exceeds that sensor's noise floor. Considering a single emission point, a relatively low-magnitude leak (low ER and M21 SV) has a higher probability of being detected by the LDSN if it happens to be located close to a sensor node. In this case, the number of molecules emitted by the leak per unit time is relatively low, but the emission plume has yet to significantly disperse, so the instantaneous plume concentration seen by the sensor may be robustly detected. Conversely, if a leak is located far from a sensor node, it must possess a larger ER to be detected (ignoring special meteorological conditions that can enhance remote detection capability, as previously discussed). The concept of a DT band is common to many NGEM techniques, for example OGI detection sensitivity is determined in part by environmental conditions outside of the operators control.[26]

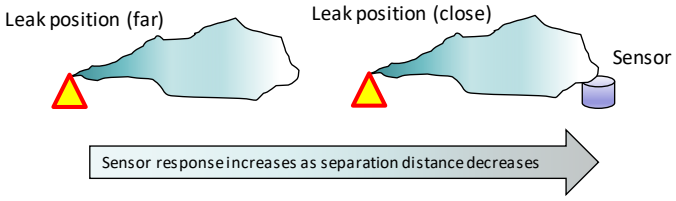

A sensor's minimum detection capability for one leaking component is not a single fixed value but forms a range called the detection threshold (DT) band.

A small mass ER leak can be easily detected if it is located close to sensor node. If the same leaking component is located farther from the sensor it may be below the sensor's DT band.

Figure 3-6. Illustration of distance effects of detection

Data from the controlled-release simulated leak trials were used to explore the DT band and implications for default node spacing as part of LDSN/DRF method development. The most informative tests were releases of isobutylene at 0.36 g/hr (two trials), 0.71 g/hr (five trials) and 1.42 g/hr (23 trials). For this subset of trials, the average release duration was 44 minutes. In Figure 3-7, the three known isobutylene mass ERs from these 30 controlled release experiments

are depicted as single points on the x-axis, with individual M21-measured SVs from the simulated leaking component shown on the y-axis. Typically, the FHR LDAR subject matter expert (SME) executed more than one M21 measurement per release trial, and the values shown were corrected for the isobutylene RF of the utilized M21 instrument (Thermo TVA 1000B FID).[27] The average values of the M21 SVs for three ERs are represented by the diamond symbols, with red bars indicating ± 1 standard deviation (± 1σ) in the data. With a precise increase in MFC-measured mass ER (moving right along the x-axis), the associated average M21 SV proxy also increases (upward on y-axis). With a mass ER increase, the signal level detected on a remote LDSN sensor node also increases (detections become easier), since the concentration of target molecules in the air parcels transported to the sensor also rises (all other factors held constant).

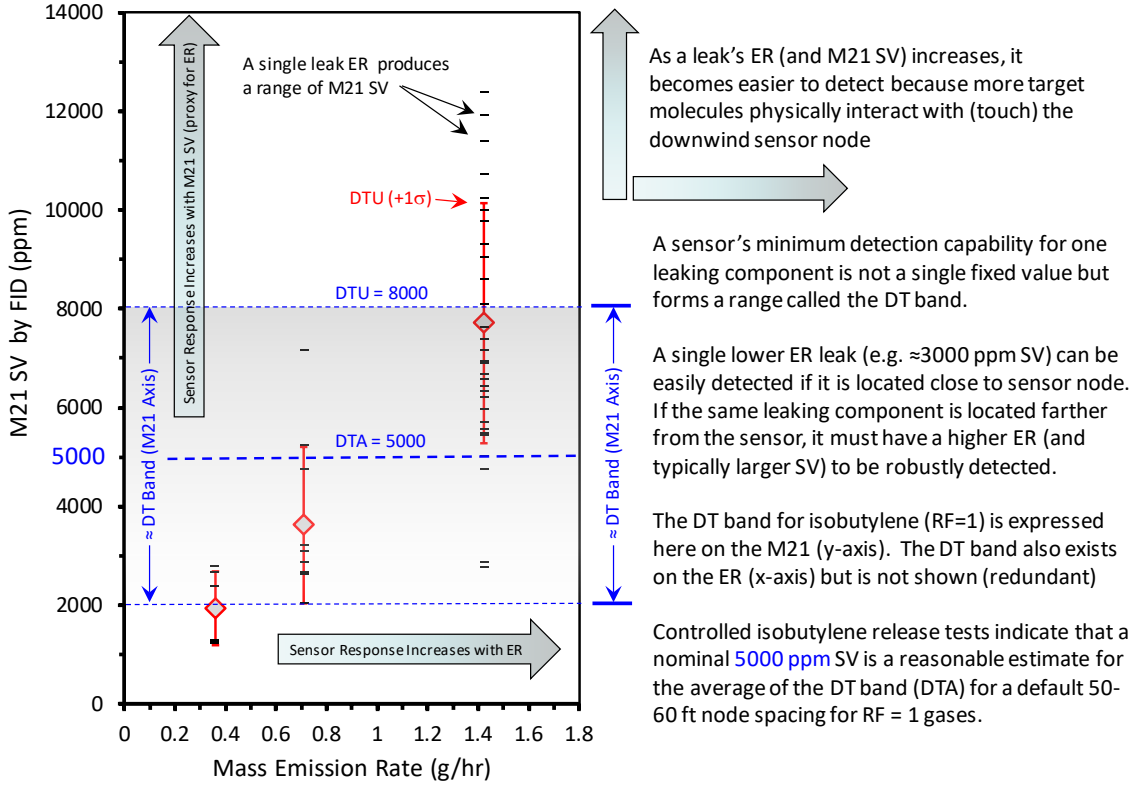

Figure 3-7. Controlled release ERs, M21 values and DT band

The controlled-release simulated leak experiments at ≤ 1.42 g/hr produced LDSN leak detections on at least one sensor node in 28 out of 30 trials. For the various spatial configurations of collocated and dispersed sensor network deployments in these trials (Figure 3-2 inset, Appendix A), a short time duration release provided potentially detectible plumes to only a subset of sensors, due to wind direction limitations. This makes overall node detection statistics difficult to express, since a lack of detection on a node may be due to insufficient plume transport to its location. This temporal sampling limitation is not present in real-world use as LDSN/DRF that provides 24/7 monitoring of the process unit, since changes in wind direction over extended periods of time naturally occur. Factors such as wind direction and distance also affect the DT for other NGEM approaches, such as OGI, where gas speciation, observation distance, wind

speed, and the relative temperature of leaked gas and background scene determine detection capability.[28-29] In Figure 3-7, LDSN detections were achieved in each of the 0.36 g/hr trials, with leak to sensor separation distances of 20 ft and 38 ft (Figure 3-3). Four of the five 0.71 g/hr trials produced detections on at least one sensor node at distances ranging from 20 to 58 ft. The trial that failed to produce a detection in this subset was relatively short duration (35 minutes) at a 39 ft separation distance, with all sensors grouped at the same location. Ambient winds speeds were low for this experiment (<1 m/s) and the lack of detection is ascribed to insufficient plume transport to the single collocated sensor location. Although LDSN node detections were observed at both 0.36 g/hr and 0.71 g/hr mass ERs, sensor signal was more robust at 1.42 g/hr, so most of the low release trials in this subset (23 of 30) were performed at this ER. At 1.42 g/hr, LDSN detections were achieved in 22 of 23 trails at 26 distinct leak point to sensor distances ranging from 5 ft to 72 ft (mean of 37 ft). The trial that failed to produce detections at this ER was at 58 ft separation distance and utilized collocated sensors, so insufficient wind transport to the single sensor location was likely a factor.

The controlled-release trials support the definition of an LDSN DT band in terms of 0.36 g/hr (weaker detection potential), 0.71 g/hr (moderate detection potential), and the 1.42 g/hr (more robust detection potential) ERs. These trials indicate that an isobutylene leak of 1.42 g/hr and higher mass ERs should be routinely detectable with an LDSN of 50-60 ft default sensor node spacing (farthest distance between nodes ≈ 100 ft). More specifically, an isobutylene leak of ER ≥1.42 g/hr should be detectable at the maximum sensor to leak separation distance in an LDSN deployment at default node spacing, given sufficient sampling time to ensure plume to sensor overlap occurs. Lower mass ERs were also detectable, with signal increasing as the leak to sensor separation distance decreased. All exploratory experiments utilized a single simulated leak emission point and sampled a relativity narrow range of lower wind speed day-time meteorological conditions under the relatively low obstruction complexity scenarios encountered in EPA ORD trials. As discussed in the methods section, continual information on the LDSN DT for a specific process unit deployment is provided through M21 measurements of the identified leaks as part of the DRF. This is a key QA feature that helps ensure LDSN detection capability is known.

In Figure 3-7, the superimposed DT band range is expressed along the M21 SV axis (y-axis) so that we may relate LDSN detection capability to M21 historical data for comparisons to the CWP (Section 4). At ≈ 8,000 ppm, corresponding to the approximate mean M21-measured value for the 1.42 g/hr releases, we define the DT band *upper* limit (DTU). The DTU provides guidance on how large a leak must be (on average, as measured by M21) to be detected at the maximum leak to sensor separation distances in a given LDSN deployment. For isobutylene at a default 50-60 ft sensor node spacing, the LDSN should detect leaks with M21 SVs above ≈ 8,000 ppm anywhere in the monitored unit. Because M21 approximates mass ER, some variability around the DTU is expected, as indicated by the red-colored ± 1σ y-axis error bars on the 1.42 g/hr ER values. Accounting for this variability, a DTU (+1σ) value ≈ 10,000 ppm is a reasonable expectation for an RF =1 gas. Also indicated in Figure 3-7, an estimate for center point of the DT band, called the DT *average* (DTA) is shown. For an RF = 1 gas, the DTA is ≈ 5,000 ppm. The DTA is useful for a variety of simple comparisons, including the basic equivalency calculations discussed in Section 4. A DT band *lower* limit (DTL) may also be defined, but this concept is less useful in practice due to the effects of leak clusters and factors subsequently described.

In real-world application, the gas streams monitored by LDSN/DRF will seldom be single component in nature. As described in Section 2.0, the 10.6 eV PID has a range of response for different compounds so the characteristics of detection will depend on the mix of gas streams potentially emitted from the specific components present in the monitored process unit. In the CRADA research to date, we have performed testing in the following gas-mix scenarios:

- *Isobutylene:* high purity RF = 1 test gas used in controlled release studies. The approximate DTA, DTL, and DTU of isobutylene are 5,000, 2,000, and 8,000 ppm respectively (Figure 3-7).
- *Ethylene:* High purity, RF ≈ 10 to 15 test gas and in impurity-mixed streams found in the FHR SLOF process unit (Section 3.3). Ethylene is difficult to monitor with the current 10.6 eV PID version of LDSN and requires high node density. The estimated DTA of an ethylene stream with typical impurities is ≈ 50,000 ppm to 75,000 ppm at default node spacing. The DTA can be reduced if sensor node density is greatly increased.
- *Meta-Xylene Aromatics:* Relatively uniform RF ≈ 0.5 to 0.8 mix of compounds found in the FHR CC Meta-Xylene (or m-Xylene) process unit (Section 3.5). Assigned a conservative RF = 0.8 value. Easily monitored by current embodiment of LDSN. The DTA, DTL, and DTU of this unit is determined by multiplying 0.8 times the isobutylene DT band values.
- *Mid-Crude Fuel gas*: Methane rich streams with effective RF > 30 (not monitored by the 10.6 eV PID version of LDSN).
- *Mid-Crude Light Petroleum Gas (LPG) Mix*: RF ≈ 3 gas streams present in FHR CC Mid-Crude that can be monitored by LDSN but with reduced sensitivity compared to isobutylene. The DTA, DTL, and DTU of this unit is determined by multiplying 3.0 times the isobutylene DT band values.
- *Mid-Crude Light Liquid Mix (gasoline, jet fuels, etc.)*: Approximately RF ≈ 1 gas streams present in Mid-Crude that can be monitored by LDSN with similar sensitively to isobutylene.
- *Mid-Crude Composite Mix*: Since the *LPG* and *Light Liquid Mix* gas streams of Mid-Crude are simultaneously monitored by the same LDSN deployment, a composite mix response factor is of RF = 2.5 is employed (estimated). The overall process unit DTA = 12,500 with the DTL and DTU typically expressed in relation to individual gas streams. Further information on the calculation of the composite RF is discussed in Section 6.

Figure 3-8 provides a simplified view of the DT band concept for isobutylene, and the FHR CC m-Xylene and Mid-Crude process units without the complexity of the mass ER and M21 SV data of Figure 3-7. Using the isobutylene (RF =1) DT band as a reference, the DT bands for the m-Xylene (RF ≈ 0.8) and Mid-Crude (composite RF ≈ 2.5) for the default 50-60 ft node density can be easily expressed. In the case of Mid-Crude, the *Light Liquid Mix* component is used to estimate the lowest DTL, whereas the *LPG* gas stream with a high RF value is used to estimate the highest anticipated DTU for the unit. The DT band concept primarily applies to single-component leak detection (as represented by the controlled release trials) and can inform expected LDSN performance in multiple ways. The DTA is a single average performance value that can be used in simple calculations and comparisons. The width of the DT band represents

the distance-specific performance factors that can take into account the spatial distribution of the sensor nodes with respect to component position (discussed in Section 4 and appendices).

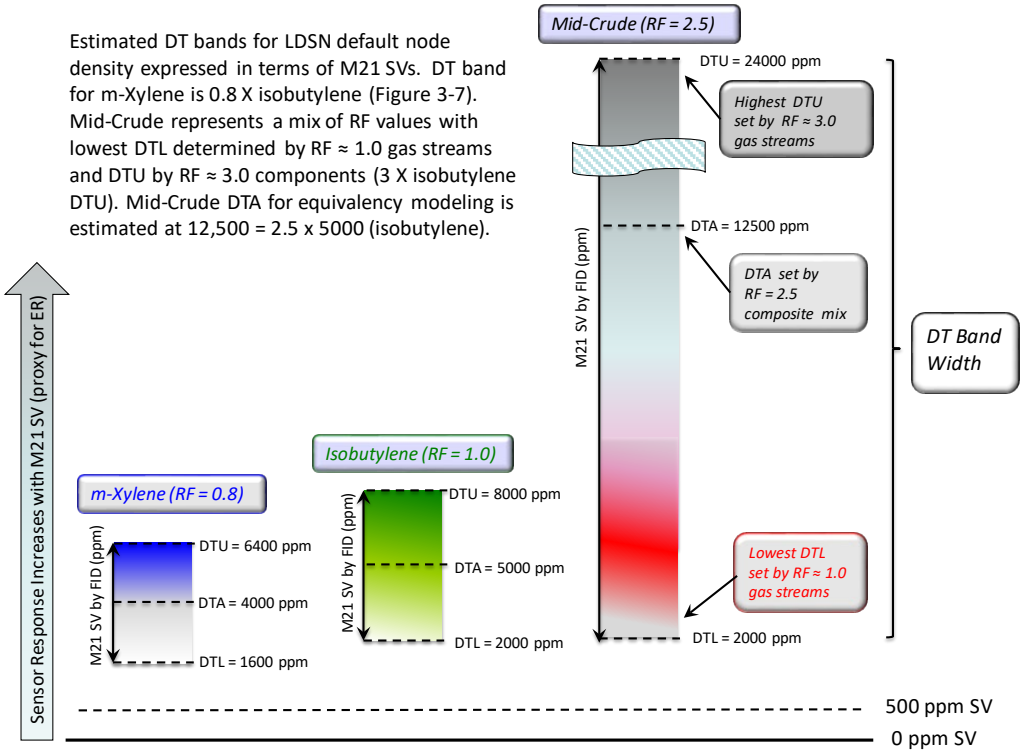

Figure 3-8. DT bands for FHR CC m-Xylene and Mid-Crude

In addition to distance-dependent single leak sensor performance, there is another detection sensitivity factor that centers on the additive effect of multiple leaking components that must be considered in LDSN/DRF method development. Figure 3-9 provides a real-world example of this effect with presentation of a layout of the first level of the m-Xylene process unit in FHR CC, detailed in Section 3.5. In addition to four LDSN node locations (blue dots), this figure shows the location of historical LDAR leaks that were discovered and repaired as part of the CWP from January 2013 through August 2019, with ranges in M21 SV levels for these documented leaks levels indicated by colored circles in the legend (e.g. red > 50,000 ppm). The values are "as reported" and have not been corrected for the M21 FID instrument RF for this process unit as this correction is typically not performed in daily LDAR.

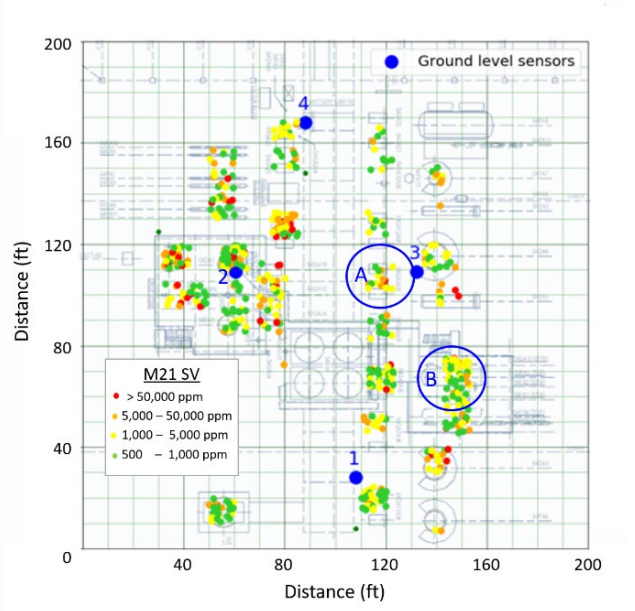

Figure 3-9. Leak clusters in historical CWP data

From the over five years of historical LDAR data, it is evident that leaks occur in clusters (over time), where component density is elevated around major equipment. As discussed in Section 5, the locations of component clusters (based on historical data or major equipment siting for new installations), along with prevailing wind directions, must be considered in the initial LDSN site deployment planning in order to optimally place sensor nodes. Illustrated here are two component clusters, labeled "A" and "B" that can be observed by LDSN node 3 under different wind conditions. From the perspective of node 3, the components located in the blue open circle labeled "A" represent proximate detection targets, with separation distances less than 20 ft from the closest sensor. This means that detection capability should be enhanced from this component cluster and M21 SVs obtained as part of the DRF should routinely include values towards the lower end of the DT band (Figure 3-7). Components in area "B" are much farther removed from node 3 (≈ 50 ft or more), so a single detected leak from this area (found solely by node 3) would likely possess a relatively large SV (e.g. > 50,000 ppm by FID).

It is important to consider that multiple simultaneous leaks of lower SVs could exist in cluster "B", with their combined effects producing a detectable signal on LDSN node 3. This real-world "*cluster*" detection potential is an important consideration in the development of the DRF and is detailed in subsequent sections. As an example-scenario in brief, the facility LDAR tech responds to a low-level LDSN node 3 detection (a PSL notification). The PSL detection box (Section 3.4) indicates that the emission is originating from Area B, and the technician is led to an approximately defined search area by the mSyte™ mobile device. The LDAR tech chooses to use OGI to screen the component cluster, looking for larger SV leaks (e.g. > 50,000 ppm). In this case, OGI fails to detect an emission so the LDAR tech uses fast-screen hand-held probe survey gear which has a ppb resolution (Figure 1-4) to check areas of the cluster. The technician identifies three probable leaking components and enters this information into the LDSN mobile device (data entry at this step is optional if M21-gear is also carried). The technician then uses M21 (at that time or at a later time) to pinpoint the three leak issues, quantify the SVs (e.g. 800 ppm, 2,000 ppm, and 5,000 ppm), and enters details into the LDSN mobile device to initiate the repair sequence under the DRF (as required). In addition to compliance and emission inventory data, the information provided by the M21 SVs is an important QA check for LDSN and is a surrogate for controlled-release studies to inform LDSN detection capability over time. In this case the *cluster* detection allows leaks that would normally be outside of the DT band (below DTL) to be found and fixed. The LDSN spatial node network coupled with the presence of multiple leaking components produces an effective increase in detection sensitivity, extending the DT band to lower values (in certain cases). This is called the DT band *cluster* limit or (DT*cluster*), and is described further in Section 4, along with other terms that are used in generation of specific emissions equivalency-modeling scenarios.

The DRF itself can help improve detection capability since even low SV leaks (e.g. 500-600 ppm) found during the PSL survey are repaired. These lower-level emissions may not significantly contribute to the PSL but represent "opportunistic finds", serving to enhance the emission control performance of LDSN/DRF. Because PSL notifications will persist if the subject leak(s) are not found, the DRF will investigate potential leak sources that would be time-prohibitive under the CWP. For example, leaks that occur from components that are exempt from regular monitoring (e.g. under insulation) may be found by LDSN/DRF, providing both emissions reduction and safety benefit. Additionally, emissions from AVO-identified leaks from

both regularly monitored and unmonitored LDAR components may be found and repaired faster using LDSN/DRF. Together these factors form the concept of overall emission control efficacy (ECE) for an NGEM-based innovative LDAR monitoring approach. In a similar manner, emissions that are not part of the LDAR program may be detected and repaired by LDSN/DRF. The LDAR ECE concept and the added benefit of non-LDAR program emissions detection and repair are discussed further in Sections 4 through 6 of this report. A summary of the basic detection performance terms for NGEM techniques like LDSN and OGI is contained in Table 3-1 with specific LDSN/DRF detection-related modeling terms contained in Table 4-1.

Table 3-1. Summary of LDSN/DRF detection sensitivity terms

LDSN/DRF Term	Acronym / Abbreviation	Description
Detection Threshold (Detection Threhold Band)	DT	A way to define the detection performance of NGEM approaches like LDSN and OGI (alternative to a single-valued method detection limit). The width of the DT band is caused by effects such as sensor to node distance for LDSN, gas to background temperature contrast for OGI, or mixes of gas RFs (for LDSN or OGI)
DT Average	DTA	The midpoint of the DT band representing the average detection performance of a single LDSN node for a single leaking component[1]
DT Upper	DTU	The upper limit of the DT band. A leak with mass ER (or M21 SV) > DTU should be detected at full node to leak separation distance[2]
DT Lower	DTL	The lower limit of the DT band. A single leaking component with mass ER (or M21 SV) < DTL is difficult to detect (low signal)[3]
DT (± 1 Standard Deviation)	DT ($\pm 1\sigma$)	Additional uncertainty in DTU or DTL when leak is documented by M21 SV measurement (a proxy for true mass ER)
Emission Control Efficacy	ECE	Conceptual term that accounts for all LDSN/DRF detection factors (distance effect, leak clusters, collaborative node detection, opportunistic DRF detections, etc.)

[1]For process units with multiple RF gas streams, DTA is estimated as a weighted average (Section 6)

[2]For process units with multiple RF gas streams, basic DTL is typically estimated using lowest RF component

[3]For process units with multiple RF gas streams, basic DTU is estimated using highest RF component with specific RFs used for compliance purposes

3.3 FHR SLOF Pilot Test

The next stage of system development involved long-term testing of prototype versions of LDSN/DRF at a working facility. The FHR SLOF in Port Arthur, TX, was selected for the first facility pilot test since it possessed real-world challenges but also was relatively small, with an open configuration that supported safe use of controlled-release testing for research purposes (not possible in larger process units). The FHR SLOF[30] is a bulk storage terminal permitted to receive, store, and distribute ethylene and propylene. Products are stored underground in natural salt dome caverns and recovered for sale through displacement by brine. When products are received from storage, the brine is displaced, degassed (controlled by flare), and placed in specially lined storage ponds for subsequent use. The SLOF process unit (Figure 3-10) includes filters, product measurement devices, filter-separators, a solid bed dehydration system, brine degassing facilities, a flare system, brine injection and transfer facilities, and other equipment.

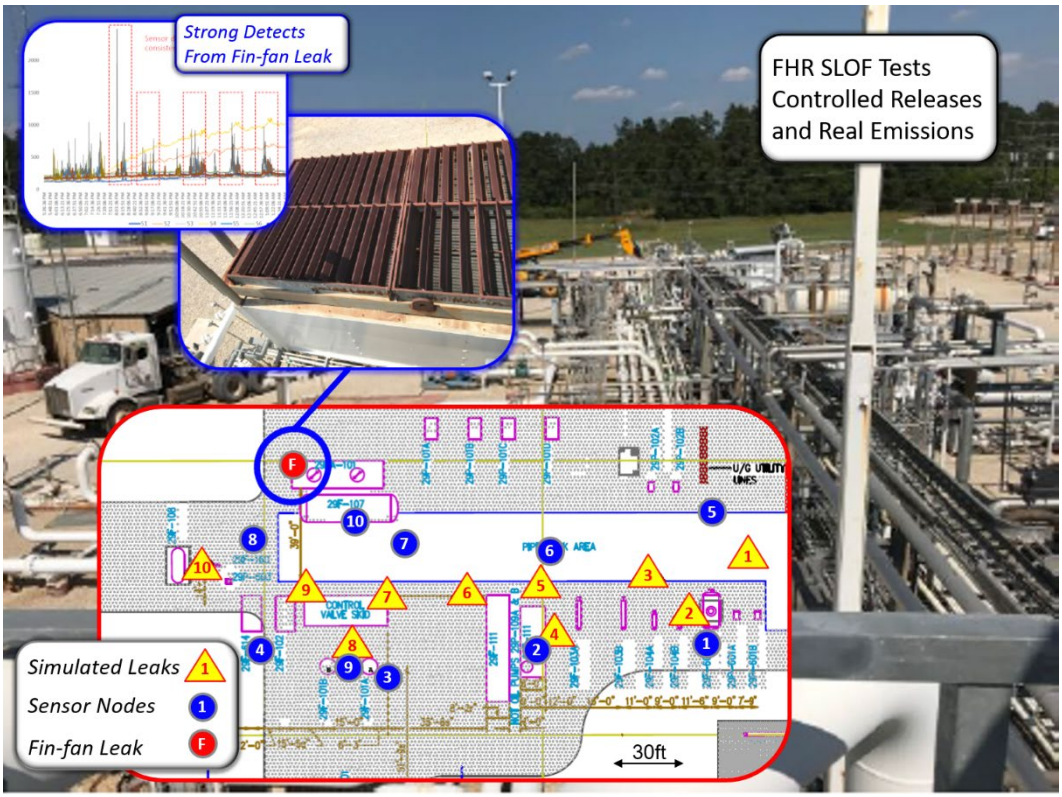

Figure 3-10. Overview of the FHR SLOF pilot test

The FHR SLOF pilot test was executed in two parts. A set up test was conducted from 5/14/2018 to 5/25/2018 and used LDSN Prototype 1 wireless sensors that were employed in the exploratory tests. This test informed aspects of sensor design and deployment as well as controlled-release point placement in the process unit to support the longer-term test to follow. The phase 1 test also helped Molex further develop the prototype multi-node wireless data handling hardware gateway, the initial version of the mSyte™ LDSN software and mobile device, while the team collaboratively advanced DRF concepts.

The primary SLOF test was executed from 9/10/2018 to 12/7/2018, using ten LDSN Prototype 2 Sensor nodes (Figure 3-5). Similar to the exploratory tests at EPA ORD, 48 controlled-release trials of 1 to 24-hour duration each were conducted in the SLOF tests to assist in understanding LDSN performance under various conditions. Figure 3-10 illustrates the controlled-release points (yellow triangles) and sensor node positions (blue circles) used in SLOF. For sense of scale, the distance between sensor node 1 and sensor 8 in Figure 3-10 is approximately 166 ft. The ten LDSN nodes were positioned at two elevations (two levels) within the process unit in preparation for the larger scale multi-level pilot test at FHR CC. To aid in source location algorithm development, wind speed and direction were measured in relatively free-flowing conditions just outside of the process unit. As with tests at EPA ORD, controlled releases of isobutylene and ethylene (separately) were executed from a single position (one release point at a time) that was moved between locations on multiple levels. Additional details on the SLOF test series are found in Appendix B.

In addition to controlled release tests using isobutylene (RF = 1), the LDSN deployment at SLOF had the objective to detect real-world process unit leaks of ethylene mix (RF ≈ 10). The RF of real-world leaks at SLOF is only approximately known since the low responding primary compound (ethylene, RF ≈ 10-15) was potentially co-emitted with small amounts of other compounds having RF < 10. LDSN sensor node spacing in SLOF was smaller due to the lower RF (average node to node separation of 30 ft). Key goals of the long-term SLOF test series were to generate important engineering data on LDSN node deployment over variety of meteorological conditions, further develop the LDSN source detection and location algorithms, and explore sensor QA response tests (called bump tests) and automated sensor health monitoring through mSyte™, further described in Section 5. These goals were largely met at SLOF, contributing advancement towards CRADA NTO 2, NTO 3, and NTO 4 (Section 1.3).

As described in the comparisons of CWP to LDSN/DRF attributes (Table 2-1), a technical strength of the latter is in the continuous discovery of significant emissions from non-LDAR program components. An example of this advantage was found at SLOF. At the initiation of the testing, the LDSN detected a strong emission source that was previously unknown to the facility. Prototype LDSN source triangulation through the initial mSyte™ algorithm provided location data to the FHR LDAR SME as a rudimentary PSL box. As part of the draft DRF, the SME scanned the PSL with OGI, but no leak was found. The OGI survey was followed by area scanning with fast hand-held probes (Figure 1-4) and further consultation with LDSN readings. Within two days the identification of a difficult to detect emission buried inside of the cooling loop of a heat exchanger “fin-fan” set was verified (location F and inset of Figure 3-8). Due to the nature of this leak, it could not be quantified with M21, as the probe could not directly contact the buried leak interface. Although M21 was not established, the level of response observed on multiple sensors to the RF ≈ 10 gas stream was indicative of a significant emission. This equipment is not part of the LDAR program so was not detected in previous M21 inspections. This particular leak could not be detected with OGI but was immediately apparent under LDSN. This delay of repair (DOR) emission could not be mitigated until the next facility shutdown (required major equipment disassembly). As a consequence, the fin-fan leak became a dominant feature in SLOF testing and was considered an “interfering source”. The fin-fan emission was used as a test case for source localization optimization and as an interfering source in controlled-release trials. Additional information on the SLOF test is found in Appendix B.

The presence of the constant fin-fan leak (as opposed to short-term tracer release tests) facilitated investigation of LDSN detection capability under a range of meteorological conditions. As discussed in Section 3-1, overnight lulls in wind speed (calms) coupled with compressed atmospheric boundary layers can significantly enhance leak detection capability. This effect is observed in Figure 3-11 where the fin-fan leak and other leaks in the SLOF process unit present a dramatically larger signal to the LDSN as the wind speed (gray trace, secondary axis) falls to well below 0.5 m/s on this evening. The presence of a significant leak in the process unit was made obvious by this diurnal effect with strong detections on a range of downwind nodes occurring as the temporal and spatial accumulation of emitted molecules in the stagnant airmass is followed by a brief “puff-flow” to the sensor node locations. Although leak detection is enhanced under these conditions, source location capability via multimode triangulation becomes more difficult under extremely low wind speeds and is the subject of future work.

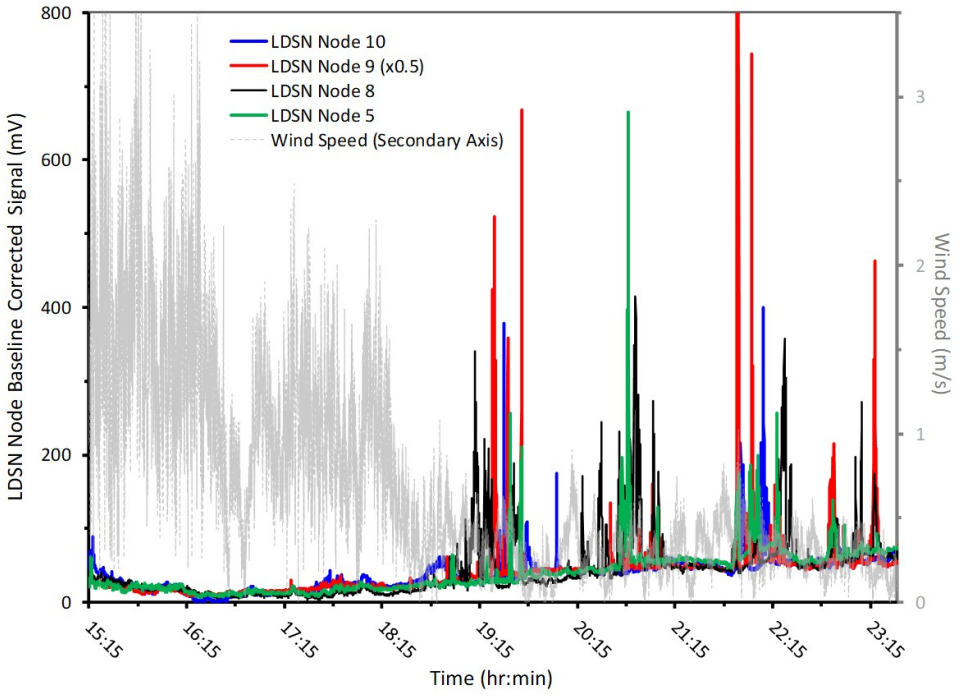

Figure 3-11. Fin-fan leak behavior over night

The fin-fan leak also allowed the ability of the early prototype mSyte™ algorithms to find and locate leaks within complex backgrounds to be developed and tested. Figure 3-12 shows an example of a daytime measurement where fin-fan leak (yellow dot) has been localized to Est. Leak Location 1 (green rectangle). Additionally, a controlled release of isobutylene at location L15 (yellow triangle) was similarly localized (green rectangle) by the early mSyte™ model. Here the mass ER of the controlled release (4.26 g/hr or 30 sccm), and other release rates for SLOF were larger than that used in the exploratory tests due to the strong fin-fan interference. The ability to LDSN/DRF to detect smaller leaks in the presence of present nearby emissions is the subject of ongoing work (Section 6).

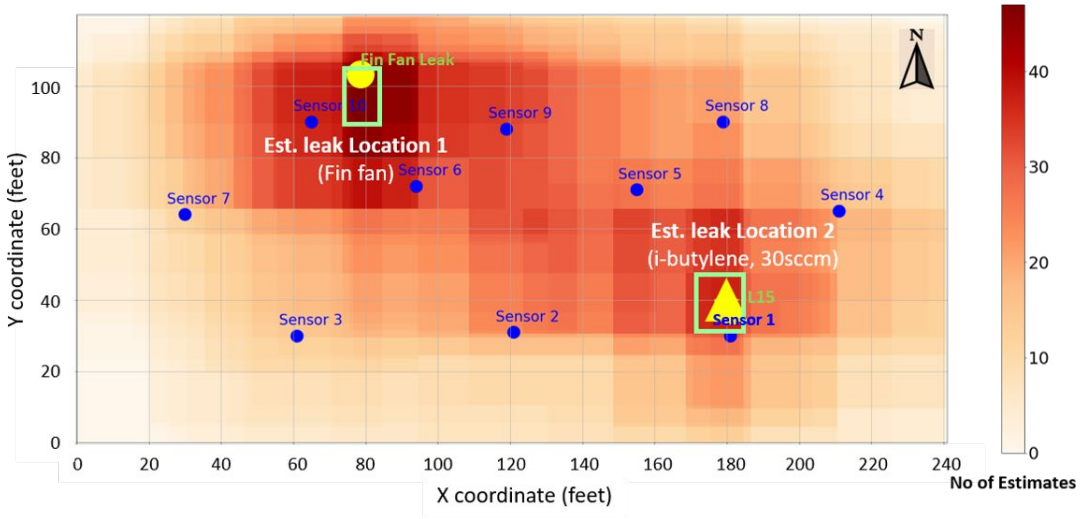

Figure 3-12. An early mSyte™ detection in complex background

3.4 LDSN/DRF Development 2

As presented in Figure 3-5, several versions of prototype sensors were developed by Molex and used in different phases of this CRADA project. Figure 3-13 provides a full picture of the pre-production version of the Molex Sensor used in the FHR CC test. This version was purposely designed to withstand harsh outdoor environmental conditions and be safe to install in refineries and other chemical plants where flammable gases may be present. These sensors take gas readings every second, and they transmit data via Wi-Fi to a local server which then forwards the data to the cloud via local wired routing. To uniquely identify sensors in the field, each sensor is assigned a Device ID based on its factory assigned MAC address. This sensor survived harsh summer conditions in the Gulf Coast and delivered consistent performance, based on regularly-conducted QA test data. A slightly improved version of the preproduction model was certified by Underwriters Laboratory (UL) in late 2019 to Class 1 Div. 2 hazardous location designation. In addition to gas sensors, the LDSN system has an integrated 3D ultrasonic anemometer mounted in open field to record the instantaneous wind direction and wind speed. It is currently believed that one properly sited anemometer that provides accurate prevailing wind data outside of the process unit is sufficient for most installations. Micro-scale wind flow patterns inside the process units are highly complex but are fundamentally determined by the prevailing wind outside of the unit. The leak triangulation (leak location) approach calculates an area of highest probability for the leak source, usually using multiple of days of prevailing wind data and sensor measurements. Leaning algorithms to account for leak source triangulation bias due to specific flow obstructions in a process unit for a given sensor network configuration is subject of ongoing research.

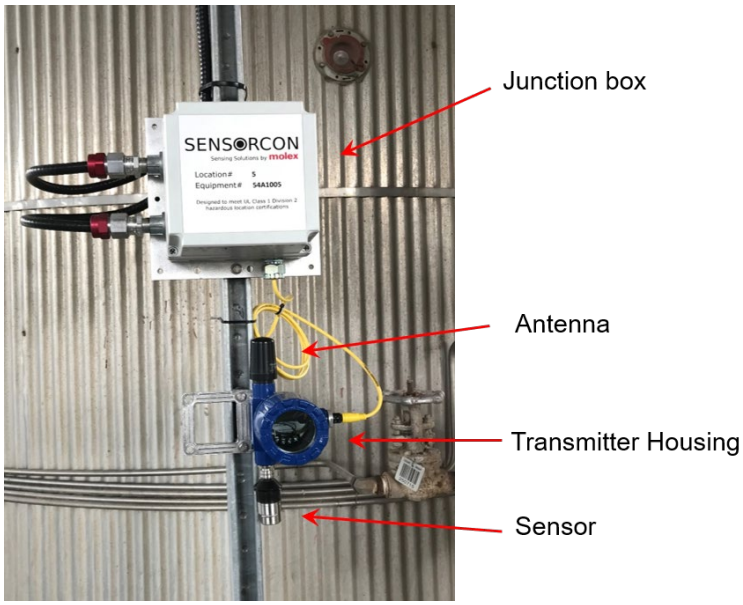

Figure 3-13. Molex's pre-production sensor - 2019

All data were stored in a MongoDB (New York, NY, USA) database on the Amazon Web Service (AWS) cloud (Seattle, WA, USA). Molex mSyte™ is a software platform that processes data from the LDSN, displays and reports the results and provides notifications based on preset rules and well-established algorithms. Molex mSyte™ also serves as a repository for all sensor data, including sensor QA and leak investigation records, as well as metadata of the plant such as

maintenance activities that may have an impact on the operation or detection results of the LDSN. Molex mSyte™ is designed to handle both LDSN and DRF requirements with some of the key elements presented in Figure 3-14.

Figure 3-15(a) is an mSyte™ screenshot of the output graph of a particular sensor node showing multiple detection peaks. The algorithm on the mSyte™ constantly analyzes the sensor data including identifying and calculating the strength of each detection peak and estimates the possible location of the leak source relative to the locations of the sensors using simultaneously measured wind data. Once the detection strengths and the number of detection events reach preset threshold values within a pre-defined time window, a notification with a PSL box is generated and sent automatically to designated personnel via emails or text messages. Figure 3-15(b) represents a screenshot of a PSL map on the mSyte™. The darker pink box represents an area where one or more leaks are most likely to be located while the lighter pink color defines an area with lower probability of leaks.

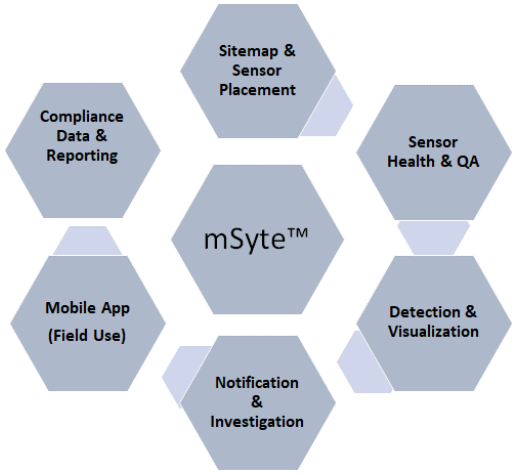

Figure 3-14. Molex's mSyte™ data platform

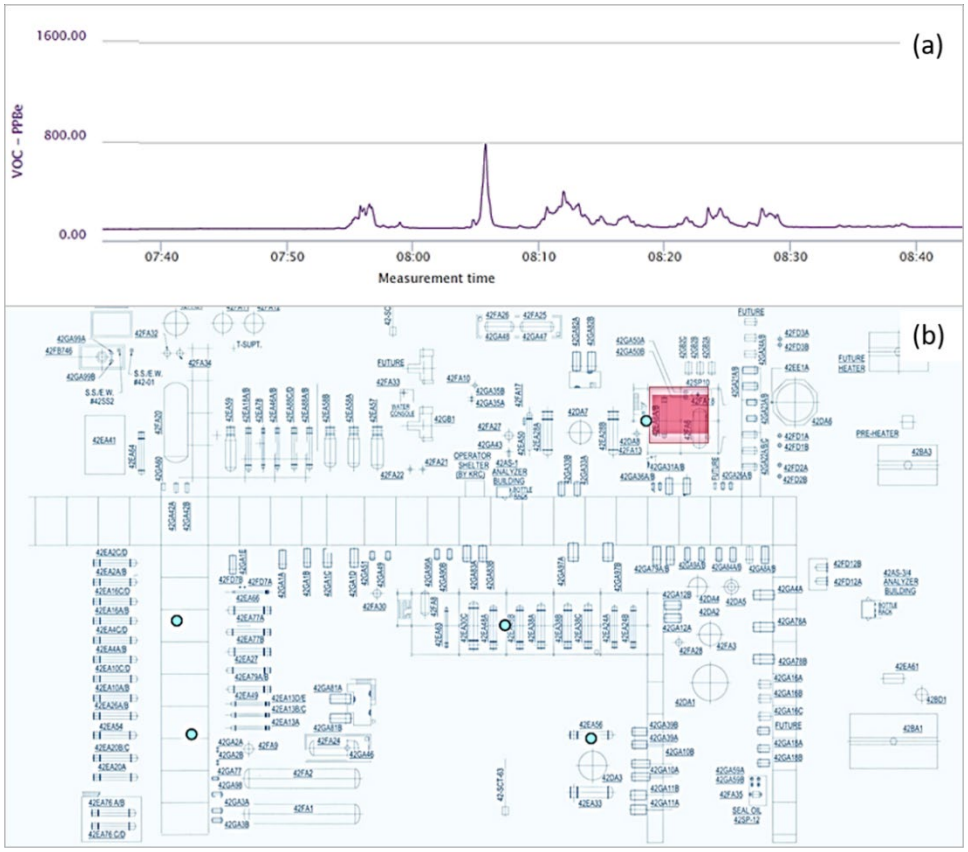

Figure 3-15. Leak detection on mSyte™ (a) sensor signal, and (b) PSL box

In the DRF following each detection notification, an LDAR technician is dispatched to the area defined by the PSL box to investigate the source(s) of emissions. While M21 equipment is a reliable way of pinpointing and identifying leaks, a hand-held ppb instrument has proven to be very effective in narrowing down the source locations given its high sensitivity, mobility, and proximity to actual leaks (typically <2 ft) in the search process. During our SLOF testing and FHR Corpus Christi pilot study, the larger leaks were typically found within 5-15 minutes, and oftentimes multiple leaks were found at each PSL. In the DRF, an LDAR technician can perform one or more investigations depending on how many leaks or emission events are identified. These investigations are numbered in sequence starting from 01 in the format of notification ID - xx. 19-SD-00005-03, for example, represents the 3rd leak investigation under notification#19-SD-0005. For each leak investigation, the component tag ID (if applicable), leak location, Method 21 ppm reading and time of the measurement, name of the technician etc. were all documented through a mobile app called mSyte™ mobile (see Figure 3-16). If no leak is found or a PSL box is found to be related to an authorized emission, for example, this info will still be entered for records. A PSL notification cannot be closed without all related investigations being closed out properly and general threshold settings being met. Figure 3-17 is a sample of mSyte™ leak investigation dashboard.

Figure 3-16. LDAR technician demonstrating the mSyte™ mobile device

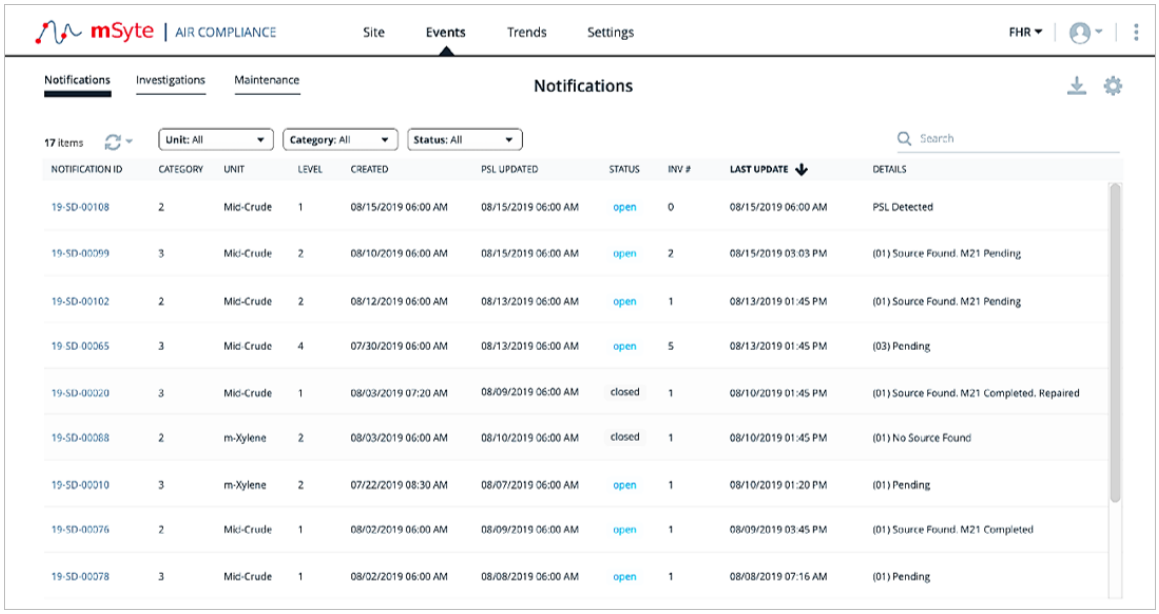

Figure 3-17. mSyte™ leak investigation dashboard

3.5 FHR CC Pilot Test

The FHR CC pilot tests were conducted in the summer and fall of 2019 in the Mid-Crude and m-Xylene process units at FHR's Corpus Christi West refinery. The primary objective of the FHR CC pilot set was to deploy and test the most advanced version of LDSN/DRF produced to date in a real-world setting. Due to safety issues, controlled release testing was not performed in these tests, but, as an alternative, information from M21-measured leaks was used to further the understanding of systems performance. Extensive planning and preparation were required to deploy the LDSN and to interface with the facility on the DRF. Factors such as placement of sensor nodes within the process units are further discussed in Section 5.

The LDSN was first implemented in the m-Xylene unit with operations beginning on 5/1/2019. The LDSN was operational in the Mid-Crude unit on 7/1/2019. The pilot test ended in both units on 11/30/2019. FHR CC Mid-Crude is a typical crude oil refining process unit, similar to that found in many refineries. The m-Xylene unit is also typical but is a finishing unit (not a full reforming process), so it exhibits a very high percentage of aromatics in the gas stream. As described in Section 3.2, these two process units have products and gas streams with 10.6 eV PID RFs of 2.5 (Mid-Crude, composite mix) and 0.8 (m-Xylene, aromatics). There are also refinery fuel gas streams in Mid-Crude that are used for process heaters with methane as a primary constituent. These fuel gas streams are typically not well suited to LDSN monitoring using the 10.6 eV PID sensor, so they were treated separately in the process unit's monitoring plan (Section 5.1). For Mid-Crude, 38 pre-production prototype LDSN sensor nodes (Figures 3-5 and 3-13) were installed in six levels. In the smaller m-Xylene unit, ten LDSN nodes were installed on four levels (Appendix C1). A view of the two process units is provided in Figure 3-18, with Figure 3-19 presenting conceptual views inside of an FHR CC process showing the DRF in action. Exact locations of sensor nodes can be found in Appendix C1.

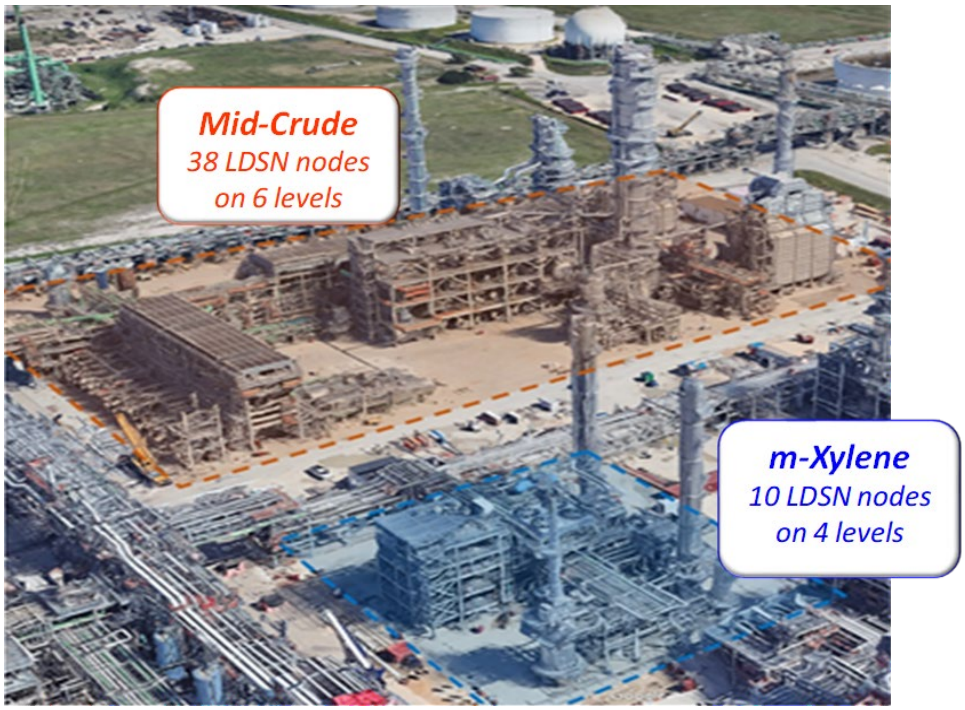

Figure 3-18. View of Mid-Crude and m-Xylene process units

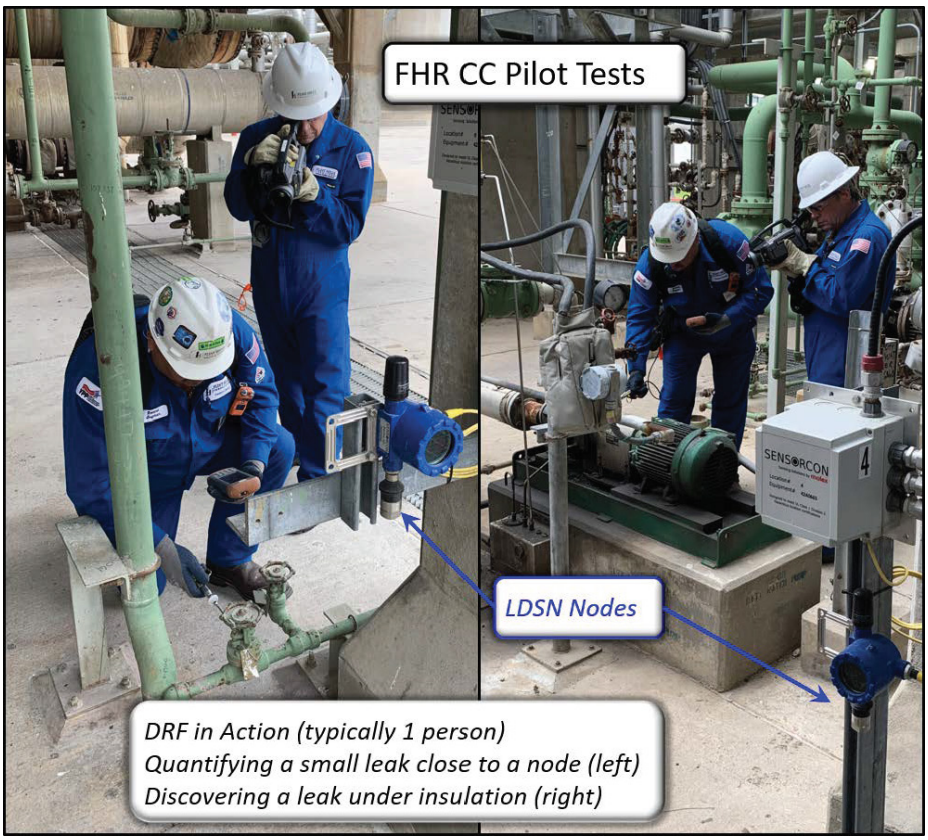

Figure 3-19. Examples of DRF leak quantification

Unlike the SLOF pilot test, both units were vertically developed, comprising up to six levels of elevations with maximum height (excluding towers) of 58 ft for m-Xylene and 92 ft for the Mid-Crude. An accurate 3D model of the process units was not available during the preliminary sensor placement planning. The CRADA team worked instead with 2D master drawings of main floors with elevated areas shown as inserts on the side of the drawings. The LDSN network node positions for the progressive levels of Mid-Crude and m-Xylene units are shown in Appendix C1, Figures C1-1 to C1-11, with small numbered red points representing sensor node locations and the colored circular regions representing a 60 ft detection radius around each sensor node. The different colors correspond to different elevations of each sensor node and were carefully chosen based on both location of a high density of LDAR program components and proximity to a local power source, while avoiding direct impact from steam present in the plant.

As detailed in Section 4, historical LDAR data can be an important tool to assist in understanding LDSN/DRF performance compared to the M21-based CWP. In brief, FHR CC Mid-Crude and m-Xylene units have 26,667 (2016-2018) and 9,313 (2014-2018) monitored LDAR components under the CWP, respectively. Excluding the high RF fuel gas-related components, there are 24,172 components in Mid-Crude and 9,313 components in m-Xylene that are relevant to the LDSN pilot studies. For this subset of components, if we consider time periods where valves, pumps, and connectors were all monitored, a 3-year historical analysis period in the Mid-Crude unit may be represented. The m-Xylene unit has a longer history of comprehensive M21 monitoring, so a 5-year historical analysis is appropriate. From 2016 through 2018, a total of 358 reportable leaks (LDSN-relevant) over 500 ppm SV were found in Mid-Crude (119 per year on average). Over a 5-year period in m-Xylene from 2014 through 2018, 563 reportable leaks were found (112.4 per year on average). Considering leaks with SVs between 30,000 ppm and 100,000 ppm (highest value reported), there were on average 11.3 and 11 such leaks per year found in Mid-Crude and m-Xylene, respectively.

Figure 3-20 provides an overview of leaks detected in the FHR CC pilot by the LDSN/DRF. A total of 39 leaks were found by the system in the Mid-Crude unit during the 5-month pilot study. In the m-Xylene process unit, 67 leaks were found by LDSN/DRF over a 7-month period. The DT band for isobutylene (RF = 1) from Figure 3-7, superimposed for discussion purposes, is close to the 10.6 eV LDSN DT band for m-Xylene for the 50-60 ft default node spacing. With an RF = 0.8, the DTA for m-Xylene is ≈ 4,000 ppm, whereas the DT band for the Mid-Crude unit (RF = 2.75) is shifted higher with DTA of ≈ 12,500 ppm (Figure 3-8). It is apparent that in both process units, the LDSN/DRF system was detecting and repairing leaks that were below the respective DTLs for the units. As detailed in other sections of this report and Appendix E, there are several factors that contribute to this expected result, including (1) presence of smaller leaks located very close to a sensor node, (2) additive effect of groups of smaller leaks DT (cluster) detections), (3) opportunistic repair of leaks discovered as part of the DRF, (4) enhancements in leak detection capability due to channeled wind flow or special meteorological conditions and/or (5) inaccuracies of M21 proxy for mass ER (integrated emissions from leak interface underestimated by point concentration measurement).

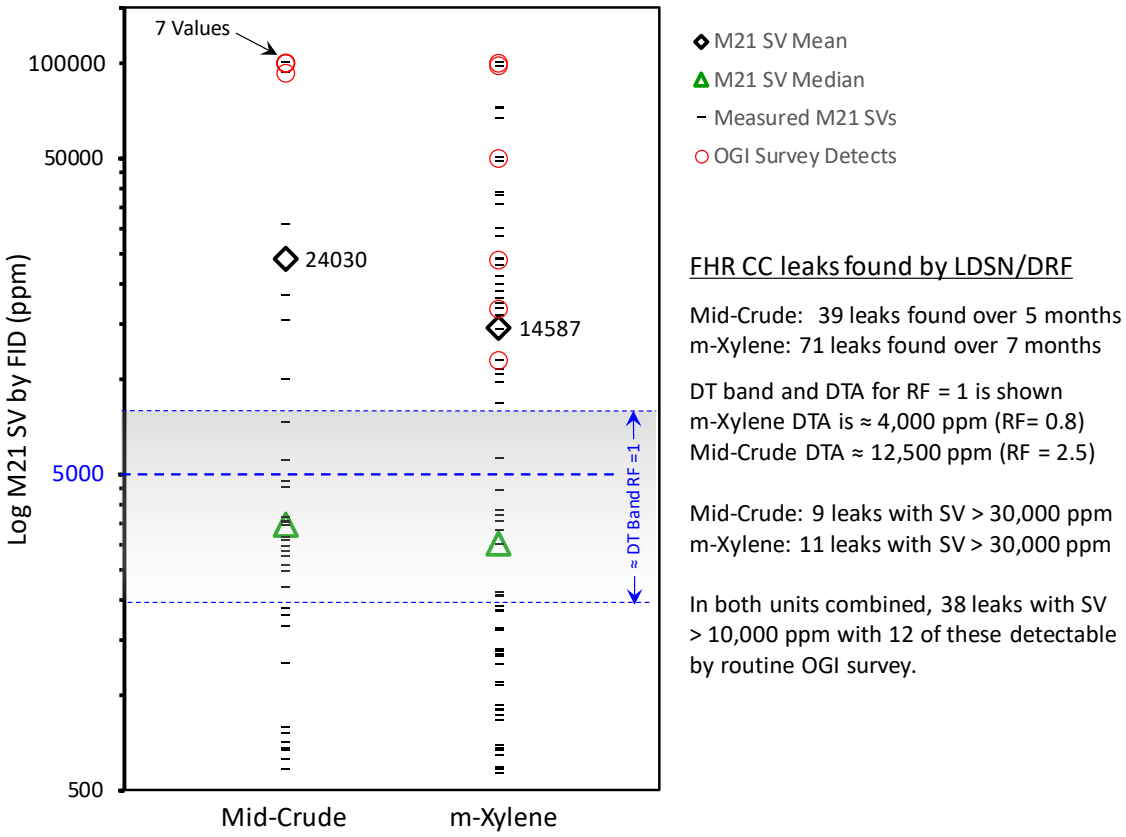

Figure 3-20. FHR CC pilot test summary

The ability to find and fix small leaks is important to support environmentally sustainable operations and also in the emissions equivalency calculations described in Section 4. However, the key benefit of LDSN/DRF is more rapid identification and repair of the larger leaks, which disproportionately drive overall process unit emission levels. In the m-Xylene unit, a total of 11 leaks were found that exceeded 30,000 ppm SV with two leaks registering at or near the maximum reported value of 100,000 ppm. In Mid-Crude, nine leaks possessed SVs above 30,000 ppm with seven of these at 100,000 ppm. In both units combined, there were 38 leaks with SV at 10,000 ppm or higher with a total of 12 of these leaks (32%) judged detectable by OGI survey, as executed by the FHR LDAR SME. An additional five of these 38 leaks were judged by the FHR SME be detectable by OGI with "high difficulty" (a term derived by the FHR SME indicating detection with OGI camera used in extreme proximity to the component with knowledge of the leak presence and exact location identified with other instruments). The lowest SV leak detected by OGI with high difficulty had an SV of 9,800 ppm. No other leaks below 10,000 ppm were detectable by OGI. For the ten leaks with SVs > 90,000 ppm, eight of these were "routinely detectable" by OGI, one leak at 100,000 ppm was in the "difficult to detect" category, and one leak at 100,000 ppm was not detectable. The routinely detectable and difficult to detect categories were derived by the FHR SME with the former indicating probable detection during a standard OGI survey. In follow-on OGI observations of several of the leaks, some were judged to be more detectable and some less detectable indicating conditions at the time of survey play a factor in the OGI DTs (assuming leak mass ER remained constant). Overall, 61% of

LDSN/DRF-discovered emissions originated from connectors, 25% from valves, and 14% from all other sources including pumps, drains, open ended lines, and components or sources that were not part of the LDAR monitoring program.

Due to resource limitations, it was not possible to execute a complete M21 inspection just prior to and directly after the FHR CC pilot efforts. However, M21 under the CWP continued to be executed (independent from DRF testing) as per standard procedures during the pilot tests in both process units. A comparison of the SV values (in ppm) for leaks detected under routine M21 inspection and by LDSN/DRF during the pilot studies is contained in Table 3-2, with "N" indicating the number found in each category. In both cases, the LDSN/DRF approach found larger numbers of high SV leaks (reflected in higher mean values). As expected, a significant number of smaller leaks were found in the areas of the process units that were subject to comprehensive (100%) CWP inspection (a technical advantage of the M21-based CWP, Table 2-1).

Table 3-2. Comparison of M21 SVs leaks detected by CWP and LDSN/DRF

	Mid-Crude found by LDSN/DRF	Mid-Crude found by CWP	m-Xylene found by LDSN/DRF	m-Xylene found by CWP
Average	24030	13302	14587	4352
Median	3463	4892	3020	945
σ	39075	20201	22527	14553
Minimum	582	540	564	500
Maximum	100000	81568	100000	100000
N	39	23	71	59

When assessing this LDSN/DRF to M21 CWP comparison, the following factors must be considered. Because this was the first test of the technology in a complex refinery unit, some adjustments to the LDSN detection algorithms acceptance levels were made during the test. As discussed in Section 5, LDSN adjustments and node placement optimization would be an expected part of an implementation start up. There were instances where LDSN identified potential leaks, but draft notification and localization thresholds were not yet reached. This process was interrupted by the standard M21 sweep through the area finding, documenting, and repairing leaks. Valuable information was learned regarding some of the larger emissions that were detected by CWP that were not robustly observed by LDSN/DRF. In total there were four leaks found by M21 CWP in Mid-Crude that were above the DTU of 24,000 ppm (Figure 3-8). Similarly, there were four leaks in m-Xylene above DTU of 6,800, using uncorrected M21 data.

A closer examination shows that seven leaks >10,000 ppm went undetected by the LDSN but were found by M21 CWP in the Mid-Crude unit. Further analyses shows that two of the leaks took place in areas outside the 50 ft sensor coverage, four were missed due to temporarily unfavorable wind conditions (a notification was yet to be issued for such a leak but it was found under the CWP), and one miss was ascribed to an ineffective search in the DRF. As a result of the analysis, six more sensors are planned to be added to the unit to provide a more complete

sensor coverage, and a more effective hand-held VOC detector was employed in the leak search of the DRF process. In order to mitigate the seasonal wind effect, the sensitivity of the LDSN was increased by reducing the number of plume detections required to generate a detection. Shortly after the sensitivity change, two new PSL notifications were issued in the 4th floor fin-fan area where three larger leaks were identified by M21 before the DRF (Appendix C3).

4.0 LDSN/DRF to CWP Equivalency

To establish an AWP, the proposed work practice must demonstrate a reduction in regulated material emissions at least equivalent to the reduction achieved under current federal requirements [40 CFR 65.8(a) and other regulations]. In this case, LDSN/DRF must deliver the same or better emissions reductions as obtained under the scheduled M21 LDAR CWP. This is typically referred to as demonstration of emissions equivalency. This section presents one possible emissions equivalency analysis approach which utilizes historical M21 SV data from the FHR CC LeakDAS® (Inspection Logic, Louisville, KY, USA) database acquired over a multiyear period. While a generalized assessment of the LDSN/DRF concept equivalency to the CWP is part of CRADA LTOs, the presented analysis considers only the currently realized form of LDSN that uses a 10.6 eV PID sensor. The following analysis focuses on the FHR CC m-Xylene (RF = 0.8) and Mid-Crude (RF = 2.5) process units with the nominal 60 ft sensor node spacing that was employed in the 2019 pilot tests, with four additional sensors that are currently operating in the Mid-Crude unit. A Monte Carlo emissions simulation approach was selected for the equivalency evaluation, consistent with the 2000 EPA equipment leak AWP approach and the later OGI evaluation.[31] Two sets of Monte Carlo emissions models are presented, the EPA ORD analysis and the Molex analysis (see Table 7-2 for acknowledgments). Section 4 consists of the following subsections:

- Section 4.1 discusses historical leak inventory data captured in LeakDAS® for the subject process units. Several types of emissions, their relation to the LDAR work practice, and how these emissions are tracked are described.
- Section 4.2 describes the procedures used in the emission equivalency comparison in general terms, starting from the processing of the LeakDAS® data, followed by the preparation of the data for Monte Carlo simulations. A nonproprietary version of the leak data used in the emission simulations is contained in Appendix E2. Section 4.2, with support from Appendices E and F, describes the EPA ORD and Molex emission equivalency simulation approaches.
- Section 4.3 discusses and compares select results for the EPA ORD and Molex emission equivalency simulations.
- Section 4.4 describes LDSN/DRF factors associated with different types of LDAR and non-LDAR program emissions described in Section 4.1. Some of these emission types that are routinely detected and mitigated under LDSN/DRF were not considered in the analyses of Sections 4.2-3 and produce additional emission reduction benefits.
- Section 4.5 summarizes the results presented in Sections 4.3 and 4.4.

As a general note, evaluating AWP performance relative to historic emissions data is not necessary to demonstrate equivalency to federally required practices (as outlined in 40 CFR 65,

Subpart F).[32] The FHR CC process units are subject to both federal and state regulations. In some cases, state regulations may be more stringent than federal requirements, and the inventories also reflect additionally protective work practices implemented voluntarily by FHR. Therefore, comparing AWP performance to historical process unit data is less favorable than a strict comparison to federal regulations. This analysis can be considered a conservative, protective evaluation, rather than a definitive determination of LDSN/DRF equivalency to the federal CWP.

4.1 Historical LDAR Monitoring Data m-Xylene and Mid-Crude

The FHR CC LDAR team maintains extensive historical records on LDAR activities across the plant in their LeakDAS® database, including a detailed inventory of M21 SV measurements. For the emission analyses subsequently described, m-Xylene LDAR program component SV measurements from January 2013 to June 2019 were consolidated to develop a list of active leaks in the 2014-2018 and 2016-2018 time frames for the m-Xylene and Mid-Crude process units, respectively. This analysis included leaks from all component categories (e.g. valves, pumps, connectors), although AVO-discovered program leaks and non-LDAR emissions are not considered in the primary analysis (see Section 4.5). The Mid-Crude analysis was limited to three years because connectors were not included in scheduled LDAR monitoring in this unit prior to 2016. The procedure for identifying historical leaks is discussed in more detail in Section 4.2 Emissions Equivalency Analysis Approachand is outlined further in Appendix E1. The lists of process unit leaks considered in this analysis are included in Appendix E3.

The LeakDAS database includes records for 27,037 and 9,474 unique component tags between 2013 and 2019 for Mid-Crude and m-Xylene respectively. Connectors, which are typically monitored on an annual basis, represent 64% and 70% of the tracked components while valves, usually monitored quarterly, comprise 34% and 29%, respectively. The remaining components, other than pumps, are typically monitored on a quarterly basis as well. Pumps are monitored monthly, and the database included 121 and 25 unique pump tags for Mid-Crude and m-Xylene, respectively.

Figure 4-1 presents a high-level summary of the historical leak populations for both the m-Xylene and Mid-Crude units for their respective modeling time periods. Figures 4-1(a) and (d) show the portion of leaks by component category. In both units, more than half of the leaks are from connectors. Given that connectors are subject to less frequent annual monitoring under the CWP, this category is likely to show more substantial benefits under the proposed AWP's continuous monitoring. Pumps are subject to monthly monitoring and therefore present less of a potential benefit due to long periods of inattention. However, their frequent leaks from a small population (<0.5% of all tracked components) do suggest that continuous monitoring could be beneficial if pump locations are accounted for in LDSN design.

Figures 4-1(b) and (e) present the general leak SV distribution while Figures 4-1(c) and (f) present the portion of leak emissions based on leak SV magnitudes for each unit. In each case, the portion of leaks with SVs greater than double the LDSN DTA is relatively small (<15%). However, these leaks, which would be both more likely to be detected and detected quickly due to their magnitude, are responsible for more than ¾ of emissions for each unit. By identifying and repairing these leaks rapidly and effectively, LDSN/DRF can more efficiently distribute LDAR resources than the CWP.

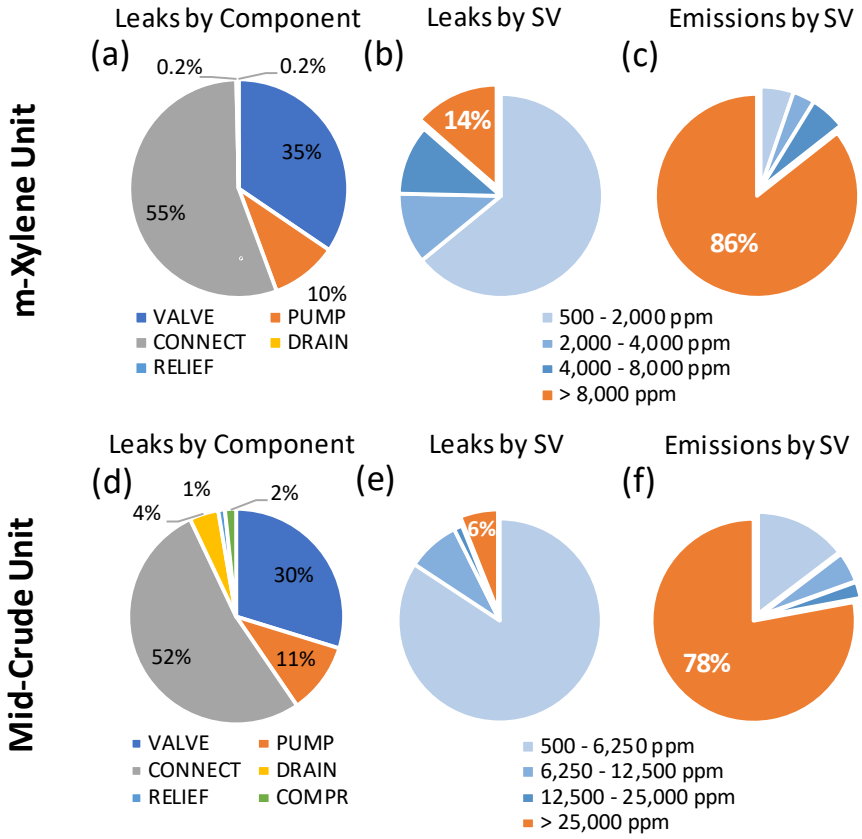

Figure 4-1. Historical LDAR leak apportionment by component category, SVs, and emissions (a-c) m-Xylene, and (d-f) Mid-Crude, respectively

Figure 4-2(a) presents the distribution of primary leak SVs in the process units. The cumulative emissions profiles are shown in Figure 4-1(b) with 100,000 being the largest reported M21 SV, as determined by FID. The total number of leaks represented in m-Xylene and Mid-Crude are 568 (5 years) and 299 (3 years), respectively. Note that these do not reflect the total number of leaks reported, but rather the number of leaks identified as appropriate for LDSN simulation. As discussed in Section 3.5, fuel gas leaks are excluded from the current analysis. In Figure 4-1(b), emissions are determined from the as-reported (uncorrected) SV values for m-Xylene units using the Synthetic Organic Chemical Manufacturing Industry (SOCMI) correlation equations, while the Mid-Crude units uses the petroleum equations.[2] These are the same procedures FHR uses to report annual emission inventories. In both cases, the process units show similarly skewed distributions. Within the simulation sample set, leaks with SVs >30,000 ppm represent < 7% of the detections for these process units and account for approximately ¾ of the emissions. Leaks with SVs >10,000 ppm represent about 10% of detections and account for >80% of emissions. The CWP's systematic approach results in identifying a large population of leaks, which invariably will include these more significant sources. However, the majority of leaks found are responsible for a small portion of leak emissions due to the skewed nature of the leak size distribution.

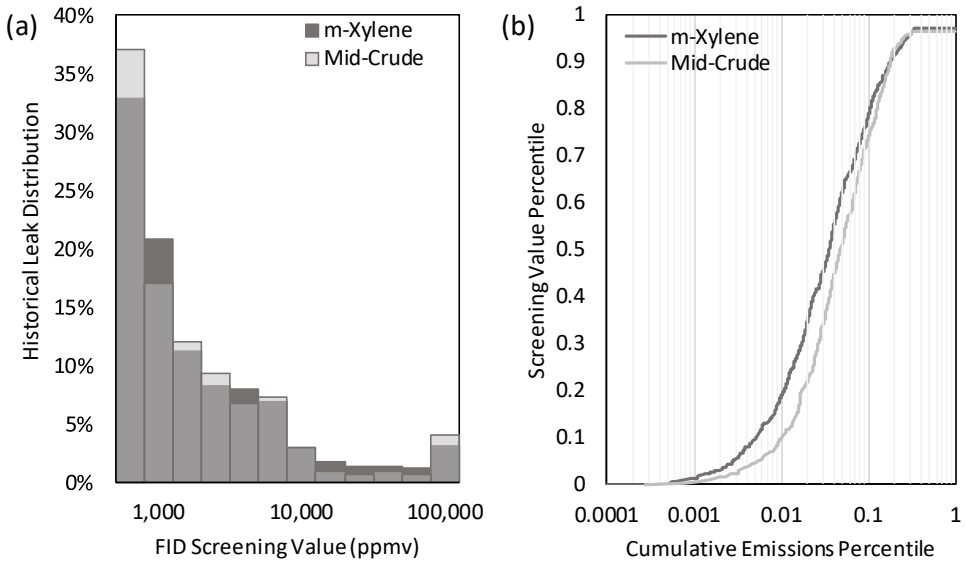

Figure 4-2. FHR CC historical leak profiles (a) SV distribution, (b) cumulative emissions

A strength of the LDSN/DRF concept is the potential to detect leaks and other emissions that are either difficult to find under the CWP or are not covered under the LDAR work practice (called non-LDAR program leaks). There are a variety of reasons why potential leak interfaces may not be included in scheduled M21 monitoring, and the emissions contributions of these leaks are comparatively poorly understood. Some potential leak interfaces would normally be part of the M21-monitoring program but are exempted because they cannot be properly accessed with the M21 contact inspection probe. Examples of this category are connectors that are covered by thermal insulation. Some components are difficult to monitor because they are elevated requiring temporary scaffolding, so they are monitored at a lower frequency. Some leak interfaces, such as components in heavy liquid service, are part of the LDAR work practice, but due to low expected emission potential, are not monitored using M21. Emissions from this category may be detected by process unit operators using AVO procedures,[33-34] with each finding and associated repair captured in LDAR documentation. Non-LDAR program leaks, for example the fin-fan leak of Section 3.3, and other emissions may also be detected by AVO, or by safety monitoring equipment in severe cases. As opposed to AVO-detected LDAR program leaks, non-LDAR program leaks/emissions are not tracked in LDAR documentation. Instead, they follow the applicable reportable and non-reportable emission event guidelines (e.g. 30 TAC 101.201).

As previously discussed, emissions from these source types can be relatively large and can go undetected for significant lengths of time. The historical AVO LDAR record offers some indication of the LDAR program leaks from unmonitored components under the CWP. For m-Xylene (2014-2018) and Mid-Crude (2016-2018) there were 24 and 42 total AVO leak detections respectively, approximately 4% and 12% percent of total leaks, which might be detectable by LDSN (Figure 4-3). The distribution of AVO leaks is not clear because, in many cases, an initial SV measurement was not taken prior to repair. However, pilot results suggest that AVO leaks may be found at a higher rate under LDSN/DRF than CWP. Moreover, the presence of these leaks indicates that there is a not-insignificant population of leaks which an

LDSN system may be able to detect far more rapidly than is currently possible.

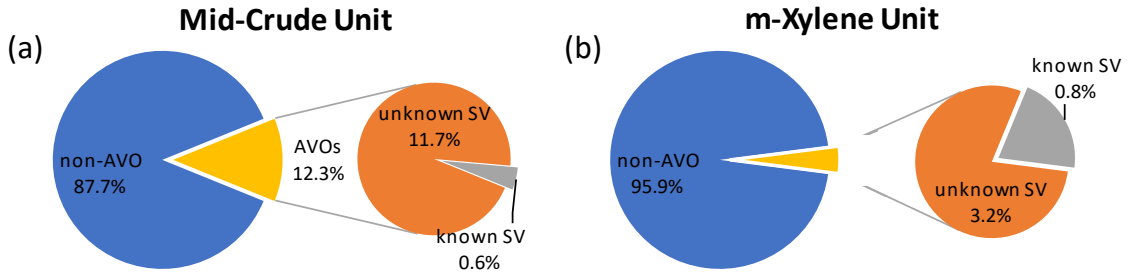

Figure 4-3. Historical AVO leak identification: a) Mid-Crude and (b) m-Xylene

While this leak inventory and the associated analysis described in the following sections are particular to the two process units, the leak data used is typical of, if not fully representative of, similar process units. Given this, the equivalency results are specific to the two FHR CC units. However, broader patterns and conclusions about the effect of the LDSN/DRF concept may be assumed to be generally applicable so long as the method limitations and caveats discussed across Section 4 are considered.

4.2 Emissions Equivalency Analysis Approach

This section describes an evaluation of leak emissions control under the scheduled M21-based CWP compared to LDSN/DRF control using a Monte Carlo simulation approach and variations on detection performance assumptions. This is called the "EPA ORD analysis" and was developed by Haley Lane as part of her Oak Ridge Institute for Science and Education (ORISE) NGEM research appointment with EPA ORD (Section 7.2). The EPA ORD analysis differs slightly in defined terms and approaches to the analysis independently developed by Molex, described in Section 4.2 and Appendices E and F.

Demonstrating equivalency relative to M21 is difficult due to associated uncertainties of the CWP and the unknown uncertainties and performance levels of a proposed AWP. EPA guidance recommends a Monte Carlo simulation approach as a useful tool for evaluating possible AWP performance. Monte Carlo simulations evaluate a broader array of scenarios and can elucidate the impact of expected variation on a method's performance. The U.S. EPA's 2000 guidance presents a method for establishing AWP equivalency and a threshold; "an alternate work practice should provide at least the same or better environmental protection as the current work practice in 67 percent of the simulated tests".[31] Two different Monte Carlo simulation models were developed to evaluate the LDSN/DRF concept equivalency relative to scheduled M21 LDAR: one by EPA ORD and one by Molex ("EPA model" and "Molex model"). Both models simulate emissions over multi-year periods in order to study the long-term performance of LDSN/DRF controls. This section is primarily focused on a summary of the EPA model results, some comparisons to the Molex approach, and a discussion of the equivalency implications. A more thorough review of both model methods and results is included in Appendix E1 and Appendix F.

4.2.1 LeakDAS Data Processing

The Monte Carlo models developed by both EPA ORD and Molex evaluated simulated multi-year emissions using FHR CC historical data. The LeakDAS dataset discussed in Section 4.1 was

chosen in order to test LDSN/DRF effectiveness with the most recent, representative dataset available for each FHR CC pilot test unit. Historical, process unit-specific SV data was chosen in lieu of a broader approach in order to focus the analysis on the pilot study and evaluate two specific, existing embodiments of the LDSN/DRF concept. In contrast, the original EPA Guidance and OGI AWP analysis used a 1993 dataset of SV measurements from 24 different units in order to characterize the SV distribution and the 1993 Petroleum Industry Bagging Data to simulate the SV to mass correlation.[35] While this analysis seeks to remain consistent with the EPA Guidance and OGI AWP approaches wherever possible, the approach was adapted to use unit-specific historical data, better evaluate LDSN/DRF benefits and limitations, and study emissions over longer time periods.

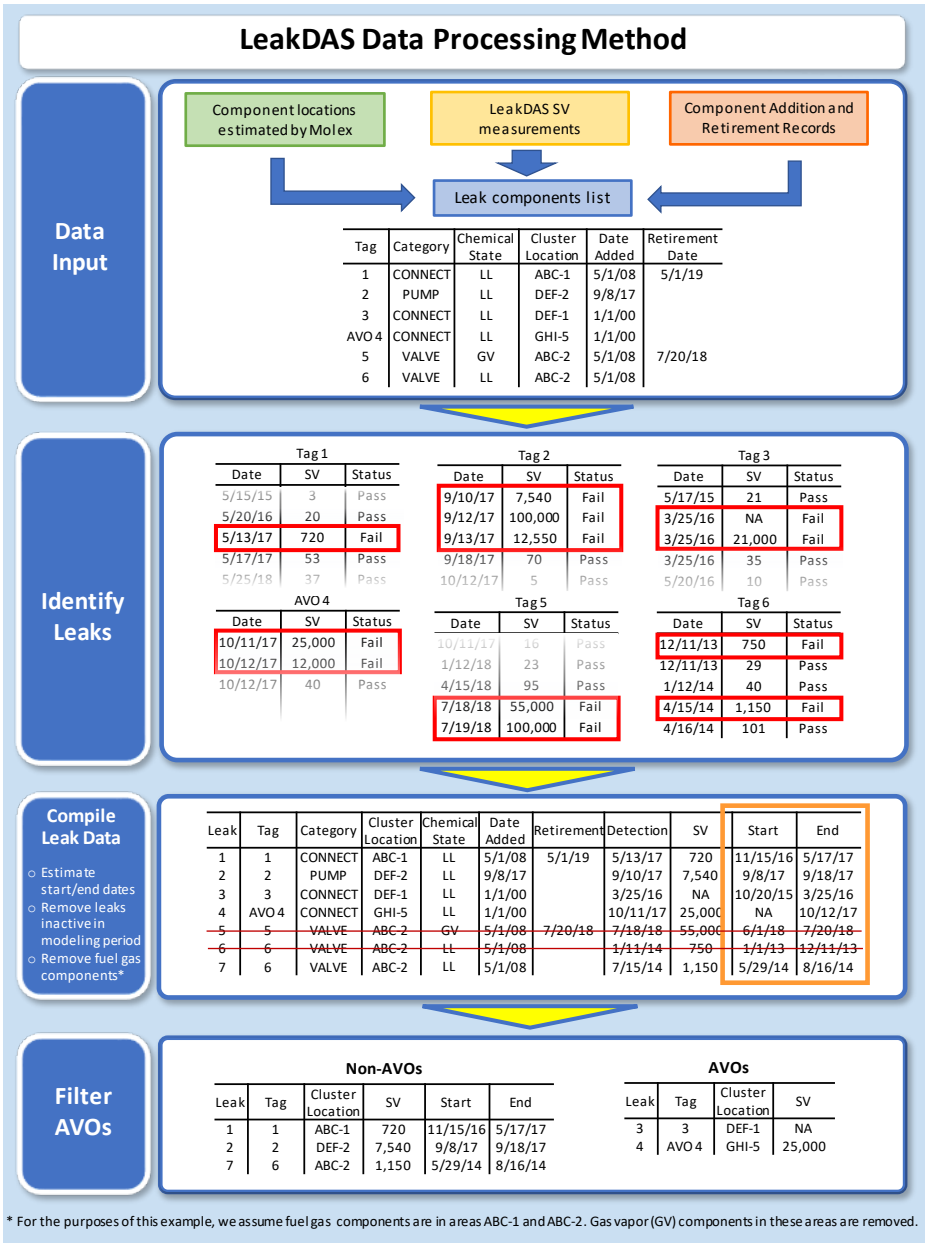

Figure 4-4. LeakDAS data processing methods

The LeakDAS inventory is a rich dataset which details a variety of LDAR activities across the FHR CC facilities over time. This analysis used Thermo Fisher Scientific TVA measurement and AVO records between the years of 2013 and 2019 to characterize m-Xylene and Mid-Crude leak profiles. Individual measurements were determined to be unsuitable for this purpose because leaking components tend to be overrepresented. While a non-leaking component is generally measured once a monitoring cycle, a leaking component may be measured several times prior to a successful repair. The dataset was processed in order to develop a list of active leaks between the years of 2014-2018 and 2016-2018 for m-Xylene and Mid-Crude, respectively. Leaks were identified based on individual component historical records, and the dataset development procedure is presented in Figure 4-4. For further discussion of EPA ORD processing methods, see Appendix E1, and see Appendix F1 for a discussion of Molex methods.

4.2.2 Emissions Calculations Methods

The equivalency analysis presented in this section derives from the methods of the original AWP Monte Carlo guidance and the subsequent OGI analysis, but it differs in significant ways. The original guidance focused on comparing the effectiveness of M21 to methods which had no reliance on M21. Given that the current DRF assumes M21 will be used to quantify each individual leak that is found, this approach was unsuitable. Emissions presented in this chapter can be considered a reflection of the SVs and leak inventory reporting rather than a simulation of true mass emissions. Moreover, the original guidance did not calculate emissions, instead focusing on total process unit emission rates. This approach would not reflect the potential benefits, nor the limitations, of the LDSN/DRF concept because its primary benefit lies in reducing the duration of large emission sources. The OGI analysis also noted this limitation and updated the Monte Carlo analysis to compare total emissions, rather than emission rates. The analysis presented in this report made an additional update by extending the length of modeling time and considering all LDAR component categories. The OGI assessment limited its scope to emissions from valves within a single quarter. Early LDSN/DRF modeling indicated that longer time frames would better demonstrate the long-term equivalency of this new AWP, and the component sample was broadened to better characterize the process units. Finally, this method differs from the two previous versions in its focus on process unit specific historical data. While a more broadly transferable equivalency analysis is possible, it was not within project scope.

The LDSN/DRF concept is a new method, and pilot testing was limited to two process units. The transferability of the approach is complicated by a variety of variables, but the overall theory of the method was established by CRADA collaborators. What remains uncertain is the exact level of performance in any given specific embodiment of the concept. Pilot testing provided important supporting data. However, the equivalency analysis sought to begin examining the long-term viability of the proposed AWP from an emissions perspective. Given the significant unknowns, three different LDSN/DRF emissions scenarios were modeled in comparison to CWP emissions. These scenarios were based on an understanding of the method theory as outlined in Section 3 and Appendix F2. A description of modeling terms used in the EPA ORD analysis is contained in Table 4-1, and terms for the Molex analysis are presented in Table 4-2.

Table 4-1. Description of EPA ORD modeling terms

EPA Modeling Term	Acronym / Abbreviation	Description
Detection Threshold - *Average* (Same as Table 3.1)	DTA	Most conservative emission modeling scenario that uses the average RF for process unit. Assumes individual leaks with SV > the process unit DTA are detected within 3 days and repaired within 7 days. See Table 3-1 for additional notes on DTA determination. This calculation approach does not require information on the position of the sensors or the leaks.
Detection Threshold - *Band* (Same as Table 3.1)	DT	More realistic emission modeling scenario that takes into account distance to sensor effects on detection threshold (accounts for DT band width) for single leaking components. See Figure 4.3 for detection distance calculation. Assumes individual leaks with SV > calculated threshold are detected within 3 days and repaired within 7 days.
Detection Threshold - *Cluster* EPA ORD Modeling Term	DTC	More realistic emission modeling scenario that combines DT with additive effect of multiple closely-spaced leaks forming a cluster (combined SVs of cluster can also exceed detection threshold). See Figure 4.3 for calculation description. Assumes individual leaks or leak clusters with SV > calculated threshold are detected within 3 days and repaired within 7 days.

Table 4-2. Description of Molex modeling terms

Molex Modeling Term	Acronym / Abbreviation	Description
Detection Threshold Average - Single Tag	DTA(tag)	The DTA(tag) modeling scenario assumes that single tag leaks with SV > DTA are detected in the fugitive emission simulation. The DRF process takes 10 days (3 days to detect and 7 days to repair).
Detection Threshold Average - Cluster	DTA(cluster)	The DTA(cluster) modeling scenario assumes a cluster of leaks with the sum of SVs > DTA are detected in the fugitive emission simulation. The DRF assumes leaks above the cluster repair threshold (3000 ppm) will be repaired one by one. If no individual leaks above this threshold are found, the model assumes that up to 3 leaks will be repaired under the defined DRF, i.e. 3 days to detect and 7 days to repair.
Detection Threshold Band - Single Tag	DT(tag)	Same as DT in EPA ORD's simulations. This is a more realistic scenario than DTA(tag) since it takes into account distance to sensor effects on detection threshold for single leak components.
Detection Threshold Band - Cluster	DT(cluster)	Same as DTC in EPA ORD's simulations. This is a more realistic modeling scenario than DTA(cluster) since it takes into account of distance to sensor effects. In this scenario, a leak closer to a sensor has a greater contribution to the total detection signal than another leak of the same size within one cluster and contributions of these leaks to the detection signal are mathematically modelled.
Equivalency-required Detection Threshold Average	eDTA	eDTA represents a target average detection threshold that LDSN/DRF as a whole must achieve in order to demonstrate M21 CWP equivalency in total fugitive emissions for a given process unit. In Molex's simulation, eDTA is conservatively calculated as the average value of DTA(tag) and DTA(cluster).
Equivalency-required Detection Threshold Upper limit	eDTU	eDTU is the DT value or smallest leak that should be detected by the sensor network at the farthest distance away from a sensor in order to achieve equivalency to M21. In Molex's simulation, eDTA is conservatively calculated as 1.5 times eDTA.

None of these approaches can be considered the definitive method at this stage of concept development. Simulations demonstrated that the LDSN/DRF systems would take time to reach steady-state control (see Section 4.2.3). Therefore, further testing is necessary to establish the exact mechanism for LDSN/DRF control and the expected performance levels. However, these scenarios were designed to provide a range of potential performance levels. While the DTA scenario is the simplest approach, the DTA value itself is an aggregate based on the varying emissions compounds, the sensor model, and sensor spacing in the process unit. It was chosen as an initial approach, similar to that applied in the OGI AWP, in order to provide an easy, straightforward performance test. Note that no modeling tested varying individual leak emissions RFs. However, testing evaluating varying DTAs is presented in Appendices E and F.

The DT and DTC scenarios were developed in order to consider the additional physical processes which would impact LDSN detection capabilities. Distance plays an important role in emission dispersion and has both positive and negative impacts for LDSN/DRF. Smaller leaks located near sensors, which would be ignored under the DTA scenario, may be detectable in practice. Conversely, larger leaks, which the DTA scenario would assume are detected, may be difficult to identify due to location. The facility layout, sensor siting, and local meteorological conditions would contribute to whether distance effects are a net benefit, and it is important to account for areas with higher component density when developing LDSNs. The location effects were modeled using a heuristic distance transformation based on the theoretical distance-concentration relationship (see Appendix F2 for additional information). The equation below presents how detection was determined for the DT scenario:

$$\text{Equation 4-1:} \quad \frac{SV}{D^2} \geq \frac{DTA}{1{,}250}$$

In Equation 4-1, D is the distance between a leaking component and the nearest sensor, and 1,250 is D^2 for the typical furthest distance anticipated with 50 ft sensor spacing ($50/\sqrt{2}$). Note that exact component locations were not known. Instead, general component areas (clusters) were determined and leak locations were randomly generated within cluster regions for each simulation iteration. The DTC scenario also used the distance heuristic with an additional effect. In practice, it was observed that groups of smaller leaks in a concentrated area could produce detections despite no single leak being above the DTA. The cluster scenario represents this effect by assuming a detection occurs when the conditions represented in Equation 4-2 are reached.

$$\text{Equation 4-2:} \quad max\left(\sum\left[\frac{SV}{D^2}\right]_{a,i}\right) \geq \frac{DTA}{1{,}250}$$

In Equation 4-2, the maximum sum of transformed SV for cluster *a* relative to any sensor *i* should be greater than the transformed DTA. Neither of these approaches is necessarily an exact representation of these physical processes as they function at FHR CC. However, they are theoretical portrayals which provide additional insight into how the LDSN/DRF will control emissions from LDAR components. Both the Molex and EPA models tested additional variations of these scenarios and several other options which are discussed in Appendices E1 and F1.
The Monte Carlo model simulated varying leak profiles in order to test a wider array of possible emissions. Control performance for these leaks was estimated for all three LDSN scenarios and compared to simulated control under the CWP. A variety of assumptions were made in order to simplify emissions simulations. These assumptions and their basis are presented below:

(1) Leak samples are representative

It was assumed that the overall leak datasets created using historical data were reflective of future leak distributions. Leak samples were created using random sampling with replacement to test a broader range of potential SV distributions. Leak start times were randomly generated within the modeling period using a unit variate. Samples were limited to 250 (Mid-Crude) and 500 (m-Xylene) leaks. It was assumed that this would be representative of potential SV distributions which might be detected by LDSN.

(2) No variability for M21

No variability was modeled for M21 measurements because both methods rely on M21 to determine the leak size. The model assumes no difference in SV if a leak is found by CWP or LDSN/DRF, regardless of differences in detection date. The first M21 measurement of a failing M21 record for a given leak was assumed to be representative of that leak's size up until the point of detection.

(3) No variability for LDSN detection

No variability was modeled for LDSN detection. This is an area for further research, but there was insufficient data to characterize LDSN variability at the time of model creation. Instead, three separate scenarios were developed to model a range of potential control scenarios. Additionally, LDSN detection was assumed to correlate directly to M21 measurements. In practice, LDSN detections may correlate more strongly to true mass emissions than M21 measurements, given the known variability of M21 and the possible variability of LDSN. This area of variation was not explored in this analysis to simplify the number of variables within the Monte Carlo models.

(4) No repeat leakers

The EPA ORD model assumed no repeat leaking components within the modeling period. In this case, leaks from the same component were each treated as separate, individual leaks within the same cluster region. This assumption was made to remain consistent with the previous OGI analysis and avoid issues which arise when simulated leaks "overlap" due to randomized start times. EPA ORD assumed that leaks which occur after an original leak cannot be assumed to occur before the first leak from that component. Molex did not make these assumptions and modeled components with multiple leaks, assuming this is a better reflection of process unit emissions. This difference in approaches constitutes the primary difference in EPA ORD and Molex emissions estimates.

(5) All components subject to the same CWP monitoring schedule

In practice, some components may be subject to varying schedules due to a variety of regulation intricacies. However, all components of a given category were assumed to be subject to the same CWP schedule—monthly pump, annual connector, and quarterly inspections for all other components. Note that both the OGI and EPA AWP Guidance only evaluated quarterly CWP monitoring because both analyses were limited to valves. The EPA ORD model assumed that inspections occurred on the first day of a given month, using dates between 1/1/2014 and 1/1/2019. The Molex model assumed inspections occurred every 30, 90, or 365 days. These approaches resulted in some differences in emission estimates which were small in the aggregate Monte Carlo results.

(6) Repair occurs seven days after detection

Regulations require that leaks be repaired within 15 days, and most leaks are repaired on the first attempt within five days of detection. Seven days was chosen as a conservative assumption and applied to all four modeling scenarios. Three extra detection days were added to the LDSN leak repair process.

(7) Analyze leakers only

Emissions for components with SVs less than 500 ppm were not considered, consistent with the OGI analysis, because the level of control is assumed to be equal under both work practices. In practice, it is possible that leaks which might be detected under LDSN due to location or cluster effects would not be identified under the CWP. However, this possibility was ignored due to the inclusion of Assumption (2). The DRF requires that any detected leak above the leak definition (typically 500 ppm) will be repaired.

(8) Constant mass emission rates

For the purposes of this analysis, emission rates were assumed to be constant for the entirety of a leak's duration. Emission rates were based on the first SV measured as a failing M21 record for historical leaks. For an exploration of non-constant emission rates, see the Molex analysis presented in Appendix F1.

While the CWP emissions are generally reflective of what would be reported emissions, they are not directly comparable to those reported numbers. First, the set of historical leaks used for simulation was a subset of the overall leaks due to limitations of the LDSN system (e.g. emissions from sources with unfavorable RFs). Emissions from components with SVs less than 500 ppm were not included because the control level was assumed to be equal under both work practices. Additionally, the component emissions were based on the first failed screening value measurement for a given leak rather than the entire history of SVs. This was done both as a simplifying assumption and to maintain consistency across model scenarios. The Molex and EPA ORD emissions estimates are also not directly comparable, primarily due to the difference in approach with respect to components with repeating leaks. For further discussion of these differences see Appendix E1.

4.2.3 Monte Carlo Simulation

The four different LDAR control scenarios (CWP, DTA, DT, and DTC) were incorporated into an emissions model that was tested using Monte Carlo simulations. The EPA ORD simulation steps are outlined in Figure 4-5, and Figure 4-6 presents the Molex simulation approach. Both the Molex and EPA ORD simulations varied the leak population sample, leak start times, and the component locations (within bounded cluster regions) for each simulation iteration. No error was applied to the SV measurements or control performance. None of the evaluated scenarios should be considered a definitive representation of LDSN/DRF or CWP emissions. Instead, they represent a likely spectrum of possible LDAR leak control efficacy in comparison to CWP performance. The potential benefits from non-LDAR leaks were not explored in this analysis, and AVO leaks were excluded due to the lack of preceding inventory measurements, as discussed in Section 4.2.1.

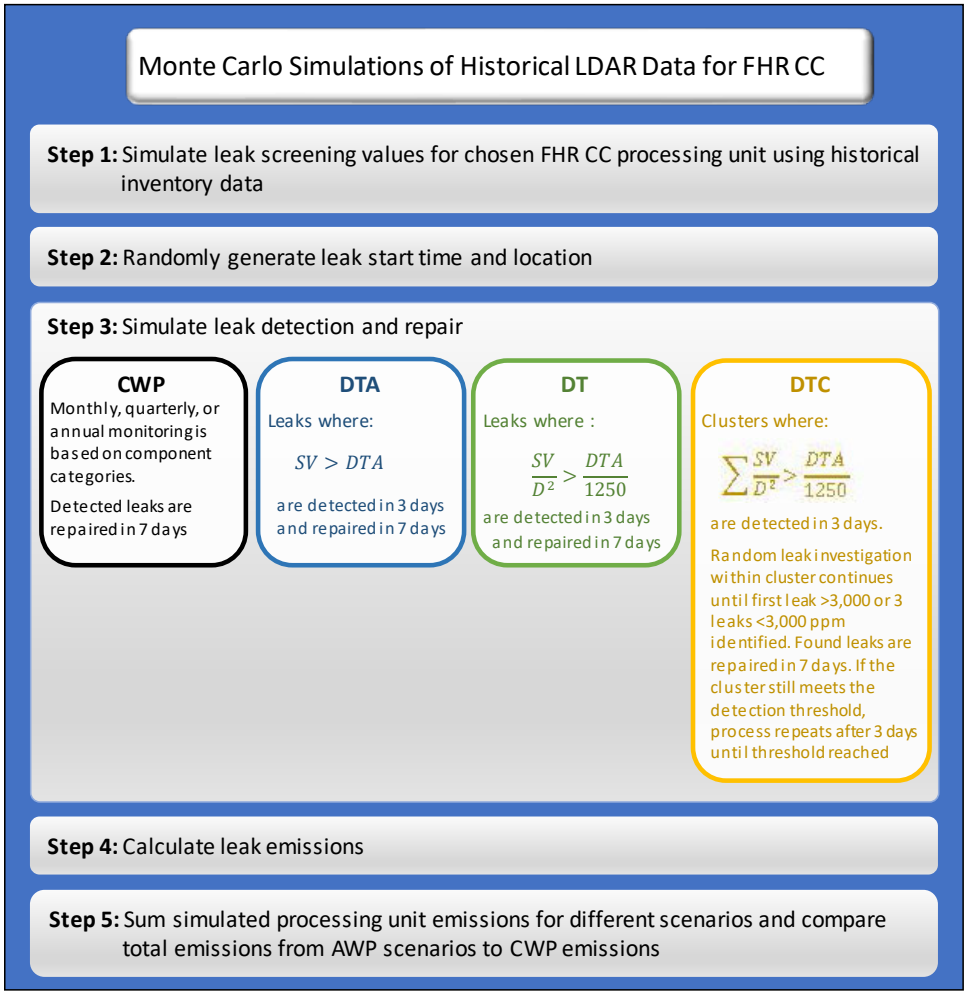

Figure 4-5. EPA ORD Monte Carlo emissions model

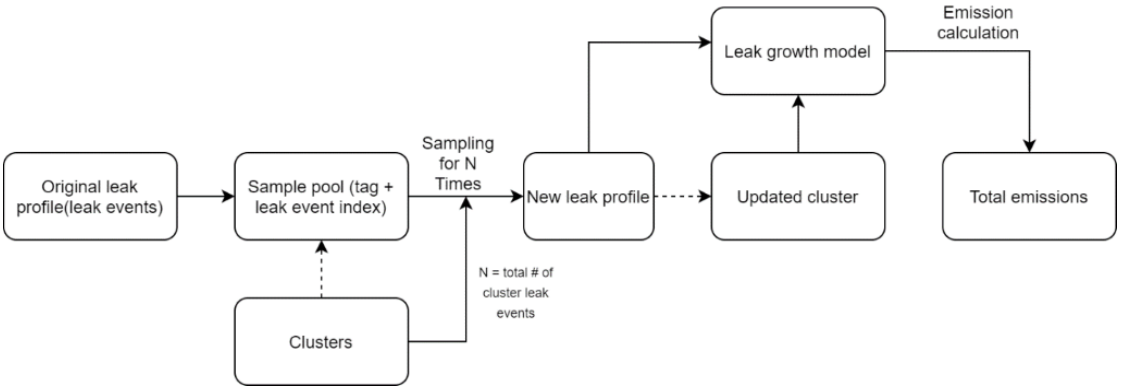

Figure 4-6. Molex Monte Carlo emissions model

In order to better understand the effects of the different emissions scenarios, individual simulation iterations were reviewed. Modeled emissions presented in Figure 4-7 and 4-8 are from a single EPA ORD model iteration but can be considered representative of the overall emissions and control patterns observed.

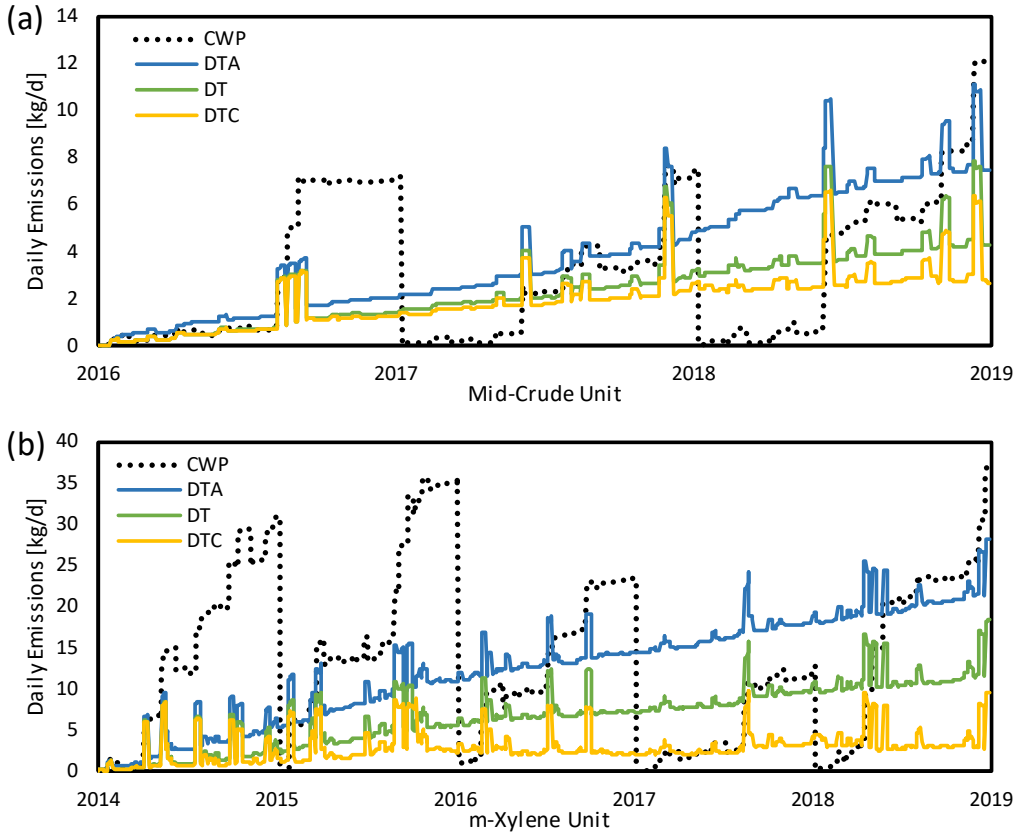

Figure 4-7. Example EPA ORD Simulation of daily emissions: (a) Mid-Crude, (b) m-Xylene

The emission rates shown in Figure 4-7 illustrate several LDSN/DRF strengths and constraints. Figure 4-7 shows the modeled daily emissions from the 3 scenarios compared to historical LDAR management. The m-Xylene unit (b) demonstrates faster detection of larger leaks, most clearly at the beginning of both 2014 and 2015. Similar performance can be seen in the Mid-Crude unit (a) mid-way through 2016. Additionally, the m-Xylene DTC model appears to reach a relatively steady state of control where the baseline level of daily emissions is reasonably stable after an initial adjustment period. This is due to low average DTA and DRF constraints which require repair of any leaks found with SVs greater than 3,000 ppm. It also illustrates that this adjustment period may need to be accounted for when developing performance thresholds. The DTA and DT model scenarios do not have a mechanism for fixing leaks which do not trigger an alert under each scenario's' detection threshold. This results in a baseline of emissions from smaller leaks which become more prominent as time goes on. It is a conservative modeling choice to not allow for repair of some leaks which do not trigger a system detection given the proposed DRF requirements (see Section 6).

Conversely, the Mid-Crude unit (a), demonstrates less effective control. The AWP scenarios are more similar for Mid-Crude than for m-Xylene, and the baseline daily emission rate increases steadily over the modeling duration. There may be some level of steady state, or near-steady state, achieved for DT and DTC, but a longer modeling period with additional data would be necessary to confirm. These examples illustrate a less effective embodiment of the LDSN/DRF

concept, and this is apparent in the net cumulative emissions as well (see Figure 4-8(a)). The modeled m-Xylene unit emissions (Figure 4-8(b)) show significant reductions relative to historical emissions for two of the three scenarios and modest reductions with DTA assumptions. Modeled Mid-Crude emissions also demonstrate equivalency for the DT and DTC cases but fail to demonstrate equivalency for the DTA scenario. For Mid-Crude DTA, the increasing daily emissions baseline produced by smaller leaks which are not detected becomes dominant relative to the reductions from quickly repaired larger leaks. The DT and DTC performance demonstrates the importance of considering distance effects both when designing a LDSN and when evaluating equivalency.

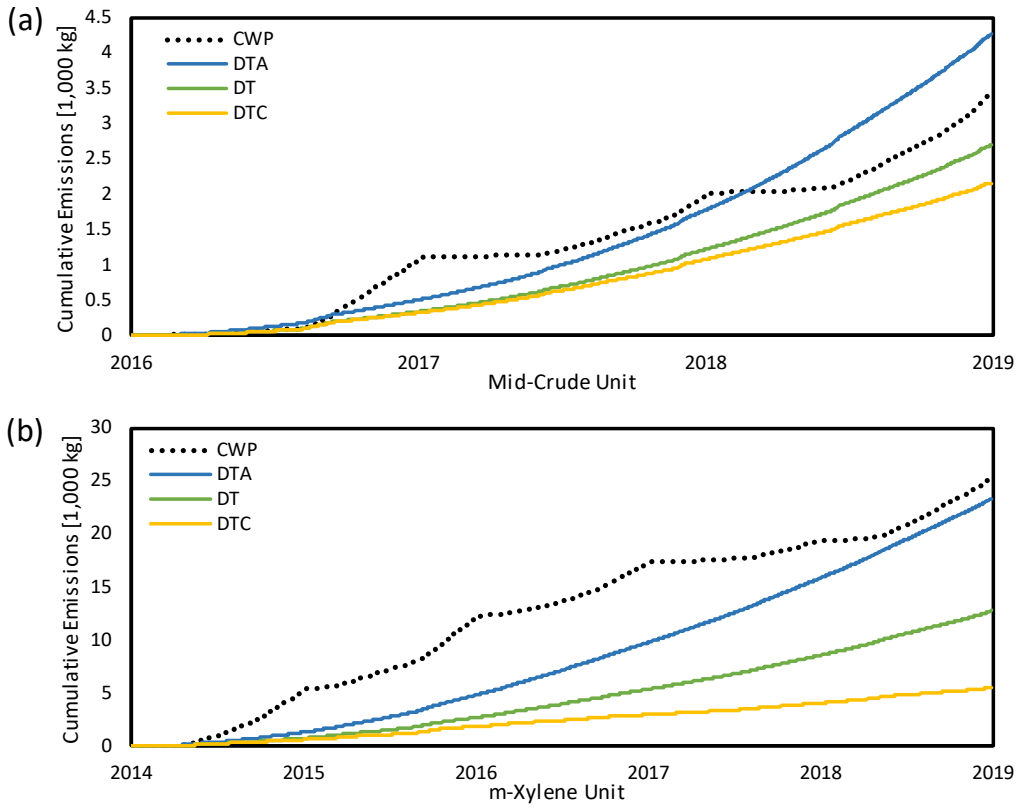

Figure 4-8. Example EPA ORD simulation of cumulative emissions: (a) Mid-Crude, (b) m-Xylene

Both the Molex and EPA ORD Monte Carlo model were used to evaluate three different LDSN/DRF control levels and analyze a variety of different system constraints and model limitations. The historical results presented are reflective of an average EPA ORD simulation iteration, and cumulative results are discussed in Section 4.3. For a discussion of additional model and control scenario analysis, see Appendices E1 and F1.

4.3 Simulation Results

This section presents results from the EPA ORD and Molex Monte Carlo models which simulated emissions under LDSN/DRF LDAR programs in order to evaluate if the existing FHR CC systems would produce equivalent control to the CWP. The simulations focused on leaks originating from LDAR program, non-AVO components given the relative lack of knowledge

about other leak sources and in order to remain consistent with previous equivalency approaches. For a discussion of emissions sources not evaluated in this simulation, see Section 4.4.

The results of this analysis suggest that the LDSN/DRF systems installed at the FHR CC facility would be equivalent under the current embodiments. Equivalency summary results are presented in Table 4-3. In 10,000 iteration simulations, the m-Xylene unit demonstrated equivalency rates greater than the 67% threshold across all three scenarios for both the Molex and EPA ORD models. In contrast, the Mid-Crude unit did not establish equivalency for the DTA scenario in either model. This is due primarily to the unit having a DTA more than double that of m-Xylene (12,500 ppm). The DTA scenario was the most simplistic; it assumed that no leaks with SVs below the DTA would be detected by the system. Pilot test results suggest that this assumption is not born out in practice. However, the lower level of equivalency does reflect the Mid-Crude system's lower level of control relative to the m-Xylene unit.

Table 4-3. Equivalency simulation results

Processing Unit	m-Xylene		Mid-Crude	
Model	**EPA**	**Molex***	**EPA**	**Molex***
n	10,000	10,000	10,000	10,000
DTA	78.0%	100%	20.7%	59.0%
DT	99.8%	100%	72.4%	93.2%
DTC**	100%	100%	92.5%	92.8%
* Non-growth emissions model ** EPA and Molex cluster models reflect different DRFs				

While the summary results indicate that the LDSN/DRF concept can demonstrate equivalency, the net emission results provide additional insight. Figure 4-9 presents boxplots of the EPA ORD simulated net emissions for the LDSN/DRF scenarios compared to scheduled-M21 LDAR. In this presentation, an equivalent simulation iteration would be less than or equal to 0 kg net emissions. The relative levels of control under each LDSN/DRF scenario are clearly demonstrated in the differences in median net emissions. All six datasets display significantly more left-tail outliers with skewness ranging from 0.26-0.42. Additionally, the net emissions illustrate the added emissions reductions needed to achieve equivalency or additional benefits of LDSN/DRF. The 67th percentile of net emissions can be considered an indicator of the additional reductions necessary to achieve the equivalency threshold. The 67th percentile of Mid-Crude DTA net emissions is 1,377 kg, approximately 40% of average M21 emissions. In contrast, this same metric for the DT and DTC scenarios is -151 and -835 kg, approximately 5% and 25% of M21 emissions respectively. It would take a significant reduction in overall emissions from LDAR component leaks for the DTA simulation to demonstrate equivalency. However, this simulation does not consider non-LDAR or AVO leaks, which provide additional benefits (see Section 4.4 for discussion). The median net emissions reductions for m-Xylene represent 15%, 49%, and 76% of scheduled-M21 for DTA, DT, and DTC, respectively. While the results indicate that the pilot study LDSN/DRF systems can demonstrate equivalency, the significant differences in scenario simulated net emissions indicate that further research is necessary to better understand the practical levels of control achieved under LDSN/DRF.

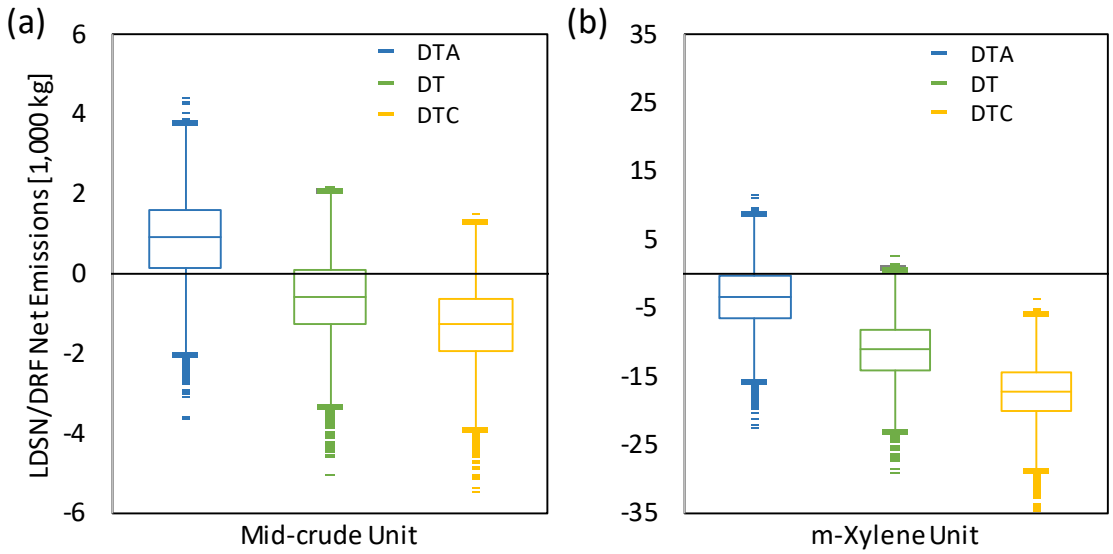

Figure 4-9. LDSN/DRF simulated net emissions compared to M21 LDAR (a) Mid-Crude and (b) m-Xylene

Evaluating LDAR performance relative to scheduled-M21 without conducting handheld monitoring of all components is complicated. Tracking the number of leaks repaired under LDSN/DRF may present one avenue for evaluating emissions control performance in practical implementations, and simulation results can provide guidance in this area. Figure 4-10 displays boxplots of the percentage of leaks repaired in the Mid-Crude (a) and m-Xylene (b) units from 10,000 iterations of the EPA ORD model. While all but one of the m-Xylene LDSN/DRF scenarios demonstrated 67% or greater equivalency, only the m-Xylene DTC scenario repaired a similar number of leaks to simulated scheduled-M21. The broader range of the Mid-Crude DTC scenario suggests that the m-Xylene unit DTC scenario was limited by the number of simulated leaks, rather than LDAR performance. The m-Xylene DT scenario was able to demonstrate equivalency for 99.8% of the simulation iterations despite fixing on average just over half the leaks repaired under DTC and CWP scenarios (averages leak repair counts are 253 for DT, 431 for DTC, and 435 for CWP). The m-Xylene DTA and Mid-Crude DT and DTC scenarios also demonstrated equivalency with average repair rates of 25%, 21%, and 43%, respectively. These results demonstrate one of the theorized strengths of the LDSN/DRF concept. Despite generally responding to and repairing significantly fewer leaks than under the CWP, the proposed work practice still results in greater emissions reductions due to its ability to quickly respond to larger leaks. This further emphasizes the importance of understanding the impacts of these significant sources.

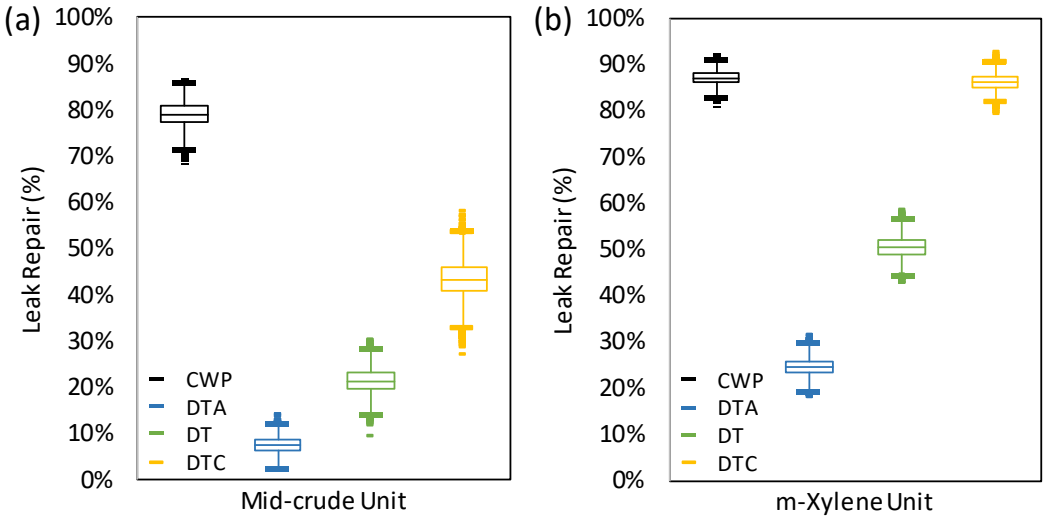

Figure 4-10. Emissions scenario leak repairs (a) Mid-Crude, (b) m-Xylene

Pegged leaks, those with screening values greater than the upper limit of the portable device in use, represent a significant portion of leak inventory emissions. This is due both in part to their magnitude and to the way in which their emissions are estimated. While other leak emission rates are calculated using correlation equations, pegged leak emissions are characterized using constant emission rates for specific component categories. The pegged emission rates provided in guidance are significantly larger than what would be used under the correlation equations. Much like for M21 overall, these leaks have been shown to vary widely in mass emission rates. However, the guidance methods were used in this analysis to remain consistent with inventory practices. Pegged leaks are both the most likely leaks to be detected under LDSN, so long as the emitted compounds have a favorable RF, and the most important to repair quickly. When considering leak repair rates as a method for evaluating performance, it is important to assess the effects of these larger sources explicitly.

The original leak datasets (methods outlined in Section 4.2.1 and distribution discussed in Section 4.1) included 18 and 12 pegged leaks in m-Xylene and Mid-Crude, respectively. Due to the Monte Carlo model's randomized sampling with replacement, the simulations tested a wider range of pegged values. A summary comparing equivalency rates to the number of simulated pegged leaks is presented in Figure 4-11. Both DTA scenarios show notable correlation between performance and the number of pegged values in a simulation, although it is not a perfect correlation [see m-Xylene (b) at 15 pegged leaks]. The m-Xylene (b) DT and DTC scenarios do not show much correlation. However, this is due to the overall high rates of equivalency. The Mid-Crude (a) DT and DTC scenarios do illustrate a correlation similar to that observed for the DTA scenarios. Notably, the scenarios indicate diminishing returns above a certain level. The shift begins when approximately 85% equivalency is reached, at 11 and 15 pegged leaks respectively. Therefore, results suggest the LDSN/DRF systems in these units are likely achieving equivalency if pegged leaks are being found at a rate similar to historical records, despite an overall reduction in the number of leaks repaired. Tracking the number of pegged leaks may be a useful performance target because a well-functioning system should be able to detect large leaks at rates equal to or higher than those achieved under CWP, and that metric is a strong indicator for equivalency.

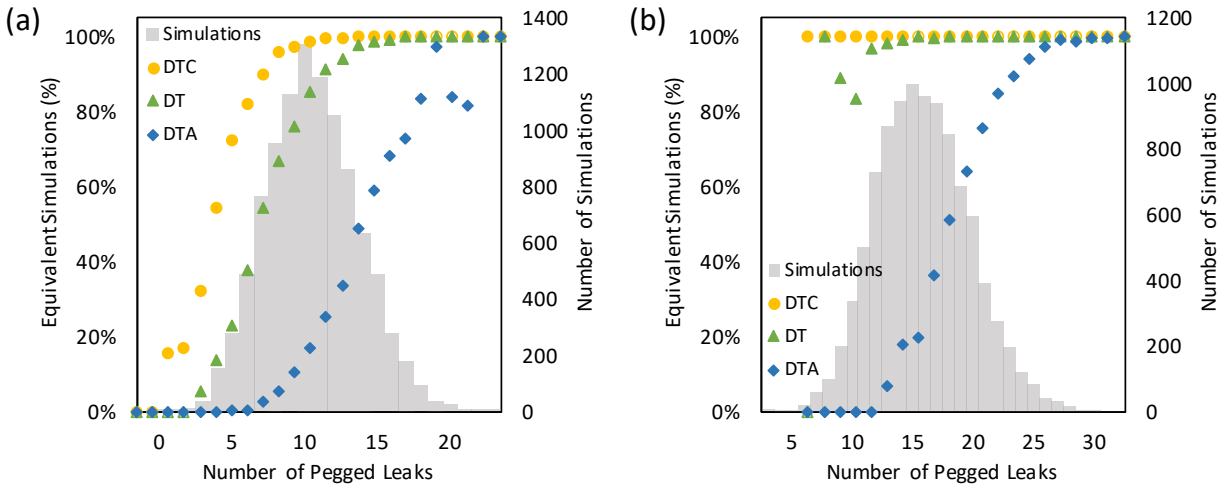

Figure 4-11. Pegged leak relation to LDSN/DRF equivalency (a) Mid-Crude, (b) m-Xylene

4.4 Additional LDSN/DRF Benefits

The emission equivalency discussion presented here considers only the projected performance of LDSN/DRF in comparison to fugitive emission control achieved using the CWP. In reality, 24/7 emissions monitoring can provide additional emission reduction benefits over a traditional M21-based LDAR monitoring program that is executed on a specific set of components on a periodic schedule (with high temporal latency).

As one example of added benefit, AVOs are leak detections that are determined by facility operators or, in more serious cases, by safety monitoring systems indicating a potentially dangerous situation. Some LDAR program components (e.g. equipment in heavy liquid service or connectors that are part of instrumentation or are covered by insulation) are not routinely monitored under the CWP. Emissions from these components may be found by AVO, but not until they reach a detectable threshold that could be well above the leak definition SV. Under the proposed LDSN/DRF approach, current AVO detection capability will not decrease. Since it can be assumed (and has been demonstrated in this CRADA) that sufficiently sensitive LDSN/DRF can detect emissions below the AVO threshold, a positive emissions reduction benefit is inherent in the approach. This added benefit is not accounted for in the current equivalency modeling.

A second example of added emission reduction benefit not considered in the current equivalency analysis centers on timely detection and mitigation of emissions from components or equipment that that are not covered by the CWP. A good example of this is the fin-fan leak described in Section 3.3. This leak was significant in size, was not a monitored LDAR component, was not detected by AVO, could not be detected by OGI, but was immediately obvious to LDSN/ DRF monitoring. This LDSN/DRF detection will likely lead to emissions reductions (when the leak source is ultimately repaired or replaced) compared to the “undetected scenario”. Several other examples of detections and repairs of emissions from non-LDAR program components were documented in pilot testing.

4.5 Conclusions

This section presented an approach for evaluating the equivalency of the FHR CC LDSN/DRF systems compared to CWP at the facility. Monte Carlo simulations demonstrated that high levels of LDAR control and emissions reduction can be achieved under the proposed work practices. Models for the m-Xylene unit were shown to be equivalent to or better than CWP for all LDSN/DRF scenarios, and significant emissions reductions were observed when distance effects were incorporated into the simulations. The Mid-Crude unit also demonstrated greater than 67% equivalency for two of the three emissions control scenarios in comparison to scheduled-M21. Non-LDAR and AVO sources are another significant source of emissions that are less effectively controlled under the CWP, and this presents an additional benefit to the continuous, extensive monitoring employed by LDSNs.

This equivalency analysis was limited to the process units included in the CRADA pilot study and was not designed to provide conclusions about other potential LDSN installations. However, the results did provide insight into what should be considered when developing broader, more transferable analyses. The SV distribution, in particular the portion of emissions generated by larger and "pegged" leaks, is especially important to evaluate when considering the proposed work practice. Additionally, the portion of emissions which originate from components subject to longer monitoring intervals or no monitoring will influence the impact of LDSN/DRF. The site layout and the feasibility of siting sensors close enough to a sufficient majority of components may also determine whether a system is cost effective. Distance plays an important role in equivalency determinations. The typical emissions compounds are also key, and a poorly designed system may not be able to achieve a sufficiently low DTA with the sensor used in this study. Future equivalency analyses and testing may be able to develop a more transferable relationship between eligible gas streams, DRF procedures, distance, and system DTAs.

Ultimately, modeling demonstrated that the LDSN/DRF approach may take time to reach a level of steady-state control. While smaller leaks may not be found at high rates initially, pre-existing AVO and non-LDAR leaks may be more prevalent during the early stages after installation. Additional and longer-term research is necessary to better understand the variation of and degree of control possible under LDSN/DRF. However, Monte Carlo simulations established that the LDSN/DRF concept can demonstrate significant emission reductions relative to CWP despite repairing fewer leaks than under CWP, thereby improving LDAR efficiency.

5.0 LDSN/DRF Methods and Quality Assurance

This section describes important aspects of LDSN/DRF methods and QA procedures that were developed under the CRADA through 2019. These procedures capture current knowledge and development status, with focus on the specific pilot implementations at the FHR CC process units. The purpose of this section is to summarize the procedures that were used, and are continuing to be refined, that will ensure ongoing LDSN/DRF emission control performance. The information in this section, along with supporting appendices, completes the documentation of research and development activities in pursuit of NTOs 1, 2, 3, and 4, described in Section 1.3. With the delivery of this report, all near-term CRADA objectives have been successfully met.

Work remains to develop a transferable embodiment of LDSN/DRF and to refine system design criteria (e.g. optimal node density) and automated QA and calibration procedures for general applications. We must further our understanding of some regulatory aspects of LDSN/DRF, such as emission inventory reporting, which would necessarily change under any potential NGEM-based LDAR AWP (Section 2). The CRADA team will continue to learn from and implement feedback received from facility operations during the pilot tests of LDSN/DRF. The team must also continue to communicate these environmentally beneficial NGEM advances to the international technical community as part of scientific discourse,[12-13] and through peer-reviewed literature, with this report representing a significant milestone. The work that remains to be done is reflected in the LTOs described in Section 1.3, with progress towards these LTOs the subject of Section 6 of this report.

Section 5 comprises five subsections that provide an overview of method progress to date.

- Section 5.1 discusses sensor placement and LDAR program component coverage design under the LDSN/DRF monitoring plan that is part an overall fugitive management plan for a facility.
- Section 5.2 describes the LDSN node preparation, factory calibration, and in-field sensor functionally checks (called bump tests) that were developed and performed as part of the pilot test to help ensure sensor operation. The use of the mSyte™ mobile interface to assist the operator in performing the bump test is also described and mSyte™ system health monitoring is also discussed.
- Section 5.3 explains the procedures followed under the DRF by facility personnel in response to an LDSN leak detection generating a PSL. The combination of fast survey checks to identify emission points combined with M21 to document the leak level is described. The DRF rules to help diagnose and document cluster detections and other real-world factors are discussed.
- Section 5.4 discusses advanced QA concepts that leverage the automated data archiving and analysis inherent in the LDSN/DRF approach along with the QA feedback provided by the M21-documented leaks under the DRF. This valuable information can help ensure ongoing systems performance and assist in understanding inventories.
- Section 5.5 provides an example of how LDSN-type data (from mSyte™ or any similar such system) may be analyzed by third parties as part of an independent auditing QA function.

5.1 LDSN/DRF Monitoring Plan Design

LDSN/DRF can represent an important part of a facility's overall fugitive emission management plan but is likely not the only LDAR tool employed. In complex industrial facilities, not all areas and types of chemical service will be monitored by LDSN/DRF at a given time. Some examples of these situations include phased LDSN deployments (LDSN coverage not yet present), large distance between few LDAR components (LDSN cost/benefit not present), chemical detectability (insufficient sensor RF), and other similar considerations. An example from the FHR CC pilot test relates to the fuel gas components for a high methane-content stream that could not be easily monitored with the current 10.6 eV PID embodiment of LDSN. In these cases, a facility could

implement an LDSN/DRF solution for portions of a facility while continuing to follow the LDAR CWP using traditional M21 or the OGI AWP in other areas. Figure 5-1 provides an overview of different elements that could potentially comprise a facility's fugitive emission management plan. Facilities would maintain records that clearly demonstrate which portions of the facility were complying with M21 CWP and which were utilizing the LDSN/DRF, for example.

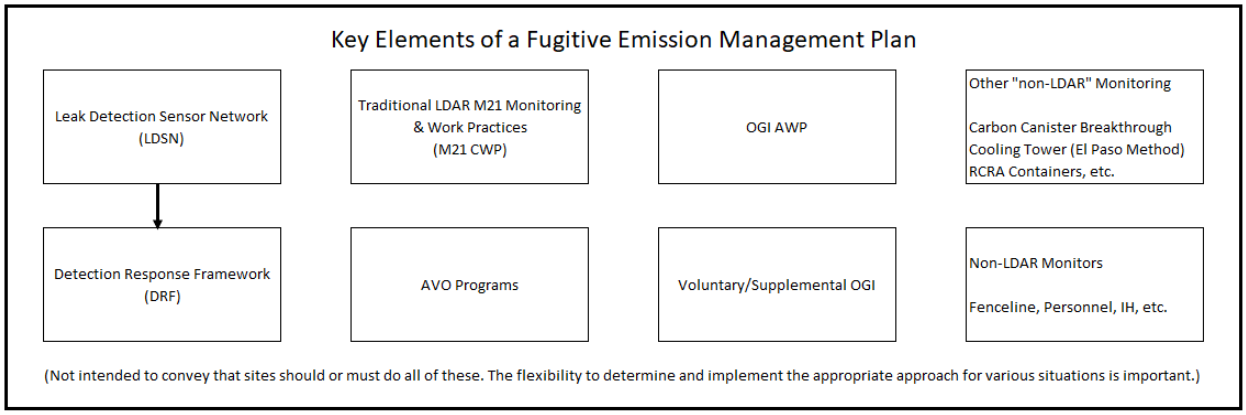

Figure 5-1. Key elements of a fugitive emission management plan

The design and implementation of the LDSN monitoring plan is the first step in successful use of LDSN/DRF as a key part of a facility's overall fugitive management strategy. The installation of LDSN nodes, supporting wireless communication infrastructure, and wind measurements in a complex refinery unit requires significant planning and engineering execution in collaboration with facility operations. Most critical among the many details that need to be considered is the strategic placement of sensor nodes within the process unit to achieve optimal coverage for the subset of components that are defined to be part of the LDSN monitoring plan. In general, component density, historical LDAR results (if available), and area meteorological conditions to optimize sensor placement must be considered. Additional factors such as emitted gas properties, wind flow obstructions and flow channeling within the process unit, multi-level placement strategies, and potential interfering effects (e.g. proximity to steam emissions) are also considered. The pilot tests in SLOF and FHR CC assisted the team in a better understanding of these factors with an LTO to form general method guidance for LDSN implementation planning (Section 6).

Figure 5-2 provides an example of a 3-dimensional view of sensor node placement planning for the FHR CC Mid-Crude pilot test, with further details provided in Appendix C. The spacing shown is based on the default 50-60 ft criteria determined from tracer release studies discussed in Section 3.2 with vertical separation differences of ± 20ft, determined by the process unit levels. One important aspect of the LDSN monitoring plan is that it may be adjusted as information on LDSN performance becomes available. For example, the initial deployment plan for FHR CC Mid-Crude (Appendix C1) was adjusted based on LDSN performance information provided by the characterization of the leaks as part of the DRF (Section 3.4, Appendix C2). This LDSN QA information, coupled with further spatial analysis of sensor placement near key component clusters, resulted in the addition of 6 strategically placed sensor nodes to ensure complete LDSN coverage (Appendix C3).

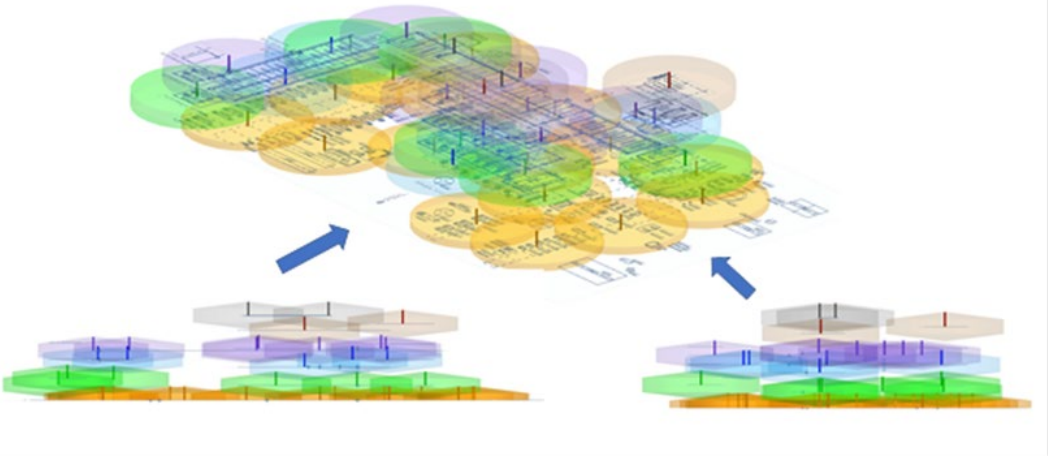

Figure 5-2. Example of LDSN node placement in FHR CC Mid-Crude

5.2 LDSN Node Pre-deployment and In-field QA Testing

Once LDSN node locations were planned and supporting infrastructure placed, the next step was to install Molex-certified sensors. The team utilized a pre-production version of the sensor for the 2019 pilot tests (Figures 3-5 and 3-13). Although still approaching final commercial form, this sensor and the mSyte™ platform were highly developed, allowing for a realistic assessment of system preparation, deployment, and long-term operational QA methods. Figure 5-3 outlines the major procedural steps that were followed in the construction and operation of the LDSN. As the manufacturer of the technology, Molex QA-screened all incoming components, produced the sensors, and performed comprehensive pre-deployment operation checks on all sensor nodes deployed in the FHR CC pilot. For these tests, Molex used a zero point and 500 ppb isobutylene (two-point) factory calibration procedure to prepare the sensors for use. Higher range tests on the 10.6eV PID utilized were performed to establish linearity up to 3 ppm (the extent of expected range), but these tests were not applied to 100% of the FHR CC pilot sensors. The establishment of uniform minimum requirements for factory calibration of LDSN sensors is further discussed in Section 6 on generalized methods.

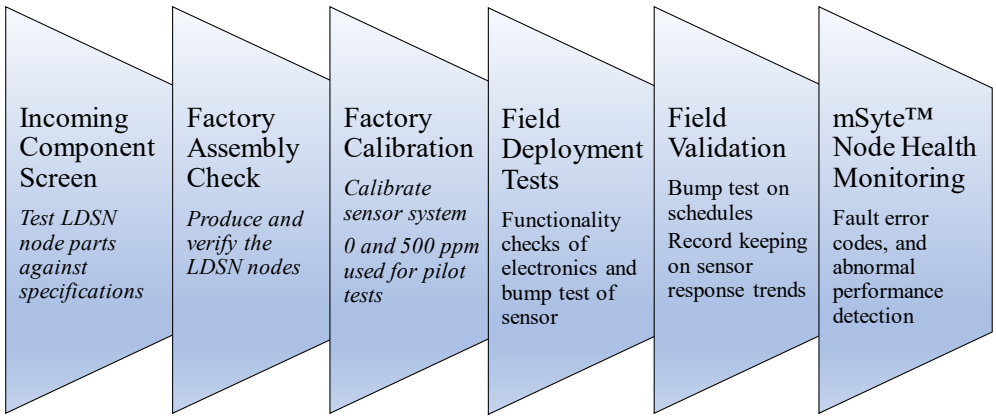

Figure 5-3. LDSN fabrication and implementation procedures

The LDSN nodes were installed in the process units, and comprehensive operational tests of the sensors and wireless communication capability were conducted. As part of these commissioning tests, an in-field sensor functionality and calibration check called a "bump test" was performed (Figure 5-4, Appendix D6). In brief, the operator attaches a special bump test fixture to the sensor inlet. The fixture is connected via a ¼ inch diameter polyurethane tubing to a small format (easily carried), certified 500 ppb isobutylene cylinder that is fitted with an on-demand regulator. The operator uses the mSyte™ mobile device to verify the identity of the sensor node to be tested, starts the bump procedure test within mSyte™ mobile app, and then releases the test gas for a short time period administered by the mobile app.

As indicated in the Figure 5-4, the sensor responds to the sudden change in concentration (the bump), and the amplitude of change in the sensor reading is compared to a preset threshold value determined in factory calibration. A successful bump test is shown by a "Pass" message on the mobile app, which currently indicates the response of the sensor exceeds 50% of the nominal value of the standard. If the first test was not successful, the test was repeated up to two additional times. If the sensor continued to fail, it was recalibrated or replaced with a pre-calibrated sensor. All the bump tests are segregated from leak detections, and the test time, test gas, test results as well as operator who performs the test are automatically logged in the mSyte™ database as a QA record and displayed to the operator.

Due to the modular design of the Molex sensor element, replacing a malfunctioned sensor with a factory-certified replacement in the field is an easy procedure, requiring no tools. To change a sensor, the lower metal cylinder PID housing shown in the "Pre-production LDSN" image of Figure 3-5 is unplugged, and a replacement sensor and housing are plugged back in. Information on the sensor change is updated in mSyte™, and the sensor is allowed to equilibrate for two hours before the commissioning bump test is performed.

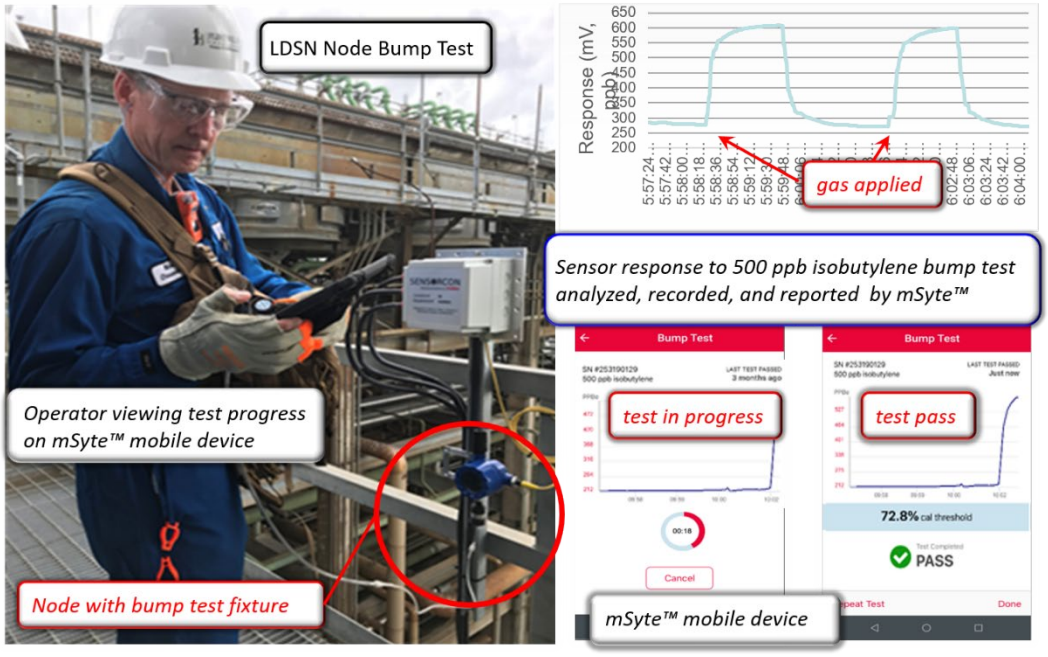

Figure 5-4. LDSN node bump test QA check

For CRADA research, bump tests were conducted more frequently than will be required in a standardized LDSN method. For the exploratory tests and SLOF pilot, bump tests were conducted once per day, in part because the test team was on site and the number of sensors were low. Based on the demonstrated reliability of the sensors during early testing and the implementation of additional automated sensor health monitoring parameters, the bump tests were conducted less frequently during the FHR CC pilot tests (once per week). For the long-term SLOF and FHR pilot tests, over 180 individual bump tests were performed. These tests show an average of a 12% drop in sensor sensitivity over three months of testing, suggesting sufficient stability in sensor performance for continual use.

For larger LDSN installations that might include hundreds of sensors spread over significant area and acreage, the resources expended to perform bump tests can be significant. For example, it could require up to one full time equivalent (FTE) just to conduct weekly bump tests for 1,000 sensors across a refinery. With final-form continuous sensor health monitoring, cross-node data comparisons, and associated automatic notifications, it is envisioned that once per quarter bump testing will be sufficient to maintain LDSN operational performance for this specific sensor type (10.6 eV PID). The health of each sensor is continuously monitored for power outage, loss of data transmission, and sensor baseline levels. The current status of each sensor is available on mSyte™. Historical data is also logged in the database. Any failure or significant deviation from preset threshold values will result in a notification being sent to appropriate facility personnel. Failed sensors should be reset, repaired, or replaced.

5.3 The DRF Procedure

The DRF describes the LDAR tools and procedures facility personnel use to respond to PSL notifications delivered by the LDSN. The DRF and the LDSN work together to locate, assess, and produce auditable records of discovered leaks and associated repairs under the envisioned AWP. As illustrated in Figures 1-2 and 1-4, fast survey gear like hand-held probes and OGI, along with calibrated M21, are part of the DRF and assist in identifying and documenting emissions. Through the DRF, facility personnel gather and input key metadata into the LDSN to inform of maintenance activities and document performance over time. The interaction of the LDSN system and facility personnel is facilitated by the mSyte™ mobile device carried by the LDAR technician into the process units (Figure 5-5). Just as the LDSN system improved over time with design iterations and continued use, the long-term pilot tests informed aspects of the DRF. Captured here are key components of the DRF employed in the pilot tests along with easily envisioned augmentations that will be incorporated into the DRF as use continues. Advanced LDSN and DRF topics are described in Section 6 in the context of CRADA LTOs.

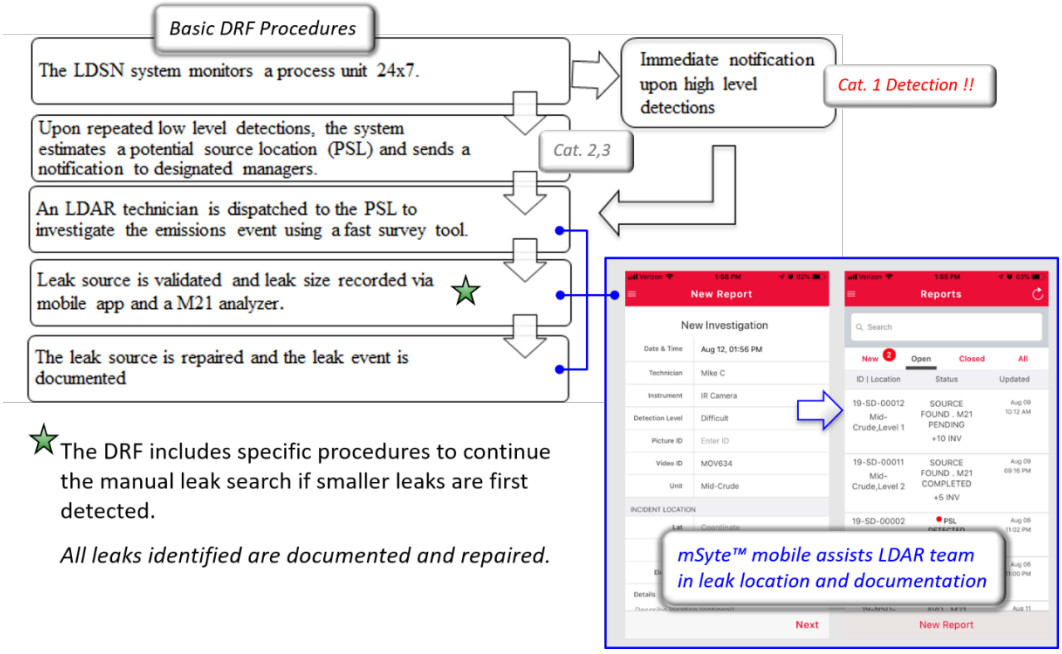

Figure 5-5. Basic DRF procedures and mobile interface

The LDSN system automatically detects, categorizes, and approximates the location of emissions in the monitored process unit based on VOC and meteorological measurements. The LDSN notifies selected facility personnel of detected emission anomalies so that appropriate action can be taken under the DRF. Those notifications are automatically classified as one of three separate categories.

Category 1 notifications are for larger potentially impactful emissions that need prompt response by facility personnel. These are anticipated to likely be associated with significant maintenance activities or unplanned emissions. The Category 1 notification protocol may include direct alarms for operators, for example phone notifications, and/or e-mail notification to appropriate personnel. During the FHR CC pilot test, all Category 1 notifications were the result of planned maintenance activities that were authorized by the facility's Maintenance, Start-up, Shutdown permits.

Instead of direct alarms to operators, Category 2 and Category 3 notifications are accompanied by a PSL box. The PSL box concept is introduced in Sections 1.4.2 and 3.4, with examples from FHR CC provided in Appendix C2. A discrete serialized identification number is automatically assigned to each new PSL. The PSL box serves as a visual representation of the area in which there is high probability that a fugitive emission anomaly has occurred. Category 2 notifications are typically medium to large leaks that can be efficiently identified during the DRF process. Category 3 notifications are often smaller and/or intermittent emissions that are more challenging to locate. Category classifications are useful when prioritizing the order in which multiple PSLs should be investigated. PSLs continue to update periodically as additional sensor readings and meteorological data are collected and analyzed. These updates can be especially helpful for Category 3 PSLs which can require more resources to pinpoint the potential leak source.

The purpose of the PSL investigation is to locate the associated potential leak source(s) so that

source identification can be made, and repair protocols initiated as required. To most efficiently locate the leak target, the technician uses emission screening gear that is easily deployed. This includes hand-held probe equipment such as VOC sniffers, OGI, or other appropriate detectors for the chemicals of interest (Figure 5-6). Once identified, the source is measured with calibrated M21-equipment to document the leak's peak concentration value and initiate repair procedures. Relevant information is entered into the mobile device and is recorded for regulatory, operational, and QA purposes. The mobile app and electronic records are the primary documentation method. However, paper records can be also used. Other metadata, such as maintenance activities which may generate emissions, can be entered into the system to facilitate intelligent LDSN operation. Through machine learning and other capability improvements, the efficiency and effectiveness of LDSN operation is expected to increase over time. Although electronic data is the primary record source, paper format is allowed to prevent delays when mobile devices or electronic systems are temporarily unavailable.

As the technician searches for the leak, each component measured by M21 that exhibits a peak SV above the regulatory leak definition is considered an actionable leak and is repaired. Once a leak has been detected that in the judgement of the technician is presumed to be the leak responsible for the generation of the PSL, the search portion of the investigation is complete. Once the leak has been effectively repaired, the PSL is allowed to close automatically after a specified time unless additional sensor data triggers the PSL to update. If additional impactful leaks are undetected during the investigation, the system will automatically generate a new or updated PSL thereby triggering a new investigation.

In some cases, a PSL notification is triggered by multiple small leaks that are in close proximity to each other. This is the result of the leak cluster aggregation effect. While each of the leaks in this leak cluster may individually be below the lower band of the DT, the combined effects of their fugitive emissions can be detected by the LDSN. Once leaks have been detected that in the judgement of the technician are presumed to be the leaks responsible for the generation of the PSL, the search portion of the investigation is complete. Once the leaks have been effectively repaired, the PSL is allowed to close automatically after a specified time unless additional sensor data triggers the PSL to update. If additional small leaks were undetected during the investigation, the system will automatically generate a new or updated PSL once the leak cluster aggregation is detected. A new or updated PSL would trigger a new investigation.

Figure 5-6. DRF in action on a leak found under insulation

5.4 Ongoing QA of LDSN

In addition to automated sensor health monitoring and periodic bump tests, a powerful QA concept inherent in the LDSN/DRF approach is the systematic review of archived data. Since all sensor, wind, and DRF leak diagnostic information (measured by M21) are retained for a five-year period, it is possible to recreate and analyze specific PSL notifications and the effects of repair procedures, for both operational and QA benefit. Figure 5-7 provides an example of LDSN/DRF informetrics where time-resolved leak detection data for two sensors in the jet fuel (RF < 1) area of the Mid-Crude process unit are examined along with wind data and DRF findings. In the upper panel (a), hourly average wind speed and direction data are plotted on the primary and secondary y-axes, respectively. In the lower panel (b), summations of all hourly peak detections are plotted on the y-axis, with the temporal location of several events noted. For this LDSN metric, the mSyte™-determined amplitudes of all leak detection peaks (in units of ppbe) are summed for each hour. In this real-world example, sensor nodes (A) and (B) were relatively quiet until 10:00 on 8/5/2019 when leak signal appeared on both units, emanating from an upwind source located to the southeast of the centroid of the nodes. A PSL notification was issued by mSyte,™ and the LDAR technician under the DRF identified and adjusted an 18.9-inch circumference control valve in heavy liquid service (on 8/8/2019, reducing the initial M21 leak SV of 3,600 ppm to < 700ppm). The valve was formally repaired (tested below 500 ppm SV) on 8/22/2019. As a method development factor of note, the leak signal was lower on both sensors during high wind speeds (hourly average over 6.0 m/s) prior to the DRF action. Sensor (A) remained relatively quiet under similar wind conditions indicating this leak mass ER was reduced by first repair attempt.

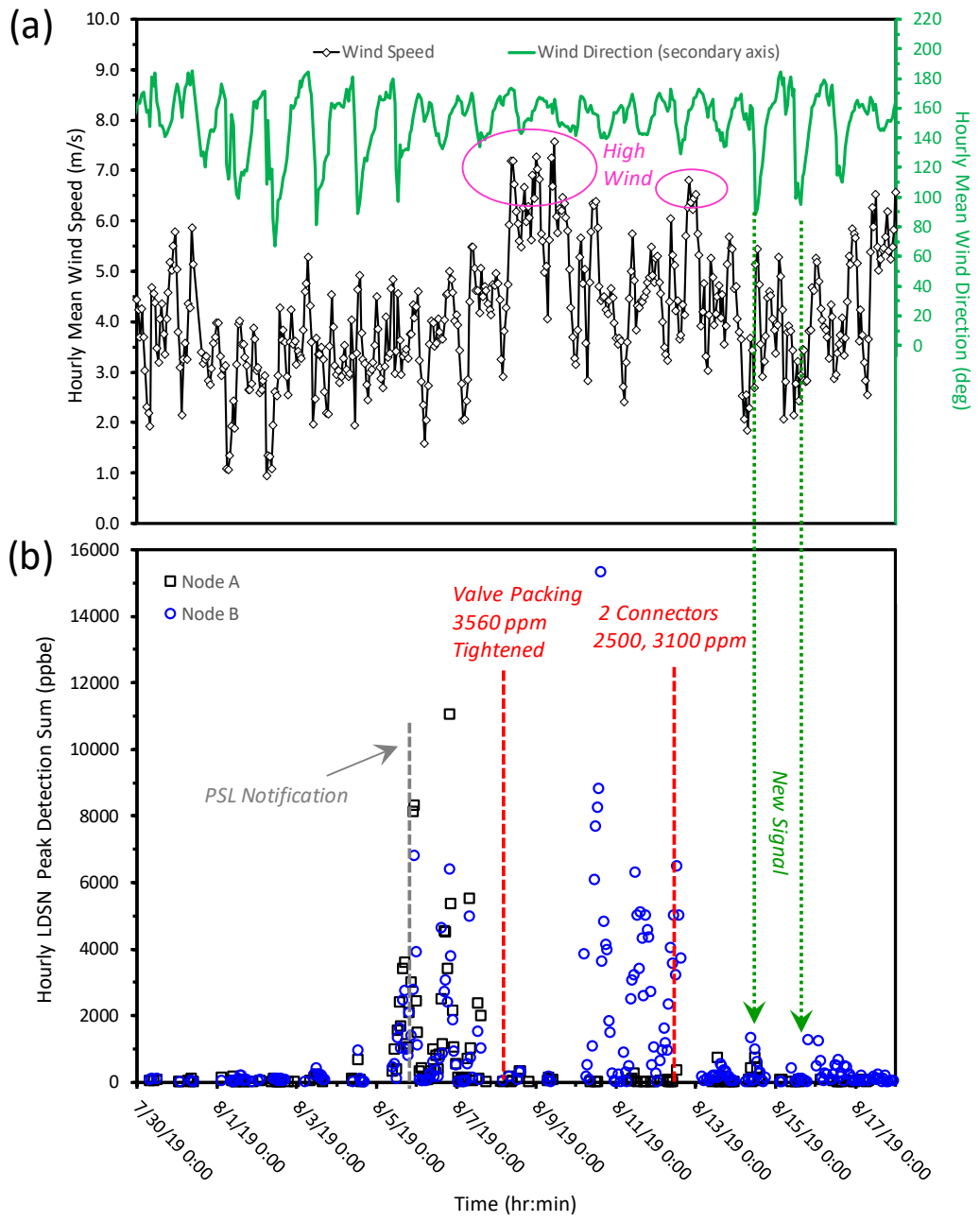

Figure 5-7. Example of LDSN data review: (a) meteorological data, (b) LDSN data

The simultaneous observation of detected leak signal on two spatially separated LDSN nodes, followed by a directed DRF action that likely resulted in the significant cessation of emissions and sensor signal, represents a powerful QA check of both LDSN detection capability and mSyte™ algorithm triangulation fidelity. On 8/10/2019, signal again appeared on Sensor (B), and the DRF response found two connector leaks (2.4-inch plugs), with SVs of 2,500 ppm and 3,100 ppm. One leak was repaired immediately and the other within one day. Under changing wind conditions sensor signal from a new direction begins to appear days later (green arrows).

Because the automated processing and summary of LDSN/DRF data is easy to accomplish through programing code, many types of performance metrics, summary statistics, and comparisons can be envisioned and are the subject of ongoing methods development research. Table 5-1 provides an example summary using the data from Figure 5-7 for the two primary periods of interest from 8/5/2019 to 8/9/2019 and 8/10/2019 to 8/13/2019. For the first leak event ascribed to the valve (3,600 ppm SV), around 60% of the 96 total monitoring hours exhibited at least one leak detection peak for Sensor (A) and (B), with a total number of detects of 1,077 and 922, respectively. A metric called "LDSN Signal Rate" can be defined as the total summation of all hourly LDSN peak detections, divided by the number of hours where detections occurred (for a subject time period). The rate is around 1,600 and 1,300 ppbe/hr for Sensors (A) and (B), respectively, for the valve leak event. The average and maximum peak heights are also easily calculated and, with the signal rate data, indicate a slightly greater plume to sensor overlap for Sensor (A) under these conditions.

Table 5-1. Summary of LDSN data review for Figure 5-6

Figure 5-6 Node	Peroid of Interest	Monitoring Period (hrs)	Percentage of Hours with Detects (%)	Total Number of Detects (N)	LDSN Signal Rate (ppbe/hr)	Average Peak Height (ppbe)	Max Peak Height (ppbe)
A	8/5/19 0:00 to 8/9/19 0:00	96	65	1077	1581	89.6	4865
B	8/5/19 0:00 to 8/9/19 0:00	96	56	922	1298	76.0	4381
A	8/10/19 0:00 to 8/13/19 0:00	72	26	49	60	23.3	364
B	8/10/19 0:00 to 8/13/19 0:00	72	76	1601	3029	104.1	6084

Whereas the first leak event from 8/5/2019 to 8/9/2019 produced somewhat similar signal on the two sensors, the second leak event was much more strongly observed by Sensor (B). This a consequence of the exact position of the leak and wind flow specific within the unit. Although a comparison of the Sensor (B) hourly LDSN peak detection sum for events one and two does not show a major difference to the eye, the LDSN signal rate metric is a factor of two greater for the latter. This comports with the presence of two connector leaks (2,500 ppm and 3,100 ppm SVs), for event two with separation distances from the leaks to Sensor (B) approximately the same.

5.4 Independent QA Audits of LDSN/DRF

One of the more powerful aspects of a performance-based sensor network leak detection approach is that the raw time-resolved data from the sensor nodes during 24/7 monitoring is continually archived and available for later analysis by either the company supplying the sensor network, the facility operating the network, or a third party for compliance or other auditing purpose. Although there is cost associated with data storage, the need for transparency and

auditability takes priority. Based on the amount of data generated during the pilot and the current cost to store and access this type of data, an expectation to maintain up to five years of sensor reading raw data (mV or ppbe) does not seem unreasonable. That data could be maintained in a manner that is easily viewed electronically and reasonably available for export upon request by the appropriate authority.

The spectrum of independent analysis options for the recorded raw data is the subject of ongoing research, but a variety of statistical calculations on individual nodes as well as comparisons between nodes are easily envisioned. Figure 5-8 provides an example of how sensor network data, from the current or any similar system, may be independently analyzed. In this case a modified version of EPA's open-source SPod fenceline sensor analysis software[17, 25, 36] is used to process 24 hours of data from the ten sensor nodes present in the m-Xylene units during a particular day when a significant leak signal was present on two sensor nodes (4 and 5).

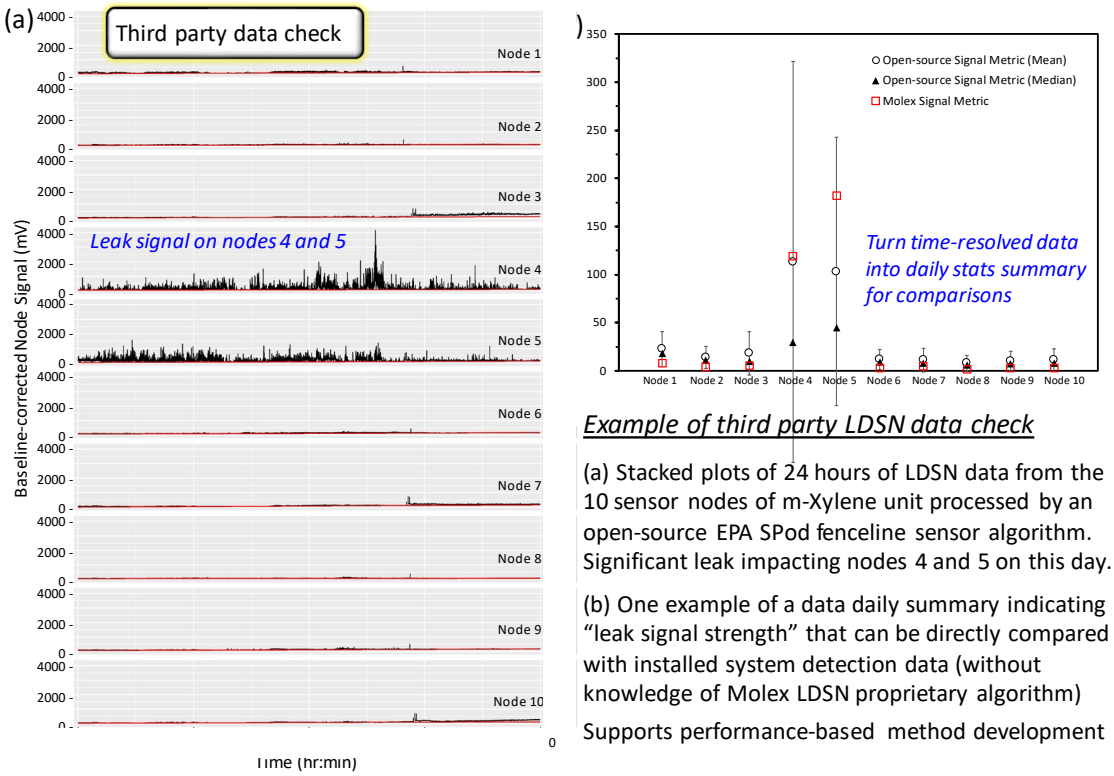

Example of third party LDSN data check

(a) Stacked plots of 24 hours of LDSN data from the 10 sensor nodes of m-Xylene unit processed by an open-source EPA SPod fenceline sensor algorithm. Significant leak impacting nodes 4 and 5 on this day.

(b) One example of a data daily summary indicating "leak signal strength" that can be directly compared with installed system detection data (without knowledge of Molex LDSN proprietary algorithm)

Supports performance-based method development

Figure 5-8. Assessment of Molex LDSN data with an open-source approach

In this example, the EPA ORD open-source algorithm automatically processes 24-hours of 1 Hz time-resolved data from the ten independent nodes and applies a baseline-correction algorithm that may be used to analyze baseline offsets if desired. The time series analysis from the open-source software is shown in Figure 5-8(a). The open-source software can calculate a variety of node-specific statistics and can determine sensor noise floors for time periods when leak signal is not present. The software can look for sensor operational anomalies indicating possible sensor maintenance issues (e.g. baseline discontinuities or unrealistically low or high sensor noise floors). In Figure 5-8(b) the mean, median, and standard deviation (± σ error bars) of the overall

24-hour times series for each of the nodes (called the open-source signal metric) is compared to a Molex signal metric, a normalized form of 24-hours of summed peak data, similar to that discussed in Figure 5-7. In this case, data derived from the Molex proprietary sensor signal processing are similar to that independently determined from the raw data.

With this approach, Molex, or another leak detection sensor network company, can provide the archived data and a representation of their leak detection analysis, without disclosure of proprietary signal processing algorithms, to a third party who can assess and document system performance through independent analysis of the data. This third-party verification potential is a significant advantage of many emerging NGEM approaches. Variations of this independent analysis is the subject of method development efforts for potential use in a performance based Other Test Method (OTM).

6.0 Summary and Future Work

An executive summary of LDAR Innovation CRADA work to date and areas for future research are provided in the following sections:

- Section 6.1 provides a bullet-list overview of major accomplishments and findings.
- Section 6.2 describes future work related to the development of transferable methods.
- Section 6.3 discusses design criteria for development of standardized methods.
- Section 6.4 discusses aspects of emission reporting and permit representations.
- Section 6.5 illustrates the power of LDSN/DRF found in forward research.

6.1 Major Accomplishments and Findings to Date

The major accomplishments and findings of this CRADA to date are as follows:

- A specific embodiment of an innovative LDAR approach called LDSN/DRF was developed and real-world tested in three working process units. Operational and QA methods were established, and the emission reduction performance against the CWP was determined. The business case for LDSN/DRF was evaluated. With the completion of this report, all CRADA NTOs described in Section 1.3 were successfully met.
- Key aspects of LDSN leak detection performance include the sensitivity of the sensor to the emitted gas stream, the node density of the network, and the factors that affect plume transport. These factors must be fully evaluated in the formulation of a LDSN monitoring approach as part of a facility's overall fugitive emissions management plan (Section 5.1). For example, the current embodiment of LDSN based on a 10.6 eV PID cannot effectively monitor methane-dominant streams such as fuel gas, so other LDAR monitoring is required in these areas of the process unit.
- Although the LDSN/DRF system focuses on rapid detection and mitigation of larger leaks soon after they occur, many smaller leaks are also found and fixed as a result of node proximity effects (DT band), leak clusters, and the DRF design.

- Tools such as hand-held probes and OGI provide value in rapidly locating leaks detected by LDSN. The facility's monitoring plan and the process unit's DRF specify the tools and procedures used in a process unit to maximize operational efficiency and data quality. The mSyte™ mobile device is a key enabling technology for LDSN/DRF.
- LDSN/DRF found and fixed leaks of various sizes (M21 SVs). Approximately 30% of leaks found with M21 SVs > 10,000 ppm were judged detectable by OGI survey.
- Feedback from facility operations on LDSN/DRF was positive. The detection of potentially hazardous emissions from non-LDAR program components (such as leaks under insulation) was described as a major benefit by facility operations.
- When considering all aspects of emission reduction performance, safety and operations benefit, and total cost of ownership, LDSN/DRF is judged to be superior to 100% manual M21 inspection under the CWP (see Section 2 for attribute comparison).
- As described subsequently, additional work remains to understand and develop transferable methods for LDSN/DRF and better understand regulatory hurdles and additional benefits found in this NGEM approach. These subjects represent LTOs for the CRADA (Section 1.3).

6.2 Development of an LDSN/DRF OTM

Whereas the NTOs of this CRADA focused on the development and assessment of an innovative LDAR approach for specific FHR process units, the LTOs of this research center on transferability and exploration of the ultimate potential of this NGEM method. The primary aspects of these objectives can be phrased in the form of a question.

- *Is it possible to develop a standardized performance-based method for LDSN (that works with a DRF) that could be generally applied to refineries, chemical facilities, and potentially smaller facilities like oil and gas production operations using other forms of sensors?*

This question can be expressed more efficiently as follows.

- *Is it possible to develop an EPA OTM for LDSN/DRF?*

The EPA's Office of Air Quality Planning and Standards (OAQPS) Category C OTM system[37] allows for submission of novel approaches for application-specific emissions quantification and source management work practice measurements. The submitted OTM is reviewed by OAQPS, and potentially by outside reviewers, and feedback to the submitter(s) is provided. When (if) OAQPS deems appropriate, the OTM is posted on the EPA's Emissions Measurement Center public website,[37] along with all relevant supporting information (e.g. this report and follow-on work from this group and others).

To date there are 42 OTMs posted on a wide range of topics. A posted OTM may be downloaded and used by any interested party, and feedback on the method is encouraged in the spirit of open exchange and scientific advancement. One purpose of the OTM repository is to serve as staging area for "methods in process" that OAQPS may draw upon (with appropriate modification) for promulgation in support of future rule making activities or work practice development. Other organizations or regulatory bodies may download and utilize a posted OTM for their own

purposes and may consult with OAQPS on the appropriateness of a given OTM for a specific application and intended use of data. An OTM that is found to have technical performance or implementation issues may be modified or removed at the discretion of EPA OAQPS.

EPA ORD, Molex, and FHR may work together under the LDAR Innovation CRADA to create and submit an LDSN/DRF OTM for posting consideration by EPA OAQPS. It is also possible for another group outside of this CRADA to submit a similar concept to OAQPS at any time. The work performed in this CRADA to date provides a solid foundation for exploration of a standardized, performance-based form of the LDSN/DRF approach that may be used beyond the specific process units that were part of the work described in this report. Some critical aspects for consideration in development of an OTM, as well some aspects potential future benefits of this technology are subsequently described.

When considering elements of a performance-based OTM for leak detection sensor networks, an issue of scope of application must be considered. This CRADA has focused on leak detection relevant to LDAR monitoring programs in refineries as an alternative to the M21-based CWP, but other applications are possible. For example, the same 10.6 eV PID sensor node and mSyte™ infrastructure would be useful for monitoring condensate storage tank emissions at upstream oil and gas sites. We do not yet know if a future OTM developed by this team will include this or other similar applications because even though the hardware and software are useful, the procedures and action levels will differ significantly from the designed use case. The same argument can be made for chemical facility fugitive applications that involve high-toxicity hazardous compounds where the sensitivity of a sensor network approach may be outside of the performance envelope thus far investigated. The reminder of this section focuses on the primary application of LDSN/DRF for refinery process units.

6.3 System Design Criteria and Method Standardization

The most critical elements of LDSN/DRF monitoring plan design for facility process units include sensor selection and sensor node placement. This is a core feature for development of an OTM. As detailed in Section 3, the DT of an individual sensor is a function of several factors including the distance of the leak from that sensor, the responsiveness of the chemicals of interest, the wind conditions, etc. In general, leaks that are closer to a sensor can be detected at smaller emission rates than leaks that are farther away. Instead of having a single method detection level like most analytical test methods, the LDSN sensors have a “DT band” that can be represented by M21-type ppm values across the sensor coverage radius.

The DTU is the upper limit of the detection threshold band and is the DT value (in ppm) that represents the smallest leak (on average) that could be detected by the sensor network at the furthest distance away from a sensor. A DTU of 18,000 ppm would indicate that on average, all ongoing leaks $\geq$ 18,000 ppm of the target chemicals of interest would trigger a PSL notification to facility personnel. In practice, the DRF process can identify actionable leaks (e.g. >500 ppm) that are still below the lower band of the DT range. Detections below the DT lower band are a function of proximity to the sensor node (in general the closer to the sensor the lower the detection limit), leak cluster aggregation effect (multiple smaller leaks whose combined emissions trigger PSL notifications), and/or opportunistic detection of leaks during the investigation portion of the DRF process.

Another critical aspect of LDSN/DRF OTM development is sensor selection. Sensor selection is based on the responsivity of the chemicals of interest. The sensor(s) used in an effective LDSN should have response factors of ≤ 10 for the targeted LDAR applicable process streams. Note that this is the same response factor required by M21. For response factors >10, leaks either could not be detected or the node density necessary to achieve acceptable DT performance would be resource prohibitive. As described in Section 2.3, the response factor is the ratio of the known concentration of a VOC compound to the measured reading of an appropriately calibrated sensor. If the process stream is a mixture, the response factor is calculated for the average composition of the process stream. Average stream compositions might be based on sample data, feed/product specifications, or process knowledge. Response factors should be based on published data, test results, or generally accepted calculation methodologies.

Sensor node placement should follow a site assessment, design, optimization, and installation process such that all components within the LDSN boundary that were previously M21 CWP applicable will have sensor coverage. Sensor coverage is defined by a DTU of 18,000 ppm or less. Figure 6-1 shows an example sensor layout plan.

Figure 6-1. Typical sensor layout plan

6.4 Emission Reporting and Permit Representations

Another area for future research is emission reporting and permit representations for NGEM systems in general. The generally accepted practice for estimating fugitive emissions from components that have been monitored in accordance with EPA M21 is to utilize correlation equations for converting the screening values into mass emission rates. This approach is included in Section 2.1.2 as an advantage of the M21-based CWP due to mandated 100% screening. For non-monitored components, the mass emission rates are estimated as the product of emission

factors and control efficiencies. Additional background and details for each of these methods can be found in Reference 2, EPA Protocol for Equipment Leak Emission Estimates. Since most industrial facilities will include monitored and unmonitored fugitive components, the air emission inventory will include both methodologies.

New Source Review and Prevention of Significant Deterioration permit applications use the latter approach. For air permits that must be issued prior to the commencement of construction activities, there is no opportunity to conduct M21 monitoring in advance of the permit application submittal.

For the portions of the facility in Texas complying with M21 CWP, fugitive emission estimates can continue to follow the methodology specified in Texas Commission on Environmental Air Quality's (TCEQ's) Emissions Inventory Guidelines (RG-360).[38] For portions of the facility utilizing LDSN/DRF, the estimated fugitive emissions can be based on an estimate of the number of fugitive emission components, the emission factors found in TCEQ's Air Permit Technical Guidance for Chemical Sources - Fugitive Guidance (APDG 6422),[39] and LDSN/DRF control efficiencies that are appropriate for a continuous fugitive monitoring system (28LAER level control percentages).

For future projects or activities that require new or amended permits and include additional LDAR type components that will be covered by an LDSN/DRF system, the permit application should include fugitive emission representations based on an estimate of the net fugitive emission component count changes, emission factors found in TCEQ's Air Permit Technical Guidance for Chemical Sources – Fugitive Guidance (APDG 6422), and LDSN-DRF control efficiencies that are appropriate for a continuous fugitive monitoring system (28LAER level control percentages).

6.5 The Power of LDSN/DRF - Forward Research

Future research may enable new capabilities in emission monitoring as additional potential benefits associated with this and other NGEM technologies can be envisioned. Once a facility has an operating LDSN that can automatically record and analyze information on a 24/7 basis, powerful data use concepts can be explored. As described in Sections 2 and 4.4, not only are more effective LDAR programs delivered from a business perspective, but emissions from leaks and malfunctions that are not part of the LDAR program can be found and mitigated, providing for significant environmental benefit. Future advanced forms of process monitoring and emissions accounting can be considered where transient events, such as actuating pressure relief devices or planned maintenance activities can be observed from both an emissions and operations point of view. An example of such a transient event is shown in Figure 6-2 where an emission is observed and tracked over multiple sensors in the network over time. This type of analysis serves as both an advanced QA check of LDSN operation and potentially the basis for a whole-facility monitoring concept for the future, benefiting industry, regulators, and communities alike.

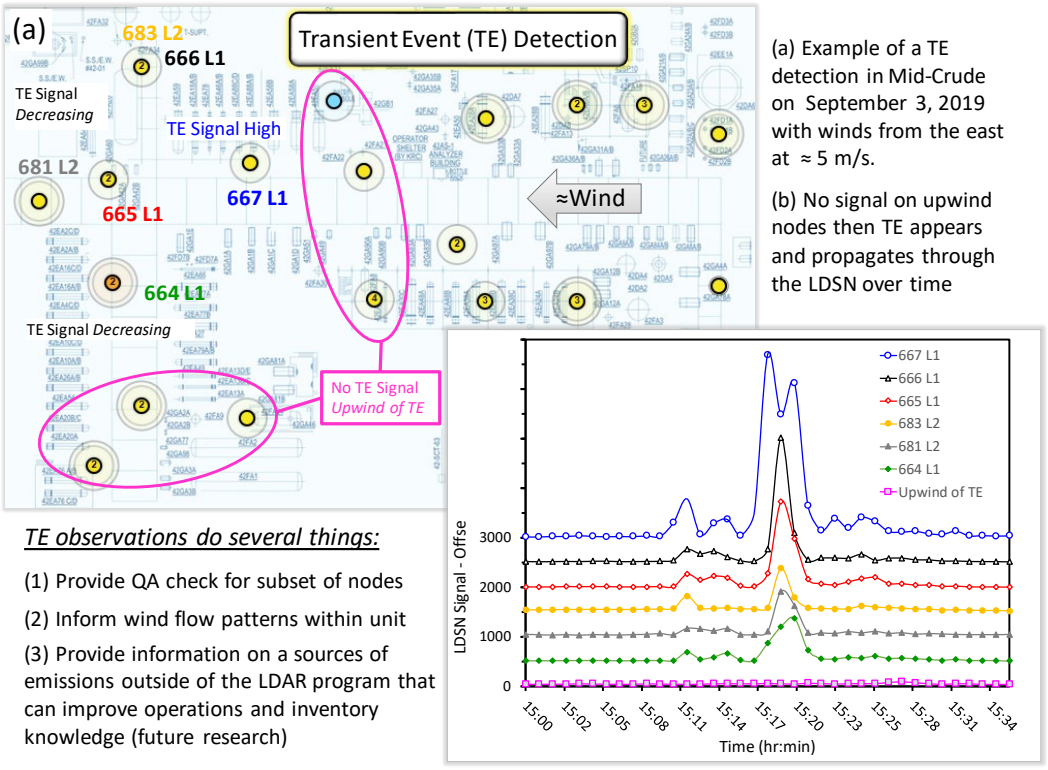

(a) Example of a TE detection in Mid-Crude on September 3, 2019 with winds from the east at ≈ 5 m/s.

(b) No signal on upwind nodes then TE appears and propagates through the LDSN over time

TE observations do several things:

(1) Provide QA check for subset of nodes

(2) Inform wind flow patterns within unit

(3) Provide information on a sources of emissions outside of the LDAR program that can improve operations and inventory knowledge (future research)

Figure 6-2. Example of a TE detection

7.0 Acronyms and Acknowledgments

Table 7-1 lists the Acronyms and abbreviations used in this report. Table 7-2 acknowledges the contributions of individuals working on this project.

Table 7-1. Acronyms and abbreviations

Acronyms or Abbreviation	Full Detail
AVO	audio, visual, or olfactory leak/emission detection
AWP	alternative work practice
AWS	Amazon Web Services
CC	FHR Corpus Christi West Refinery (or FHR CC), the site of pilot testing
CEMM	Center for Environmental Measurement and Modeling (EPA ORD)
CFD	computational fluid dynamics (flow field model simulations)
CFR	Code of Federal Regulations
CRADA	cooperative research and development agreement
CWP	current work practice
DOR	delay of repair
DRF	detection response framework
DT	Detection Threshold (DT band), general - Table 3.1, modeling - Table 4.1
DTA	The midpoint of the DT band, general - Table 3.1, modeling - Table 4.1

Acronyms or Abbreviation	Full Detail
DTC	DT band with cluster detects, EPA modeling term - Table 4.1
DTL	DT band lower limit, general term - Table 3.1
DTU	DT band upper limit, general term - Table 3.1
DT(+1σ)	DT band uncertainty, general term - Table 3.1
DT(cluster)	Molex equivalency modeling term - Table 4.2
DT(tag)	Molex equivalency modeling term - Table 4.2
DTA(cluster)	Molex equivalency modeling term - Table 4.2
DTA(tag)	Molex equivalency modeling term - Table 4.2
eDTA	Molex equivalency modeling term - Table 4.2
eDTU	Molex equivalency modeling term - Table 4.2
ECE	Emissions Control Efficacy, general term – Table 3.1
EPA	U.S. Environmental Protection Agency
ER	emission rate (typically by mass)
eV	electron Volt
FHR	Flint Hills Resources Corpus Christi Refinery LLC (the company)
FHR CC	Flint Hills Resources Corpus Christi West Refinery, site of pilot testing
FHR SLOF	Flint Hills Resources Sour Lake Olefins Facility, site of pilot testing
FID	flame ionization detector
FLIR	forward looking infrared
FTE	full time equivalent
g/hr	grams per hour
hr	hour(s)
HAP	hazardous air pollutant
HC	hydrocarbon
Hz	Hertz (1 Hz is a rate of once per second)
ID	identification
IP	ionization potential
IR	infrared
LDAR	leak detection and repair
LDSN	leak detection sensor network
LDL	lower detection limit
LPG	light petroleum gas
LTO	longer-term objective (for CRADA 914-16)
M21	EPA Method 21
MDL	method detection limit
MET	meteorological
MFC	mass flow controller
min	minutes
Molex	Molex, LLC
mSyte™	Molex prototype LDSN data upload and management platform
NGEM	next generation emissions measurement
NTO	near-term objective (for CRADA 914-16)
OAQPS	Office of Air Quality Planning and Standards
OAR	Office of Air and Radiation
OGI	optical gas imaging

Acronyms or Abbreviation	Full Detail
ORD	Office of Research and Development
ORISE	Oak Ridge Institute of Science and Education
OTM	Other Test Method
PDF	portable document format
PID	photoionization detector
ppbv	part(s) per billion by volume (also listed as ppb)
ppbe	ppb equivalent (a sensor's digital output unit)
ppmv	part(s) per million by volume (also listed as ppm)
PSL	potential source location (leak detection output from mSyte™ LDSN)
QA	quality assurance
QAM	quality assurance manager
QC	quality control
R6	EPA Region 6
RF	response factor
RH	relative humidity
RPD	relative percent difference
RSD	relative standard deviation
RTP	Research Triangle Park
sccm	standard cubic centimeter per minute
SV	screening value (M21-dtermined peak concentration)
SLOF	FHR Sour Lake Olefins Facility (or FHR SLOF), the site of pilot testing
SME	subject matter expert
S/N	signal to noise ratio
SOCMI	Synthetic Organic Chemical Manufacturing Industry
Stdev	standard deviation
σ	standard deviation
3σ	3 times the standard deviation (sensor noise floor)
SSD	solid state drive
TBD	to be determined
TCEQ	Texas Commission on Environmental Quality
UL	Underwriters Laboratory
U.S.	United States
VOC	volatile organic compound

Table 7-2 provides a summary of contributor effort using the following project-specific role key: (A) report authorship, (B) report editing (C) concept development, (D) EPA ORD equivalency model development (E) Molex emission simulation and equivalency model development, (F) LDSN/mSyte™ hardware and software development, (G) data acquisition and analysis (H) project/program management, (I) quality assurance, (J) technical consultation, (PI) organization principle investigator.

Table 7-2. Acknowledgment of contributions

Name	Affiliation	Contribution Area
Eben Thoma	EPA/ORD/CEMM	A, B, C, D, G, H, I, PI EPA
Haley Lane	ORISE (EPA ORD)	A, B, C, D*, G, I
Carlowen Smith	ORISE (EPA ORD)	B
Megan MacDonald	ORISE (EPA ORD)	B
Libby Nessley	EPA/ORD/CEMM	B, I, J
Casey Bray	EPA/OAR/AQAD	I
Jason Dewees	EPA/OAR/AQAD	J
Wenfeng Peng	Molex LLC	A, B, C, E, F, G, H, I, PI (Molex)
Ling-Ying Lin	Molex LLC	A, B, C, E, F, G, I
Alex Chernyshov	Molex LLC	A, B, C, E, F, G
Miao Xu	Molex LLC	A, B, C, E
Dave Massner	Molex LLC	C, F, G,
Arun RajuGanesan	Molex LLC	C, F
Ray Haskell	Molex LLC	F, H
Ben Madoff	Molex LLC	F
Barry Kelley	Koch Industries	A, B, C, E, F, G, H, I, PI (FHR)
Mike Clausewitz	Koch Industries	A, B, C, G, I, J
Deb Cartwright	Flint Hills Resources	A, B, C, G, H, I
Kurt Anderson	Flint Hills Resources	A, B, C, G, H, I
Roland Guzman	Flint Hills Resources	G, I
Austin Narverud	Flint Hills Resources	B, C, J
Brent Sorensen	Flint Hills Resources	B, H

*H. Lane led the development of the EPA ORD equivalency analysis as part of her NGEM ORISE research appointment with EPA ORD.

8.0 References and Endnotes

1. EPA, U. S., Reference Method 21, Determination of volatile organic compound leaks. U.S. Government Printing Office, Washington, D.C.: Federal Register 40 CFR Part 60, Appendix A-7 , Electronic Code of Federal Regulations, 1990.
2. EPA, U. S., Protocol for equipment leak emission estimates. U.S. EPA, Office of Air and Radiation, Office of Air Quality Planning and Standards, Research Triangle Park, North Carolina 27711: 1995.
3. EPA, U. S., Leak detection and repair, A best practices guide. U.S. EPA, Office of Compliance, Office of Enforcement and Compliance Assurance, 1200 Pennsylvania Avenue, NW, Washington, DC 20460 2007; pp 2014-02.
4. EPA, U. S., Alternative work practice to detect leaks from equipment. U.S. Code of Ferderal Register: 40 CFR Parts 60, 63, 65; 73 FR 78199, EPA-HQ-OAR-2003-0199, p78199-78219, 2008.

5. EPA, U. S., Technical support document, optical gas imaging protocol U.S. Code of Federal Register: 40 CFR Parts 60, Appendix K, EPA-HQ-OAR-2010-0505-4949, 2015.
6. Furry, D.; Harris, G.; Ranum, D.; Anderson, E.; Carlstrom, V.; Sadik, W.; Shockley, C.; Siegell, J.; Smith, D., Evaluation of instrument leak detection capabilities for smart LDAR application: Refinery testing. *Environmental Progress & Sustainable Energy: An Official Publication of the American Institute of Chemical Engineers* **2009,** *28* (2), 273-284.
7. Ravikumar, A. P.; Wang, J.; Brandt, A. R., Are optical gas imaging technologies effective for methane leak detection? *Environmental Science & Technology* **2016,** *51* (1), 718-724.
8. Robinson, D. R.; Luke-Boone, R.; Aggarwal, V.; Harris, B.; Anderson, E.; Ranum, D.; Kulp, T. J.; Armstrong, K.; Sommers, R.; McRae, T. G., Refinery evaluation of optical imaging to locate fugitive emissions. *Journal of the Air & Waste Management Association* **2007,** *57* (7), 803-810.
9. Albertson, J. D.; Harvey, T.; Foderaro, G.; Zhu, P.; Zhou, X.; Ferrari, S.; Amin, M. S.; Modrak, M.; Brantley, H.; Thoma, E. D., A mobile sensing approach for regional surveillance of fugitive methane emissions in oil and gas production. *Environmental science & technology* **2016,** *50* (5), 2487-2497.
10. Snyder, E. G.; Watkins, T. H.; Solomon, P. A.; Thoma, E. D.; Williams, R. W.; Hagler, G. S. W.; Shelow, D.; Hindin, D. A.; Kilaru, V. J.; Preuss, P. W., The changing paradigm of air pollution monitoring. *Environmental science & technology* **2013,** *47* (20), 11369-11377.
11. Somov, A.; Baranov, A.; Spirjakin, D.; Spirjakin, A.; Sleptsov, V.; Passerone, R., Deployment and evaluation of a wireless sensor network for methane leak detection. *Sensors and Actuators A: Physical* **2013,** *202*, 217-225.
12. W. Peng, D. M., L. Lin, A. Chernyshov, B. Kelley, M. Clausewitz, D. Cartwright, A. Narverud, K. Anderson, E. Thoma, In *A Sensor Network System for Process Unit Emissions Monitoring*, Preceedings of the 2019 Air and Waste Managment Association Air Quality Measurement Methods and Technology Conference, Durham NC, April 2-4. U.S EPA Science Inventory, Record 345869, https://cfpub.epa.gov/si/ , Accessed Februray 18, 2020.
13. W. Peng, D. M., L. Lin, A. Chernyshov, B. Kelley, M. Clausewitz, D. Cartwright, K. Anderson, H. Lane, E. Thoma, In *An Automated Sensor Network System and Innovative Approach for VOC Leak Detection*, 2019 American Fuel and Petrochemical Manufactures (AFPM) Environmental Conference, Salt Lake City, UT, October 27 - 29, 2019; U.S. EPA Science Inventory, Record 348039, https://cfpub.epa.gov/si/ , Accessed Februray 18, 2020.
14. Weimer, J.; Krogh, B. H.; Small, M. J.; Sinopoli, B., An approach to leak detection using wireless sensor networks at carbon sequestration sites. *International Journal of Greenhouse Gas Control* **2012,** *9*, 243-253.
15. Murphy, C. F.; Allen, D. T., Hydrocarbon emissions from industrial release events in the Houston-Galveston area and their impact on ozone formation. *Atmospheric Environment* **2005,** *39* (21), 3785-3798.
16. Smith, R., Detect Them Before They Get Away: Fenceline Monitoring's Potential To Improve Fugitive Emissions Management. *Tulane Environmental Law Journal* **2015**, 433-

453.

17. Thoma, E.; George, I.; Duvall, R.; Wu, T.; Whitaker, D.; Oliver, K.; Mukerjee, S.; Brantley, H.; Spann, J.; Bell, T., Rubbertown Next Generation Emissions Measurement Demonstration Project. *International journal of environmental research and public health* **2019,** *16* (11), 2041.
18. Webster, M.; Nam, J.; Kimura, Y.; Jeffries, H.; Vizuete, W.; Allen, D. T., The effect of variability in industrial emissions on ozone formation in Houston, Texas. *Atmospheric Environment* **2007,** *41* (40), 9580-9593.
19. Zavala-Araiza, D.; Lyon, D.; Alvarez, R. n. A.; Palacios, V.; Harriss, R.; Lan, X.; Talbot, R.; Hamburg, S. P., Toward a functional definition of methane super-emitters: Application to natural gas production sites. *Environmental science & technology* **2015,** *49* (13), 8167-8174.
20. Endnote_1:, The EPA ORD National Risk Management Research Laboratory (NRMRL) was the original signatory for CRADA #914-16. EPA ORD NRMRL became EPA ORD CEMM in October 2019, with no change in personnel, for continued execution of the CRADA.
21. Endnote_2:, Information on the Federal Technology Transfer Act and the CRADA process with EPA ORD can be found at https://www.epa.gov/ftta/collaborating-epa-through-federal-technology-transfer-act, Accessed February 18, 2020.
22. Endnote_3:, Elements of standardized methods generally refer to factors such as instrument technology performance (e.g. sensor sensitivity), siting criteria, calibration and QA, general documentation, and use limitations, presented in the context of performance-based method (not limited to the specific embodiment demonstrated in this CRADA). The DRF is envisioned to be application specific (differs by process unit) but the presence of a DRF to for example, provide QA feedback to ensure ongoing operation of an LDSN, is believed to be required and therefore will likely be part of a standardized method in some form.
23. API, Analysis of Refinery Screening Data, API Publication No. 310, American Petroleum Institute: Washington, DC, 1997.
24. Endnote_4:, Published 10.6 eV RFs for individual compunds can vary by manufacturer. Table 2-2 contains 10.6 eV PID RF values from Technical/Application Article 02 by Ion Science Inc., 2019 https://www.ionscience.com/wp-content/uploads/2017/03/TA-02-Ion-Science-PID-Response-Factors-UK-V1.14.pdfElements , Accessed March 21, 2020
25. Thoma, E. D.; Brantley, H. L.; Oliver, K. D.; Whitaker, D. A.; Mukerjee, S.; Mitchell, B.; Wu, T.; Squier, B.; Escobar, E.; Cousett, T. A., South Philadelphia passive sampler and sensor study. *Journal of the Air & Waste Management Association* **2016,** *66* (10), 959-970.
26. Stovern, M.; Murray, J.; Schwartz, C.; Beeler, C.; Thoma, E. D., Understanding oil and gas pneumatic controllers in the Denver–Julesburg basin using optical gas imaging. *Journal of the Air & Waste Management Association* **2020,** *70* (4), 468-480.
27. Thermo, TVA 1000 Response Factors, P/N 50039, Version 8-23-2000, Thermo Environnmental Instrumnets Inc., Franklin Massachusetts;

http://www.petersonenvironmental.com/ThermoTVA1000ResponseFactors.pdf , Accessed Febrary 18, 2020. .

28. Zeng, Y.; Morris, J., Detection limits of optical gas imagers as a function of temperature differential and distance. *Journal of the Air & Waste Management Association* **2019,** *69* (3), 351-361.
29. Zeng, Y.; Morris, J.; Sanders, A.; Mutyala, S.; Zeng, C., Methods to determine response factors for infrared gas imagers used as quantitative measurement devices. *Journal of the Air & Waste Management Association* **2017,** *67* (11), 1180-1191.
30. Endnote_5:, In the fourth qaurter of 2019, Motiva (headquartered in Houston TX, a subsidiary of the Saudi Arabian national oil company Saudi Aramco), acquireed the SLOF site from FHR
31. EPA, U. S., Monte Carlo Simulation Approach for Evaluating Alternative Work Practices for Equipment Leaks. Office of Air and Radiation, Office of Air Quality Planning and Standards, Draft report. Attachment C to EPA-HQ-OAR-2003-0199-0008, Statistical Methods and Analysis of Sample Size Determination for a Generic Alternative Method. 1999.
32. EPA, U. S., Alternative Means of Emission Limitation, (40 CFR 65.102), Subpart F - Equipment Leaks, Electronic Code of Federal Regulations, https://gov.ecfr.io/cgi-bin/text-idx?SID=9f493e42caba260d8ee3ce742f537eec&mc=true&node=se40.17.65_1102&rgn=div8 , Accessed 04/29/2020 2020.
33. EPA, U. S., Standards: Pumps, Valves, Connectors, and Agitators in Heavy Liquid Service; Instrumentation Systems; and Pressure Relief Devices in Liquid service., (40 CFR 63.169), Subpart H—National Emission Standards for Organic Hazardous Air Pollutants for Equipment Leaks, Electronic Code of Federal Regulations, https://gov.ecfr.io/cgi-bin/text-idx?SID=09693ea334c7dc0a99aafcd5d381c353&mc=true&node=se40.11.63_1169&rgn=div8 , Accessed 04/29/2020 2020.
34. EPA, U. S., Instrument and Sensory Monitoring for Leaks.[65.017(b)(4), 65.107(e)(1)(v), & 65.104(a)(2)], Subpart F -Equipment Leaks, Electronic Code of Federal Regulations, https://gov.ecfr.io/cgi-bin/text-idx?SID=9f493e42caba260d8ee3ce742f537eec&mc=true&node=sp40.17.65.f&rgn=div6#se40.17.65_1104, Accessed 04/29/2020 2020.
35. API, 1993 Study of Refinery Fugitive Emissions from Equipment Leaks, Volumes I, II, and III, Radian DCN No. 93-209-081-02, Prepared by Radian Corporation for Western States Petroleum Association, Glendale, CA, and American Petroleum Institute, Washington, D.C. 1994.
36. Thoma E.D., M. B. A., Squier B., Daly R., Brantley H. L., Deshmukh P., Wille, G., Cansler J. , U.S. EPA Science Communication, Science in Action Fact Sheet: SPod Fenceline Sensors Under Development, Next Generation Emissions Measurements, 2016, https://www.epa.gov/air-research/spod-fact-sheet , Accessed February 18, 2020.
37. EPA, U. S., United States Environmental Protection Agency Air Emission Measurement Center (EMC), EMC Other Test Methods, https://www.epa.gov/emc/emc-other-test-

methods , Accessed Frebruary 18, 2020.

38. TCEQ, 2013 Emission Inventory Guidelines, Appendix A: Technical Supplements, 2015, https://www.tceq.texas.gov/assets/public/comm_exec/pubs/rg/rg360/rg36012/appendix_a.pdf , Accessed Februray 18, 2020.
39. TCEQ, Air Permit Technical Guidance for Chemical Sources, Fugitive Guidance, APDG 6422, 2018, https://www.tceq.texas.gov/assets/public/permitting/air/Guidance/NewSourceReview/fugitive-guidance.pdf , Accessed Februray 18, 2020.

Appendix A: Exploratory Tests

Appendix A consists of two summary presentations reviewing select aspects of the two exploratory tests conducted at the EPA RTP outdoor test range. Appendix A1 (pages A2 to A16) reviews RTP Test 1, conducted 11/27/17 to 12/7/17). Appendix A2 (pages A17 to A51) summarizes RTP Test 2, conducted 2/26/18 to 3/7/18.

The following was originally developed as part of internal CRADA team communications and has been modified in places to remove proprietary information and to improve clarity for use in this report. This appendix does not intend to capture all efforts performed in these tests but provides the reader with a sense of the type of work accomplished.

.

Appendix A1
RTP Test 1 Summary

Tests Conducted November 27, 2017 to December 7, 2017

Outline

- Intro to PID and sensors used in Test 1
- Review and analysis of test data
- Summary of Test 1
  - What we have learned
  - Next steps

What is PID?

- Photoionization detector (PID) is a type of sensor that utilizes vacuum UV to ionize gas molecules, and then measures the electric current to determine the concentration of the gas.

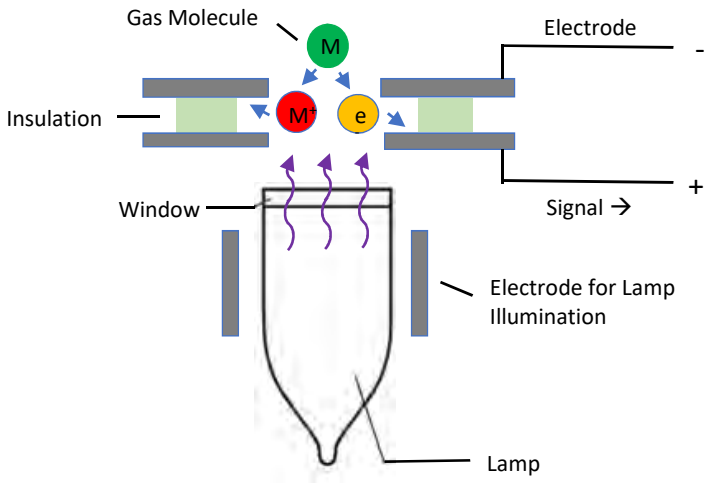

CMI Technologies Evaluated

- TVA-1000B by Thermo Fisher (Method 21)

- OGI camera by FLIR (AWP)

- Photoionization Detector (PID)
  - Falco Area Monitors by Ion Science
    - Molex unit, white cap sensor, diffusion model
    - EPA unit, white cap sensor, sample draw model
  - Falco Area Monitor by Ion Science (sample drawing, EPA unit)
  - S-Pod fenceline monitor by EPA
  - PID data acquisition systems by Molex

EPA Test Range

Test area

Mezzanine w/ sensor mounting rack

Calibration station

Test Set-up

Valves

- 100% Isobutylene was used as the test gas.
- Mass flow controllers were used to control the leak rate.
- Every leak was measured by TVA-1000B/M21 (some also by FLIR OGI).
- All sensors were placed together in one or two locations, while the leak location differs.

Sensor set-up

Mass flow controllers

Flanged spool piece (8”)

Overall Layout

- 22 tests (one aborted) with 15 sensors. Of them 18 tests have all sensors at 4.5ft off the ground, and 4 tests have half the sensors at 4.5ft and half at 13ft above the ground.

- Bubbles mark leak locations – size corresponds to maximum mass flow rate. Dotted lines connect leaks to sensors (located on grey bar).

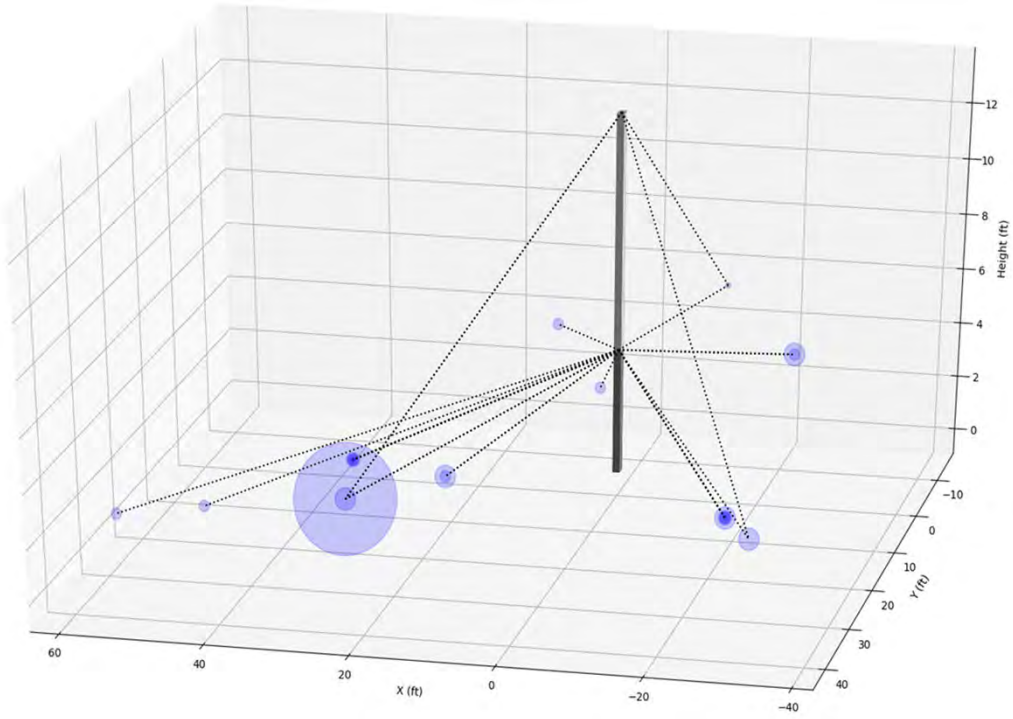

Statistics of Wind Data

- There was positive (from leak towards sensor) and negative wind of varying speed during each test.

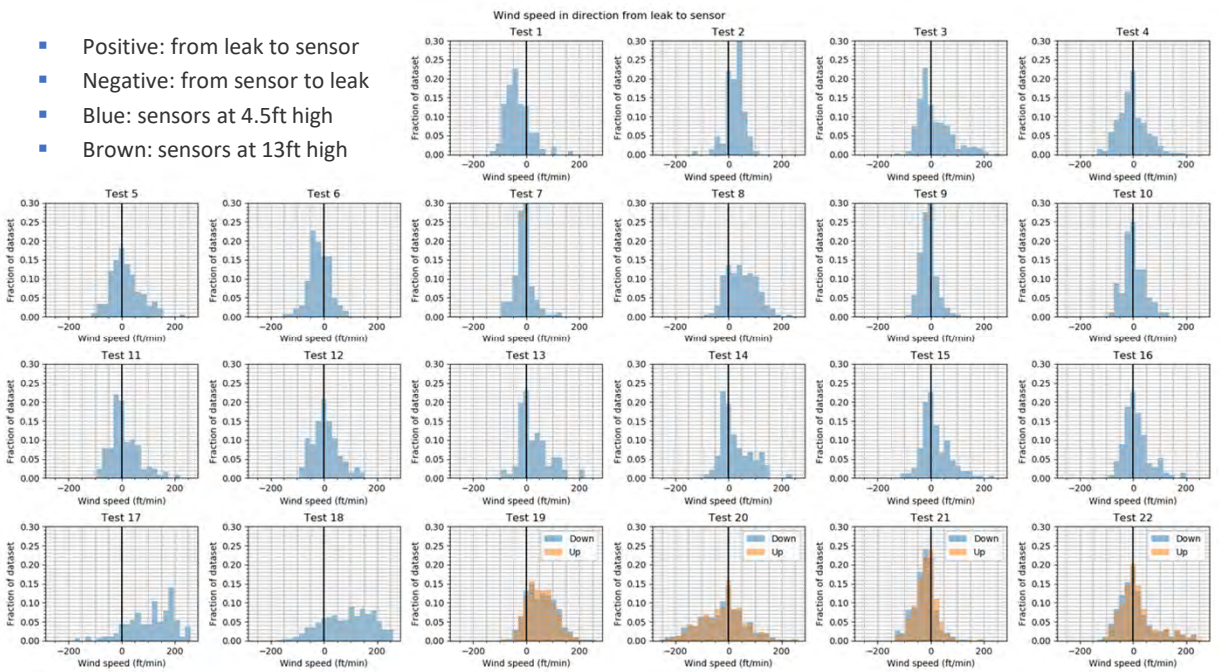

Sensor Output Plots

- Multiple detects were observed during this 1 hour test session.
- All sensors responded in the same way regardless of types and sensitivities.

Test Conditions:

- 10sccm leak rate
- Dry gas meter
- TVA = 8,000ppm
- Leak was 4’ high, and 7’ east of sensors

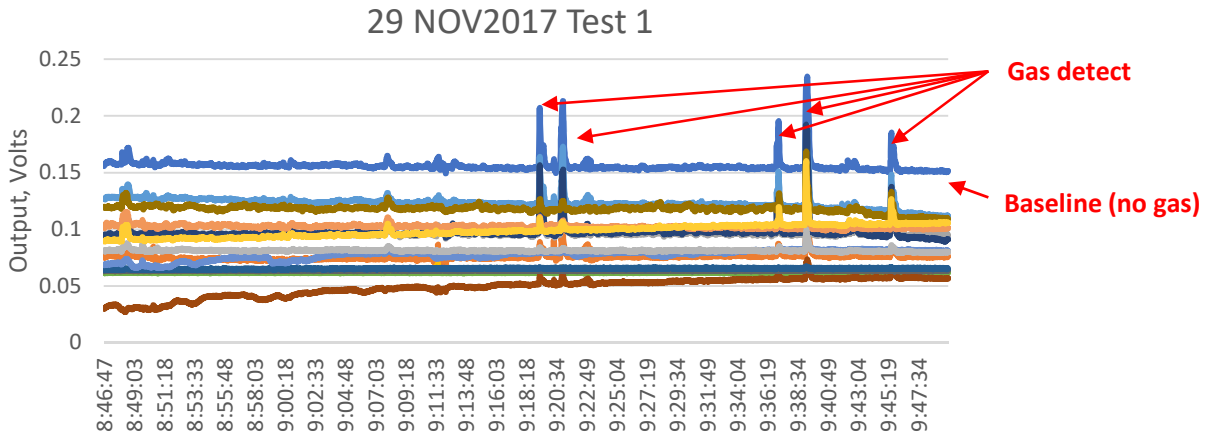

Distance and Leak Rate Test

- Valve Bonnet as the leak source 3’6’’ above the ground and 37’10” NE of sensors.
- Significant gas detects were observed at a leak rate of 5.0sccm or even as low as 2.5sccm.

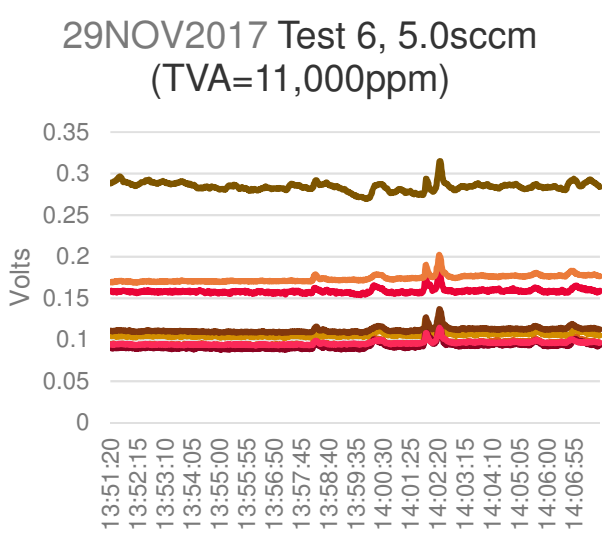

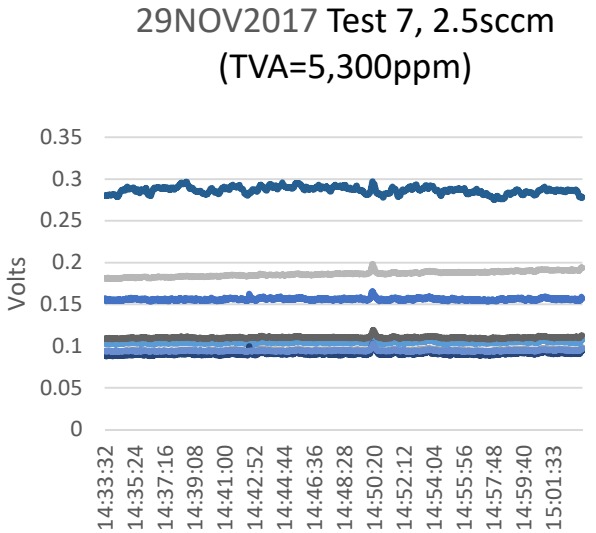

Foggy Morning (High RH) Test

- 20sccm leak, Valve Bonnet, TVA>100,000 ppm, leak was 22” high and 40’ SE of sensors. Intermittent fan.
- Sensors responded to gas while their baseline output was drifting.

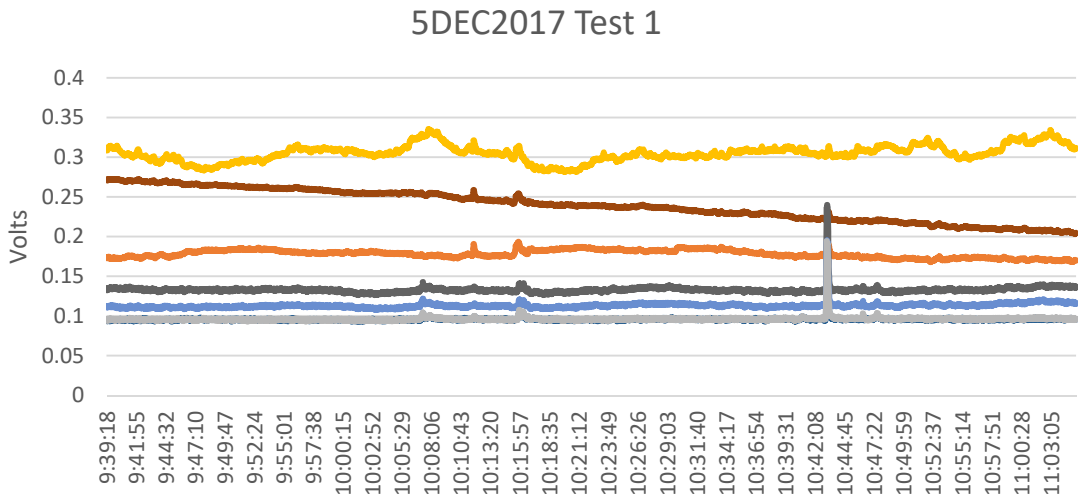

Forced Air Flow Test

- Directional flow of air generated by a fan from the leak to sensors created a large response to gas on some sensors

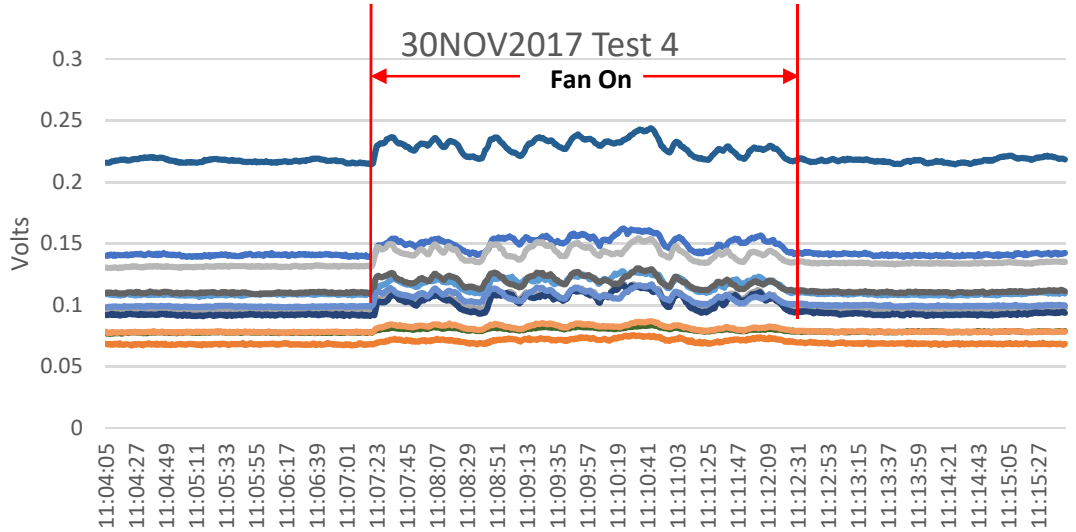

Test Conditions:

- 13sccm leak rate
- Valve Bonnet
- TVA = 43,000ppm
- Leak was 22' high, and 33' SE of sensors

Wind Effects

- Below are plots of sensor readings (Blue, left y-axis) and wind speed from leak to sensor (Red, right y-axis) from Test 1, 2, and 3 on November 29. Test 1 and 3 seem to show a possible relationship between wind speed and detection, but Test 2 has no obvious relationship.

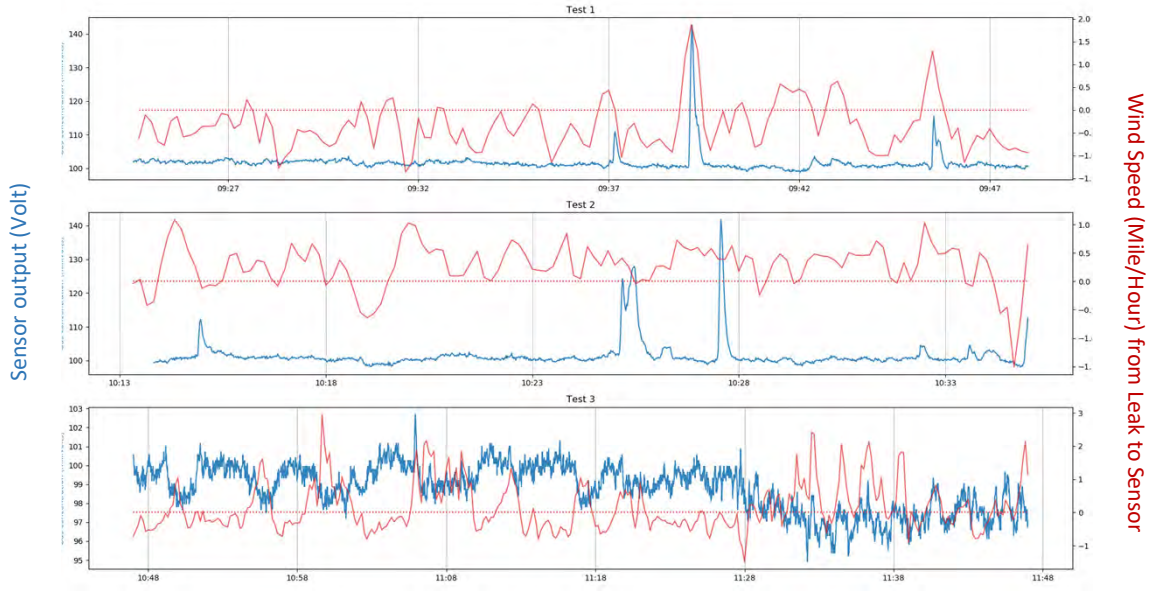

Summary (what we have learned)

- The PID does detect gas leaks remotely in fluctuating wind conditions. Each detection is a statistically significant change in the sensor output within a short time period, e.g. seconds to minutes.
- Our preliminary test results show the PID can reliably detect gas leaks at 5sccm at 20C within a radius of 30ft.
- The preliminary test shows the correlation between the leak rate and the signal response size. The relationship between them is, however, dependent on many factors.*
- Limited trials with intentional obstruction between emission source and sensors show sensors were still able to detect leaks.
- Some sensors have showed drift in the baseline due to environmental changes. Even so, the PID sensors were still found to respond to gas.
- The PID sensor was found to respond to the exhaust from a forklift truck running nearby.
- The PID was able to detect small leaks outside the normal operating regime of the OGI.

_____

* Factors may include atmosphere stability, wind speed, plume sensor overlap statistics, distance between sensor and source, sensor responsivity for a mixture of compounds, time resolution of sensor, impedance of gas transportation, etc.

Next Steps

- Study correlation between gas response and wind etc.
- Build test prototype for further study
- Evaluate each type of PID sensors in the lab
- Develop test plans for the next few months
- Identify action items prior to each test

Appendix A2
RTP Test 2 Summary

Tests Conducted February 26, 2018 to March 7, 2018

Outline

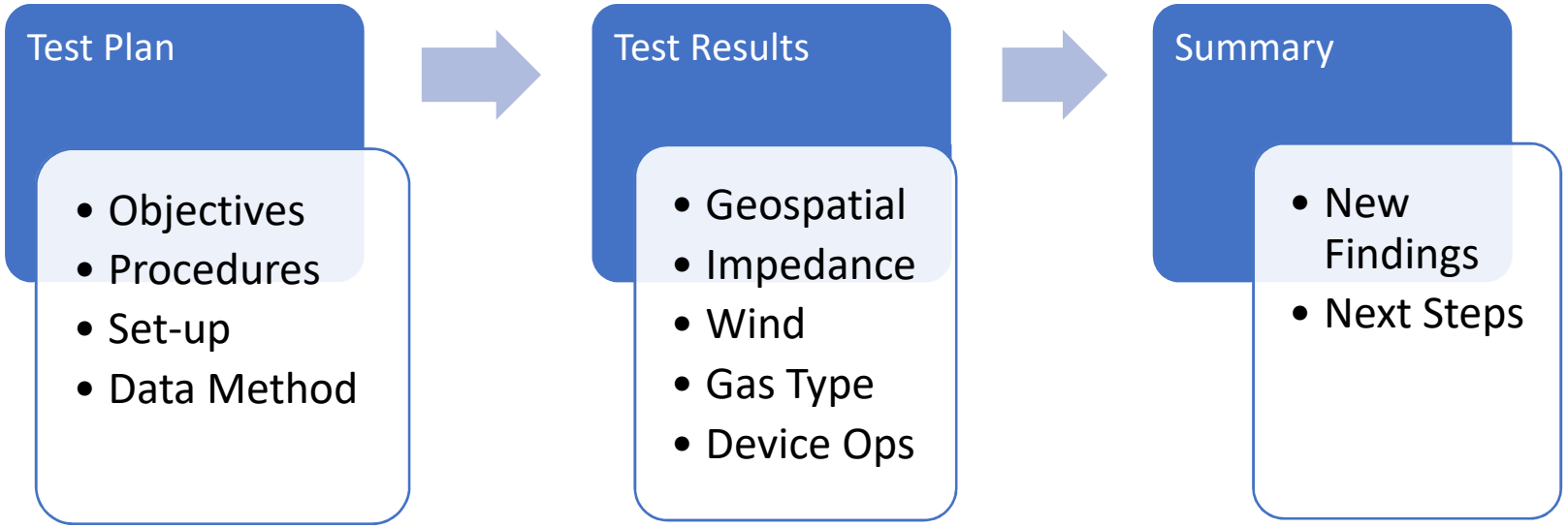
Test Plan
• Objectives
• Procedures
• Set-up
• Data Method
Test Results
• Geospatial
• Impedance
• Wind
• Gas Type
• Device Ops
Summary
• New Findings
• Next Steps

Test Objectives

- Further validate a highly sensitive photoionization detector (PID) technology for detecting plumes of volatile organic compounds (VOC).

- Explore spatial distribution application of sensors and feasibility of triangulating back to the leak source. Gain insights into variables that will help establish a relationship between each gas response and the leak source, and the significance of variables impacting remote sensor leak detection.

- Obtain knowledge about ethylene detection and wireless sensor operation, and information required for EPA's Quality Assurance Project Plan (QAPP) to further document the CRADA's Phase 1 activities.

Test Matrix

Test ID	Test # Planned	Layout	Gas	Leak Rate, sccm	Variable
1	1	A-0	iso-butylene	2.5	Leak Rate
2	2	A-0	iso-butylene	5.0	Leak Rate
3	3	A-0	iso-butylene	10	Leak Rate
4	4	A-0	iso-butylene	20	Leak Rate
5	9	A-1	iso-butylene	10	Leak Point
6	10	B-0	iso-butylene	10	Spatial Distribution
7	11	B-1	iso-butylene	10	Leak Point
8	12	C-0	iso-butylene	10	Spatial Distribution
9	13	C-1	iso-butylene	10	Leak Point
10	14	D-0	iso-butylene	10	Spatial Distribution
11	15	D-1	iso-butylene	10	Leak Point
12	16	E (5ft)	iso-butylene	10	Spatial Distribution
13		E (5ft)	Ethylene	10	Gas
14	17	F (10ft)	iso-butylene	10	Spatial Distribution
15		F (10ft)	Ethylene	10	Gas
16	18	G (20ft)	iso-butylene	10	Spatial Distribution
17		G (20ft)	Ethylene	10	Gas
18		H (30ft)	iso-butylene	10	Spatial Distribution
19	19	N/A	N/A	N/A	Heat Strip/Operation

Note: Tests 5-8 (ethylene leak rate test) in the original plan was replaced by Tests 13, 15 and 17.

Sensor Layout Examples

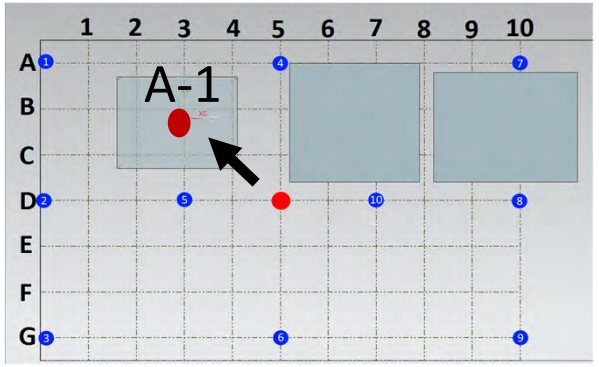

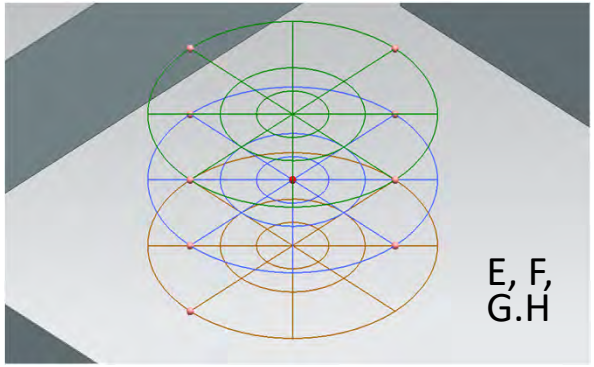

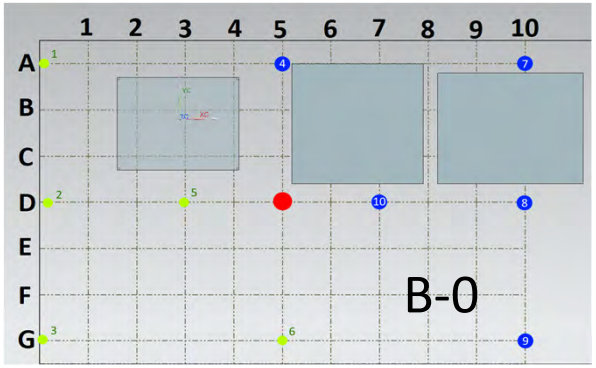

Blue dots: sensors @ 5' height
Green dots: sensors @ 10' height
Red dot: leak point
Gray boxes: buildings
Scale: grid lines 10ft

Test Set-up

- Either 100% iso-butylene or 100% ethylene was used as the test gas, and a 4” valve was used as the leaking component. The leak rate was controlled by an Alicat mass flow controller.
- The test area structure was de-energized and monitored constantly with area gas monitors. A manual power shutoff device was placed at the power output in case one of the monitors goes off at 10% LEL.
- Sensor placement, leak source location, gas or leak rate were adjusted according to the test plan and actual test results.
- Detection results were monitored via data acquisition system and displayed for real time evaluation.

Isobutylene Gas Tank

Mass flow controllers

Leaking Valve

Wireless Sensor Transmitters

RTP test site with wireless sensors mounted on tripods

Leak partly surrounded by impedance

Leak in open field & Method 21 inspection

EPA SPod and Molex sensors at same location

Molex Data Processing Method

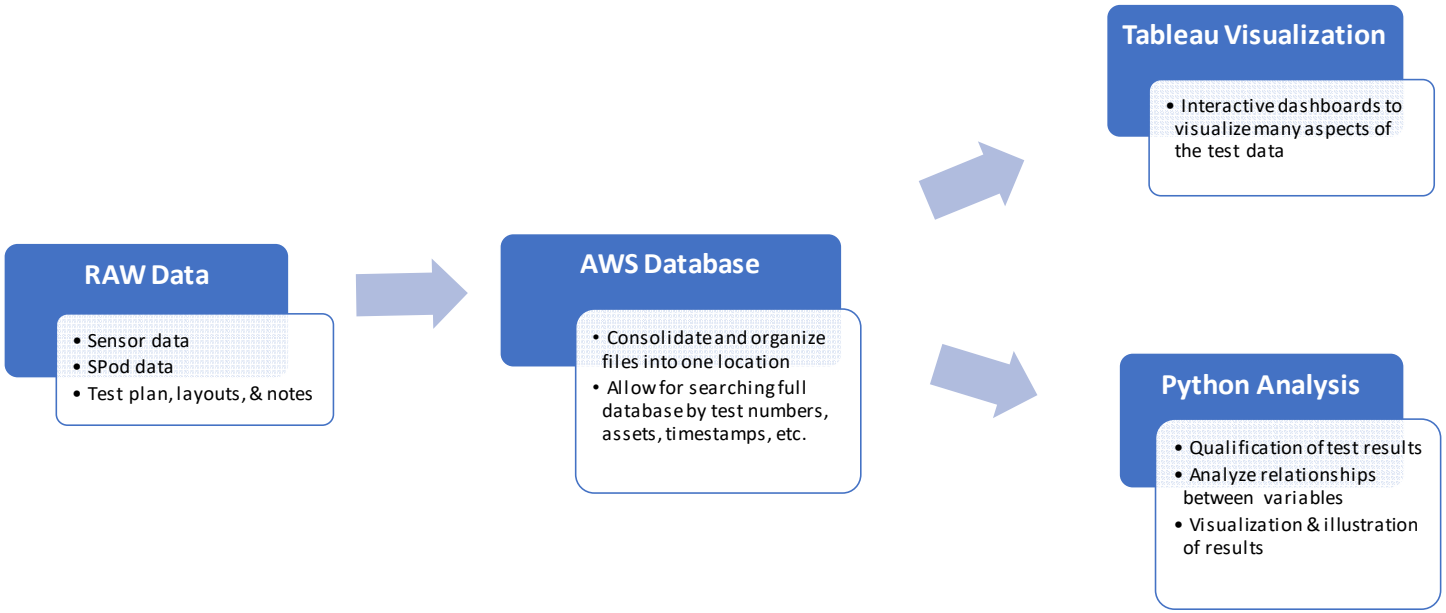

Leak Rate Interpretation

Iso-butylene (C4H8, MW=56.11)

- 10 sccm = 24.2mg/min, or 1.452g/hr @50F, 1atm
- 10 sccm = 23.7mg/min, or 1.422g/hr @60F, 1atm

- 1 gallon liquid = 2.226kg @ 588g/ml = 1565 hours or 65 days @10sccm, 60F

Ethylene (C2H4, MW=28.05)

- 10 sccm = 12.1mg/min, or 0.726g/hr @50F, 1atm
- 10 sccm = 11.8mg/min, or 0.708g/hr @60F, 1atm

- FLIR GasFindIR minimum detection for ethylene: 4.4g/hr in a controlled setting (source: http://www.flir.co.uk/ogi/display/?id=30866)

Sensitivity Checks

Proprietary Information has been removed from this section

Bump Test, Diffusion Mode

- In passive sampling mode, sensors still showed similar gas responses from each other.

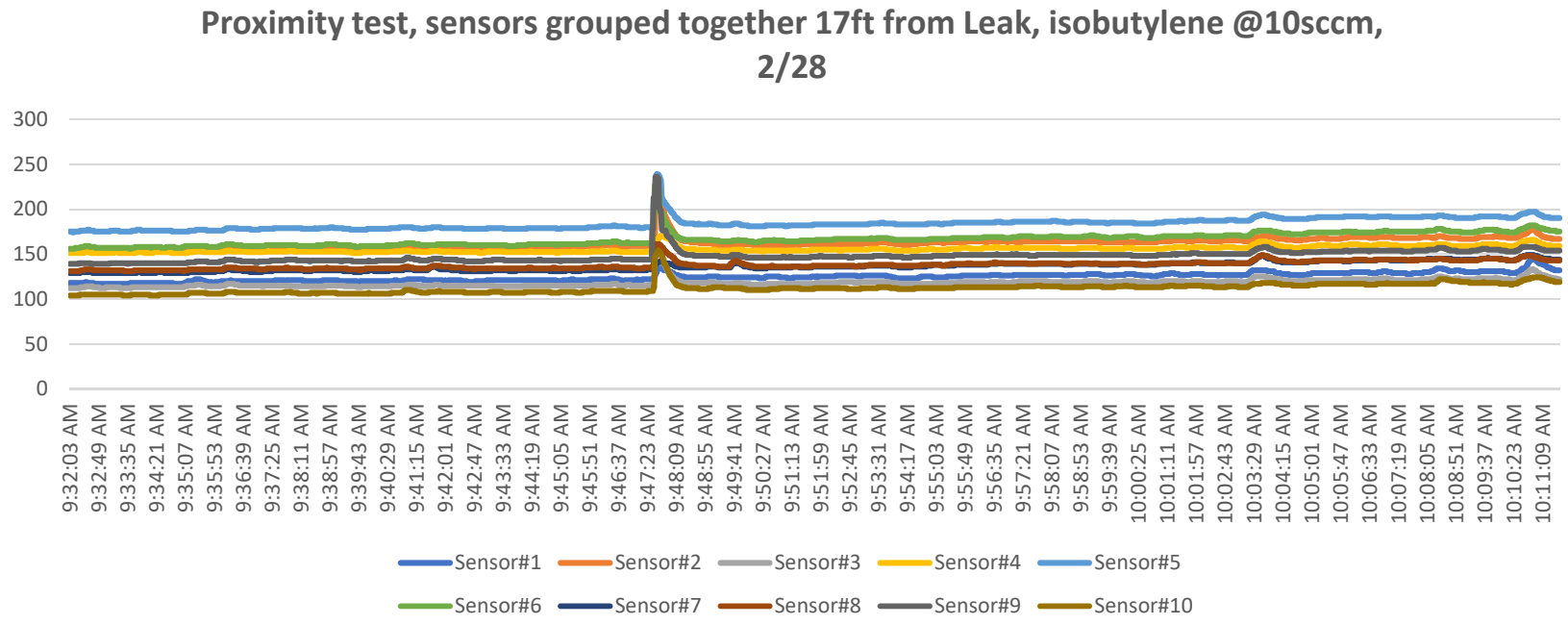

Leak Rate

Proprietary Information has been removed from this section

Leak Rate Tests

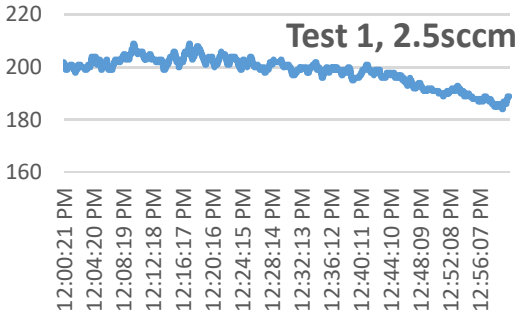

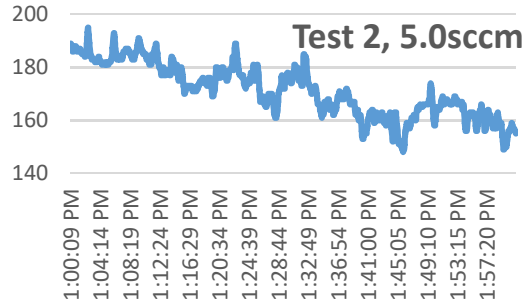

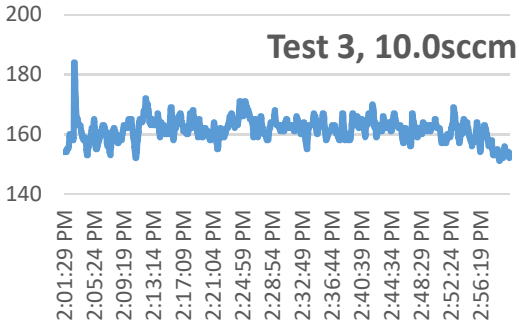

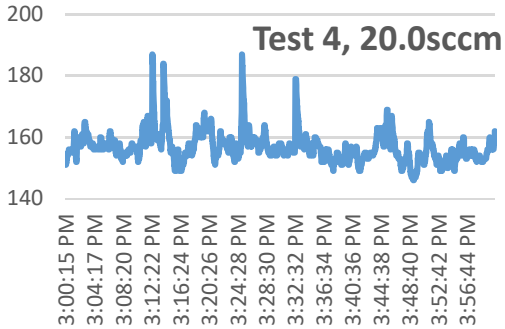

- Sensor #5, Layout A-0, 20ft, isobutylene, rain, 2/26

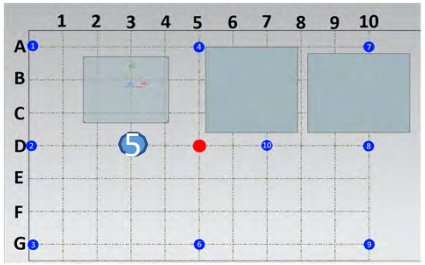

Leak Rate vs. Detection

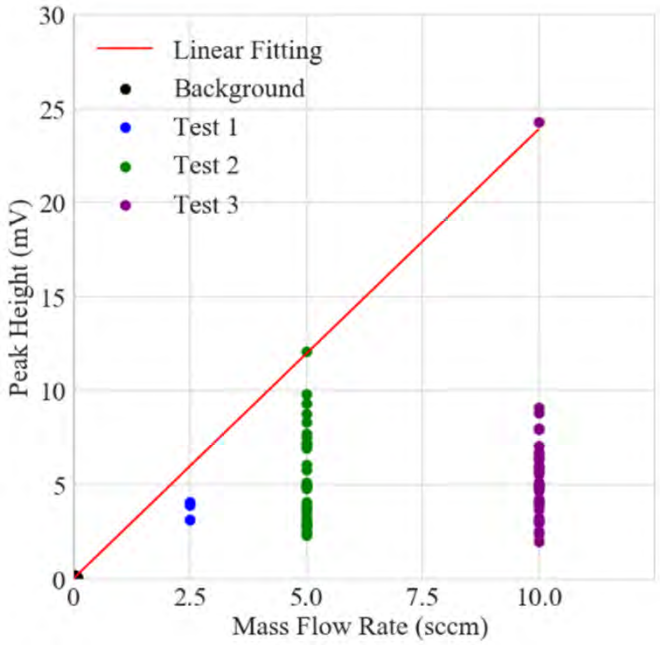

- Although weather condition kept changing during the tests, the graph below still shows that the detection signal increased with increasing leak rate overall.

Sensor #5 in Tests 1-3, Layout A-0, 20ft, isobutylene, rain, 2/26

Leak Distance

Proprietary Information has been removed from this section

Distance Change

- Sensor #5, 5ft height, Isobutylene, 10sccm

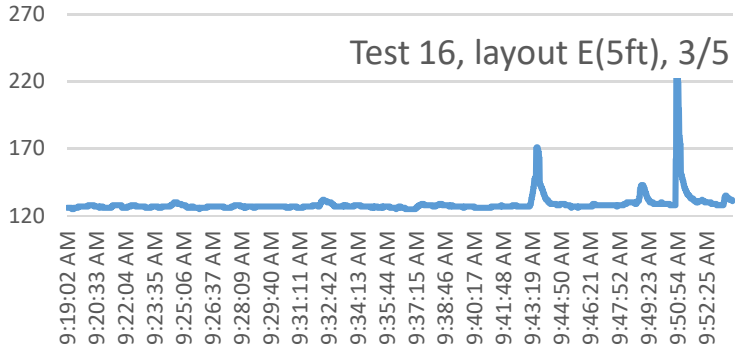

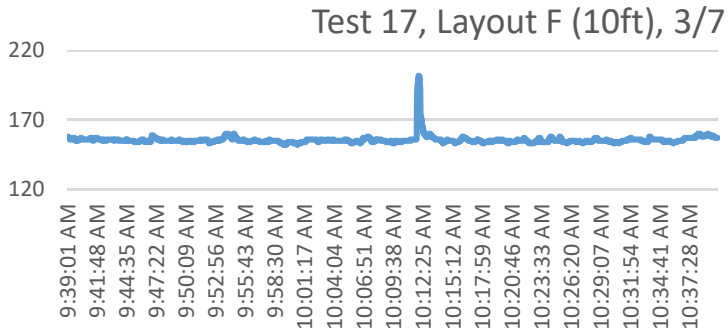

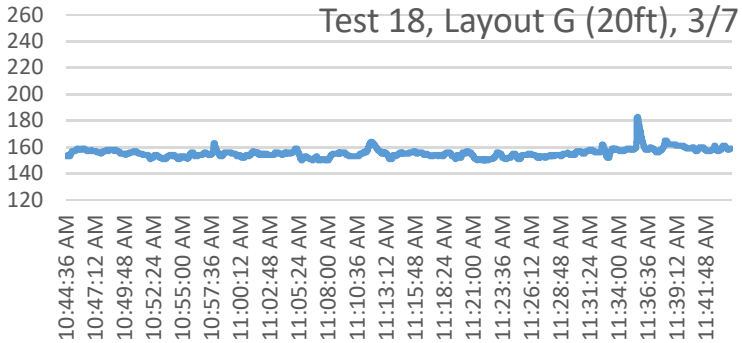

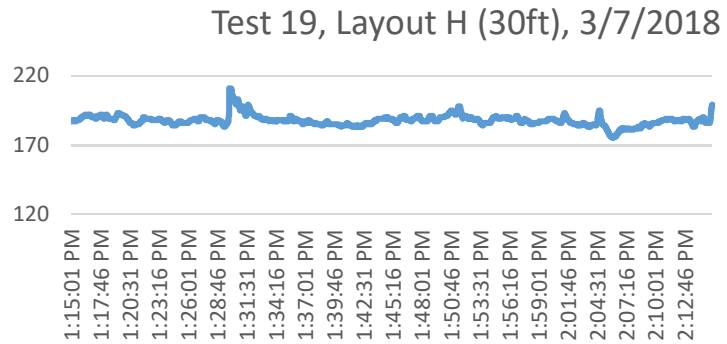

Multi-Peak Detection

- In a close range, some detections have two or more overlapping peaks.

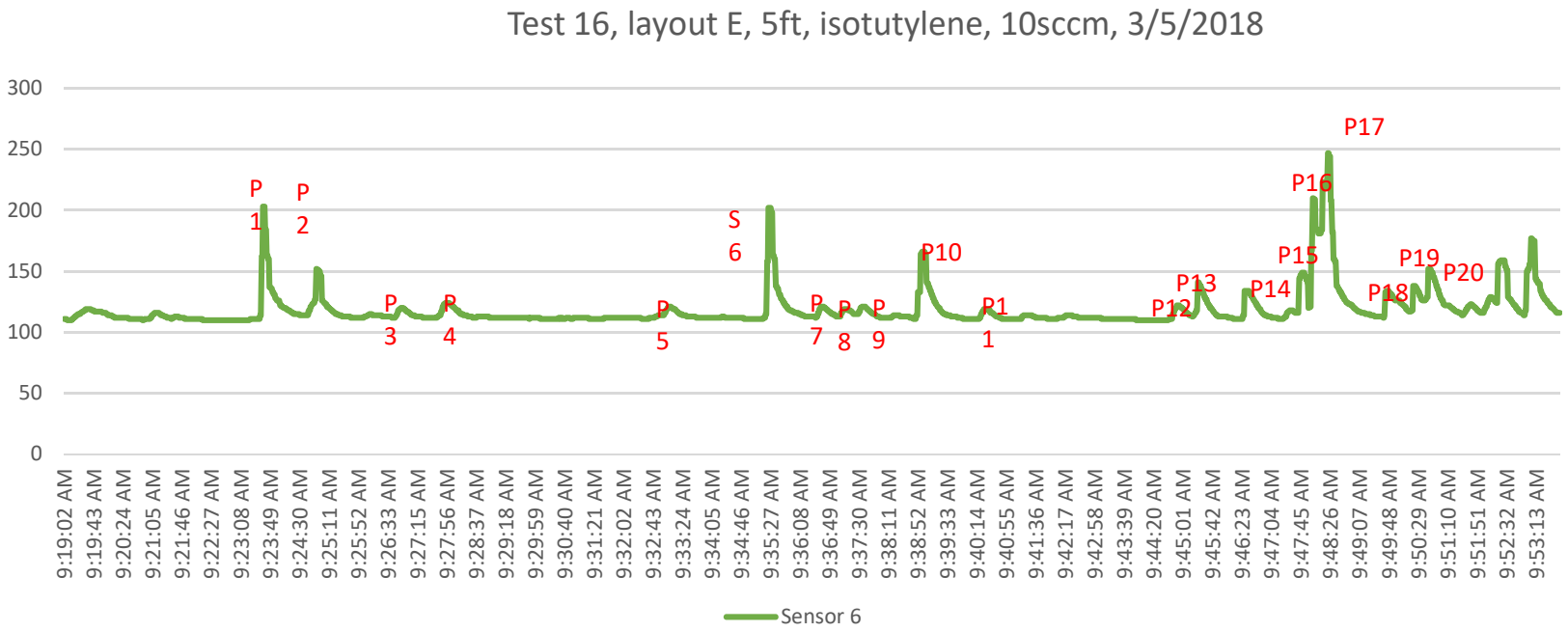

Sensors Aligned w/ Leak

- Sensor 8 showed lower detection than sensor 10, which is closer to the leak point

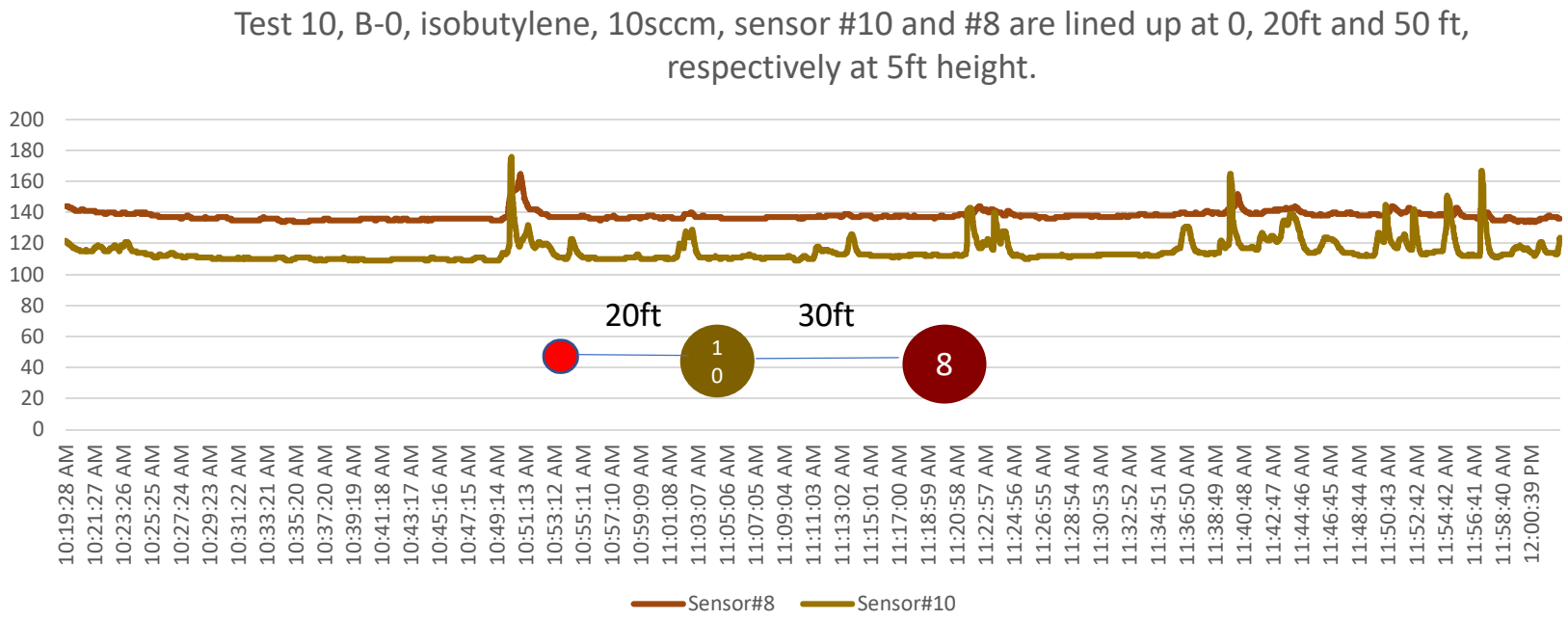

Long Distance

- Sensors 58 ft away showed visible detections.

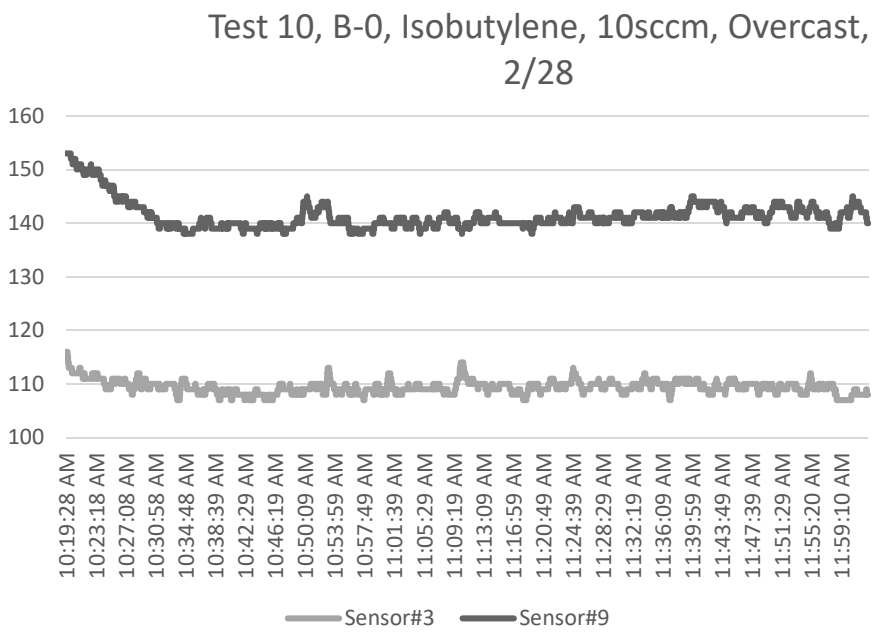

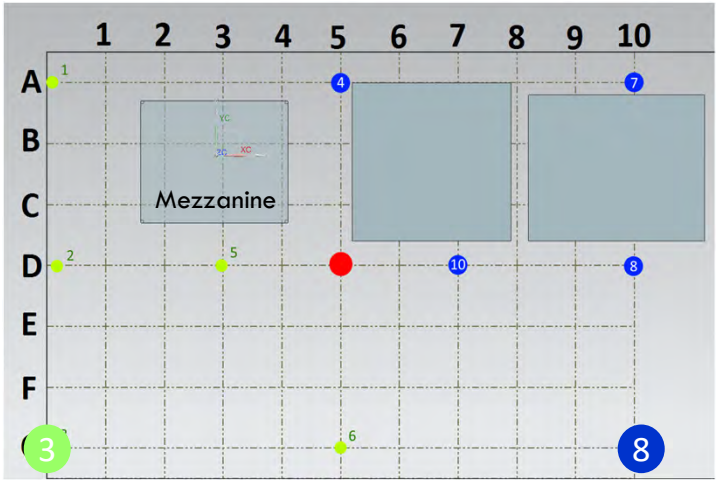

Blue dots: sensors @ 5' height
Green dots: sensors @ 10' height
Red dot: leak point
Gray boxes: buildings
Scale: grid lines 10ft

Leak Distance vs. Detection

- The longer the distance, the lower the detection magnitude. The width of the detection peak appears to increase with distance.

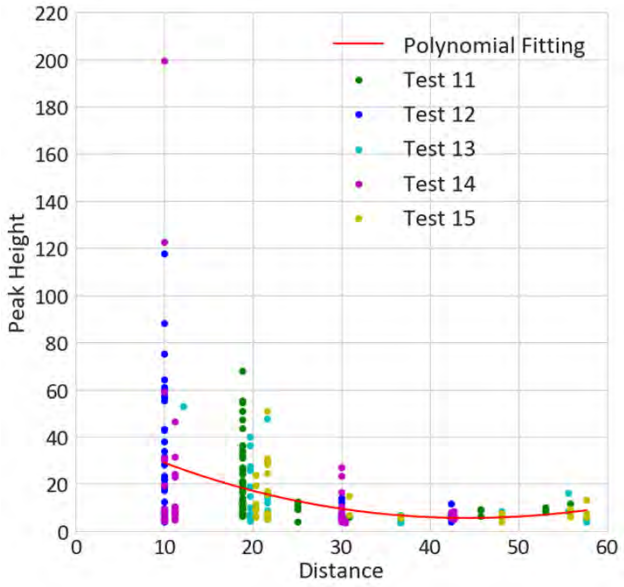

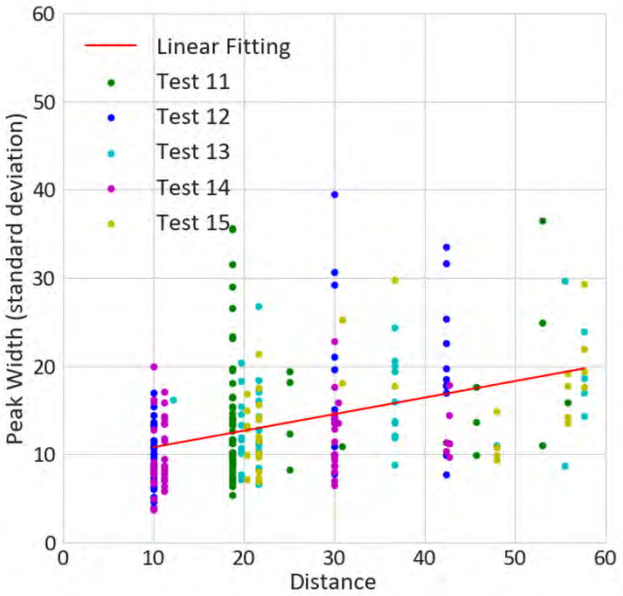

Sensor Height

Proprietary Information has been removed from this section

Sensors @ Different Heights

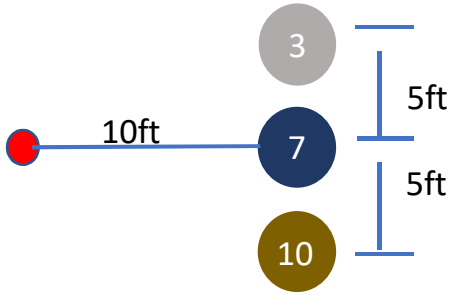

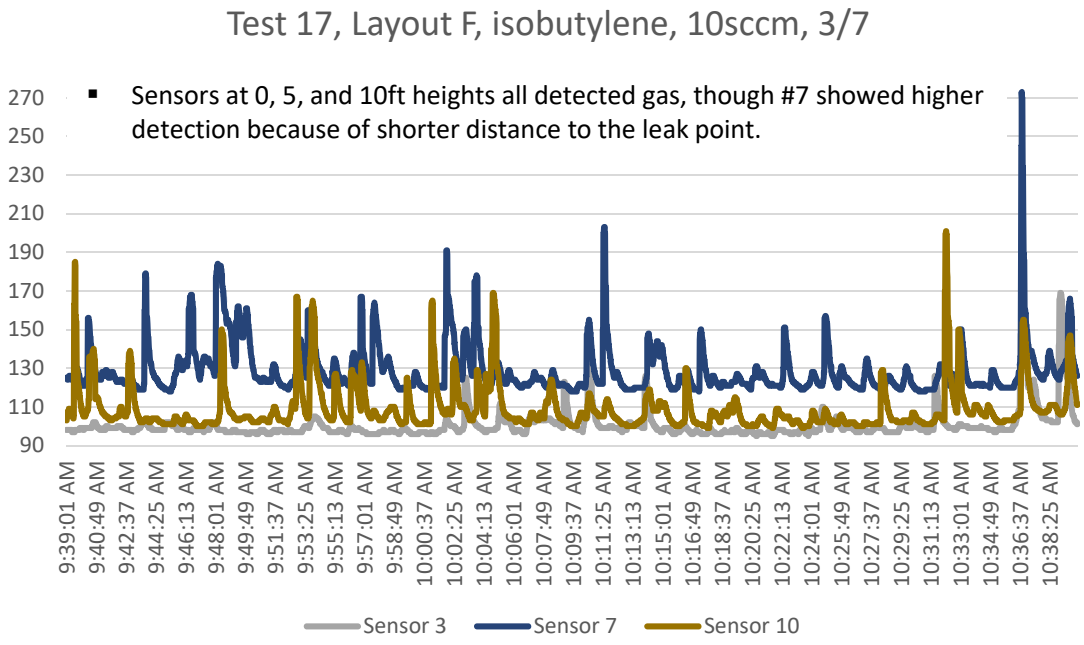

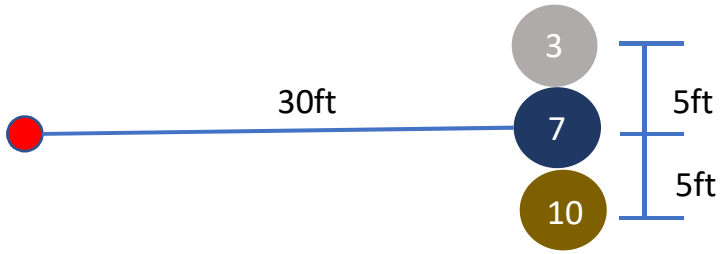

- The sensor at 10ft height had lowest detection possibly because the molecular weight of gas became a bigger factor in gas distribution with increasing time (longer distance means more time to travel).

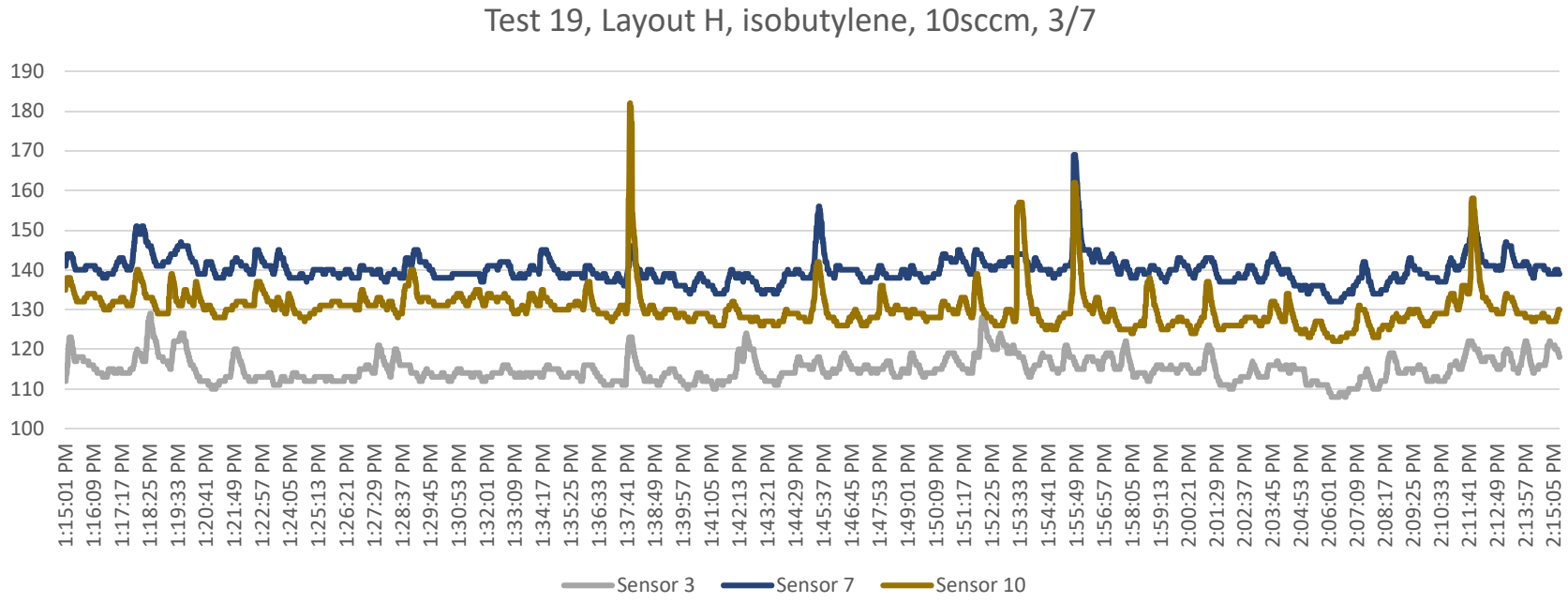

Impedance

Proprietary Information has been removed from this section

Sensor Behind Building

- The sensor at 10ft height had lowest detection possibly because the molecular weight of gas became a bigger factor in gas distribution with increasing time (longer distance means more time to travel).

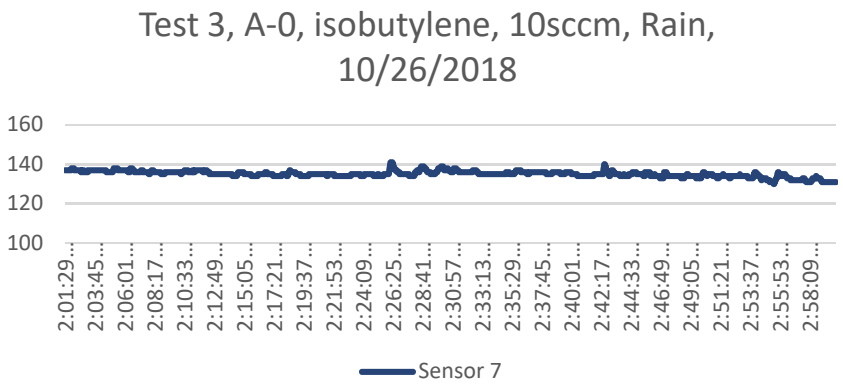

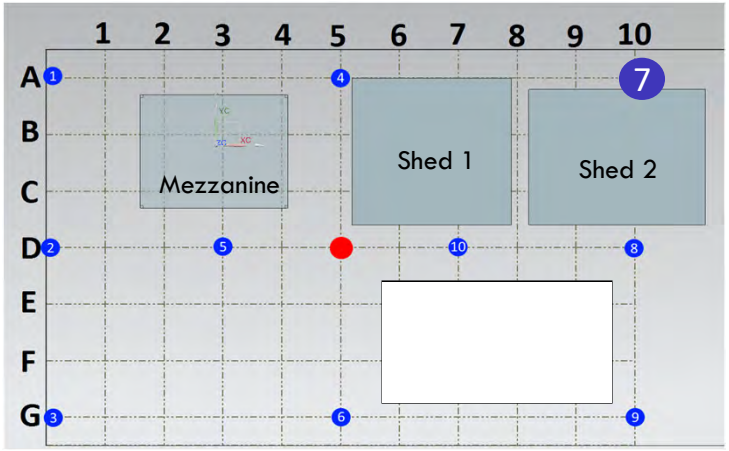

Leak Inside Mezzanine

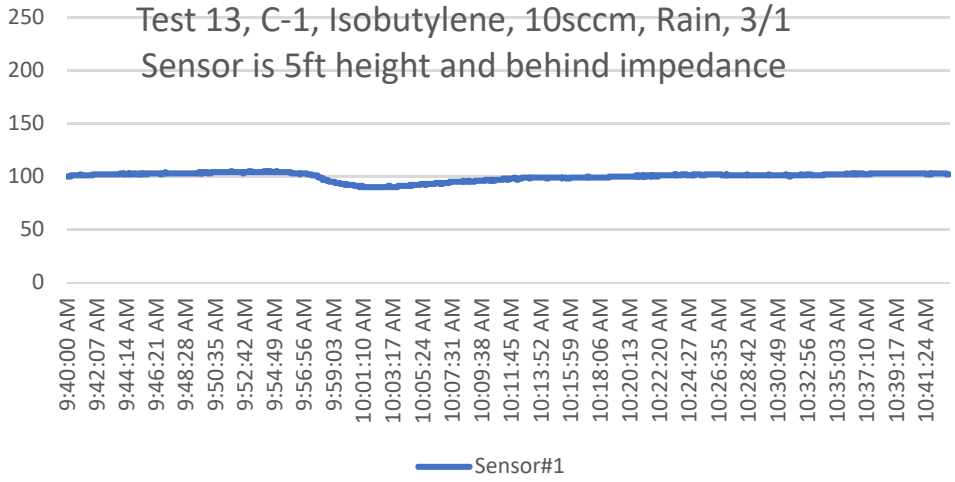

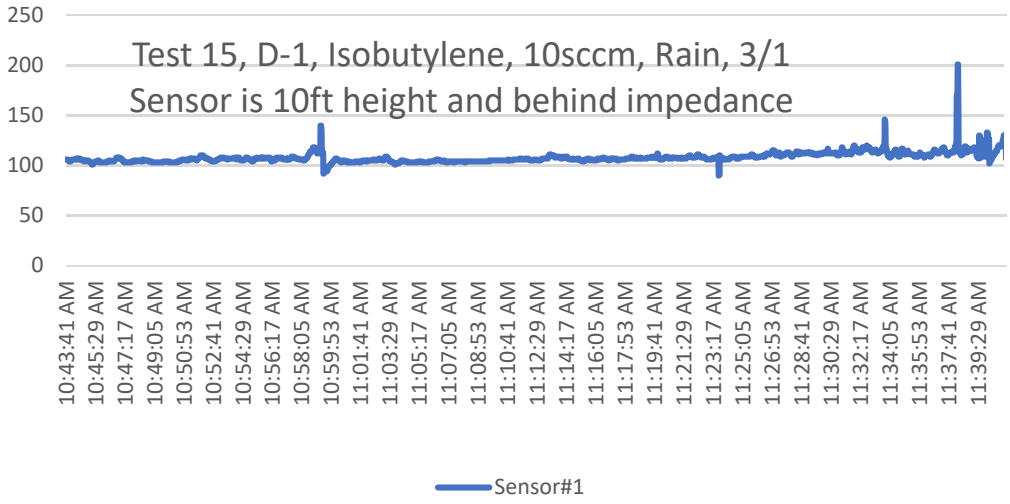

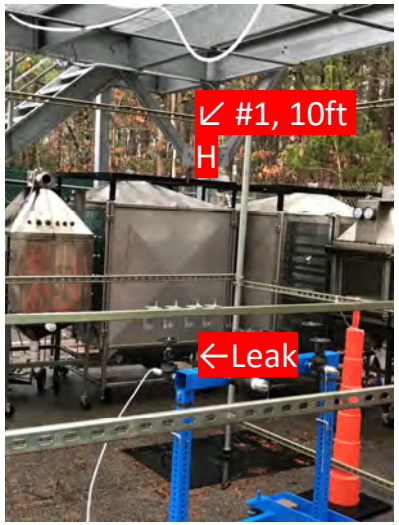

- Sensor #1 didn't detect gas when it was placed at 5ft height behind metal chambers, but it showed detections after being raised above the chambers.

Wind

Proprietary Information has been removed from this section

Ethylene

Proprietary Information has been removed from this section

Ethylene Leak @10ft Radius

- Ethylene was detected from sensors placed 10 ft away from the leak point.

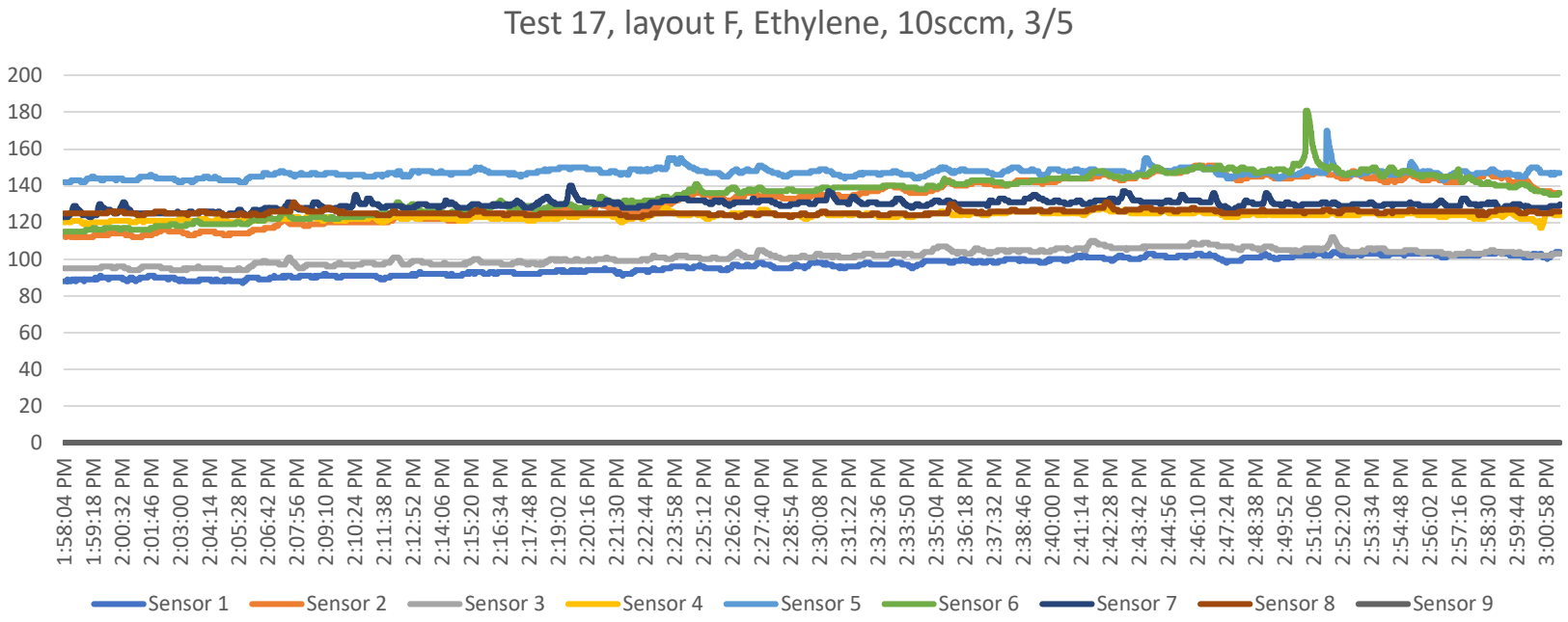

Ethylene vs. iso-Butylene @20ft Radius

- Visible detections were observed from sensors 20ft away from ethylene leak. The detection signals were about 1/10- 1/5 of isobutylene's.

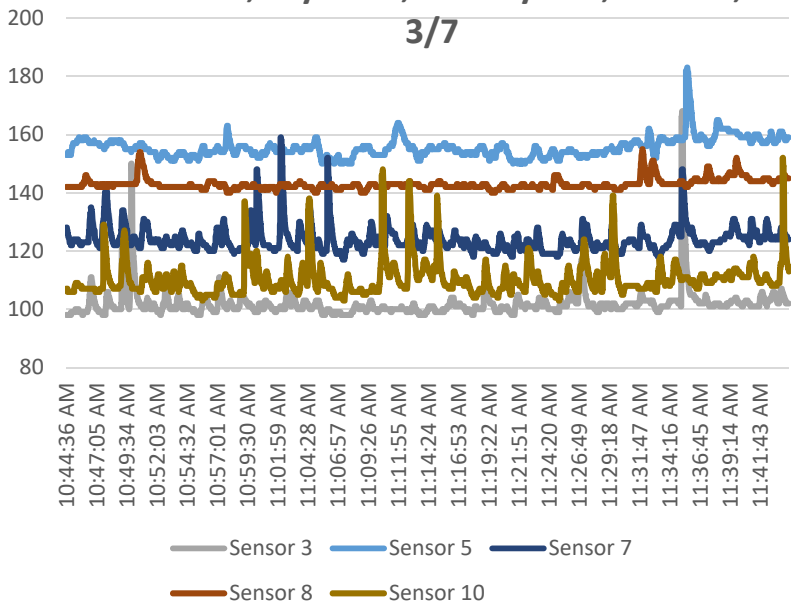

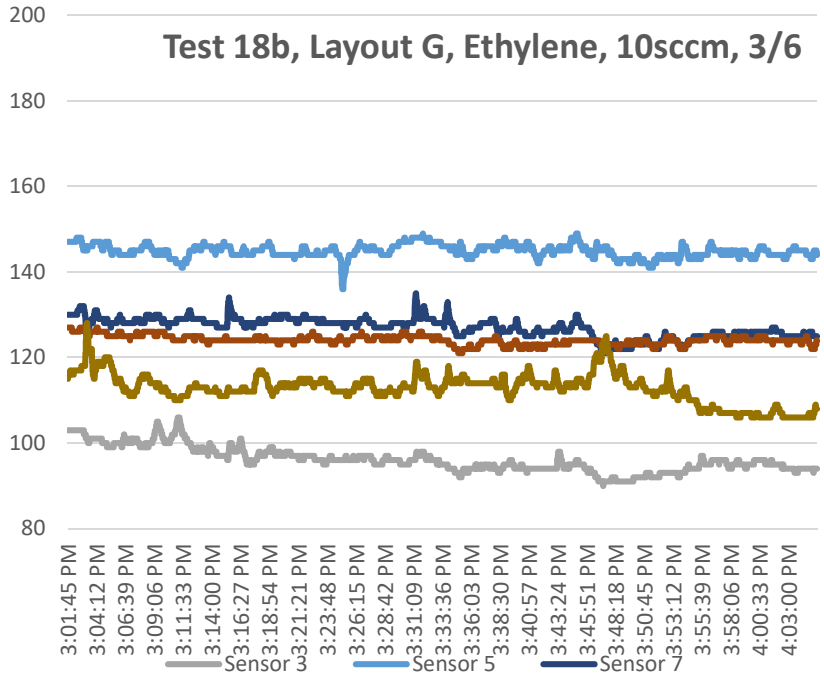

Device Comparison

Proprietary Information has been removed from this section

Method 21 Techniques

- Data suggests current M21 measurements are inaccurate. TVA has better accuracy than MiniRAE. Dilution tubes should not be used when gas concentrations are within TVA measuring range.

Isobutylene, ppm	MiniRAE, ppm	TVA, ppm	RF	TVA w/ RF, ppm	TVA w/ Dilution Probe, ppm	TVA Dilution w/ RF, ppm
101	**104**	137	0.66	**90**	140	**92**
510	**412**	692	0.64	**443**	650	**416**
2011	**1258**	3070	0.58	**1781**	2500	**1450**
5050	**2465**	10200	0.45	**4590**	6750	**3038**
9999	**3300**	31800	0.24	**7632**	14400	**3456**

Notes: 1. Testing was performed by Mike Clausewitz on March 1, 2018.
2. MiniRAE was calibrated to 100ppm isobutylene; TVA was calibrated to 500, 2000, and 10,000ppm methane.

Summary (what we have learned)

- The PID has continuously demonstrated near-source detectability of VOC emissions. At 40-60^{o}F and low wind speeds, visible detections were observed for isobutylene leak at 10sccm, or approximately 1.4g/hr at a distance of 50ft without obstruction.
- Sensor detection is affected by leak rate, distance, height, impedance, and wind etc. Sensors close to the leak source have large detection signals. Sensors farther away and /or behind impedance have smaller detection signals.
- Detection of gases 5ft below and 5ft above the leak point suggests that a gas not only travels laterally, but also disperses vertically.
- There appear to be good correlations between sensor response and wind direction. In general, sensors downwind respond to gas and when there are multiple sensors aligned downwind, the one closer to the leak shows higher response than the one farther away.
- A sensor network provides enhanced detection coverage, and info about probable location of the leak source.
- Ethylene leak at 10sccm or 0.71g/hr @60F was detected by sensors 20 ft away at 1/10-1/5 of the magnitude of isobutylene's response. This leak rate is about 6 times of the reported minimum detection limit (4.4g/hr) of FLIR gas imaging cameras.
- Double or multi-peak detection often occurs when a sensor is close to the leak source.

Next Steps

- Continue studying impact of different variables and relationships between them
- Update Test 2 Summary
- Develop plan for Test 3 Phase 1 test
- Sour Lake safety plan
- Sour Lake Management of Change (MOC)
- Update EPA Quality Assurance Project Plan (QAPP)
- Develop Molex PID transmitter for Test 3
- Develop algorithms to calculate detection signals on mSyte
- Continue testing PID sensors in the lab

Appendix B: FHR SLOF Tests

Appendix B consists of two summary presentations reviewing select aspects of the two LDSN Pilot tests conducted at FHR SLOF (called Test 3). Appendix B1 (pages B2 to B26) reviews SLOF Test 3.1 , conducted 5/14/18 to 5/23/18. Appendix B2 (pages B27 to B55) summarizes SLOF Test 3.2 , conducted 9/10/18 to 12/7/18. These presentations were developed as an internal CRADA communication and have been modified for use in this report.

The following was originally developed as part of internal CRADA team communications and has been modified in places to remove proprietary information and to improve clarity for use in this report. This appendix does not intend to capture all efforts performed in these tests but provides the reader with a sense of the type of work accomplished.

Appendix B1
Sour Lake Test 3.1 Summary

Tests Conducted May 14, 2018 to May 23, 2018

Outline

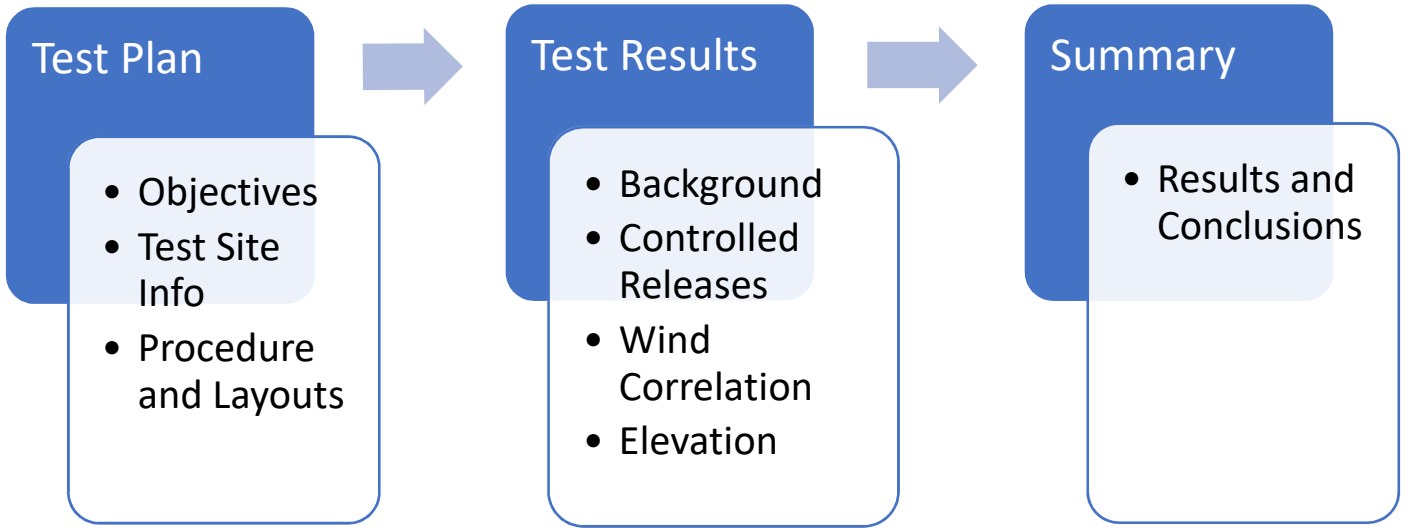
Test Plan
• Objectives
• Test Site Info
• Procedure and Layouts
Test Results
• Background
• Controlled Releases
• Wind Correlation
• Elevation
Summary
• Results and Conclusions

Test Plan & Setup

Test Objectives

- Conduct experiments to optimize sensor setup, including total number of sensors and geospatial grid arrangement.
- Continue to validate feasibility of triangulation of leak source location.
- Conduct experiments to evaluate the background level of ethylene and possible impact to Test 3.2. Validate and improve the test method and experimental plan for Test 3.2.
- Continue to gain additional knowledge about the design of a robust field sensor device.
- Test WIFI and other hardware and infrastructure required for Test 3.2.
- Develop infrastructure SOW for Test 3.2 – sensor locations, mounting requirements, conduit/wire scope, remote power relay scope, other scope.

Test Site Introduction

- Flint Hills Resources Port Arthur's (FHR's) Sour Lake Olefins Facility (SLOF) is a bulk storage facility located in Sour Lake, TX. The facility is permitted to receive, store, and distribute ethylene and propylene.
- Products are stored in underground storage caverns and recovered from the caverns for sale through displacement by brine.
- The equipment used at the SLOF includes filters, product measurement devices, filter-separators (liquid coalescers), a solid bed dehydration system, brine degassing facilities, a flare system, brine injection and transfer facilities, brine ponds, air compressors, utility equipment, and a control building.

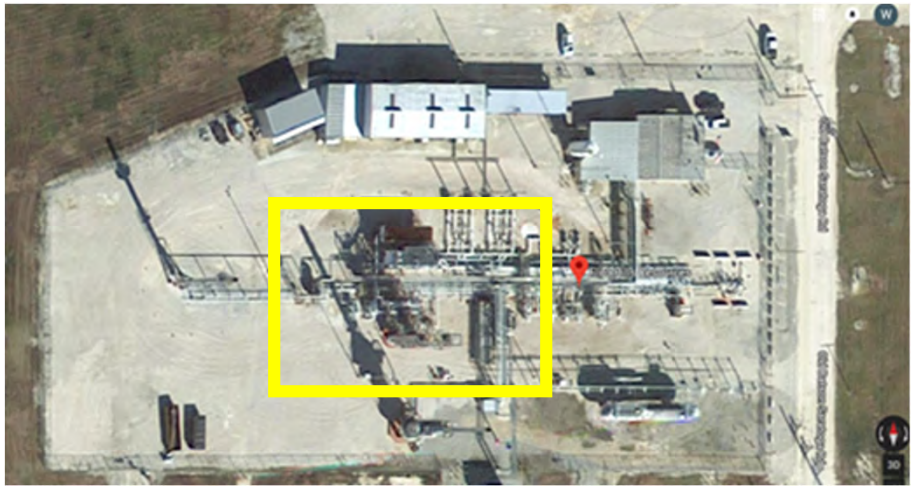

* The marked location is the designated test area.

Additional Info During Test

- Plant shut down, but 1500psi pressure of ethylene in pipes.
- Maintenance activities on and off.
- Interference from adjacent plant.
- High temp, high humidity; low wind speeds most of the time.

General Test Procedure

- Position sensors per planned layout.
- Calibrate equipment and bump test sensors.
- Place leak valve in designated location and barricade the leak area.
- Record sensor background readings.
- Release gas at a preset flow rate and record sensor readings.
- Perform Method 21 measurements.
- Stop gas flow and bag the leak point.
- Move on to the next leak location or test.

Omega Transmitter & Refitted Housing

EPA SPod Wind Sensor

Gas & Mass Flow Controllers

3/4” Valve (Leak Component)

Layout A

Note: All sensors were placed at 5’ above grade except sensors #9 at 11’ and #10 at 21’ respectively. Leak points L2,L4,L8 were 3’ above grade, the rest were 1’ above grade.

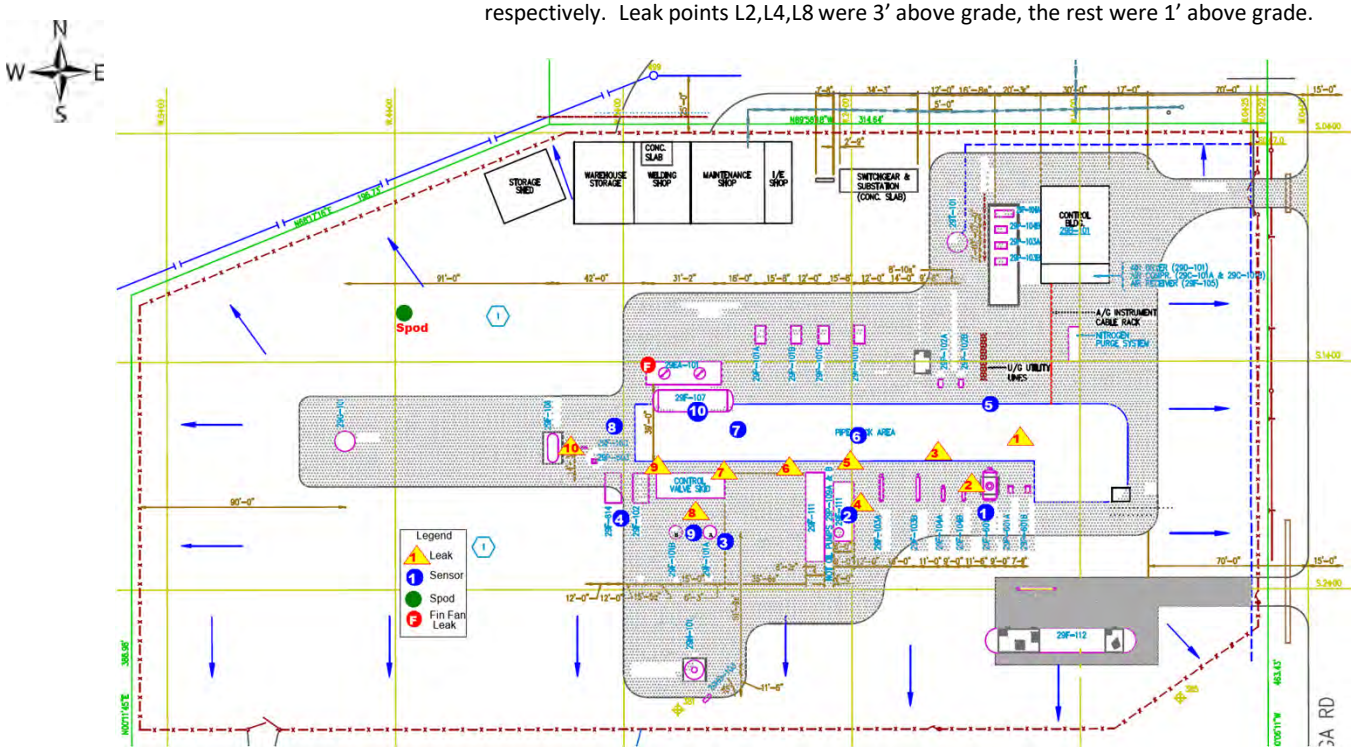

Test Matrix

Test #	Layout	Leak Location	Gas Type	Leak Rate, SCCM	Test Time, Minutes
0 (5/15)	A (1)	N/A	Background	0	120
1 (5/15)	A (1)	L1	Iso-butylene	10	30
2 (5/15)	A (1)	L2	Iso-butylene	10	30
3 (5/16)	A (1)	L3	Iso-butylene	10	30
4 (5/16)	A (1)	L4	Iso-butylene	10	30
5 (5/16)	A (1)	L5	Iso-butylene	10	30
6 (5/16)	A (1)	L6	Iso-butylene	10	30
7 (5/16)	A (1)	L7	Iso-butylene	10	30
8 (5/15, 16)	A (1)	L8	Iso-butylene	10	30
9 (5/16)	A (1)	L9	Iso-butylene	10	30
10 (5/16)	A (1)	L10	Iso-butylene	10	30
1 (5/17)	A (1)	L10	Iso-butylene	200, 0	15, 15
2 (5/17)	A (1)	L10	Iso-butylene	150, 0	15, 15
3 (5/17)	A (1)	L10	Iso-butylene	100, 0	15, 15
4 (5/17)	A (1)	L10	Iso-butylene	50, 0	15, 15
5 (5/17)	A (1)	L10	Iso-butylene	20, 0	15, 15
6 (5/17)	A (1)	L10	Iso-butylene	10, 0	15, 15
1 (5/18)	C	L11	Iso-butylene	100, 0	60, 15
2 (5/18)	C	L12	Iso-butylene	100, 0	60, 15
1 (5/21)	D	L13	Iso-butylene	30, 0	180, 15
2 (5/21)	D	L14	Iso-butylene	30, 0	90, 15
1 (5/22)	D	L14	Iso-butylene	30, 0	60, 15
2 (5/22)	D	L15	Iso-butylene	30, 0	120, 15
1(5/23)	E	L16	Ethylene	100, 0	60, 30

Layout C

Note: Same as layout A except sensor #9 was relocated and set at 5’ above grade. The leak points L11-12 were 1’ above grade.

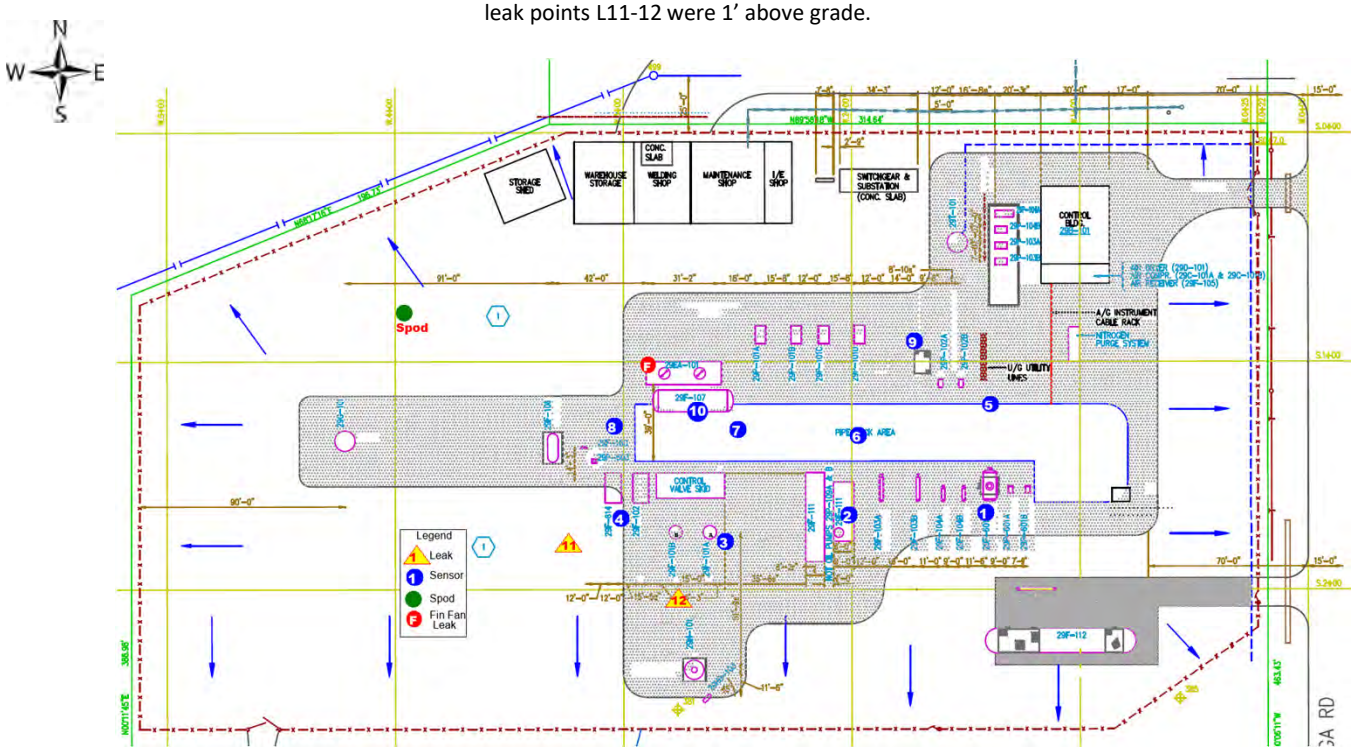

Layout D

Note: All the sensors and leak points were place at 5’ and 1’ above grade, respectively.

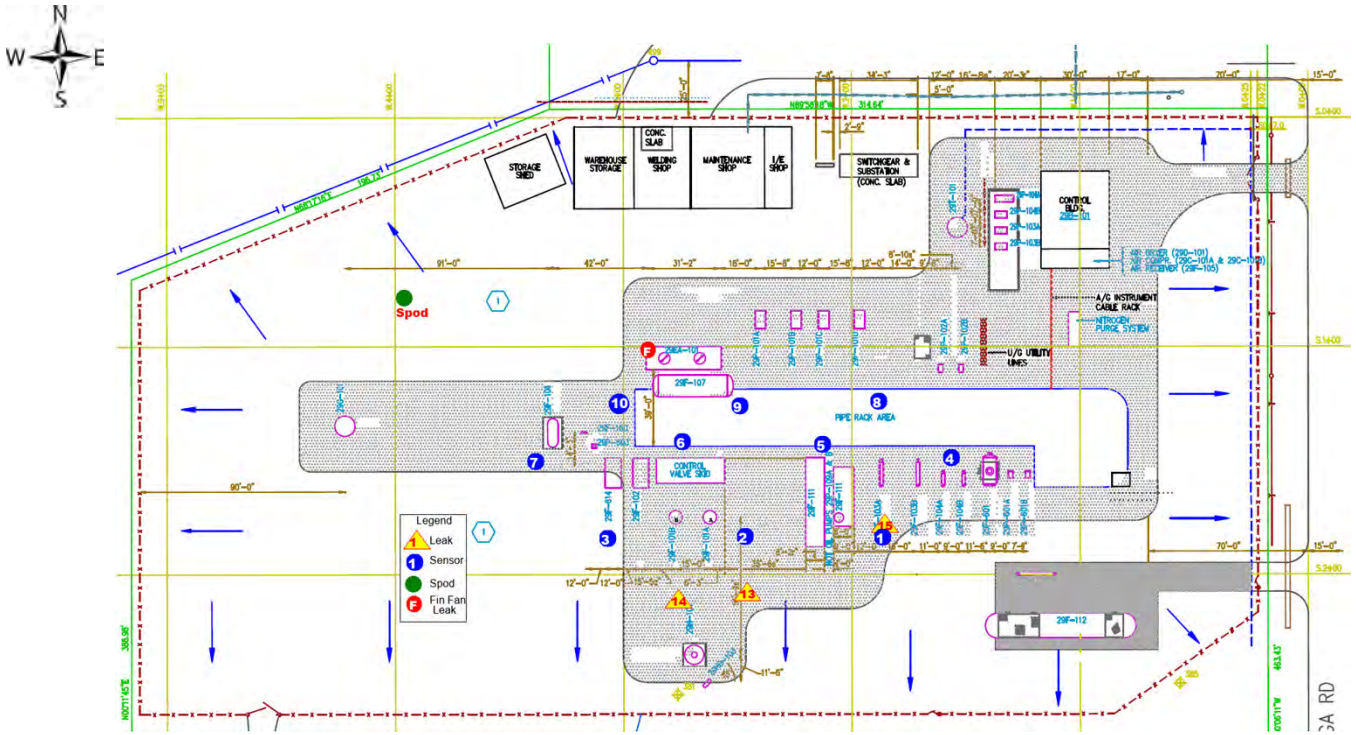

Background Test

Overnight Background Test (Layout A, 5-15-2018)

Significant detects were witnessed without controlled gas releases in the area.

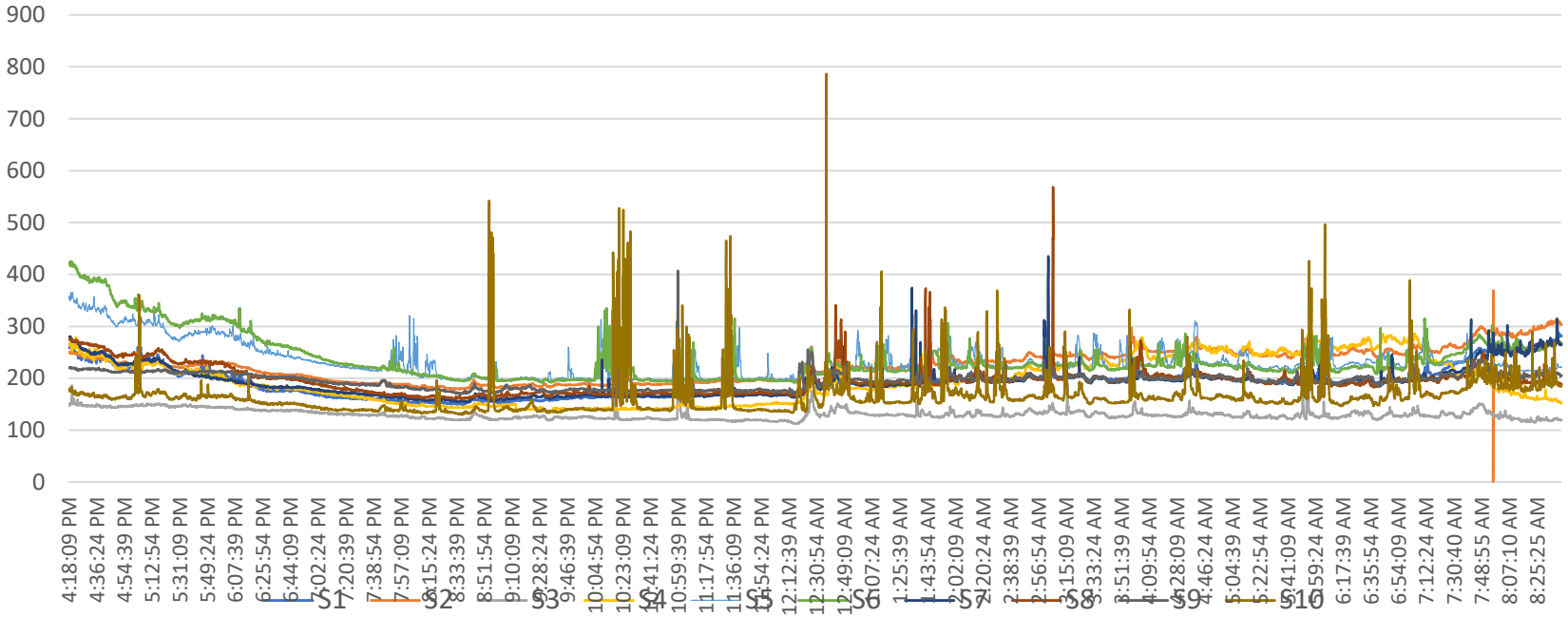

Overnight Background Test (Layout D, 5-21-2018)

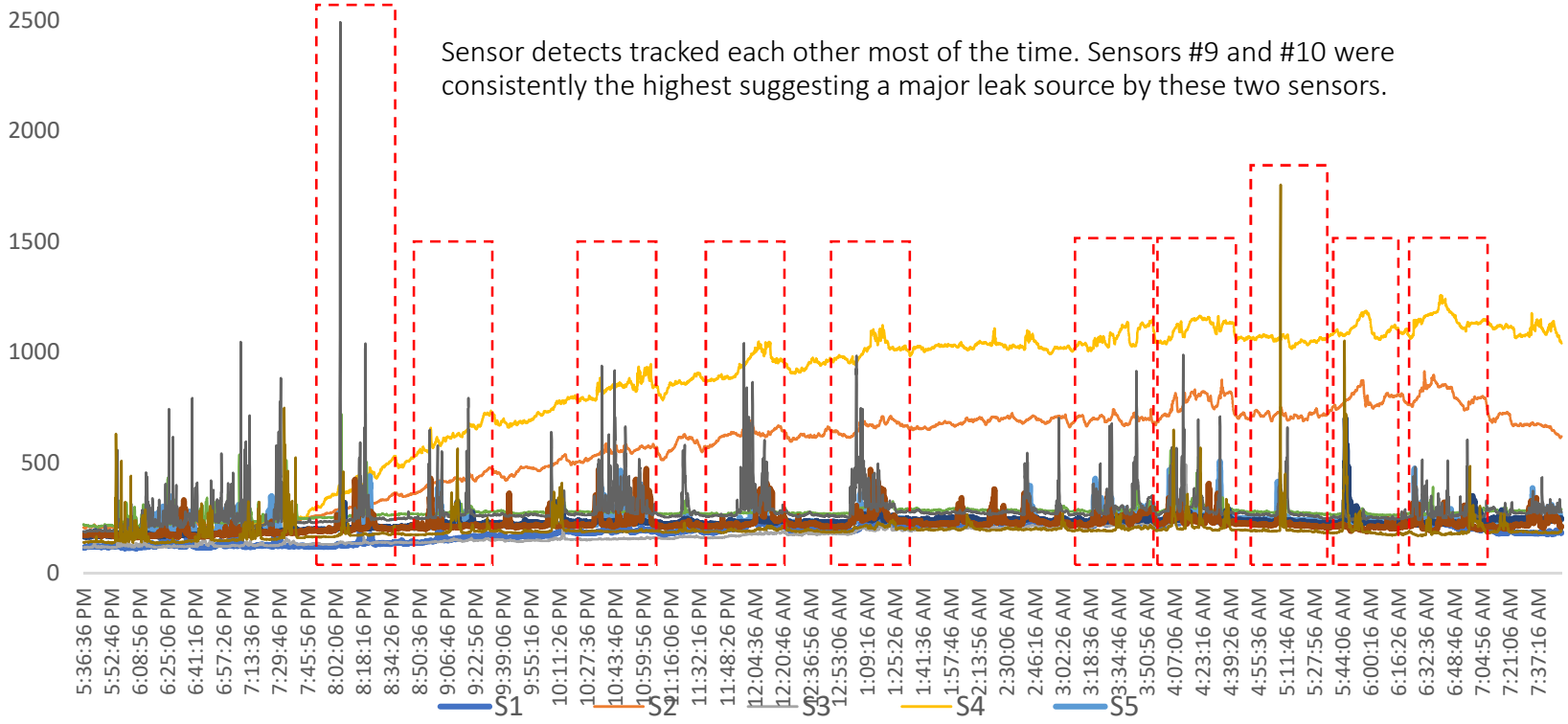

Leak Source Identification

Fin fan

Flare

Top of fin fan

Initially, we thought a flare on the west side had caused the detection signals. Upon investigation with portable devices including the TVA, we were able to pinpoint the leak source to a fin fan bank above a degassing drum.

Overnight Background Test (layout D, 5-22-2018)

A close examination of one cluster reveals that all the sensors showed detects, including sensor #1 and #4 that were 120-150ft away from the fin fan leak.

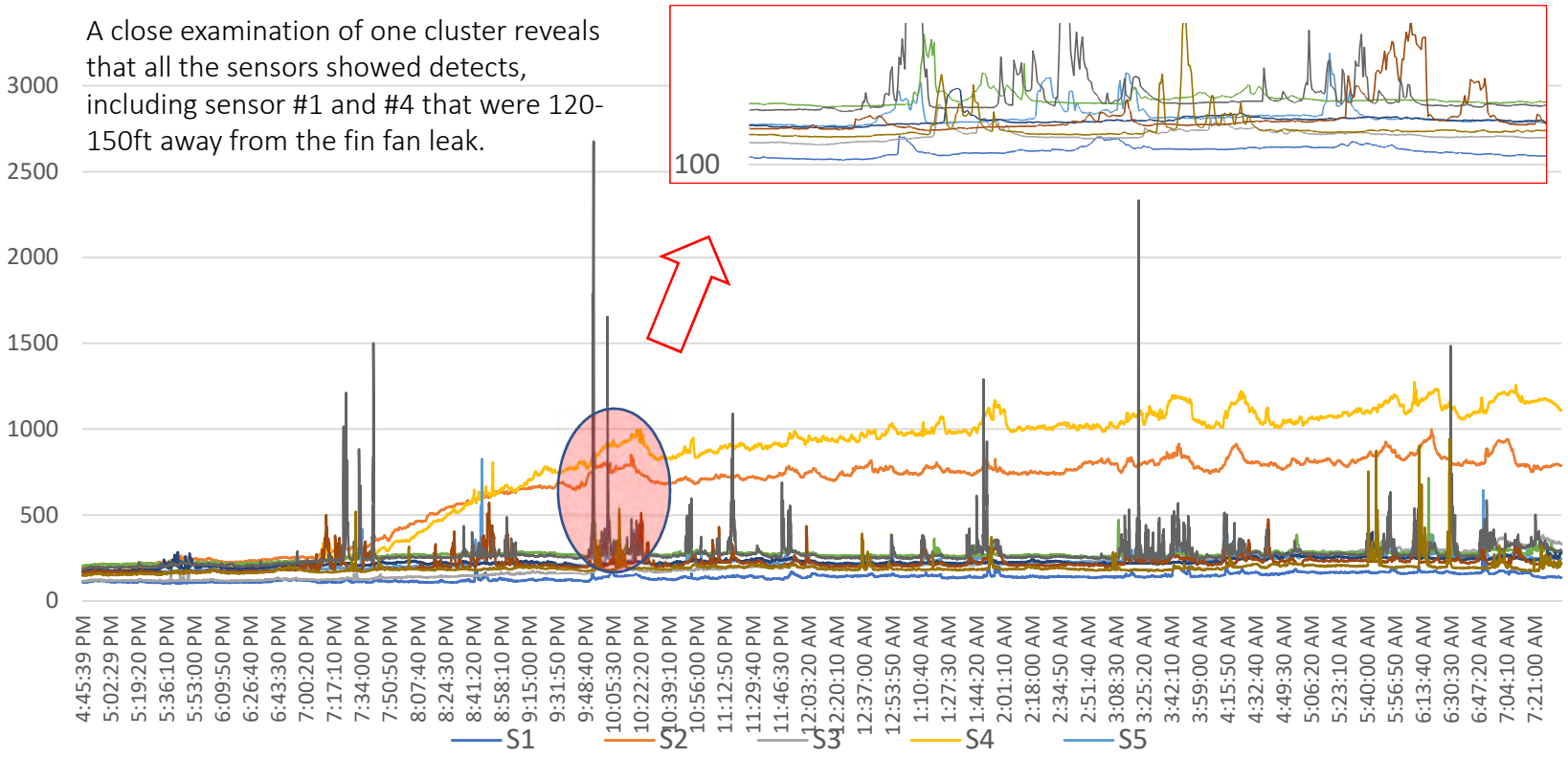

Controlled Gas Releases

30sccm Isobutylene Leak Test (Layout D, L15, 5-22-2018 Test 2)

While the fin fan leak (represented by sensors #9 and #10) continued to show up in the sensor data, we observed significant detections of sensors #4 and #8 that were not part of the fingerprints of the fin fan leak.

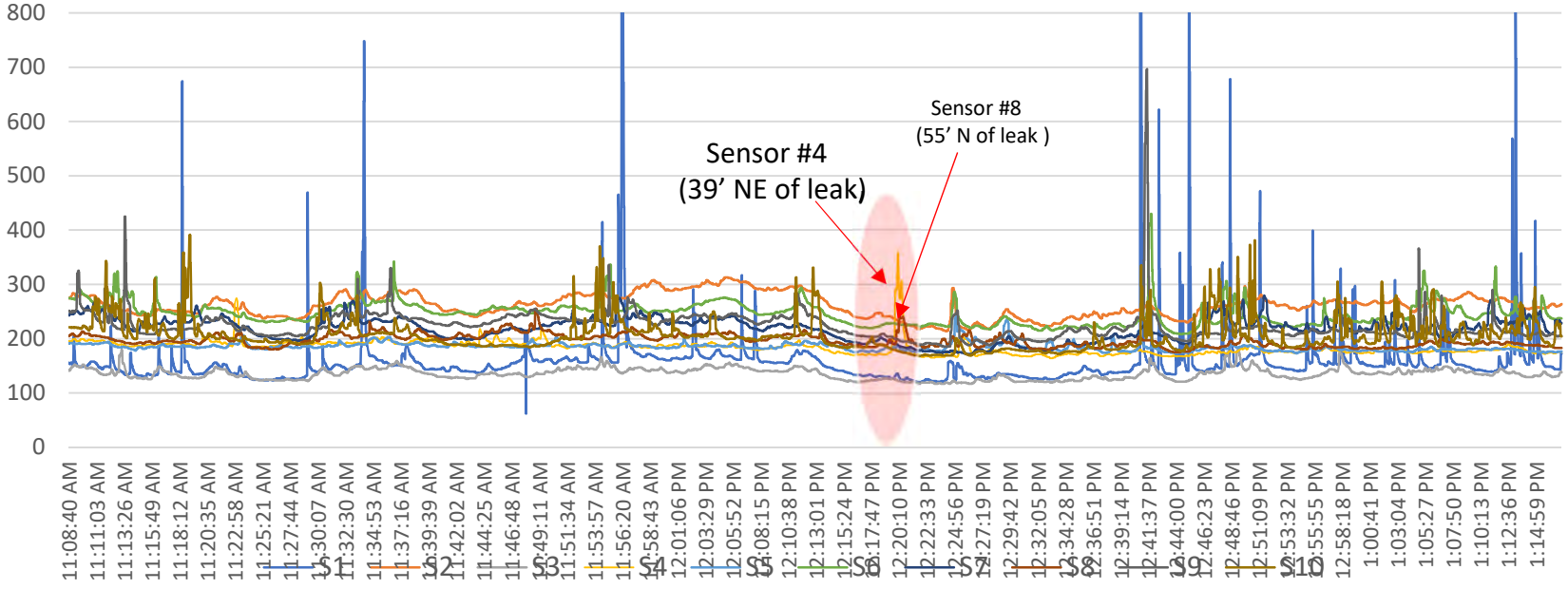

Leak Source Confirmation

The controlled release L15 was located 5’ north of sensor #1, but south of #8 and southwest of #4. Therefore, we are confident that the detection signals of sensors #4 and #8 came from this leak source.

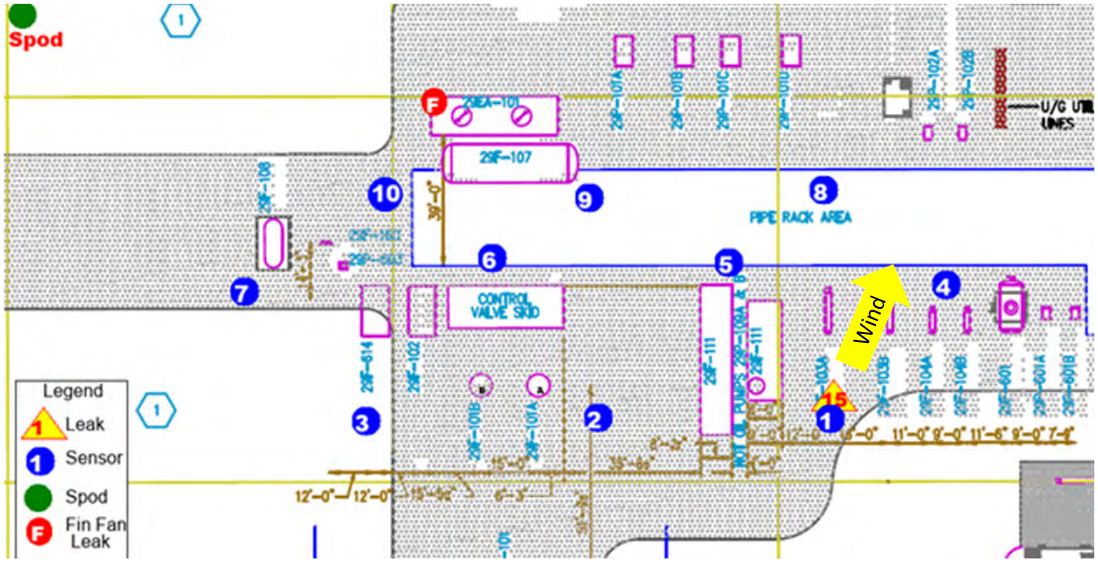

Wind Correlation

Proprietary Information has been removed from this section

Elevation

Layout E

- Test was performed in an open area upwind of the fin fan.
- Sensors were paired and placed at varying distances from a 100sccm ethylene leak at 1’ above grade.
- In each pair, sensors were set at 1’ and 5’ above grade respectively.

100sccm Ethylene Test (Layout E, L16, 5-23-2018 Test 1)

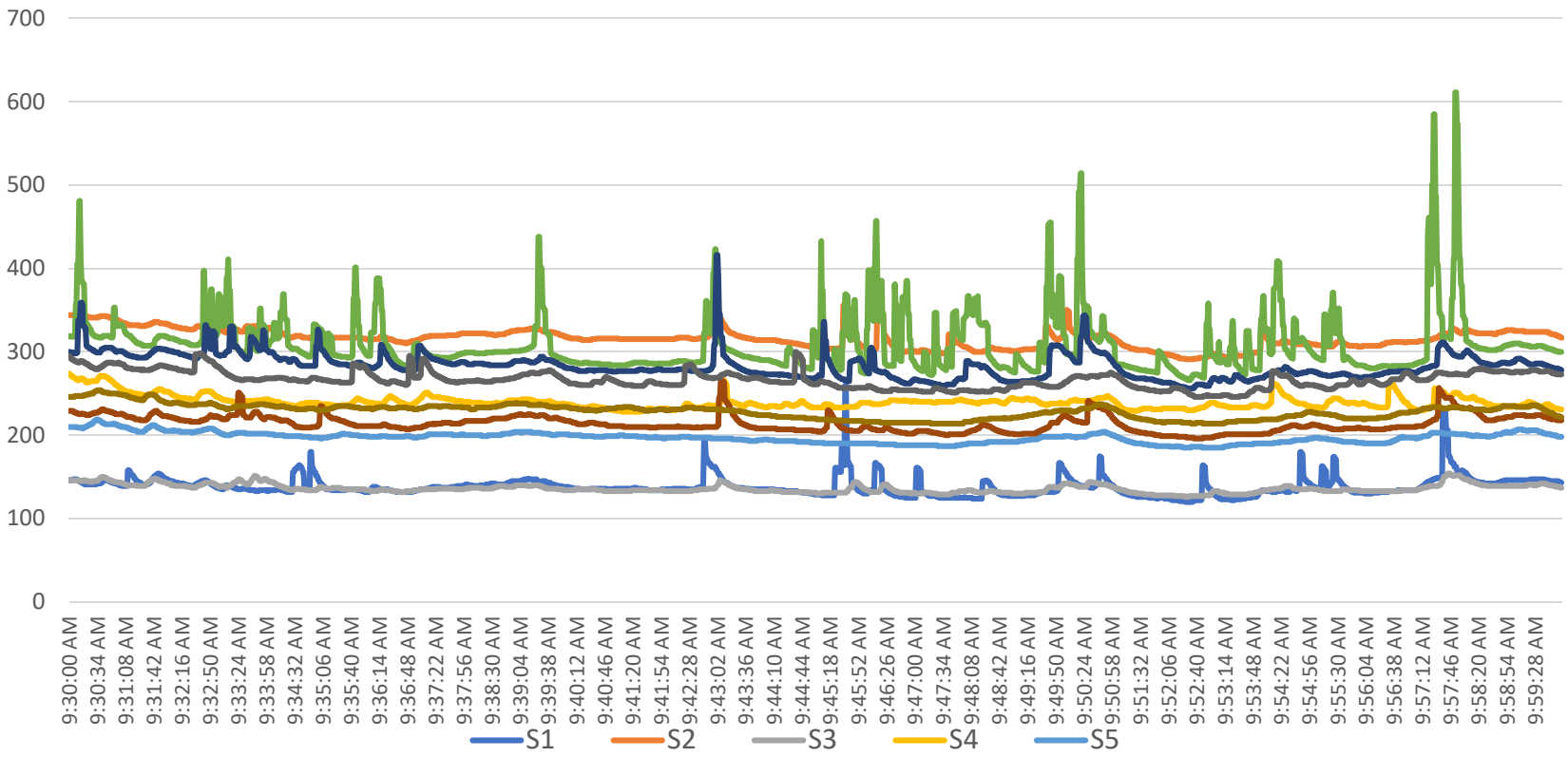

Sensors at the same elevation as the leak, i.e. 1’ above grade, appeared to have higher detection signals than those at a higher elevation (5’) within the tested distance of 34’ from the leak location. Gases heavier than ethylene are likely to follow the same rule.

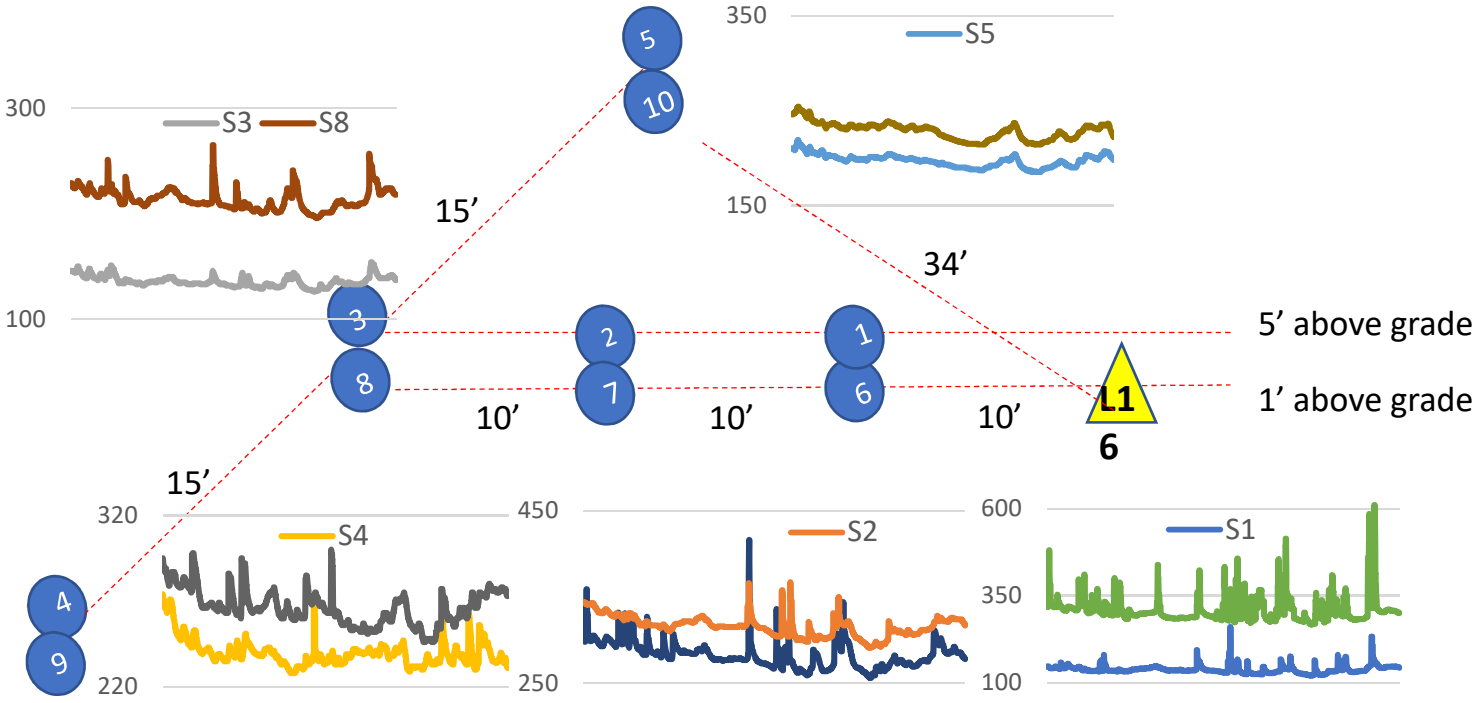

Results Summary

- Leak detectability is determined by 1) leak size, 2) sensor performance, 3) gas transport (meteorological conditions) and 4) capability of sensor collaboration in the network.
  - Test 3.1 continues to advance our understanding of elements 1 through 3 while we begin work on element 4.
  - Test 3.1 yielded positive, encouraging results supporting the area sensor concept.
- An unplanned, significant leak which was not part of Method 21 program was discovered immediately at the beginning of test 3.1 by our sensor network.
  - This leak was not detectable by OGI due to its location (fin fan).
- Overnight (extended time period) testing shows diurnal meteorological conditions that will play an important part in detection strategies.
  - Night or stable conditions appear to be more favorable for detectability.
  - Data shows that sensors placed as far as 130-150 ft away in the plant responded to the fin fan leak.
- Proven capability to decipher 30 SCCM (4.0g/hr@90F) isobutylene leaks against background emissions (fin fan leak).
- The equivalency argument for regulatory method use is developing and remains viable.

molex FLINT HILLS resources EPA United States Environmental Protection Agency ORD

Appendix B2
SLOF Test 3.2 Summary

Tests Conducted September 10, 2018 to December 7, 2018

Outline

Test Plan	Test Results	Summary
Objectives	New Leak Detection	Conclusions & Recommendations
Sensor Info	Controlled Releases	
Sensor Layout	Sensor Elevation	
Test Matrix	Sensor Performance	

Test Plan & Set-Up

Test Objectives

- Field Test Molex 1st Gen Sensor Hardware System
- Validate performance & durability of 1st Gen Sensors
- Validate MET sensors correlation to detection & leak location
- Test upload data to Molex mSyte data platform
- Continue to develop algorithms to detect and triangulate new leaks (offline)
    - Single & Multiple leak releases
    - Test for mobile vehicle emissions
    - Longer release times – (1) 24-hour test
    - Blind leak test – challenge data science model
- Capture requirements for a site assessment for sensor array configuration

Test 3.2 Layout

- Yellow pins – Sensor Locations
- Red Triangles – Leak Locations

(Sensors are about 3’ above grade)

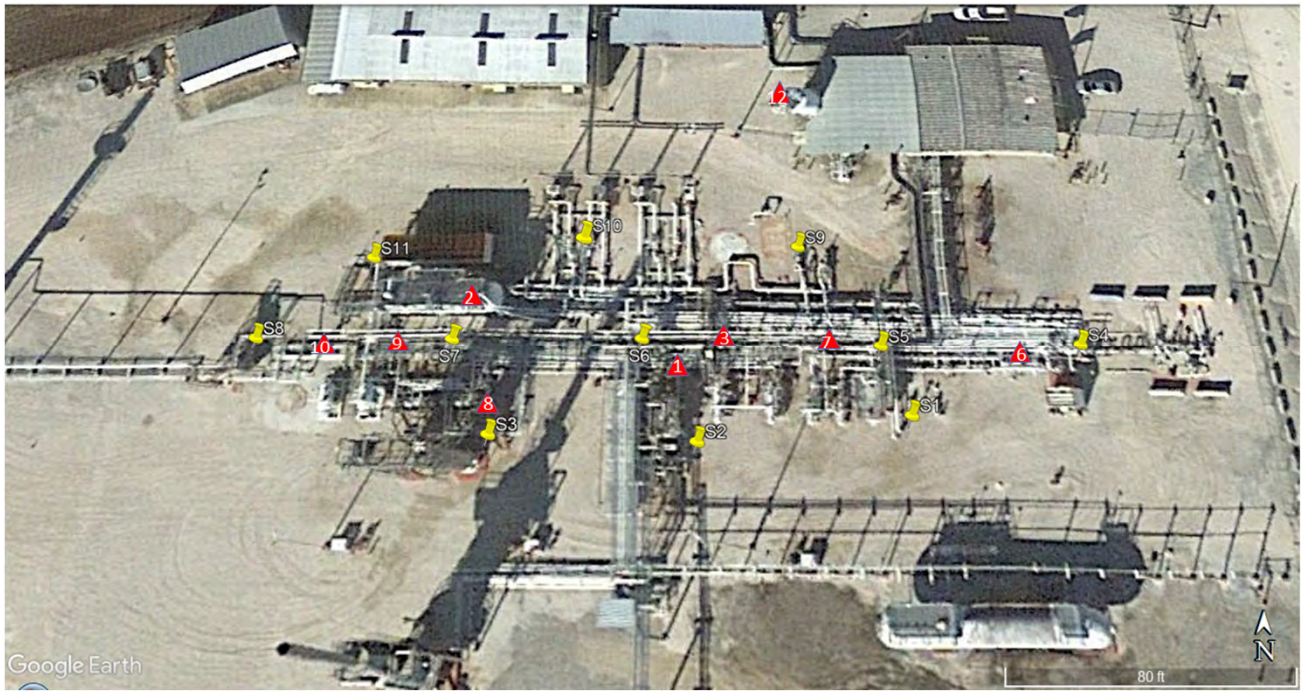

Test 3.2 Schedule

Test Name	Date	Test Focuses
Test 3.2.1	Sep 10 - Sep 21, 2018	Collected sensor performance data Collected data for algorithm development Validated new bump test method
Test 3.2.2	Oct. 15 - Oct. 19, 2018	Tested sensor durability Tested leak elevation
Test 3.2.3	Dec. 3 - Dec. 7, 2018	Tested sensor durability Investigated sensor placement vs. gas species

Test Matrix (1)

Test ID	Leak Location	Leak Elevation, ft	Gas Type	Gas Leak Rate, SCCM	Test Duration, Hr
Coverage Validation					
2-1	LL1	3	Isobutylene	50	1.5
2-2	LL2	21	Isobutylene	50	1
2-3	LL3	10	Isobutylene	50	1
2-4	LL4	4.5	Isobutylene	50	1
2-5	LL5	6	Isobutylene	50	1
Min Detect of Isobutylene					
3-1	LL1	3	Isobutylene	10	1
3-2	LL1	3	Isobutylene	20	1
3-3	LL1	3	Isobutylene	30	1
3-4	LL1	3	Isobutylene	40	1
Min Detect of Ethylene					
4-1	LL1	3	Ethylene	25	1
4-2	LL1	3	Ethylene	50	1
4-3	LL1	3	Ethylene	75	1
4-4	LL1	3	Ethylene	100	1
4-5	LL1	3	Ethylene	150	1
4-6	LL1	3	Ethylene	200	1

Test Matrix (2)

Test ID	Leak Location	Leak Elevation, ft	Gas Type	Gas Leak Rate, SCCM	Test Duration, Hr
Data for Algorithm Development					
5-1	LL6	2.5	Isobutylene	30	2
5-2	LL7	4.9	Isobutylene	30	2
5-3	LL8	3	Isobutylene	50	2
5-4	LL9	4.5	Isobutylene	30	1
5-5	LL10	4.5	Isobutylene	30	2
Extended Release Test					
6-1	LL1	3	Isobutylene	30	24
Multiple Leak Test					
7-1	LL1, LL7	3 & 4.5	Isobutylene	30, 30	2
7-2	LL3, LL8	3 & 4.5	Isobutylene	30, 50	2
Blind Test					
9-1		6	Isobutylene	30	2
9-2		3	Isobutylene	30	2
9-3		4.5	Isobutylene	30	2
9-4		3	Isobutylene	30	2
9-5		4.5	Isobutylene	50	2
Leak Elevation Test					
10-1	LL2	21	Isobutylene	50	2
Extended Release Test @ High Elevation					
11-1	LL12	23	Isobutylene	50	24

Test Matrix (3)

Test ID	Leak Location	Leak Elevation, ft	Gas Type	Gas Leak Rate, SCCM	Test Duration, Hr
Data for Algorithm Development					
12-1	LL7	4.75	Isobutylene	50	1
12-2	LL8	3	Isobutylene	50	2
12-3	LL10	4.5	Isobutylene	50	2
Blind Test					
13-1		10	Isobutylene	30	2
13-2		5	Isobutylene	30	2
13-3		5	Isobutylene	20	2
13-4		5	Isobutylene	30	2
Response Factor Test					
14-1	LL7	4.75	Isobutylene	30	2
14-3	LL7	4.75	Ethylene	150	2
14-6	LL7	4.75	Ethylene	300	1
14-7	LL7	4.75	Ethylene	300	2
14-8	LL7	4.75	iso-butylene	30	2
17-1	LL5	6	Ethylene	500	1
17-2	LL5	6	Ethylene	250	1
17-3	LL5	6	Ethylene	100	1
Leak Elevation Test					
16-1	LL12	23	Isobutylene	50	4.5
16-2	LL12	23	Isobutylene	100	2.5
16-3	LL3	10	Isobutylene	50	7

Sensors and Equipment

- 1st generation of Molex wireless sensors
- 1st version of Molex's mSyte software platform

Molex Sensor Transmitter

Gateway Computer

Meteorological Station

Controlled Gas Release Set-Up

- Controlled gas release testing was done the same way as in Test 3.1.
- Isobutylene or Ethylene was used as the test gas.
- Each gas release was quantified and recorded with EPA Method 21.

Gas and Mass Flow controllers

4” Valve as Leak Component

Method 21 Measurement

Test Observers

- Eben Thoma (EPA ORD CRADA PI) and Jason Dewees from the EPA discussed sensors and investigate the fin fan leak. Mike Miller, EPA R6 conducted a QA audit.

- Beth Akers, Xuan Zhao, and Emily Johnson from TCEQ watched sensor validation tests.

- Lucinda Legel dropped in to provide guidance.

New Leak Detection

Proprietary Information has been removed from this section

New Leak Detection in September

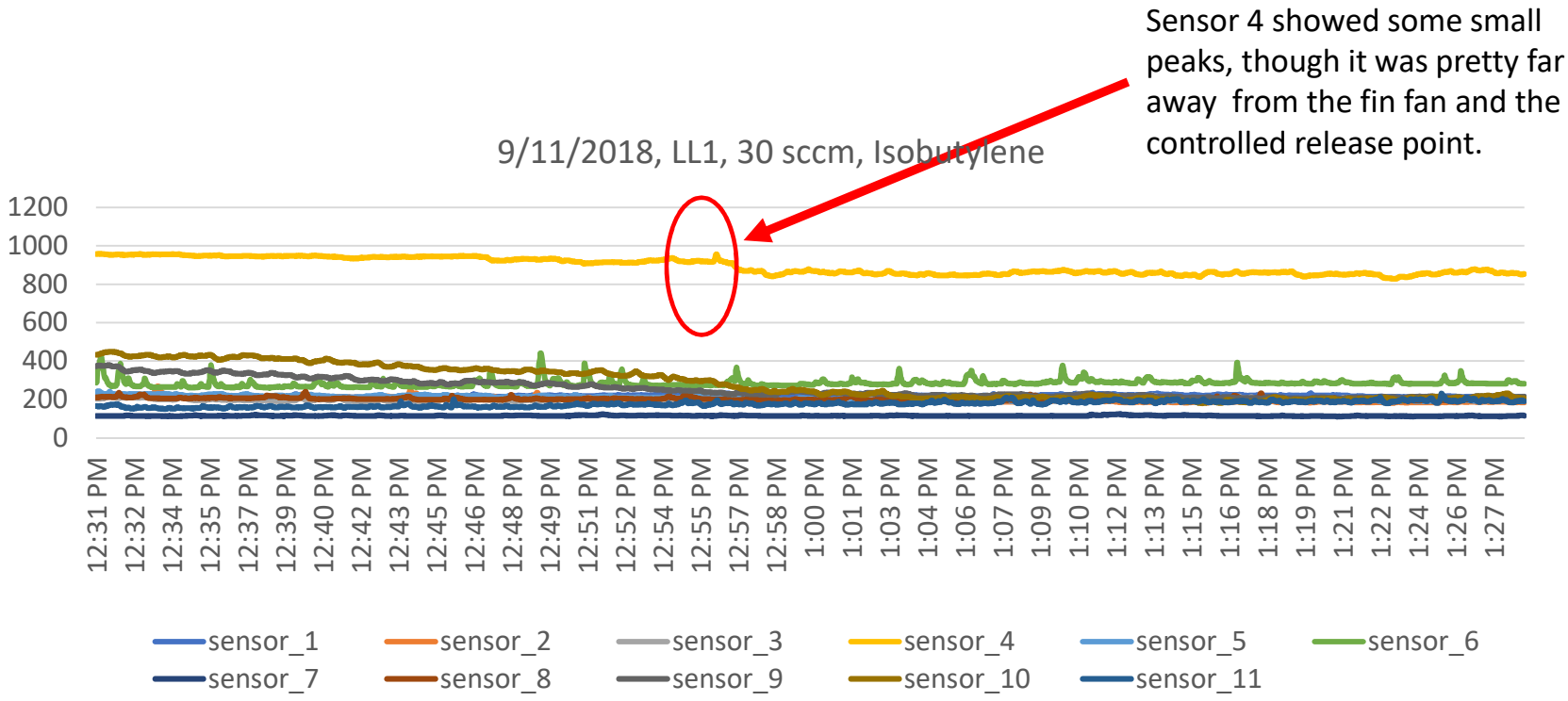

Valve Bonnet Leak Found

- Portable PID and AVO led us to a 6” valve (LDAR tag #18542) between S1 and S4.
- Leak was found within 5-10 min.
- TVA = 60,000ppm. OGI difficult.

View from S1 back to valve leak (~40’)

New Leak Detection in October

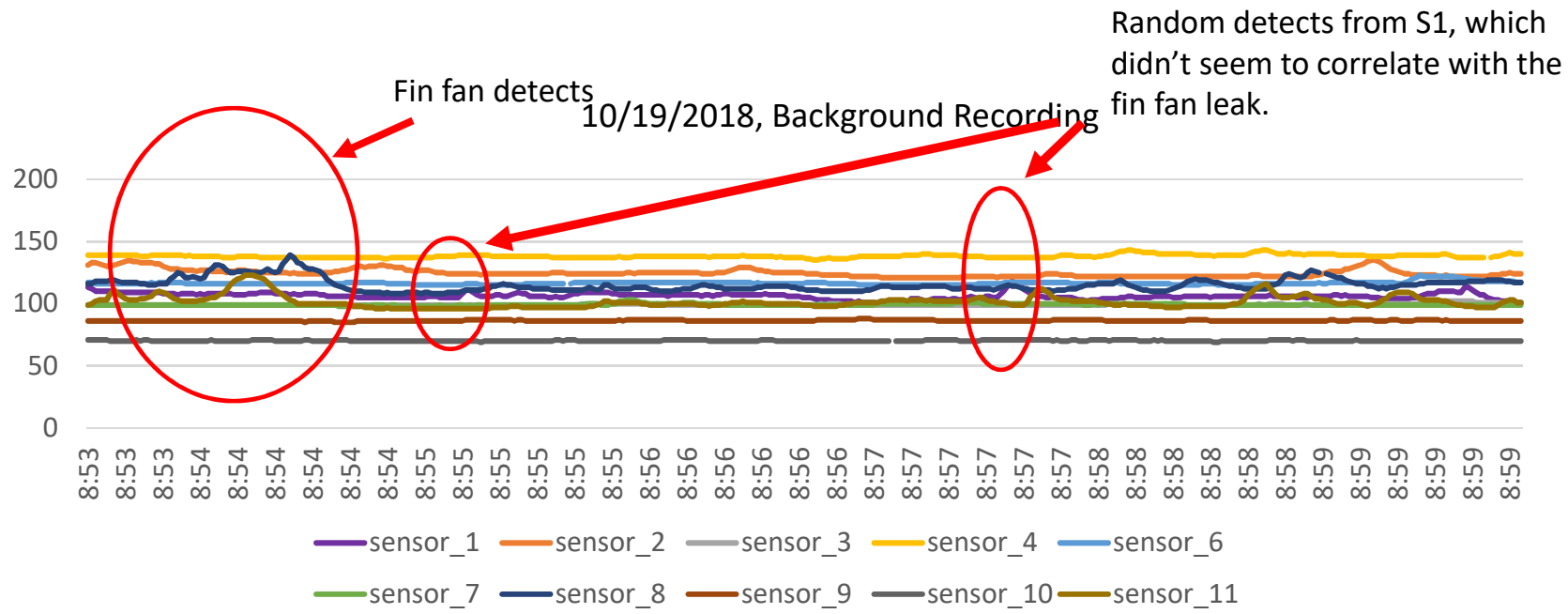

Valve Plug Leak Found

- Within 5-10 min, we were able to narrow down the leak location via AVO and a portable PID (PID>100ppm).
- TVA flame-out; IR Camera recorded a plume from a vent hole in the valve plug.

Controlled Releases & Triangulation

Proprietary Information has been removed from this section

Wind data comparison of all wind sensors

- All 5 wind sensors showed consistent wind patterns.
- The “A” Met station would be the best location to represent the wind condition of the Sour Lake Facility.

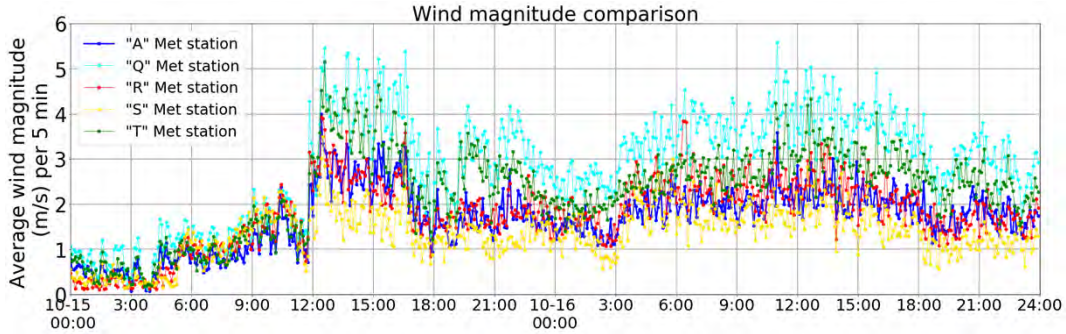

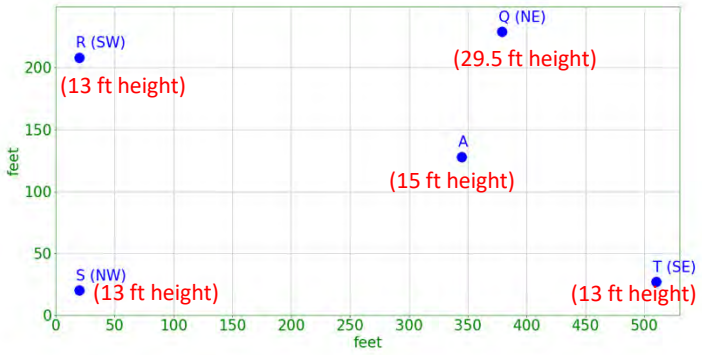

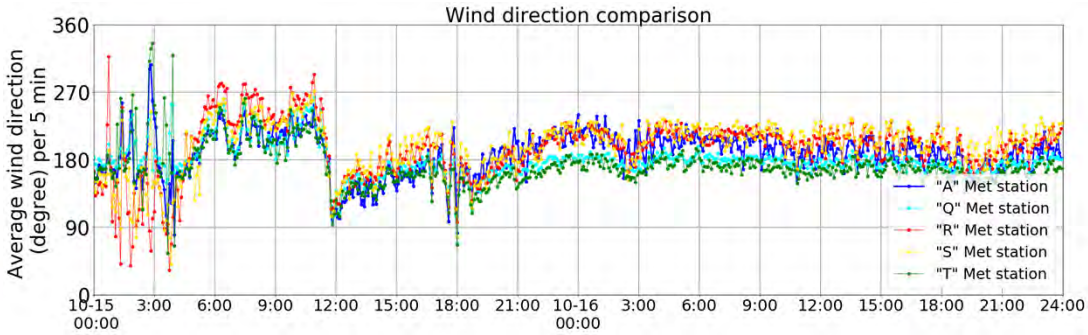

Data source : 2018/10/15 00:00 - 2018/10/17 00:00

Wind vs. Temperature

In general, low temperature, low wind speeds, and more diverse wind directions were seen during night times.

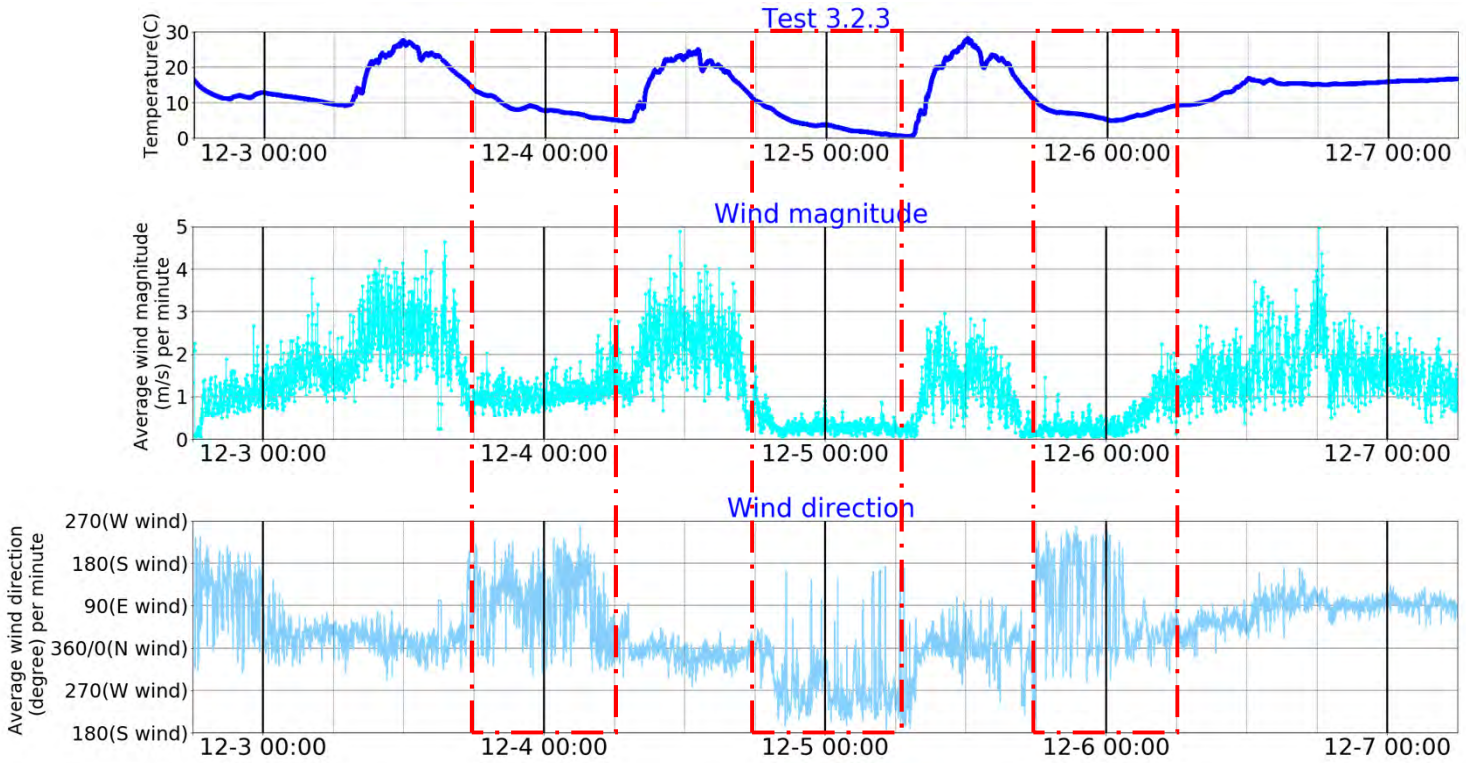

Data source : 2018/12/2 18:00 - 2018/12/7 06:00

Leak Location Approximation

- Molex's algorithm of leak location approximation has successfully triangulated a fin fan leak , a valve leak as well as a controlled release leak of 30 sccm Isobutylene marked as "LL1".

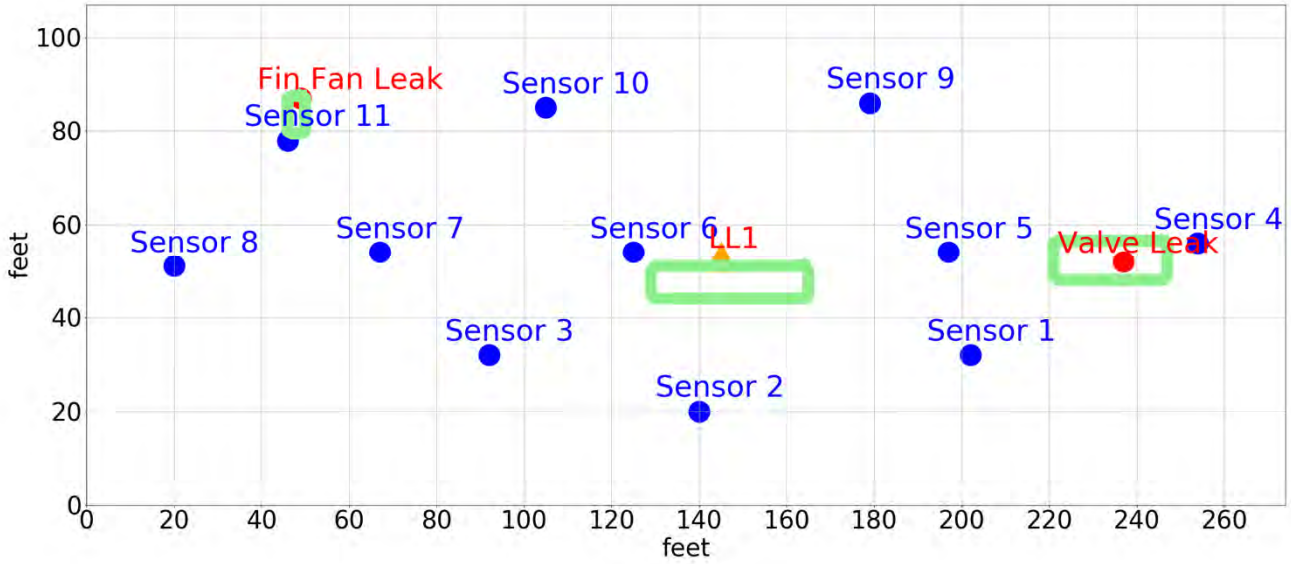

: Possible leak area

Data source : 2018/9/19 9:30 - 2018/9/19 12:00

Elevation Study

Proprietary Information has been removed from this section

Leak @ 23’ Elevation

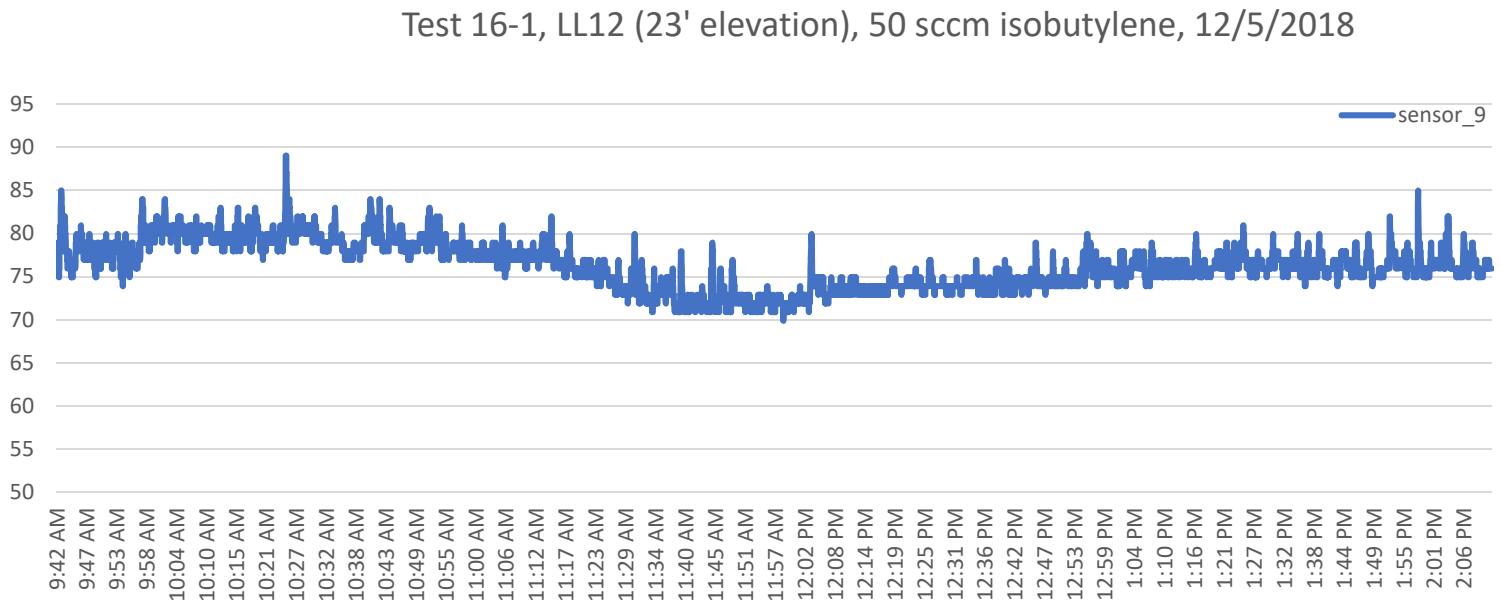

- Multiple detections were seen from Sensor #9 which was 62' from the leak and 2.5’ above grade.

Gas Plumes of Different Leaks

- Light molecules tend to go up, heavy molecules tend to go down in the air.
- The molecular weight effect decreases with increasing wind speed.

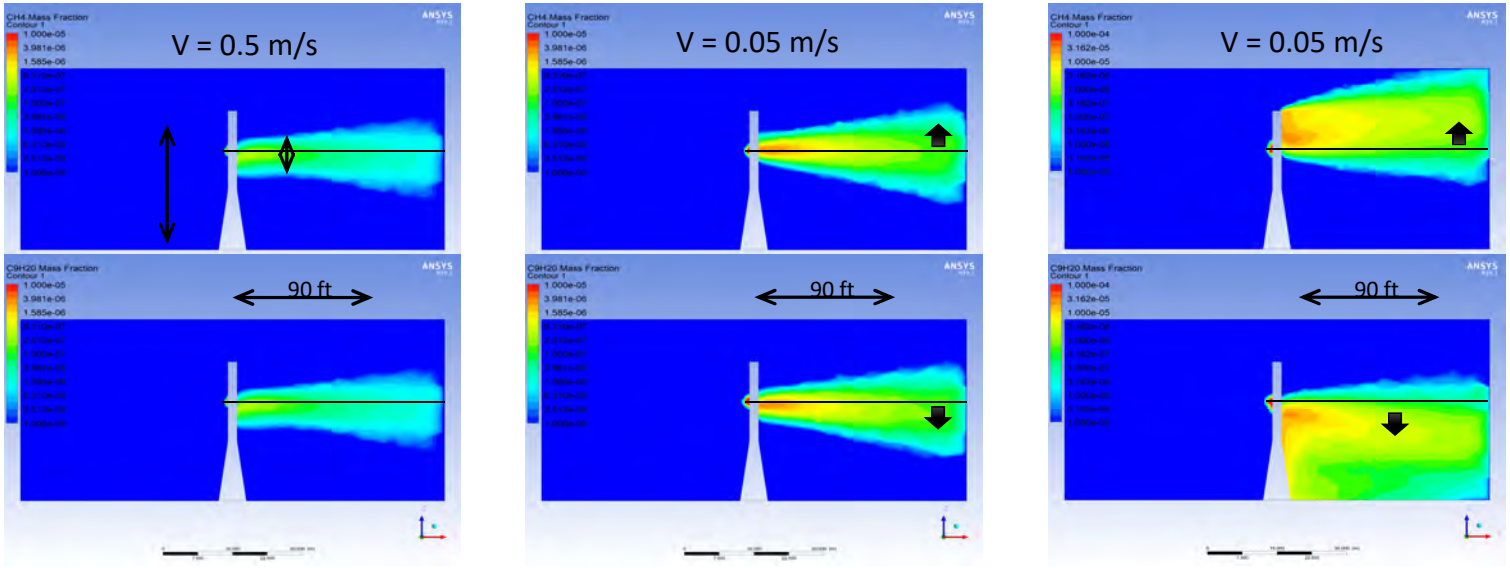

Leak size = 3.6 g/hour

Leak size = 36 g/hour (×10)

Sensor Performance

Proprietary Information has been removed from this section

Bump Test Data

Date	Sensor 1	Sensor 2	Sensor 3	Sensor 4	Sensor 5	Sensor 6	Sensor 7	Sensor 8	Sensor 9	Sensor 10	Sensor 11
9/10/2018	316	286	242	225	296	448	280	225	211	259	398
9/11/2018	259	256	259	257	268	321	230	275	369	301	270
9/12/2018	275	203	269	209	275	354	233	258	314	156	272
9/13/2018	301	307	342	236	344	372	317	316	329	271	299
9/14/2018	268	286	314	191	307	325	278	266	314	254	285
9/17/2018	273	158	310	213	283	318	280	289	289	206	275
9/18/2018	280	326	311	218	279	324	287	288	309	222	284
9/19/2018	274	280	306	199		312	282	281	300	234	266
9/20/2018	200	223	242	164		265	220	235	243	208	247
9/21/2018	197	227	243	208		242	221	229	240	221	223
10/15/2018	236	253	261		275*	268	237		237	207	222
10/16/2018	253	234	275	181	294	293	261	251	261	243	212
10/17/2018	265	138	280	83	144	288	267	241	267	227	191
10/18/2018	276	289	282	203	311	328	285	284	285	274	267
10/19/2018	271	282	290	181	296	316	279	276	279		260
12/3/2018	260	259	269	210	259	313	257	259	254	260	230
12/4/2018	155	155	166	139	157	192	159	238	155	163	194
12/5/2018	130	161	167	143	159	203	161	230	159	166	204
12/6/2018	102	155	148	131	160	192	154	242	138	158	207
12/7/2018	125	138	156	74	132	150	147	213	128	136	197

* Sensor was replaced due to an issue with wireless communication.

Sensor Stability over 3 Months

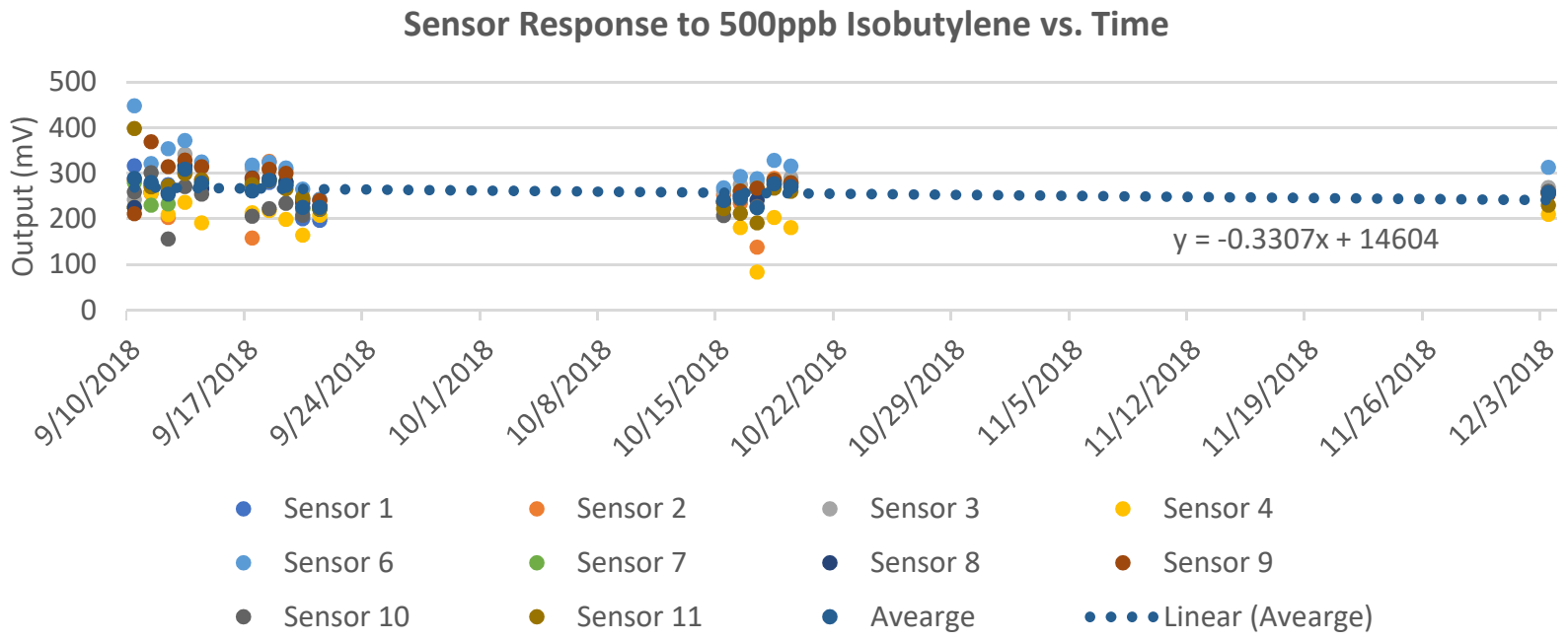

Summary & Recommendations

Proprietary Information has been removed from this section

Summary of Findings and Progress

- ✓ Found two large component leaks between LDAR cycles at SLOF. Through exercises, we developed a preliminary leak-search process involving a portable PID and Method 21 instruments, that allows us to quickly narrow down, pin-point, and validate the leak source.
- ✓ Sensor density determines sensor sensitivity and time to detect large leaks, and the ability to differentiate new leaks from authorized emission sources. The sensor detection signal is a function of leak size, distance and the gas type under similar wind conditions.
- ✓ Developed and validated software algorithms for leak location approximation. Operating offline, Molex's model has successfully triangulated a valve bonnet leak, a valve plug leak, and the fin fan leak, as well as several controlled gas releases in SLOF.
- ✓ Bump test results were fairly consistent, with an average change of -12% in sensor sensitivity over 3 months suggesting excellent stability of sensors in the field.

molex FLINT HILLS resources EPA United States Environmental Protection Agency ORD

Appendix C: FHR CC Tests

Appendix C consists of three sets of figures and tables summarizing select aspects of the FHR CC pilot tests conducted in 2019. Appendix C1 (pages C2 to C13) presents the sensor node layout planning for the Mid-Crude and m-Xylene process units. Appendix C2 (pages C14 to C48) provides summary tables of LDSN/DRF information and figures illustrating the potential source location (PSL) boxes determined by mSyte™, along with M21 screening values (SVs) determined under the DRF. Appendix C3 (pages C49 to C59) presents an updated version of the sensor locations that will be used in the process units on an ongoing basis. In the case of Mid-Crude, this includes six additional sensors that improve leak detection coverage based on pilot test results (described in report).

The following was originally developed as part of internal CRADA team communications and has been modified in places to remove proprietary information and to improve clarity for use in this report. This appendix does not intend to capture all efforts performed in these tests but provides the reader with a sense of the type of work accomplished.

Appendix C1
LDSN Node Layouts for FHR CC Tests

Tests Conducted May 1, 2019 to November 30, 2019 (m-Xylene unit)
and July 1, 2019 to November 30, 2019 (Mid-Crude Unit)

FHR CC Mid-Crude Process Unit (Level 1)

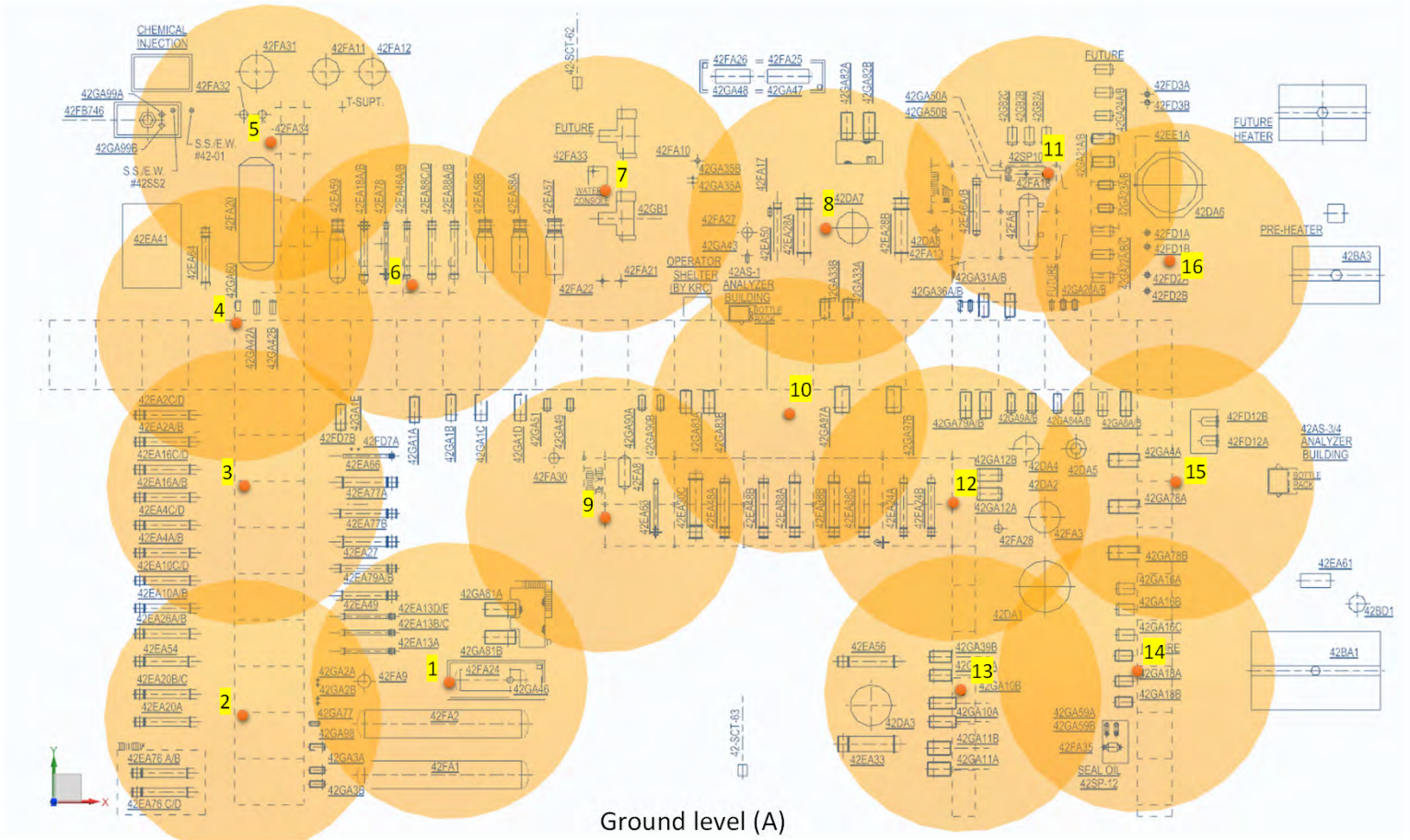

Figure C1-1. Mid-Crude sensor locations (ground level, level 1). The sensor nodes are represented by the red dots and are sequentially numbered for each process unit. The colored circles surrounding each sensor node indicates a 60 ft radius and represents an approximate detection coverage by individual LDSN nodes for an RF = 1 gas. These are the approximate node locations during the 2019 pilot test and do not reflect the any additional nodes added after the pilot test (described in report).

FHR CC Mid-Crude Process Unit (Level 2)

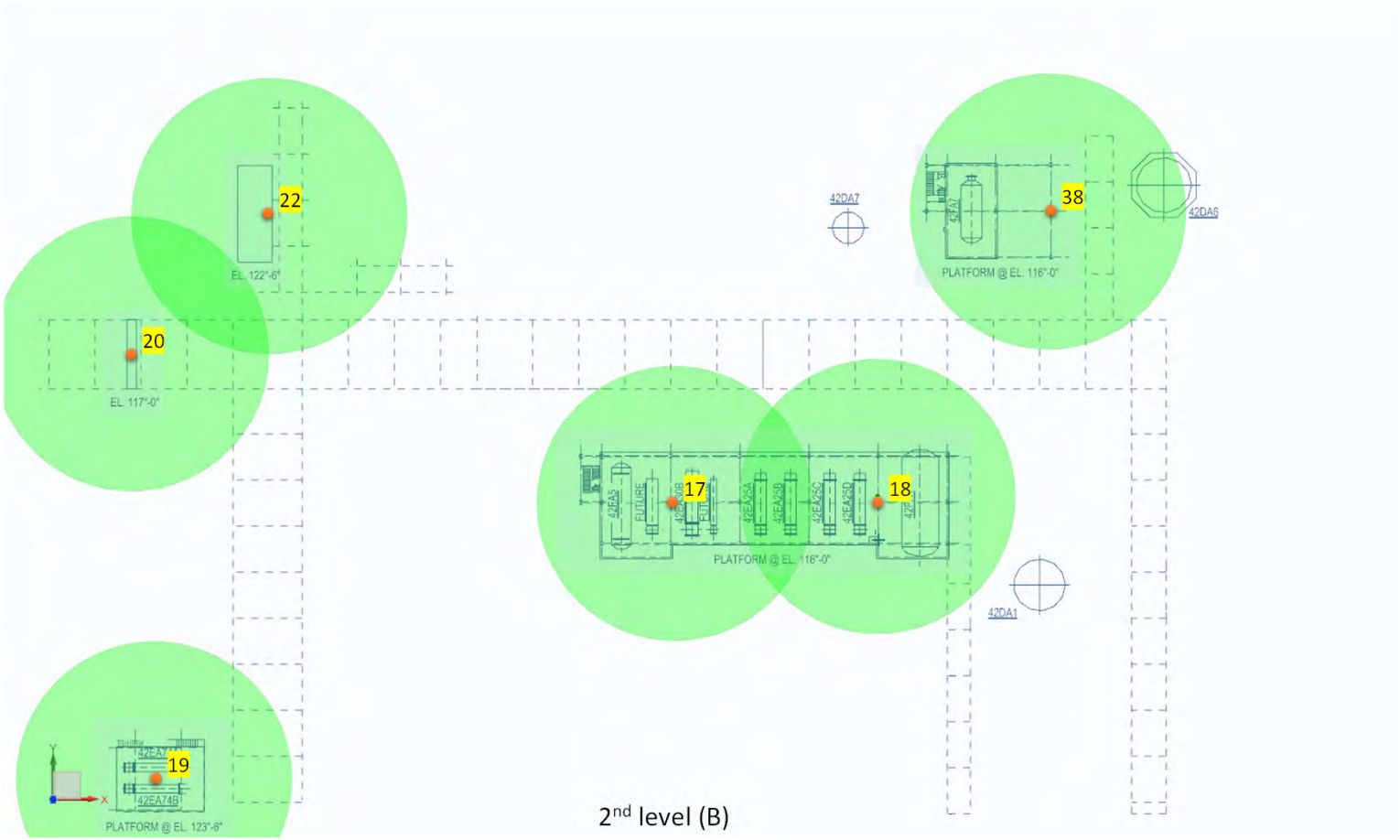

Figure C1-2. Mid-Crude sensor locations (level 2). These are the node location during testing and do not reflect the additional nodes added after the pilot test.

FHR CC Mid-Crude Process Unit (Level 3)

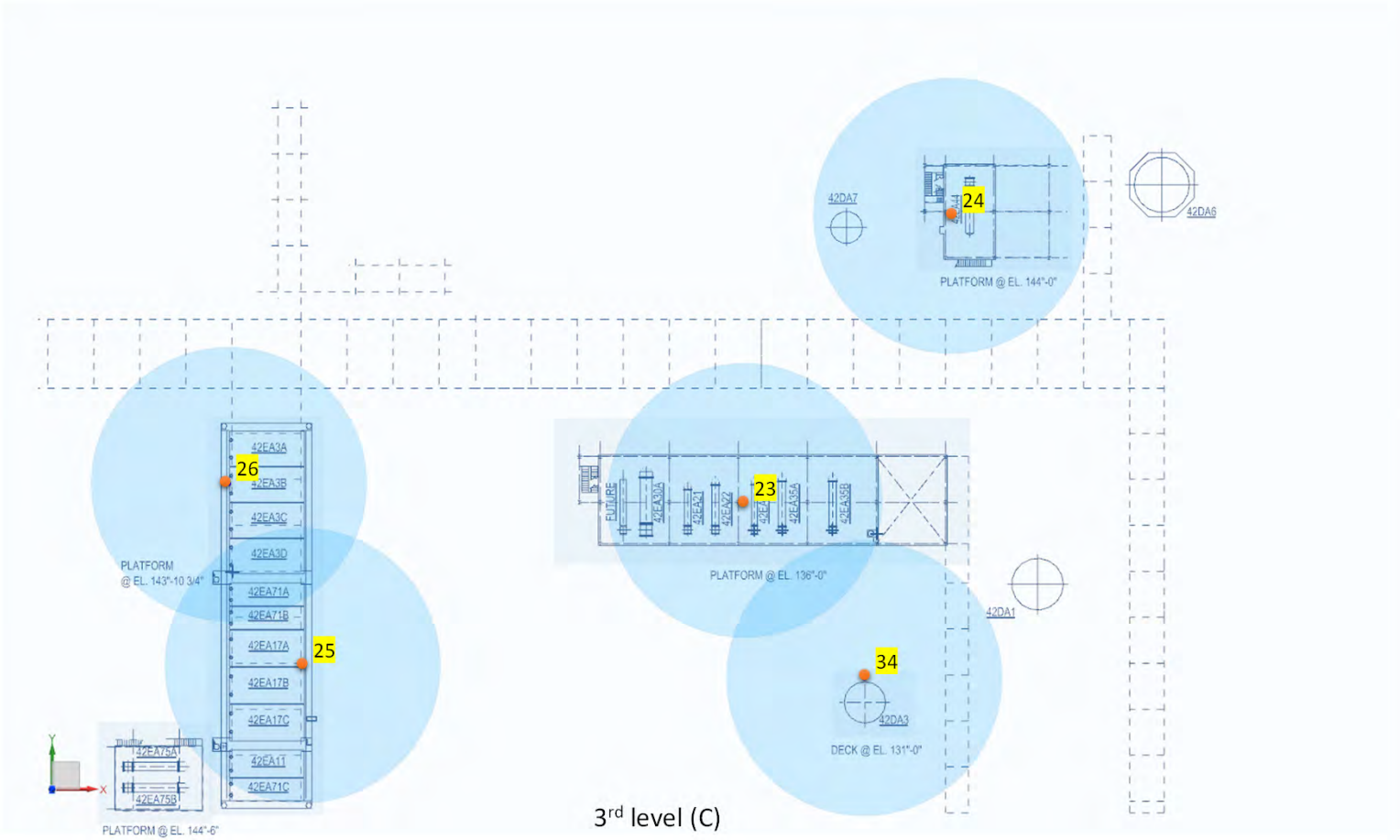

Figure C1-3. Mid-Crude sensor locations (level 3). These are the node location during testing and do not reflect the additional nodes added after the pilot test.

FHR CC Mid-Crude Process Unit (Level 4)

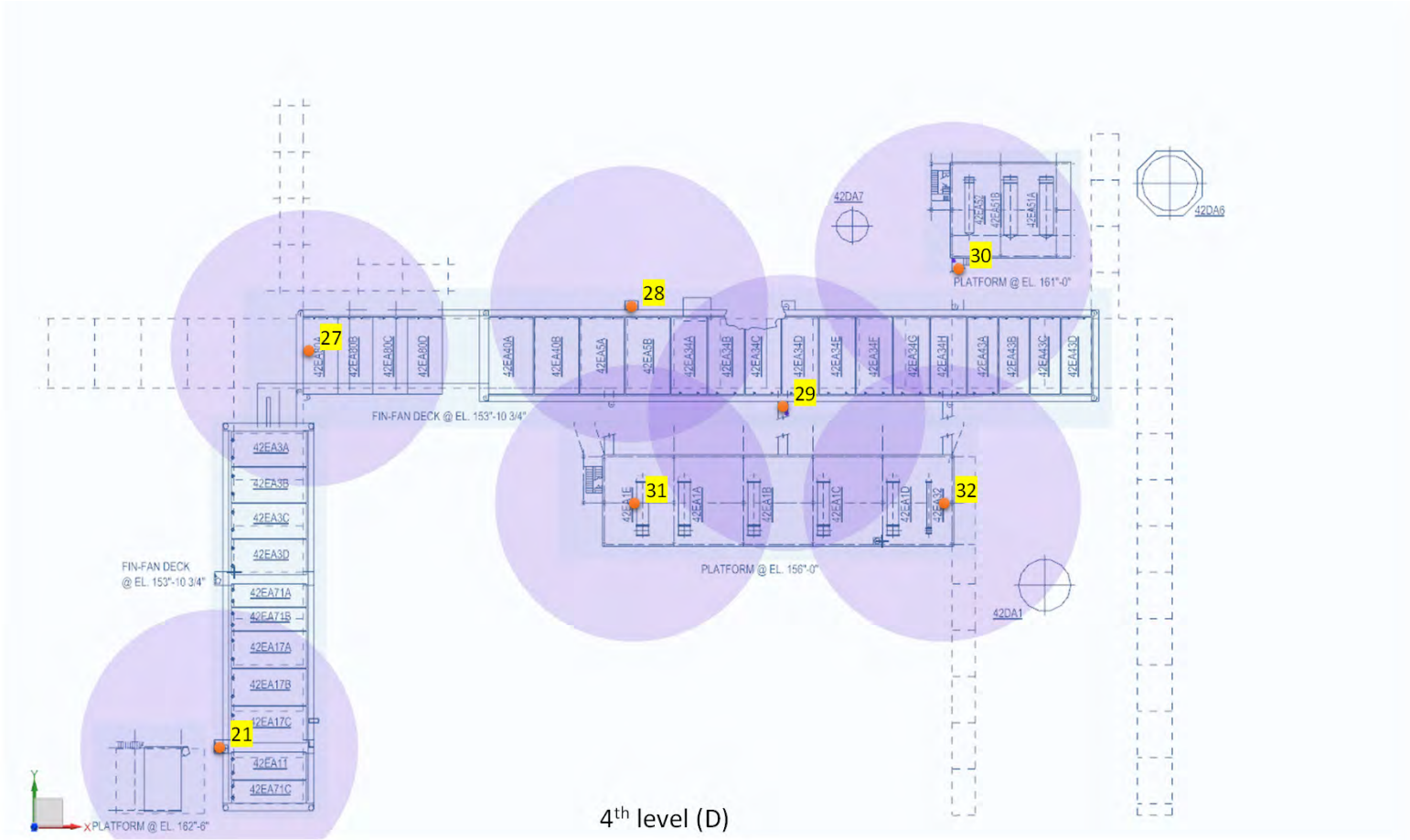

Figure C1-4. Mid-Crude sensor locations (level 4). These are the node location during testing and do not reflect the additional nodes added after the pilot test.

FHR CC Mid-Crude Process Unit (Level 5)

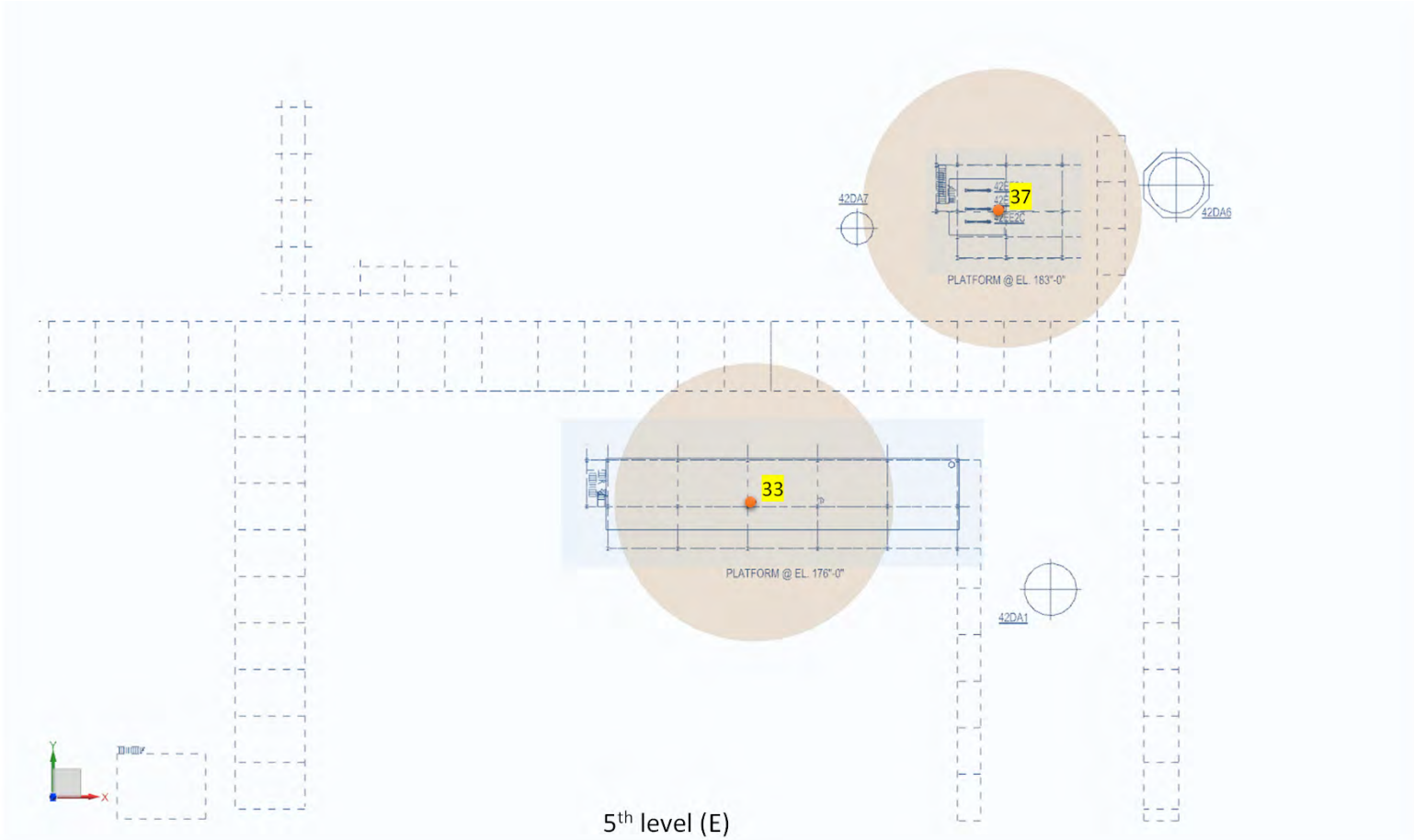

Figure C1-5. Mid-Crude sensor locations (level 5). These are the node location during testing and do not reflect the additional nodes added after the pilot test.

FHR CC Mid-Crude Process Unit (Level 6)

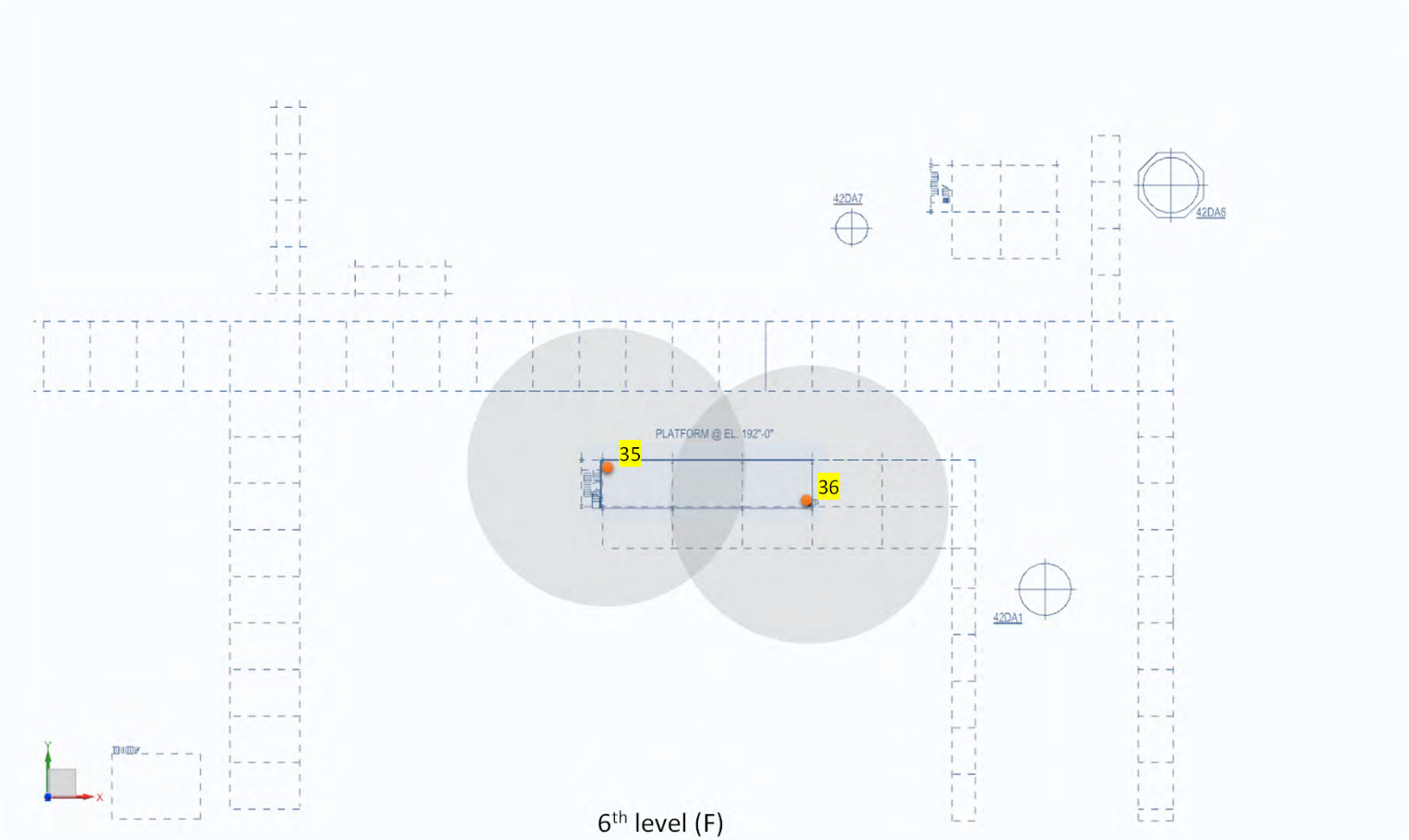

Figure C1-6. Mid-Crude sensor locations (level 6). These are the node location during testing and do not reflect the additional nodes added after the pilot test.

FHR CC Mid-Crude Process Unit - All Levels

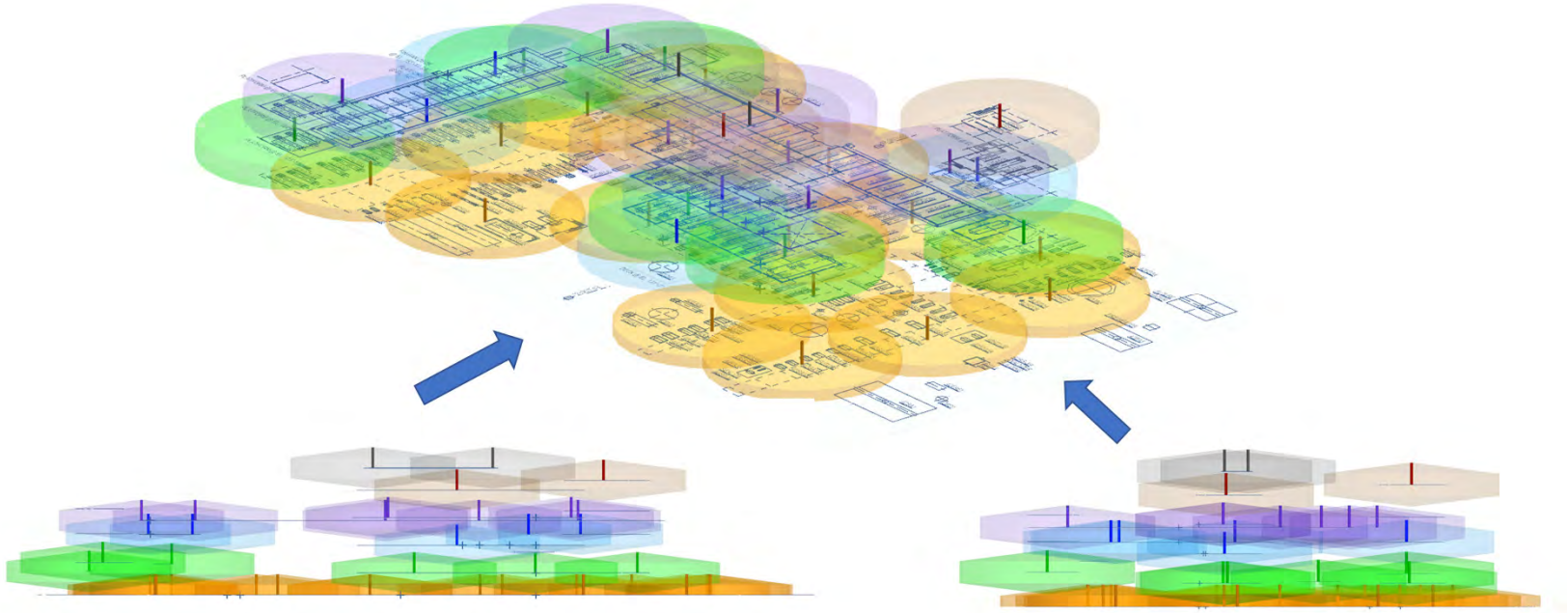

Figure C1-7. Three dimensional representation of the LDSN nodes on different elevations within Mid-Crude unit reflected in Figures C1-1 trough C1-6. The colors represent different elevations within the process unit. These are the node location during testing and do not reflect the additional nodes added after the pilot test.

FHR CC m-Xylene Process Unit (Level 1)

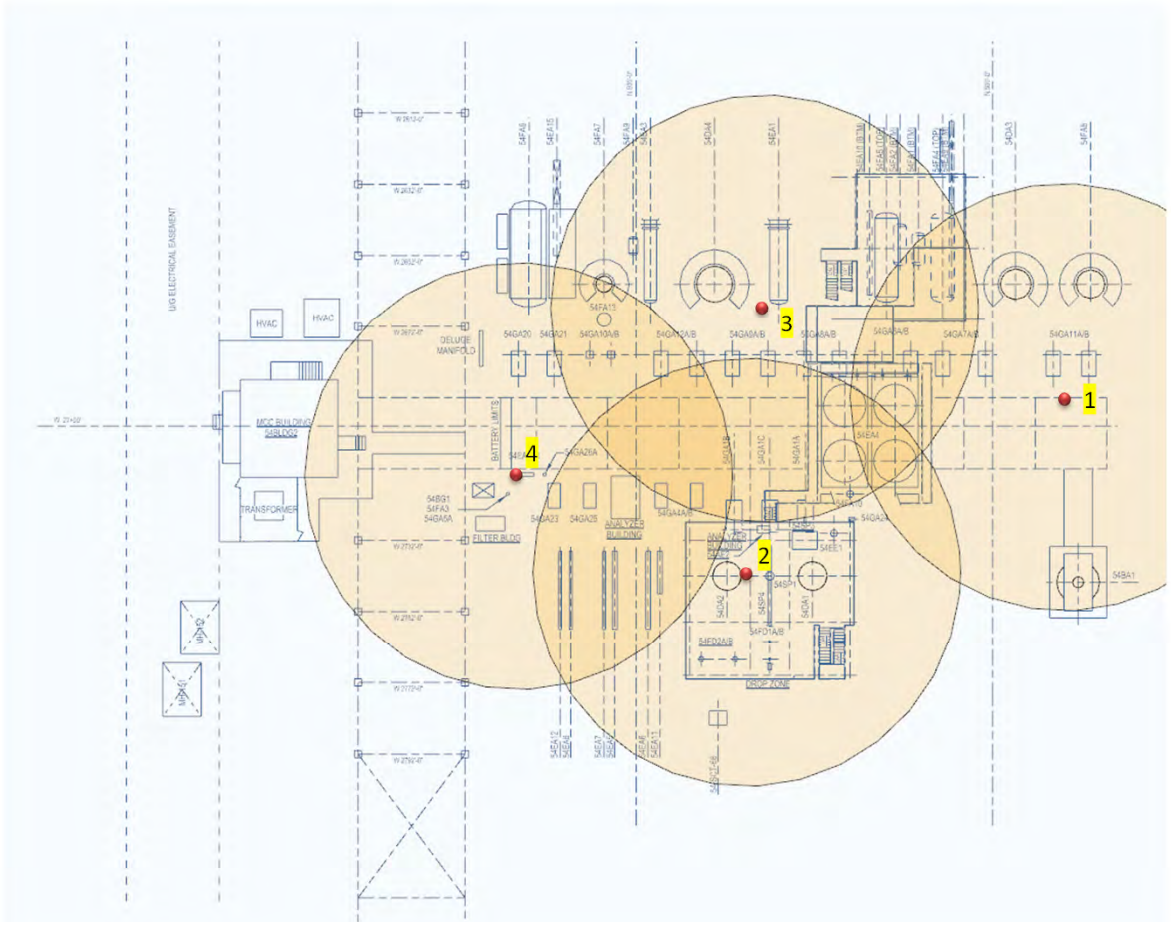
1
2
3
4
HVAC
HVAC
TRANSFORMER
FILTER BLDG
ANALYZER BUILDING
DEHYDRATOR BUILDING
DEHYDRATOR BUILDING
DEHYDRATOR

FHR CC m-Xylene Process Unit (Level 2)

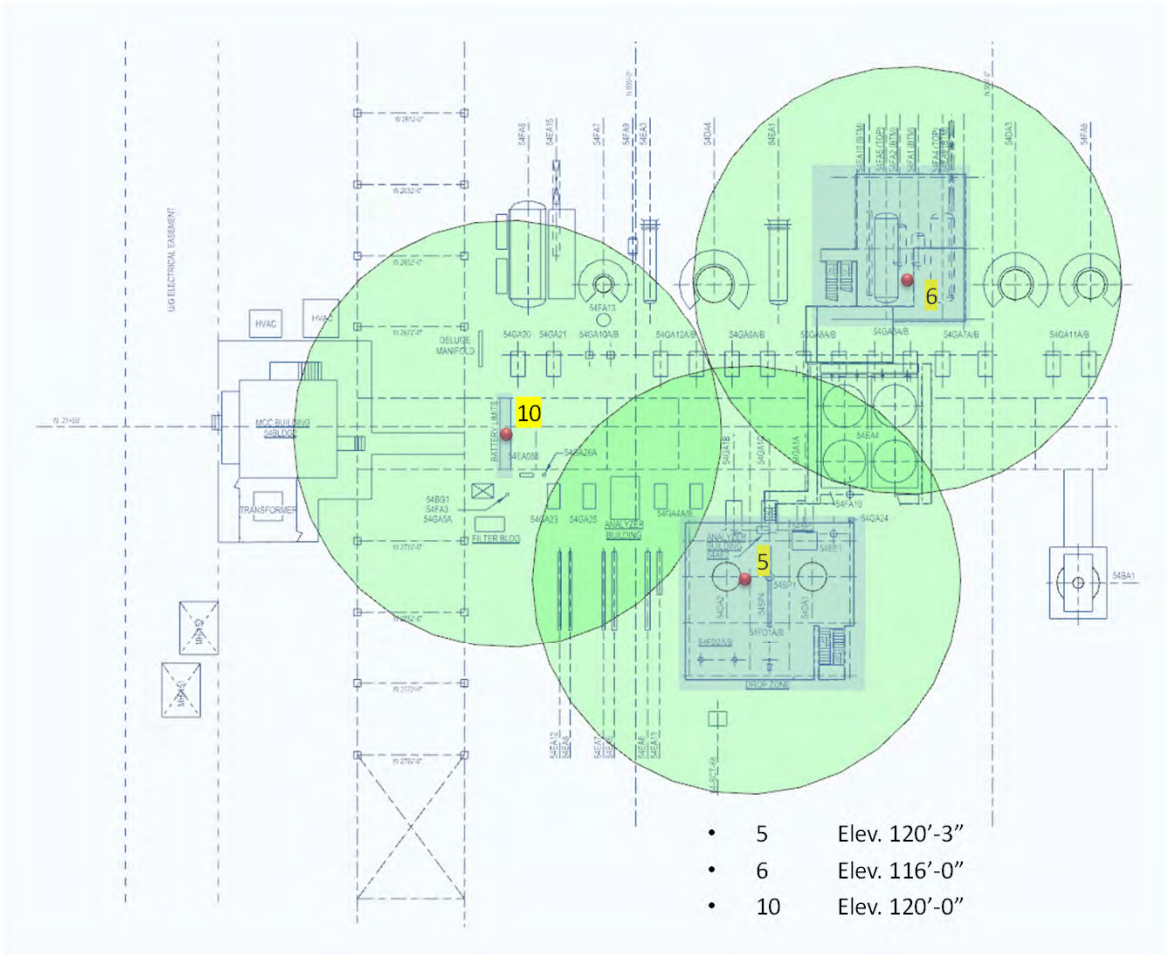

Figure C1-9. m-Xylene sensor locations (level 2). These are the node location during testing and do not reflect the additional nodes added after the pilot test.

FHR CC m-Xylene Process Unit (Level 3)

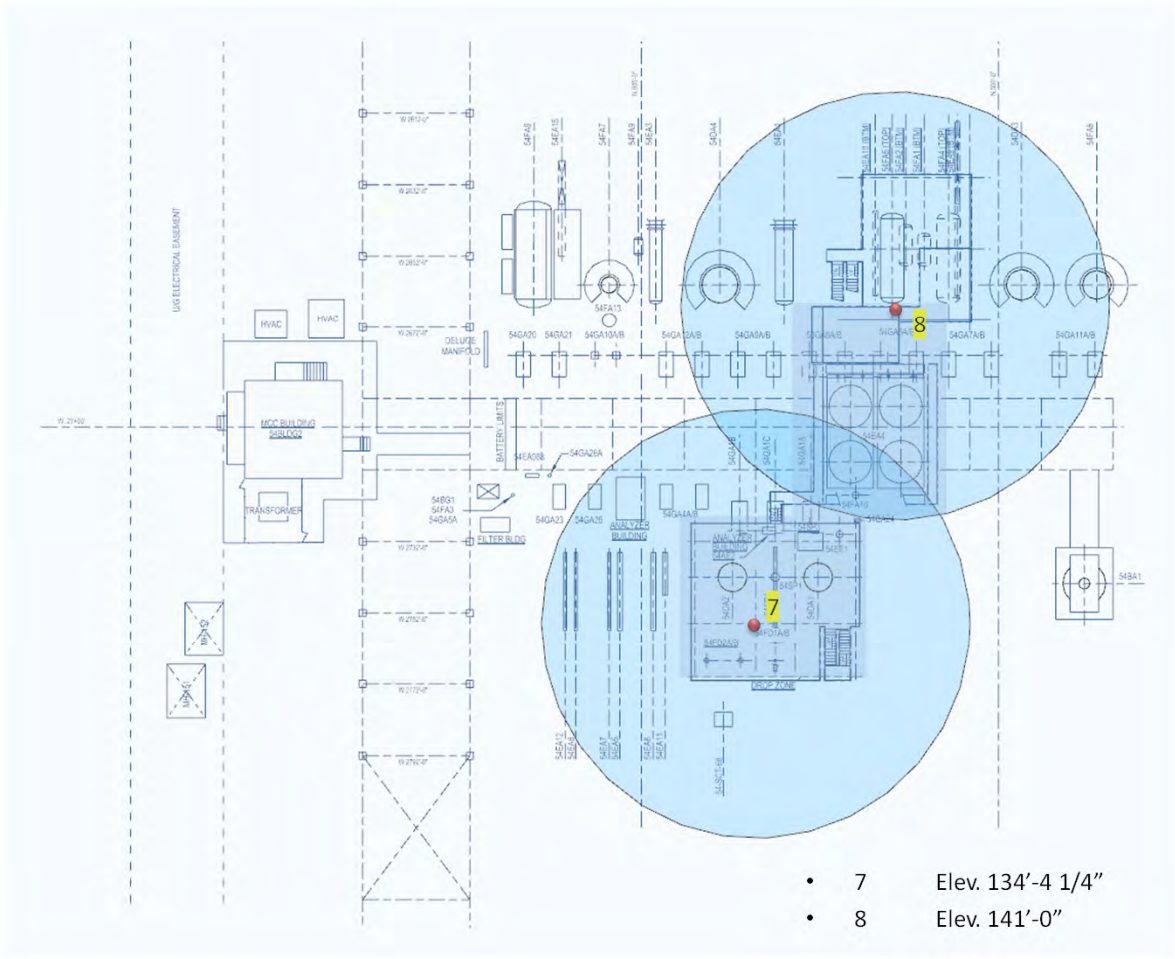

Figure C1-10. m-Xylene sensor locations (level 3). These are the node location during testing and do not reflect the additional nodes added after the pilot test.

FHR CC m-Xylene Process Unit (Level 4)

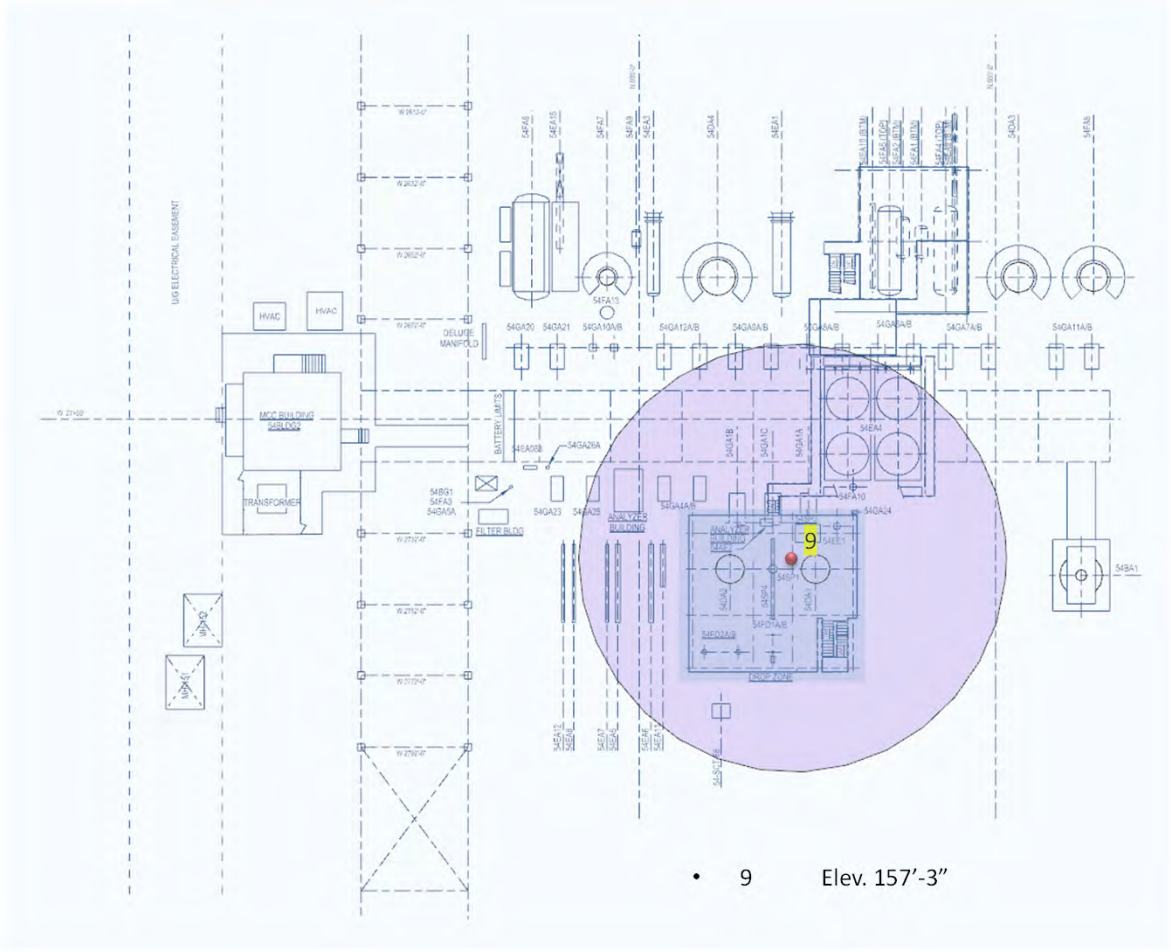

Figure C1-11. m-Xylene sensor locations (level 4). These are the node location during testing and do not reflect the additional nodes added after the pilot test.

Appendix C2
Summary of LDSN PSLs and DRF SVs

Tests Conducted May 1, 2019 to November 30, 2019 (m-Xylene unit)
and July 1, 2019 to November 30, 2019 (Mid-Crude Unit)

FHR CC Mid-Crude Process Unit PSL Summary

Table C2-1. PSL summary table for the LDSN/DRF pilot test in the FHR CC Mid-Crude process unit from 7/1/2019 to 11/30 2019. Table is sorted by ascending DRF SV values.

LDSN PSL ID	PSL/DRF Investigation ID	Process Unit Level	DRF Date Found	Date Repaired	LDAR Component Tag	Type of component	≈ Dist. To LDSN Node (ft)	DRF SV (ppm)	OGI Detection Result
19-SD-00045	3	1	11/6/2019	11/8/2019	105180A.1	Connector	23	582	No Detect
19-SD-00011	1	2	7/11/2019	7/24/2019	112357	Connector	36	626	No Detect
19-SD-00014	4	1	10/30/2019	11/4/2019	111636	Valve	19.2	664	No Detect
19-SD-00030	3	2	11/6/2019	11/20/2019	114788A	Valve	46.7	681	No Detect
19-SD-00056	2	1	11/26/2019	11/27/2019	102078	Pump	50	713	No Detect
19-SD-00059	1	2	11/5/2019	11/20/2019	106351	Valve	48	756	No Detect
19-SD-00042	1	1	8/26/2019	9/4/2019	112800	Connector	38	792	No Detect
19-SD-00043	1	1	8/27/2019	8/28/2019	113910B.1	Connector	24	1262	No Detect
19-SD-00045	1	1	9/5/2019	9/9/2019	AVO 018748	Connector	44	1652	No Detect
19-SD-00058	2	1	11/4/2019	11/7/2019	118887	Valve	48	1783	No Detect
19-SD-00012	1	1	7/18/2019	7/18/2019	Near 112144	OEL	72	1896	No Detect
19-SD-00021	1	1	7/11/2019	7/15/2019	105282.1	Connector	24	2186	No Detect
19-SD-00033	2	1	8/12/2019	8/13/2019	AVO 018726	Connector	25	2451	No Detect
19-SD-00014	8	1	11/19/2019	11/20/2019	112011.1	Connector	63	2572	No Detect
19-SD-00052	1	3	11/6/2019	11/10/2019	108260.1	Connector	23	2742	No Detect
19-SD-00030	2	2	9/18/2019	9/21/2019	AVO 018786	Connector	46.7	2836	No Detect
19-SD-00045	2	1	10/30/2019	10/30/2019	AVO 018989	Connector	38.6	2946	No Detect
19-SD-00033	3	1	8/12/2019	8/14/2019	AVO 018728	Connector	25	3082	No Detect
19-SD-00052	3	4	11/6/2019	11/7/2019	Non LDAR	Non LDAR	40	3153	No Detect
19-SD-00014	6	1	11/5/2019	11/7/2019	AVO 018235	Connector	18.4	3463	No Detect
19-SD-00058	1	1	10/29/2019	10/31/2019	AVO 018987	Connector	30.5	3520	No Detect
19-SD-00033	1	1	8/8/2019	8/22/2019	AVO 018740	Valve	25	3559	No Detect
19-SD-00025	5	1	9/11/2019	9/12/2019	105803.1	Connector	52	3654	No Detect
19-SD-00052	4	4	11/6/2019	11/7/2019	Non LDAR	Non LDAR	40	4535	No Detect
19-SD-00053	1	4	10/9/2019	10/10/2019	Near 109280	Non LDAR	42	4751	No Detect
19-SD-00014	5	1	11/5/2019	11/7/2019	111575	Compressor	19	5526	No Detect
19-SD-00014	7	1	11/19/2019	11/20/2019	112082	Valve	72	7287	No Detect
19-SD-00014	3	1	9/18/2019	9/24/2019	AVO 018724	Valve	20	9951	No Detect
19-SD-00020	2	1	7/2/2019	7/17/2019	AVO 018743	Connector	15	15231	No Detect
19-SD-00038	1	2	9/12/2019	9/17/2019	AVO 018985	Connector	10	18330	No Detect
19-SD-00042	3	1	8/26/2019	8/27/2019	119746.1	Connector	54	30876	No Detect
19-SD-00020	1	1	7/11/2019	7/14/2019	103056R.1	Connector	25	93106	Moderate Detect
19-SD-00024	1	1	7/23/2019	7/24/2019	108940.1	Connector	63	100000	Easy Detect
19-SD-00014	2	1	7/30/2019	8/19/2019	111575	Compressor	19	100000	Moderate Detect
19-SD-00014	9	1	7/23/2019	7/24/2019	111961.1	Connector	63	100000	No Detect
19-SD-00014	1	5	11/19/2019	11/25/2019	111972	Pump	48	100000	Easy Detect
19-SD-00042	2	1	8/26/2019	8/27/2019	119674.1	Connector	49	100000	Moderate Detect
19-SD-00052	2	4	11/6/2019	11/7/2019	Non LDAR	Non LDAR	38.6	100000	Difficult Detect
19-SD-00056	1	1	10/24/2019	10/24/2019	Non LDAR	Non LDAR	5	100000	Easy Detect

FHR CC Mid-Crude Process Unit

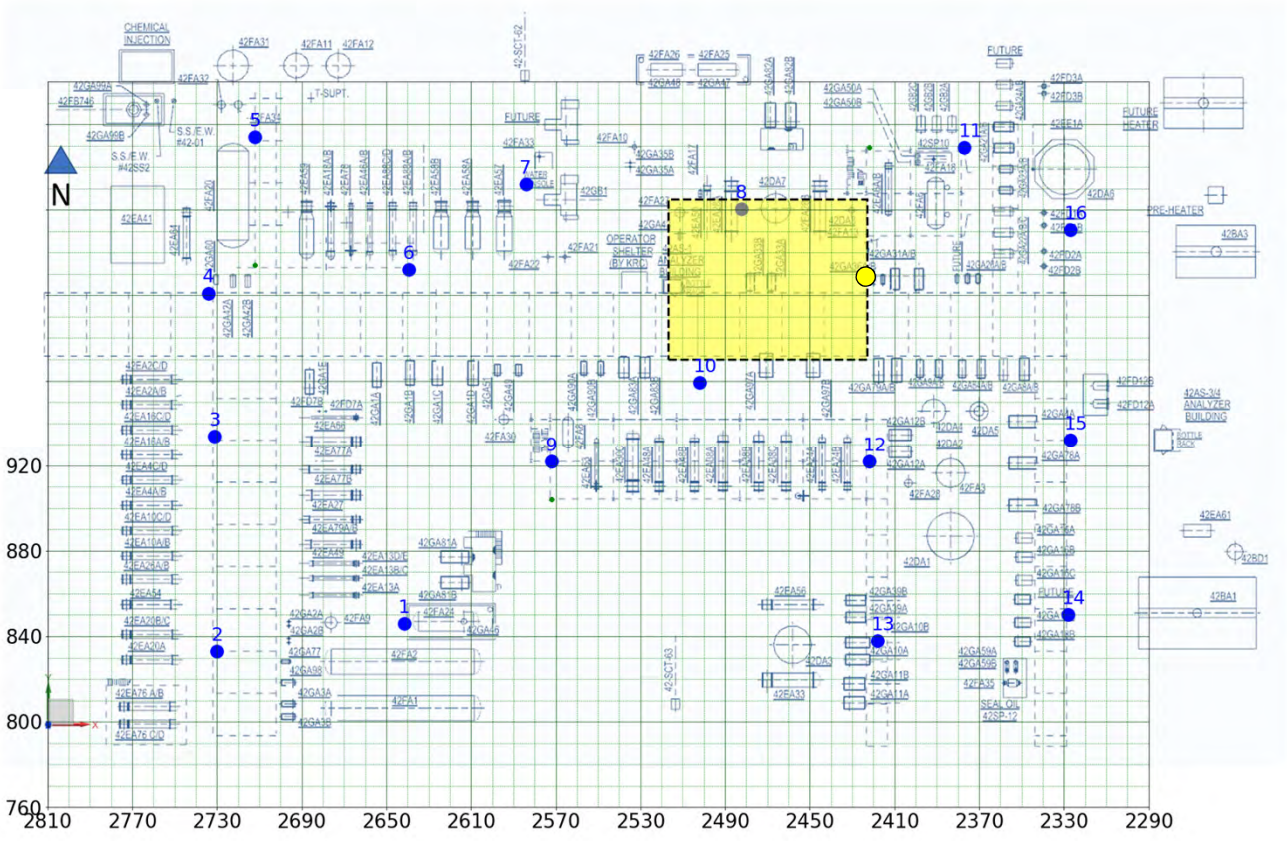

19-SD-00012

Created : 2019-06-08 19:00:00
Site/Unit : Mid-Crude
Elevation Level: 1
Detection Category : 3

Leak size (ppm)

- > 50,000
- 5,000 – 50,000
- 1,000 – 5,000
- 500 – 1,000

Gas sensor

Cat. 2 PSL

Cat. 3 PSL

Scale : 10ft x10ft

Figure C2-1. Mid-Crude PSL 19-SD-00012

FHR CC Mid-Crude Process Unit

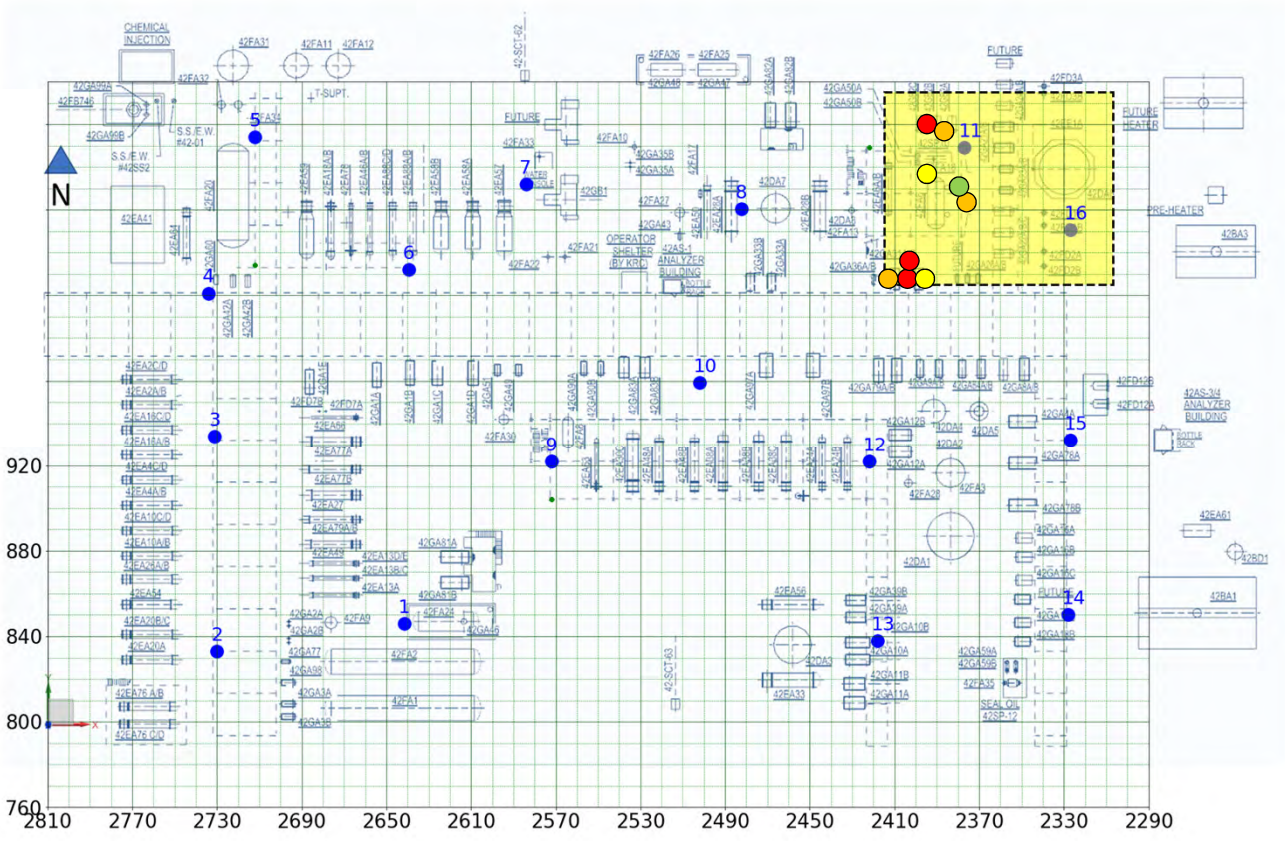

19-SD-00014

Created : 2019-06-10 19:00:00
Site/Unit : Mid-Crude
Elevation Level: 1
Detection Category : 3

Leak size (ppm)

- > 50,000
- 5,000 – 50,000
- 1,000 – 5,000
- 500 – 1,000

Gas sensor

Cat. 2 PSL

Cat. 3 PSL

Scale : 10ft x10ft

Figure C2-2. Mid-Crude PSL 19-SD-00014

FHR CC Mid-Crude Process Unit

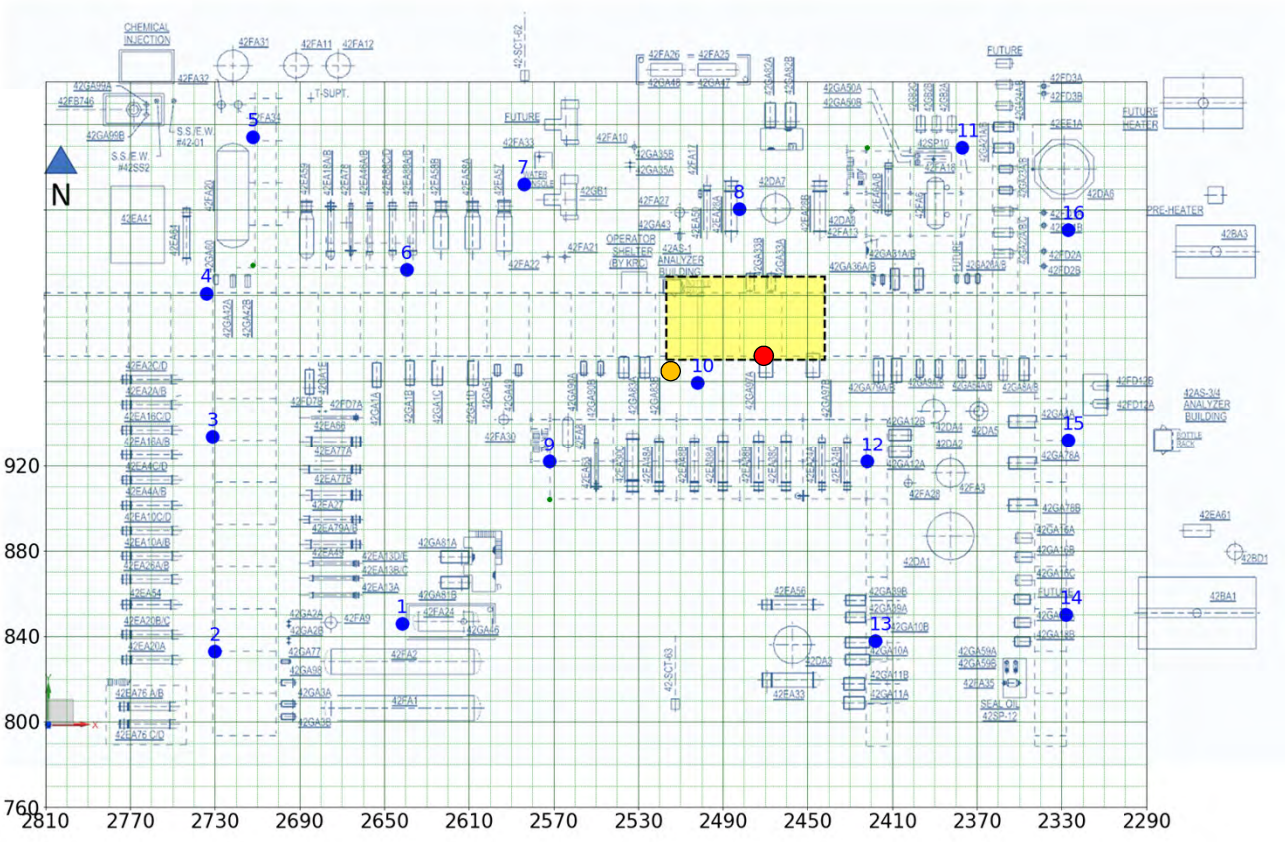

19-SD-00020

Created : 2019-06-26 19:00:00
Site/Unit : Mid-Crude
Elevation Level: 1
Detection Category : 3

Leak size (ppm)

- > 50,000
- 5,000 – 50,000
- 1,000 – 5,000
- 500 – 1,000

Gas sensor

Cat. 2 PSL

Cat. 3 PSL

Scale : 10ft x10ft

Figure C2-3. Mid-Crude PSL 19-SD-00020

FHR CC Mid-Crude Process Unit

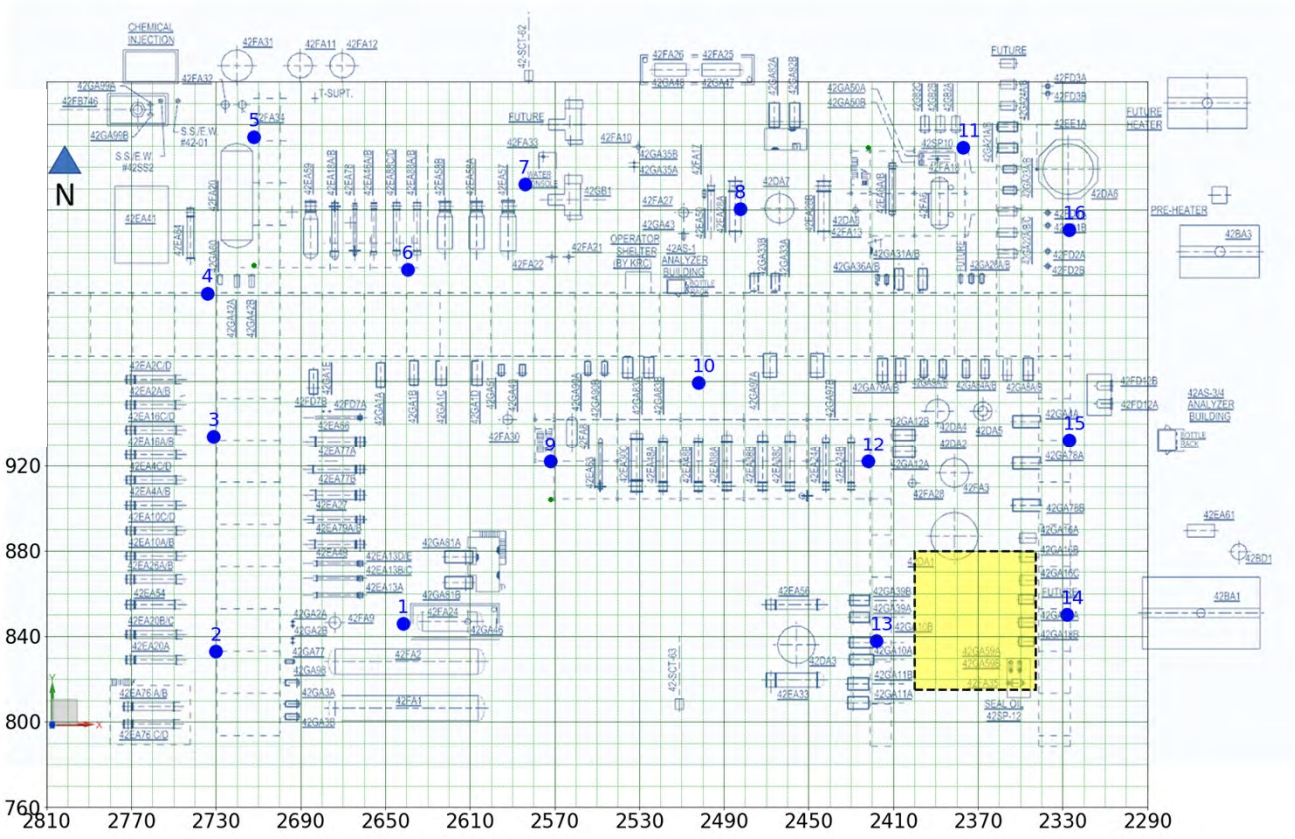

19-SD-00021

Created : 2019-07-05 19:00:00
Site/Unit : Mid-Crude
Elevation Level: 1
Detection Category : 3

Leak size (ppm)

- > 50,000
- 5,000 – 50,000
- 1,000 – 5,000
- 500 – 1,000

Gas sensor

Cat. 2 PSL

Cat. 3 PSL

Scale : 10ft x10ft

Figure C2-4. Mid-Crude PSL 19-SD-00021

FHR CC Mid-Crude Process Unit

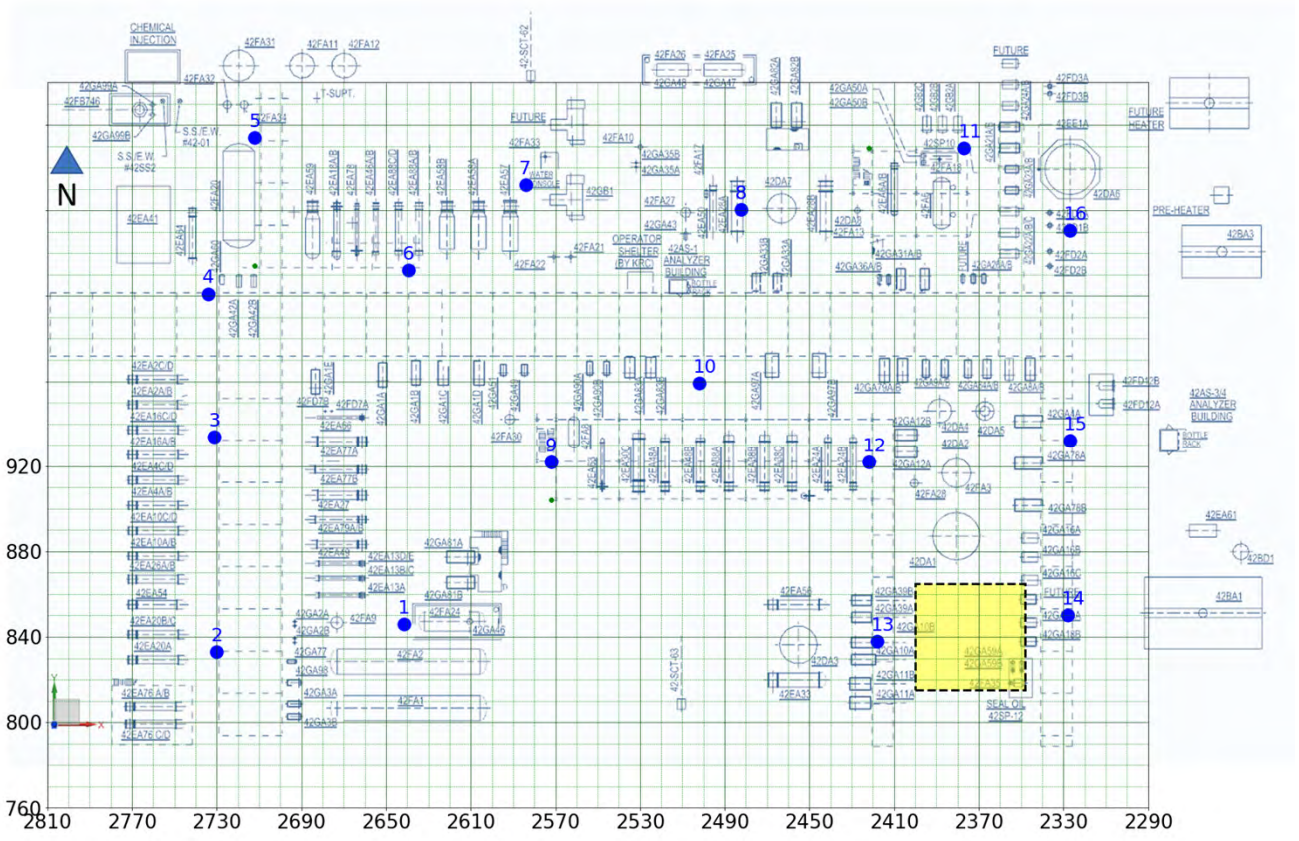

19-SD-00025

Created : 2019-07-21 19:00:00
Site/Unit : Mid-Crude
Elevation Level: 1
Detection Category : 3

Leak size (ppm)

- > 50,000
- 5,000 – 50,000
- 1,000 – 5,000
- 500 – 1,000

Gas sensor

Cat. 2 PSL

Cat. 3 PSL

Scale : 10ft x10ft

Figure C2-5. Mid-Crude PSL 19-SD-00025

FHR CC Mid-Crude Process Unit

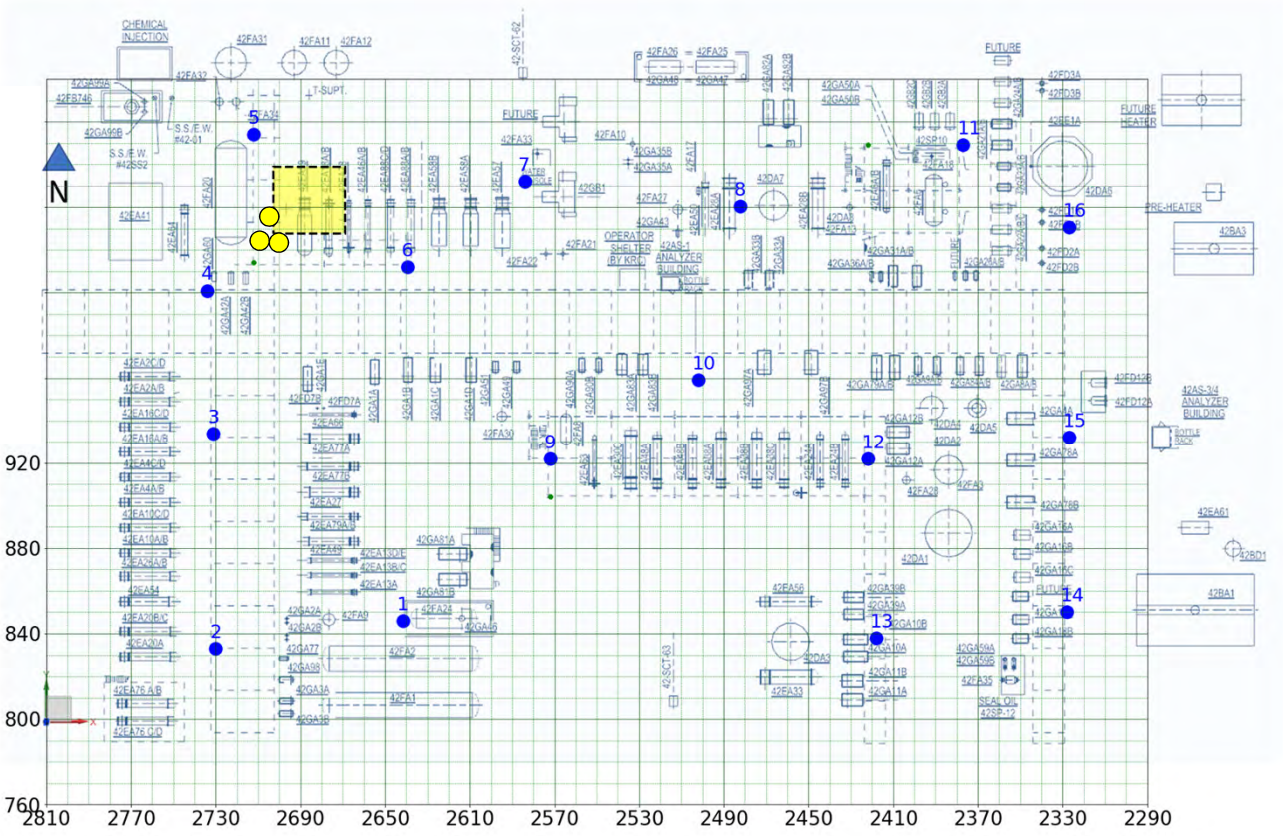

19-SD-00033

Created : 2019-08-07 19:00:00
Site/Unit : Mid-Crude
Elevation Level: 1
Detection Category : 3

Leak size (ppm)

- > 50,000
- 5,000 – 50,000
- 1,000 – 5,000
- 500 – 1,000

Gas sensor

Cat. 2 PSL

Cat. 3 PSL

Scale : 10ft x10ft

Figure C2-6. Mid-Crude PSL 19-SD-00033

FHR CC Mid-Crude Process Unit

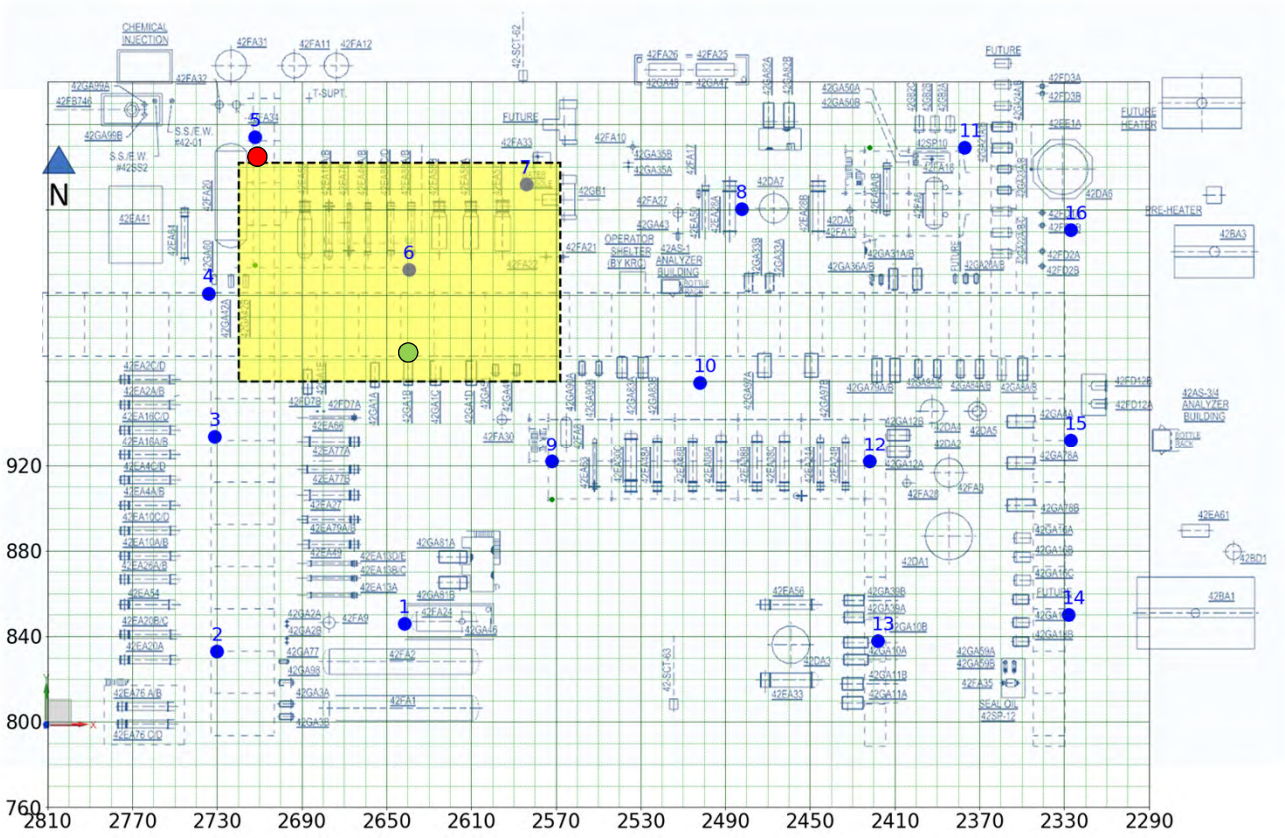

19-SD-00056

Created : 2019-10-23 19:00:00
Site/Unit : Mid-Crude
Elevation Level: 1
Detection Category : 3

Leak size (ppm)

- > 50,000
- 5,000 – 50,000
- 1,000 – 5,000
- 500 – 1,000

Gas sensor

Cat. 2 PSL

Cat. 3 PSL

Scale : 10ft x10ft

Figure C2-7. Mid-Crude PSL 19-SD-00056

FHR CC Mid-Crude Process Unit

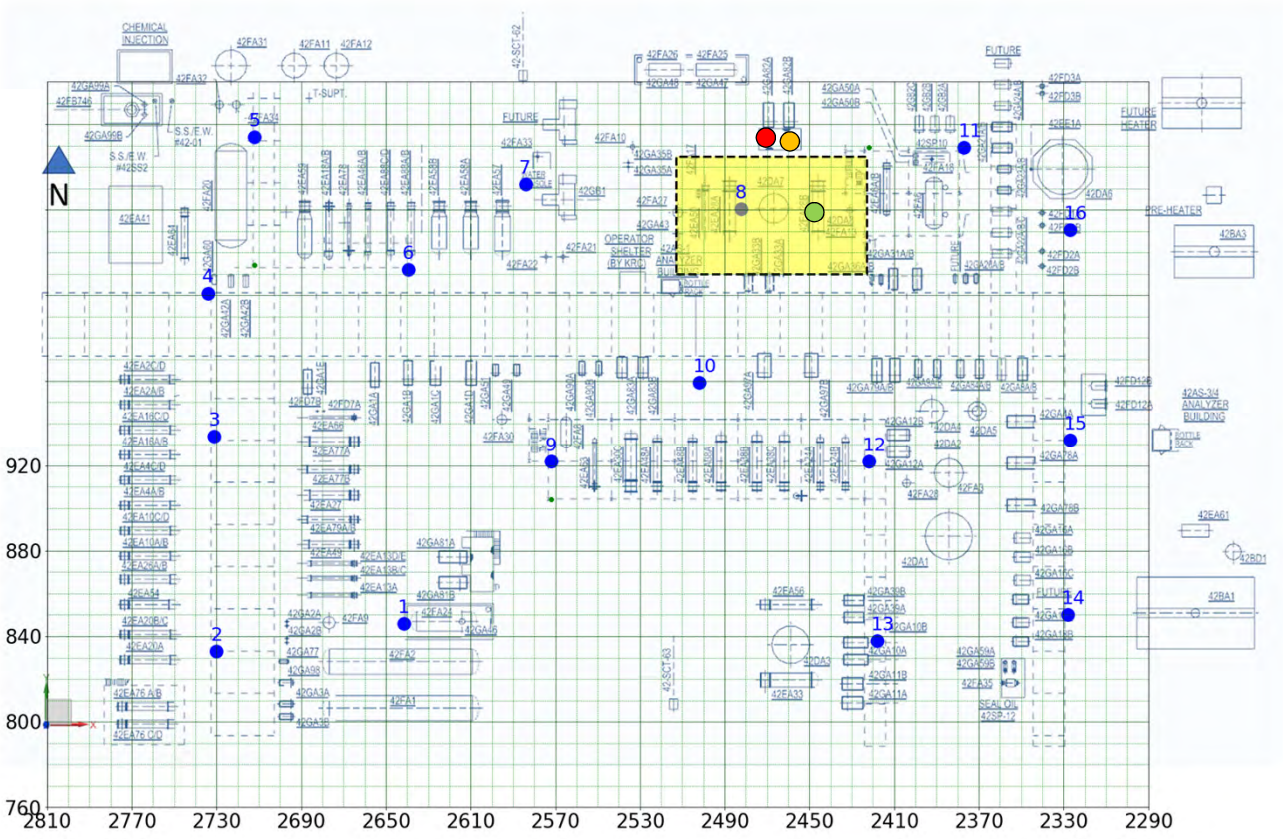

19-SD-00042

Created : 2019-08-23 19:00:00
Site/Unit : Mid-Crude
Elevation Level: 1
Detection Category : 3

Leak size (ppm)

- > 50,000
- 5,000 – 50,000
- 1,000 – 5,000
- 500 – 1,000

Gas sensor

Cat. 2 PSL

Cat. 3 PSL

Scale : 10ft x10ft

Figure C2-8. Mid-Crude PSL 19-SD-00042

FHR CC Mid-Crude Process Unit

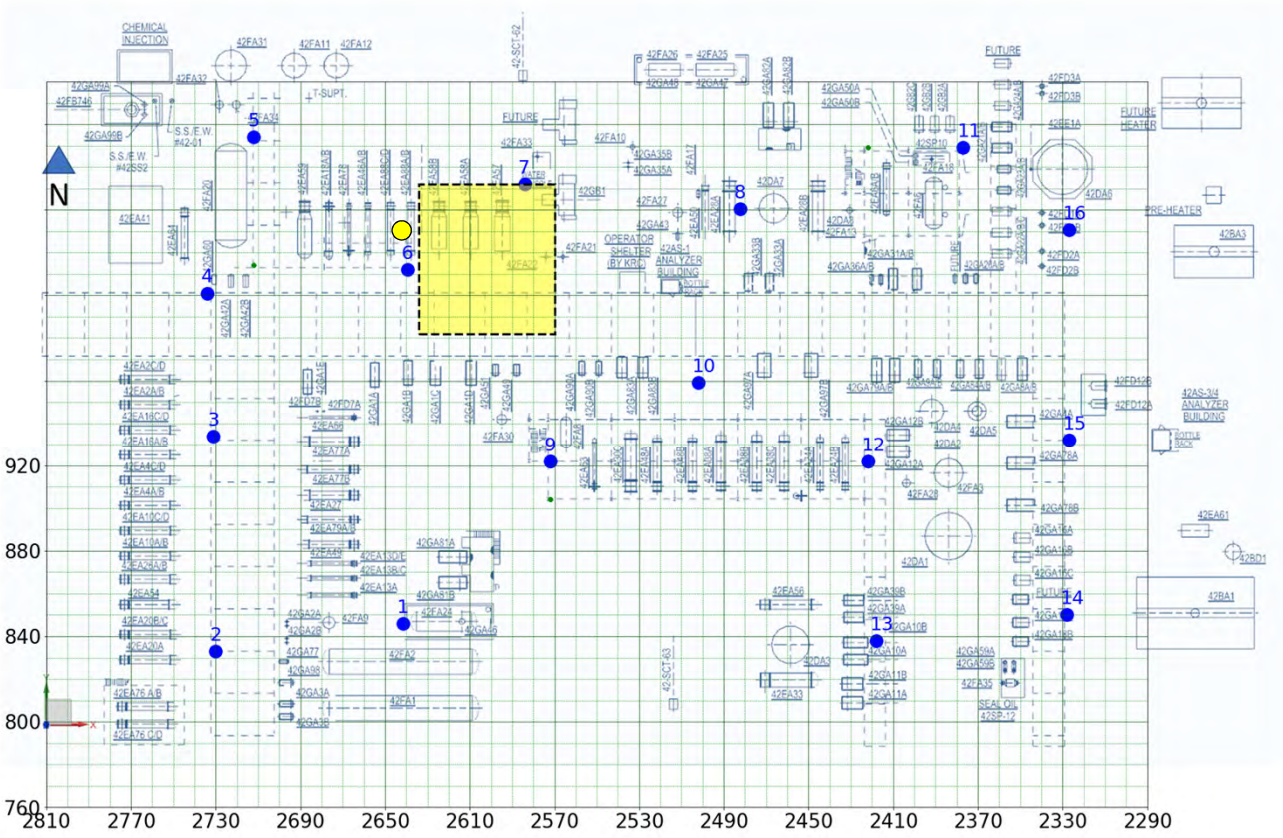

19-SD-00043

Created : 2019-08-23 19:00:00
Site/Unit : Mid-Crude
Elevation Level: 1
Detection Category : 3

Leak size (ppm)

- > 50,000
- 5,000 – 50,000
- 1,000 – 5,000
- 500 – 1,000

Gas sensor

Cat. 2 PSL

Cat. 3 PSL

Scale : 10ft x10ft

Figure C2-9. Mid-Crude PSL 19-SD-00043

FHR CC Mid-Crude Process Unit

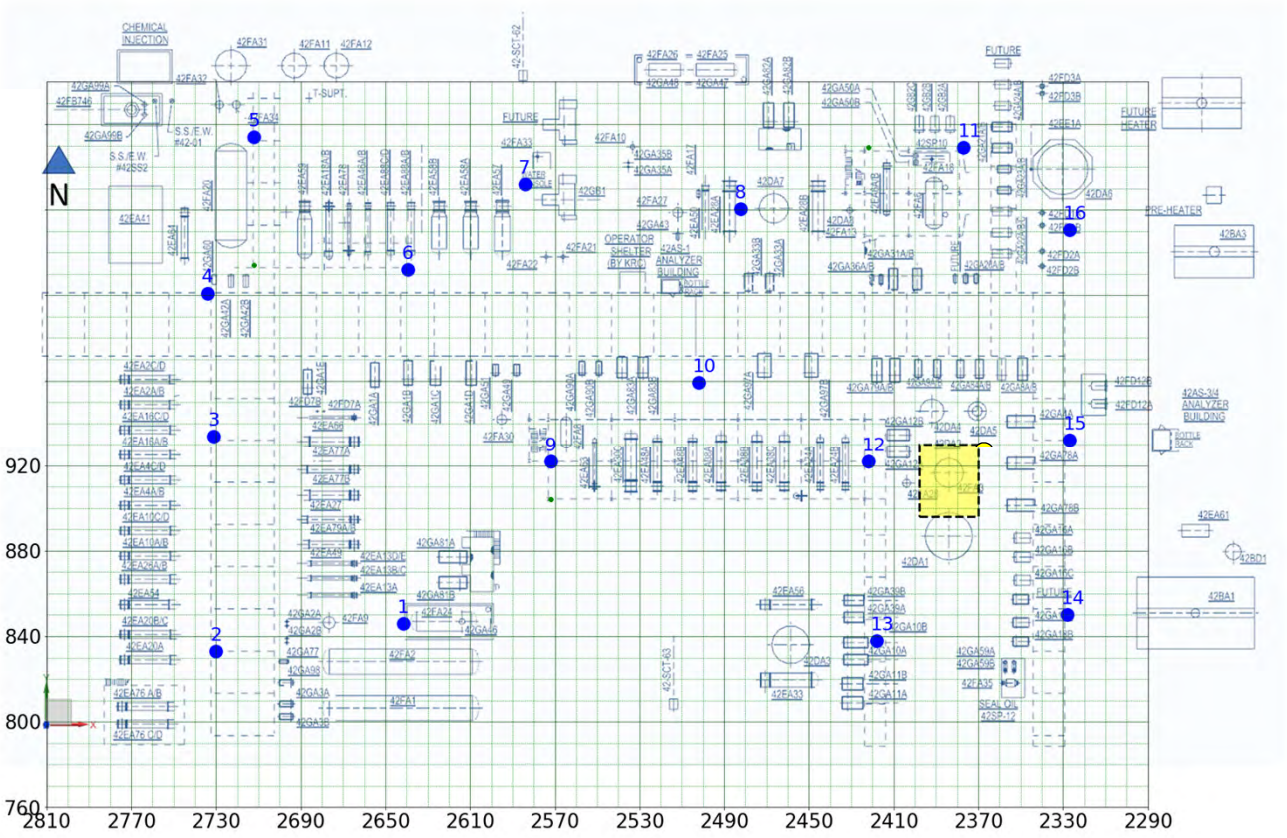

19-SD-00045

Created : 2019-09-03 19:00:00
Site/Unit : Mid-Crude
Elevation Level: 1
Detection Category : 3

Leak size (ppm)

- > 50,000
- 5,000 – 50,000
- 1,000 – 5,000
- 500 – 1,000

Gas sensor

Cat. 2 PSL

Cat. 3 PSL

Scale : 10ft x10ft

Figure C2-10. Mid-Crude PSL 19-SD-00045

FHR CC Mid-Crude Process Unit

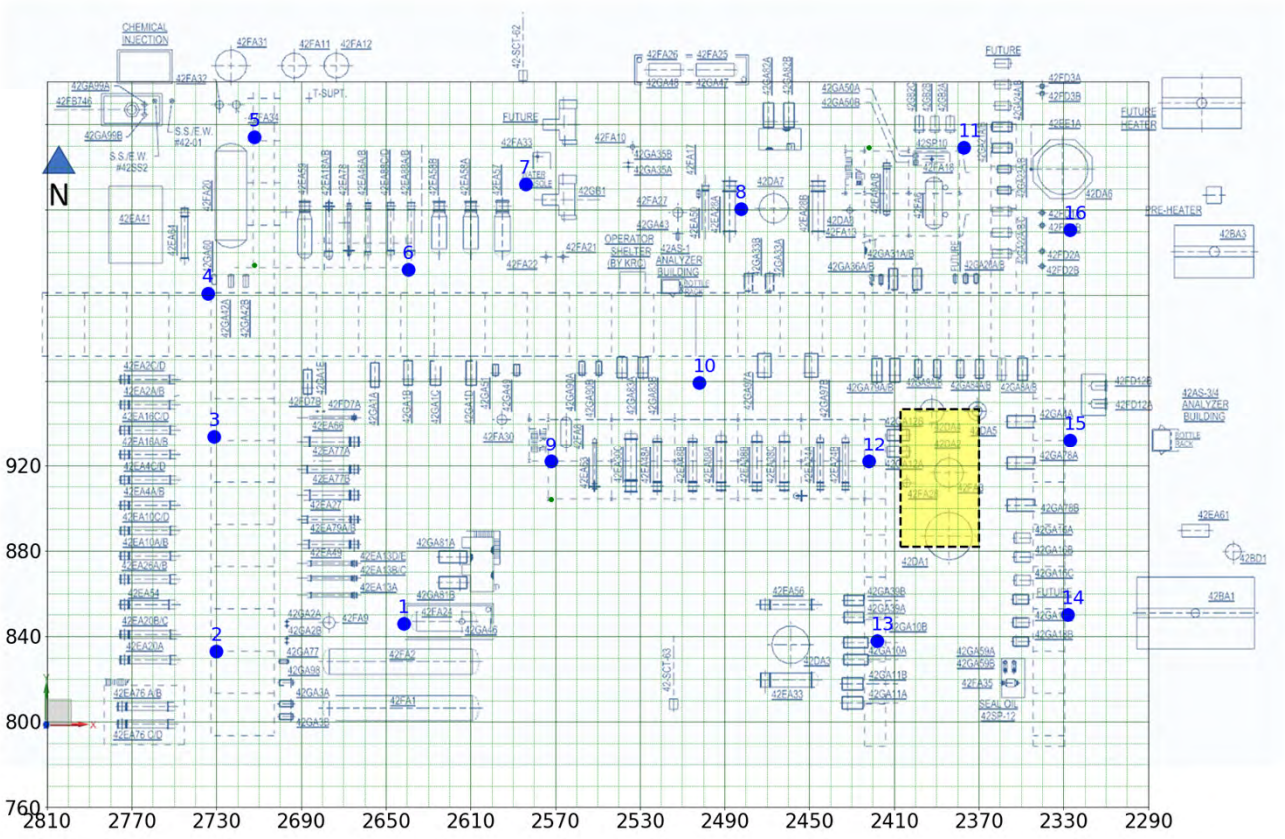

19-SD-00059

Created : 2019-10-31 19:00:00
Site/Unit : Mid-Crude
Elevation Level: 1
Detection Category : 3

Leak size (ppm)

- > 50,000
- 5,000 – 50,000
- 1,000 – 5,000
- 500 – 1,000

Gas sensor

Cat. 2 PSL

Cat. 3 PSL

Scale : 10ft x10ft

Figure C2-11. Mid-Crude PSL 19-SD-00059

FHR CC Mid-Crude Process Unit

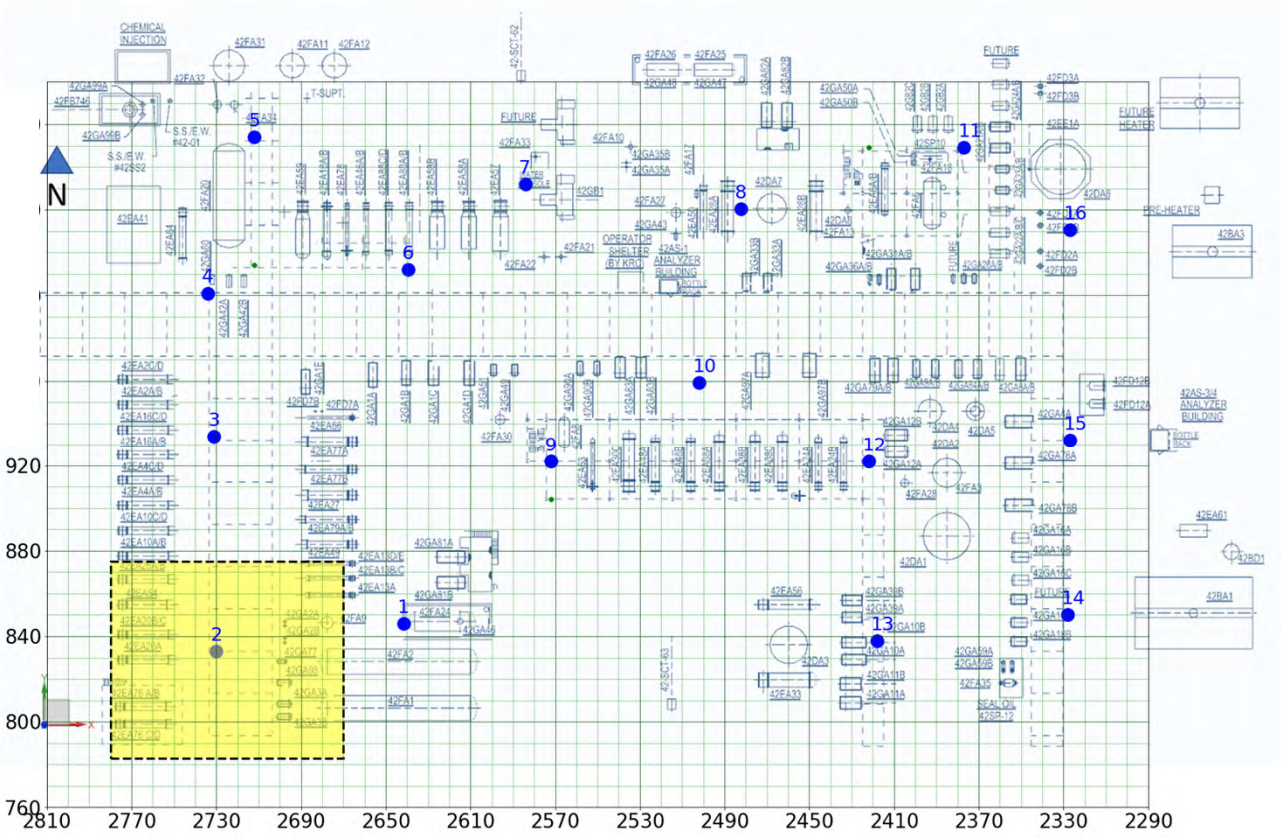

19-SD-00058

Created : 2019-10-25 19:00:00
Site/Unit : Mid-Crude
Elevation Level: 1
Detection Category : 3

Leak size (ppm)

- > 50,000
- 5,000 – 50,000
- 1,000 – 5,000
- 500 – 1,000

Gas sensor

Cat. 2 PSL

Cat. 3 PSL

Scale : 10ft x10ft

Figure C2-12. Mid-Crude PSL 19-SD-00058

FHR CC Mid-Crude Process Unit

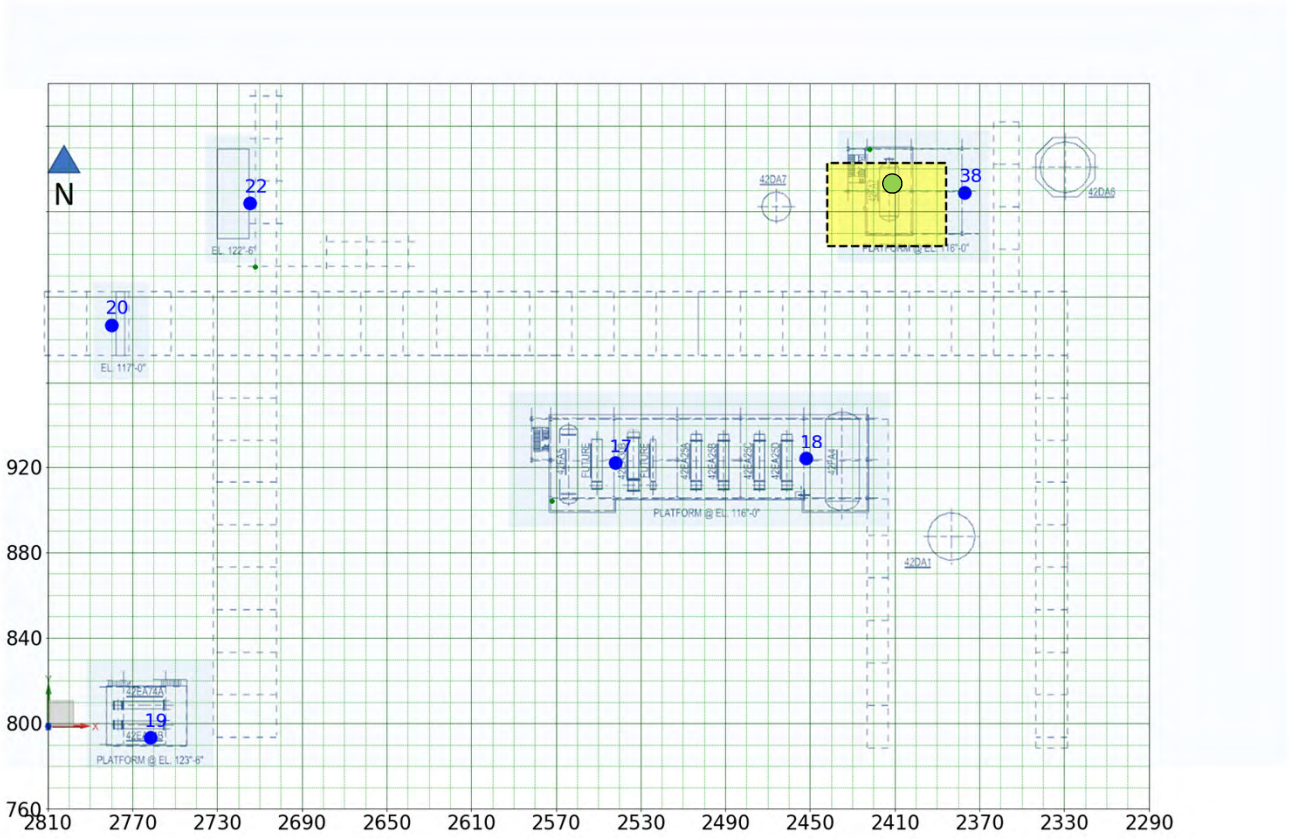

19-SD-00011

Created : 2019-06-07 19:00:00
Site/Unit : Mid-Crude
Elevation Level: 2
Detection Category : 3

Leak size (ppm)

- > 50,000
- 5,000 – 50,000
- 1,000 – 5,000
- 500 – 1,000

Gas sensor

Cat. 2 PSL

Cat. 3 PSL

Scale : 10ft x10ft

Figure C2-13. Mid-Crude PSL 19-SD-00011

FHR CC Mid-Crude Process Unit

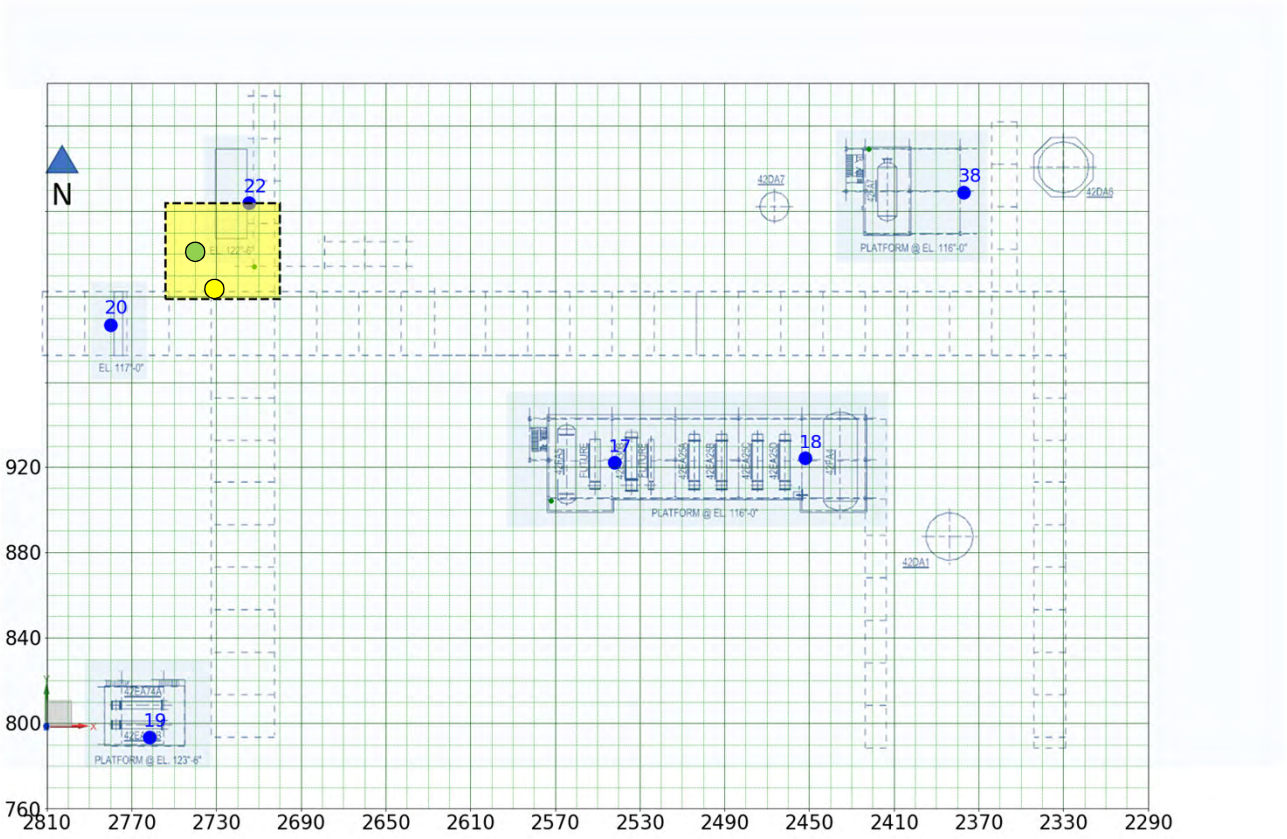

19-SD-00030

Created : 2019-08-06 19:00:00
Site/Unit : Mid-Crude
Elevation Level: 2
Detection Category : 3

Leak size (ppm)

- > 50,000
- 5,000 – 50,000
- 1,000 – 5,000
- 500 – 1,000

Gas sensor

Cat. 2 PSL

Cat. 3 PSL

Scale : 10ft x10ft

Figure C2-14. Mid-Crude PSL 19-SD-00030

FHR CC Mid-Crude Process Unit

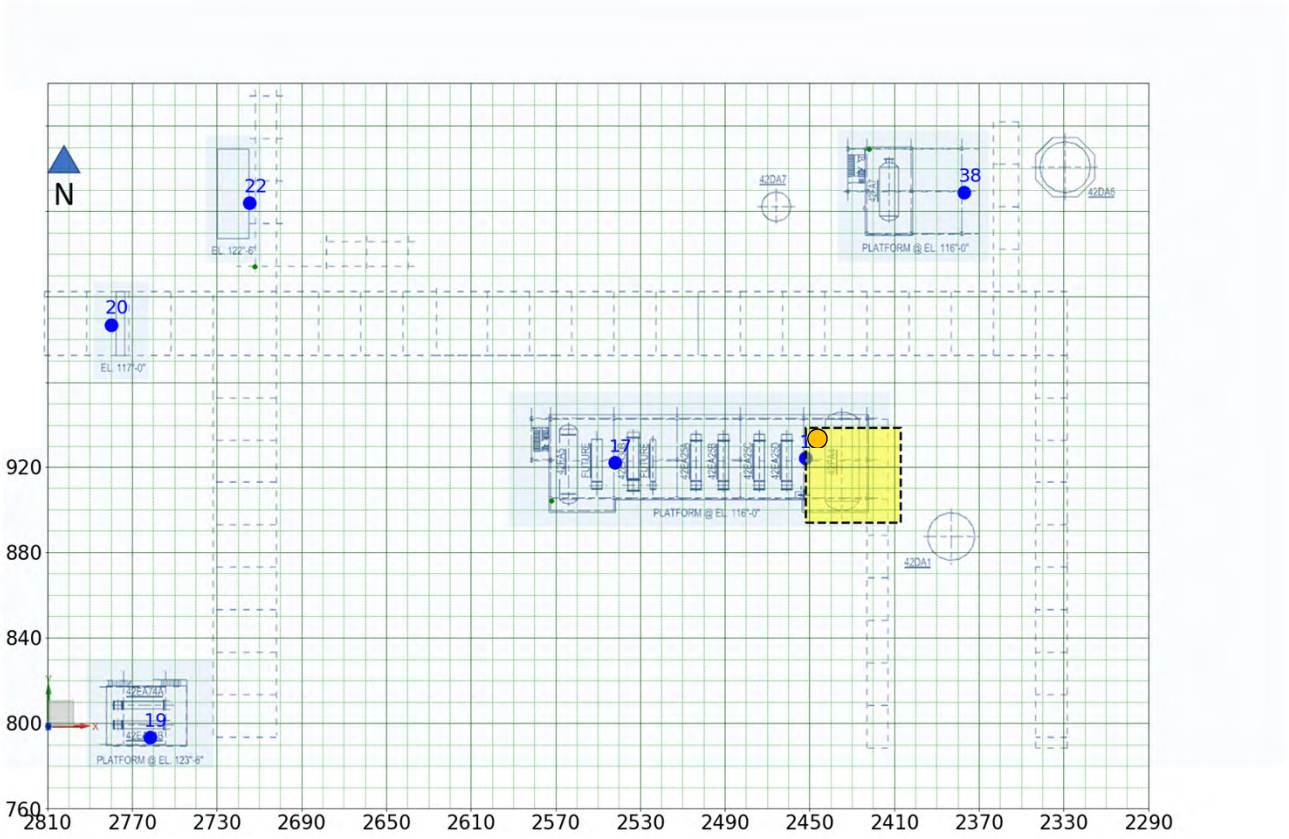

19-SD-00038

Created : 2019-08-14 19:00:00
Site/Unit : Mid-Crude
Elevation Level: 2
Detection Category : 3

Leak size (ppm)

- > 50,000
- 5,000 – 50,000
- 1,000 – 5,000
- 500 – 1,000

Gas sensor

Cat. 2 PSL

Cat. 3 PSL

Scale : 10ft x10ft

Figure C2-15. Mid-Crude PSL 19-SD-00038

FHR CC Mid-Crude Process Unit

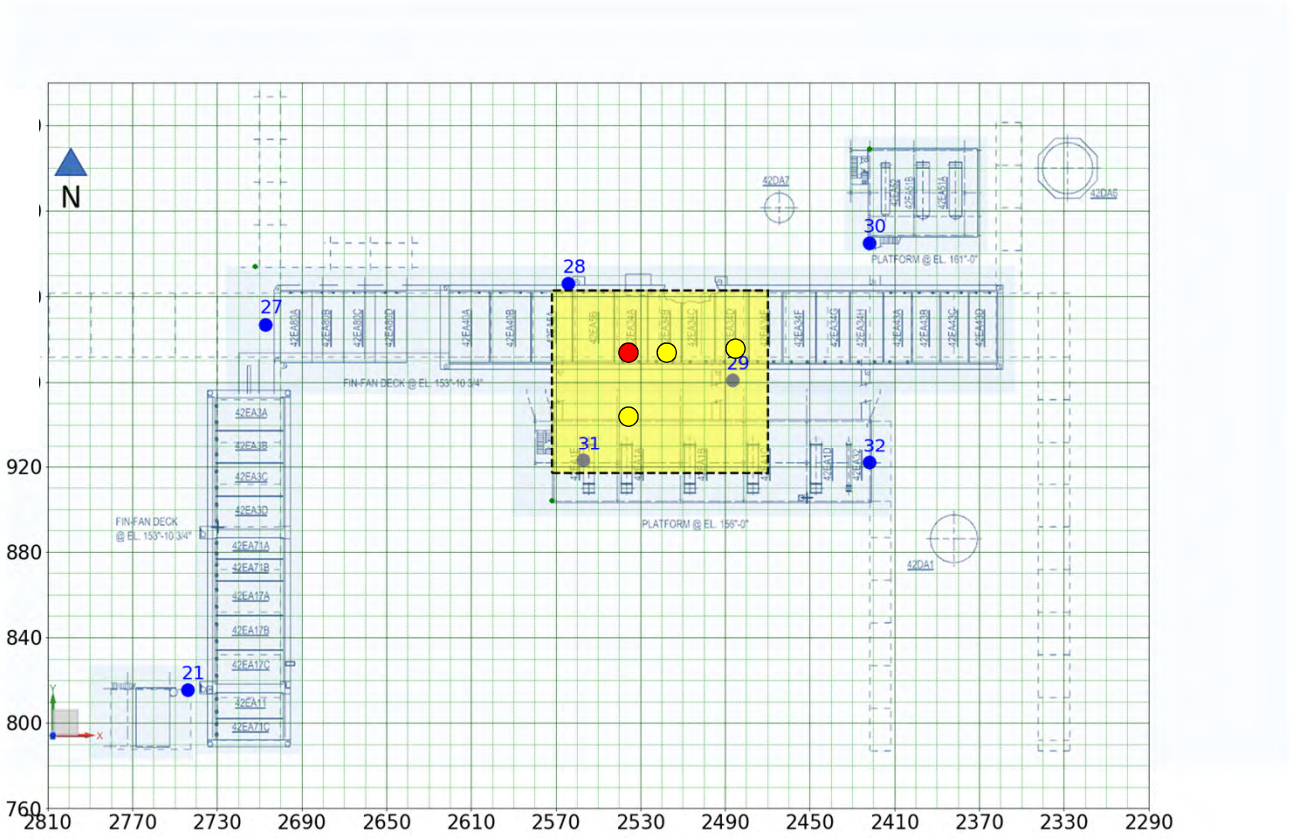

19-SD-00052

Created : 2019-10-08 19:00:00
Site/Unit : Mid-Crude
Elevation Level: 4
Detection Category : 3

Leak size (ppm)

- > 50,000
- 5,000 – 50,000
- 1,000 – 5,000
- 500 – 1,000

Gas sensor

Cat. 2 PSL

Cat. 3 PSL

Scale : 10ft x10ft

Figure C2-16. Mid-Crude PSL 19-SD-00052

FHR CC Mid-Crude Process Unit

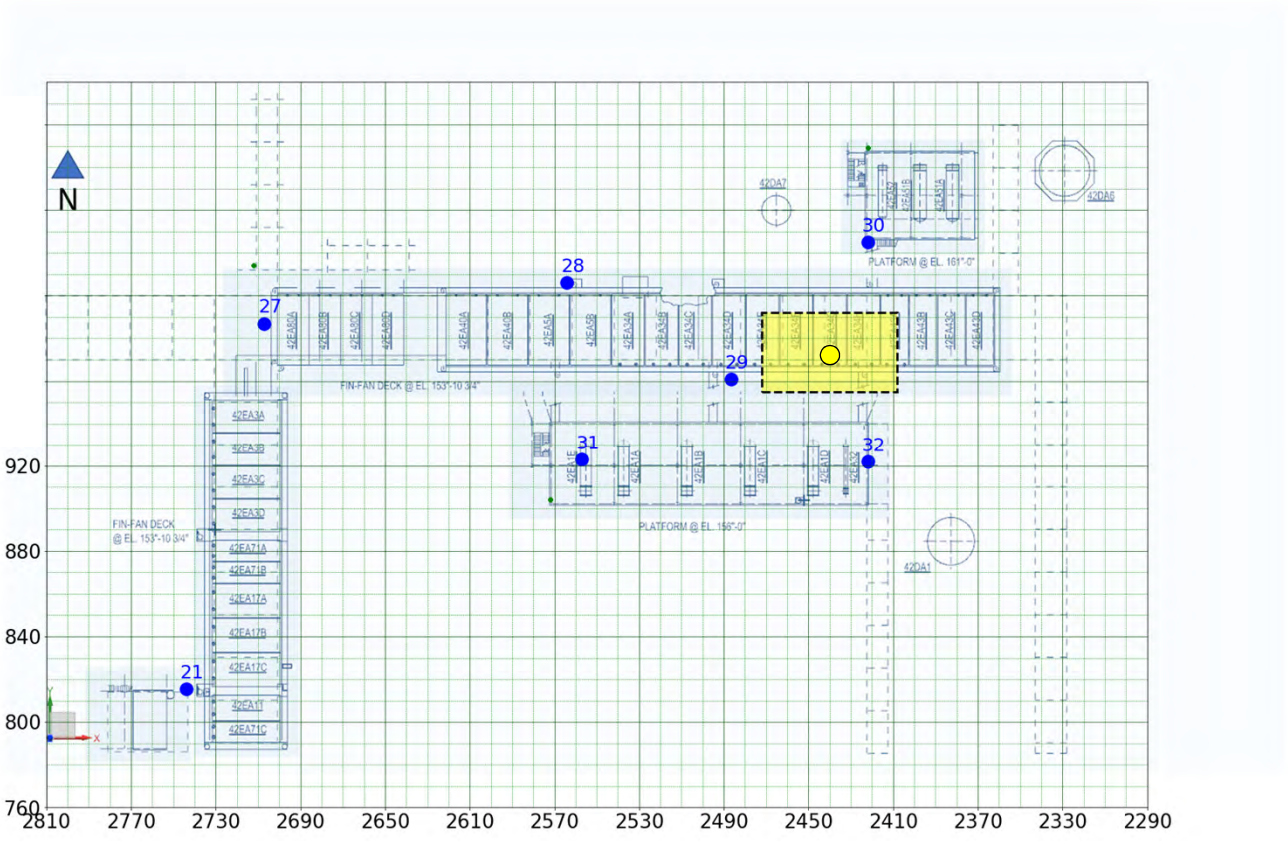

19-SD-00053
Created : 2019-10-08 19:00:00
Site/Unit : Mid-Crude
Elevation Level: 4
Detection Category : 3

Leak size (ppm)

- > 50,000
- 5,000 – 50,000
- 1,000 – 5,000
- 500 – 1,000

Gas sensor

Cat. 2 PSL

Cat. 3 PSL

Scale : 10ft x10ft

Figure C2-17. Mid-Crude PSL 19-SD-00053

FHR CC Mid-Crude Process Unit

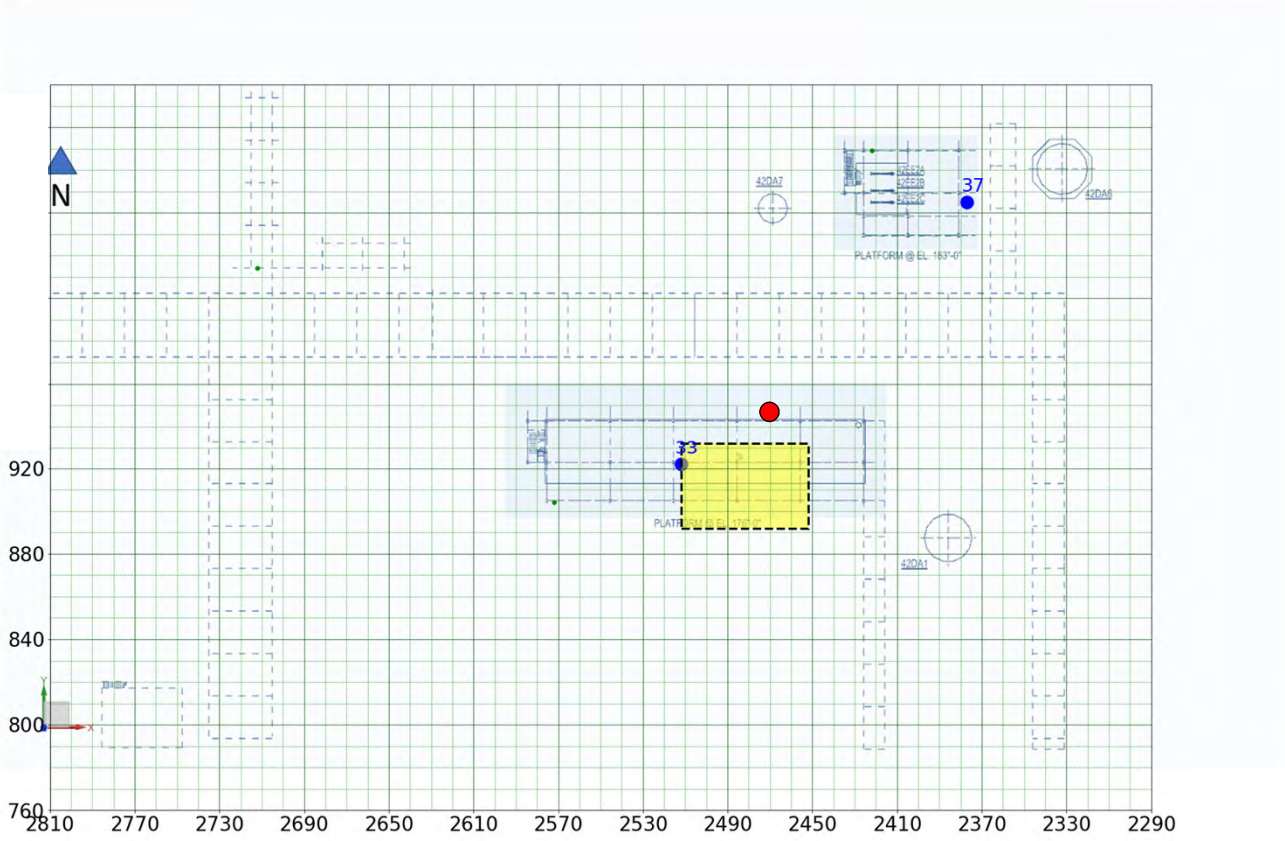

19-SD-00024
Created : 2019-07-18 19:00:00
Site/Unit : Mid-Crude
Elevation Level: 5
Detection Category : 3

Leak size (ppm)

- > 50,000
- 5,000 – 50,000
- 1,000 – 5,000
- 500 – 1,000

Gas sensor

Cat. 2 PSL

Cat. 3 PSL

Scale : 10ft x10ft

Figure C2-18. Mid-Crude PSL 19-SD-00024

FHR CC m-Xylene
Process Unit
PSL Summary

Table C2-2. PSL summary table (1 of 2) for the LDSN/DRF pilot test in the FHR CC m-Xylene process unit from 5/1/2019 to 11/30 2019. "DRF-Pre" entries represent leak detected by LDSN prior to implementation of PSL ID system. Table is sorted by ascending DRF SV values.

LDSN PSL ID	PSL/DRF Investigation ID	Process Unit Level	DRF Date Found	Date Repaired	LDAR Component Tag	Type of component	≈ Dist. To LDSN Node (ft)	DRF SV (ppm)	OGI Detection Result
19-SD-00028	15	1	11/18/2019	11/19/2019	249694	Valve	6	564	No Detect
19-SD-00029	1	1	8/6/2019	8/19/2019	253195	Connector	26	583	No Detect
19-SD-00029	5	1	8/20/2019	8/21/2019	253213	Drain	26	590	No Detect
19-SD-00028	4	1	8/22/2019	8/23/2019	253442.2	Connector	24	643	No Detect
19-SD-00029	8	1	10/15/2019	10/18/2019	253342	Valve	15	665	No Detect
19-SD-00051	1	3	10/12/2019	10/22/2019	251183	Connector	17	676	No Detect
19-SD-00029	3	1	8/12/2019	8/13/2019	252682.1	Connector	42	692	No Detect
19-SD-00050	6	2	10/28/2019	11/4/2019	252885	Valve	11	828	No Detect
19-SD-00028	14	1	10/22/2019	10/23/2019	253677.1	Connector	35	863	No Detect
19-SD-00057	7	2	11/21/2019	11/23/2019	250925	Valve	16	890	No Detect
19-SD-00028	7	1	9/17/2019	9/19/2019	248889.1	Connector	15	894	No Detect
19-SD-00035	7	1	11/21/2019	11/27/2019	252776	Valve	45	903	No Detect
19-SD-00035	6	1	10/22/2019	10/30/2019	252796	Valve	45	924	No Detect
19-SD-00055	4	1	11/18/2019	11/21/2019	252574	Valve	51	1071	No Detect
19-SD-00028	9	1	9/17/2019	9/19/2019	248875.1	Connector	15	1073	No Detect
19-SD-00055	1	1	10/17/2019	10/21/2019	252577	Valve	51	1073	No Detect
19-SD-00057	3	2	11/21/2019	11/26/2019	250968	Connector	16	1103	No Detect
19-SD-00057	4	2	11/21/2019	11/26/2019	250964	Connector	16	1254	No Detect
19-SD-00029	11	1	11/11/2019	11/21/2019	AVO 018950	Connector	18	1316	No Detect
19-SD-00028	17	1	11/18/2019	11/19/2019	249906	Valve	24	1320	No Detect
DRF-Pre			`		AVO 018732	Connector		1332	
19-SD-00035	2	2	8/29/2019	9/3/2019	252228	Valve	32	1341	No Detect
19-SD-00055	6	1	11/18/2019	11/21/2019	252555	Valve	51	1342	No Detect
19-SD-00028	12	1	10/11/2019	10/16/2019	248881	Connector	15	1371	No Detect
19-SD-00055	5	1	11/18/2019	11/21/2019	252602	Valve	42	1398	No Detect
19-SD-00029	2	1	8/6/2019	10/11/2019	Near 253317	Non LDAR	16	1607	No Detect
DRF-Pre			`		253329.1	Connector		1635	
DRF-Pre			`		AVO 018733	Connector		1842	
Leak ID #5	3	1	5/8/2019	5/9/2019	AVO 018744	Connector	15	1848	No Detect
19-SD-00050	3	2	10/15/2019	10/17/2019	252827	Valve	11	1903	No Detect
19-SD-00047	2	1	9/18/2019	9/24/2019	249354.1	Connector	17	2048	No Detect
19-SD-00028	13	1	10/22/2019	10/24/2019	248701	Connector	9	2050	No Detect
19-SD-00055	3	1	10/21/2019	11/5/2019	252682	Valve	42	2072	No Detect
19-SD-00028	11	1	10/11/2019	10/16/2019	248835	Pump	9	2109	No Detect
19-SD-00028	18	1	11/18/2019	11/21/2019	249883.1	Connector	24	3014	No Detect
19-SD-00028	1	1	8/6/2019	8/8/2019	253410.1	Connector	15	3020	No Detect

FHR CC m-Xylene
Process Unit
PSL Summary

Table C2-3. PSL summary table (2 of 2) for the LDSN/DRF pilot test in the FHR CC m-Xylene process unit from 5/1/2019 to 11/30 2019. "DRF-Pre" entries represent leak detected by LDSN prior to implementation of PSL ID system. Table is sorted by ascending DRF SV values.

LDSN PSL ID	PSL/DRF Investigation ID	Process Unit Level	DRF Date Found	Date Repaired	LDAR Component Tag	Type of component	≈ Dist. To LDSN Node (ft)	DRF SV (ppm)	OGI Detection Result
19-SD-00057	2	2	10/28/2019	11/6/2019	250735	Connector	6	3315	No Detect
19-SD-00028	6	1	8/29/2019	9/3/2019	249216.1	Connector	27	3555	No Detect
19-SD-00029	10	1	10/15/2019	10/17/2019	253195	Connector	26	3718	No Detect
19-SD-00035	3	2	8/29/2019	9/4/2019	252164.1	Connector	57	3861	No Detect
19-SD-00050	5	3	10/22/2019	11/5/2019	252945	Valve	34	4465	No Detect
19-SD-00028	10	1	10/1/2019	10/7/2019	248701	Other (Lid)	9	5590	No Detect
19-SD-00028	16	1	11/18/2019	11/21/2019	AVO 018951	Connector	10	8381	No Detect
Leak ID #5	1	1	5/8/2019	5/9/2019	AVO 018730	Connector	15	9776	Difficult Detect
19-SD-00028	8	1	9/17/2019	9/19/2019	248881	Connector	15	10285	No Detect
19-SD-00050	2	1	10/12/2019	10/17/2019	AVO 018787	Connector	5	10724	No Detect
19-SD-00035	5	1	10/11/2019	10/16/2019	252783	Connector	45	11416	Moderate Detect
19-SD-00029	7	1	8/26/2019	8/28/2019	253255.1	Connector	16	14383	No Detect
19-SD-00028	19	1	11/18/2019	11/21/2019	250012	Connector	25	15834	No Detect
19-SD-00050	4	3	10/15/2019	10/17/2019	252945	Valve	34	16733	Easy Detect
19-SD-00028	5	1	8/26/2019	8/28/2019	248720.1	Connector	9	17437	No Detect
19-SD-00050	1	3	10/1/2019	10/8/2019	AVO 018727	Connector	50.4	17988	Difficult Detect
19-SD-00057	1	2	10/28/2019	11/8/2019	AVO 018988	Connector	10	18850	No Detect
19-SD-00057	5	2	11/21/2019	11/26/2019	AVO 018990	Connector	15	19987	No Detect
19-SD-00047	5	1	10/28/2019	11/8/2019	249905	Connector	24	21031	No Detect
19-SD-00029	6	1	8/22/2019	8/23/2019	253343.2	Connector	15	21040	No Detect
19-SD-00008	1	3	6/13/2019	8/7/2019	252951	Valve	34	22797	Difficult Detect
19-SD-00054	1	1	10/16/2019	10/30/2019	252782	Valve	45	23820	Moderate Detect
19-SD-00055	2	1	10/17/2019	10/31/2019	252552	Valve	51	24102	No Detect
19-SD-00001	1	2	6/13/2019	10/22/2019	250735	Connector	6	28317	No Detect
19-SD-00047	4	1	10/22/2019	10/23/2019	Non LDAR	Non LDAR	5	30102	No Detect
19-SD-00035	4	1	9/25/2019	9/26/2019	252783	Connector	45	35690	No Detect
19-SD-00029	9	1	10/15/2019	10/17/2019	AVO 018741	Connector	20.6	38147	No Detect
19-SD-00029	4	1	8/15/2019	8/24/2019	252682	Valve	42	38878	No Detect
Leak ID #5	2	1	5/8/2019	5/9/2019	AVO 018721	Connector	15	48893	Difficult Detect
19-SD-00028	2	1	8/6/2019	8/6/2019	253399.1	OEL	15	50042	Moderate Detect
19-SD-00047	1	1	9/18/2019	9/24/2019	249331.1	Connector	17	66720	No Detect
19-SD-00028	3	1	8/15/2019	8/19/2019	253329.1	Connector	15	71744	No Detect
19-SD-00035	1	1	8/12/2019	8/13/2019	252766	Connector	45	72203	No Detect
DRF-Pre			`		AVO 018731	Connector		98000	Easy Detect
19-SD-00057	6	2	11/21/2019	11/25/2019	AVO 017056	Connector	10	100000	Easy Detect

FHR CC m-Xylene Process Unit

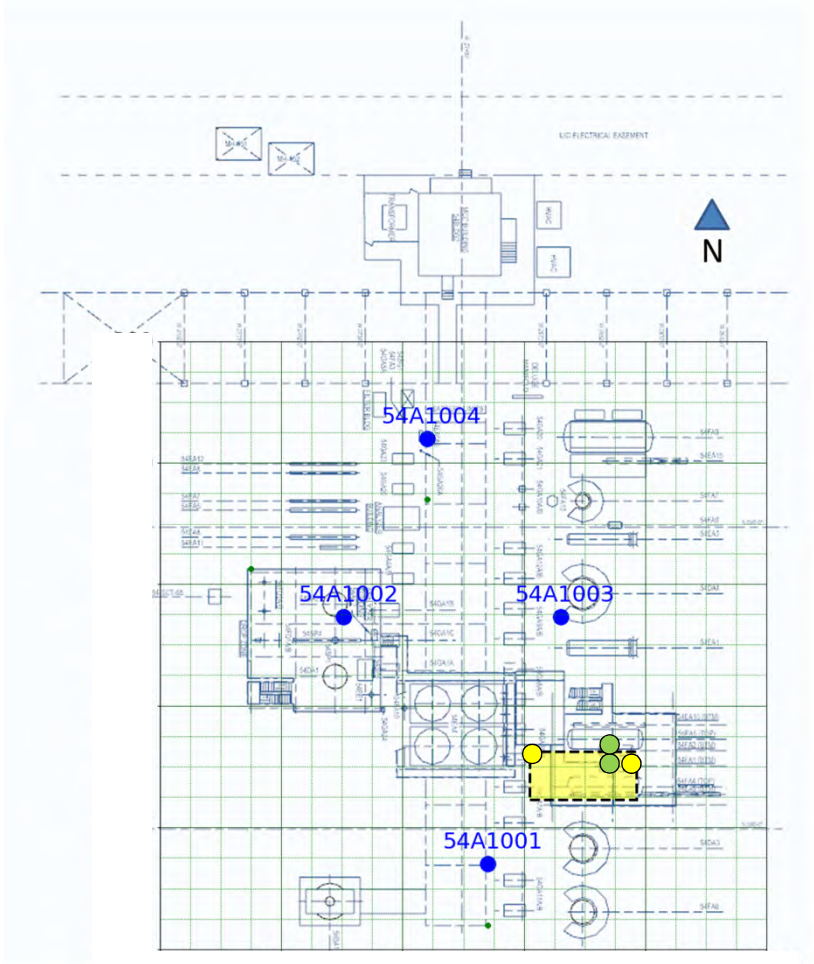

19-SD-00005
Created : 2019-06-06 19:00:00
Site/Unit : m-Xylene
Elevation Level: 1
Detection Category : 3

Leak size (ppm)

- > 50,000
- 5,000 – 50,000
- 1,000 – 5,000
- 500 – 1,000

Gas sensor

Cat. 2 PSL

Cat. 3 PSL

Scale : 10ft x10ft

Figure C2-19. m-Xylene PSL 19-SD-00005

FHR CC m-Xylene Process Unit

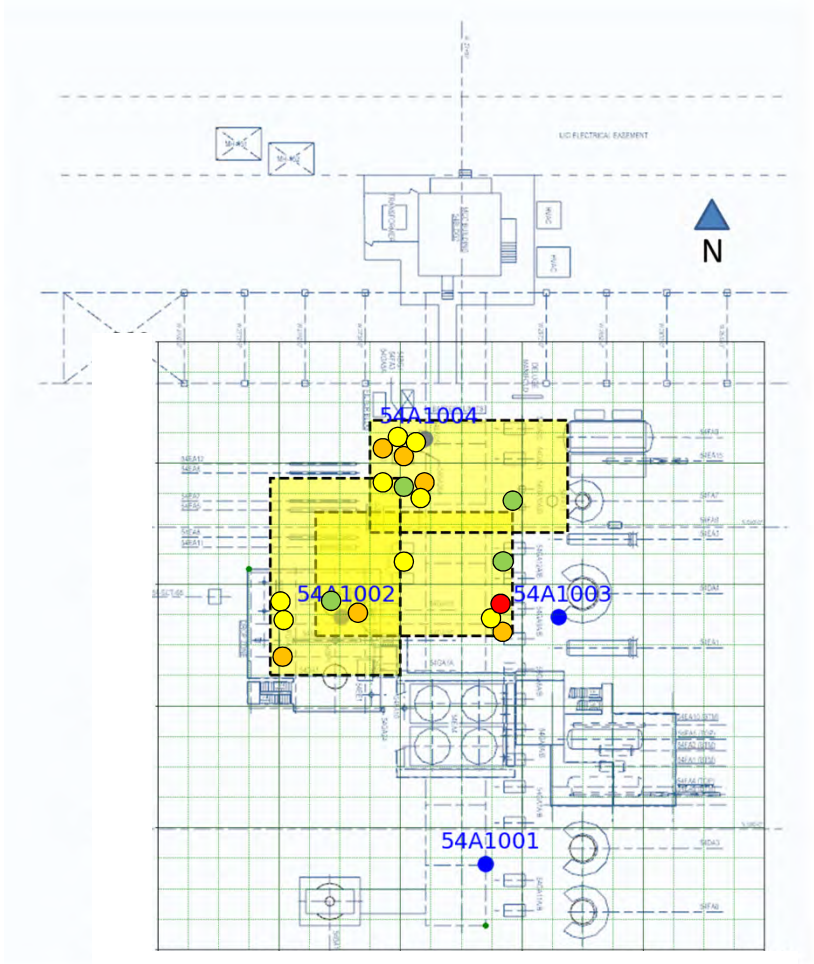

19-SD-00028
Created : 2019-07-27 19:00:00
Site/Unit : m-Xylene
Elevation Level: 1
Detection Category : 3

Leak size (ppm)

- > 50,000
- 5,000 – 50,000
- 1,000 – 5,000
- 500 – 1,000

Gas sensor

Cat. 2 PSL

Cat. 3 PSL

Scale : 10ft x10ft

Figure C2-20. m-Xylene PSL 19-SD-00028

FHR CC m-Xylene Process Unit

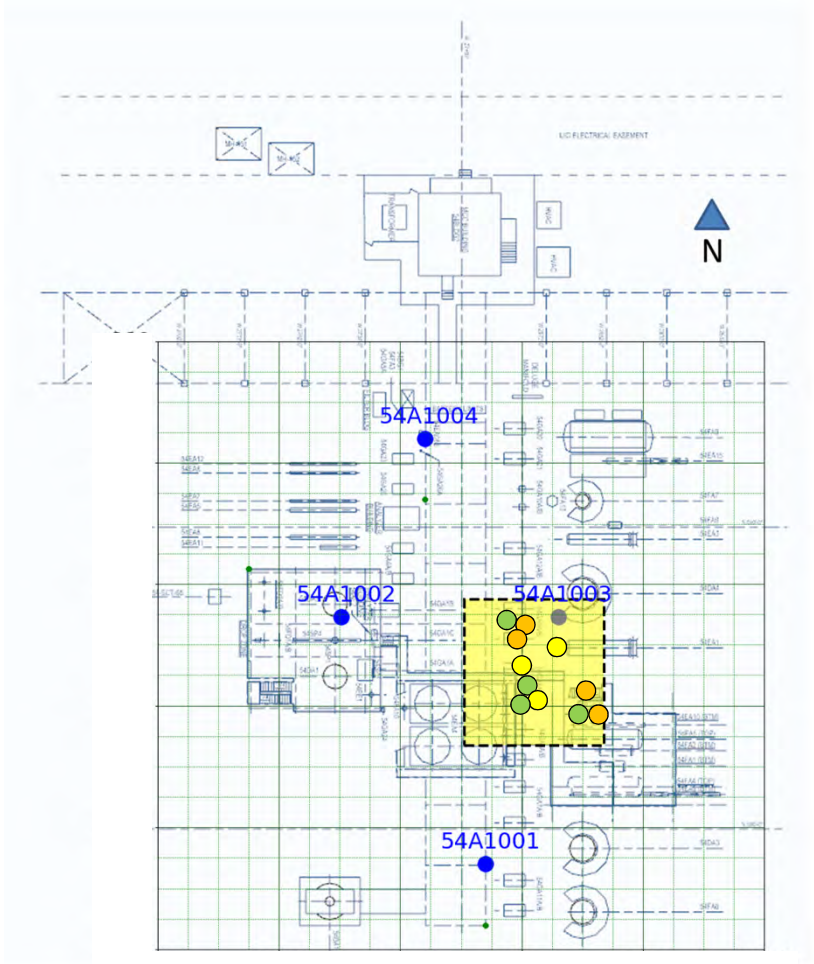

19-SD-00029
Created : 2019-08-05 19:00:00
Site/Unit : m-Xylene
Elevation Level: 1
Detection Category : 3

Leak size (ppm)

- > 50,000
- 5,000 – 50,000
- 1,000 – 5,000
- 500 – 1,000

Gas sensor

Cat. 2 PSL

Cat. 3 PSL

Scale : 10ft x10ft

Figure C2-21. m-Xylene PSL 19-SD-00029

FHR CC m-Xylene Process Unit

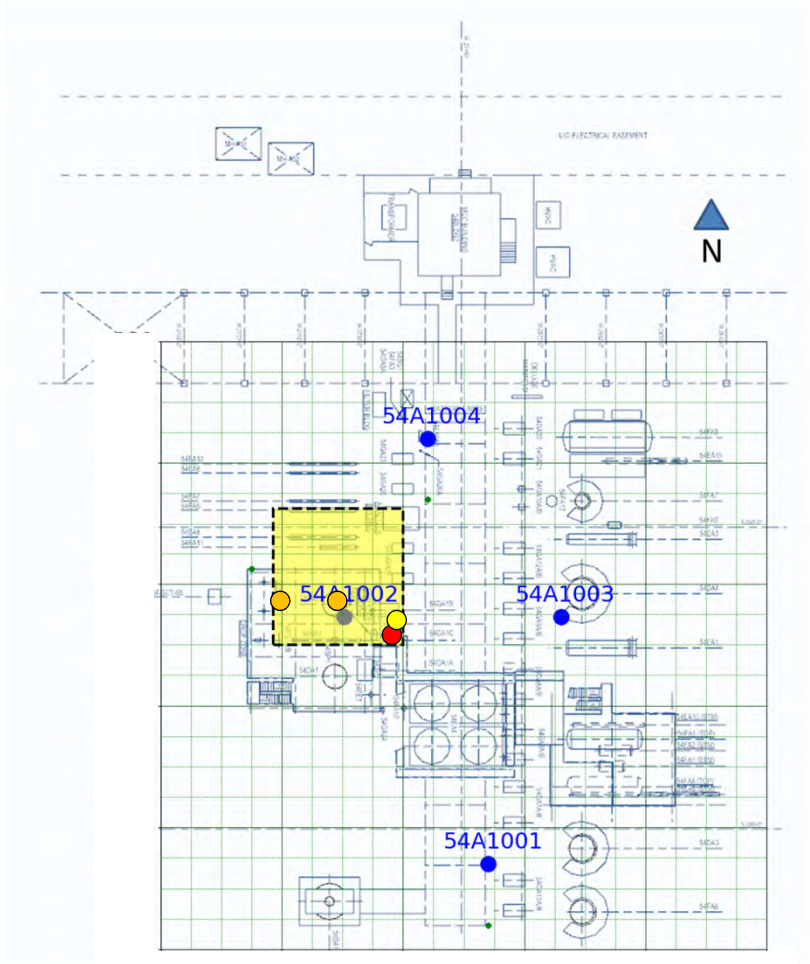

19-SD-00047
Created : 2019-09-17 19:00:00
Site/Unit : m-Xylene
Elevation Level: 1
Detection Category : 3

Leak size (ppm)

- > 50,000
- 5,000 – 50,000
- 1,000 – 5,000
- 500 – 1,000

Gas sensor

Cat. 2 PSL

Cat. 3 PSL

Scale : 10ft x10ft

Figure C2-22. m-Xylene PSL 19-SD-00047

FHR CC m-Xylene Process Unit

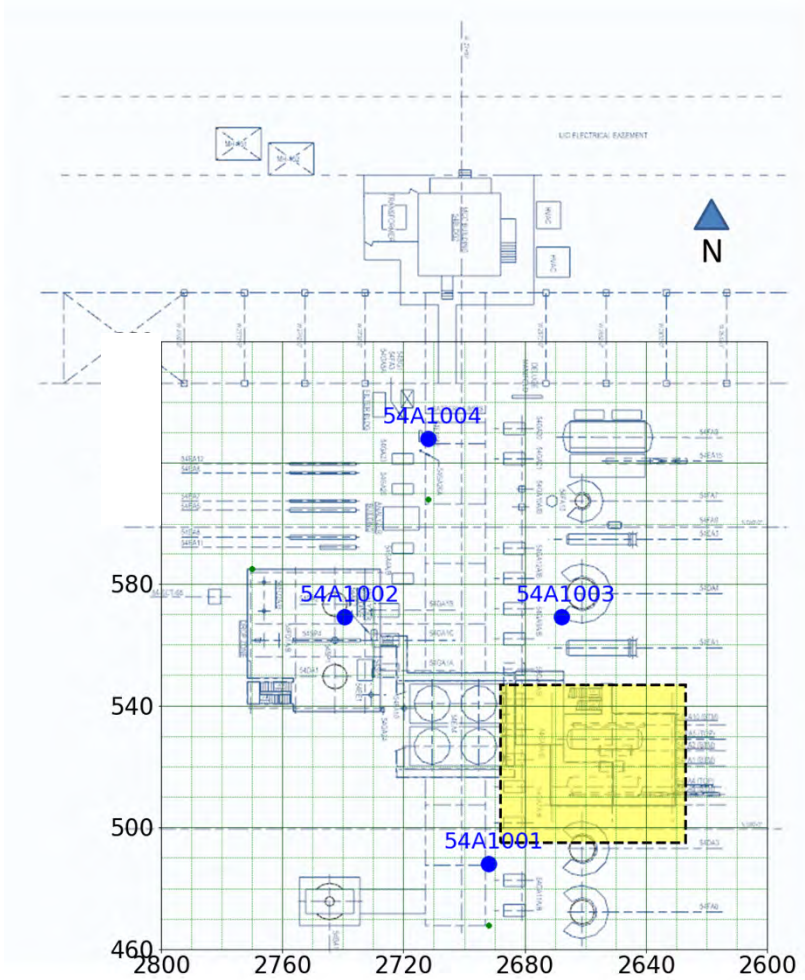

19-SD-00055
Created : 2019-10-16 19:00:00
Site/Unit : m-Xylene
Elevation Level: 1
Detection Category : 3

Leak size (ppm)

- > 50,000
- 5,000 – 50,000
- 1,000 – 5,000
- 500 – 1,000

Gas sensor

Cat. 2 PSL

Cat. 3 PSL

Scale : 10ft x10ft

Figure C2-23. m-Xylene PSL 19-SD-00055

FHR CC m-Xylene Process Unit

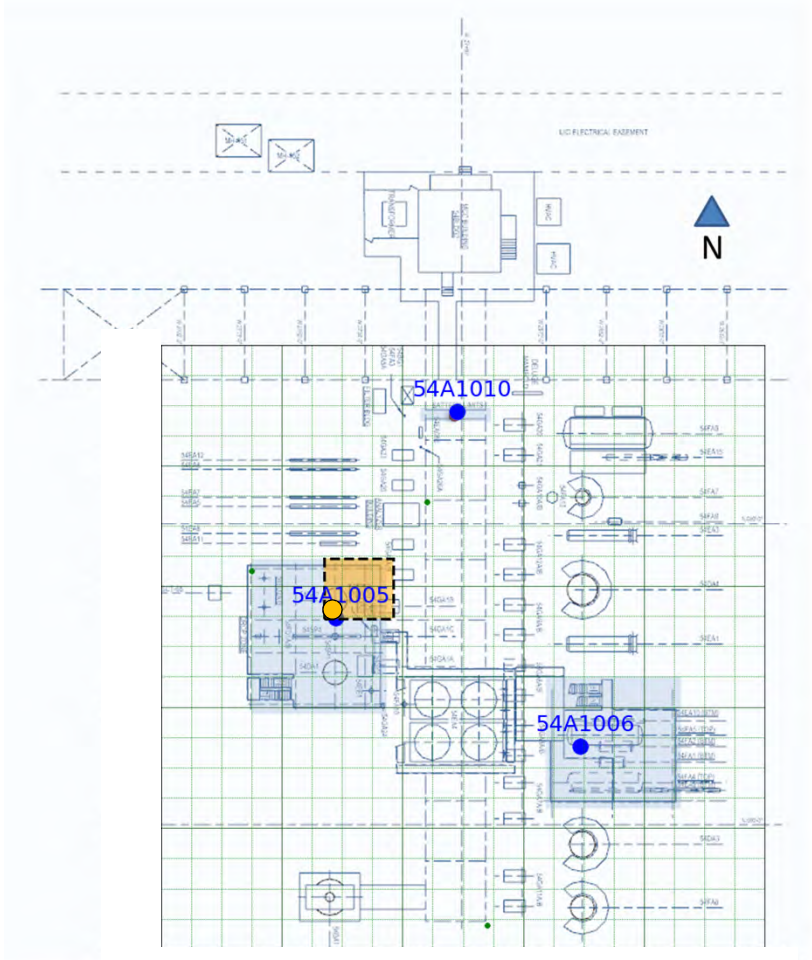

19-SD-00001
Created : 2019-06-05 19:00:00
Site/Unit : m-Xylene
Elevation Level: 2
Detection Category : 2

Leak size (ppm)

- > 50,000
- 5,000 – 50,000
- 1,000 – 5,000
- 500 – 1,000

Gas sensor

Cat. 2 PSL

Cat. 3 PSL

Scale : 10ft x10ft

Figure C2-24. m-Xylene PSL 19-SD-00001

FHR CC m-Xylene Process Unit

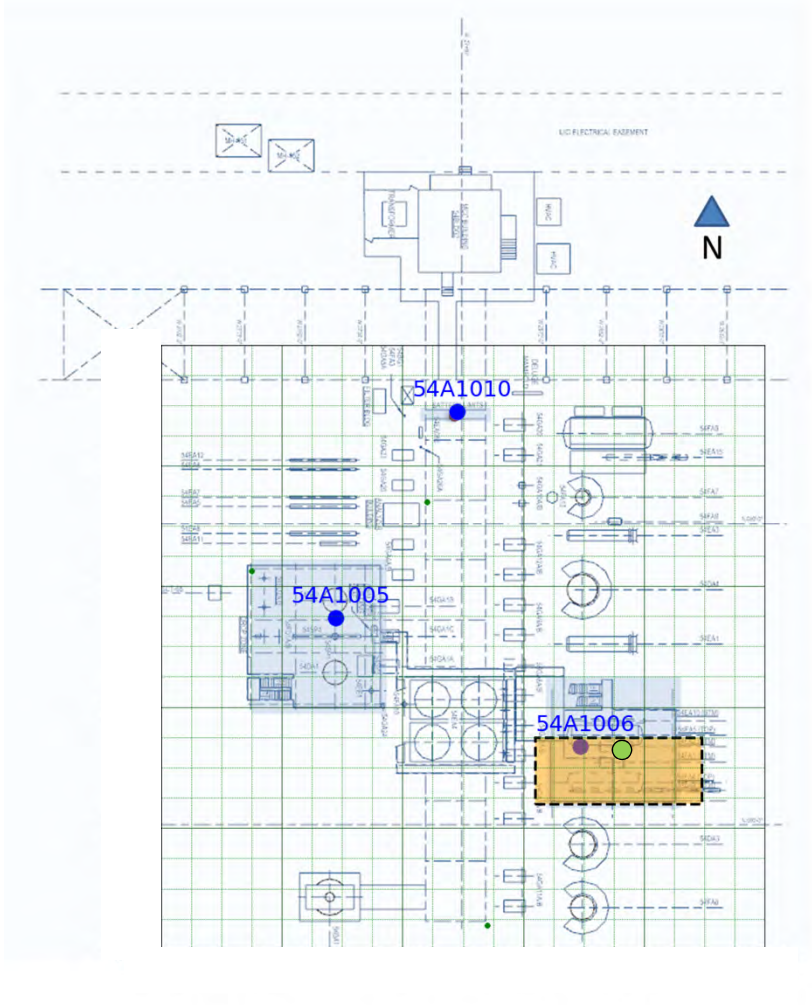

19-SD-00006
Created : 2019-06-06 19:00:00
Site/Unit : m-Xylene
Elevation Level: 2
Detection Category : 2

Leak size (ppm)

- > 50,000
- 5,000 – 50,000
- 1,000 – 5,000
- 500 – 1,000

Gas sensor

Cat. 2 PSL

Cat. 3 PSL

Scale : 10ft x10ft

Figure C2-25. m-Xylene PSL 19-SD-00006

FHR CC m-Xylene Process Unit

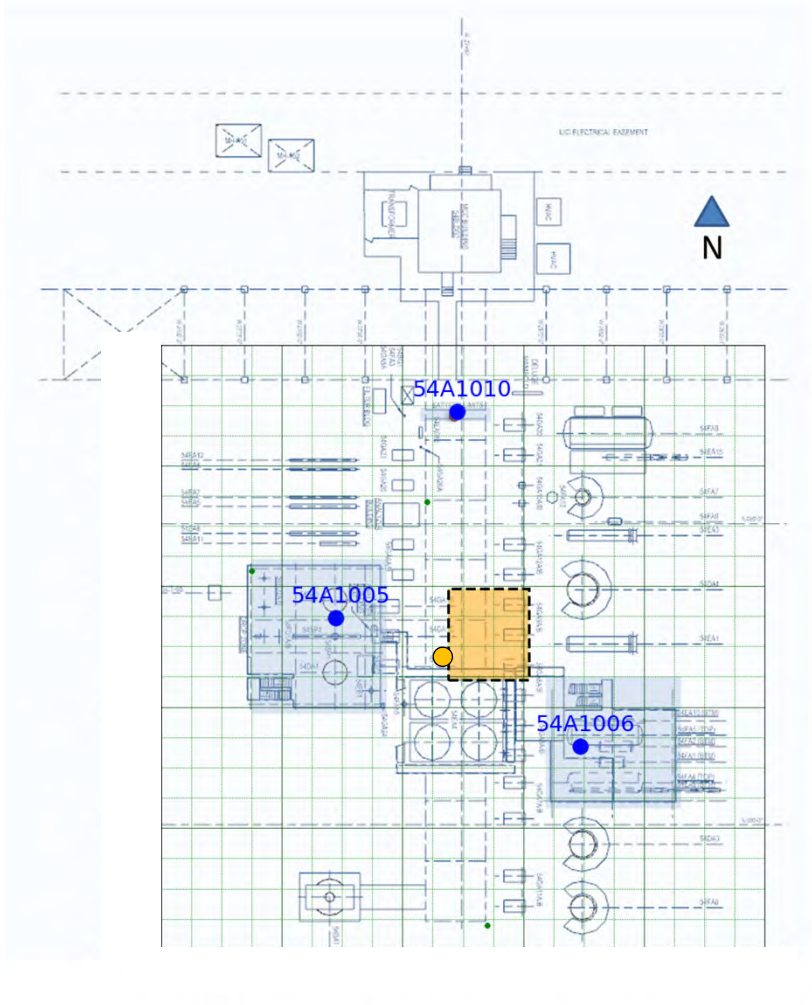

19-SD-00008
Created : 2019-06-07 19:00:00
Site/Unit : m-Xylene
Elevation Level: 2
Detection Category : 2

Leak size (ppm)

- > 50,000
- 5,000 – 50,000
- 1,000 – 5,000
- 500 – 1,000

Gas sensor

Cat. 2 PSL

Cat. 3 PSL

Scale : 10ft x10ft

Figure C2-26. m-Xylene PSL 19-SD-00008

FHR CC m-Xylene Process Unit

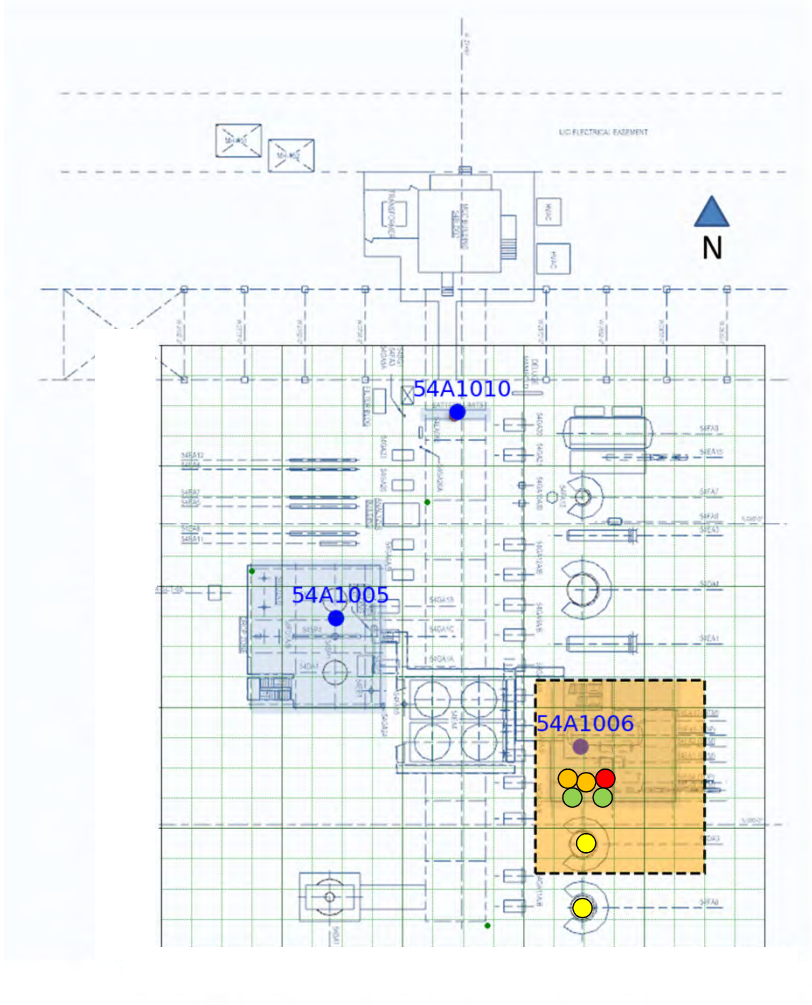

19-SD-00035
Created : 2019-08-08 19:00:00
Site/Unit : m-Xylene
Elevation Level: 2
Detection Category : 2

Leak size (ppm)

- > 50,000
- 5,000 – 50,000
- 1,000 – 5,000
- 500 – 1,000

Gas sensor

Cat. 2 PSL

Cat. 3 PSL

Scale : 10ft x10ft

Figure C2-27. m-Xylene PSL 19-SD-00009

FHR CC m-Xylene Process Unit

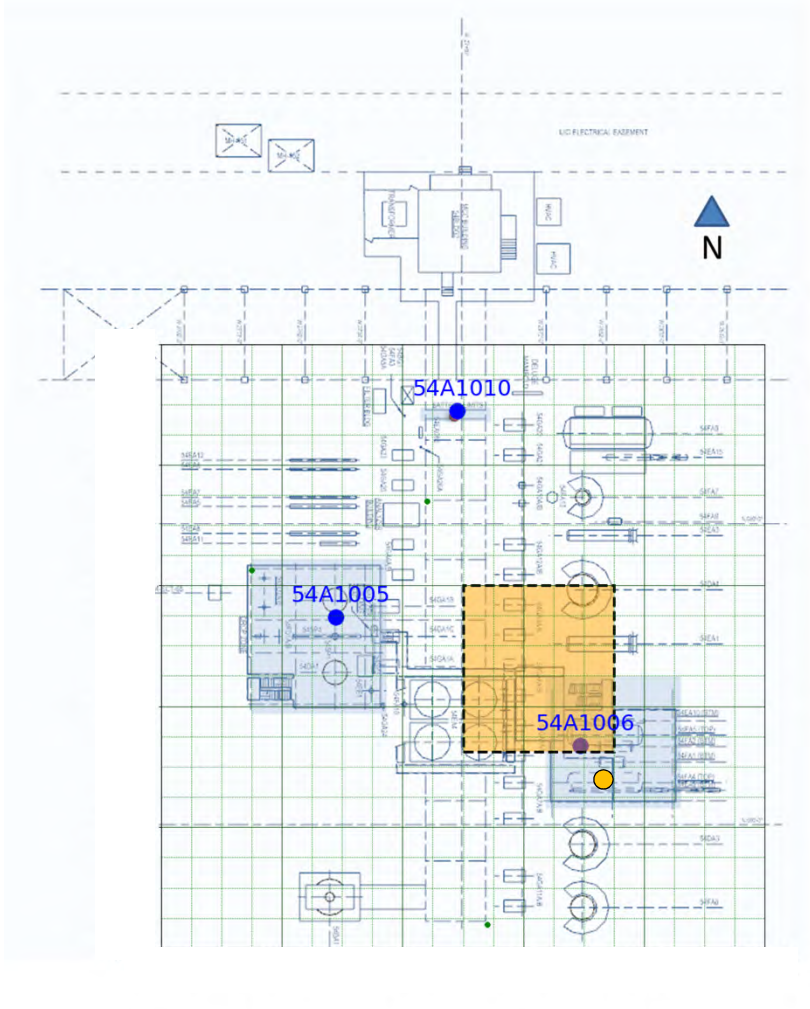

19-SD-00054
Created : 2019-10-15 19:00:00
Site/Unit : m-Xylene
Elevation Level: 2
Detection Category : 2

Leak size (ppm)

- > 50,000
- 5,000 – 50,000
- 1,000 – 5,000
- 500 – 1,000

Gas sensor

Cat. 2 PSL

Cat. 3 PSL

Scale : 10ft x10ft

Figure C2-28. m-Xylene PSL 19-SD-00054

FHR CC m-Xylene Process Unit

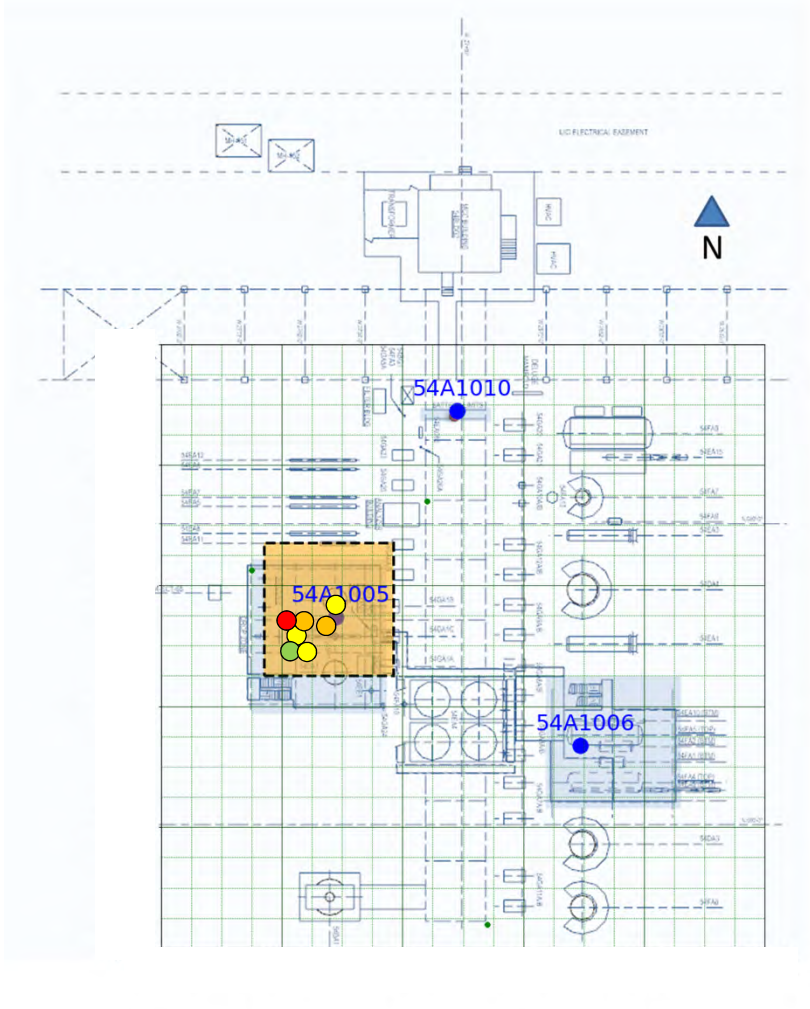

19-SD-00057
Created : 2019-10-25 19:00:00
Site/Unit : m-Xylene
Elevation Level: 2
Detection Category : 2

Leak size (ppm)

- > 50,000
- 5,000 – 50,000
- 1,000 – 5,000
- 500 – 1,000

Gas sensor

Cat. 2 PSL

Cat. 3 PSL

Scale : 10ft x10ft

Figure C2-29. m-Xylene PSL 19-SD-00057

FHR CC m-Xylene Process Unit

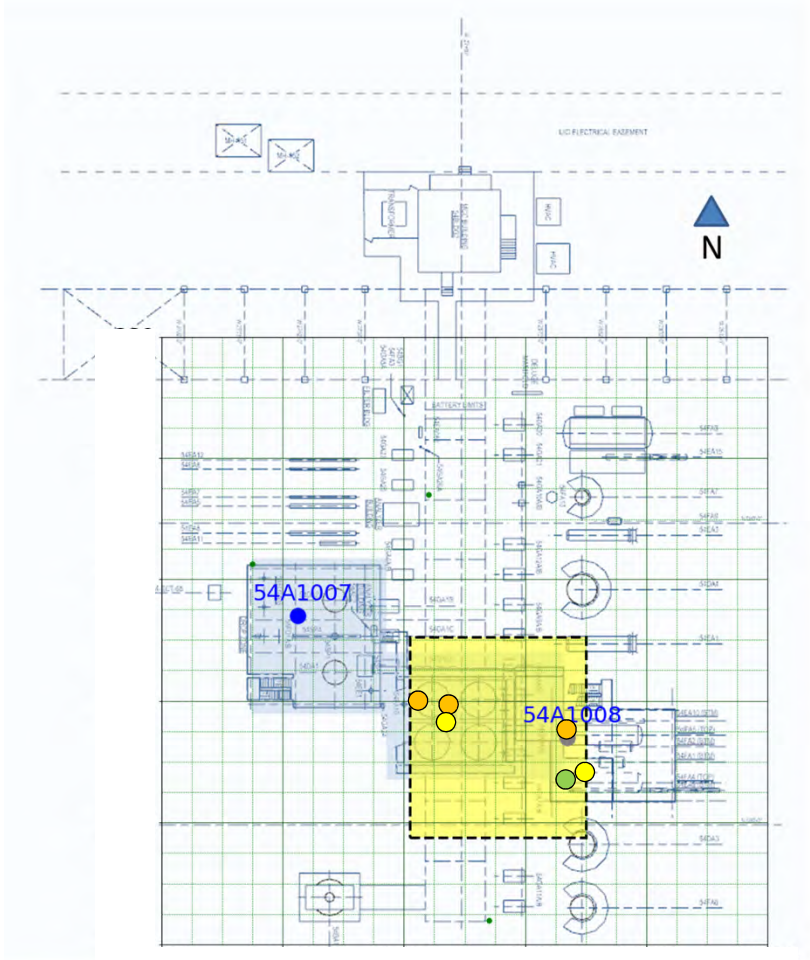

19-SD-00050
Created : 2019-09-26 19:00:00
Site/Unit : m-Xylene
Elevation Level: 3
Detection Category : 3

Leak size (ppm)

- > 50,000
- 5,000 – 50,000
- 1,000 – 5,000
- 500 – 1,000

Gas sensor

Cat. 2 PSL

Cat. 3 PSL

Scale : 10ft x10ft

Figure C2-30. m-Xylene PSL 19-SD-00050

FHR CC m-Xylene Process Unit

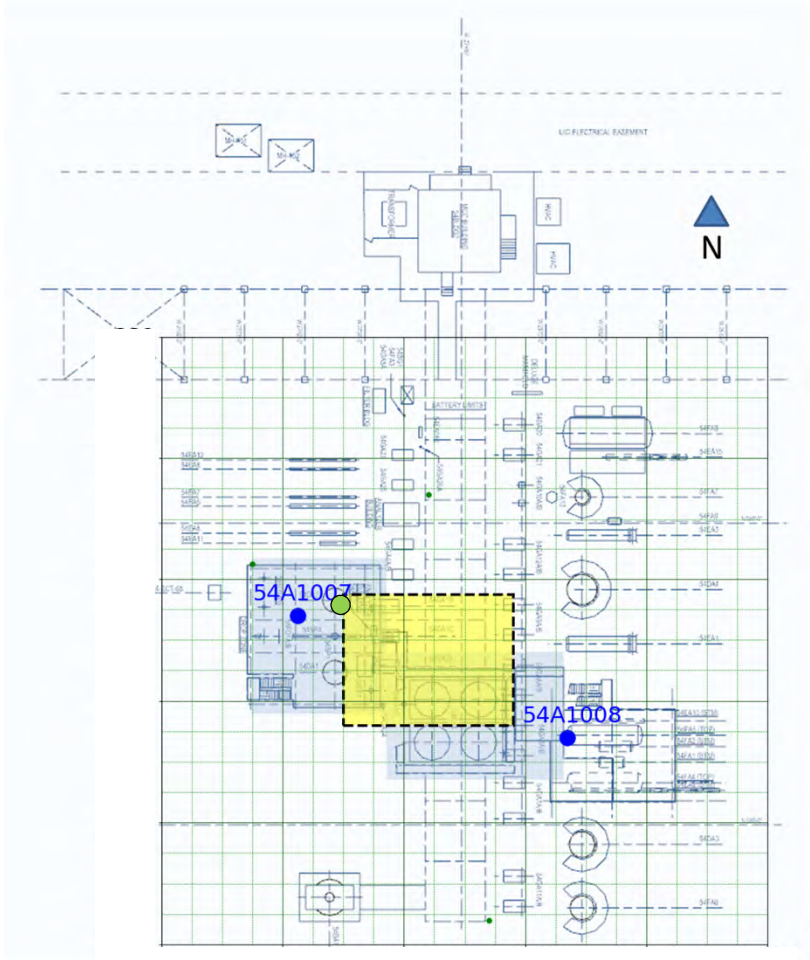

19-SD-00051
Created : 2019-09-26 19:00:00
Site/Unit : m-Xylene
Elevation Level: 3
Detection Category : 3

Leak size (ppm)

- > 50,000
- 5,000 – 50,000
- 1,000 – 5,000
- 500 – 1,000

Gas sensor

Cat. 2 PSL

Cat. 3 PSL

Scale : 10ft x10ft

Figure C2-31. m-Xylene PSL 19-SD-00051

Appendix C3
Revised LDSN Node Layouts for FHR CC

Appendix C3 presents an updated version of the sensor locations that will be used in the process units on an ongoing basis. In the case of Mid-Crude, this include six additional sensors that improve leak detection coverage based on pilot test results (described in report).

FHR CC Mid-Crude Process Unit (Level 1)

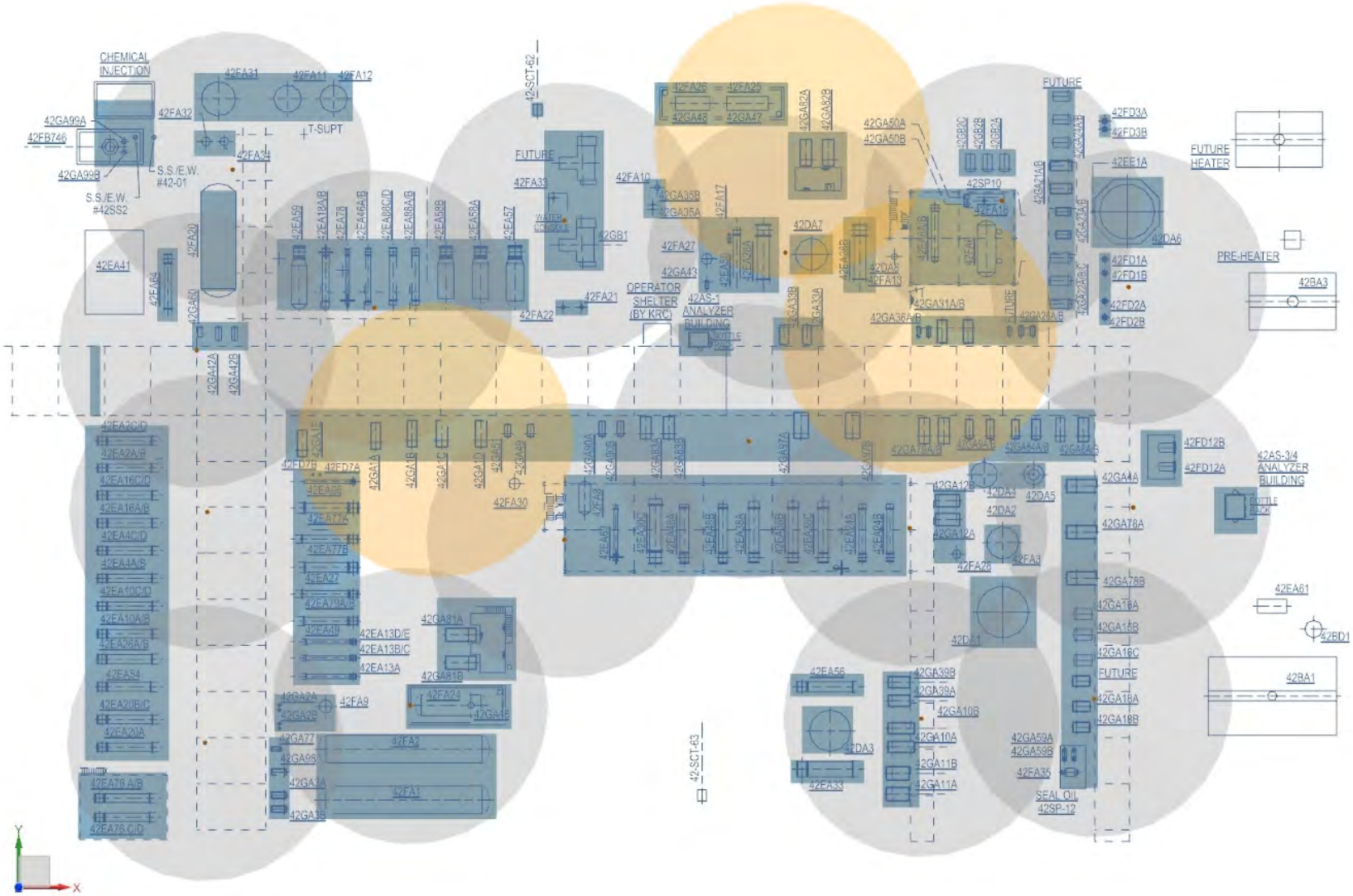

Figure C3-1. Mid-Crude sensor locations (level 1). The four added nodes are beige colored.

FHR CC Mid-Crude Process Unit (Level 2)

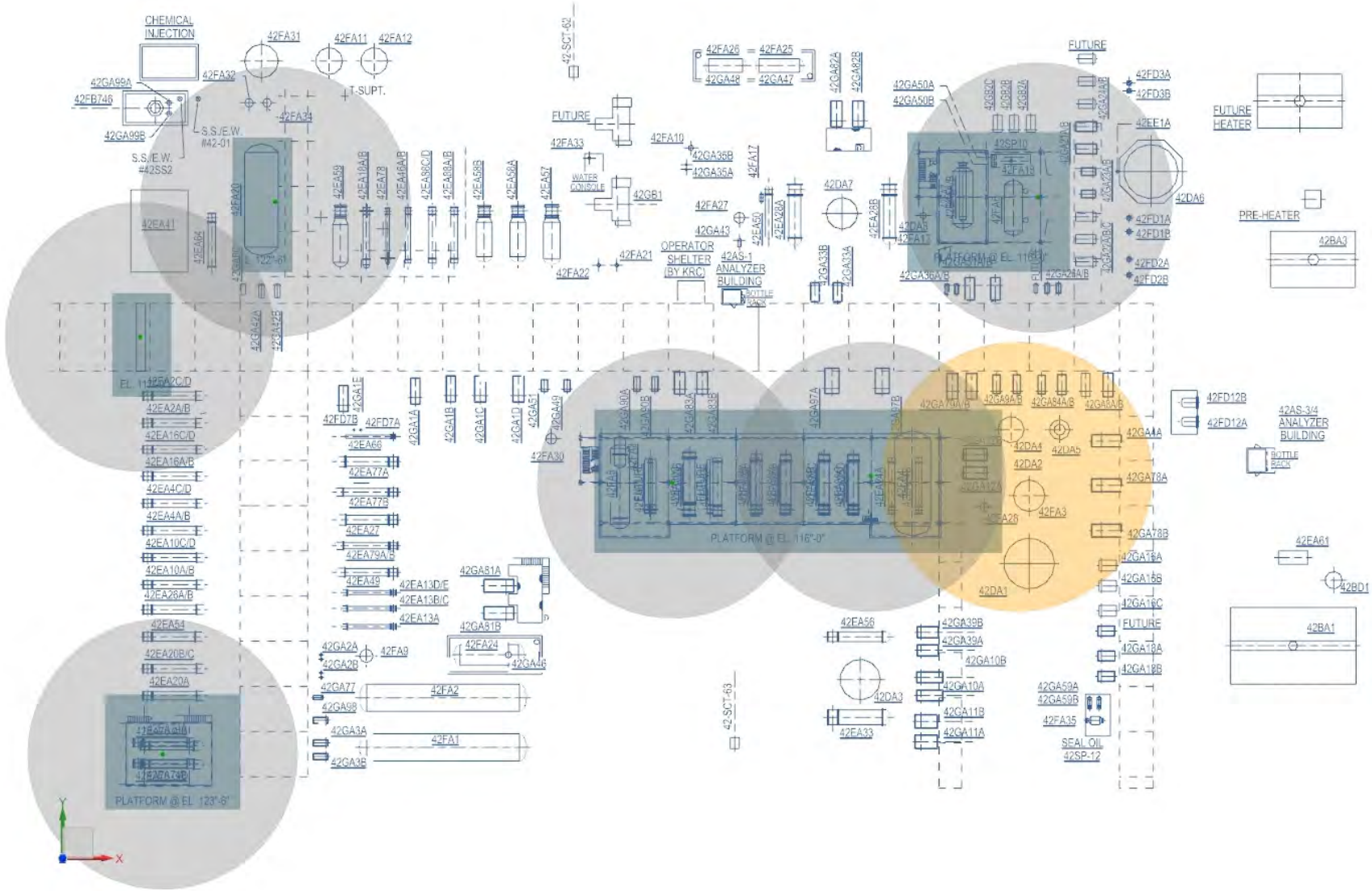

Figure C3-2. Mid-Crude sensor locations (level 2). The added node is beige colored.

FHR CC Mid-Crude Process Unit (Level 3)

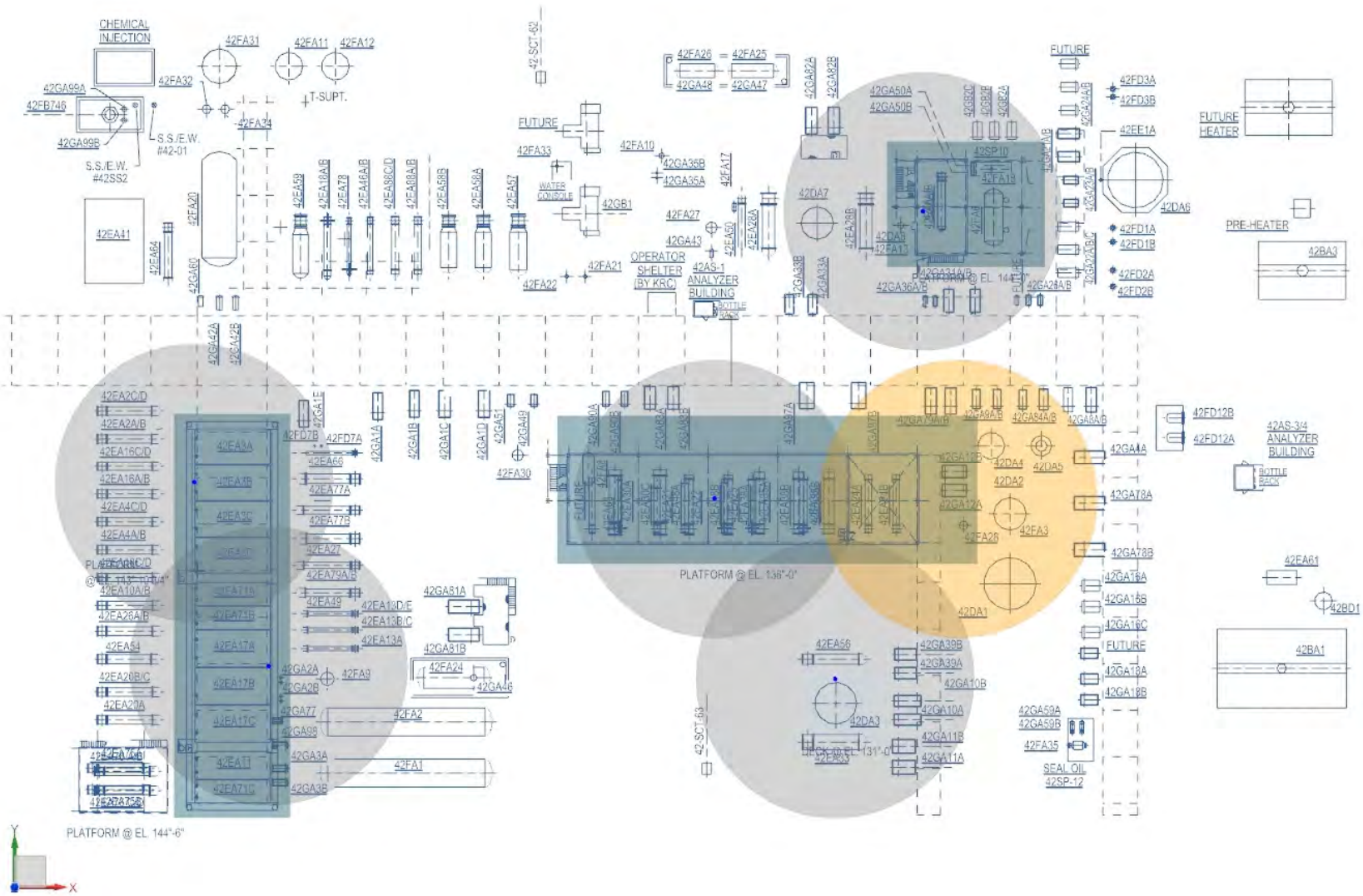

Figure C3-3. Mid-Crude sensor locations (level 3). The added node is beige colored.

FHR CC Mid-Crude Process Unit (Level 3)

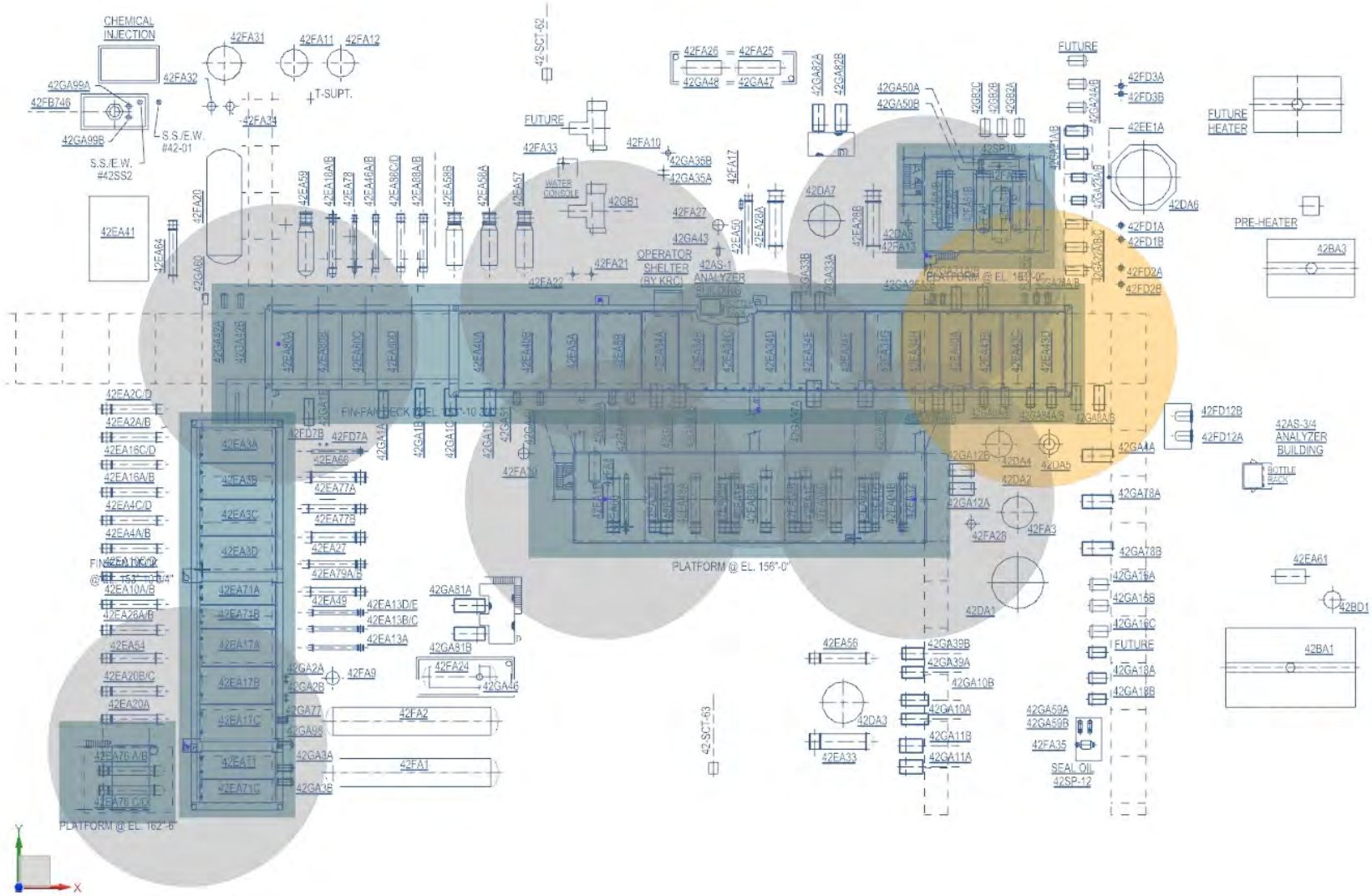

Figure C3-4. Mid-Crude sensor locations (level 4). The added node is beige colored.

FHR CC Mid-Crude Process Unit (Level 5)

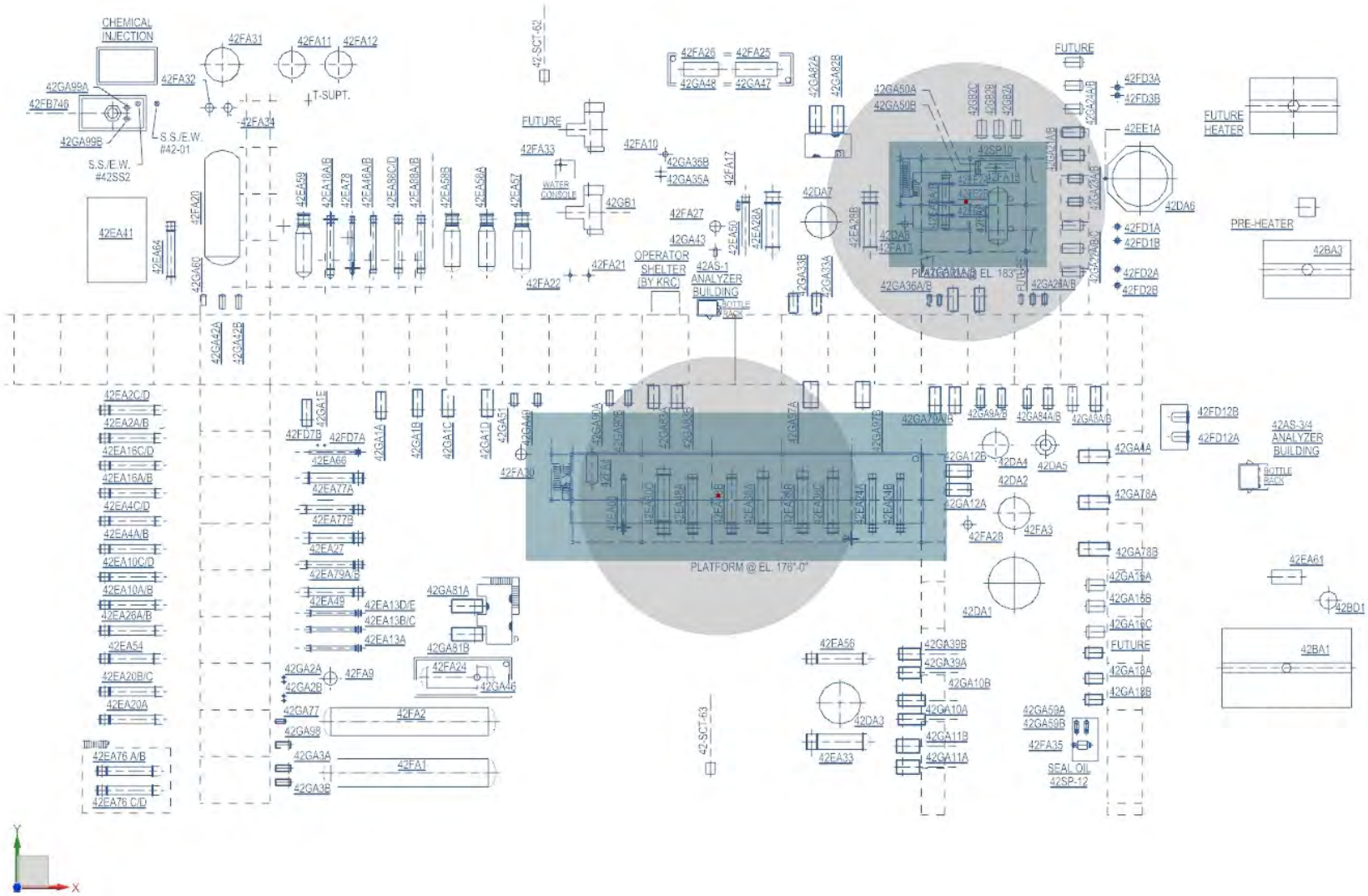

Figure C3-5. Mid-Crude sensor locations (level 5).

FHR CC Mid-Crude Process Unit (Level 6)

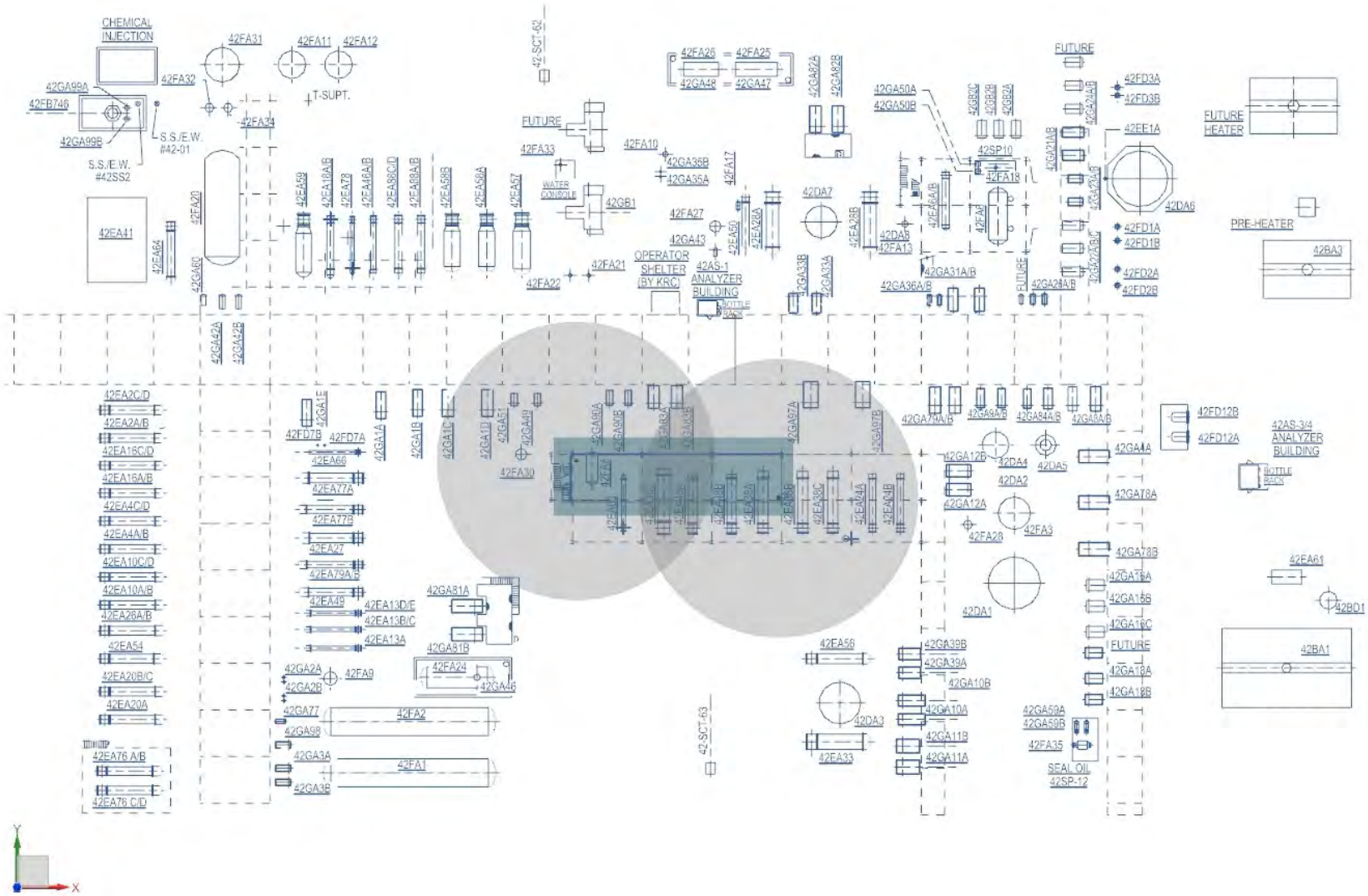

Figure C3-6. Mid-Crude sensor locations (level 6).

FHR CC m-Xylene Process Unit (Level 1)

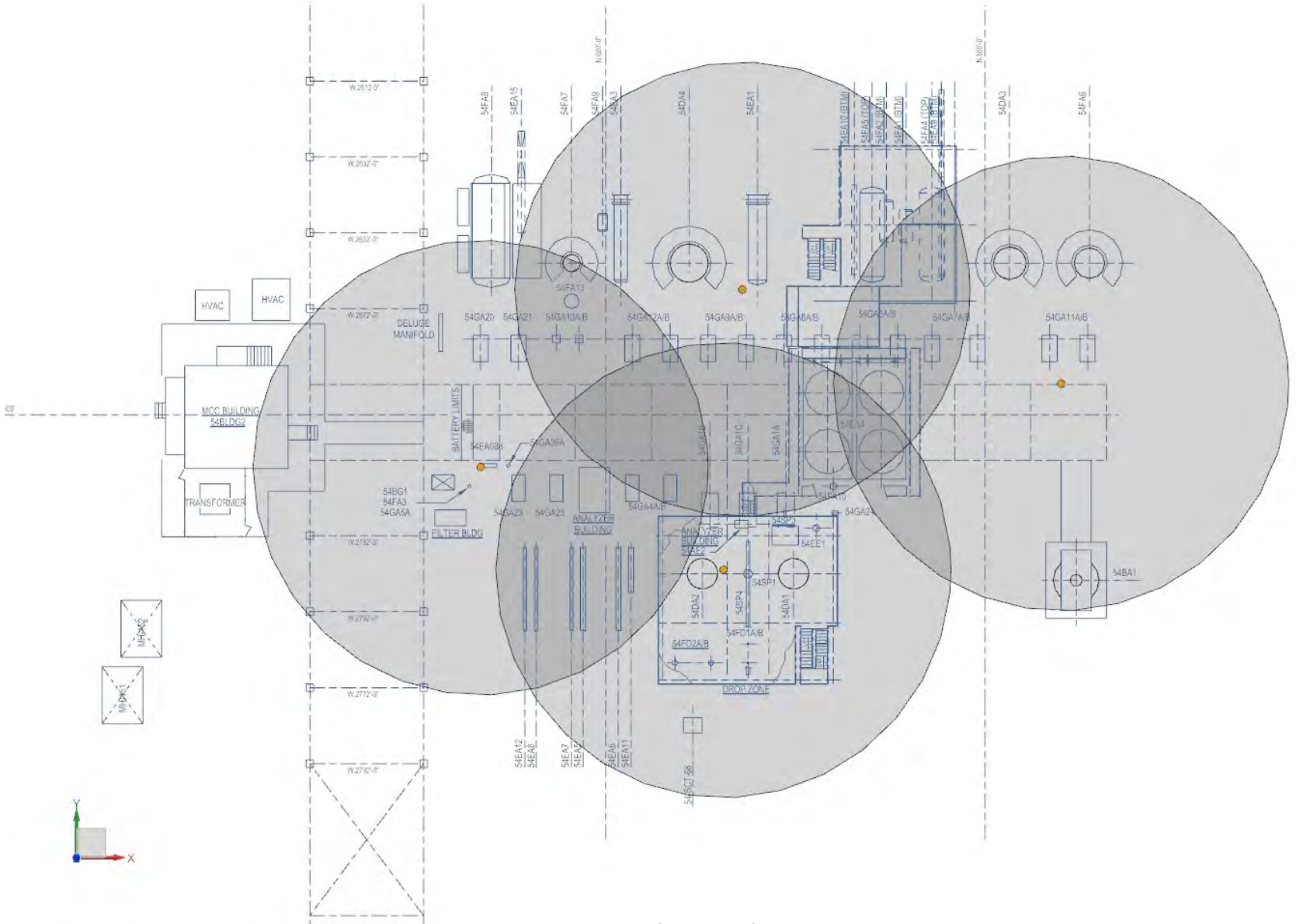

Figure C3-7. m-Xylene sensor locations (level 1).

FHR CC m-Xylene Process Unit (Level 2)

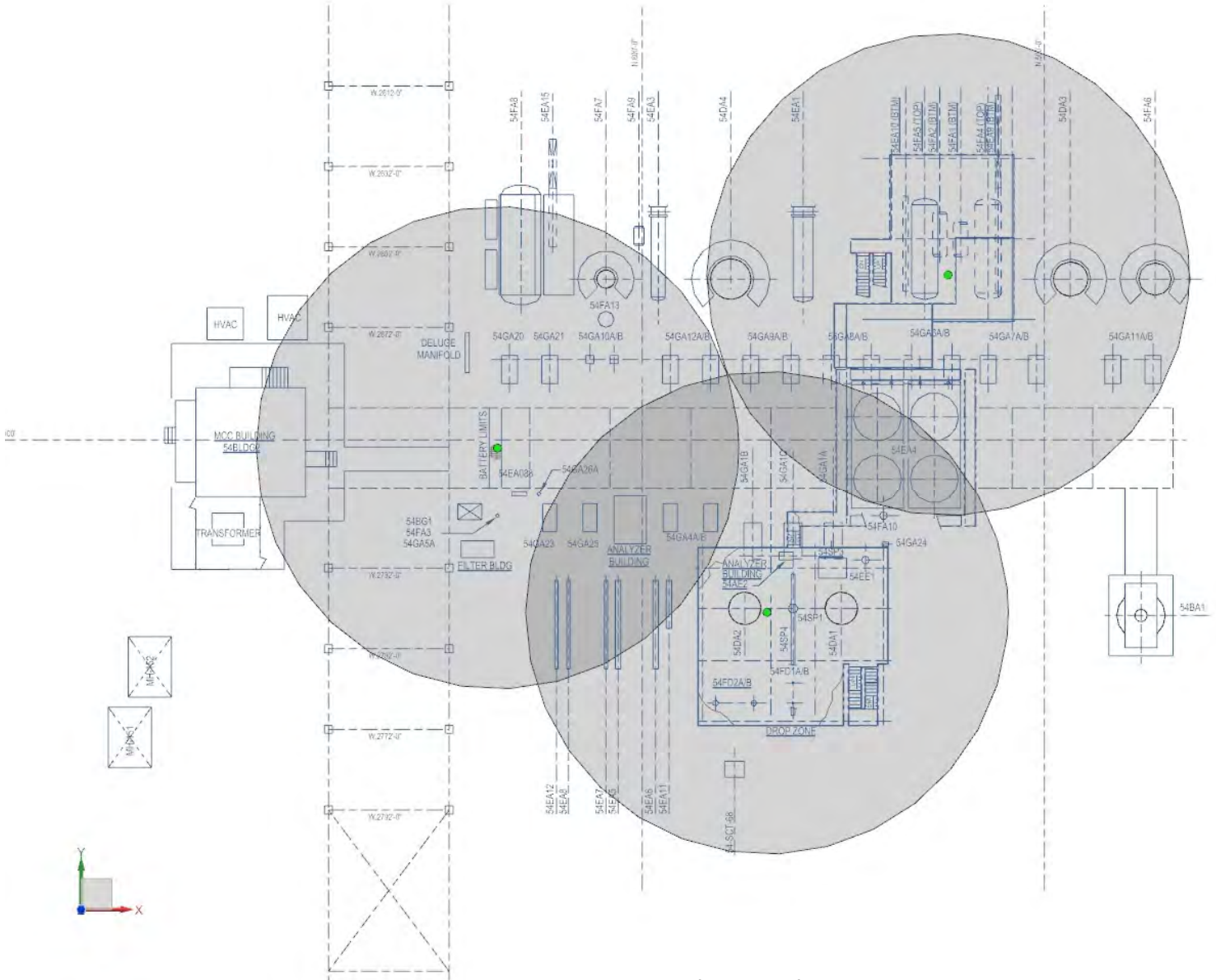

Figure C3-8. m-Xylene sensor locations (level 2).

FHR CC m-Xylene Process Unit (Level 3)

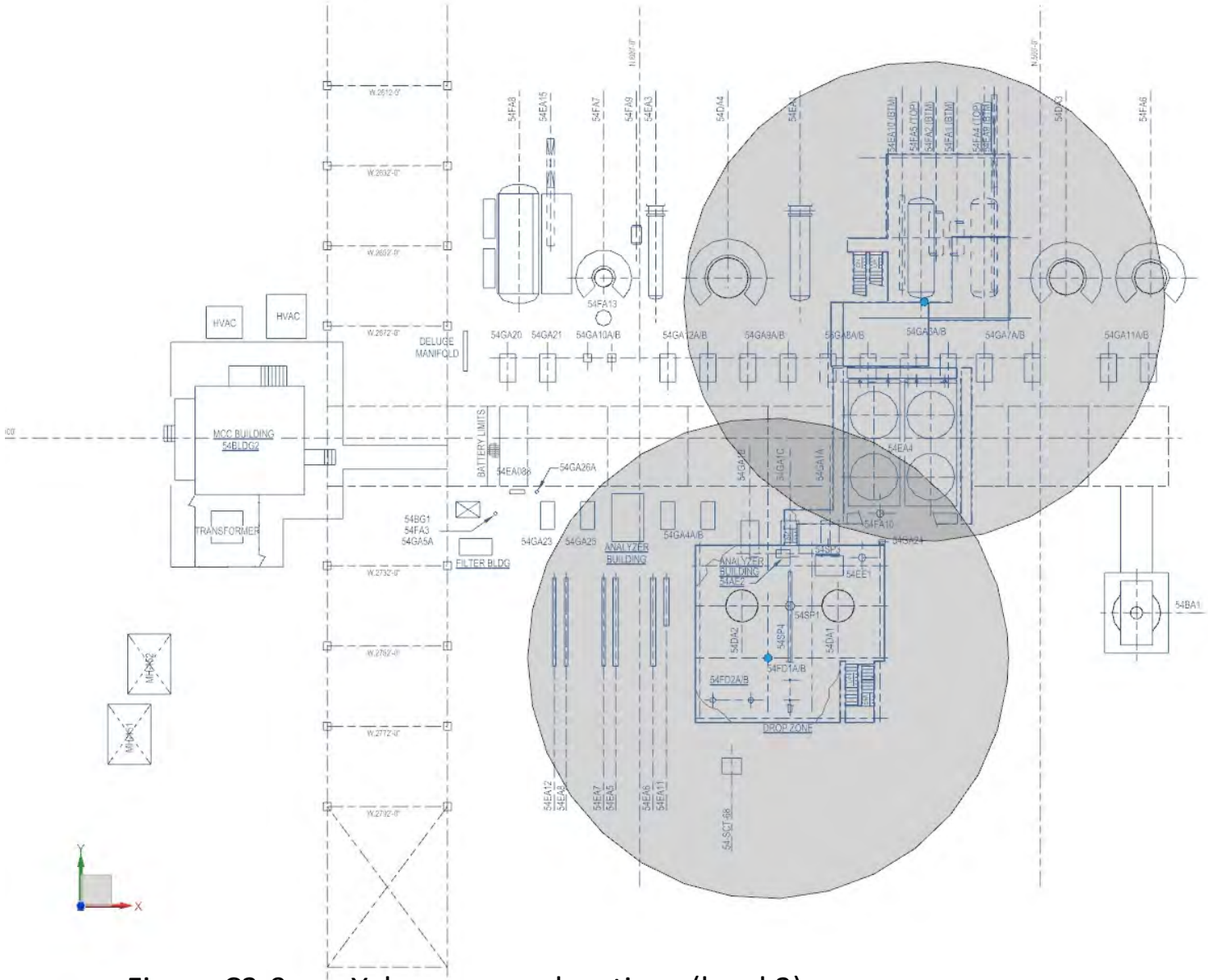

Figure C3-9. m-Xylene sensor locations (level 3).

FHR CC m-Xylene Process Unit (Level 4)

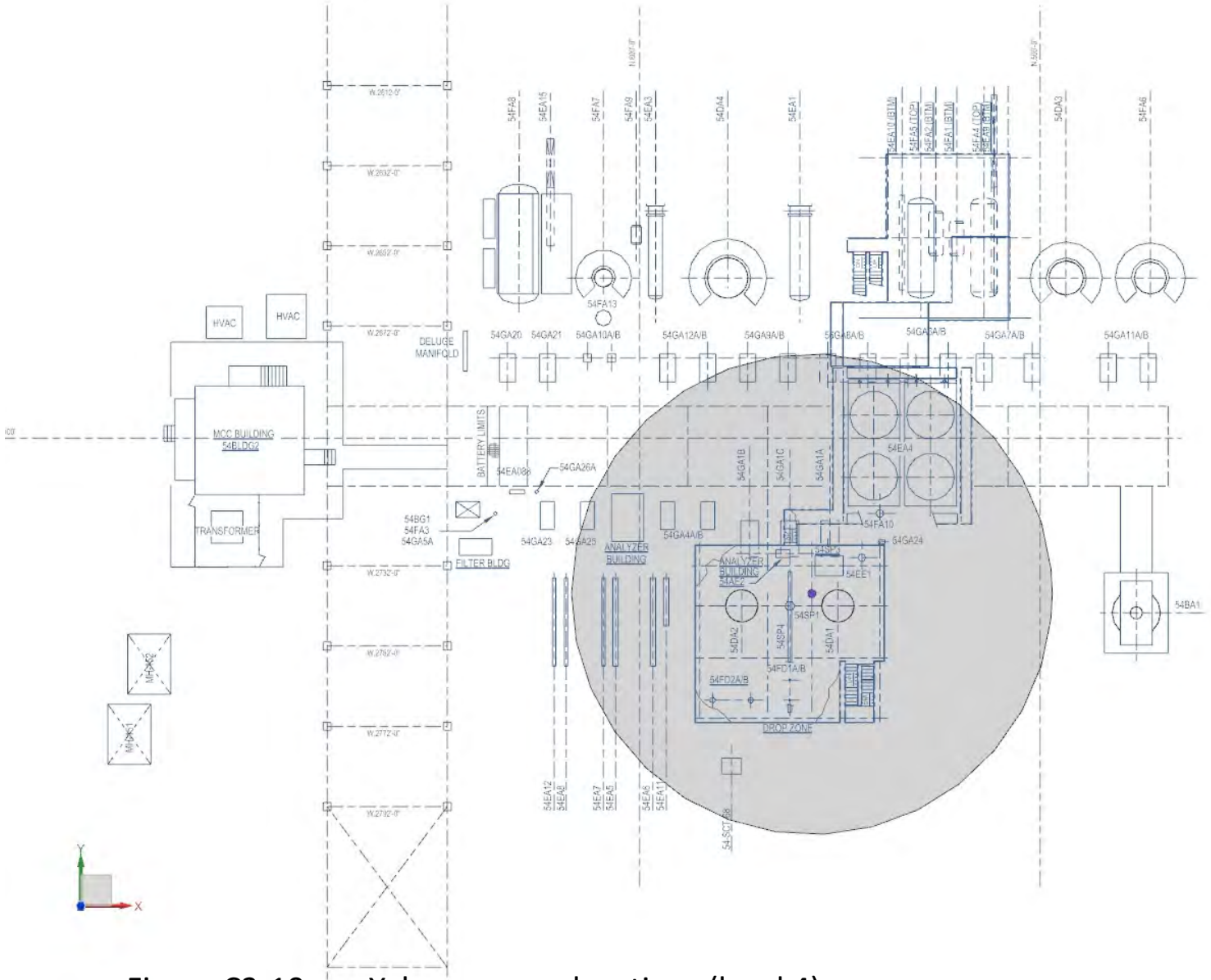

Figure C3-10. m-Xylene sensor locations (level 4).

Appendix D

Test Methods and Procedures

Appendix D1

EPA Method 21 Procedures

METHOD 21—DETERMINATION OF VOLATILE ORGANIC COMPOUND LEAKS

1.0 Scope and Application

1.1 Analytes.

Analyte	CAS No.
Volatile Organic Compounds (VOC)	No CAS number assigned.

1.2 Scope. This method is applicable for the determination of VOC leaks from process equipment. These sources include, but are not limited to, valves, flanges and other connections, pumps and compressors, pressure relief devices, process drains, open-ended valves, pump and compressor seal system degassing vents, accumulator vessel vents, agitator seals, and access door seals.

1.3 Data Quality Objectives. Adherence to the requirements of this method will enhance the quality of the data obtained from air pollutant sampling methods.

2.0 Summary of Method

2.1 A portable instrument is used to detect VOC leaks from individual sources. The instrument detector type is not specified, but it must meet the specifications and performance criteria contained in section 6.0. A leak definition concentration based on a reference compound is specified in each applicable regulation. This method is intended to locate and classify leaks only, and is not to be used as a direct measure of mass emission rate from individual sources.

3.0 Definitions

3.1 *Calibration gas* means the VOC compound used to adjust the instrument meter reading to a known value. The calibration gas is usually the reference compound at a known concentration approximately equal to the leak definition concentration.

3.2 *Calibration precision* means the degree of agreement between measurements of the same known value, expressed as the relative percentage of the average difference between the meter readings and the known concentration to the known concentration.

3.3 *Leak definition concentration* means the local VOC concentration at the surface of a leak source that indicates that a VOC emission (leak) is present. The leak definition is an instrument meter reading based on a reference compound.

3.4 *No detectable emission* means a local VOC concentration at the surface of a leak source, adjusted for local VOC ambient concentration, that is less than 2.5 percent of the specified leak definition concentration. that indicates that a VOC emission (leak) is not present.

3.5 *Reference compound* means the VOC species selected as the instrument calibration basis for specification of the leak definition concentration. (For example, if a leak definition concentration is 10,000 ppm as methane, then any source emission that results in a local concentration that yields a meter reading of 10,000 on an instrument meter calibrated with methane would be classified as a leak. In this example, the leak definition concentration is 10,000 ppm and the reference compound is methane.)

3.6 *Response factor* means the ratio of the known concentration of a VOC compound to the observed meter reading when measured using an instrument calibrated with the reference compound specified in the applicable regulation.

3.7 *Response time* means the time interval from a step change in VOC concentration at the input of the sampling system to the time at which 90 percent of the corresponding final value is reached as displayed on the instrument readout meter.

4.0 Interferences [Reserved]

5.0 Safety

5.1 Disclaimer. This method may involve hazardous materials, operations, and equipment. This test method may not address all of the safety problems associated with its use. It is the responsibility of the user of this test method to establish appropriate safety and health practices and determine the applicability of regulatory limitations prior to performing this test method.

5.2 Hazardous Pollutants. Several of the compounds, leaks of which may be determined by this method, may be irritating or corrosive to tissues (*e.g.,* heptane) or may be toxic (*e.g.,* benzene, methyl alcohol). Nearly all are fire hazards. Compounds in emissions should be determined through familiarity with the source. Appropriate precautions can be found in reference documents, such as reference No. 4 in section 16.0.

6.0 Equipment and Supplies

A VOC monitoring instrument meeting the following specifications is required:

6.1 The VOC instrument detector shall respond to the compounds being processed. Detector types that may meet this requirement include, but are not limited to, catalytic oxidation, flame ionization, infrared absorption, and photoionization.

6.2 The instrument shall be capable of measuring the leak definition concentration specified in the regulation.

6.3 The scale of the instrument meter shall be readable to ±2.5 percent of the specified leak definition concentration.

6.4 The instrument shall be equipped with an electrically driven pump to ensure that a sample is provided to the detector at a constant flow rate. The nominal sample flow rate, as measured at the sample probe tip, shall be 0.10 to 3.0 l/min (0.004 to 0.1 ft^3/min) when the probe is fitted with a glass wool plug or filter that may be used to prevent plugging of the instrument.

6.5 The instrument shall be equipped with a probe or probe extension or sampling not to exceed 6.4 mm (¼ in) in outside diameter, with a single end opening for admission of sample.

6.6 The instrument shall be intrinsically safe for operation in explosive atmospheres as defined by the National Electrical Code by the National Fire Prevention Association or other applicable regulatory code for operation in any explosive atmospheres that may be encountered in its use. The instrument shall, at a minimum, be intrinsically safe for Class 1, Division 1 conditions, and/or Class 2, Division 1 conditions, as appropriate, as defined by the example code. The instrument shall not be operated with any safety device, such as an exhaust flame arrestor, removed.

7.0 Reagents and Standards

7.1 Two gas mixtures are required for instrument calibration and performance evaluation:

7.1.1 Zero Gas. Air, less than 10 parts per million by volume (ppmv) VOC.

7.1.2 Calibration Gas. For each organic species that is to be measured during individual source surveys, obtain or prepare a known standard in air at a concentration approximately equal to the applicable leak definition specified in the regulation.

7.2 Cylinder Gases. If cylinder calibration gas mixtures are used, they must be analyzed and certified by the manufacturer to be within 2 percent accuracy, and a shelf life must be specified. Cylinder standards must be either reanalyzed or replaced at the end of the specified shelf life.

7.3 Prepared Gases. Calibration gases may be prepared by the user according to any accepted gaseous preparation procedure that will yield a mixture accurate to within 2 percent. Prepared standards must be replaced each day of use unless it is demonstrated that degradation does not occur during storage.

7.4 Mixtures with non-Reference Compound Gases. Calibrations may be performed using a compound other than the reference compound. In this case, a conversion factor must be determined for the alternative compound such that the resulting meter readings during source surveys can be converted to reference compound results.

8.0 Sample Collection, Preservation, Storage, and Transport

8.1 Instrument Performance Evaluation. Assemble and start up the instrument according to the manufacturer's instructions for recommended warmup period and preliminary adjustments.

8.1.1 Response Factor. A response factor must be determined for each compound that is to be measured, either by testing or from reference sources. The response factor tests are required before placing the analyzer into service, but do not have to be repeated at subsequent intervals.

8.1.1.1 Calibrate the instrument with the reference compound as specified in the applicable regulation. Introduce the calibration gas mixture to the analyzer and record the observed meter reading. Introduce zero gas until a stable reading is obtained. Make a total of three measurements by alternating between the calibration gas and zero gas. Calculate the response factor for each repetition and the average response factor.

8.1.1.2 The instrument response factors for each of the individual VOC to be measured shall be less than 10 unless otherwise specified in the applicable regulation. When no instrument is available that meets this specification when calibrated with the reference VOC specified in the applicable regulation, the available instrument may be calibrated with one of the VOC to be measured, or any other VOC, so long as the instrument then has a response factor of less than 10 for each of the individual VOC to be measured.

8.1.1.3 Alternatively, if response factors have been published for the compounds of interest for the instrument or detector type, the response factor determination is not required, and existing results may be referenced. Examples of published response factors for flame ionization and catalytic oxidation detectors are included in References 1-3 of section 17.0.

8.1.2 Calibration Precision. The calibration precision test must be completed prior to placing the analyzer into service and at subsequent 3-month intervals or at the next use, whichever is later.

8.1.2.1 Make a total of three measurements by alternately using zero gas and the specified calibration gas. Record the meter readings. Calculate the average algebraic difference between the meter readings and the known value. Divide this average difference by the known calibration value and multiply by 100 to express the resulting calibration precision as a percentage.

8.1.2.2 The calibration precision shall be equal to or less than 10 percent of the calibration gas value.

8.1.3 Response Time. The response time test is required before placing the instrument into service. If a modification to the sample pumping system or flow configuration is made that would change the response time, a new test is required before further use.

8.1.3.1 Introduce zero gas into the instrument sample probe. When the meter reading has stabilized, switch quickly to the specified calibration gas. After switching, measure the time required to attain 90 percent of the final stable reading. Perform this test sequence three times and record the results. Calculate the average response time.

8.1.3.2 The instrument response time shall be equal to or less than 30 seconds. The instrument pump, dilution probe (if any), sample probe, and probe filter that will be used during testing shall all be in place during the response time determination.

8.2 Instrument Calibration. Calibrate the VOC monitoring instrument according to section 10.0.

8.3 Individual Source Surveys.

8.3.1 Type I—Leak Definition Based on Concentration. Place the probe inlet at the surface of the component interface where leakage could occur. Move the probe along the interface periphery while observing the instrument readout. If an increased meter reading is observed, slowly sample the interface where leakage is indicated until the maximum meter reading is obtained. Leave the probe inlet at this maximum reading location for approximately two times the instrument response time. If the maximum observed meter reading is greater than the leak definition in the applicable regulation, record and report the results as specified in the regulation reporting requirements. Examples of the application of this general technique to specific equipment types are:

8.3.1.1 Valves. The most common source of leaks from valves is the seal between the stem and housing. Place the probe at the interface where the stem exits the packing gland and sample the stem circumference. Also, place the probe at the interface of the packing gland take-up flange seat and sample the periphery. In addition, survey valve housings of multipart assembly at the surface of all interfaces where a leak could occur.

8.3.1.2 Flanges and Other Connections. For welded flanges, place the probe at the outer edge of the flange-gasket interface and sample the circumference of the flange. Sample other types of nonpermanent joints (such as threaded connections) with a similar traverse.

8.3.1.3 Pumps and Compressors. Conduct a circumferential traverse at the outer surface of the pump or compressor shaft and seal interface. If the source is a rotating shaft, position the probe inlet within 1 cm of the shaft-seal interface for the survey. If the housing configuration prevents a complete traverse of the shaft periphery, sample all accessible portions. Sample all other joints on the pump or compressor housing where leakage could occur.

8.3.1.4 Pressure Relief Devices. The configuration of most pressure relief devices prevents sampling at the sealing seat interface. For those devices equipped with an enclosed extension, or horn, place the probe inlet at approximately the center of the exhaust area to the atmosphere.

8.3.1.5 Process Drains. For open drains, place the probe inlet at approximately the center of the area open to the atmosphere. For covered drains, place the probe at the surface of the cover interface and conduct a peripheral traverse.

8.3.1.6 Open-ended Lines or Valves. Place the probe inlet at approximately the center of the opening to the atmosphere.

8.3.1.7 Seal System Degassing Vents and Accumulator Vents. Place the probe inlet at approximately the center of the opening to the atmosphere.

8.3.1.8 Access door seals. Place the probe inlet at the surface of the door seal interface and conduct a peripheral traverse.

8.3.2 Type II—"No Detectable Emission". Determine the local ambient VOC concentration around the source by moving the probe randomly upwind and downwind at a distance of one to two meters from the source. If an interference exists with this determination due to a nearby emission or leak, the local ambient concentration may be determined at distances closer to the source, but in no case shall the distance be less than 25 centimeters. Then move the probe inlet to the surface of the source and determine the concentration as outlined in section 8.3.1. The difference between these concentrations determines whether there are no detectable emissions. Record and report the results as specified by the regulation. For those cases where the regulation requires a specific device installation, or that specified vents be ducted or piped to a control device, the existence of these conditions shall be visually confirmed. When the regulation also requires that no detectable emissions exist, visual observations and sampling surveys are required. Examples of this technique are:

8.3.2.1 Pump or Compressor Seals. If applicable, determine the type of shaft seal. Perform a survey of the local area ambient VOC concentration and determine if detectable emissions exist as described in section 8.3.2.

8.3.2.2 Seal System Degassing Vents, Accumulator Vessel Vents, Pressure Relief Devices. If applicable, observe whether or not the applicable ducting or piping exists. Also, determine if any sources exist in the ducting or piping where emissions could occur upstream of the control device. If the required ducting or piping exists and there are no sources where the emissions could be vented to the atmosphere upstream of the control device, then it is presumed that no detectable emissions are present. If there are sources in the ducting or piping where emissions could be vented or sources where leaks could occur, the sampling surveys described in section 8.3.2 shall be used to determine if detectable emissions exist.

8.3.3 Alternative Screening Procedure.

8.3.3.1 A screening procedure based on the formation of bubbles in a soap solution that is sprayed on a potential leak source may be used for those sources that do not have continuously moving parts, that do not have surface temperatures greater than the boiling point or less than the freezing point of the soap solution, that do not have open areas to the atmosphere that the soap solution cannot bridge, or that do not exhibit evidence of liquid leakage. Sources that have these conditions present must be surveyed using the instrument technique of section 8.3.1 or 8.3.2.

8.3.3.2 Spray a soap solution over all potential leak sources. The soap solution may be a commercially available leak detection solution or may be prepared using concentrated detergent and water. A pressure sprayer or squeeze bottle may be used to dispense the solution. Observe the potential leak sites to determine if any bubbles are formed. If no bubbles are observed, the source is presumed to have no detectable emissions or leaks as applicable. If any bubbles are observed, the instrument techniques of section 8.3.1 or 8.3.2 shall be used to determine if a leak exists, or if the source has detectable emissions, as applicable.

9.0 Quality Control

Section	Quality control measure	Effect
8.1.2	Instrument calibration precision check	Ensure precision and accuracy, respectively, of instrument response to standard.
10.0	Instrument calibration	

10.0 Calibration and Standardization

10.1 Calibrate the VOC monitoring instrument as follows. After the appropriate warmup period and zero internal calibration procedure, introduce the calibration gas into the instrument sample probe. Adjust the instrument meter readout to correspond to the calibration gas value.

NOTE: If the meter readout cannot be adjusted to the proper value, a malfunction of the analyzer is indicated and corrective actions are necessary before use.

11.0 Analytical Procedures [Reserved]

12.0 Data Analyses and Calculations [Reserved]

13.0 Method Performance [Reserved]

14.0 Pollution Prevention [Reserved]

15.0 Waste Management [Reserved]

16.0 References

1. Dubose, D.A., and G.E. Harris. Response Factors of VOC Analyzers at a Meter Reading of 10,000 ppmv for Selected Organic Compounds. U.S. Environmental Protection Agency, Research Triangle Park, NC. Publication No. EPA 600/2-81051. September 1981.

2. Brown, G.E., *et al.* Response Factors of VOC Analyzers Calibrated with Methane for Selected Organic Compounds. U.S. Environmental Protection Agency, Research Triangle Park, NC. Publication No. EPA 600/2-81-022. May 1981.

3. DuBose, D.A. *et al.* Response of Portable VOC Analyzers to Chemical Mixtures. U.S. Environmental Protection Agency, Research Triangle Park, NC. Publication No. EPA 600/2-81-110. September 1981.

4. Handbook of Hazardous Materials: Fire, Safety, Health. Alliance of American Insurers. Schaumberg, IL. 1983.

17.0 Tables, Diagrams, Flowcharts, and Validation Data [Reserved]

Appendix D2

FHR TVA 1000-B FID Calibration Procedure

The following procedure refers to the model TVA-1000B (Thermo Fisher Scientific, Waltham MA, USA) flame ionization detector (FID) typically used for EPA Method 21 (M21) Leak Detection and Repair (LDAR) inspections in Flint Hills Resources (FHR) facilities. This procedure also applies to alternate EPA Method 21 FID systems. For example, this procedure is used for the model Phx42™, manufactured by LDARtools (Dickinson, TX, USA), discussed in Appendix D3. The TVA-1000-B FID was the M21 instrument used for the exploratory tests (Appendix A), the SLOF tests (Appendix B), and in generation of historical LDAR data discussed in this report. The Phx42™ was the predominate M21 instrument used in the 2019 FHR CC Pilot tests. At the end of this procedure, a typical example of an instrument calibration record set is provided.

Environmental Policy/Procedure Manual
Issued: December 2001
Revision Date: January 27, 2015
Revision No: 1
Last Reviewed: September 25, 2014

I. Purpose

The purpose of this procedure is to outline the necessary steps for performing the daily calibration and drift test on the TVA 1000-B analyzer.

II. Scope

This procedure is to be used by all LDAR Environmental Monitoring Technicians.

III. Pre-requisites

1. Ensure certification sheets for calibration gasses are filed in the correct location and accurately reflect the calibration gas bottles.
2. Update the Daily Calibration Form (found on the info-net under environmental policies, procedures, forms and tools, Program: LDAR) to reflect current gas concentrations and Cylinder Identification.
3. Verify the calibration gas cylinders contain enough gas to last a full shift.

IV. Procedure

1.0 Before Beginning Calibration

1. Ensure filters are clean so possible contamination does not interfere with calibration results & flow of instrument.
2. Ensure hydrogen tank is filled.
3. Ensure probe assembly is properly attached.
4. Check machine filter and ensure flame arrestor is tightly secured.
5. Make sure program settings are set correctly. Reference set-up guide in “check off list” box as needed.
6. If a dilution probe will be calibrated to the machine that is being set up, check the 100,000 ppm box next to “scale”. All machines without a dilution probe will have the 10,000 ppm box checked.
7. Make sure all “blanks” and check boxes are filled in appropriately on the Daily Calibration form.

2.0 Calibration Steps

1. Turn machine on and open hydrogen supply valve. Allow 5 minutes for electronic warm-up and to ensure proper hydrogen flow.

2. Then press 1 = Run. This will ignite the unit and display readings. If a flame out message appears, clear the message (press exit), wait a moment, and repeat this step.

3. Check the instrument sample flow rate using the rotometer. The flow rate must be within 0.1 and 3.0 liters/minute to pass per method 21. Document the flow rate on the Daily Calibration form.

4. Allow at least 30 minutes for warm-up.

5. Unplug machine.

6. Press exit until main menu appears.

7. Press 2 = Set up.

8. Press 1 = Calibration.

9. Press 3 = Zero to zero the instrument.

10. Introduce zero gas into the analyzer through the probe.

11. Press enter to start.

12. Wait for minimal change in values (about 15 seconds). Typically, the sample is stable when the first two digits of the reading do not change for 4-5 seconds. The values or counts should be between 2000 and 5000.

13. Press enter to accept, and then press 1 to save.

14. Exit to Main Menu, Press 1 = Run. Record the reading with Zero Gas still attached to the analyzer through the probe.

15. Document results on “Daily Calibration Log”.

16. Exit to Main Menu.

17. Press 2 = Set up.

18. Press 1 = Calibration.

19. Press 4 = Span.

20. Follow screen prompts. The first gas introduced is the 500 ppm (methane).

21. Wait for readings to stabilize at least 15 seconds.

22. Press enter to accept, and then press 1 to save.

23. Exit to Main Menu, Press 1 = Run, record your reading with 500 ppm Gas still attached into the analyzer through the probe.

24. Before moving on to the next calibration gas, introduce the Zero gas again to zero out the analyzer.

25. Repeat Steps 16-24 for the other gases. The other gases used for calibration are 2000 ppm and 10,000 ppm.

26. On analyzers specifically used for carbon canisters, a 100 ppm gas will be used for span 1, with the 500 ppm, 2000 ppm, and 10,000 ppm gases following in that order.

27. TVA must be calibrated within 10% of the known calibration value as per method 21.

28. Per FHR-CC internal policy, the TVA should be calibrated within ±4% of the known calibration value.

29. Calibration results will be documented on the "Daily Calibration Log". Place your initials in appropriate column after calibrating analyzer, print your name in appropriate column and record the time.

30. Exit to main menu. Press 2 = Set up, 1 = Calibrate and 5 = RFO

31. Confirm that the response factor says "RFO: DEFAULT". If not, set to this value.

32. If for any reason the wrong gas is introduced to the wrong span, repeat Steps 6-23.

3.0 Calibrating Dilution Probe

Check the dilution probe assembly for loose fittings, worn out O-rings, and the hose for cracks or tears.

The Dilution Probe operates by drawing ambient air through an activated charcoal scrubber, then through a length of tubing, then through the dilutor sidearm and finally into the TVA. The dilutor orifice allows samples to be drawn at a fixed ratio of 10:1. Standard probe allows 100 mL of air through sidearm for each 10 mL of air through dilution probe, expanding accuracy of the TVA between 10,000 ppm and 100,000 ppm.

1. To begin calibrating the Dilution Probe, place Dilutor fitting on the Close Area Sampler of the TVA.

2. Introduce 10,000 ppm gas or equivalent.

3. Using the Fine Metering Valve of the Dilution Probe, adjust reading to 10% of calibration gas value.

4. Note: Opening the Fine Metering Valve dilutes the samples, allowing adjustments to be lowered; whereas adjusting to the closed position restricts air flow, allowing adjustments to be higher.

4.0 Calibration Drift Analysis Test (CDAT)

The CDAT is conducted at the end of each workday. FHR has the option of also performing a mid-day CDAT. The results are documented in the "Calibration Drift Assessment Test" section of the "Daily Calibration Log". This test indicates how far the instrument has drifted off its calibration.

1. Have analyzer in "Run" mode.

2. Introduce 500 ppm gas to Analyzer through probe. Document reading on the appropriate CDAT column of the "Daily Calibration Log".

3. Introduce the zero gas to the analyzer and repeat step 2, introducing the 500 ppm gas and documenting your second reading. Zero out the analyzer a third time and introduce the 500 ppm gas a third time, again documenting the reading on the "Daily Calibration Log".

4. Take the average of the three documented 500 ppm gas readings by adding them together and dividing by 3. Follow the CDAT % formula on the back of the daily calibration form to determine the percentage of drift from the original calibration value.

5. Repeat the same steps for the 2000 ppm and 10,000 ppm gasses.

6. If FHR is performing the optional mid-day CDAT and the drift is ±4% or greater on any of the three gasses, the analyzer must be re-calibrated and documented on calibration paperwork.

7. If the drift is at -10% or lower on any of the three gasses, this will constitute a negative drift. When a negative drift occurs, each component that was monitored after the most recent calibration that resulted in readings of 50 ppm or greater must be re-monitored. Notify FHR data managers and the FHR technician in charge of calibrations for the week. Reference the negative drift guidelines on how to build an "over 50's" package and for each FHR technician's responsibilities.

8. If for whatever reason, a CDAT cannot be performed due to a mechanical failure, all components must be re-monitored. Inform the data-managers as soon as possible so they can review data in quarantine before it is processed.

9. Reference approved wording and examples on both negative drifts and mechanical failures for proper documentation.

IV. References

Refer to FHR form FEF-AQ-100 (Daily Calibration Form).
Refer to the LDAR Daily Checklist in the Environmental Share Drive.
Refer to set up guide and TVA 1000B Quick Start and Calibration Guide.

Environmental Policy/Procedure Manual
Issued: December 2001
Revision Date: January 27, 2015
Revision No: 1
Last Reviewed: September 25, 2014

Calibration of TVA 1000-B
Procedure No: FEP-AQ-100

Environmental Procedure Approval

This procedure has been reviewed and approved for distribution by Flint Hills Corpus Christi, LLC.

_____ _____
Environmental Director Date

FLINT HILLS RESOURCES

Environmental Policy/Procedure Manual
Issued: December 2001
Revision No: 2.0

Daily Calibration Form
Form No: FEF-AQ-100
Page: 1 of 1

Date Instrument Calibrated: 5/15/18 Technician Signature: Mike S. Chapman

Instrument Model: TVA 1000B Instrument ID#: 69443

Calibration Gas Standards

	Zero	500 ppmv	2,000 ppmv	10,000 ppmv
Calibration Gas Bottle Certification No.	Lot Number: 856697	Lot Number: TLBH-150A-500-3	Lot Number: TLBH-150A-2000-1	Lot Number: TLBH-150A-9950-1
Calibration Gas Concentration (ppmv)	0	512	2020	9940

Checklist:

☑ Checked the probe filter ☑ Checked the machine filter ☑ Checked o-rings

☑ Program spans set correctly ☑ Checked expiration dates of calibration gases

TVA start time: 7:20 AM

Instrument Readings of Calibration Gases

	Time	Zero	500 ppmv	2,000 ppmv	10,000 ppmv	w/ Dilution Probe
Start Shift	8:00 AM	Ø	508	2032	10,000	1007
Mid Shift CDAT (optional)						
Mid Shift Calibration (if needed)						
End Shift CDAT	4:20 PM		538	2131	10,800	

Instrument sample flow rate = 1.5 liters/min. Must be between 0.1 and 3 liters/min to pass.

Notes:

1. *Recalibrate if any instrument readings vary greater than 10% from the gas standards.*
2. *A calibration drift assessment test (CDAT) must be performed at the end of the monitoring shift and a mid-shift CDAT is optional.*
3. *If the CDAT instrument reading is less than 10% of the gas standard, re-monitor all components screened greater than 50ppm since the last acceptable calibration check.*
4. *If a dilution probe is to be used during the monitoring shift, it must be calibrated with the instrument and recorded on this form. Do not use the probe if it does not calibrate within the above standards. Use 10,000ppm gas to calibrate dilution probe.*

Comments:

Daily Calibration Form

Date Instrument Calibrated: 5-3-2018 Instrument Model (check one): ☑ TVA ☐ PID ☐ Other_____

Instrument ID#: 69443 Scale: ☐ 10,000 PPM ☑ 100,000 PPM ☐ Other_____

Technician initials: JF Name (print): JOEL FLORES

Calibration Gas Standards

	Zero	500 ppmv	2,000 ppmv	10,000 ppmv
Calibration Gas Cylinder Identification	856697	TLBH-150A-500-3	TLBH-150A-2000-1	TLBH-150A-9950-1
Calibration Gas Concentration (ppmv)	0	512	2020	9940
Calibration Gas Certification Date	See Gas Certification	See Gas Certification	See Gas Certification	See Gas Certification

Checklist:

☑ Checked the flame arrestor prior to starting TVA
☑ Checked the probe filter
☑ Program spans set correctly
☑ Checked o-rings and connections are airtight
☑ Checked the machine filter
☑ Checked expiration dates of calibration gases

Start time for TVA warm up: 10:00 AM / PM
Instrument sample flow rate: 1 liters/min. (Must be between 0.1 and 3 liters/min to pass)

Notes:

1. *The battery charger should be disconnected from the instrument during all tests (Calibration, CDAT and Quarterly tests).*
2. *If a dilution probe is to be used during the monitoring shift, it must be calibrated with the instrument and recorded on this form. Use 10,000 ppmv gas to calibrate dilution probe.*
3. *A CDAT must be performed at the end of the monitoring shift and a mid-shift CDAT is optional. This applies to LDAR leak definitions only (500 ppmv, 2000 ppmv and 10,000 ppmv).*
4. *If the CDAT shows a negative drift of more than 10 percent from the last calibration value, then all components screened greater than 50 ppmv since the last acceptable calibration check must be remonitored. This applies to LDAR leak definitions only (500 ppmv, 2000 ppmv and 10,000 ppmv)*
5. *FHR Corpus Christi only uses purchased certified calibration gases.*
6. *In the comment section below, describe any corrective action taken if the meter readout could not be adjusted to correspond to the calibration gas value in accordance with section 10. 1 of Method 21 of appendix A-7 of this part.*

Comments:_____

QA/QC review completed by (print name):_____ Date:_____

Instrument Readings of Calibration Gases

Instrument Calibration

Technician initials: JF Technician name (print): JOEL FLORES Time: 11:30 AM / PM

Calibration in-house target is between +/- 4% of the calibration gas value.

	Zero		500 ppmv	2,000 ppmv	10,000 ppmv	w/ Dilution Probe
PPMV	1		513	2027	10,000	994

Calibration Drift Assessment Test (CDAT)

Technician initials: JF Technician name (print): JOEL FLORES Time: 12:45 AM / PM

	PPMV value (A)	PPMV value (B)	PPMV value (C)	Average PPMV (D) = (A+B+C)/3	Last Cal. Value (E)	CDAT % = [(D-E)/E] * 100
500 PPMV	501	518	514	512	513	.19
2000 PPMV	2030	2039	2056	2042	2027	.74
10,000 PPMV	10400	10400	10400	10400	10,000	4.00

Recalibrate if any instrument readings vary greater than negative 10% from the last calibration value or in-house instruction is +/- 4% of the calibration gas value prior to any additional monitoring. If CDAT shows a negative drift of more than 10% see (Note 4.) on front page for remonitor requirements.

Instrument Calibration

Technician initials:_____ Technician name (print):_____ Time:_____ AM / PM

Calibration in-house target is between +/- 4% of the calibration gas value.

	Zero	100 ppmv	500 ppmv	2,000 ppmv	10,000 ppmv	w/ Dilution Probe
PPMV						

Calibration Drift Assessment Test (CDAT)

Technician initials:_____ Technician name (print):_____ Time:_____ AM / PM

	PPMV value (A)	PPMV value (B)	PPMV value (C)	Average PPMV (D) = (A+B+C)/3	Last Cal. Value (E)	CDAT % = [(D-E)/E] * 100
500 PPMV						
2000 PPMV						
10,000 PPMV						

Recalibrate if any instrument readings vary greater than negative 10% from the last calibration value or in-house instruction is +/- 4% of the calibration gas value prior to any additional monitoring. If CDAT shows a negative drift of more than 10% see (Note 4.) on front page for remonitor requirements.

FLINT HILLS resources
Corpus Christi Refineries

Environmental Policy/Procedure Manual
Issued: December 2001
Revised: 5/2005 (Revision No. 2)
Reviewed: 5/2013

Instrument Certification Form
Form No. FEF-AQ-101

Certifier's Name: Joel Flores

☑ ROUTINE 3-MONTH CERTIFICATION
☐ REPLACEMENT INSTRUMENT
☐ MAINTENANCE PERFORMED

Date of Test: 5-3-18

Instrument ID#: 69443

Zero Air Cylinder Number: 856697

Calibration Test Results

1	Cylinder #:		Expiration Date:	
	TLBH-150A-500-3		11-08-2021	
Test	Zero air reading ppmv	500 ppm cal gas mixture ppmv (A)	Meter reading ppmv (B)	Absolute delta ppmv (A-B)[1]
1	0	512	521	9
2	0	512	522	10
3	0	512	525	13
			Total (C)=	32
		D= ((C/3)/A)*100=		2.08

2	Cylinder #:		Expiration Date:	
	TLBH-150A-2000-1		11-08-2021	
Test	Zero air reading ppmv	2,000 ppm cal gas mixture ppmv (A)	Meter reading ppmv (B)	Absolute delta ppmv (A-B)[1]
1	0	2020	2041	21
2	0	2020	2046	26
3	0	2020	2049	29
			Total (C)=	76
		D= ((C/3)/A)*100=		1.25

3	Cylinder #:		Expiration Date:	
	TLBH-150A-9950-1		11-08-2021	
Test	Zero air reading ppmv	10,000 ppm cal gas mixture ppmv (A)	Meter reading ppmv (B)	Absolute delta ppmv (A-B)[1]
1	0	9940	10100	160
2	0	9940	10200	260
3	0	9940	10200	260
			Total (C)=	680
		D= ((C/3)/A)*100=		2.28

If (D) is less than or equal to 10%, the machine passes;

[1] In this case, the absolute difference is always a positive value

Response Time Test

Calibration gas mixture (A) x .90 = 461
This is your 90% response reading that is required.
Test 1: 4.29 Seconds (B)
Test 2: 4.41 Seconds (B)
Test 3: 4.75 Seconds (B)
13.45 Total Seconds (E)
(E) divided by 3= 4.48 Seconds (F)

Calibration gas mixture (A) x .90 = 1818
This is your 90% response reading that is required.
Test 1: 4.97 Seconds (B)
Test 2: 5.03 Seconds (B)
Test 3: 4.85 Seconds (B)
14.85 Total Seconds (E)
(E) divided by 3= 4.95 Seconds (F)

Calibration gas mixture (A) x .90 = 8946
This is your 90% response reading that is required.
Test 1: 5.79 Seconds (B)
Test 2: 6.06 Seconds (B)
Test 3: 6.56 Seconds (B)
18.41 Total Seconds (E)
(E) divided by 3= 6.14 Seconds (F)

If all values for (F) are less than or equal to 30 seconds, the machine passes;

Maximum/highest response time obtained during tests: 6.14 Seconds

Sample Flow Test

Instrument sample flow rate = 1 liters/min. Must be between 0.1 and 3 liters/min to pass.

Certification

INSTRUMENT PASSES CERTIFICATION: ☑ YES ☐ NO

This instrument meets the specifications outlined in reference Method 21 and is therefore certified for use by:

Signature: Joel Flores Date: 5-3-18

Accessories attached during test:
DILUTION PROBE

Appendix D3

Phx42™ FID Use and Calibration Procedures

The user instruction manual, maintenance information, and response factors for the EPA Method 2(M21) flame ionization detector (FID), model Phx42, manufactured by LDARtools (Dickinson, TX, USA) can be found at the below web address, last accessed February 21, 2019 (version of manual used in FHR CC 2019 studies).

http://www.ldartools.com/#resources

Calibration Procedure

The calibration procedures for the LDARtools Phx42™ starting on page 4 of the manual. See Appendices D1 and D2 for further information on FHR M21 FID calibration procedures and record keeping.

Clarification on use

The LDARtools Phx42™ was the primary M21 screening value quantification tool used during the 2019 FHR CC pilot studies but early CRADA tests and historical M21data was primarily acquired with the TVA-1000B (Thermo Fisher Scientific, Waltham MA, USA)

Version

2

LDARtools

Cal5.0 Manual

Rev. Date: November 26, 2018

To confirm that this is the most current version, please go to www.LDARtools.com/#support, then check the Resources section.
OR
Go to the Customer Support Portal and Open the “Docs” section.

Table of Contents

Settings 2
- Cylinder Set-up and Management 2
- Extension Probes 3
- Daily Calibration 4
- Drift 5
- Precision Calibration 6
- Exporting Calibration Records via USB 7
- Automatic wireless export of Calibration Records 7
- Manual wireless export of Calibration Records 7

Managing Updates 8
- Update Cal5.0 8
- Update the Device Settings 8
- Update License 8
- Changing Wireless Network 9

Troubleshooting 10
- Responding to Errors 10
- Reporting an Issue 12
- Exporting Logs 13
- Shutdown/Restart 13

Section 1

Settings

Cylinder Set-up and Management

NOTE: A Cal5.0 Parameter Form is available for you to use to develop and document your Calibration Settings. See LDARtools.com>Support>Resources.

1. Add a Cylinder:
    a. Tap Menu (the “hamburger” icon).
    b. Tap Manage Cylinders.
    c. Tap Add Cylinder.
    d. Fill in the fields appropriate to your cylinder:
        i. Certification day – The day your cylinder was certified
        ii. Expiration date – The day the certification on the cylinder will expire
        iii. Manufacturer’s or Cylinder Serial Number – The ID you want to use to refer to this cylinder
        iv. Actual PPM – The actual PPM of the cylinder
        v. Target PPM – The target PPM or the Leak Definition associated with this cylinder
    e. Tick the following checkboxes that apply:
        i. The Calibration checkbox means that this cylinder will be used for Daily and Precision.
        ii. The Drift checkbox means that this cylinder will be used for all drifts.
        i. Continue adding cylinders until finished. (NOTE: At this point, Cal5.0 will automatically assign the ports from least to greatest concentrations.)

ii. Verify that each cylinder's port number corresponds to the port number its gas line is connected to in the back. (The Port number is in the top left corner of every cylinder.)

iii. Tap Done.

2. Deleting a Cylinder

    f. Tap the Delete button next to cylinder.

3. Temporarily Suspending the use of a Cylinder.

    g. Uncheck the Calibration and Drift checkboxes.

    h. Tap Done.

4. Adding Technicians:

    a. Tap Menu.

    b. Tap Manage Technicians.

    c. Tap the textbox and enter the Technician's name.

    d. Tap Add.

    e. Tap Done.

5. Removing Technicians:

    a. Tap Menu.

    b. Tap Manage Technicians.

    c. Tap the X next to a technician's name.

    d. Tap Done.

Extension Probes

In order to calibrate extension probes on a SpanBox5 you will need to contact support@ldartools.com for instructions on modifying the box settings.

NOTE: The response time of the phx42 with an extension probe exceeds the cut-off for the default settings and may result in the units being assigned to the wrong port during calibration.

Daily Calibration

1. Confirm that you have been certified according to the Cal5.0 Mastery Document.
2. For the initial use of the SpanBox5, a best practice is to “assign” each phx42 to a specific port on the SpanBox5. You should label each port with the serial number of the phx42 that you will use on that port for all Daily and Precision Calibration and Drifts.
3. Ignite the phx42 using the 3-button-press ignition before attaching the device to the SpanBox5.

NOTE: Throughout the calibration process, avoid kinking, bending, or blocking probes at any time!

4. Check the Probe Flow of all your units and record the results for later entry into Cal5.0. Do this before you attach the phx42s to the SpanBox5.
5. Tap Daily Calibration.
6. Select phx42(s) on Connection screen, then tap Next.

   If connection or firmware error appears, tap Yes to Retry Connection.

   After a successful Connection, Self-check will begin

   If there are any Self-check issues, acknowledge them by marking the associated Check Boxes. Then tap OK.
7. Tap Next.
8. Verify that the cylinder information is correct, then tap Next on the Cylinders screen. Otherwise, tap Manage Cylinder to remove or add cylinders.

   At the four-minute mark of the warm-up, the Hunting process will administer gases through each port and ID the phx42 that “recognizes” that gas has been released. This will confirm which port each phx42 is on.

   Once the warm-up period is over, the unit will start calibrating the assigned cylinders.

   Afterwards, the calibration confirmation process will verify if the unit is calibrated to each gas correctly.

   Once the units pass or fail Calibration, the Maintenance Report screen will appear.
9. Select your Tech Name from the dropdown and sign, then tap Next.
10. Check the box next to any non-critical self-check issues that may have occurred.
11. Select Tech Name from the dropdown list, sign, then tap Next.

12. Tap OK.

13. Daily Calibration of Filter Detection

Immediately after the last step of your calibration/confirmation process or right before your phx42 goes out into the field:

1. Remove the probe filter.
2. Wait 5 seconds (the pumps will shut off).
3. Replace the same probe filter and continue with your work day.

REMINDER: If you do not do this within 30 minutes of calibration you will receive ERROR CODE 24.

Drift

1. Make sure that the phx42 is ignited and warmed-up before attaching it to the SpanBox5.

2. Make sure that the phx42 is attached to its assigned port: THE SAME PORT with which it was calibrated earlier in the day.

3. Tap the Drift box on the Home Screen.

   Analyzers that have a Daily Calibration from today will appear.

   On the right of each analyzer, the latest EOD and Noon drift results will be shown.

4. Check the boxes next to the analyzers to be drifted:

   If the analyzer can't be discovered, it will be greyed out.

   If the analyzer is in range, wait a minute for the SpanBox5 to discover and connect.

5. Check either Noon or End of Day at the bottom.

6. Tap Next.

   If a drift of the same type (Noon or EOD) has already been performed on a unit, it will prompt you to confirm that the previous drift will be overwritten. Only do this if you are an experienced user and understand the consequence.

7. If the Cylinder information is correct, tap Next. Otherwise, tap Manage Cylinders.

   The Drift process will begin.

   Units will be drifted to the selected cylinders that were assigned.

If you are running a standard drift, each gas will be applied once.

If you are running a VVa, each gas will be applied 3 times.

If a unit fails on one gas, it will continue testing any other gases you might have selected.

8. Once complete, select a Tech from dropdown, sign, then tap OK.

Precision Calibration

1. Make sure that each phx42 is attached to its assigned port: THE SAME PORT with which it was calibrated earlier in the day.

2. Tap the Precision Calibration box on the Home screen.

   Analyzers that have a Daily Calibration from today will show.

   On the right of each analyzer, the latest Precision Calibration result will be shown.

3. Check the boxes next to the analyzers to be Precision Calibrated.

   If analyzer cannot be discovered, it will be greyed out.

4. Tap Next.

   REMINDER: If you ever run an extra Precision Calibration on the same day, you will be warned that you will be overwriting the previous record for that day. Only do this if you are an experienced user and understand the consequence.

   The Calibration Precision process will automatically `begin.

   Each gas response time will be tested 3 times each.

   If a unit fails at any time, it will be skipped for the remainder of the tests but remain on-screen. The other units will continue.

   A notice at the end of the Precision Cal will display the phx42 number and what gas it failed at on the Cal Precision Report screen.

5. Select Tech from dropdown, sign, and tap OK.

Exporting Calibration Records via USB

1. Insert a USB drive into SpanBox5.
2. On the Home Screen, tap Export Records.
3. Select the desired date range.
4. Tap OK.
5. Wait until the “Successfully exported records to USB” prompt appears.
6. Tap OK.
7. Remove the USB from SpanBox5 and connect it to a computer.

   The Record files can be found in the Cal5 Records folder with either of these filename formats:

   - Cal5 Record DD.MM.YYYY-DD.MM.YYYY
   - Cal5 Record DD.MM.YYYY

Automatic wireless export of Calibration Records

Cal5.0 can scheduled to transmit your calibration records to your LTI Desktop Manager or Chateau database daily at a time of your choosing.

Please contact support@ldartools.com for sync credentials and setup instructions.

Manual wireless export of Calibration Records

Cal5.0 can manually transmit calibration records to your LTI Desktop Manager or Chateau database if sync credentials have been enabled.

Obtain your credentials from your Site Supervisor or contact support@ldartools.com to enable this feature.

1. On the Home screen, tap Reports.
2. Tap Manual Sync.
3. Select the desired date range.
4. Tap OK.
5. Once upload process is complete, tap OK.

Section 2

Managing Updates

Update Cal5.0

1. Tap Menu.
2. Tap Update Cal5.0.

   If a newer version is available, it will show a prompt to download the update.
3. Tap OK.

   Once the download is complete, it will automatically update and restart Cal5.0.

Update the Device Settings

1. Email support@ldartools.com with the desired change.

   LDARtools Technical Support will complete the change.
2. Once you are notified of the change, tap Menu.
3. Tap Settings.
4. Wait, then once the updated prompt appears, tap OK.
5. Tap Menu.
6. Tap Home.
7. Tap OK to close the prompt.

Update License

1. Tap Menu.
2. Tap License.
3. Tap Update Online.

4. Once the Success prompt appears, tap OK.
5. Tap Done.

Changing Wireless Network

1. Request the Super-Secret Password from support@ldartools.com.
2. Tap Menu.
3. Tap Manage Networks.
4. Enter the Super-Secret Password.
5. Tap OK.
6. Tap Search.
7. Select the Wi-Fi name.
8. Enter the password, then tap Connect.
9. Tap Test Connection.
10. Once successful, tap Done.

Section 3

Troubleshooting

Responding to Errors

Error: Could not get Unit and product settings from support portal or database cache.	Two things are happening: • This phx42 is not being calibrated on its assigned SpanBox5. • This SpanBox5 can't communicate with the LDARtools Support Portal to download settings. 1. Check if the SpanBox5 can grab settings from the Support Portal: a. Tap Menu. b. Tap Settings. c. Wait, then do either: • If a successful prompt appears, tap OK. Try calibrating again, there may have been a temporary loss of network connection. • If you do not get a successful prompt, then proceed to next step. 2. Verify that the SpanBox5 is connected to a wireless network: a. Follow Steps 1-8 of the Changing Wireless Network section. Once the wireless network is selected and a Disconnect button appears, then the network is connected b. Tap Test Connection to verify that the connection is good. c. Do either: • If successful, navigate to the Home screen, then start Daily Calibration. • If unsuccessful, submit a software support ticket and be sure to attach the Cal5.0 logs.

Error: No phx mapped to port	1. Contact Support if you do not use 10k ppm gas. This is the first step! 2. Check the gas lines. Verify that all gases going from left to right (when facing the back of the SpanBox5) are arranged in order of least to greatest concentration. REMINDER: SpanBox5 uses the highest span g to determine the phx42 port assignment. 3. Verify that the gases selected in the Manage Cylinders screen are the ones connected to the SpanBox5: a. Open the Manage Cylinders screen. The Port number is in the top left corner of every cylinder. b. Verify that each cylinder's port number corresponds to the port number its gas line is connected to in the back. 4. If these are correct and the problem persists, submit a software support ticket and be sure to attach the Cal5.0 Logs.
Critical Self-check Issues Critical Self-check issues prevent the calibration process.	1. If the problem is a Sample Pump Shutdown error: a. Check for tears and leaks in the probe. b. Perform Probe Integrity test. c. If there is a probe problem, Submit a Hardware support ticket. (Do not use the 42App to report this issue.) Describe the problem in the comment field. 2. If problem is an HPH2 error: a. Fill the analyzer with Hydrogen and rerun the Daily Calibration. b. If the problem persists, connect with the 42App. c. Run the Self-check and Report an Issue on the Support Portal. d. Attach the phx42 logs from the SpanBox5 to the Support ticket. 3. If the problem is neither of the above: a. Connect with the 42App. b. Run the Self-check and Report an Issue on the Support Portal. c. Attach the phx42 logs from the SpanBox5 to the Support ticket.

Non-Critical Self-Check Issues	1. If this is a Charge or Battery issue: a. Make sure the units are on chargers overnight. b. If the battery shows "uncharged" after 12 hours on the charger, connect to the 42App. c. Run the Self-check and Report an Issue on the Support Portal. d. Attach the phx42 logs from the SpanBox5 to the Support ticket. 2. If this is a Heater issue: a. Connect with the 42App. b. Run the Self-check and Report an Issue on the Support Portal. c. Attach the phx42 logs from the SpanBox5 to the Support ticket.
Failed Connection / Signal Strength Problems	1. If Bluetooth strength is not OK after 60 seconds, go back to the Home screen, then continue. 2. If that does not resolve it, submit a software support ticket and be sure to attach the Cal5.0 Logs.
Flame-out or ignition problems during warm-up	1. Connect with the 42App. 2. Run the Self-check. 3. Do either: • If it passes, put it back on the SpanBox5 and calibrate. • If it fails, Report an Issue on the Support Portal.

Reporting an Issue

1. Tap Menu.
2. Tap Report an Issue.
3. Enter Support Portal Credentials.
4. Select type of issue:
    a. Cal5.0 issue
    b. Analyzer issue
5. If Analyzer issue, select serial number from dropdown.
6. Select Date of issue.

7. In the Issue text box, enter a description of the issue.
8. Tap submit.

Exporting Logs

NOTE: When reporting an issue through Cal5.0, logs will automatically be attached. Only use the steps below if you are submitting updated logs for an existing support case.

1. Tap Menu.
2. Tap Copy Log files to USB.
3. Wait until the “Successfully exported logs to USB” popup appears.
4. Tap OK.
5. Remove the USB from SpanBox5 and connect it to a computer.
6. On the computer’s File Explorer, navigate to the USB drive.

   The logs can be found in the Logs folder. The file name includes the phx42 serial number followed up by the type of Log file and the date.

Shutdown/Restart

Note: Only shutdown the SpanBox5 when instructed to do so by LDARtools support or when preparing to move the unit.

1. Tap Menu.
2. Scroll down Menu.
3. Tap Shutdown/Restart.

5/21/2019

DailyCal Report

Analyzer ID	Date	Calibrate	Cylinder	Cyl. Mfr. ID	Conc.	Reading	Pass	Ext Probe	Drift 1	Drift 1a	Drift 1b	Drift 1c	Drift Pct1	Pass	Drift 2	Drift 2a	Drift 2b	Drift 2c	Drift Pct2	Probe Flow	Pass	Warm up	Tech ID	Warm Up Duration
phx42-1745	4/15/2019	10:47 AM	Zero 0	5625377Y	0.00	1.12	Yes	No	-	-	-	-	-	-	-	-	-	-	-	0.25	-	10:31 AM	Mike Charles	15 min
phx42-1745	4/15/2019	10:47 AM	Methane 500	EB0106513	495.00	497.00	Yes	No	11:51 AM	496	496	503	0.3	Yes	4:51 PM	504	501	502	1.1	0.25	Yes	10:31 AM	Mike Charles	15 min
phx42-1745	4/15/2019	10:47 AM	Methane 2000	CC400156	2,021.00	2,013.00	Yes	No	11:53 AM	2014	2007	2018	0.0	Yes	4:52 PM	1996	2005	1998	-0.7	0.25	Yes	10:31 AM	Mike Charles	15 min
phx42-1745	4/15/2019	10:47 AM	Methane 10000	CC82984	9,890.00	9,738.00	Yes	No	11:54 AM	9712	9768	9809	0.3	Yes	4:53 PM	9741	9748	9771	0.2	0.25	Yes	10:31 AM	Mike Charles	16 min

Personnel have performed the required daily calibration, for all working Analyzers on site, to every calibration span gas.
Zero gas was used to purge after the initial calibration process and between all samples during the drift assessment

Precision Calibration Record

Analyzer	Cal. Date	Tech ID	Gas	Span	Conc	Pass	Test 1	Test 2	Test 3	Prec.	Resp 1	Resp 2	Resp 3	Avg Resp	Anlz SN	Cyl. Man. ID	Cyl. Exp Date
phx42-1745	4/15/2019 10:54:00 AM	Mike Charles	Methane	500	495	Yes	501	500	502	1.212%	03.77	03.92	03.77	03.82	phx42-1745	EB0106513	9/18/2026
phx42-1745	4/15/2019 10:55:00 AM	Mike Charles	Methane	2000	2021	Yes	2006	2024	2018	0.247%	03.82	04.01	03.73	03.85	phx42-1745	CC400156	10/16/2022
phx42-1745	4/15/2019 10:56:00 AM	Mike Charles	Methane	10000	9890	Yes	9838	9821	9832	0.603%	04.08	03.81	03.96	03.95	phx42-1745	CC82984	8/1/2020

Zero gas was used to purge after the initial calibration process and between all samples during the drift assessment and precision calibration processes.

Signature:_____ _____
Print:_____ Date
Field Supervisor

Signature:_____ _____
Print:_____ Date
Site Administrator

Signature:_____ _____
Print:_____ Date
Client Rep. (optional)

Appendix D4

MiniRAE 3000 and Cub PID Information and Procedures

The hand-held probe (HHP) MiniRAE 3000 10.6 eV photoionization detector (PID), manufactured by Honeywell Rae Systems Inc. (Sunnyvale, CA USA) and the Cub personal VOC monitor (10.6 eV PID), manufactured by Ion Science Inc. (Stafford TX, USA) may be used as supporting diagnostics (non-critical data) for assessment of leaks/emissions in Test 4. A product brochure and a calibration procedure for the MiniRAE 3000 is contained on the following pages D32-D34. A product brochure for the Cub is contained on pages D35-D36.

The user's manual for the MiniRAE 3000 is found at the flowing web address, last accessed February 21, 2019 (version FHR CC pilot tests):

https://www.raesystems.com/sites/default/files/content/resources/3G%20PID%20User%27s%20Guide%20Rev%20A_English_0.pdf

The user's manual for the Ino Science Cub is found at the flowing web address, last accessed February 21, 2019 (version FHR CC pilot tests):

https://www.ionscience.com/products/cub-personal-voc-detector/#downloads

Honeywell

THE POWER OF **CONNECTED**

ppbRAE 3000 +

Portable Handheld VOC Monitor

The compact ppbRAE 3000 + is a comprehensive VOC gas monitor and datalogger for hazardous environments. The ppbRAE 3000 + is one of the most advanced handheld VOC monitors available for parts-per-billion detection. This third-generation patented PID device monitors VOCs using a photoionization detector with a 9.8 eV, 10.6 eV UV-discharge lamp.

Workers can easily measure VOCs and wirelessly transmit readings up to 2 miles/3 km away.

The built-in wireless modem allows real-time data connectivity with the command center located up to two miles/3 km away (with optional RAELink3 portable modem) from the detector.

- Accurate VOC measurement in all operating conditions
- Easy access to lamp and sensor in seconds without tools
- Patented sensor and lamp autocleaning reduces maintenance
- Monitors real-time readings and location of people
- Low Cost of Ownership: 3-year 10.6 eV lamp Warranty
- BLE module and dedicated APP for enhanced datalogging function

FEATURES & BENEFITS

Proven PID Technology
- 3-second response time
- Extended range from 1 ppb to 10,000 ppm with highly acute linearity
- Humidity compensation with integral humidity and temperature sensors
- Reflex PID Technology™

Integrated
- Highly connectivity capability through multiple wireless module options
- Integrated Correction Factors list of 220 compounds—more than any other PID
- Includes flashlight for dark conditions
- Large graphic display presents gas type, Correction Factor and concentration

Durable
- Easy access to battery, lamp and sensor in seconds without tools
- Rugged housing withstands use in harsh environments
- IP-67 waterproof design for easy cleaning and decontamination

APPLICATIONS

- Oil & Gas
- HazMat
- Industrial Safety
- Civil Defense
- Environmental & Indoor Air Quality

Download on the App Store

GET IT ON Google Play

Instrument Specifications

Size	10" L x 3.0" W x 2.5" H (25.5 x 7.6 x 6.4 cm)
Weight	26 oz (738 g)
Sensors	Photoionization sensor with standard 10.6 eV or optional 9.8 eV lamp
Battery	• Rechargeable, external field-replaceable Lithium-Ion battery pack • Alkaline battery adapter
Running time	16 hours of operation (12 hours with alkaline battery)
Display Graphic	4 lines, 28 x 43 mm, with LED backlight for enhanced display readability
Keypad	1 operation and 2 programming keys, 1 flashlight on/off
Direct Readout	Instantaneous reading • VOCs as ppm by volume or mg/m3 (3 in upper case for cubic) • STEL, TWA and PEAK • Battery and shutdown voltage • Date, time, temperature
Alarms	95 dB (at 12"/30 cm) buzzer and flashing red LED to indicate exceeded preset limits • High: 3 beeps and flashes per second • Low: 2 beeps and flashes per second • STEL and TWA: 1 beep and flash per second • Alarms latching with manual override or automatic reset • Additional alarm for low battery and pump stall
EMI/RFI	Highly resistant to EMI/RFI Compliant with EMC Directive 89/336/EEC
IP Rating	• IP-67 unit off and without flexible probe • IP-65 unit running
Datalogging	Standard 6 months at one-minute intervals
Calibration	Two-point or three-point calibration for zero and span. Reflex PID Technology™ Calibration memory for 8 calibration gases
Sampling Pump	• Internal, integrated flow rate at 500 cc/mn • Sample from 100' (30m) horizontally and vertically
Low Flow Alarm	• Auto pump shutoff at low-flow condition
Communication & Data Download	• Download data and upload instrument set-up from PC through charging cradle or using BLE module and dedicated APP • Wireless data transmission through built-in RF modem
Wireless Network	Mesh RAE Systems Dedicated Wireless Network
Wireless Range (Typical)	Up to 15 ft (5m) for BLE EchoView Host: LOS > 660 ft (200 m) ProRAE Guardian & RAEMesh Reader: LOS > 660 ft (200 m) ProRAE Guardian & RAELink3 Mesh: LOS > 330 ft (100 m)
Safety Certifications	• **US and Canada:** UL, cUL, Classified as Intrinsically Safe for use in Class I, Division 1 Groups A, B, C, D • **Europe:** ATEX Ex II 2GEx ia IIC/IIB T4 • IECEx: Ex ia IIC/IIB T4
Temperature	-4° to 113° F (-20° to 50° C)
Humidity	0% to 95% relative humidity (non-condensing)
Attachments	Durable black rubber boot with straps

Instrument Specifications

Warranty	3-year warranty for 10.6 eV lamp, 1 year for pump, battery, and instrument
Wireless Frequency	ISM license-free band. IEEE 802.15.4 Sub 1GHz IEEE 802.11 bands b/g 2.4 GHz
Wireless Approvals	FCC Part 15, CE R&TTE, Others[1]
Radio Module	Supports Bluetooth or RM900 or BLE

[1] Contact RAE Systems for country-specific wireless approvals and certificates. Specifications are subject to change.

Sensor Specifications

Gas Monitor	Range	Resolution	Response Time T90
VOCs	0 to 9999 ppb	1 ppb	< 3 s
	10 to 99 ppm	0.01 ppm	< 3 s
	100 to 999 ppm	0.1 ppm	< 3 s
	1000 to 9999 ppm	1 ppm	< 3 s

MONITOR ONLY INCLUDES:

- ppbRAE 3000 + Monitor
- Wireless communication module built in, as specified
- Charging/download adapter
- Organic vapor zeroing kit
- Tedlar® bag for calibration
- Flex-I-Probe™
- External filter
- Rubber boot with straps
- Alkaline battery adapter
- Lamp-cleaning and tool kit
- Soft leather case

MONITOR WITH ACCESSORIES KIT:

- Hard transport case with pre-cut foam padding
- Charging/download cradle
- 5 Porous metal filters and O-rings
- Gas outlet port adapter and tubing

OPTIONAL CALIBRATION KIT ADDS:

- 10 ppm isobutylene calibration gas, 34L
- Calibration regulator and flow controller

OPTIONAL GUARANTEED COST-OF-OWNERSHIP PROGRAM:

- 4-year repair and replacement warranty
- Annual maintenance service

For more information
www.honeywellanalytics.com
www.raesystems.com

Europe, Middle East, Africa
Life Safety Distribution GmbH
Tel: 00800 333 222 44 (Freephone number)
Tel: +41 44 943 4380 (Alternative number)
Middle East Tel: +971 4 450 5800 (Fixed Gas Detection)
gasdetection@honeywell.com

Americas
Honeywell Analytics Distribution Inc.
Tel: +1 847 955 8200
Toll free: +1 800 538 0363
detectgas@honeywell.com
Honeywell RAE Systems
Phone: +1 408 952 8200
Toll Free: +1 888 723 4800

Asia Pacific
Honeywell Analytics Asia Pacific Tel:
+82 (0) 2 6909 0300
India Tel: +91 124 4752700
China Tel: +86 10 5885 8788-3000
analytics.ap@honeywell.com

Technical Services
EMEA: HAexpert@honeywell.com
US: ha.us.service@honeywell.com
AP: ha.ap.service@honeywell.com

Datasheet_ppbRAE 3000_+_DS-1018-_EN
©2018 Honeywell International Inc.

Mini Rae 3000 Calibration Procedures

1. To turn on hold down “ON/Mode” key for a couple of seconds. When the PID is turned on it will go thru a short range of information. You will see the word Ready across your screen go ahead and press “Y/+” key. At this point it will go thru a short warm up phase and straight into the survey mode. PID is now ready to calibrate.

2. Next, hold down the “MODE” and “N/-” keys at the same time for a couple of seconds. You will see “Calibrate/select gas?” across your screen; press “Y/+” key, it will take you to “Fresh air calibrate?” press “Y/+” key again. Connect your zero air to end of probe; the mini will do an automatic 20 second countdown. After 20 seconds are complete leave your bag on the probe and it will show the reading/results for zero gas. You can wait until it prompts you to the next gas or you can press “Y/+” to move on to your gas calibration.

2.1 You will see “Span Cal?” connect your gas to end of probe, the Mini Rae will do an automatic 20 second countdown; after 20 seconds are complete leave your bag on probe and it will show your reading/results. The Mini Rae will not record your results so you must remember and document. *Note: See step 4.1 for multiple gasses.

3. If you are only calibrating 1 span gas (100ppm) you are complete with calibration. Press “Mode” key until it takes you to the display screen. PID is ready to use. For other span gases proceed to strep 4.

4. For multiple span calibrations: after you have completed the first gas calibration, your screen should take you to “Select Cal Memory” here press “Y/+” key. It will show you the cal memory you are currently on. Example “Mem #??” Here you will press “N/-” key to take you to your next cal memory. Your screen should read “Mem #??” press “Y/+” then press “Y/+” again to save memory. The PID will ask questions “Change span value” and “Modify cal memory” “Change correction factor” you should press “N/-” to these questions. You will be asked for “fresh air cal?” If you have calibrated you zero gas in the first span you can skip this by pressing “N/-” key. Now repeat step 2.1.

4.1 Repeat step 4 to calibrate multiple spans.

5. Once you have calibrated all span gases you can return to display screen by pressing “Mode” key until it appears. To change the cal memory you’re in return to the calibration screen. Enter “Y/-” when “Calibrate/select gas?” screen appears; now using your “N/-” key scroll until you find Select cal memory key. Use “Y/+” or “N/-” to select memory you want. When you get the memory you want save it by pressing “Y/+” key. Now use your Mode key to return to display screen.

FLINT HILLS RESOURCES

Environmental Policy/Procedure Manual
Issued: December 2001
Revision No: 2.0

Daily Calibration Form
Form No: FEF-AQ-100
Page: 1 of 1

Date Instrument Calibrated: 12-5-17 Technician Signature: Mike S. Clemens

Instrument Model: Mini Rae 3000 Instrument ID#: 592-912541 (Rental Unit from Airgas)

Calibration Gas Standards

	Zero	100 ppmv
Calibration Gas Bottle Certification No. or Lot No.	Lot Number: 856697	Lot Number: 854049
Calibration Gas Concentration (ppmv)	0	101

Checklist:

☑ Checked the probe filter ☑ Checked the machine filter ☑ Checked o-rings

☑ Program spans set correctly ☑ Checked expiration dates of calibration gases

Instrument Readings of Calibration Gases

	Time	Zero	100 ppmv
Start Shift	8:51	Ø	103
Mid Shift CDAT (optional)	11:07	Ø	89
Mid Shift Calibration (if needed)	11:08	Ø	104
End Shift CDAT	2:01	Ø	93

Instrument sample flow rate = .5 liters/min. Must be between 0.1 and 3 liters/min to pass.

Notes:

1. *Recalibrate if any instrument readings vary greater than 10% from the gas standards.*
2. *A calibration drift assessment test (CDAT) must be performed at the end of the monitoring shift and a mid-shift CDAT is optional.*
3. *If the CDAT instrument reading is less than 10% of the gas standard, re-monitor all components screened greater than 50ppm since the last acceptable calibration check.*
4. *If a dilution probe is to be used during the monitoring shift, it must be calibrated with the instrument and recorded on this form. Do not use the probe if it does not calibrate within the above standards. Use 10,000ppm gas to calibrate dilution probe.*

Comments: _____

FLINT HILLS RESOURCES

Environmental Policy/Procedure Manual
Issued: December 2001
Revision No: 2.0

Daily Calibration Form
Form No: FEF-AQ-100
Page: 1 of 1

Date Instrument Calibrated: 11/15/17 Technician Signature: Jose Medellin

Instrument Model: Mini Rae 3000 Instrument ID#: 592-912541

Calibration Gas Standards

	Zero	100 ppmv
Calibration Gas Bottle Certification No.	TW05-87795	IL3010
Calibration Gas Concentration (ppmv)	0	100

Checklist:

☑ Checked the probe filter ☑ Checked the machine filter ☑ Checked o-rings

☑ Program spans set correctly ☑ Checked expiration dates of calibration gases

Instrument Readings of Calibration Gases

	Time	Zero	100 ppmv
Start Shift	1:02 pm	0	100
Mid Shift CDAT (optional)			
Mid Shift Calibration (if needed)			
End Shift CDAT	1:28 pm	0	103

Instrument sample flow rate = 0.5 liters/min. Must be between 0.1 and 3 liters/min to pass.

Notes:

1. *Recalibrate if any instrument readings vary greater than 10% from the gas standards.*
2. *A calibration drift assessment test (CDAT) must be performed at the end of the monitoring shift and a mid-shift CDAT is optional.*
3. *If the CDAT instrument reading is less than 10% of the gas standard, re-monitor all components screened greater than 50ppm since the last acceptable calibration check.*
4. *If a dilution probe is to be used during the monitoring shift, it must be calibrated with the instrument and recorded on this form. Do not use the probe if it does not calibrate within the above standards. Use 10,000ppm gas to calibrate dilution probe.*

Comments: PID calibrated for certification

FLINT HILLS resources
Corpus Christi Refineries

Environmental Policy/Procedure Manual
Issued: December 2001
Revised: 5/2005 (Revision No. 2)
Reviewed: 5/2013

Instrument Certification Form
Form No. FEF-AQ-101

Certifier's Name: Jose Medellin

☑ ROUTINE 3-MONTH CERTIFICATION
☐ REPLACEMENT INSTRUMENT
☐ MAINTENANCE PERFORMED

Date of Test: 11/15/17

Instrument ID#: 592-912541

Zero Air Cylinder Number: TW05-877950

Calibration Test Results

1	Cylinder #:		Expiration Date:	
	LL3010		3/8/19	

Test	Zero air reading ppmv	100 ~~500~~ ppm cal gas mixture ppmv (A)	Meter reading ppmv (B)	Absolute delta ppmv (A-B)[1]
1	8	100	107	7
2	8	100	100	8
3	0	100	99	1
			Total (C)=	8
		D= ((C/3)/A)*100=		2.67

2	Cylinder #:		Expiration Date:	

Test	Zero air reading ppmv	2,000 ppm cal gas mixture ppmv (A)	Meter reading ppmv (B)	Absolute delta ppmv (A-B)[1]
1				
2				
3				
			Total (C)=	
		D= ((C/3)/A)*100=		

3	Cylinder #:		Expiration Date:	

Test	Zero air reading ppmv	10,000 ppm cal gas mixture ppmv (A)	Meter reading ppmv (B)	Absolute delta ppmv (A-B)[1]
1				
2				
3				
			Total (C)=	
		D= ((C/3)/A)*100=		

If (D) is less than or equal to 10%, the machine passes;

[1] In this case, the absolute difference is always a positive value

Response Time Test

Calibration gas mixture (A) x .90 = 90
This is your 90% response reading that is required.
Test 1: 3.87 Seconds (B)
Test 2: 4.28 Seconds (B)
Test 3: 4.59 Seconds (B)
12.74 Total Seconds (E)
(E) divided by 3= 4.25 Seconds (F)

Calibration gas mixture (A) x .90 = _____
This is your 90% response reading that is required.
Test 1: _____ Seconds (B)
Test 2: _____ Seconds (B)
Test 3: _____ Seconds (B)
_____ Total Seconds (E)
(E) divided by 3= _____ Seconds (F)

Calibration gas mixture (A) x .90 = _____
This is your 90% response reading that is required.
Test 1: _____ Seconds (B)
Test 2: _____ Seconds (B)
Test 3: _____ Seconds (B)
_____ Total Seconds (E)
(E) divided by 3= _____ Seconds (F)

If all values for (F) are less than or equal to 30 seconds, the machine passes;

Maximum/highest response time obtained during tests: 4.25 Seconds

Sample Flow Test

Instrument sample flow rate = 0.5 liters/min. Must be between 0.1 and 3 liters/min to pass.

Certification

INSTRUMENT PASSES CERTIFICATION: ☑ YES ☐ NO

This instrument meets the specifications outlined in reference Method 21 and is therefore certified for use by:

Signature: Jose Medellin Date: 11/15/17

Accessories attached during test: Water Trap

Cub Personal PID Monitor

Personal safety monitor for hazardous & toxic gases.

The world's smallest, lightest, most sensitive personal PID monitor for hazardous and toxic compounds.

Best available photoionization (PID) detection

- PID independently verified as best performing on the market
- Unrivaled sensitivity detects down to ppb levels
- Widest range detects gases 1 ppb – 5,000 ppm
- In-built humidity resistance with no need to compensate
- Anti-contamination design for extended field operation
- Measures 480 selectable compounds (10.6 eV lamp)

Safety

- Fastest (<13 second) response to hazardous gases & vapors
- Clear audio, visual and vibrating alarms
- Large LCD display for clear readings
- Longest battery life (16 hours)
- Meets ATEX, IECEx (US & Canadian certification pending)

Ease of use

- Smallest, lightest personal PID monitor available
- Simple one button operation
- Intuitive software and simple calibration routine
- Easy to service
- Easily upgrade your instrument

Low cost operation

- Inexpensive consumables and parts
- Free 2 year warranty when instrument registered online

Cub is the world's smallest, lightest personal PID monitor for the accurate detection of volatile organic and total aromatic compounds. With market leading parts-per-billion (ppb) sensitivity, Cub gives an indication of harmful gases including benzene before they reach levels which are harmful.

Cub is available in three distinct variants; ppm, ppb and TAC mode. Choose a ppb or ppm instrument with 10.6 eV lamp for accurately detecting a wide range of VOCs dependent on your sensitivity requirements. Cub^{TAC} with 10.0 eV lamp gives accurate detection of total aromatic compounds (TACs) down to ppb levels.

Small, compact and lightweight Cub is robust yet comfortable and unobtrusive to wear. Cub has a dynamic range of 1 ppb to 5000 ppm, the widest on the market measuring 480 selectable compounds.

When worker exposure exceeds pre-set limits the instrument's audible, vibrating and flashing LED alarms alert you to the gases present. Readings are displayed in ppb and ppm on its bright, back-lit LCD display with selectable data logging time.

Cub's linked together within their docking stations.

Upgradeable ppb sensitivity can be purchased quickly and easily. CubDoc docking stations are available for USB communication, charging and calibrating your instrument, dependent on your requirements.

The instrument's PID sensor technology has been independently verified as best performing for speed, accuracy and humidity resistant operation. Its unique Anti-contamination and patented Fence Electrode Technology provide extended run time in the most challenging environments, giving you accurate results you can truly rely on.

Applications include

• Industrial hygiene • Chemical and petrochemical plants • Oil & gas
• Pharmaceuticals • Health & safety • Hazardous materials • First response
• Environmental

Accessories

Cub is supplied with an exclusive range of accessories.
Visit www.ionscience.com/cub for more info.

Distributed by:

CUB TECHNICAL SPECIFICATION

SENSITIVITY
0.001 ppm (isobutylene equivalent) *Model dependent
0.002 mg/m³ (isobutylene equivalent) *Model dependent

ACCURACY
±5% display reading + one digit

RESPONSE TIME
<13 seconds (T90)

APPROVALS
Europe: ATEX: CE, Ex II 1G, Ex ia IIC T4; -20 °C ≤ Ta ≤ 55 °C
IECEx: Ex ia IIC T4 -20 °C ≤ Ta ≤ 55 °C
China: Ex ia IIC T4 -20 °C ≤ Ta ≤ 55 °C
US and Canadian approvals: Class I, II and III, Division I, Hazardous (Classified) Locations

BATTERY
Battery life up to 16 hours
Battery charge time 4 hours

PID LAMP OPTIONS
10.6 eV, 10.0 eV

DATA LOGGING
30,000 readings

COMMUNICATION
USB 2.0

ALARM
LEDs, audio and vibrate
Sounder 86 dB @ 300mm
Pre-programmed TWA & STEL. Work exposure alarm levels on all models.

TEMPERATURE
Operating: -20 to 55 °C, -4 to 131 °F
Humidity handling: Fence Electrode Technology

WEIGHT & DIMENSIONS
111g (3.91 oz)
61 x 66 x 59 mm (2.4 x 2.6 x 2.3")

RESOLUTION
0.001 ppm

RANGE
ppm 0.1 - 5,000 ppm
ppb 0.001 - 5,000 ppm
TAC 0.01 - 5,000 ppm

CALIBRATION
2 point calibration via docking station

UPGRADEABLE
Upgrade ppm to ppb

IP RATING
Designed to IP65 (heavy rain)

LCD DISPLAY
Back lit multi colour

FLOW RATE
N/A (no pump)

DOCKING STATION OPTIONS
Charge only
Charge and USB communication
Charge, USB communication and calibration

*Model dependant

Cub V1.6. This publication is not intended to form the basis of a contract and specifications can change without notice.

Ion Science LLC
4153 Bluebonnet Drive,
Stafford, TX 77477, USA
Toll free: 1 877 864 7710
E: info@ionscienceusa.com

Appendix D5

Optical Gas Imaging Procedures

General Optical Gas Imaging Procedures

March 2019

Contents

1.0 Scope and Applicability 3
2.0 Summary of Method 3
3.0 Definitions 3
4.0 Health and Safety Warnings 3
5.0 Cautions 4
6.0 Interferences 4
7.0 Personnel Qualifications 4
8.0 Equipment and Supplies 4
9.0 Procedure 5
10.0 Data and Records Management 10
11.0 Quality Control and Quality Assurance 10
12.0 References and Supporting Documentation 11

Figures

Figure 1. GF320 back of hand grip with Power, Menu Joystick, and Menu buttons 6
Figure 2. GF320 top of hand grip with Auto/Manual/HSM, Focus/Zoom, and Save/Start-Stop Recording buttons 7
Figure 3. GF320 top of camera with Programmable button, Temperature Range, and Camera Dial 7
Figure 4. GF320 front left side of camera with Manual Image Focus, Visible Image, and Laser buttons ... 8
Figure 5. GF320 back of camera with battery, battery release latch, battery compartment release, and camera SD card and data storage. 8

Tables

Table 1. GF320 Infrared Camera Buttons, Locations, and Functions 5

1.0 Scope and Applicability

1.1 The purpose of this procedure is to describe the use and operation of the FLIR GF320 infrared (IR) camera during for field measurement activities. The FLIR GF320 is used to locate leaks of hydrocarbon vapors from simulated leaking valves and connectors.

1.2 This procedure is for personnel using the GF320 for the leak screening purposes.

1.3 This procedure is a general guide. For more complete information on FLIR GF320 series IR camera functionality, please consult the manufacturer's manual.

1.4 Please consult the quality assurance project plan (QAPP) for test-specific procedures and record keeping requierenments.

2.0 Summary of Method

The GF320 is designed to identify emissions of hydrocarbon gases using an IR detector. The detector has been designed to capture IR radiation emitted within a narrow IR spectral range corresponding to several hydrocarbon gases. The images of these hydrocarbon emissions, which appear as either black or white "smoke" depending on polarity settings and background, are displayed in a viewfinder in real time. Lower emission detection limits can often be obtained using the manual mode or high-sensitivity mode (HSM). The user should be familiar with these operating modes prior to use in the field.

For the typical use, the GF320 capabilities will be implemented for two main purposes: (1) The IR camera [or optical gas imager (OGI)] is used to conduct a visual site survey to identify any potential hazards to health and safety. (2) perform leak detection surveys of with potential emissions.

This procedure was prepared by persons deemed technically competent by management based on their knowledge, skills, and abilities. The procedure has been validated in practice and reviewed in print by a subject matter expert.

3.0 Definitions

QAPP	quality assurance project plan
HSM	high-sensitivity mode
IR	infrared
OGI	optical gas imaging
SD	secure digital

4.0 Health and Safety Warnings

4.1 This document does not attempt to address all potential safety concerns associated with the use of the IR camera. It is the responsibility of the user of this procedure to establish appropriate safety and health practices.

4.2 Always observe proper safety procedures when using the IR camera. The operator must be familiar with the safety aspects associated with the instrument's operation, as outlined in the instrument's operating manual.

4.3 The IR camera is not intrinsically safe and might require additional site-specific monitoring prior to operation. Refer to any pertinent site-specific health and safety plans for guidelines on safety precautions. These guidelines, however, should only be used to complement the judgment of an experienced professional.

4.4 Minimize exposure to potential health hazards by use of protective clothing, and eyewear.

5.0 Cautions

5.1 If the camera is not working properly and a reboot of the camera does not alleviate the problem, red-tag it and remove it from use.

5.2 Operate the camera only in appropriate environmental conditions. Temperatures above 50 °C (122 °F) can damage the camera.

5.3 Read the operational manual and fully understand all aspects of its use before attempting to operate the IR camera.

5.4 Avoid pointing the camera at strong energy sources, including the sun, as these could negatively affect the detector.

6.0 Interferences

6.1 For accurate measurements, allow the camera a 15-minute cool down period before use.

6.2 Avoid pointing the camera at strong energy sources, including the sun, as these could negatively affect accuracy and possibly damage equipment.

6.3 Steam plumes and very hot backgrounds present potential interferences

7.0 Personnel Qualifications

7.1 Field personnel must only operate equipment for which they are trained and authorized to use. Personnel must be trained by qualified operators.

7.2 Operators of the instrument must read the manufacturer's manual and this operating procedure and demonstrate that they fully understand how to properly operate the instrument.

7.3 Before use, the training of the operator must be suitably documented. The level of training (proficiency of operator) is related to data quality objectives of the QAPP.

8.0 Equipment and Supplies

- Infrared camera (FLIR Systems model GF320)
- Infrared camera telephoto lens (FLIR Systems GF320 fixed lens; Standard 24° x 18°)
- FLIR Systems user's manual (FLIR GF3xx Series)
- Spare rechargeable lithium-ion batteries
- Laptop with secure digital (SD) storage

9.0 Procedure

9.1 Camera Startup

Table 1 provides a summary of IR camera operations. Users should refer to the GF320 IR camera operator's manual for additional information on keypad and button functions, level/gain control, and thermal image recording.

Table 1. GF320 Infrared Camera Buttons, Locations, and Functions

Button	Location	Function
S	Top of hand grip	Allows the user to save an image when in picture mode or start and stop the recording of video when in video mode.
A/M	Top of hand grip	Switches camera mode between Automatic -Level and Gain, Manual - Level and Gain, and High Sensitivity Mode (HSM).
FOCUS/ZOOM	Top of hand grip	Allows the user to focus the image when in video or picture mode and zoom in on an image that has been saved.
P	Top of camera	A programmable button that can be set to control the color palette, change zoom factor, invert polarity, or hide/show graphics.
Temperature Range	Top of camera	Allows the user to adjust the temperature range. Typical setting is 50–140 °F.
Menu	Back of hand grip	Allows the user to bring up the menu. Pressing menu a second time closes the menu or backtracks.
Menu Joystick	Back of hand grip	Allows the user to navigate menus. Pushing in selects menu option.
Power	Back of hand grip	Allows the user to turn the camera on and off.
Visible Image	Front left side of camera	Toggles the camera between visible imagery and IR imagery.
Laser	Front left side of camera	Allows the user to aim/identify. Holding down produces a laser dot for aiming/identifying.
Camera Dial	Back left side of camera	Used to switch between camera mode, video mode, file archive, program, and settings.

To operate the infrared camera:

1. Ensure that a fully charged battery has been inserted into the camera.
2. Turn the power on and allow 5 minutes for the camera to reach operating temperature. The message in the viewfinder will read "Cool down in progress" during this time.
3. After cool-down is complete, verify that the date and time settings are correct.
4. To set the date and time, turn the camera dial to settings, use the menu joystick to navigate to "set date and time," and press joystick to change the date and time.
5. Remove the lens cap and select AUTO, MANUAL, or HSM mode by pressing the A/M button:
    - In AUTO mode, the camera sets the level and gain based on scene content, which can also be described as the temperature of the objects in the scene.
    - In MANUAL mode, the user adjusts the level and gain manually to optimize the image in the viewfinder. Adjusting level and gain is done by using the menu joystick (up/down adjusts level; left/right adjusts gain).

- In HSM mode, level and gain are set by the camera along with a higher image integration rate to allow imaging of smaller leaks.

6. Adjust the focus using the FOCUS/ZOOM button (or the black ring near the lens) to produce the clearest thermal image.
7. Ensure the camera is functioning properly (operation verification) by viewing the presence of a hydrocarbon plume through the eyepiece. This can be accomplished by the use of a butane lighter or other hydrocarbon source. Document this verification in the field logbook.

The camera is now ready for thermal imaging.

Figures 1–5 show the control buttons for the Infrared Camera.

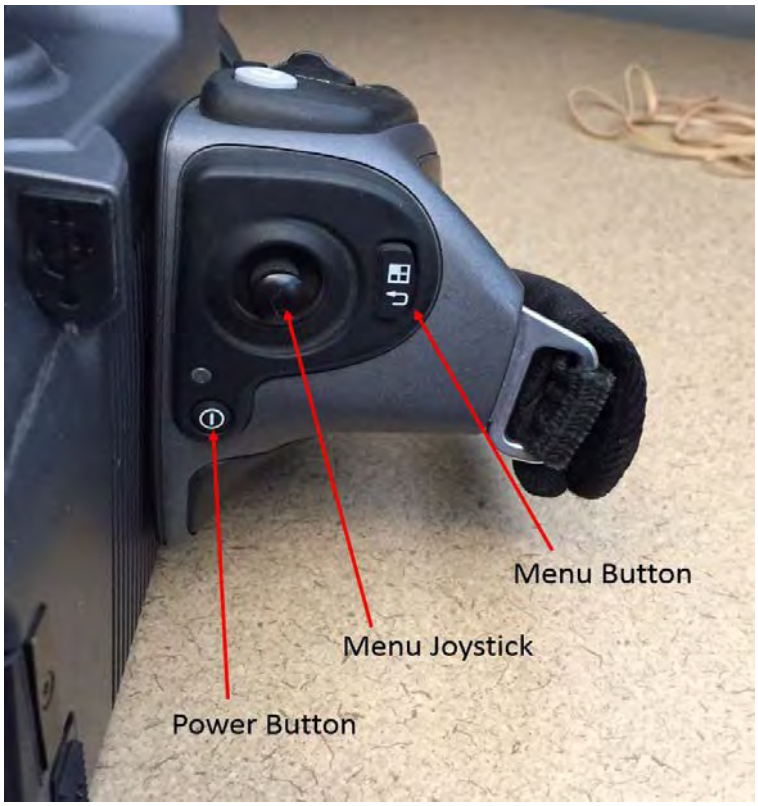

Figure 1. GF320 back of hand grip with Power, Menu Joystick, and Menu buttons.

Figure 2. GF320 top of hand grip with Auto/Manual/HSM, Focus/Zoom, and Save/Start-Stop Recording buttons.

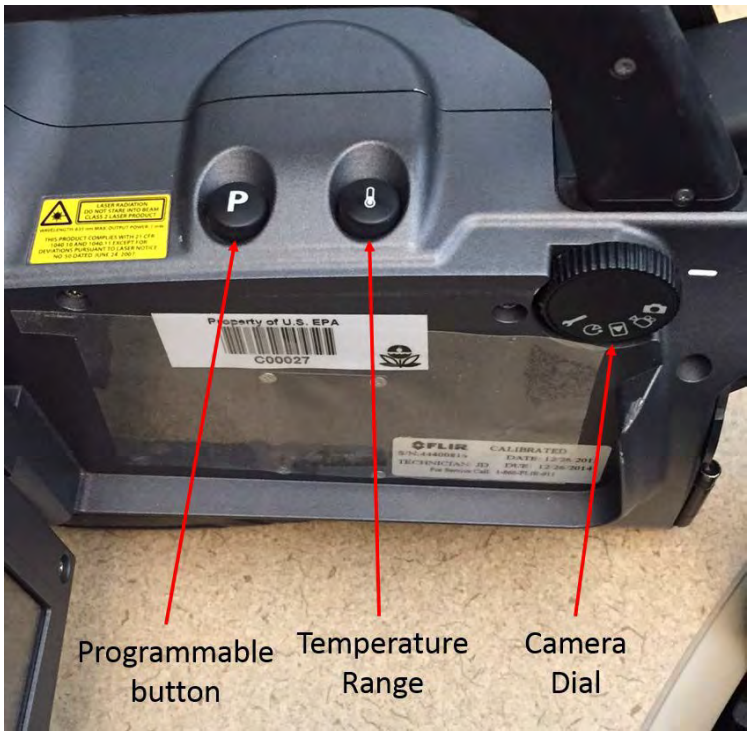

Figure 3. GF320 top of camera with Programmable button, Temperature Range, and Camera Dial.

Figure 4. GF320 front left side of camera with Manual Image Focus, Visible Image, and Laser buttons.

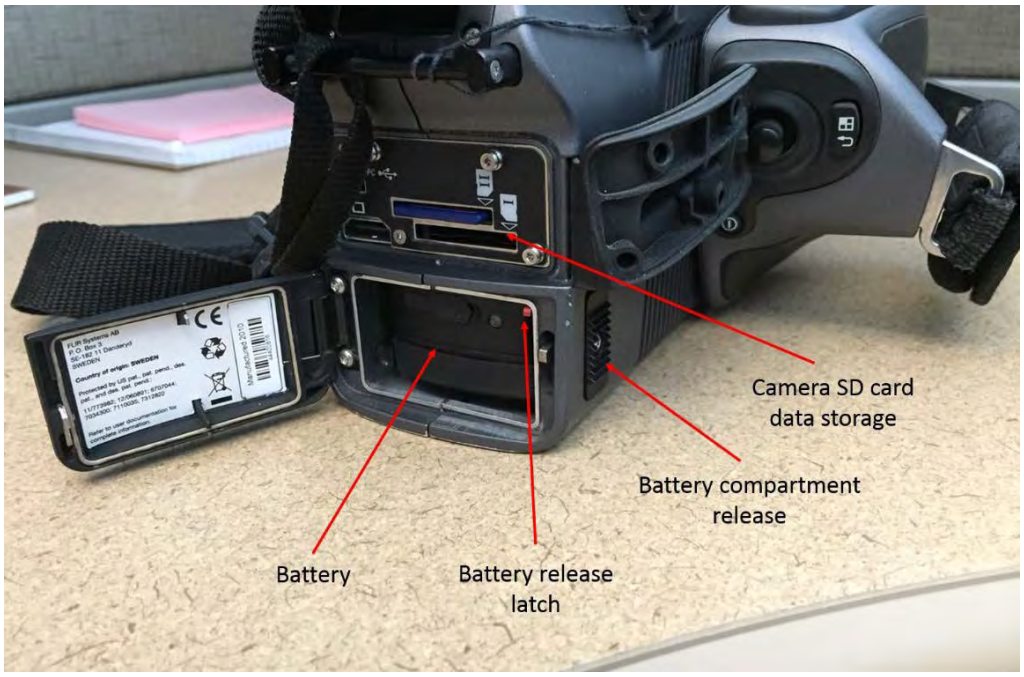

Figure 5. GF320 back of camera with battery, battery release latch, battery compartment release, and camera SD card and data storage.

9.2 Safety Site Survey

1. Use the GF320 to identify any substantial hydrocarbon vapor plumes that might pose significant danger to health and safety by scanning the site upon arrival.
2. Once the safety site survey is completed and no hazardous conditions are identified, begin OGI survey as per QAPP.

9.3 Component Leak Source Identification

Upon completion of the safety site survey procedure, execute screening as per the QAPP. Screen the components for hydrocarbon emitting leak source using the IR camera.

1. For each test, thoroughly inspect the entire component from different angels so as to achive different backgrounds.
2. When a leak source is observed to be emitting (releasing hydrocarbon emissions), document visibility (1. Easy, 2. Moderate, 3. Difficult) as per QAPP.
3. Execute any required video saving and associated record keeping as per the QAPP

9.4 Reserved section

Reserved section

1. N/A

9.5 Camera Battery Replacement

1. Open the battery compartment, located at the back of the camera by using the battery door release located just to the right of the battery compartment.
2. Press down on the battery release hatch (the small red lever located in the top right corner of the battery compartment).
3. Remove the old battery.
4. Insert a new battery with contacts up, facing towards the camera body.
5. Close the battery compartment door.

10.0 Data and Records Management

Information generated by field personnel must be organized and accounted for in accordance with established records management procedures of the QAPP. Data recorded in the project forms and electronic files shall include, but are not limited to, the following:

- IR camera serial number
- Project name
- Camera operator name
- Date and time
- Recorded video file number
- Description of recorded video
- Weather conditions
- Remarks

11.0 Quality Control and Quality Assurance

Important factors in establishing quality requirements include the sensitivity and specificity of the detection system used. Quality requirements include ensuring that equipment is ready for use as follows:

- Operating instructions and/or manuals from the manufacturer are available for each piece of equipment.
- Equipment used for field activities must be handled, transported, shipped, stored, and operated in a manner that prevents damage and deterioration. Equipment must be handled, maintained, and operated in accordance with the manufacturer's operating instructions.

Field personnel are responsible for maintaining a central, comprehensive list of all field equipment subject to this procedure. The equipment inventory list for each instrument or piece of equipment must include the following:

- The description/identity of the equipment (e.g., IR camera, IR camera lens)
- Manufacturer's or vendor's name
- Equipment serial number or other manufacturer identification number
- The manufacturer's instructions or a reference to their location
- Record of damage, malfunctions, modifications, and/or repairs to the equipment

Any problems or abnormalities observed during use of the instrument must be recorded in the field notebook. If the instrument does not appear to be operating properly, red-tag it and remove it from service. Record pertinent information in the project logbook, including date, time, video file number and description, location, and camera operator name.

12.0 References and Supporting Documentation

NEICPROC/11-005. FLIR GasFindIR GF320 Infrared Cameras. 1-23-2012.

FLIR GF3xx Series User's Manual, Publ. No. T559157, Revision a506, December 21, 2010.

FLIR Systems, http://www.flir.com (last accessed December 13, 2016). Users can view training videos and download manuals from FLIR Systems.

Optical Gas Imaging Daily Validation and Log Sheet

Daily Validation	
Date and Time: 10/19/18 8:07 AM	Project Name: SOUR LAKE 3.2.2.
IR Camera Serial Number: 44401015	Camera Operator Name: Mike Clausewitz
Weather Conditions: PARTLY SUNNY, TEMP 62°, HUMIDITY 82%, WIND 3MPH	
Validation test 1 distance: 5'	Validation test 1 recorded video file number: 2773
Validation test 2 distance: 15'	Validation test 2 recorded video file number: 2775
Description of recorded video:	
Remarks:	

Video Recording	
Time: ~ 9:05 AM	Camera Operator Name:
Recorded video file number: DC 2777 – MOV 2780	
Weather Conditions: PARTLY SUNNY, TEMP 70°, HUM 69%, WIND NE 5 MPH	
Description of recorded video: LL 4 AT 30 SCCM	
Remarks:	

Optical Gas Imaging Daily Validation and Log Sheet

Video Recording	
Time: ~ 9:45 AM	Camera Operator Name:
Recorded video file number: 02782	
Weather Conditions: Temp Hum WSW PARTLY SUNNY, 71°, 69%, ENE 5 MPH	
Description of recorded video: TAG 16217 - VALVE PLUG - Weep hole	
Remarks:	

Video Recording	
Time:	Camera Operator Name:
Recorded video file number:	
Weather Conditions:	
Description of recorded video:	
Remarks:	

Video Recording	
Time:	Camera Operator Name:
Recorded video file number:	
Weather Conditions:	
Description of recorded video:	
Remarks:	

Appendix D6

Node Field Test Procedures - Sensor Bump Test and Calibration

Molex Gas Sensor Bump Test Procedure (used in FHR CC Pilot test)

Equipment

- Calibration gas cylinder (500 ppb isobutylene balanced with zero air)
- Positive flow regulator, single stage, 0.3 - 8.0 LPM selectable flow
- Calibration cup
- Calibration tubing (with air conditioning assembly)
- Mobile device with “mSyte” application installed

PPE

Compliance with the worksite’s requirements

Frequency

Bump test to be executed once per quarter or as per specific project guidance (e.g. QAPP) period.

Pass/Fail Threshold Limits

±50% of the nominal value of the gas

Preparation

Hold the regulator, turn the calibration gas cylinder in a clockwise direction to tighten; connect either end of the calibration tubing to the regulator’s barb fitting; connect the other end of the calibration tubing to the calibration cup.

Procedure

1. Open the "mSyte" application, select the target device, click the “Bump Test” button in the “mSyte” application to enter the “Bump Test” mode.
2. Click the “Start” button to initiate the actual bump test, the first count down clock (10s) will be activated.
3. When an “Apply Gas” message appears, turn on the calibration gas cylinder, set the flow rate as “0.3” LPM, and place the calibration cup over the sensor orifice, push the calibration cup onto the orifice to secure the connection.
4. The second countdown clock (30s) will be activated.

5. Once the count down clock is finished, the mobile device will display “Pass” or “Fail” result; the device will return to the “Operation” mode. Turn off the calibration gas and remove the calibration cup from the sensor orifice.

6. Perform another bump test if the first bump test result is “Fail.”
7. Follow the attached process flow chart for additional operations if the sensor doesn’t pass the bump test.

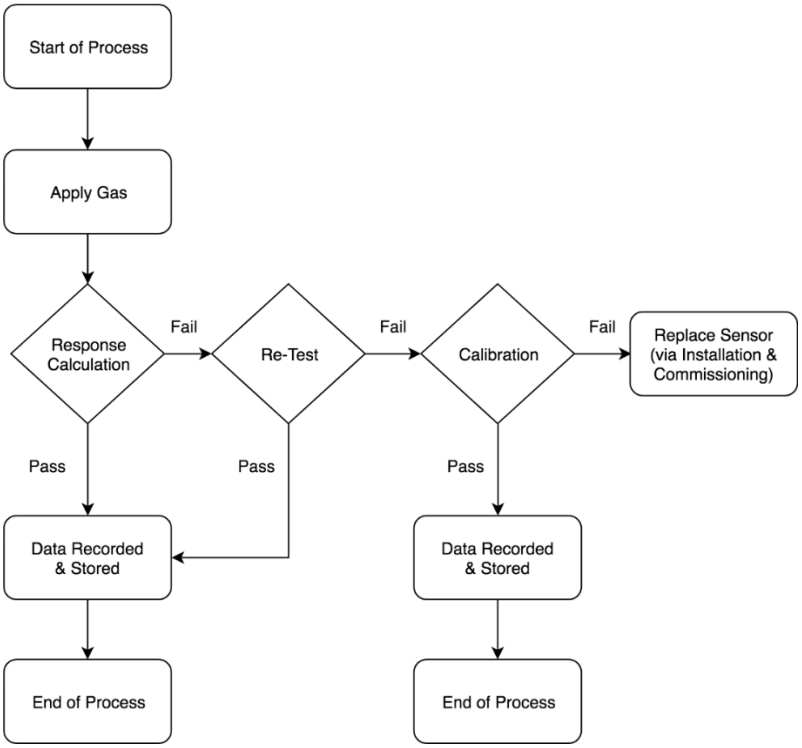

Molex Gas Sensor Calibration Procedure

Equipment List

- Calibration gas cylinder (500 ppb isobutylene balanced with zero air)
- Positive flow regulator, single stage, 0.3 – 8.0 LPM selectable flow
- Calibration cup
- Calibration tubing (with air conditioning assembly)
- Mobile device with “mSyte” application installed

PPE

Compliance with the worksite’s requirements

Frequency

Once a year or when sensors fails bump test, whichever comes first.

Preparation

Hold the regulator, turn the calibration gas cylinder in a clockwise direction to tighten; connect either end of the calibration tubing to the regulator's barb fitting; connect the other end of the calibration tubing to the calibration cup.

Procedure

1. Open the "mSyte" application, select the target device, click the "Calibration" button in the "mSyte" application to enter the "Calibration" mode
2. Click the "Start" button to initiate the actual calibration process, the first countdown clock (30s) will be activated.
3. When an "Apply Gas" message appears, turn on the calibration gas cylinder, set the flow rate as "0.3" LPM, and place the calibration cup over the sensor orifice, push the calibration cup onto the orifice to secure the connection.
4. The second countdown clock (90s) will be activated.
5. Once the countdown clock is finished, the mobile device will display "Pass" or "Fail" result; the device will return to the "Operation" mode. Turn off the calibration gas and remove the calibration cup from the sensor orifice.
6. Perform another calibration if the calibration result is "Fail".
7. Follow the attached flow chart for additional operations if calibration fails again.

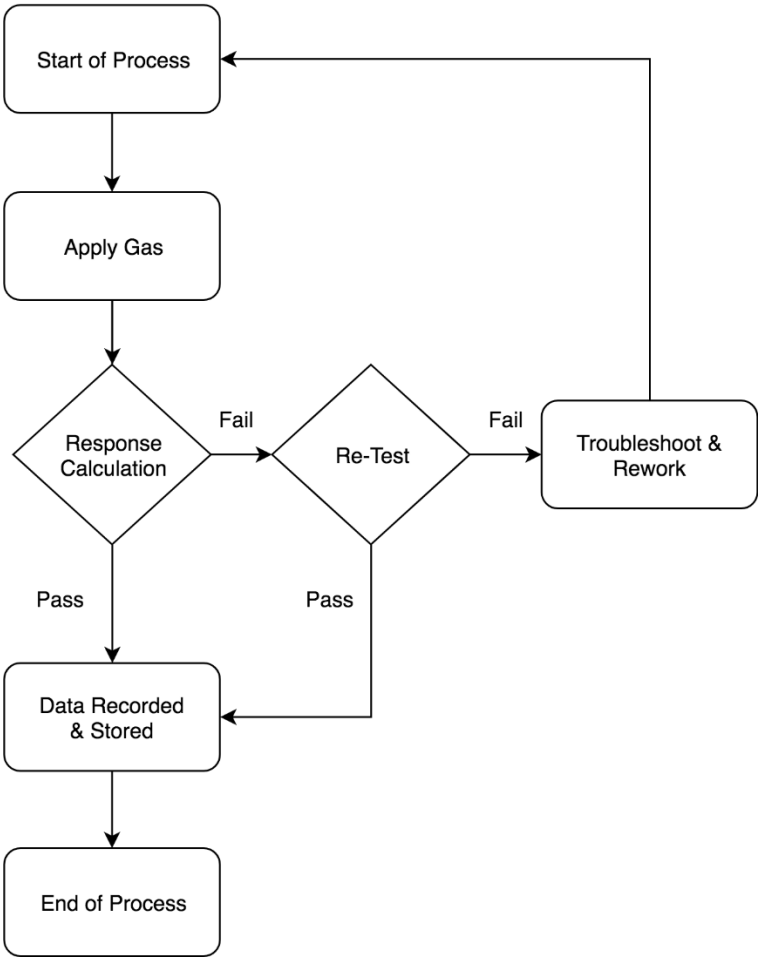

Appendix D7

Simulated Leak Test Gas Release Procedures (Controlled Release Procedures)

Example Controlled Release Apparatus and Test Matrix

This is an example of the controlled gas release apparatus and the test matrix for FHR SLOF trials (Appendix B). The same equipment and similar procedures were used in the exploratory trial at the EPA RTP test range (Appendix A). Due to safety concerns, controlled test gas release were not performed in the FHR CC trials but the M21 readings from found leaks provided feedback on LDSN performance in that case.

Gas Release Apparatus

In the FHR SLOF tests, either 100% isobutylene gas or 100% ethylene were used as the simulated leak gas, and an intentionally loosened valve was the leaking component. As with the exploratory tests, isobutylene (RF = 1) was the primary controlled release gas used in > 90% of the trials. A two stage CGA590 regulator was fitted to the gas tank to release gas at a reduced pressure. A gas flow control box was connected to the gas delivery line between the gas tank and the leaking component using polyurethane tubing. The gas flow controller box consisted of 4 MC series digital mass flow controllers (MFCs) of varying flow rate ranges, i.e. 0-10 sccm (standard cubic centimeters per minute), 0-50 sccm, 1-500 sccm, and 0-2000 sccm made by Alicat Scientific, Inc, Tucson, AZ

Alicat MC series MFCs are based on the accurate measurement of volumetric flow. The volumetric flow rate is determined by creating a pressure drop across a unique internal restriction, known as a laminar flow element, and measuring differential pressure across it. Per manufacturer's datasheet:

http://www.alicat.com/documents/specifications/Alicat_Mass_Controller_Specs.pdf

(last accessed 03/14/2020), the mass flow controllers can be operated at -10 to 60 °C, and accurately controls the flow rate of gas to ± 0.4% of Reading + 0.2% of Full Scale. They also have a list of gases built in to correct for possible errors when used for a gas different from the calibration gas, typically nitrogen. In these tests, we set the gas type to either isobutylene or ethylene depending on which gas is used. All these mass controllers used in the test had a Class 1 Div. 2 rating. A picture of the Alicat MFC is shown in Figure D7-1 below with the

actual set of controllers used in testing shown Figure D7-2. Note these MFCs are specially designed to handle isobutylene gas.

Figure D7-1. Alicat Scientific MC series MFC

Figure D7-2. Set of Alicat Scientific MC series MFCs used in tests

In exploratory test (Appendix A), a flow rate between 5 and 20 sccm was primarily used. In the FHR SLOF tests (Appendix B), flow the presence of an interfering source (fin fan leaks) necessitated the use of higher test gas release flow rates. When no pressure is built up in the downstream, the actual flow rate displayed by the MFC is an indication of the leak rate of the gas through the leaking component. For the purpose of comparison and documentation, every leak was measured by the TVA-1000B FID and the MiniRAE 3000 PID following the EPA M21 procedure, and by a FLIR model GF320 OGI camera. The TVA-1000B and MiniRAE PID instruments that were calibrated every day before use as per M21 requirements.

Isobutylene and ethylene are flammable gases. They have a lower explosive limit (LEL) of 1.8% and 2.7% by volume, respectively. For safety reasons, the test site and particularly the leak point were monitored by four Industrial Scientific Corporation model Radius BZ1 area monitors. Each monitor is equipped with an oxygen sensor, a combustible gas sensor that has a resolution of 1% LEL, and a PID sensor that has 1ppm resolution. The oxygen and combustible gas sensors have their low-level alarm points set at 19.0% O2 and 10%LEL, respectively. As is specified in the in CRADA Safety Plan, all the safety monitors were bump tested each day to known concentration gases before use to ensure proper working order.

For Test 3 at SLOF, 100% isobutylene and 100% ethylene was released, controlled and monitored utilizing CGA510 single-stage regulator and Alicat Scientific MFCs. Portable LEL Monitors were set up at release gas cylinders, Alicat flow controller unit, and at leak point locations. A manual power shutoff to the flow controller would have been performed if LEL readings reach 10% LEL. Controlled releases were only be performed while test team was on site. A total of ten (10) sensors and one (1) spare sensor were used for Test 3.1. Sensor placement, leak location and isobutylene or ethylene mass flow rates were adjusted based on actual test results. Detection results were monitored in real time for the SLOF test via a data acquisition system and displayed for evaluation and adjustments. This testing approached helped the team better understand sensor node spatial relationship to detectability, mass flow rate and concentration correlations, impedance impact on plume characteristics and PID performance for remote detection of near-source emissions under changing meteorological conditions.

Example Test Procedures Matrix for Test 3.1 (Appendix B1)

This section contains information on the test procedures used for Test 3.1 (an example)

Test Procedure: Geospatial Sensor Placement

Purpose: Study correlation between sensor locations and detectability for both isobutylene and ethylene. Test and optimize sensor locations so that any leak within the defined perimeter can be detected by one or more of the sensors.

Test Preparation (daily):

1. Conduct Safety Meeting (Safety Plan)
2. Establish Communication Protocol and Task Assignments
3. Review Test Plan, Procedure and Safety Measures

4. Conduct parameter space assessment in single sensor node mode
5. Set up and calibrate equipment, baseline test sensors against background
6. Conduct functional test and sensor bump test (dry run)

Data Collection Procedure and Instructions:

1. Establish and record primary test set up parameters
   1.1. Sensors / emission geospatial position for Test #1 (performed for each node)

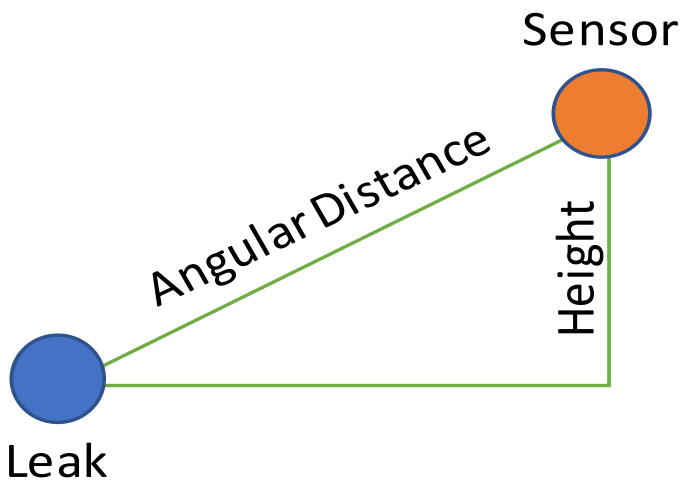

Figure D7-3. Example of placement geometry

Each controlled release or background experiment (Test) was documented with layout map containing the physical locations and separation measurements for each sensor node and emission point. Here the layout map for the Test #1 (and all subsequent tests with the same sensor locations) is signified as "A" in Table D7-1. The controlled release or documented physical leak position (uniformly called "leak location"), is recorded in the layout map and carries the Test # (e.g. L1 for Test #1).

   1.2. Gas type (or known natural leak details)
   1.3. Mass flow rate to be used for the trial (or details of know natural leak)

2. Initiate recording of other test parameters (data logger)
   2.1. Meteorological Data
   2.2. Sensor Baseline Readings

3. Start gas flow at predetermined flow rate for release gas (if required)

3.1. Start gas flow and record gas flow start time
3.2. Wait 5 min and then perform Method 21 and record TVA & MiniRAE readings, and IR Camera results.
3.3. Record sensor readings and the reading time
3.4. MOLEX Sensor and SPod will be electronically data logging
3.5. Continue taking readings until predetermined test time, (e.g. 30 min), is completed

4. Stop gas flow and record time ending Test #1

5. Reposition sensors and/or leak to geospatial position #2 for Test #2 (or subsequent tests if necessary).

6. Examine controlled release gas type change requirements for Test#2 (or subsequent test). ***If no controlled releases gas type change is required***, repeat Step 1 to document new layout and gas release parameters for Test #2, repeat Step 2 (if not already operating), and repeat Steps 3-5 to complete Test 2# (use the same procedure for subsequent tests).

7. ***If controlled release gas type change is required***, switch source gas and reset the gas type in MFC as required and perform required line purging procedure after gas change.

8. With the new controlled release gas type, repeat Step 1 to document new layout and gas release parameters for Test #2, repeat Step 2 (if not already operating), and repeat Steps 3-5 to complete Test 2# (use the same procedure for subsequent tests).

Example Test Matrix for Test 3.1

This section contains an example of the controlled release test matrix used for Test 3.1 (Appendix B1). Compared to SLOF Test 3.2 (Appendix B2), Test 3.1 was more exploratory in nature with the results obtained during initial days of testing providing feedback on decisions for testing on subsequent days. Controlled release tests were conducted over a base 30-minute time frame, which could extend to 2 hours, depending on conditions. Due to changing daily meteorological conditions, the exact deployment plan (sensor and leak placements) was not rigidly set beforehand but was determined at the beginning of each day based on the wind forecast and thoroughly documented. Other parameters, such as sensor operating settings, were varied. A basic example test matrix is showed in Table D7-1 with meteorological conditions (e.g. wind speed and wind direction) recorded the onsite met station and the EPA SPod (not descried here). See Appendix B for additional details.

Table 7-1. Example Planned Test Matrix for Test 3.1 (initial release rates increased to 30 sccm min due to fin fan leak interference)

Test #	Layout	Leak Location	Gas Type	Leak Rate, SCCM	Test Time, Min
1	A	N/A	Background	0	120
2	A	L1	ISO	10	30
3	A	L2	ISO	10	30
4	A	L3	ISO	10	30
5	A	L4	ISO	10	30
6	A	L5	ISO	10	30
7	A	L6	ISO	10	30
8	A	L7	ISO	10	30
5	A	L4	ISO	10	30
6	A	L5	ISO	10	30
7	A	L6	ISO	10	30
8	A	L7	ISO	10	30
9	A	L8	ISO	10	30
10	A	L9	ISO	10	30
11	A	L10	ISO	10	30
12-16	B	Selected*	ISO	10	30
17-18	C	Selected*	ISO	10	60
19-20	D	Selected*	ISO	10	60
21	E	Selected*	ISO	10	60
22	E	N/A	Background	0	Weekend
23-33	E	L1-L10	ETH	20	60
34-35	F	Selected*	ETH	20	60
36	F	Selected*	ISO	10	60

* Leak locations adjusted to matched new sensor locations

Appendix E

EPA ORD Equivalency Simulations

Appendix E1

EPA ORD Simulation Approach

Appendix E1

EPA ORD Simulation Approach

Table of Contents

1 Introduction 5
2 Previous Guidance 6
3 LeakDAS Inventory 7
3.1 Inventory Characteristics 7
3.2 Methods 12
3.3 Leak Sample Characteristics 16
4 Monte Carlo Model 18
4.1 Methods 18
4.2 Model Comparison 22
4.3 Model Sensitivity 24
5 Simulation Results 25
6 References 28

Figures

Figure 3-1: LeakDAS TVA Measurement Distribution 10
Figure 3-2: LeakDAS Data Processing Method 13

Tables

Table 3-1: Mid-Crude Unit LeakDAS Records Summary 8
Table 3-2: m-Xylene Unit LeakDAS Records Summary 9
Table 3-3: Mid-Crude Unit Component Records Summary 11
Table 3-4: m-Xylene Unit Component Records Summary 12
Table 3-5: Mid-Crude Unit Leak Summary 16
Table 3-6: m-Xylene Unit Leak Summary 17
Table 4-1: EPA ORD Model Input Variables 20
Table 4-2: EPA ORD and Molex Simulation Comparison, Median Emissions 22
Table 4-3: EPA ORD and Molex Simulation Comparison, Equivalency 23
Table 4-4: Model Sensitivity, emissions distribution statistics 24
Table 5-1: Simulation results 25
Table 5-2: Simulation results, alternate CWP scenario 25
Table 5-3: Simulation results, LDSN DTA 26
Table 5-4: Simulation results, detection time 27

1 Introduction

To establish an alternate work practice (AWP), the proposed leak detection and repair (LDAR) approach must demonstrate a reduction in regulated material emissions at least equivalent to the reduction achieved under current federal requirements (40 CFR 65.8(a)). This Appendix outlines an equivalency determination approach which compares LDSN/DRF emissions reductions to those achieved under the current work practice (CWP), scheduled Method 21 (M21) LDAR.

Previous guidance provides a rubric for evaluating equipment leak control relative to the CWP, but previous models were designed such that they cannot comprehensively evaluate the strengths and weaknesses of the LDSN/DRF concept. A new Monte Carlo model, rooted in previous approaches, was developed in order to better evaluate the long-term controls of LDSN/DRF and reflect the continued use of M21 Toxic Vapor Analyzer (TVA) measurements. Additionally, historical process unit-specific data was used to better reflect the specific conditions of the Flint Hills Resources, Corpus Christi (FHR CC) pilot study. This site-specific equivalency approach was deemed most suitable by the CRADA team for evaluation of the LDSN/DRF concept at the current stage of development. Development of a less specific and more transferable equivalency evaluation approach for LDSN/DRF is the subject of ongoing research.

This Appendix includes additional support for the equivalency analysis presented in Section 4 of the report. Appendix E is structured as follows:

E1 EPA ORD Simulation Approach (*written summary*)

- Section 2 discusses previous equivalency approaches developed for evaluating new Leak Detection and Repair (LDAR) methods.
- Section 3 describes the historical database used to characterize processing unit leaks, data processing methods, and the simulation leak dataset characteristics.
- Section 4 describes the Monte Carlo model approach and discusses model sensitivities.
- Section 5 reviews emissions simulation results.

E2 EPA ORD Software Code (*R code*)

E3 LeakDAS Database (*.csv tables*)

2 Previous Guidance

Two different equivalency approaches were reviewed when developing the pilot study LDSN/DRF equivalency evaluation. The first is the 1999 EPA document *Monte Carlo Simulation Approach for Evaluating Alternative Work Practices for Equipment Leaks* (referred to as "1999 EPA Approach" in this Appendix) (U.S. EPA, 1999). This document presents a Monte Carlo simulation tool available for petitioners to use when proposing AWPs to replace the CWP (scheduled, manual M21 LDAR management for all components). The tool was designed to compare M21 to other means of detection—distinguishing between the 'true mass emission rate' and the emission rate derived from screening value (SV) correlations.

While the emphasis on mass emissions is important given the significant uncertainty associated with M21, it was not as easily applicable to the proposed LDSN/DRF method without introducing additional uncertainty in comparisons. In this case, both the CWP and proposed alternative are dependent on M21 to characterize individual leaks. Since M21 is part of the LDSN/DRF approach and part of the CWP, it serves as a stable point of comparison for site-specific evaluation with existing historical data.

The difference in approach is focused on distribution and efficiency of M21-based LDAR resources rather than elimination of M21 entirely. Given this difference, true mass emissions were not considered for the approach presented in this report, and M21 measurement uncertainty was not included. This was a simplifying assumption, but it was deemed a reasonable simplification because both the CWP and LDSN/DRF would have the same level of uncertainty in individual M21 leak measurements. The focus on M21 uncertainty instead of leak duration limited the suitability of the 1999 EPA Approach for this analysis. However, the document provides important initial guidance. The 1999 EPA Approach establishes a Monte Carlo modeling framework which creates simulated facility leak profiles, models different leak detection methods, and applies a useful equivalency benchmark wherein at least 67% of simulations must demonstrate emissions equivalency for an AWP to be defined as equivalent. While the 1999 EPA Approach created a helpful framework, later work provides adjustments more applicable for the LDSN/DRF method.

The 2000 document *Monte Carlo Simulation Evaluation of Gas Imaging Technology* (referred to in this report as "OGI Evaluation") built upon the equivalency determination method presented in the 1999 EPA Approach using an updated version of the original simulation code. Similar to the original model, the OGI Evaluation considered M21 uncertainties relative to a detection method dependent on 'true mass emissions.' Unlike LDSN, the proposed OGI AWP still depended on scheduled monitoring, but the method did evaluate the impact of different monitoring intervals to allow for a higher detection threshold. The OGI Evaluation also updated the equivalency determination to compare cumulative emissions instead of cumulative emission rates. It also ignored emissions from components which would not be subject to repair under either work practice by assuming equivalent control levels would be achieved—simplifying modeling. While the introduction of emissions and varying leak durations was very important for evaluating LDSN/DRF, the OGI Evaluation was limited to estimating quarterly emissions. The

approach did not seek to demonstrate long-term equivalency, and LDSN/DRF modeling suggested contributions from smaller leaks are not always insignificant if the number of unrepaired leaks increases with time. Ultimately, incorporating leak emissions was an important factor in developing an LDSN/DRF equivalency analysis.

While each of the previous approaches provided some guidance in equivalency determination methods, neither was thought to be the single best approach for evaluating the LDSN/DRF concept. For example, the FHR CC pilot study process units include a variety of component categories in their LDAR programs which are often subject to different monitoring intervals. Both the 1999 and 2000 approaches were limited to modeling valves subject to quarterly monitoring. Moreover, an LDSN's ability to detect leaks is inherently based in the sensors locations chosen for a specific system. Neither previous analysis created space for more specific evaluations, instead focusing on the most broadly applicable leak detection simulations. The equivalency determination approach presented in this appendix seeks to address the limitations of the previous analyses and provide a method which considers the particulars of the LDSN/DRF concept.

3 LeakDAS Inventory

The LeakDAS inventory is a database system which FHR uses as a tracking tool for all LDAR activities which occur at FHR, CC West. Records from 2013-2019 for the two pilot study process units, Mid-Crude and m-Xylene, were used to characterize leaks subject to LDAR management. Multiple years were chosen to provide sufficient data for a long-term multiyear analysis, and the most recent available data was used in order to most closely reflect the current process units. Both TVA measurement and AVO detection records were reviewed because both must be considered in order to effectively compare the CWP and LDSN/DRF concept.

The inventory of TVA measurements was processed to produce a final sample of process unit leak SVs more similar to the 1993 OAG multi-unit dataset used in the 1999 EPA Approach and OGI Evaluation [American Petroleum Institute, 1995; Epperson, 2000]. This section outlines the dataset characteristics and processing methods used.

3.1 Inventory Characteristics

The LeakDAS inventory for the FHR CC Mid-Crude and m-Xylene units includes 148,692 and 106,275 relevant LDAR records, respectively, between the years of 2013-2019. Initial investigations of the dataset were limited to the years 2014-2018 in order to create a 5-year leak profile for each unit. However, data from adjacent years was ultimately incorporated in order to better characterize leaks events which occurred over the 5-year period. A summary of Mid-Crude LeakDAS measurements is included in Table 3-1, and a summary for m-Xylene measurements is included in Table 3-2.

In both units, there were very few AVO-Visual detections, and the majority of TVA measurements were very small (< 10 ppmv). For comparison, the leak definition for a component

is, at minimum, defined as 500 ppmv. Measurements over a component threshold are recorded as "Failed" and comprised 1.24% and 1.55% of TVA measurements in Mid-Crude and m-Xylene, respectively. Leaks are also slightly overrepresented in the LeakDAS database relative to their physical presence because a component with an active leak may be measured several times prior to repair (accounted for in the analysis). In contrast, a component without an active leak is unlikely to be measured more than once in a monitoring interval. Some components, for example in heavy liquid service or under insulation, are not routinely monitored and leaks may only be detected through AVO. The low proportion of "failed" TVA measurements in comparison to the vast number of measurements executed illustrates the significant inefficiencies associated with the CWP. While the comparatively small population of active leaks in a process unit during a given period may be found effectively under the CWP, the majority of scheduled-M21 LDAR efforts are focused on non-leaking components.

Table 3-1: Mid-Crude Unit LeakDAS Records Summary

Database Records Summary								
Unit	**Mid-Crude**							
Component Class	**Valve**	**Pump**	**Drain**	**Relief Valve**	**Connector**	**Compressor**	**Piping**	**Total**
Total Measurements	66,261	3,319	5,656	2,462	70,844	149	1	**148,692**
Failed Measurements	428	204	27	4	1,156	27	1	**1,847**
AVO-Visual Records	30	95	0	0	56	13	1	**195**
Calendar Year								
2013	10,434	493	879	293	1,775	12	0	**13,886**
2014	11,297	574	838	363	2,840	22	0	**15,934**
2015	9,283	446	1,099	333	5,968	21	0	**17,150**
2016	6,368	375	731	303	13,679	21	0	**21,477**
2017	12,381	437	721	344	16,723	20	1	**30,627**
2018	8,387	517	696	414	15,097	30	0	**25,141**
2019	8,111	477	692	412	14,762	23	0	**24,477**
TVA Measurements								
0 ppmv	2.5%	5.3%	9.5%	14%	3.4%	3.7%		**3.5%**
1 - <10 ppmv	87%	64%	76%	82%	84%	31%		**85%**
10 - <100 ppmv	8.8%	21%	12%	4.1%	9.3%	32%		**9.4%**
100 - <1,000 ppmv	1.3%	6.0%	1.7%	0.1%	1.9%	21%		**1.7%**
1,000 - <10,000 ppmv	0.3%	2.6%	0.2%	0.08%	0.9%	10%		**0.7%**
10,000 - <100,000 ppmv	0.02%	0.6%	0%	0%	0.1%	0.7%		**0.08%**
100,000 ppmv	0.01%	0.4%	0%	0%	0.08%	1.5%		**0.05%**

Table 3-2: m-Xylene Unit LeakDAS Records Summary

Database Records Summary								
Unit	**m-Xylene**							
Component Class	**Valve**	**Pump**	**Drain**	**Relief Valve**	**Connector**	**Compressor**	**Piping**	**Total**
Total Measurements	67,388	2,143	925	807	35,011	0	1	**106,275**
Failed Measurements	774	140	3	3	727		1	**1,648**
AVO-Visual Records	6	22	0	0	24		1	**53**
Calendar Year								
2013	9,398	303	129	111	5,088		0	**15,029**
2014	9,891	319	126	136	5,431		0	**15,903**
2015	9,372	331	143	115	5,225		0	**15,186**
2016	10,556	315	136	112	6,911		1	**18,031**
2017	9,258	310	129	112	4,047		0	**13,856**
2018	9,162	288	129	113	4,164		0	**13,856**
2019	9,751	277	133	108	4,145		0	**14,414**
TVA Measurements								
0 ppmv	3.2%	1.3%	3.9%	6.4%	3.0%			**3.2%**
1 - <10 ppmv	68%	40%	78%	82%	76%			**70%**
10 - <100 ppmv	25%	35%	16%	11%	17.5%			**22%**
100 - <1,000 ppmv	3.7%	18%	2.2%	0.4%	2.4%			**3.5%**
1,000 - <10,000 ppmv	0.4%	4.6%	0.2%	0.1%	1.1%			**0.7%**
10,000 - <100,000 ppmv	0.03%	1.5%	0%	0%	0%			**0.1%**
100,000 ppmv	0.01%	0%	0%	0%	0%			**0.04%**

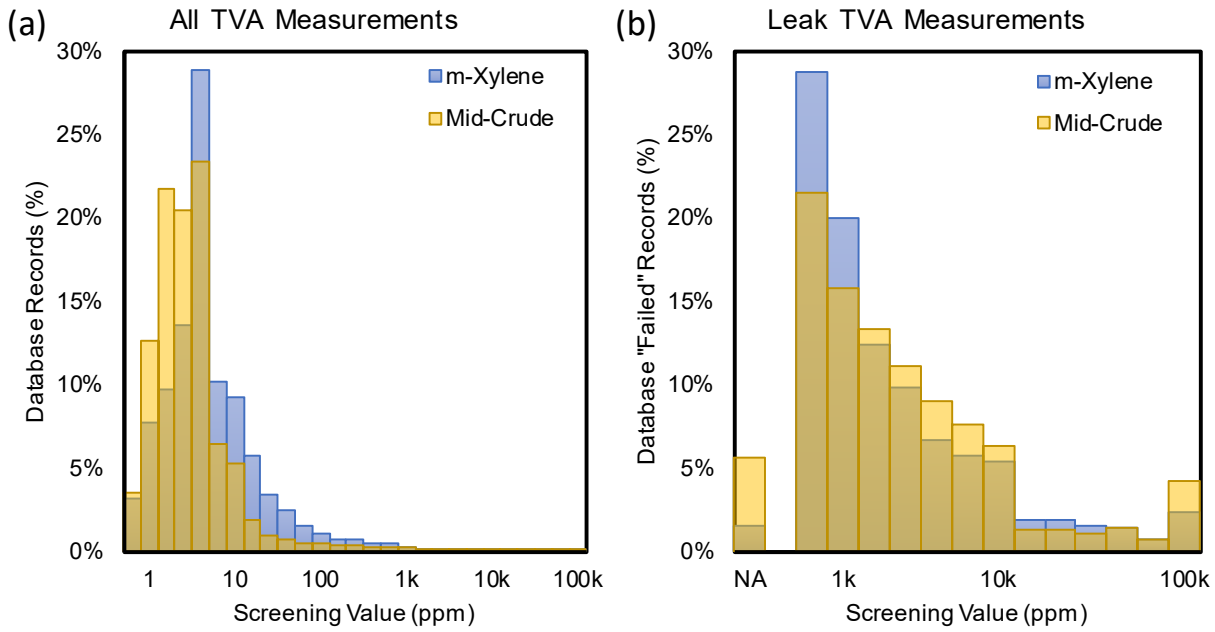

Figure 3-1: LeakDAS TVA Measurement Distribution

Equipment leak magnitudes typically follow a skewed, often lognormal, distribution. Both the overall TVA measurement inventories, shown in Figure 3-1(a), and the subset of "Failed" TVA measurements from leaks, shown in Figure 3-1(b), illustrate this pattern. The points at which the "Failed" measurements show gaps in this pattern, 10,000 and 100,000, are points at which TVA measurement methods change. TVA measurements with SVs greater than 10,000 ppmv are accomplished using a dilution probe, and measurements of 100,000 ppmv indicate a "flameout" occurred, where the concentration from emissions is higher than can be measured with the handheld instrument. Leaks detected through AVO techniques are often not measured prior to the first repair attempt, and these LeakDAS records are included in Figure 3-1(b) under SV label "NA".

While reviewing the body of measurements as a whole is helpful in characterizing the LeakDAS inventory, different categories of components are measured at different intervals. The different CWP monitoring schedules result in relative oversampling of pumps which are monitored on a monthly basis, relative to connectors, which are subject to annual monitoring, or other components subject to quarterly monitoring. A summary of records on a component tag basis is included for Mid-Crude, Table 3-3, and m-Xylene, Table 3-4. The majority of tagged components within both units are connectors. Records for the Mid-Crude unit indicated that a large portion of the connectors were added into LeakDAS in 2015. This was due to a change in requirements for which more components within the unit were subject to scheduled-M21 monitoring. Prior to 2015, these components were monitored as AVO components, and the variance in annual measurements shown in Table 3-1 reflect this change in practice.

The significant variation in connector monitoring was a limitation in the LeakDAS dataset. In order to reflect the alteration in monitoring practices, the Mid-Crude leak sample was limited to 2016-2018 while the m-Xylene dataset reflects leaks from 2014-2018. See Section 2.2 for additional discussion of leak dataset processing method development.

Table 3-3: Mid-Crude Unit Component Records Summary

Component Records Summary								
Unit	**Mid-Crude**							
Component Class	**Valve**	**Pump**	**Drain**	**Relief Valve**	**Connector**	**Compressor**	**Piping**	**Total**
Total Components	9,325	145	220	120	17,553	4	1	27,368
Leaking Components	149	52	13	2	619	4	1	840
AVO Tags	31	84	0	1	80	0	1	197
Fuel Gas Components	443	0	0	0	1,540	0	0	1,983
Chemical State								
GV	2,881	0	0	114	6,076	4	0	9,075
HL	31	84	0	1	38	0	0	154
LL	6,413	61	220	5	11,439	0	1	18,139
Components Added								
2013	14	17	0	1	19	0	0	51
2014	103	13	0	2	958	0	0	1,076
2015	1,101	9	1	0	10,797	0	0	11,908
2016	2	11	0	0	10	0	0	23
2017	3,050	36	0	55	4,513	0	1	7,655
2018	7	14	0	0	10	0	0	31
2019	7	10	0	0	55	0	0	72
Total	4,284	110	1	58	16,362	0	1	20,816
Components Removed								
2013	21	11	1	1	20	0	0	54
2014	43	18	34	0	30	0	0	125
2015	265	20	5	0	196	0	0	486
2016	20	10	0	0	74	0	0	104
2017	907	24	7	27	2,841	0	1	3,807
2018	119	14	0	0	215	0	0	348
2019	1	7	0	0	7	0	0	15
Total	1,376	104	47	28	3,383	0	1	4,939

Table 3-4: m-Xylene Unit Component Records Summary

Component Records Summary								
Unit	**m-Xylene**							
Component Class	**Valve**	**Pump**	**Drain**	**Relief Valve**	**Connector**	**Compressor**	**Piping**	**Total**
Total Components	2,764	25	32	29	6,631	0	1	9,482
Leaking Components	187	14	3	1	339		1	545
AVO Tags	0	0	0	0	26		1	27
Fuel Gas Components	76	0	0	0	0		0	76
Chemical State								
GV	636	0	0	26	1,018		0	1,680
HL	0	0	0	0	2		0	2
LL	2,128	25	32	3	5,611		1	7,800
Components Added								
2013	1	0	0	0	18		0	19
2014	41	0	0	1	99		0	141
2015	10	0	0	0	59		0	69
2016	302	0	0	0	1,661		1	1,964
2017	3	0	1	0	10		0	14
2018	31	1	0	2	42		0	76
2019	49	0	0	0	99		0	148
Total	437	1	1	3	1,988		1	2,431
Components Removed								
2013	1	0	0	0	3		0	4
2014	16	0	0	0	26		0	42
2015	0	0	0	0	42		0	42
2016	35	0	0	0	727		1	763
2017	429	0	0	0	2,251		0	2,680
2018	18	1	0	3	39		0	61
2019	3	0	0	0	24		0	27
Total	502	1	0	3	3,112		1	3,619

3.2 Methods

In order to produce lists of SVs for leaks which occurred between 2014-2018 and 2016-2018 for the m-Xylene and Mid-Crude units, respectively, the historical LeakDAS data needed to be evaluated chronologically on a component-by-component basis. An algorithm was developed for reviewing each component's measurement history and identifying individual leaks. This algorithm is outlined in Figure 3-2 and the R code used to process the measurement data is included in Appendix E2 (referred to as *Identify_Leaks*). Both the input files and the output leak sample datasets are included in Appendix E3.

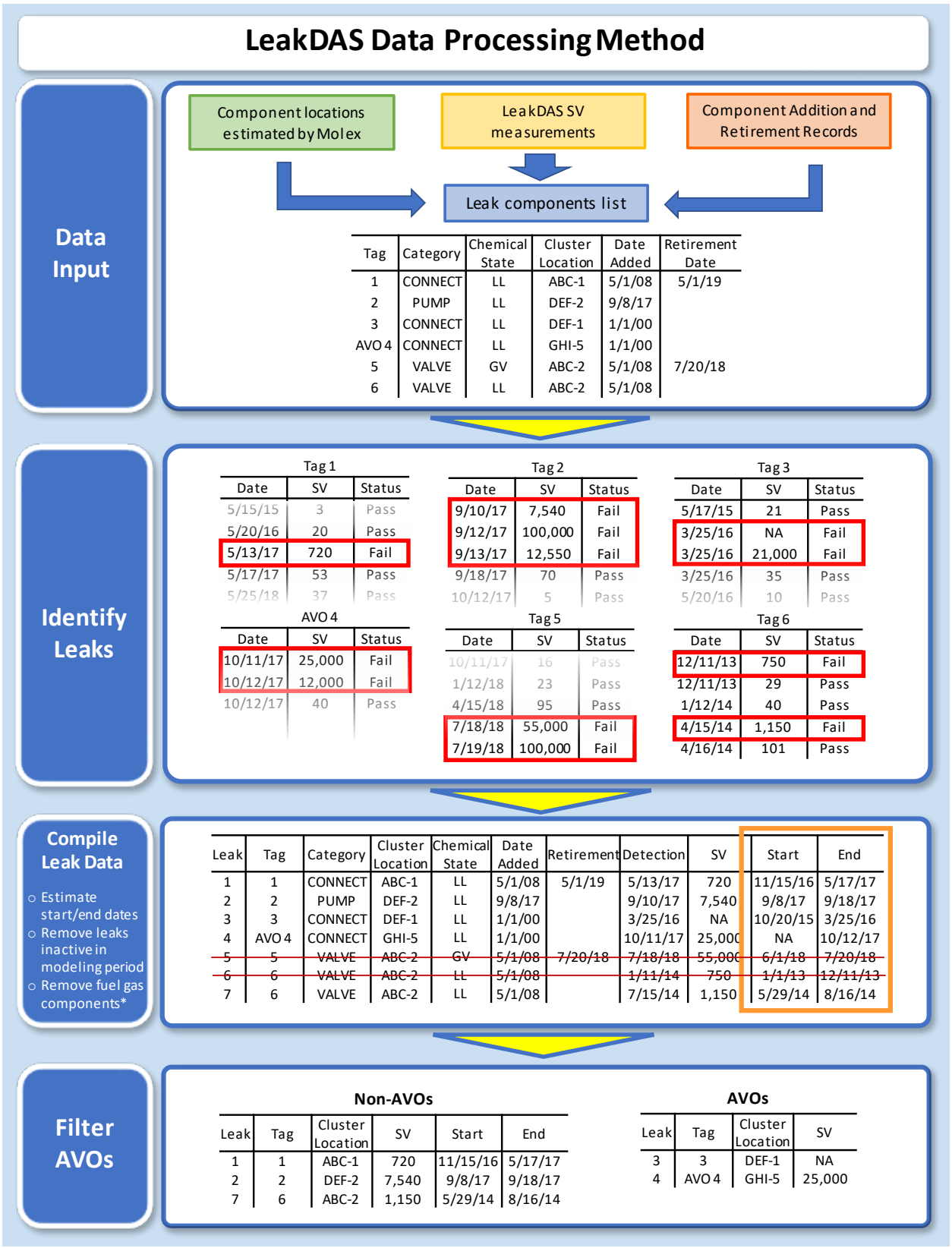

Tag	Category	Chemical State	Cluster Location	Date Added	Retirement Date
1	CONNECT	LL	ABC-1	5/1/08	5/1/19
2	PUMP	LL	DEF-2	9/8/17	
3	CONNECT	LL	DEF-1	1/1/00	
AVO 4	CONNECT	LL	GHI-5	1/1/00	
5	VALVE	GV	ABC-2	5/1/08	7/20/18
6	VALVE	LL	ABC-2	5/1/08	

Tag 1

Date	SV	Status
5/15/15	3	Pass
5/20/16	20	Pass
5/13/17	720	Fail
5/17/17	53	Pass
5/25/18	37	Pass

Tag 2

Date	SV	Status
9/10/17	7,540	Fail
9/12/17	100,000	Fail
9/13/17	12,550	Fail
9/18/17	70	Pass
10/12/17	5	Pass

Tag 3

Date	SV	Status
5/17/15	21	Pass
3/25/16	NA	Fail
3/25/16	21,000	Fail
3/25/16	35	Pass
5/20/16	10	Pass

AVO 4

Date	SV	Status
10/11/17	25,000	Fail
10/12/17	12,000	Fail
10/12/17	40	Pass

Tag 5

Date	SV	Status
10/11/17	16	Pass
1/12/18	23	Pass
4/15/18	95	Pass
7/18/18	55,000	Fail
7/19/18	100,000	Fail

Tag 6

Date	SV	Status
12/11/13	750	Fail
12/11/13	29	Pass
1/12/14	40	Pass
4/15/14	1,150	Fail
4/16/14	101	Pass

Leak	Tag	Category	Cluster Location	Chemical State	Date Added	Retirement	Detection	SV	Start	End
1	1	CONNECT	ABC-1	LL	5/1/08	5/1/19	5/13/17	720	11/15/16	5/17/17
2	2	PUMP	DEF-2	LL	9/8/17		9/10/17	7,540	9/8/17	9/18/17
3	3	CONNECT	DEF-1	LL	1/1/00		3/25/16	NA	10/20/15	3/25/16
4	AVO 4	CONNECT	GHI-5	LL	1/1/00		10/11/17	25,000	NA	10/12/17
~~5~~	~~5~~	~~VALVE~~	~~ABC-2~~	~~GV~~	~~5/1/08~~	~~7/20/18~~	~~7/18/18~~	~~55,000~~	~~6/1/18~~	~~7/20/18~~
~~6~~	~~6~~	~~VALVE~~	~~ABC-2~~	~~LL~~	~~5/1/08~~		~~1/11/14~~	~~750~~	~~1/1/13~~	~~12/11/13~~
7	6	VALVE	ABC-2	LL	5/1/08		7/15/14	1,150	5/29/14	8/16/14

Non-AVOs

Leak	Tag	Cluster Location	SV	Start	End
1	1	ABC-1	720	11/15/16	5/17/17
2	2	DEF-2	7,540	9/8/17	9/18/17
7	6	ABC-2	1,150	5/29/14	8/16/14

AVOs

Leak	Tag	Cluster Location	SV
3	3	DEF-1	NA
4	AVO 4	GHI-5	25,000

Figure 3-2: LeakDAS Data Processing Method

Seven input files, three for each process unit and one additional, are used to analyze unit leak histories. These files are available in Appendix E3 and include:

1. **LeakDAS LDAR Records** provided by FHR. A condensed version which provides all data relevant to the *Identify_Leaks* is included in this report.
2. **LeakDAS Deletion Records** provided by FHR. A condensed version which provides data relevant to the *Identify_Leaks*, limited to data from 2013-2019, is included in this report.
3. **Component Location and Cluster Designations** developed by Molex using site maps and LeakDAS records provided by FHR. A summary file is included in Appendix E3. See Appendix F for additional information.
4. **Emission Factor Correlation Equation Constants** based on 1995 EPA Guidance and FHR inventory practices [U.S. EPA, 1995].

The LDAR records are used to create a list of unique components with discovered leaks during 2013-2019. Non-leaking components are not evaluated because emissions from components with SV less than 500 are assumed to have equivalent levels of control under both the CWP and LDSN/DRF. The fields 'ComponentTag', 'Pass_Fail', and 'LocationDescription' are used to develop the list of leaking components. 'LocationDescription' is necessary to distinguish between AVO leaks without unique component tags (labeled as only "AVO").

Identify_Leaks reviews the LeakDAS history for each of the identified components sequentially. The algorithm recognizes a series of "Failed" measurements for a given component as a single leak and records the first, maximum, and average SV for the leak. The code also includes a process for bounding the leak duration. In cases where the set of "Failed" SVs is preceded and followed by "Passed" measurements, those inspection dates are recorded (ex. Tag 1 and Tag 3 in Figure 3-2). If this condition is not fulfilled for either boundary, the "DateAdded" and any deletion records are considered. In these cases, those component specific dates are used unless they are beyond the bounds of the dataset time period (2013-2019). If no other suitable dates are identified, the dates of 1/1/2013 and 1/1/2019 are used. This condition primarily affects leaks outside of the simulation periods (2014-2018 and 2016-2018) for which a preceding measurement may have been in 2012 or the subsequent measurement had not yet occurred.

The leak bounds outlined above are used to estimate start and end dates for a given leak. This is necessary to create a leak dataset representative of active leaks during the simulation period for a given process unit. The start date is estimated to be halfway between the initial leak bound and the first "Failed" record. This method was chosen based on the assumption that the occurrence of leaks is equally likely at any given point in time. It is also consistent with Texas environmental guidance for emissions estimation which allow for using half the interval between measurements assuming a constant emission rate [Texas Commission on Environmental Quality, 2020]. Repair dates are conservatively assumed to be the end time determined above. This was decided because often a first "Passed" measurement for a component is conducted immediately after a successful repair attempt. Leaks with start dates after 1/1/19 or repair dates prior to 1/1/14 or 1/1/16 for m-Xylene and Mid-Crude, respectively, are included in the *_all.R* files but are excluded from the Monte Carlo leak datasets. An exception is made for components with leaks found in 2019 with

preceding “Passed” measurements in 2018 because a change in the connector monitoring month in 2019 resulted in more connectors having estimated leak start dates in January 2019 rather than in late 2018, as had been the case for previous years. See Figure 3-2 for several examples of different cases and Appendix E2 for the processing code.

A constant emission rate was calculated for each leak using the SOCMI and refinery correlation equations, for the m-Xylene and Mid-Crude units respectively, consistent with the 1995 EPA Emissions Guidance and FHR Inventory practices [U.S. EPA, 1995]. Correlation equation selection was based on component category and the chemical state designation, as outlined in the 1995 Guidance. In cases where a designation was not clear, FHR correlation designations were used. See the emission factors input file, provided in Appendix E3, for specific designations.

Identify_Leaks includes 4 additional filters for the data at various points within the processing algorithm. Components in Mid-Crude labeled “Pre Flash” for the field ‘Drawing’ are removed because these components are in an area outside the process unit which is not covered by the current LDSN system. Components in the fuel gas area are removed based on location descriptors if the ‘Chemical State’ field is “GV’ (gas vapor). This filter removes leaks from components for which emissions are assumed to be primarily natural gas because the current sensors cannot detect methane, the primary gas, effectively. Under a new LDAR program, these components would still be subject to scheduled-M21 despite broader LDSN/DRF implementation. For an LDSN implementation using the current sensor (10.6 eV PID that does not respond to methane), the comminution of comprehensive M21 monitoring of fuel gas component CWP is specified in the facility’s fugitive management plan. Components for which no location could be determined are also removed, eliminating 14 Mid-Crude and 31 m-Xylene leaks (also reflects as approximately 5% of total). AVO leaks are not removed but instead directed to a separate file for independent analysis. AVO leaks are not included in this specific Monte Carlo analysis due to the lack of reliable initial SV measurements and the added uncertainty for estimating leak start times.

The final *Identify_Leaks* code is available in Appendix E2 and output files are included in Appendix E3.

3.3 Leak Sample Characteristics

In total, the processing method identified 1,115 and 904 unique leaks between 2013-2019 and produced a final list of 285 and 568 leaks for simulation for Mid-Crude and m-Xylene, respectively. A summary of the leak datasets is included in Table 3-5, Mid-Crude, and Table 3-6, m-Xylene. The m-Xylene unit demonstrated a relatively similar leak rate to Mid-Crude, despite the latter having almost three times the number of tagged components. Ultimately, the Mid-Crude unit simulation sample set is significantly smaller due to both the shortened 3-year simulation period and the much larger population of fuel gas components (excluded from the analysis). Both units demonstrated skewed SV distributions. However, due to the lower LDSN DTA, 25% of leaks within the m-Xylene dataset are greater than the DTA, 4,000 ppmv, while only 8% are above the DTA for Mid-Crude, 12,500 ppmv. The units demonstrate similar proportions of pegged SVs (100,000 ppmv), but it is notable that m-Xylene pegged values are almost entirely connector leaks while Mid-Crude had pegged leaks from a variety of component categories over a shorter time duration. Pump leaks, the category with the shortest CWP monitoring interval, comprised about 10% of both datasets while connector leaks, the category with the largest interval, comprised more than half of all leaks. Both Monte Carlo input files are provided in Appendix E3.

Table 3-5: Mid-Crude Unit Leak Summary

Leak Summary								
Unit	**Mid-Crude**							
Component Class	**Valve**	**Pump**	**Drain**	**Relief Valve**	**Connector**	**Compressor**	**Piping**	**Total**
Total Leaks	182	117	25	3	768	19	1	1115
AVO Leaks*	17	51	0	0	56	6	1	131
Fuel Gas Leaks	23	0	0	0	539	0	0	562
Simulated Leaks								
Count	79	32	13	3	153	5		285
Median Duration	183	20	47	53	109	49		100
Median Repair Time	1.9	6.2	1.1	4.2	2.0	3.1		2.0
Calendar Year *								
2016	15	3	9	1	60	0		88
2017	34	10	3	1	52	2		102
2018	22	17	1	1	26	3		70
2019	8	2	0	0	15	0		25
First Failed TVA Measurement								
500 - <6,250 ppmv	90%	75%	100%	100%	82%	80%		84%
6,250 - <12,500 ppmv	5.1%	16%	0%	0%	9.2%	0%		8%
12,500 - <25,000 ppmv	1.3%	3.1%	0%	0%	1.3%	0%		1%
12,500 - <100,000 ppmv	0%	3.1%	0%	0%	3.3%	0%		2%
100,000 ppmv	3.8%	3.1%	0%	0%	4.6%	20%		4%

* Note that this includes AVOs between 2013-2015 when connectors were not subject to scheduled monitoring.

* First failed detection record for final simulation leak set

Table 3-6: m-Xylene Unit Leak Summary

Leak Summary								
Unit	**m-Xylene**							
Component Class	**Valve**	**Pump**	**Drain**	**Relief Valve**	**Connector**	**Compressor**	**Piping**	**Total**
Total Leaks	374	85	3	1	440	0	1	904
AVO Leaks*	1	11	0	0	35		1	48
Fuel Gas Leaks	17	0	0	0	0		0	17
Simulated Leaks								
Count	196	56	1	1	314			568
Median Duration	45	21	49	68	182			54
Median Repair Time	1.9	4.1	1.1	13	3.8			3.0
Calendar Year *								
2014	45	12	0	0	46			103
2015	32	12	0	1	69			114
2016	35	11	1	0	81			128
2017	32	8	0	0	36			76
2018	41	11	0	0	43			95
2019	11	2	0	0	39			52
First Failed TVA Measurement								
500 - <2,000 ppmv	86%	43%	100%	100%	54%			64%
2,000 - <4,000 ppmv	6.6%	18%	0%	0%	13%			11%
4,000 - <8,000 ppmv	4.1%	20%	0%	0%	14%			11%
8,000 - <100,000 ppmv	3.1%	20%	0%	0%	13%			10%
100,000 ppmv	0.51%	0%	0%	0%	5.4%			3.2%

* First failed detection record for final simulation leak set

4 Monte Carlo Model

The Monte Carlo model developed for this equivalency analysis was designed to satisfy several different needs. The simulation aims to approximate previous methods presented in the 1999 EPA Approach and the OGI Evaluation while addressing the limitations of those methods and adjusting the analysis to better evaluate the specific strengths and weaknesses of the LDSN/DRF concept [U.S. EPA, 1999; Epperson, 2000]. As is noted above, this analysis was constrained to a process unit specific evaluation due to the current stage of LDSN/DRF development. Future analyses may be able to develop broader equivalency evaluations as continued research establishes a more thorough understanding of the level of control achievable under different LDSN/DRF embodiments.

This section discusses the equivalency evaluation approach developed for this report and presents some emissions comparisons to verify agreement between the EPA ORD and Molex equivalency determinations.

4.1 Methods

For the purposes of this report, a process unit specific Monte Carlo model was developed for the two CRADA pilot study units. This model simulates process unit leak profiles for 3-year (Mid-Crude) and 5-year (m-Xylene) simulation periods using historical data—see Section 3 for a discussion of leak list development. Four different control regimes were included to compare the CWP control performance to three different LDSN/DRF control scenarios. Multiple leak control scenarios were developed for LDSN/DRF because the exact level of control is not fully understood at the time of this report. The three LDSN/DRF emissions control scenarios are as follows:

1. **Detection Threshold Average (DTA)**
   This scenario assumes individual leaks for which

   $$SV \geq DTA_F \qquad \text{[Equation 1]}$$

   where DTA_F is the LDSN DTA for process unit F, are detected and repaired. It assumes all leaks for which $SV < DTA_F$ are not repaired. This is the most conservative and simplistic control scenario.

2. **Detection Threshold (DT)**
   This scenario assumes individual leaks for which

   $$\frac{SV}{D^2} \geq \frac{DTA_F}{1{,}250} \qquad \text{[Equation 2]}$$

   where D is the distance from the leaking component to the nearest sensor, are detected and repaired. It assumes all leaks for which Equation 2 is not true are not repaired. This scenario is considered more realistic due to its incorporation of distance effects. However, the heuristic used here should be considered a useful tool, rather than a definitive characterization of distance effects on LDSN detection capabilities. See Appendix F2 for a review of the development of this scenario approach.

3. **Detection Threshold – *Cluster* (DTC)**
   This scenario assumes a cluster of leaks triggers an LDSN alert when

$$max\left(\sum\left[\frac{SV}{D^2}\right]_{a,i}\right) \geq \frac{DTA}{1{,}250} \qquad \text{[Equation 3]}$$

   where the sum of individual DT designations in a localized cluster of leaks, *a*, are summed for each sensor *i* and the maximum of the sums is used to determine if a LDSN alert occurs. This heuristic should also be considered a useful tool for characterizing a physical phenomenon observed during the pilot study, rather than a definition (discussed further in Appendix F2). Unlike the other 2 scenarios, the DTC scenario also incorporates DRF conditions. A randomized search method within a cluster is used such that the model simulates finding smaller leaks in the process of searching for larger leaks which trigger LDSN alerts. These smaller leaks are repaired based on defined DRF conditions. Results presented in this report simulated the following condition:

   - ❖ When an LDSN alert occurs, an investigator must continue searching until either three leaks with SV < 3,000 ppmv or one leak with SV > 3,000 ppmv is found. Any leaks found with SV > 500 ppmv are repaired, and an investigation is closed.

   The model assumes that this process will continue to repeat after each round of repairs is completed until the condition outlined in Equation 3 is no longer true.

In order to run the model, initial variables must be defined. Table 4-1 lists the input variables, acceptable values where applicable, and default values chosen for this analysis. While different numbers of model iterations were run, the analysis presented in Section 4 of the primary report is focused on 10,000 iteration simulations. The repair time was conservatively assumed to be 7 days because regulations require that non-DOR leaks be repaired within 15 days [40 CFR 63.168(f)(1); 40 CFR 60.482-7(d)(1)]. In practice, the majority of leaks are repaired within 5 days, and the historical leaks included in the simulation datasets had a median repair time of 2 and 3 days for Mid-Crude and m-Xylene, respectively (see Table 3-5 & Table 3-6). The model reads in an input file, created using the *Identify_Leaks* code discussed in Section 2, based on variables 'FACIL' and 'SV_metric' and a list of FHR CC sensor IDs and coordinates which are filtered based on 'FACIL.'

Table 4-1: EPA ORD Model Input Variables

Variable Name	Acceptable Values	Default	Description
SV_metric	"first" "max" "ave"	"first"	Screening value used to characterize each leak *The first leak SV was assumed to best characterize the leak prior to detection and before repair atempts.*
FACIL	"META" "MIDCRUDE"	--	FHR CC Process Unit
LEAK_DEF	500-100,000	4,000 12,500	LDSN Detection Threshold Average (DTA) [ppmv]
s	> 0	500 250	Number of leaks sampled in each model iteration *Default values were ~12% reduction from total list length to increase the variation of leak profiles tested.*
n	> 0	--	Number of model iterations
t_detect	≥ 0	3	LDSN detection time
t_repair	≥ 0	7	Repair time *Applied equally to CWP and LDSN/DRF.*
SV_DRF*	500 - LEAK_DEF	3,000	DRF threshold for leak investigations
x_lk*	> 0	3	DRF condition: number of leaks found below SV_DRF before closing an investigation

* These variables are based on DRF conditions and are only used for the DTC scenario

The model is iterative and follows a 5-step process for each of the *n* iterations. The steps are as follows:

Step 1: Simulate leak screening values

A process unit leak profile is created by randomly sampling, with replacement, 's' leaks from the input file leak list.

Step 2: Randomly generate leak start time and location

Leak start times are generated using a uniform variate to create a list of randomly distributed times between the simulation start, 1/1/2014 or 1/1/2016 depending on the process unit, and end date, 1/1/2019. Each leak location is simulated by separately generating x and y coordinates within each leak's cluster box range. The x and y coordinates are each created using a uniform variate between 0 and 1 which is used to generate a number between the minimum and maximum box values ('xmin' – 'xmax' and 'ymin' – 'ymax'). Note that both duplicate leaks and unique leaks with the same component tag are each treated as if they are from separate components within the same cluster. This simplifying assumption—no repeat leakers—is consistent with the 1999 EPA Approach and the OGI Evaluation.

Step 3: Simulate leak detection and repair

Leak detection and repair is simulated for the CWP and three different LDSN/DRF control scenarios. LDSN/DRF detection and repair follows the methods discussion above. The CWP scenario applies monitoring intervals (monthly, quarterly, or annually) based on the component category. Monitoring is assumed to occur on the first of the month; see Appendix F1 for an analysis of the impact of monitoring interval date variation. Note that the model also includes an additional CWP scenario which simulates scheduled M21 without connector monitoring. Results from this scenario are not presented in Section 4 of the report but are summarized in Section 5, below. The simulation assumes a constant repair time across all modeled scenarios. An end date of 1/1/2019 is applied for leaks which are not repaired during the modeling period.

Step 4: Calculate leak emissions

Emissions are calculated on an individual leak basis for each of the four leak scenarios using the following equation.

$$E_{i,m} = ER * \left(end_{i,m} - start_i\right) \quad \text{[Equation 4]}$$

$E_{i,m}$: *Emissions from leak i under control scenario m [kg]*

ER : *Emission rate [kg/day]*

$\left(end_{i,m} - start_i\right)$: *Leak duration [days]*

Step 5: Sum and compare CWP and LDS/DRF total emissions

Individual leak emissions are summed to determined total emissions for each scenario. LDSN scenarios are compared to CWP emissions. An LDSN scenarios is defined as equivalent to CWP for that iteration if total leak emissions are less than or equal to CWP total leak emissions.

The simulation code outlined above is available for review in Appendix E2 and input files are included in Appendix E3.

4.2 Model Comparison

While the EPA ORD model is the principal focus of Section 4 of the primary report, two models were considered in the overall evaluation. Molex produced an independent analysis using a separate model developed in-house, presented in Appendix F. The EPA ORD and Molex models were developed in tandem to ensure the models were comparable, but the two simulations vary in approach.

Comparison studies between the two simulations provided additional insight and quality assurance, and mistakes in both codes were identified and corrected during the comparison process. While there are a variety of smaller variations between the two methods, the most significant difference is the approach to components with multiple leaks. The EPA ORD model treats each simulated leak as if it originates from a unique component within a cluster area, consistent with the OGI Equivalency approach. In contrast, the Molex model does evaluate components with multiple leaks and includes conditions for "overlapping" leaks when another simulated leak occurs prior to the repair of a previously simulated leak. Each method has its limitations. It is unclear whether leaks which occurred after an initial leak should actually be modeled independently of one other, or if later leaks can be simulated as occurring prior to the original leak on the same component. It was decided that including both approaches would be preferable to choosing only one, given the uncertainty in which simulation approach is preferable.

Molex created several different versions of its simulation code in order to more closely mimic the EPA ORD approach. Table 4-2 presents the median emissions from 1,000 Mid-Crude unit simulations for several model versions. Note that the Molex simulations used the same leak profiles created using the EPA ORD Code so as to create an exact comparison.

Table 4-2: EPA ORD and Molex Simulation Comparison, Median Emissions

Model Version	Repeat Leakers?	DRF Model Conditions	Median Emissions by Control Scenario			
			M21	DTA	DT	DTC
			kg			
EPA ORD	No	EPA	3,170	3,959	2,450	1,751
Molex*	No	EPA	3,169	3,977	2,471	2,080
		Molex	3,169	3,977	2,471	2,049
	Yes	EPA	2,874	2,285	1,524	1,543
		Molex	2,874	2,285	1,520	1,543

* Only non-growth results were included in this direct comparison test

In Table 4-2, the EPA ORD model is consistent with the model presented in the primary report. The Molex models are divided based on whether multiple simulated leaks from the same component are modeled independently or with "overlap" conditions. Additionally, Molex provided results from two different cluster algorithms. The "EPA" method does not prioritize finding larger leaks and uses a purely random search (note that the Molex version of the "EPA" Cluster is not fully identical to the EPA model). The "Molex" model prioritized larger leaks in its random search cluster approach. See Appendix F1 for a more thorough explanation of these differentiations.

The emissions presented in Table 4-2 illustrate that the overall EPA ORD and Molex emissions methods are similar when the repeat leaks conditions align. Note that there are more significant differences in the DT and DTC simulations because the two methods simulate distance effects and the cluster model DRFs differently. Notably, the individual simulation iterations are not as closely aligned due to smaller variations in approach. For example, an individual simulation may have significantly different M21 emissions if a pegged valve leak is simulated as occurring on 6/25/2017. The EPA ORD Model would detect it on the first of the month, 7/1, but the Molex model would detect it based on a set interval of 90 days, finding no leak when testing on 6/24 and detecting the leak on 9/22. Conversely, the Molex model might find a leak earlier due to the same monitoring interval deviations. Ultimately, the smaller differences which affect individual iterations were found to have minimal impact on overall results, as demonstrated by the similar median emissions and the equivalency results (see Table 4-3).

Table 4-3: EPA ORD and Molex Simulation Comparison, Equivalency

Model Version	Repeat Leakers?	DRF Model Conditions	Equivalency by Control Scenario		
			DTA	DT	DTC
			% Iterations Equivalent		
EPA ORD	No	EPA	22.6%	77.1%	95.0%
Molex*	No	EPA	22.5%	76.7%	88.0%
		Molex	22.5%	76.7%	88.8%
	Yes	EPA	76.3%	96.1%	95.8%
		Molex	76.3%	96.5%	96.1%

* Only non-growth results were included in this direct comparison test

4.3 Model Sensitivity

While comparisons to the Molex model provided quality assurance, it was also important to understand the impact different variables have on EPA ORD simulations. Three variations of the original simulation code were created to test the primary variables randomized for the Monte Carlo simulation:

1. Leak SV samples
2. Leak Start Time
3. Component/Leak Location

For each model version, the tested variable was still randomized while the other two variables were adjusted to remain constant. For the sample testing, a single set of randomized start times and leak coordinates was used for all simulation iterations while the SV sample was varied. For the other two model versions, the original base SV dataset was used, rather than a single randomized sample. The three models were each run twice, once for each process unit.

Variable-specific modeling results are summarized in Table 4-4. The table presents the coefficient of variation and skewness for each control scenario across all 6 model runs. The SV sample test demonstrated the largest coefficient of variation across all scenarios, and CWP emissions exhibited the largest variation. This is likely due to CWP emissions being related to both leak start time and the SV distribution. Conversely, LDSN/DRF emissions, particularly those from larger leaks, are more closely linked to SV size, and start time would only impact emissions from smaller, less impactful leaks. Location had no impact on CWP and DTA because distance effects are not incorporated into those control scenarios. Start time did not demonstrate a strong skew for most scenarios, but a strong skew was found for m-Xylene DTC. Given the slightly negative skew for Mid-Crude DTC, no specific relationship was demonstrated. However, this could possibly be based in the different process unit layouts and cluster densities. Both SV sample and location testing demonstrate a right tail skew.

Table 4-4: Model Sensitivity, emissions distribution statistics

Variable	Unit	Coefficient of Variation				Skewness			
		CWP	DTA	DT	DTC	CWP	DTA	DT	DTC
SV Sample	m-Xylene	19%	6%	8%	10%	0.34	0.31	0.15	0.27
	Mid-Crude	29%	12%	10%	11%	0.47	0.36	0.30	0.23
Start Time	m-Xylene	9%	4%	5%	6%	0.02	0.05	0.11	0.45
	Mid-Crude	14%	6%	6%	6%	0.02	0.17	0.04	-0.07
Location	m-Xylene	0%	0%	4%	4%	N/A	N/A	0.22	0.57
	Mid-Crude	0%	0%	6%	5%	N/A	N/A	0.55	0.21

5 Simulation Results

The data processing and simulation methods discussed in this Appendix were all developed to serve an overall equivalency evaluation. Because a Monte Carlo approach was used, equivalency is determined based on the proportion of simulation iterations for which LDSN/DRF simulated emissions are less than or equal to CWP emissions. An analysis determines the proposed approach is equivalent if the alternate work practice demonstrates equivalency for at least 67% of the simulation iterations [Steering Committee for Alternative Leak Detection Work Practices, 1999]. Molex and EPA ORD simulation results from 10,000 iteration model runs are presented in terms of "% equivalent" in Table 5-1. Both models demonstrated equivalency for the m-Xylene unit across all three LDSN/DRF scenarios. Equivalency was demonstrated for two of the three scenarios for the Mid-Crude unit. These results demonstrate the impact the process unit DTA may have on equivalency determinations because Mid-Crude's DTA is just over three times larger than that for m-Xylene.

Table 5-1: Simulation results

Processing Unit	m-Xylene		Mid-Crude	
Model	EPA	Molex*	EPA	Molex*
Scenario	% Equivalent			
DTA	78.0%	100%	20.7%	59.0%
DT	99.8%	100%	72.4%	93.2%
DTC**	100%	100%	92.5%	92.8%

* Non-growth emissions model

** EPA and Molex cluster models reflect different DRFs

A secondary CWP scenario was also simulated in which no connectors are repaired. Results using this CWP option are presented in Table 5-2. Both process units demonstrated robust equivalency in this scenario because a majority of leaks identified in the LeakDAS Inventory were connector leaks.

Table 5-2: Simulation results, alternate CWP scenario

Scenario	Processing Unit	
	m-Xylene	Mid-Crude
	% Equivalent	
DTA	100%	94.6%
DT	100%	99.6%
DTC	100%	100%

The final analysis presented above focuses on the process unit DTAs of 4,000 ppmv and 12,500 ppmv for m-Xylene and Mid-Crude, respectively. However, using a single DTA is limited given that detection is better described physically as a "detection threshold band." This was the justification for incorporating the DT and DTC scenarios. While the DTAs used in this report were representative of the LDSN systems in place during the pilot study, a system with a different emissions-sensor response factor or closer sensor spacing would not have the same DTA. Different DTA model runs were completed to provide a broader understanding of the impact process unit DTA has on equivalency. Results from these 1,000 iteration runs are presented in Table 5-3. The DTA and DT scenarios demonstrate equivalency at similar LDSN DTAs (~5,000 ppmv and >15,000 ppmv respectively). This is likely because the leak samples for both units demonstrated similar SV distributions. Conversely, m-Xylene demonstrates a much higher rate of equivalency at 25,000 ppmv. This is probably due to the process unit density and larger number of detectable leaks. While both units demonstrated similar historical leak discovery rates, a large number of Mid-Crude leaks emit fuel gas and are not detectable by the current LDSN system. Additionally, m-Xylene is a smaller unit—creating a stronger cluster effect because smaller leaks are more likely to be located near other active leaks at any given time.

Table 5-3: Simulation results, LDSN DTA

(a)

Model DTA Sensitivity			
Unit	m-Xylene		
LDSN DTA	DTA	DT	DTC
ppmv	% Equivalent		
1,000	100%	100%	100%
2,000	99%	100%	100%
3,000	91%	100%	100%
4,000	78%	100%	100%
6,000	27%	97%	100%
8,000	6%	90%	100%
16,000	0%	41%	99%
25,000	0%	12%	91%

(b)

Model DTA Sensitivity			
Unit	Mid-Crude		
LDSN DTA	DTA	DT	DTC
ppmv	% Equivalent		
3,125	91%	99%	100%
6,250	58%	89%	99%
9,375	28%	81%	96%
12,500	19%	71%	93%
18,750	18%	57%	84%
25,000	13%	43%	73%
50,000	6%	18%	37%

One other variable which was not studied in the primary analysis was LDSN detection time. Demonstrating an ability to detect large leaks quickly is an important aspect of any LDSN system's performance, and the value may vary by facility and detection algorithm. The primary analysis assumed a detection time of 3 days, which was identified as reasonably conservative based on a qualitative review of pilot study data. Table 5-4 presents m-Xylene simulation results from 1,000 iteration model runs with varying detection times. All scenarios demonstrate equivalency with a modeled LDSN detection time of 12 days or less. The DT scenarios remains equivalent for all detection times, but there is significant improvement from 60 to 30 days. The DTA scenario, the most conservative, does not meet equivalency standards when a detection time of 15 days is assumed.

Table 5-4: Simulation results, detection time

Unit	m-Xylene		
Detection Time	DTA	DT	DTC
days	% Equivalent		
1	79%	100%	100%
3	76%	99.9%	100%
6	75%	99.9%	100%
9	74%	99.9%	100%
12	68%	99.5%	100%
15	66%	99.6%	100%
30	47%	98%	100%
60	12%	81%	100%

Overall, the variety of simulation results presented in this Appendix and the primary report suggest that the LDSN/DRF systems installed during the CRADA FHR CC pilot study would be equivalent to scheduled M21 over multi-year time periods. Moreover, the simulations demonstrate that a system with targeted leak repair, rather than scheduled monitoring, may be both equivalent and produce significant long-term emissions reductions relative to the CWP. Further research is needed to understand exactly what level of control should be modeled for LDSN/DRF equivalency evaluations. However, the strong equivalency results, particularly for the m-Xylene unit, demonstrate that the LDSN/DRF concept has the potential to significantly reduce emissions and improve LDAR program efficiency relative to the CWP.

6 References

American Petroleum Institute, 1995: *Emission Factors for Oil and Gas Production Operations*, API Publication Number 4615, prepared by Star Environmental for API.

Epperson, David (prepared by), 2000: *Monte Carlo Simulation Evaluation of Gas Imaging Technology*, Columbus, IN 47203.

Steering Committee for Alternative Leak Detection Work Practices, 1999: *Demonstrating Alternative Work Practices for Fugitive Leak Detection and Repair (LDAR) Programs*. Unofficial report.

Texas Commission on Environmental Quality, 2020: *2019 Emissions Inventory Guidelines*, Appendix A. Air Quality Division, RG-360/19. Austin, TX 13087. Available at: https://www.tceq.texas.gov/assets/public/comm_exec/pubs/rg/rg360/rg360-19/rg360.pdf

U.S. EPA, 1995: *1995 Protocol for Equipment Leak Emission Estimates*, Office of Air and Radiation, Office of Air Quality Planning and Standards, EPA-453/R-95-017. Research Triangle Park, NC 27711.

U.S. EPA, 1999: *Monte Carlo Simulation Approach for Evaluating Alternative Work Practices for Equipment Leaks*, Office of Air and Radiation, Office of Air Quality Planning and Standards, Draft report. Research Triangle Park, NC 27711.

U.S. EPA. Alternative work practice to detect leaks from equipment. U.S. Code of Federal Register: 40 CFR Parts 60, 63, 65; 73 FR 78199, EPA-HQ-OAR-2003-0199, 2008.

Appendix E2

EPA ORD Software Code

Appendix E1

EPA ORD Simulation Approach

Table of Contents

Identify_Leaks.R..... 31
Monte_Carlo.R..... 35

Identify_Leaks.R

```
1   ##############################################################################################
2   # 2020/03 HLane
3   # Version: April 1, 2020
4   #
5   # This code uses formatted LeakDAS data archives to identify leak events within a
6   # processing unit.
7   #
8   ##############################################################################################
9
10  rm(list = ls())
11
12  # Select Processing Unit
13  unit <- "mX"    # mX, MC
14
15  library(svMisc)
16  library(tidyverse)
17  library(lubridate)
18
19
20  setwd("C:/Users/hlane/Documents/FHR-Molex CRADA/Report/Appendix E/E.3")
21
22  # Load Files
23  {
24    pathI <- c("C:/Users/hlane/Documents/FHR-Molex CRADA/Report/Appendix E/E.3/")
25    start_all <- as.POSIXct(ymd(strptime(c("1/1/2013"),"%m/%d/%Y"),
26                                tz="America/Chicago"))
27    EF <- read.csv(paste0(pathI,"Equation_FHR.csv"))
28    if(unit=="mX"){
29      LkDAS <- read.csv(
30        paste0(pathI,"LeakDAS Records/Meta Inspections 2013 thru 2019.csv"))
31      L_del <- read.csv(paste0(pathI,"LeakDAS Records/mXylene_Inactive.csv"))
32      loc1  <- read.csv(paste0(pathI,"Location Info/output_META.csv"))
33      loc2  <- read.csv(paste0(pathI,"Location Info/mXylene_leaks3.csv"))
34      EF <- filter(EF,Category=="SOCMI")
35      filename <- "mXylene"
36      time_all <- as.POSIXct(ymd(strptime(c("1/1/2014","1/1/2019"),"%m/%d/%Y"),
37                                 tz="America/Chicago"))}
38    if(unit=="MC"){
39      LkDAS <- read.csv(
40        paste0(pathI,"LeakDAS Records/Mid Crude Inspections 2013 thru 2019.csv"))
41      L_del <- read.csv(paste0(pathI,"LeakDAS Records/MidCrude_Inactive.csv"))
42      loc1  <- read.csv(paste0(pathI,"Location Info/output_MIDCRUDE_04012020.csv"))
43      loc2  <- read.csv(paste0(pathI,"Location Info/midCrude_leaks2.csv"))
44      EF <- filter(EF,Category=="REFIN")
45      filename <- "MidCrude"
46      time_all <- as.POSIXct(ymd(strptime(c("1/1/2016","1/1/2019"),"%m/%d/%Y"),
47                                 tz="America/Chicago"))}
48  }
49
50  # Clean Files
51  {
52    LkDAS <- LkDAS[,c( "InspectionHistoryID","ComponentID","UnitDescription",
53                       "ComponentTag","ComponentClass","InspectionDate",
54                       "TypeDescription","NetReading","Pass_Fail","LocationDescription",
55                       "PlantDescription","ChemicalState","DateAdded","Drawing")]
56    LkDAS[,"Date"]      <- as.POSIXct(
57      ymd_hms(strptime(as.character(LkDAS$InspectionDate),"%m/%d/%y %H:%M:%S"),
58              tz="America/Chicago"))
59    LkDAS[,"DateAdded"] <- as.POSIXct(
60      ymd(    strptime(as.character(LkDAS$DateAdded)     ,"%m/%d/%Y"),
61              tz="America/Chicago"))
```

```
62
63    L_del <- L_del[,c( "Component.Tag","Component.Class","Unit.Description",
64                       "Activity_Level","Component.ID","Component.Type","Chemical.State",
65                       "Component.Stream","Location.Description","Plant.Description",
66                       "Date.Added","Status.Description","Status.Date",
67                       "Last.M21Inspection.Date","Last.Visual.Inspection.Date",
68                       "Leak.Definition")]
69    L_del[,"Date"] <- as.POSIXct(
70      ymd(strptime(as.character(L_del$Status.Date),"%m/%d/%Y"),tz="America/Chicago"))
71  }
72
73  # Initialize data
74  {
75    tags <- unique(
76      filter(LkDAS,Pass_Fail=="Failed" & Drawing != "Pre Flash")[,c(
77        "ComponentTag","ComponentClass","TypeDescription",
78        "LocationDescription","ChemicalState")])
79
80    # Leak Data Frame
81    Leak <- data.frame("ComponentTag"       =tags$ComponentTag,
82                       "ComponentClass"     =tags$ComponentClass,
83                       "TypeDescription"    =tags$TypeDescription,
84                       "LocationDescription"=tags$LocationDescription,
85                       "ChemicalState"      =tags$ChemicalState,
86                       MaxSV=c(0),AveSV=c(0),SV0=c(0),SV1=c(0),SVr=c(0),
87                       t0=LkDAS$Date[1],t1=LkDAS$Date[1],tn=LkDAS$Date[1],
88                       tr=LkDAS$Date[1],ta=LkDAS$Date[1],te=LkDAS$Date[1],
89                       count=c(0))
90    Leak <- Leak[0,names(Leak)]
91  }
92
93  # Review each component
94  k <- 0
95  for(i in 1:length(tags[,1])){
96    tmp <- filter(LkDAS,ComponentTag==tags$ComponentTag[i] &
97                    LocationDescription==tags$LocationDescription[i])
98    tmp <- tmp[order(tmp$Date),]
99
100   row.names(tmp) <- c(1:length(tmp[,1]))
101   x <- as.numeric(row.names(tmp[tmp$Pass_Fail=="Failed",]))
102
103   # Identify Leaks
104   if(sum(tmp$Pass_Fail=="Failed")>0){
105     for(j in 1:length(x)){
106       # Identify 1st measurement
107       if((j==1)|isTRUE((x[j]-x[j-1])>1)){
108         k <- k+1                                                  # leak count
109         m <- 0                                                    # start meas. count
110         Leak[k,"t1"]                <- tmp$Date[x[j]]             # 1st measurement time
111         Leak$ComponentTag[k]        <- tmp$ComponentTag[1]        # component tag
112         Leak$ComponentClass[k]      <- tmp$ComponentClass[1]      # component class
113         Leak$TypeDescription[k]     <- tmp$TypeDescription[1]     # location description
114         Leak$LocationDescription[k] <- tmp$LocationDescription[1] # type description
115         Leak$ChemicalState[k]       <- tmp$ChemicalState[1]       # chemical state
116         Leak$SV1[k]                 <- tmp$NetReading[x[j]]       # 1st leak meas.
117         Leak$ta[k]                  <- tmp$DateAdded[x[j]]        # date component added
118         if(sum(L_del$Component.Tag==as.character(tmp$ComponentTag[1]))>0){
119           Leak$te[k] <- L_del$Date[
120             L_del$Component.Tag==as.character(tmp$ComponentTag[1])][1]
121         }
122         if(x[j]==1){
123           #  Leak$t0[k]    <- -1                                    # start time bounding
124           #  Leak$SV0[k]   <- -1                                    # previous measurement
125         }else{
126           Leak$t0[k]<-tmp$Date[x[j]-1]                            # start time bound
127           Leak$SV0[k]<-tmp$NetReading[x[j]-1]                     # previous passing meas.
```

```
128         }
129       }
130
131       # Record measurement
132       { m <- m + 1  # measurement count
133         if(!is.na(tmp$NetReading[x[j]])){
134           Leak$MaxSV[k] <- max(Leak$MaxSV[k],tmp$NetReading[x[j]],na.rm=TRUE)
135           # max measurement
136           Leak$AveSV[k] <- sum(Leak$AveSV[k],tmp$NetReading[x[j]],na.rm=TRUE)}
137         # ave measurement*m
138       }
139       # Identify last measurement
140       if((j==length(x))|isTRUE(x[j+1]!=(x[j]+1))){
141         Leak$count[k] <- m                          # measurement count
142         Leak$AveSV[k] <- Leak$AveSV[k]/m            # calculate average SV
143         Leak$tn[k] <- tmp$Date[x[j]]                # last measurement time
144
145         if(x[j]==length(tmp[,1])){
146
147         }else{
148           Leak$tr[k]  <- tmp$Date[x[j]+1]           # repair time
149           Leak$SVr[k] <- tmp$NetReading[x[j]+1]}    # repaired screening value
150       }
151     }
152   }
153 }
154
155 # Remove Fuel Gas
156 {
157   if(unit=="MC"){
158     r <- (1:length(Leak[,1]))*(
159       (lengths(strsplit(as.character(Leak$LocationDescription),"42BA"))>1)|
160         (lengths(strsplit(as.character(Leak$LocationDescription),"42-BA"))>1)|
161         (lengths(strsplit(as.character(Leak$LocationDescription),"42 BA"))>1)|
162         (lengths(strsplit(as.character(Leak$LocationDescription),"BLW HTR-3"))>1))*
163       (Leak$ChemicalState=="GV")
164   }else{
165     r <- (1:length(Leak[,1]))*
166       (lengths(strsplit(as.character(Leak$LocationDescription),"54BA1"))>1)*
167       (Leak$ChemicalState=="GV")
168   }
169   r <- r[r!=0]
170
171   write.csv(Leak[r,],paste0(filename,"_leaks_FG.csv"))
172   if(length(r)>0){Leak <- Leak[-r,]}
173 }
174
175 # Add Location
176 {
177   Leak[,c("Level","y1","y2","x1","x2")]<- c(0)
178   Leak[1:2,"cluster"] <- as.character(loc1$obj[1:2])
179
180   for(i in 1:length(Leak[,1])){
181     tmp <- filter(loc1,tag==as.character(Leak$ComponentTag[i]))
182     if(as.character(Leak$ComponentTag[i])=="AVO"){
183       tmp <- filter(loc1,tag==as.character(Leak$ComponentTag[i])&
184                     loc==as.character(Leak$LocationDescription[i]))}
185     if(length(tmp[,1])==0){
186       tmp <- filter(loc2,tag==as.character(Leak$ComponentTag[i]))
187       if(as.character(Leak$ComponentTag[i])=="AVO"){
188         tmp <- filter(loc2,tag==as.character(Leak$ComponentTag[i])&
189                       loc==as.character(Leak$LocationDescription[i]))}}
190     if(length(tmp[,1])>0){
191       Leak[i,c("Level","y1","y2","x1","x2")] <- tmp[1,c("level","W","E","S","N")]
192       Leak[i,"cluster"] <- as.character(tmp$obj[1])
193     }
```

```
194   }
195 }
196
197 # Calculate Emission Rates
198 {
199   Leak[,"ER_ID"] <- c(0)
200   for(r in 1:length(EF[,1])){
201     if(EF$Class[r]==""){r ->Leak[,"ER_ID"]
202     }else{
203       if(EF$Chem.State[r]==""){
204         r -> Leak[c(1:length(Leak[,1]))*
205                     (Leak$ComponentClass==as.character(EF$Class[r])),"ER_ID"]
206       }else{
207         r -> Leak[c(1:length(Leak[,1]))*
208                     (Leak$ComponentClass==as.character(EF$Class[r]))*
209                     (Leak$ChemicalState ==as.character(EF$Chem.State[r])),"ER_ID"]
210       }
211     }
212   }
213   # Fix Mid-Crude Screwed Connectors
214   if(unit=="MC"){
215     Leak[(str_detect(as.character(Leak$TypeDescription),"SCREW"))&
216            (Leak$ComponentClass=="CONNECT"),"ER_ID"] <- as.numeric(
217              row.names(EF[EF$Type=="SCREWD",]))
218   }
219   Leak[,c("ER_kgpd.max","ER_kgpd.ave","ER_kgpd.1")
220        ] <- EF$constant[Leak$ER_ID]*(Leak[,c("MaxSV","AveSV","SV1")]^
221                                        EF$exponent[Leak$ER_ID])*24
222   Leak[(Leak$MaxSV==1e5)&(!is.na(Leak$MaxSV==1e5)),
223        "ER_kgpd.max"] <- EF$P100k[Leak$ER_ID[(Leak$MaxSV==1e5)&
224                                                (!is.na(Leak$MaxSV==1e5))]]*24
225   Leak[(Leak$AveSV==1e5)&(!is.na(Leak$AveSV==1e5)),
226        "ER_kgpd.ave"] <- EF$P100k[Leak$ER_ID[(Leak$AveSV==1e5)&
227                                                (!is.na(Leak$AveSV==1e5))]]*24
228   Leak[(Leak$SV1  ==1e5)&(!is.na(Leak$SV1  ==1e5)),
229        "ER_kgpd.1"  ] <- EF$P100k[Leak$ER_ID[(Leak$SV1  ==1e5)&
230                                                (!is.na(Leak$SV1  ==1e5))]]*24
231 }
232
233 # Save _all Files
234 write.csv(Leak,paste0(filename,"_leaks_all.csv"))
235
236 # Filter Data
237 {
238   # create leak start/end time
239   c1 <- c(1:length(Leak[,1]))*(!is.na(Leak$te))
240   c1 <- c1[c1>0]
241   Leak[c1*(Leak$te[c1]<Leak$t1[c1]),"te"] <- NA
242
243   Leak[,"ts"] <- pmax(Leak$t0,Leak$ta,na.rm=TRUE)
244   Leak[,"ts"] <- pmax(Leak$ts,start_all,na.rm=TRUE)
245   Leak[,"start"] <-  (Leak$t1-Leak$ts)/2+Leak$ts
246   Leak[,"start"] <- pmax(Leak$start,start_all,na.rm=TRUE)
247   Leak[,"repair"] <- pmin(Leak$tr,Leak$te,na.rm=TRUE)
248   Leak[is.na(Leak$repair),"repair"] <- time_all[2]
249
250   Leak_all <- Leak
251
252   # Filter out by timestamps
253   # repair < modeling start date
254   # start  > modeling end date
255   Leak <- filter(Leak,ts<time_all[2] & repair>time_all[1])
256
257   # Remove leaks w/out location data
258   Leak <- filter(Leak,y1!=0)
259   # Separate AVOs
```

```
  Leak_AVO <- Leak[ ((lengths(strsplit(as.character(Leak$ComponentTag),
                                       "AVO"))>1)|(is.na(Leak$SV1))),]
  Leak_M21 <- Leak[!((lengths(strsplit(as.character(Leak$ComponentTag),
                                       "AVO"))>1)|(is.na(Leak$SV1))),]
}

# Save Simulation Data
{
  Leak_M21.tmp <- data.frame(
    "ComponentClass"      = Leak_M21$ComponentClass,
    "ComponentTag"        = Leak_M21$ComponentTag,
    "PreviousInspection"  = as.character(Leak_M21$t0),
    "StartDate"           = as.character(Leak_M21$start),
    "InspectionDate"      = as.character(Leak_M21$t1),
    "RepairDate"          = as.character(Leak_M21$repair),
    "NetReading"          = Leak_M21$MaxSV,
    "LocationDescription" = Leak_M21$LocationDescription,
    "ChemicalState"       = Leak_M21$ChemicalState,
    "ComponentType"       = Leak_M21$TypeDescription,
    "object"              = Leak_M21$cluster,
    "Level"               = Leak_M21$Level,
    "y1"                  = Leak_M21$y1,
    "y2"                  = Leak_M21$y2,
    "x1"                  = Leak_M21$x1,
    "x2"                  = Leak_M21$x2,
    "cluster"             = Leak_M21$cluster,
    "ER_kgpd"             = Leak_M21$ER_kgpd.max
  )
  write.csv(Leak_M21.tmp,paste0(filename,"_leaks_M21.max.csv"))

  Leak_M21.tmp[,c("NetReading","ER_kgpd")] <- Leak_M21[,c("AveSV","ER_kgpd.ave")]
  write.csv(Leak_M21.tmp,paste0(filename,"_leaks_M21.ave.csv"))

  Leak_M21.tmp[,c("NetReading","ER_kgpd")] <- Leak_M21[,c("SV1","ER_kgpd.1")]
  write.csv(Leak_M21.tmp,paste0(filename,"_leaks_M21.first.csv"))

  write.csv(Leak_AVO,paste0(filename,"_leaks_AVO.csv"))
}
```

Monte_Carlo.R

```
1   ##############################################################################
2   # 2020/02 HLane
3   # Version: March 25, 2020
4   #
5   # Monte Carlo model which simulates leak emissions control for the m-Xylene and
6   # Mid-Crude units at the FHR CC facility. The model simulates 5 different LDAR
7   # control scenarios:
8   #     1.  M21 - CWP, scheduled M21
9   #     2.  C21 - CWP, scheduled M21 without connector control
10  #     3.  DTA - LDSN/DRF, system DTA
11  #     4.  DT_ - LDSN/DRF, system DTA with distance effects
12  #     5.  DTC - LDSN/DRF, system DTA with distance and cluster effects
13  #
14  # See Appendix E1 for a full description of input variables and methods.
15  #
16  ##############################################################################
17
18  rm(list = ls())
19
20  SV_metric <- "first" # max, ave, or first
```

```
21
22  # META ###################################
23  #FACIL    <- "META"   # META or MIDCRUDE
24  #LEAK_DEF <- 4e3      # [ppmv]
25  #s        <- 500      # sample size of leaks
26
27  # MIDCRUDE ###############################
28  FACIL    <- "MIDCRUDE" # META or MIDCRUDE
29  LEAK_DEF <- 12.5e3     # [ppmv]
30  s        <- 250        # sample size of leaks
31
32  # Initialize Variables
33  n        <- 1000          # iterations
34  t_detect <- 3             # [days]
35  t_repair <- 7             # [days]
36  SV_DRF   <- 3000          # [ppmv] DRF threshold
37  x_lk     <- 3             # No. leaks to be found below DRF threshold before
38  # closing PSL
39  SV_THRES <- LEAK_DEF/1250 # Distance detection
40  # [ppmv/ft^2]
41
42  # Load Libraries
43  {
44    library(tidyverse)
45    library(lubridate)
46    library(svMisc)
47  }
48
49  # Load Files
50  {
51    setwd("C:/Users/hlane/Documents/FHR-Molex CRADA/Report/Appendix E/E.3")
52    s_loc <- read.csv("sensor_locations.csv")
53    if(FACIL=="META"){
54      leaks <- read.csv(
55        paste0("Identify_Leaks.R outputs/mXylene_leaks_M21.",SV_metric,".csv"))
56      time_all <- c("2014-01-01 00:00:00","2019-01-01 00:00:00") # start and end date
57    }
58    if(FACIL=="MIDCRUDE"){
59      leaks <- read.csv(
60        paste0("Identify_Leaks.R outputs/MidCrude_leaks_M21.",SV_metric,".csv"))
61      time_all <- c("2016-01-01 00:00:00","2019-01-01 00:00:00") # start and end date
62    }
63    setwd("../Monte Carlo")
64  }
65
66  # Set up
67  {
68    # Create function which calculates distance
69    distance <- function(x_1,x_2,y_1,y_2){sqrt(((x_2-x_1)^2)+((y_2-y_1)^2))}
70
71    # Convert Time to POSIXct
72    leaks[,"start" ] <- as.POSIXct(ymd_hms(strptime(as.character(leaks$StartDate ),
73                                                    "%m/%d/%Y %H:%M:%S")))
74    leaks[,"repair"] <- as.POSIXct(ymd_hms(strptime(as.character(leaks$RepairDate),
75                                                    "%m/%d/%Y %H:%M:%S")))
76    time_all <- as.POSIXct(ymd_hms(time_all),tz="EST")
77
78    # Set times to min/max for any NAs
79    leaks$start[is.na(leaks$start)]   <- time_all[1]
80    leaks$repair[is.na(leaks$repair)] <- time_all[2]
81
82    # Create unique Cluster ID for each non-cluster leak
83    n.na <- sum(is.na(leaks$cluster))
84    leaks[,"cluster"] <- as.character(leaks$cluster)
85    leaks$cluster[is.na(leaks$cluster)] <- length(
86      unique(leaks$cluster,na.rm=TRUE))+c(1:n.na)
```

```
87    leaks[,"cluster"] <- as.factor(leaks$cluster)
88
89    # Assume Leaks w/out Level are Level 1 (most common)
90    leaks$Level[is.na(leaks$Level)] <- 1
91
92    # Pull Unit Sensors
93    s_loc <- filter(s_loc,Unit==FACIL)
94
95    # Create Results data frames
96    E_all <- data.frame("n"=c(1:n),"M21"=c(0),"C21"=c(0),
97                        "DTA"=c(0),"DT_"=c(0),"DTC"=c(0)) # summary emissions
98    C_all <- E_all                                        # summary repair counts
99    C_all[,"P_100k"] <- c(0)                              # pegged value count
100 }
101
102 # Run n_i Monte Carlo iterations
103 for(n_i in 1:n){
104   progress(n_i,max.value = n)
105
106   # Initialize
107   {
108     # Randomize sample of s leaks
109     s_i <- sample(1:length(leaks[,1]),s,replace=TRUE)
110
111     # Create data frame
112     leak_i <- leaks[s_i,c("ComponentClass","ComponentTag",
113                           "Level","cluster","NetReading","ER_kgpd")]
114
115     # Generate leak start times
116     leak_i[,"start"] <- runif(length(s_i),0,as.numeric(
117       difftime(time_all[2],time_all[1],units = "secs")))+time_all[1]
118
119     # Generate leak location (note y1>y2 and x2>x1)
120     leak_i[,"x"] <- leaks$x1[s_i]+((leaks$x2[s_i]-leaks$x1[s_i])*runif(length(s_i)))
121     leak_i[,"y"] <- leaks$y2[s_i]+((leaks$y1[s_i]-leaks$y2[s_i])*runif(length(s_i)))
122
123     # Organize
124     leak_i <- leak_i[order(leak_i$start),]
125     leak_i[,"ID"] <- 1:s
126   }
127
128   # Determine Leak Repair Times
129   {
130     # M21 Detection
131     {
132       leak_i[,"M21"] <- leak_i$start
133       leak_i[(leak_i$start <=time_all[1]),"M21"] <- time_all[1]+1
134
135       leak_i$M21[leak_i$ComponentClass=="PUMP"]    <- ceiling_date(
136         leak_i$M21[leak_i$ComponentClass=="PUMP"],   unit="1 month")
137       leak_i$M21[leak_i$ComponentClass!="PUMP"]    <- ceiling_date(
138         leak_i$M21[leak_i$ComponentClass!="PUMP"],   unit="3 months")
139       leak_i$M21[leak_i$ComponentClass=="CONNECT"] <- ceiling_date(
140         leak_i$M21[leak_i$ComponentClass=="CONNECT"],unit="12 months")
141
142       # Federal standard (no connectors)
143       leak_i[,"C21"] <- leak_i$M21
144       leak_i$C21[leak_i$ComponentClass=="CONNECT"] <- time_all[2]
145
146       # Add repair time
147       leak_i[,c("M21","C21")] <- leak_i[,c("M21","C21")] + t_repair*24*3600
148     }
149
150     # Distance Effects
151     {
152       for(m in 1:length(s_loc[,1])){
```

```
153         leak_i[,paste("D",m,sep="_")] <- leak_i$NetReading/(
154           distance(leak_i$x,s_loc$x[m],
155                    leak_i$y,s_loc$y[m])^2)
156         leak_i[leak_i$Level!=s_loc$L[m],paste("D",m,sep="_")] <- 0
157       }
158       leak_i[,"D_max"] <- apply(leak_i[,paste("D",(1:length(s_loc[,1])),sep="_")],
159                                 MARGIN=1,FUN=max)
160     }
161
162     # DTA Scenario
163     {
164       leak_i[,"DTA"] <- max(time_all)
165       leak_i[leak_i$NetReading>LEAK_DEF,
166              "DTA"] <- pmax(leak_i[leak_i$NetReading>LEAK_DEF,"start"],
167                             min(time_all))+(t_detect+t_repair)*24*3600
168       leak_i[,"DTA"] <- pmin(max(time_all),leak_i[,"DTA"])
169     }
170
171     # DT Scenario
172     {
173       leak_i[,"DT_"] <- max(time_all)
174       leak_i[leak_i$D_max>SV_THRES,
175              "DT_"] <- pmax(leak_i[leak_i$D_max>SV_THRES,"start"],
176                             min(time_all))+(t_detect+t_repair)*24*3600
177       leak_i[,"DT_"] <- pmin(max(time_all),leak_i[,"DT_"])
178     }
179
180     # Cluster Scenario
181     {
182       leak_i[,"DTC"] <- max(time_all)    # initialize repair date
183       detect.s <- unique(leak_i$cluster) # cluster IDs
184
185       # Cluster Loop
186       for(i in 1:length(detect.s)){
187         # Initialize leaks
188         tmp <- filter(leak_i,cluster==detect.s[i])
189         tmp <- arrange(tmp,start)
190         tmp$start[tmp$start<min(time_all)] <- min(time_all)
191
192         # Similify to start to days
193         #     does make detection time slightly more conservative
194         #     (e.g. could be detection time + 23 hrs)
195         tmp$start <- ceiling_date(tmp$start,unit="day")
196
197         # Leaks within cluster i loop
198         for(j in 1:length(tmp[,1])){
199           if(j==1){x_log<-TRUE
200           }else{
201             if(tmp$start[j]!=tmp$start[j-1]){x_log<-TRUE
202             }else{x_log<-FALSE}}
203           if(x_log){
204             t_B <- tmp$start[j]
205             D_x   <- data.frame("B"=c(1:length(s_loc[,1]))*0)
206             D_x$B <- colSums(filter(tmp,(start<=t_B) & (DTC>t_B))[,paste(
207               "D",(1:length(s_loc[,1])),sep="_")])
208             D_s   <- sum(filter(tmp,(start<=t_B) & (DTC>t_B))[,"NetReading"])
209
210             # Apply Cluster Algorithm
211             x<- 0
212             while(max(D_x$B)>=SV_THRES){
213               t_B <- t_B + t_detect*24*3600
214
215               if(x>0){t_B <- t_B + t_repair*24*3600}
216               # Add repair times after 1st round of investigations
217               # (cannot detect until previous leaks repaired)
218
```

```
219              r_B <- row.names(tmp[(tmp$start<=t_B) & (tmp$DTC>t_B),])
220              r <- sample(r_B,min(length(r_B),x_lk),replace = FALSE)
221              SV <- 0
222              k  <- 1
223              while((SV<(SV_DRF))&(k <= length(r))){
224                tmp$DTC[as.numeric(r[k])] <- t_B
225                SV <- tmp$NetReading[as.numeric(r[k])]
226                k=k+1
227              }
228              D_x$B <- colSums(filter(tmp,(start<=t_B) & (DTC>t_B))[,paste(
229                "D",(1:length(s_loc[,1])),sep="_")])
230              x <- x+1
231            }
232          }
233        }
234        leak_i$DTC[tmp$ID] <- tmp$DTC
235      }
236      leak_i[,"DTC"] <- pmin(max(time_all),leak_i[,"DTC"]+(t_repair)*24*3600)
237    }
238  } # end leak repair times section
239
240  # Leak Repair Count
241  {
242    C_all[n_i,"M21"]    <- sum(leak_i$M21 < time_all[2])
243    C_all[n_i,"C21"]    <- sum(leak_i$C21 < time_all[2])
244    C_all[n_i,"DTA"]    <- sum(leak_i$DTA < time_all[2])
245    C_all[n_i,"DT_"]    <- sum(leak_i$DT_ < time_all[2])
246    C_all[n_i,"DTC"]    <- sum(leak_i$DTC < time_all[2])
247    C_all[n_i,"P_100k"] <- sum(leak_i$NetReading==1e5)
248  }
249
250  # Calculate Emissions
251  {
252    E_all[n_i,"M21"] <- sum(leak_i$ER_kgpd*
253                              pmax(0,difftime(
254                                pmin(time_all[2],leak_i$M21),
255                                pmax(time_all[1],leak_i$start),
256                                units="days")))
257
258    E_all[n_i,"C21"] <- sum(leak_i$ER_kgpd*
259                              pmax(0,difftime(
260                                pmin(time_all[2],leak_i$C21),
261                                pmax(time_all[1],leak_i$start),
262                                units="days")))
263
264    E_all[n_i,"DTA"] <- sum(leak_i$ER_kgpd*
265                              pmax(0,difftime(
266                                pmin(time_all[2],leak_i$DTA),
267                                pmax(time_all[1],leak_i$start),
268                                units="days")))
269
270    E_all[n_i,"DT_"] <- sum(leak_i$ER_kgpd*
271                              pmax(0,difftime(
272                                pmin(time_all[2],leak_i$DT_),
273                                pmax(time_all[1],leak_i$start),
274                                units="days")))
275
276    E_all[n_i,"DTC"] <- sum(leak_i$ER_kgpd*
277                              pmax(0,difftime(
278                                pmin(time_all[2],leak_i$DTC),
279                                pmax(time_all[1],leak_i$start),
280                                units="days")))
281  }
282
283  # Save individual iteration files for review
284  if(n_i<=100){
```

```
285     write.csv(leak_i[,c("ComponentClass","ComponentTag","NetReading",
286                         "Level","cluster","ID","x","y","D_max","ER_kgpd",
287                         "start","M21","C21","DTA","DT_","DTC")]
288               ,paste0("i100/",FACIL,".",SV_metric,".",LEAK_DEF,"_n",n,"_i",n_i,".csv"))
289
290   }
291
292 } # end Monte Carlo loop
293
294 # Save Summary Files
295 {
296   base <- paste0("n",n,"/",FACIL,".",SV_metric,".",LEAK_DEF,"_n",n)
297
298   write.csv(E_all,paste0(base,      ".csv"))
299   write.csv(C_all,paste0(base,"_count.csv"))
300
301   SUMM <- data.frame("DTA"=c(0,0),"DT_"=c(0,0),"DTC"=c(0,0))
302   row.names(SUMM) <- c("M21","C21")
303   SUMM[1,] <- colSums((E_all[,c("DTA","DT_","DTC")]-E_all$M21)<=0)/n*100 # percentage
304   SUMM[2,] <- colSums((E_all[,c("DTA","DT_","DTC")]-E_all$C21)<=0)/n*100 # percentage
305   print(SUMM)
306
307   write.csv(SUMM,paste0(base,"_SUMM.csv"))
308 }
309 #### End ##############################################################################
```

Appendix E3

Simulation Files

List of accompanying LeakDAS and simulation software I/O CSV files with PDF-attached compressed file "Appendix E3_Leak Database and IO Files.zip" containing the files.

Filename	Description
Equation_FHR.csv	FHR correlation equation constants for emission factor calculation.
sensor_locations.csv	LDSN/DRF sensors active at FHR CC facility with location coordinates
LeakDAS Records	
Mid Crude Inspections 2013 thru 2019.csv	LeakDAS TVA and AVO LDAR records for the FHR CC Mid-Crude unit
Meta Inspections 2013 thru 2019.csv	LeakDAS TVA and AVO LDAR records for the FHR CC m-Xylene unit
MidCrude_Inactive.csv	LeakDAS deletion records for the FHR CC Mid-Crude unit
mXylene_Inactive.csv	LeakDAS deletion records for the FHR CC m-Xylene unit
Location Info	
midCrude_leaks2.csv	Mid-Crude component location information provided by Molex
mXylene_leaks3.csv	m-Xylene component location information provided by Molex
output_MIDCRUDE_04012020.csv	Mid-Crude component location information provided by Molex
output_META.csv	m-Xylene component location information provided by Molex
***Identify_Leaks.R* outputs**	
MidCrude_leaks_all.csv	All leaks for Mid-Crude unit found in 2013-2019 records
MidCrude_leaks_AVO.csv	AVO leaks for Mid-Crude unit within the filtering parameters
MidCrude_leaks_FG.csv	All fuel gas area GV leaks for Mid-Crude unit found in 2013-2019 records
MidCrude_leaks_M21.first.csv	Simulation leaks for Mid-Crude unit within the filtering parameters, first SV
mXylene_leaks_all.csv	All leaks for m-Xylene unit found in 2013-2019 records
mXylene_leaks_AVO.csv	AVO leaks for m-Xylene unit within the filtering parameters
mXylene_leaks_FG.csv	All fuel gas area GV leaks for m-Xylene unit found in 2013-2019 records
mXylene_leaks_M21.first.csv	Simulation leaks for m-Xylene unit within the filtering parameters, first SV

Appendix F

Molex Equivalency Simulations

Appendix F1

Molex Simulation Approach

Appendix F1

Leak Simulations Based on FHR Corpus Christi LeakDAS™ Data

Executive Summary

Molex investigated the emission control equivalency of the proposed LDSN-DRF concept relative to the M21-based CWP for the FHR CC Meta-Xylene and Mid-Crude process units. The two LDAR methods were compared using a series of emission simulations with a randomized historical simulation and a Monte Carlo approach. The model simulated process unit leaks using historical facility LeakDAS™ LDAR data and calculated emissions based on both non-growth and linear-growth leak rate models and the assumed control for four different LDSN detection sensitivity performance scenarios, i.e. detection from single tag leaks represented by DTA(tag), detection from clustered leaks represented by DTA(cluster), detections from single leaks with actual distances from nearest sensors represented by DT(tag), and detection from multiple leaks with actual distances from the nearest sensors represented by DT(cluster). The historical measurement data was transformed into datasets of leaks occurring during 2014-2018 in Meta-Xylene and 2016-2018 in Mid-Crude. These leaks were simulated with randomized leak start times to compare LDSN-DRF and CWP multi-year cumulative emissions. A Monte Carlo approach was used to understand variation and to test LDSN-DRF to CWP emission control equivalency, defined as >67% of 10000 trials showing benefit.

The average detection threshold value necessary to demonstrate M21 CWP equivalency is the eDTA. Based on the most conservative approach (i.e. using average DTA(tag)) in the simulation analysis, an eDTA of 10,625 –12,500 ppm is generated from the historical leak event randomization simulation, while the Monte-Carlo method alone suggests an eDTA of 11,250 ppm for the Meta-Xylene unit, and an eDTA of 12,500 for the Mid-Crude unit. This data suggests a DTU as high as 16,875 ppm (DTA 11,250 ppm) for equivalency to the M21 CWP. At the eDTA of 12,500 ppm, LDSN-DRF also demonstrated significant emission reduction potential. For instance, LDSN-DRF emissions reduction ranged from 29% to 67% over 5 years for the Meta-Xylene unit, and 29% to 41% over 3 years for the Mid-Crude unit. These ranges are based on the simulation analysis of the more realistic DT(tag) and DT(cluster) detection scenarios in which actual distances between leaking components and sensors were taken into consideration. These comparisons did not include the emission reduction benefits from early detection and repair of other LDAR program leaks (such as AVOs) or non LDAR emissions. Although the model was limited to the duration of the simulation periods, the relative rates of change in cumulative emissions suggest the LDSN-DRF system would continue to demonstrate emission reductions relative to scheduled M21 performance.

This appendix describes the simulations in detail and presents the framework for systematically determining the eDTA. This approach allows LDSN-DRF design practices to be leveraged for other process units with similar historical leak profiles and response factors.

1 Introduction

Method 21 is an EPA protocol for detecting and quantifying leaks of volatile organic compounds in LDAR. Method 21 inspections are conducted on schedules, typically monthly for pumps, quarterly for valves, and annually for connectors. In the M21 procedure, each component interface is scanned with a calibrated flame ionization detector (FID) or photoionization detector (PID) and the highest screening value (SV) is recorded. If the screening value is equal to or greater than EPA's leak definition, this component fails the inspection and is considered as a leaking component; an effective repair must be completed within a 15-day period unless classified as a delay-of-repair (DOR) component. All Method 21 data is recorded in a database system such as LeakDAS™ including the date and time of each monitoring event, the M21 results, repair information, as well as the component tag number and chemical stream information. The LeakDAS™ software includes an emission calculation module which utilizes built-in EPA emissions factors and correlation equations to allow total fugitive emissions to be estimated for use in annual emission inventories and other mandated reports.

A leak detection sensor network (LDSN) combined with the detection response framework (DRF) provides a totally different approach to LDAR. The LDSN monitors process units by detecting small gas plumes generated by component leaks. When sensor detection signals reach preset threshold criteria, a detection notification is issued and the DRF process is initiated. Due to continuous operation, the LDSN-DRF approach is able to identify large leaks sooner, and therefore perform equally or better in total emission control when designed and operated with an appropriate average detection sensitivity.

In order to implement an alternative work practice (AWP), the new work practice "must achieve a reduction in regulated material emissions at least equivalent to the reduction in emissions achieved" under current federal regulations (40 CFR 65.8(a)). This document presents an emission analysis which seeks to assess equivalency based on our current understanding of potential LDSN-DRF performance which has been gained through controlled releases and actual leaks in laboratory, test range, and complex industrial facilities. Leak simulations were conducted assuming LDSN-DRF was employed instead of routine scheduled M21 for the past few years. Based on the LDSN-DRF design, operation, and a set of reality-based assumptions, the total fugitive emissions were calculated at different sensitivity or detection threshold average (DTA) levels. By comparing with data from the scheduled Method 21 current work practice (M21 CWP) required by applicable federal regulations, an appropriate DTA value called eDTA was determined. The eDTA represents the threshold value that the new method must achieve in order to demonstrate equivalency to the CWP for each of the two pilot test units at FHR Corpus Christi West Refinery.

1.1 Definitions of Leaks and Leak Model Assumptions

- **Emission Duration**

  The emission duration of any particular LDAR component is defined as the period from the leak start time to the repair finish time.

  The fugitive emissions total from each component is the sum of its daily emissions during the simulation time period.

- **Baseline Screening Value (SV)**

  The Method 21 screening value (SV) of a component prior to any leak or after any successful repair event is defined as 0 ppm.

- **Leak Definition**

  Based on Method 21 leak definitions in applicable federal regulations, once the SV of a component is 500 ppm or greater, it is considered a leak event for that component. An exception is that the SV value for a leak event on pumps in synthetic organic chemical manufacturing industry (SOCMI) service is 1000 ppm or greater.

- **Time-To-Repair in Method 21 and in LDSN-DRF**

  For both M21 CWP and the LDSN-DRF, the model assumes that once a specific leak has been detected it will be repaired 7 days later. This assumption is based on historical records and the requirement under both methods to conduct an initial repair attempt within 5 days of a leak being detected and a final effective repair no later than 15 days after the leak was detected. Thus, the model maintained the leak at a constant emission rate for 7 days after the leak existed for the M21 simulation. There is some anticipated time lapse between initial LDSN potential source location (PSL) notification and the time that a specific leak is detected utilizing DRF activities. So, while both the M21 and the LDSN-DRF simulations similarly assumed 7 days from leak detection until leak repair, the LDSN-DRF simulation also conservatively included 3 additional days at the elevated rates to account for time from leak existence until leak detection.

- **Calculation of Historical Emissions**

  Historical emissions are calculated from LeakDAS™ data, by using the daily SV and duration for each individual component and then converting to an hourly emission rate (kg/hr) and a daily emission amount (kg).

- **Linear Growth Model**

  This model assumes the SV will grow with time and that the growth rate is a constant. This model is designed to represent progressive leaks such as corrosion-initiated leaks and leaks related to wear of seals and seating surfaces from repeated cycling. For each individual component, the growth rate is defined as

$$Leak\ Growth\ Rate = \frac{the\ first\ failing\ SV - the\ previous\ passing\ SV}{time\ between\ first\ failing\ M21\ scan\ and\ previous\ passing\ M21\ scan}$$

  The start time is defined as the date and time of the last passing M21 monitoring record in the LeakDAS™ database. For any randomized simulation, the leak event is assumed to have randomly occurred during the simulation period.

- **Non-growth model**

  This model assumes that the SV for a leaking component remains constant at the measured value above the leak definition until it is repaired. This model theoretically represents leaks related to single point mechanical failures with no progression or cascading effects.

  In the non-growth model, the leak start time is defined as half the time between the date and time of the last passing M21 monitoring record and the date and time of the first failing M21 monitoring record in the LeakDAS™ database. For any randomized simulation, the leak event is assumed to have randomly occurred during the simulation period.

- **Components with Multiple Leaks**

  In the simulation, if a new leak event occurred before the previous leak event on the same component was repaired, the larger leak growth rate (or SV for non-growth model) is assumed to supersede the current simulated leak growth rate (or SV for non-growth model) starting from the new leak event start time. If the new leak event starts during the previous event's repair time, the current repair is assumed to correct both leaks. As shown in Figure B-1 (top), the 3rd historical leak (HF3) will be fixed during the repair of first historical leak (HF1) and the second historical leak (HF2).

  For the Monte Carlo simulation, there are several considerations that justify addressing those components in the dataset that have overlapping leaks in this manner: (1) each set of leak records is from a single process unit and each component tag has a distinct physical location assigned; (2) in the field, it is common for a new leak to be detected on a component during subsequent routine scheduled monitoring after an earlier leak has been repaired. In common parlance, these are called "repeat leaks" or "chronic leakers" and should be reflected in the simulation; (3) since M21 results are used to validate the repair status in the model, all overlapping leaks on a component are considered to have been corrected after the successful repair.

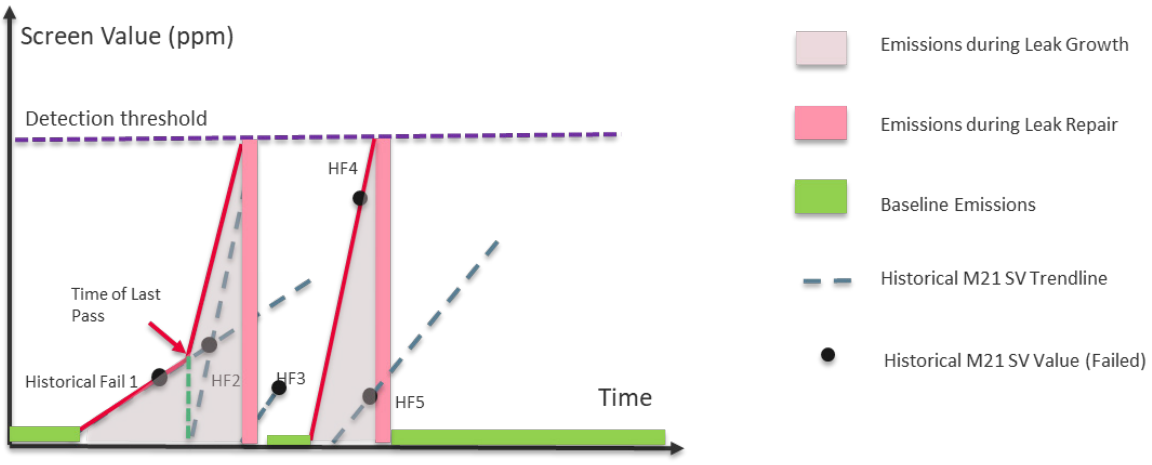

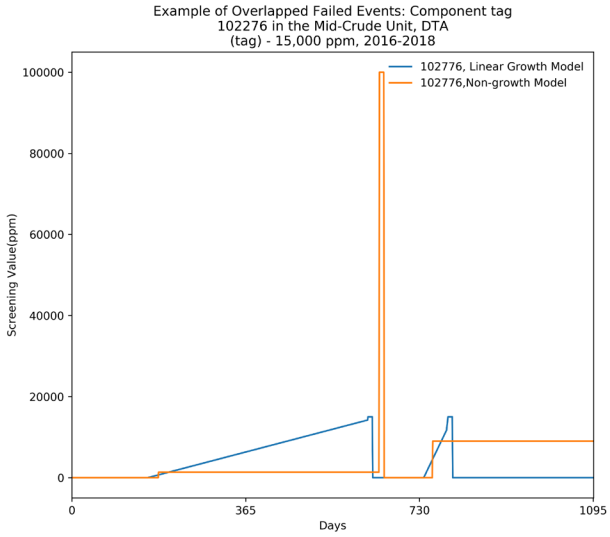

Figure B-1. Illustration of Simulating Overlapped Leak Events for a Single Component (Top Depiction, Linear Growth Model); Example of Overlapped Leak Events on Actual Component (Tag#102776 in the Mid-Crude Unit, Bottom Graph)

- **Cluster of Multiple Leaks**

  The LDSN is a chemical plume or emissions monitoring system. When multiple leaks occur from different leak interfaces on a single component such as a pump, the combined impacts of these leaks can be anticipated to contribute to the overall size of the plume and the sensor detection signals. A similar effect can result due to small leaks emanating from different components that are co-located within a small area of sensor coverage. This leak cluster aggregation effect can be evaluated through a cluster simulation.

  In the cluster simulation, the sum of SVs or distance (D) weighted SVs from a cluster of components is compared to an assigned threshold to determine if the LDSN has triggered a detection event. Cluster grouping is determined by both "unit ID" and elevation levels. For examples about leak clusters found by M21 and detailed analysis, see Appendix C.

- **Cluster Repair Threshold**

  Whenever a detection event has occurred in the cluster simulation, it is assumed that leaks above the Cluster Repair Threshold will be repaired one by one. If no individual leaks above this threshold are found, the model assumes that up to three leaks will be repaired under the defined DRF. The sum of the SV values is assumed to be greater than the cluster repair threshold.

- **Emission Rate Correlation**

The emission factors and correlation equations shown in Table B-1 are used in the emission rate calculation. These are based on information in the EPA Protocol for Equipment Leak Emission Estimates and TCEQ Technical Supplements to Emission Inventory Guidelines.

Table B-1. Emission Factors used in SOCMI equation

Equation Set Details Report (R801_9) LeakDAS Report Date: 11/2/2018

Equation Set	Class	Type	Chem State	Default Zero	Pegged 10K	Pegged 100K	Multiplier	Exponent	Default Factor
SOCMI				.00000750	.140	.620	.00001900	.8240	.22800000
SOCMI	AG			.00000750	.140	.620	.00001900	.8240	.01990000
SOCMI	AG		HL	.00000750	.140	.620	.00001900	.8240	.01990000
SOCMI	AG		LL	.00000750	.140	.620	.00001900	.8240	.01990000
SOCMI	COMPR			.00000750	.140	.620	.00001900	.8240	.22800000
SOCMI	COMPR		GV	.00000750	.140	.620	.00001900	.8240	.22800000
SOCMI	CONNECT			.00000061	.044	.220	.00000305	.8850	.00183000
SOCMI	CONNECT		GV	.00000061	.044	.220	.00000305	.8850	.00183000
SOCMI	CONNECT		HL	.00000061	.044	.220	.00000305	.8850	.00183000
SOCMI	CONNECT		LL	.00000061	.044	.220	.00000305	.8850	.00183000
SOCMI	RELIEF			.00000750	.140	.620	.00001900	.8240	.10400000
SOCMI	RELIEF		GV	.00000750	.140	.620	.00001900	.8240	.10400000
SOCMI	RELIEF		HL	.00000750	.140	.620	.00001900	.8240	.00403000
SOCMI	RELIEF		LL	.00000750	.140	.620	.00001900	.8240	.00023000
SOCMI	SAMPL			.00000750	.140	.620	.00001900	.8240	.01990000
SOCMI	SAMPL		HL	.00000750	.140	.620	.00001900	.8240	.01990000
SOCMI	SAMPL		LL	.00000750	.140	.620	.00001900	.8240	.00862000
SOCMI	VALVE			.00000066	.024	.150	.00000187	.8730	.00597000
SOCMI	VALVE		GV	.00000066	.024	.110	.00000187	.8730	.00597000
SOCMI	VALVE		HL	.00000049	.036	.150	.00000641	.7970	.00403000
SOCMI	VALVE		LL	.00000049	.036	.150	.00000641	.7970	.00023000

Table B-2. Emission Factors used in Refining Industry equation

Equation Set Details Report (R801_9) LeakDAS Report Date: 11/2/2018

Equation Set	Class	Type	Chem State	Default Zero	Pegged 10K	Pegged 100K	Multiplier	Exponent	Default Factor
FHR Refining				.00000400	.073	.110	.00001360	.5890	.00000000
FHR Refining	COMPR		GV	.00000400	.073	.110	.00001360	.5890	.63600000
FHR Refining	CONNECT	FLG		.00000031	.085	.084	.00000461	.7030	.00025000
FHR Refining	CONNECT	SCREWD		.00000750	.028	.030	.00000153	.7350	.00025000
FHR Refining	PUMP			.00002400	.074	.160	.00005030	.6100	.11400000
FHR Refining	RELIEF			.00000400	.073	.110	.00001360	.5890	.16000000
FHR Refining	VALVE		GV	.00000780	.064	.140	.00000229	.7460	.02680000
FHR Refining	VALVE		LL	.00000780	.064	.140	.00000229	.7460	.01090000

1.2 Definitions of Detection Terminology

- **Detection Threshold (DT)**

The detectability or Detection Threshold (DT) of individual sensors is dependent on the distance of the leak from the nearest sensor or sensors under similar wind conditions. Leaks closer to a sensor, for example, can be detected at a smaller size than leaks farther away. For each sensor that is part of an appropriate sensor placement plan, there is a DT band across the sensor coverage radius. DT is expressed in ppm based on FID measurements per EPA Method 21 procedure.

- **Detection Threshold Average (DTA)**

  Detection Threshold Average (DTA) is the average value of the DT band and is expressed as DTA=*avg* (DT1, DT2, …). The DTA is an average measure of LDSN-DRF's sensitivity for the process unit.

- **Detection Threshold Average required for Equivalency (eDTA)**

  To differentiate DTA from actual sensor performance, eDTA is used to represent a target sensitivity level that LDSN-DRF as a whole must achieve in order to demonstrate M21 CWP equivalency in total fugitive emissions for a given process unit. The eDTA value is generated by simulations.

- **Detection Threshold Upper Limit (DTU)**

  DTU is the upper limit of the DT band and is expressed as DTU = *max* (DT1, DT2, …). The DTU represents the DT value or smallest leak that could be detected by the sensor network at the farthest distance away from a sensor. Figure B-2 illustrates the relationship between DTA and DTU assuming even distribution of components within the sensor coverage. DTU is typically greater than 1.5 x DTA because the smallest value in the DT band can be very small (particularly when a leak takes place right next to a sensor).

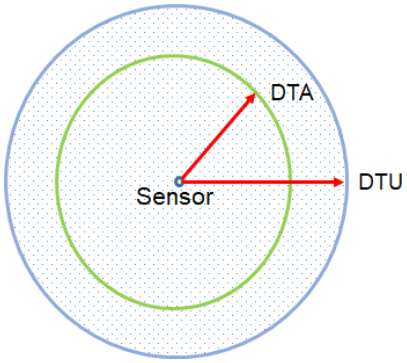

Figure B-2. Illustration of DTA and DTU within Sensor Coverage

- **Emission Rate (ER)**

  The emission rate (ER) is total emissions per hour, in kg/hr.

1.3 Description of Leak Detection Scenarios for Simulations

- **Emission Calculation with DTA(tag)**

  A detection event is defined as the SV of a single component tag reaching DTA.

- **Emission Calculation with DTA(cluster)**

  A detection event is defined as the sum of SVs from multiple leaks within one cluster reaching DTA.

- **Emission Calculation with DT(tag)**

  A detection event is defined as the SV of a single component reaching the DT value at the actual distance of the component from the closest sensor or sensors. In the DT(tag) simulation, a distance-related threshold SV/D^2, where D is the shortest distance to nearby sensors, is used to determine if the LDSN has a detection event. In this scenario, leaks farther away from sensors have smaller detection signals than leaks of the same size closer to the sensors. For details about the distance relationship, please refer to Appendix C.

- **Emission Calculation with DT(cluster)**

  A detection event occurs when the sum of SV/D^2 from a cluster of components reaches the detection threshold. In this scenario, a leak closer to a sensor has a greater contribution to the total detection signal than another leak of the same size within one cluster and their contributions to the detection signal are mathematically modelled.

2 Simulation of Historical M21 Leaks

The simulations used 2014 - 2018 data from the LeakDAS™ database to calculate historical emissions in the Meta-Xylene unit. Figure B-3 shows the daily fugitive emissions of components with leak events in that process unit. Yearly emission "cycles" can be seen which correspond to annual scheduled M21 activities. The Mid-Crude unit used 2016-2018 data for simulations. The shorter time period was considered to be more representative than previous years. This is because routine connector monitoring was added to the Mid-Crude LDAR program in 2016. The daily fugitive emissions of components with leak events in the Mid-Crude unit are also shown in Figure B-3. The cumulative emissions of these two process units were plotted to illustrate the total emission development trend for the corresponding periods (Figure B-4).

Some points of interest identified when developing the simulations and comparing the simulated M21 results to historical data recorded in LeakDAS™ include:

(1) In the historical data, a new leak event starts with one failing monitoring result and ends with one passing monitoring result. Each of the results has corresponding inspection dates and times. Those dates are primarily based on EPA's mandated inspection schedules. There is still some inherit variation associated with the inspection dates in historical date because a component requiring quarterly monitoring might be monitored earlier in the quarter or later during subsequent quarters. This variation in monitoring schedule can be impacted by weather ("rain-out" conditions in the field), LDAR components being temporarily out service, the availability of monitoring personnel, periodic restrictions on access to process units due to safety considerations during start-ups, etc. In contrast to periodic scheduled monitoring, components may have multiple leak events during the LDSN simulations, before they were repaired. When the simulated inspection date is different from the historical data, a component's leak events may overlap with each other if the component had multiple leak events. For larger process units where the number of components is over 10,000, one uniform inspection date for every component cannot be set. The direct consequence is that the simulated M21 emissions are highly dependent on the selection of an inspection date because of the potential for overlapping leaks. This phenomenon is illustrated in Figure B-5. The blue line shows the historical leak events of component number 251537 (a connector in the Meta-Xylene unit) by connecting all the historical M21 SVs with the actual installation time and passing values. The yellow line (assumes the annual M21 inspection starts on Jan. 1st) and green line (assumes the annual M21 inspection starts on June 1st) are the simulated M21 SVs without the real installation time and randomization of leak start time. As expected, the yellow and green lines extend to the whole simulation period due to the exclusion of actual installation time. All three lines have the same leak start time, which coordinates with our assumptions on how the leak developed under the linear growth model. The M21 inspection schedule for connectors is annual, so the historical leak (blue line) was detected during the annual inspection and repaired shortly after. For the simulated M21, the component was repaired earlier for the green line than the yellow line because of the different initial M21 inspection dates (the middle vs. the start of a year). In this case, because the historical leak events was based on an annual schedule, a different simulated M21 initial date will generate different simulated M21 emissions.

(2) LeakDAS™ emission calculations include several parameters for actual field conditions, i.e., the component service time (installation, removal, and "out of service" time for each LDAR component), passing SVs, and failing SVs. The yearly emissions reported are based on field measurements and component service time during the given year, which is different from the simulation data. For a simulated leak event, consideration must be given for how best to model a component that may have been removed from service during the leak event. The LeakDAS™ emission calculation module is most typically used to calculate emission estimates for annual reporting (January 1st - December 31st). However, for longer-term models, the simulated leak events can occur across yearly boundaries. The emissions from a leaking component might start during Oct. 2015 but not be detected until routine scheduled monitoring was conducted at some time in the next calendar quarter which would be in 2016. In this example, the LeakDAS™ emission calculation results for CY2015 would not account for the increased emission trend of a component that was next monitored outside the calculation range.

(3) It is not uncommon for audio visual olfactory (AVO) leaks on LDAR components to be entered into databases such as LeakDAS™. This approach allows the facility to follow the normal leak repair protocols and maintain records to show compliance with applicable regulations. When an AVO leak is found in the field by operations personnel, an initial repair attempt is conducted. If this corrects the AVO indications, the component is considered repaired. If the repair does not seem effective, then a monitoring technician is dispatched to conduct a M21 inspection to provide a M21 result for comparison with applicable leak definitions. As expected, the raw LeakDAS™ datasets used for these simulations included several AVO leak records without a M21 measurement. The LeakDAS™ emission calculator module includes an option to "include failed visuals at 10,000 ppm". Unless that option is selected, the AVO leaks are not assigned a numerical SV for inclusion in emission calculations performed in LeakDAS™. The raw datasets include readings that range from thousands of ppm to 100,000 ppm for M21 monitoring that occurred shortly after AVO discovery.

(4) The leak event duration is the time between the initial failing M21 monitoring results and the follow-up passing M21 results. The leak event duration varies among components with an average duration of 5.6 days and 11.5 days in the Mid-Crude unit and Meta-Xylene unit respectively. For leaking components that have been isolated from VOC service or that will require a process unit shutdown to complete an effective repair, there can be an allowance to go beyond the 15-day repair deadline. If failing records in the dataset that last more than 30 days are excluded, the average duration is 3.5 days and 5.0 days for these process units.

In response to the items of interest listed above, several different methods have been employed to address each issue and to conservatively estimate M21 results during the modeled simulations. These methods include:

(1) The worst-case SV is assumed for the overlapped leak events during the simulation. In both non-growth and linear growth models, this worst case is conservatively assumed, i.e., the largest leak growth slope or the leak value will replace the smaller ones if overlap occurs. In this way, if there are multiple leak events for a component, all will be considered in the model. This approach avoids the potential under-estimation of the emissions from those leak events.

(2) The component installation date and removal date parameters are not included in the simulation. Components are assumed to be emitting during all simulation periods. Component removal dates from the raw datasets are not modeled as a zero emitter. Instead, the leak event start times were randomized thousands of times. The resulting simulated average emissions should not be impacted by variations in M21 scheduling.

(3) It is reasonable to assume that through the use of a continuous monitoring system such as LDSN, the AVO leaks can be detected sooner and while they are still smaller than those that could be identified by human senses during general operator or AVO rounds in an operating facility. Earlier detection of large leaks can provide considerable emission reductions. Due to the complexity of comparing LDSN detections to non-scheduled AVO detections, the simulations did not include leaks associated with AVOs. Demonstrating M21 CWP equivalency without the added benefit of early AVO detections of an LDSN is a more conservative approach and likely understates the overall potential emission reductions available through the LDSN-DRF approach.

(4) In the M21 simulation, the leak event duration is assumed to be 7 days from the date of leak detection to the date the leak was repaired. For the LDSN models, a similar 7-day leak duration from leak detection to leak correction is used. However, because there can be some lapse between the time that an emission anomaly is detected by the LDSN and the time that a field technician identifies a specific leaking component in the field, three additional days were added to the detection time in the LDSN-DRF.

The methodology and assumptions described above were applied to the historical LeakDAS™ data in order to model M21 emissions for comparison to LDSN models using similar assumptions. Understandably, emission estimates based solely on the raw M21 SVs and correlation equations differ from the simulated M21 results. However, by applying the simulation assumptions neutrally to all simulations including the M21, DTA(tag), DTA(cluster), DT(tag) and DT(cluster), the results of the simulations can be fairly used to establish emission control equivalency. Although it is of interest that traditional M21 emission estimation methods don't provide identical results to M21 simulations, it is more important for this equivalency discussion to ensure the results of the M21 simulation and the LDSN simulations provide for a fair and equitable comparison of emission control effectiveness.

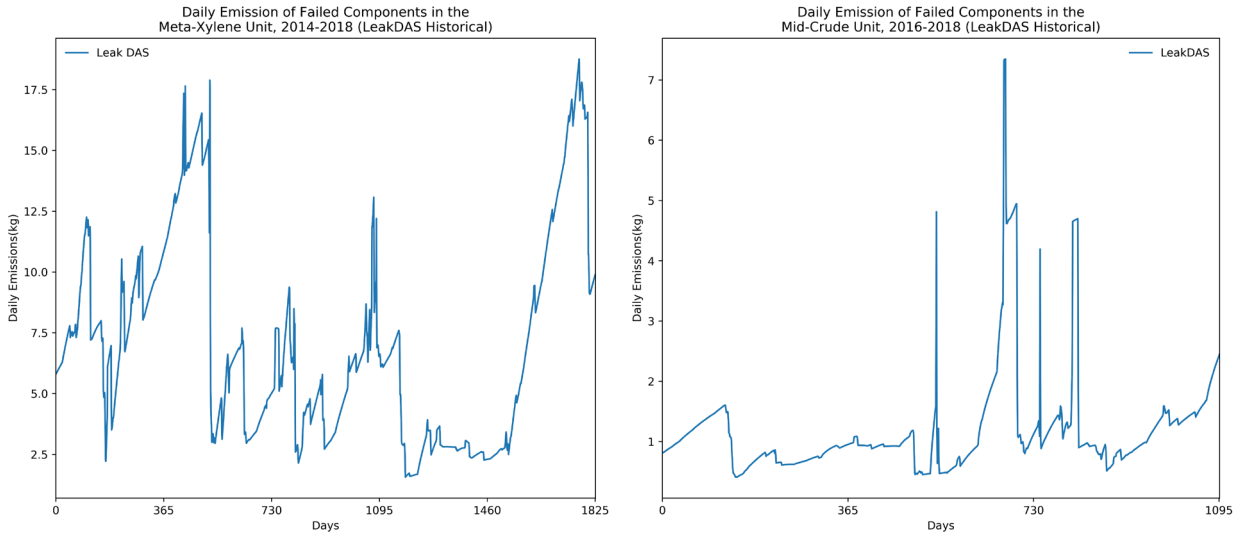

Figure B-3 Daily emissions of failed components in the Meta-Xylene Unit 2014-2018 (Left, LeakDAS™) and Mid-Crude Unit, 2016-2018 (Right, LeakDAS™)

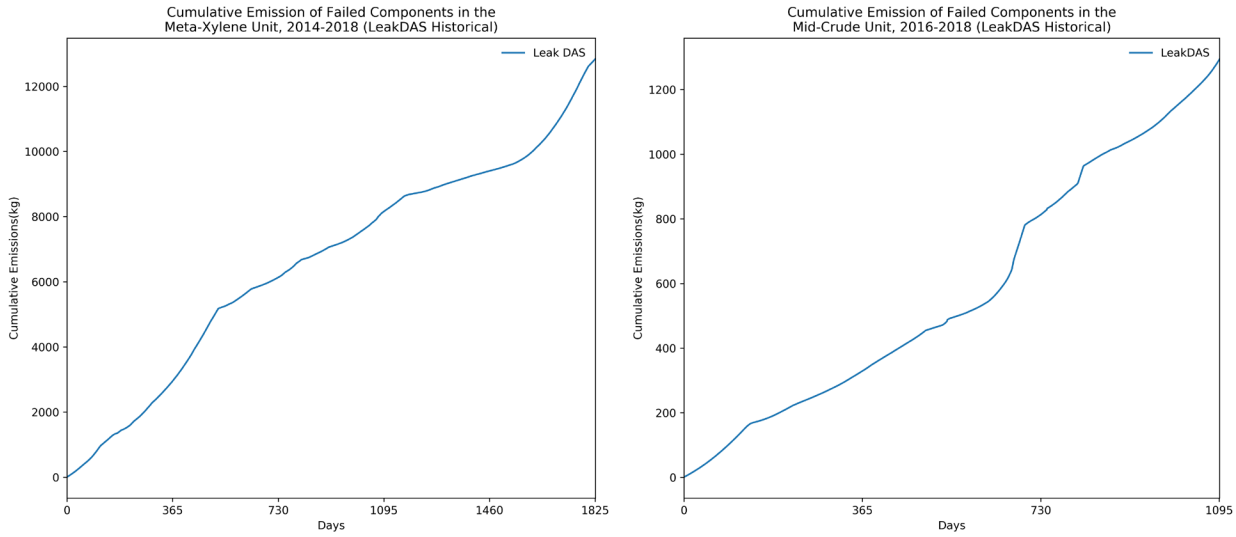

Figure B-4 Cumulative Emissions of Failed Components in the Meta-Xylene Unit, 2014-2018 (Left, Leak DAS™) and the Mid-Crude Unit, 2016-2018 (Right, LeakDAS™)

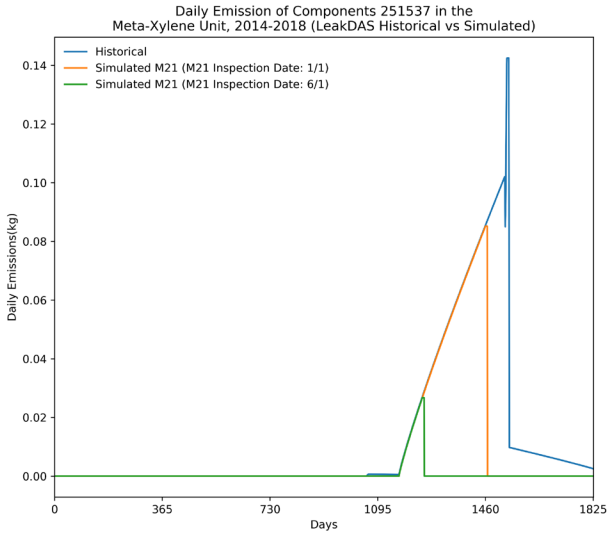

Figure B-5. LeakDAS™ Data vs. Simulated M21 Daily Emissions of Tag 251537 in Meta-Xylene Unit, 2014-2018 (Linear Growth Model)

3 Emission Simulation of Randomized Historical Leaks

Leak events were randomized for all the historical leaks for three reasons: (1) to minimize the impact of the variation in the historical M21 schedule on the emission calculation; (2) to determine the detection level that is equivalent to scheduled M21 emissions under different scenarios; (3) to validate the effectiveness and the robustness of the LDSN. A randomized leak events profile was generated by randomizing both the leak event start time and the leak event sequence.

An additional goal was to identify the theoretical detection threshold that would generate equal or less emissions than CWP. The DTA value that creates equal or less emissions compared to CWP is referred to as the "eDTA".

3.1 Simulation Basics of Scheduled M21 Emissions

Simulated scheduled M21 emissions were used as the "baseline" for the emission comparison: (1) All historical leak events were randomized based on the guidelines outlined in the 2000 EPA's Monte Carlo guiding principles [1], (2) the typical EPA M21 schedule (Table B-3) was used to allow the simulation to be readily applicable and leverageable to other process units. Based on historical data analysis, it is assumed that leaks detected by scheduled M21 will be repaired in 7 days after the leak was identified. A simulation example of the Meta-Xylene unit (Table B-4), shows that the scheduled M21 emissions of the randomized leaks have much less variance than the historical leaks. A similar situation occurs in the simulated M21 results of the Mid-Crude unit shown in Table 5. In the following simulations, January 1, 2014 (for the Meta-Xylene unit) and January 1, 2016 (for the Mid-Crude unit) are used as the first inspection date for scheduled M21 inspections.

Table B-3. EPA & Modeled M21 Schedules

Component Type	EPA Monitoring Frequency	Modeled M21 Schedule (days)
Connector	Annual	365
Pump	Monthly	30
Valve	Quarterly	90
Others	Quarterly	90

Table B-4. Simulated Scheduled M21 Emissions of the Meta-Xylene Unit, 2014-2018, Linear Growth Model

Simulated Total M21 Emissions (kg)		
Inspection Date	**Historical Data**	**Randomized (10000 trials)**
1-1	27816	29551
2-1	32750	29799
3-1	37179	30293
4-1	33597	31288
5-1	39057	32551
6-1	44697	34227
Average	35849.2	31285.0
STD	16.2%	5.8%

Table 5 Simulated Scheduled M21 Emissions of the Mid-Crude Unit, 2016-2018, Linear Growth Model

Simulated Total M21 Emissions (kg)		
Inspection Date	**Historical Data**	**Randomized (10000 trials)**
1-1	3932	3445
2-1	4676	3483
3-1	4938	3591
4-1	5533	3790
5-1	6314	4047
6-1	5636	4405
Average	5171.4	3793.5
STD	16.2%	9.8%

3.2 Emission Simulation on the Meta-Xylene Unit

The following conditions are used for the Meta-Xylene unit simulation:

	Simulation Setting
Simulation period	2014/1/1-2018/12/31
Components	Components with failed events in simulation period
Emission equation	SOCMI
DRF time for LDSN	10 days
Repair time for M21	7 days
Allow leak overlap	Yes
Leak overlap handling	As described in Section 1
M21 inspection starting date	2014-1-1
AVO-visual records	AVO-visual records related failed events are excluded
Cluster repair threshold	3000 ppm
Component location	Randomized within cluster
Component installation/removal time	Excluded
Number of trials	10000
Leak events profile	Randomize leak start time and sequence for the same tag

The Molex LDSN solution demonstrates a reduction in the total fugitive emission of the Meta-Xylene unit by shortening the duration of large leaks. To explore the effectiveness of the LDSN solution, four scenarios were simulated using two leak growth models (linear growth and non-growth) for the Meta-Xylene unit. The scenarios include DTA(tag), DTA(cluster), DT(tag), and DT(cluster). In Tables B-6 and B-7, each scenario is compared to the simulated scheduled M21 results. In these scenarios, DTA(tag) and DTA(cluster) are used to simulate single tag leak events and clusters of leaks in local areas, respectively. DT(distance) is used in simulations based on distance of the leak from the nearest sensor and DT(cluster) is used for simulations based on both the distance and the cluster assumptions. The DTA(tag) simulation is the most straight forward model. It relies on the simplest assumptions for the detection event definition. The DTA(cluster) model considers the additive effects associated with multiple leaks within a small area, which are known to contribute to the development of plumes detected by the LDSN. Both DT(tag) and DT(cluster) consider the actual distances of components from the nearest sensors, but DT(cluster) also considers the cluster effect while DT(tag) does not.

From the sensor sensitivity testing that FHR, Molex, and EPA ORD conducted using controlled releases of isobutylene which has a response factor of 1, the LDSN DT band for the Meta-Xylene units is 1,600-6,400 ppm, with a DTA of 4,000 ppm. The simulation results indicate that the average emissions for DTA(tag) 4,000 ppm are much less (43 - 70%) than the scheduled M21 emissions for both linear growth and non-growth models. After applying the distance-based detection threshold to the simulation (with DTA of 4,000 ppm), the average total emissions are estimated to be reduced by at least 60% for the non-growth model and 80% for the linear growth model when compared to the scheduled M21 emissions. From the current simulation results, the DTA(tag) is ~7,500 – 12,500 ppm for the Meta-Xylene unit which is higher than the DT band results based on relative RF. This demonstrates that the DTA of the installed system is lower than the DTA(tag) and is indicative of an LDSN that is more effective at controlling fugitive emissions than M21 CWP. The simulation results (with the a DTA level of 12,500ppm) for DT(tag) and DT(cluster) show that the total fugitive emissions of the Meta-Xylene unit were reduced by 29 - 66% when compared to the simulated M21 CWP. The simulation results demonstrate that the LDSN is easily equivalent to or better than the simulated M21 CWP.

Table B-6 Average Total Emissions (2014-2018) of the Meta-Xylene Unit with Randomized Leak Events (Linear Growth Model, 10000 trials)

PPM	DTA(tag), kg	DTA(cluster), kg	DT(tag), kg	DT(cluster), kg	M21, kg
4000	8886	3871	5212	4077	29546
5000	11156	5285	6601	4727	
7500	16639	9094	10001	6488	
10000	21678	12397	13325	8289	
12500	26119	15327	16637	10124	
15000	30114	18088	20112	11994	
17500	33849	20741	23596	13891	
20000	37329	23283	26721	15759	
22500	40629	25745	29550	17617	
25000	43728	28118	32202	19464	

Table B-7 Average Total Emissions (2014-2018) of the Meta-Xylene Unit with Randomized Leak Events (Non-growth Model, 10000 trials)

PPM	DTA(tag), kg	DTA(cluster), kg	DT(tag), kg	DT(cluster), kg	M21, kg
4000	14391	8536	9391	8183	25224
5000	17198	9993	10808	8876	
7500	22081	14483	13842	10751	
10000	26593	17910	16035	12267	
12500	27637	20234	17910	13566	
15000	29376	22611	19418	14647	
17500	30344	24107	20686	15577	
20000	31594	25326	21768	16323	
22500	32362	26963	22685	17008	
25000	33323	27811	23509	17641	

Figures B-6 and B-7 show comparisons of the daily emission rate and cumulative emission rate for both models. From Figure B-6, the daily emission rates of the various simulation scenarios are generally more consistent than the scheduled M21 emission rates. This relatively larger peaks associated with simulated M21 daily emissions are the result of new leaks accumulating over time until the periodic scheduled M21 identifies the leaks that developed since the previous monitoring cycle. Thus, the continuous monitoring of the LDSN-DRF solution not only helps reduce the cumulative emissions over the 5-year period but it also reduces the peak short-term emissions associated with the maximum daily emission rate. The trend of the cumulative fugitive emission differences between scheduled M21 and DTA(cluster), DT(tag) and DT(cluster) from Figure B-7 either becomes constant or expands over time. This suggests that the LDSN solution will continue to result in lower emissions relative to M21 CWP even beyond the duration of the modelled scenarios.

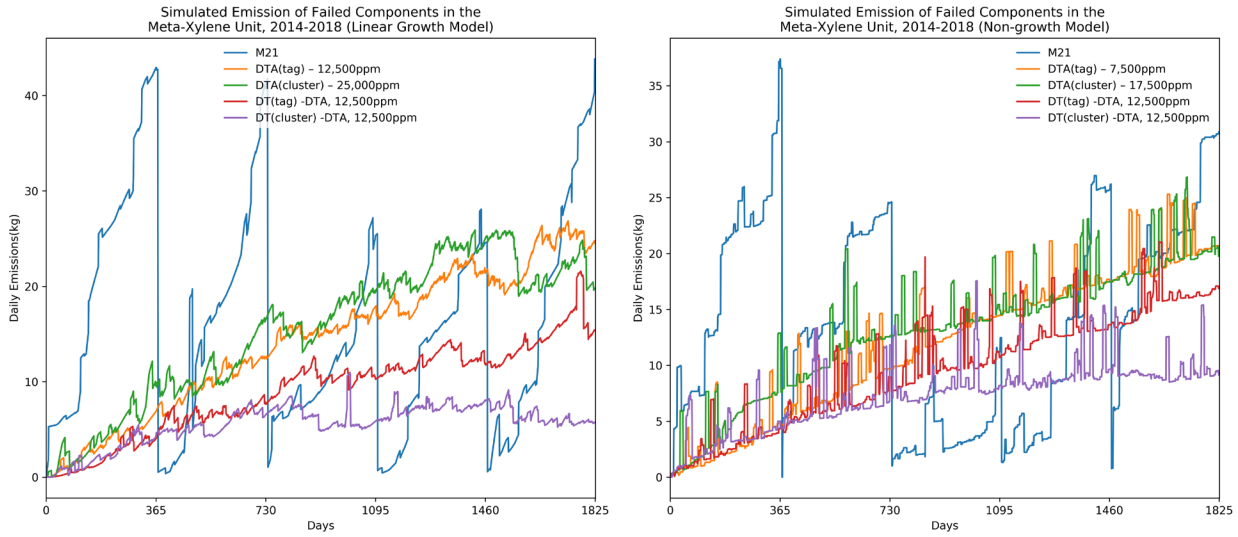

Figure B-6. Daily Fugitive Emission Rate of the Meta-Xylene Unit: Linear Growth Model (Left) and Non-growth Model (Right)

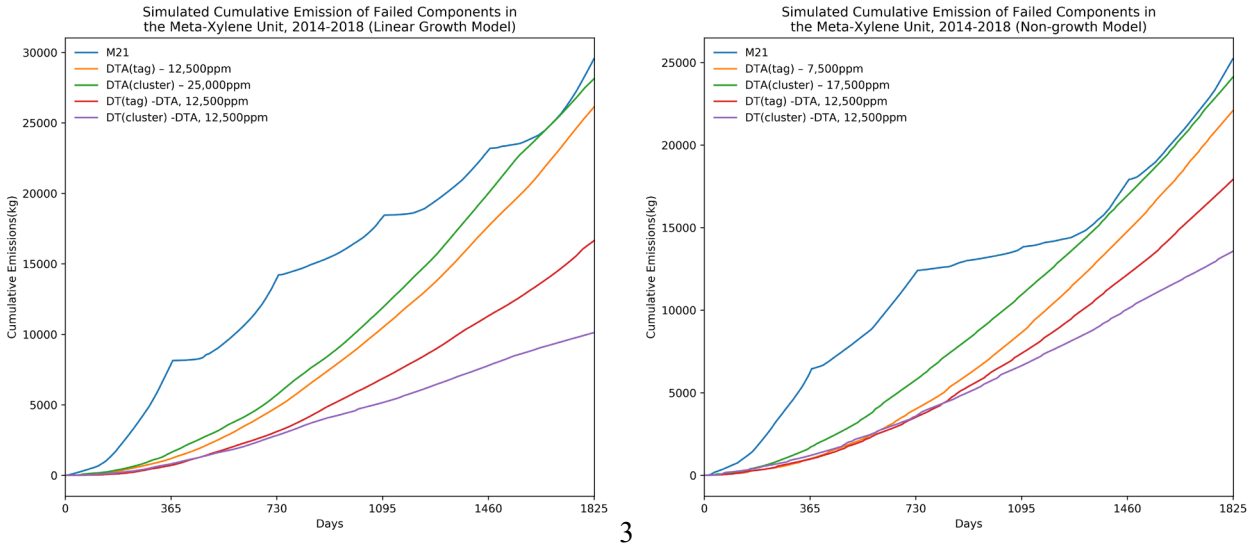

Figure B-7. Cumulative Fugitive Emissions of the Meta-Xylene Unit (2014 - 2018): Linear Growth Model (Left) and Non-growth Model (Right)

The probability of achieving equal or lower total fugitive emissions was examined by comparing different detection thresholds with the scheduled M21 emissions under the same, randomized leak profiles. Simulations were repeated numerous times, resulting in a certain percentage of the simulations achieving the desired

outcome (in this case, estimating the same amount or lower fugitive emissions than M21 CWP). Confidence level (CL) is the percentage of times that the total fugitive emissions resulting from the LDSN would be less than or equal to the total fugitive emissions of M21 CWP. CL is a measurement of the reliability of the LDSN solution under different leak profiles. In general, the resulting CL decreased as the values for DTA(tag) (Figure B-8 blue) and DTA(cluster) (Figure B-8 orange) increased. The values for DT(tag) (Figure B-8 green) and DT(cluster) (Figure B-8 red) represent distance-based DT bands covering varying DT values represented as a DTA. As shown in Figure B-8, the CL is over 67% (EPA guideline target CL) when the DTA(tag) is 7500 – 12500 ppm (non-growth and linear growth models). A DTA(cluster) of 17,500 - 25,000 ppm will achieve the 67% target CL. The CL's for DT(tag) and DT(cluster) consistently show over 67% up to 20,000 ppm DTA. This is the result of the relatively high sensitivity of the LDSN to the gas species (represented by low response factor) and relatively high sensor density in the Meta-Xylene unit. The simulation results suggest that LDSN-DRF is a robust and reliable emission monitoring system and is equivalent to or better than the M21 CWP with the current system design and sensor placement.

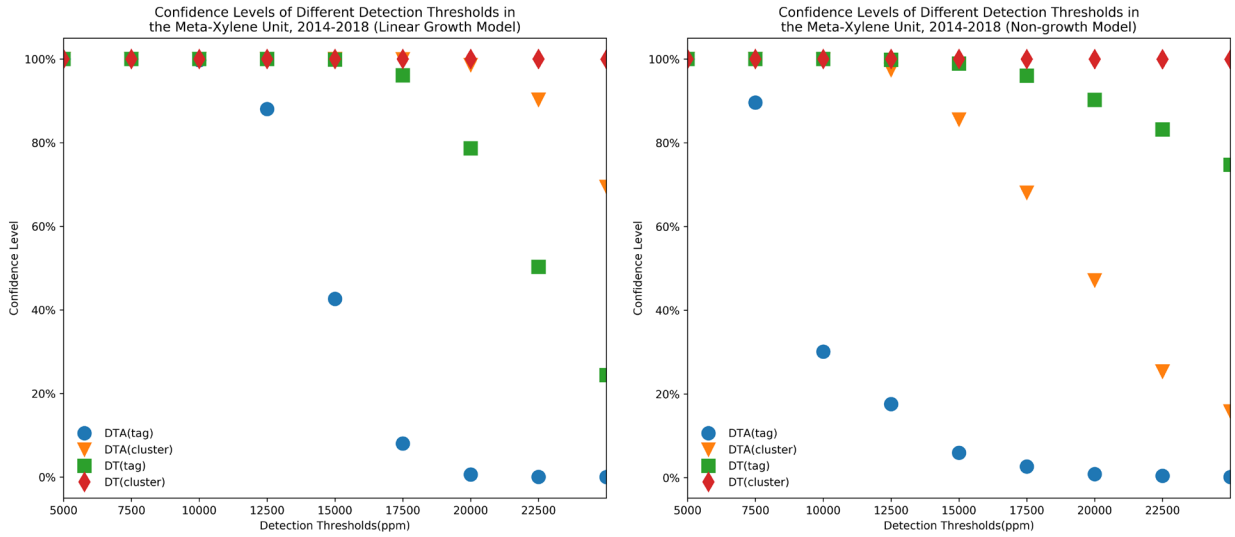

Figure B-8. CL With Different Detection Simulation Methods (Meta-Xylene Unit, 2014-2018): Linear Growth Model (Left) and Non-growth Model (Right)

3.3 Mid-Crude Unit

For the Mid-Crude unit, the following assumptions and settings are used:

	Simulation Setting
Simulation period	2016/1/1-2018/12/31
Components	Components with failed events in simulation period
Emission equation	Petro industry
DRF time for LDSN	10 days
Repair time for scheduled M21	7 days
Allow leak overlap	Yes
Leak overlap handling	As described in part 1
M21 inspection starting date	2016-1-1
AVO-Visual records	AVO-visual records related failed events are excluded
Cluster repair threshold	3000 ppm
Component location	Randomized within cluster
Number of trials	10000
Leak events profile	Randomize leak start time and sequence for the same tag

Simulations similar to those previously described for the Meta-Xylene unit were performed for the Mid-Crude unit. Adjustments required for the Mid-Crude model included: (1) two large heater units are excluded from the emission calculation. (2) the simulation period is 3 years (2016-2018) instead of 5 years. Since routine connector monitoring was added to the Mid-Crude LDAR program in 2016, these years were considered more representative than prior years.

The effectiveness of the LDSN was first validated utilizing an average total fugitive emission simulation. Table B-8 and Table B-9 summarize the results of this simulation: (1) with a DTA(tag) of between 7,500ppm and 17,500 ppm, the LDSN provides a reduction in total fugitive emissions when compared to the simulated M21. This is true for both the linear growth and non-growth models; (2) if distance factor is included in the simulation, the average total fugitive emissions will be further reduced; (3) An LDSN with a DTA(cluster) of 12,500 -17,500 ppm will also reduce the total emissions based on both leak models (linear growth and non-growth). Fugitive emission reductions were previously shown in the simulation results for the Meta-Xylene unit which has an average response factor of ~0.8. Although the response factor for some LDAR streams in the Mid-

Crude unit can be as high as 3 (range is 0.7-3.0), the LDSN-DRF simulations still demonstrate total fugitive emission reductions for this unit when compared to the M21 CWP.

Table B-8 Average Total Emissions (2016 -2018) of the Mid-Crude Unit with Randomized Leak Events (Linear Growth Model, 10000 trials)

PPM	DTA(tag), kg	DTA(cluster), kg	DT(tag), kg	DT(cluster), kg	M21, kg
5000	1403	1200	1357	1363	3437
7500	1859	1665	1815	1744	
10000	2246	2048	2078	1969	
12500	2586	2382	2304	2178	
15000	2887	2677	2496	2362	
17500	3165	2948	2700	2563	
20000	3417	3189	2904	2761	
22500	3659	3416	3122	2973	

Table B-9 Average Total Emissions (2016-2018) of the Mid-Crude Unit with Randomized Leak Events (Non-growth Model, 10000 trials)

PPM	DTA(tag), kg	DTA(cluster), kg	DT(tag), kg	DT(cluster), kg	M21, kg
5000	2270	1980	1698	1809	3222
7500	2597	2292	1965	2008	
10000	3144	2673	2147	2140	
12500	3308	2897	2287	2234	
15000	3309	3103	2418	2331	
17500	3365	3160	2518	2415	
20000	3367	3264	2599	2491	
22500	3391	3304	2688	2575	

The trend of the cumulative fugitive emission differences between scheduled M21 in the Mid-Crude unit and DTA(tag), DTA(cluster) (with corresponding detection thresholds), DT(tag), and DT(cluster) from Figure B-9 either becomes constant or expands over time. This suggests that the LDSN solution will continue to result in lower emissions relative to M21 CWP during and even beyond the duration of the modelled scenarios.

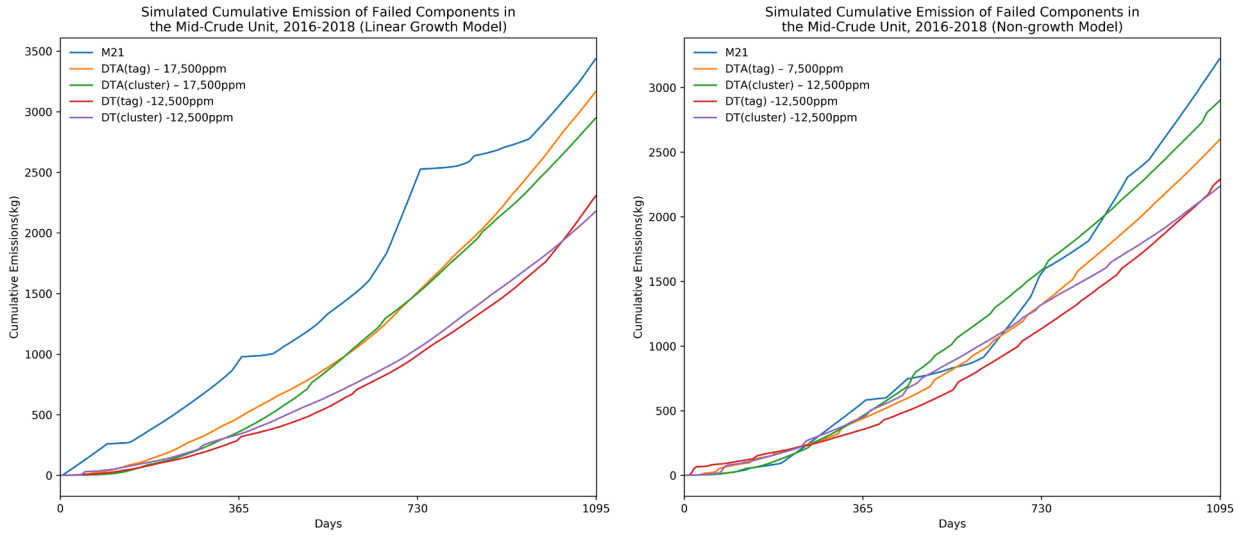

Figure B-9. Cumulative Emissions of the Mid-Crude Unit (2016-2018): Linear Growth Model (Left) and Non-growth Model (Right)

The CLs of the Mid-Crude unit were calculated for different detection threshold values. To achieve a 67% CL, the DTA(tag) and DTA(cluster) values are approximately 7,500 – 17,500 ppm from the non-growth model and 12,500 – 17,500 ppm from the linear growth model, respectively. The CLs of DT(tag) and DT(cluster) at a DTA of 12,500 ppm are over 95% in both the linear growth and non-growth models. The CLs in the Mid-Crude simulation results indicate that LDSN-DRF can be an effective and reliable method to reduce total fugitive emissions when compared to M21 CWP.

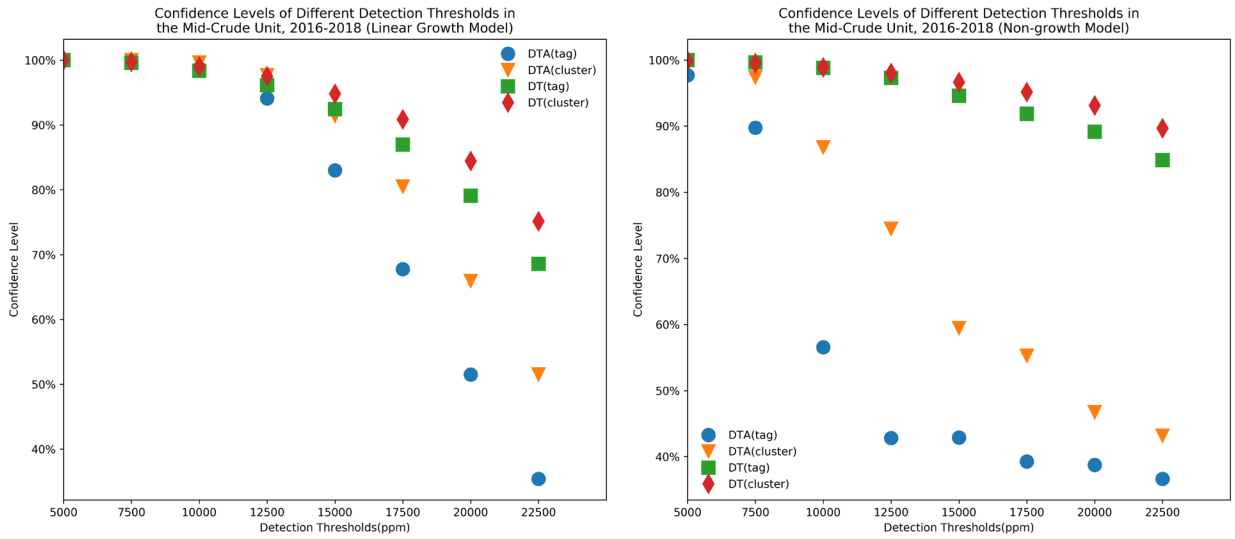

Figure B-10. CL with Different Detection Thresholds (Mid-Crude Unit, 2016-2018): Linear Growth Model (Left) and Non-growth Model(Right)

4 Emission Simulation by the Monte-Carlo Method

A Monte-Carlo simulation method was developed to further validate the robustness of the LDSN solution. This method employs random sampling to generate a profile of leak events and then uses this profile to calculate total fugitive emissions under different emission scenarios. The CL is used to evaluate the performance of LDSN-DRF. We performed 10,000 trials for both unit in the Monte-Carlo simulation.

4.1 Basic Assumptions in the Monte-Carlo (MC) Simulation

The original leak profile (all leak events plus the index of the leak events) is used to generate a sample pool (indexed leak events) based on the input set of components. In each simulation trial, randomized sampling was performed for a determined time period (known as sampling number) and a randomized leak start time was assigned for every leak event sample to build a new leak profile. The new leak profile is used to calculate the simulated total fugitive emissions.

- **Input Set of Components**

  The clusters to simulate are used as the input set of components.

- **Sample Pool of Leak Events**

A sample pool contains all the leak events from the input set of components. The leak records in the sample pool are indexed to back-track the original leak growth rate or leak size.

- **Sampling Number**

The sampling number is determined by the total number of the leak events within the input set of components.

- **Updated Cluster**

The input set of components might be different from the updated cluster because of the randomized sampling process. From the generated new leak profile, an updated cluster is made up of components with valid leak events after the sampling process.

Emission Calculation

A flowchart of the simulation process is shown in Figure B-11. Once a new leak profile is generated, the total fugitive emissions are calculated using DT(tag), DTA(tag), DT(cluster), and DTA(cluster) in a similar method to that described in previous sections.

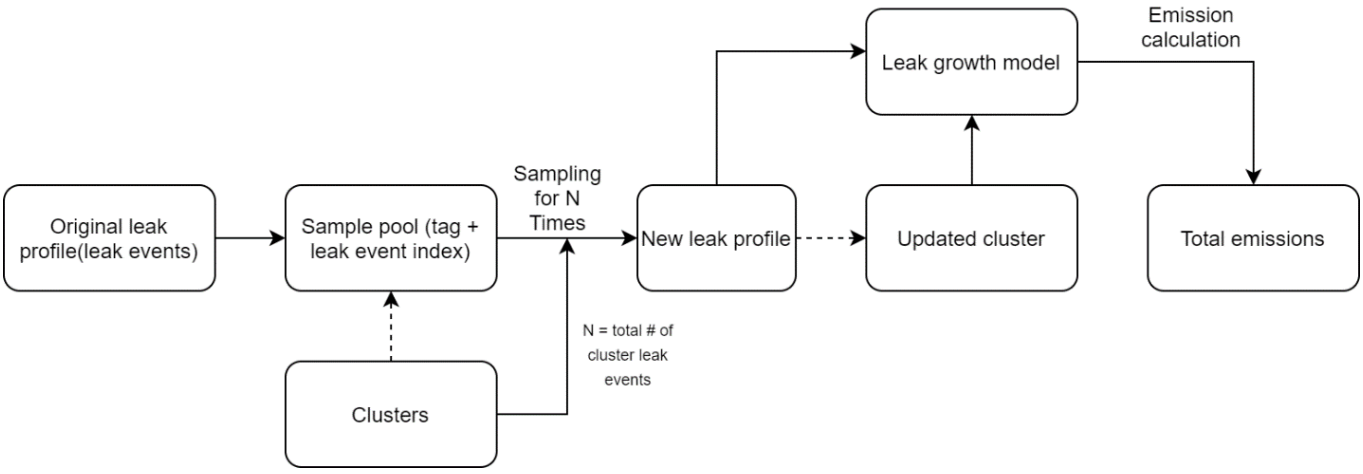

Figure B-11 Monte-Carlo Simulation Process

4.2 Monte Carlo Simulation Results

The CL is calculated using different thresholds for both process units to validate the effectiveness and reliability of the LDSN solution (Figure B-12 and Figure B-13). The CL of a DTA(tag) of 10,000 - 12,500 ppm for the Meta-Xylene unit Monte-Carlo simulation is over 67%. The DTA(cluster) level is approximately 20,000 – 25,000 ppm with the 67% as the target CL. The DT(distance) and DT(cluster), which take the DT band into consideration, are more similar to field conditions, and therefore the CL level is more representative of the anticipated performance of the LDSN. From the MC simulation results of DT(tag) and DT(cluster), the CLs are mostly over 67% (except for DT(tag) with a DTA(tag) level of 25,000 ppm). This corresponds to the low response factor and high sensor density in the Meta-Xylene unit. The MC simulation results are similar to the results of the randomized leak events simulation and provide additional confirmation of the effectiveness and robustness of LDSN in the Meta-Xylene unit.

The Mid-Crude unit simulation is more complicated due to the fact that the response factor of some of the LDAR streams are about three times higher than the Meta-Xylene unit. The sensor layout in the Mid-Crude unit is also less dense than in the Meta-Xylene unit. The CL of a DTA(tag) is around 7,500 – 17,500 ppm using the 67% rule. The DTA(cluster) level is around 12,500 – 17,500 ppm when using 67% as the target CL. The average total fugitive emissions of DT(tag) and DT(cluster) at a DTA of 12,500 ppm are estimated to be approximately 38% less than the simulated M21 CWP emissions. The simulations indicate that the LDSN-DRF solution can significantly reduce the total fugitive emission of the Mid-Crude unit when compared to routine scheduled M21 monitoring.

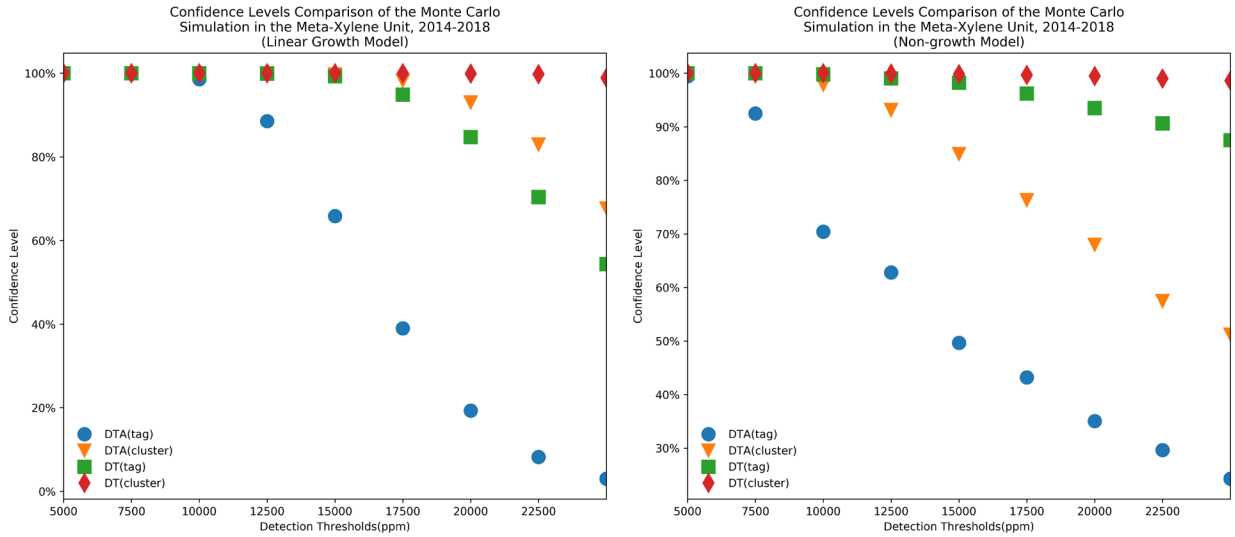

Figure B-12. CL with Different Detection Thresholds (Meta-Xylene Unit, 2014-2018): Linear Growth Model (Left) and Non-growth Model(Right)

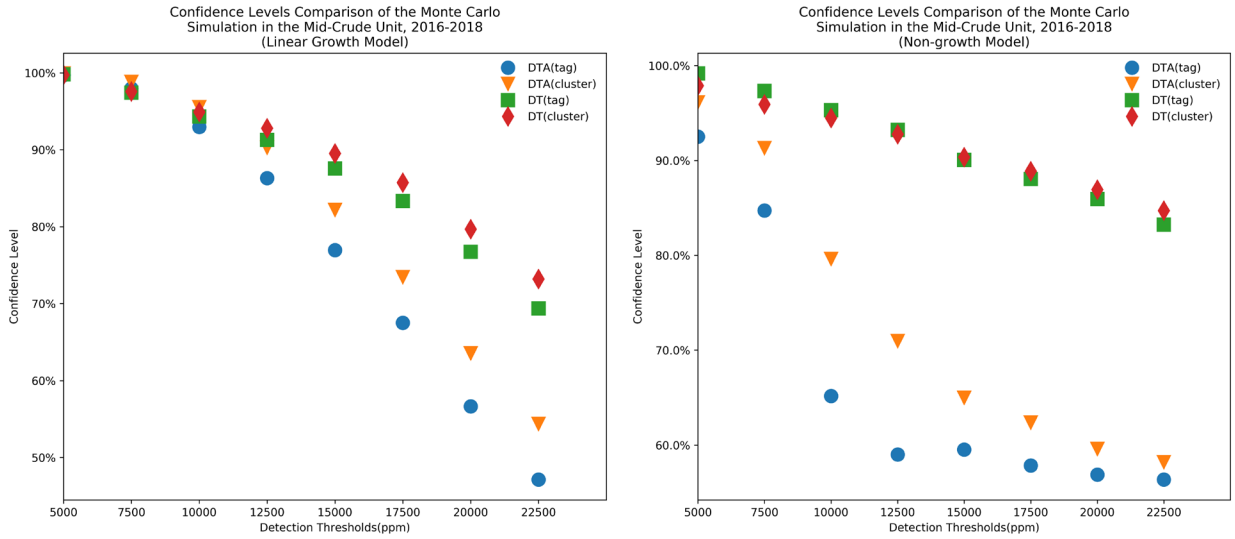

Figure B-13. CL with Different Detection Thresholds (Mid-Crude Unit, 2016-2018): Linear Growth Model (Left) and Non-growth Model (Right)

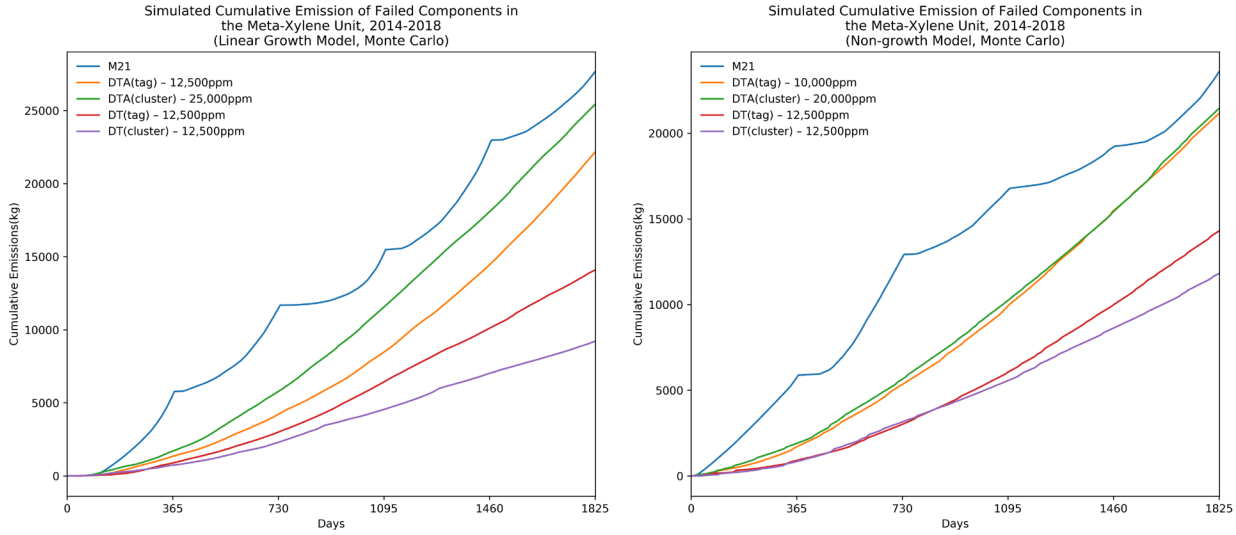

Figure B-14. Monte Carlo Simulated Cumulative Fugitive Emissions of the Meta-Xylene Unit (2014 - 2018): Linear Growth Model (Left) and Non-growth Model (Right)

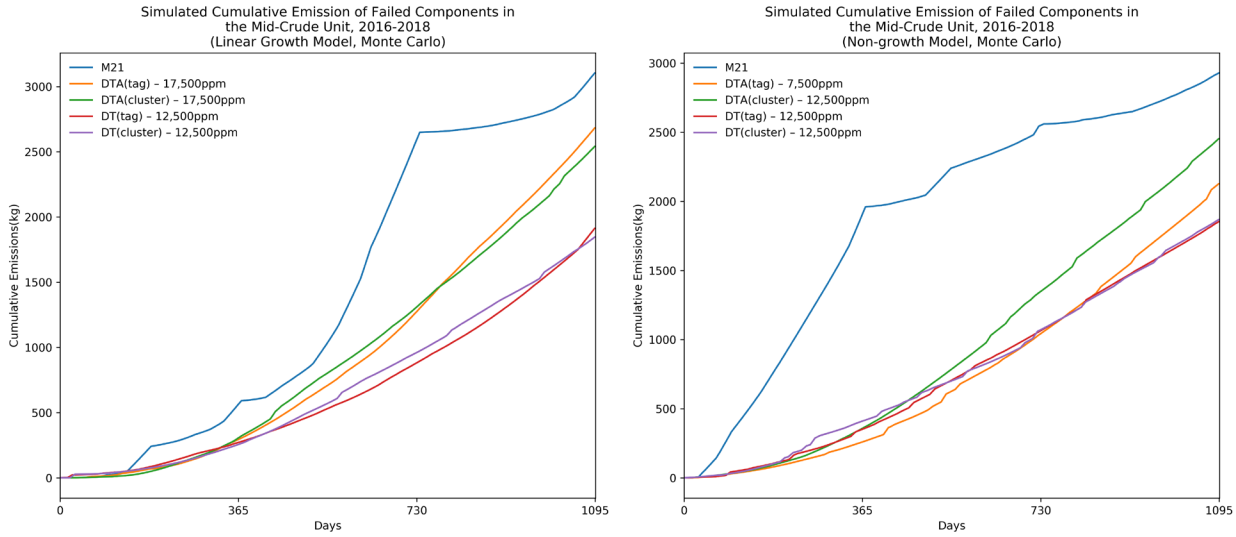

Figure B-15. Monte Carlo Simulated Cumulative Fugitive Emissions of the Mid-Crude Unit (2016 - 2018): Linear Growth Model (Left) and Non-growth Model (Right)

Although the modeling was limited to the duration of the simulation period of time, the relative rates of change in cumulative emissions shown in Figure B-14 and Figure B-15 suggest the LDSN-DRF system would continue to demonstrate emissions reductions relative to scheduled M21 performance.

Figure B-16 shows a comparison between average emissions calculated from M21 and from 4 different detection scenarios under two leak models (linear growth and non-growth). The DTA values are chosen based on passing simulations which means CL's>67%. Clearly, all the detection scenarios in both leak models demonstrate significant reductions in total fugitive emissions. This includes a 39 - 49% reduction from the DT(tag) simulation and 50-67% reduction from the DT(cluster) simulation at the DTA level of 12,500ppm. These numbers are comparable to 29% - 44% reduction from DT(tag) and 46% - 66% reduction from DT (cluster) demonstrated during the randomized historical leak simulations.

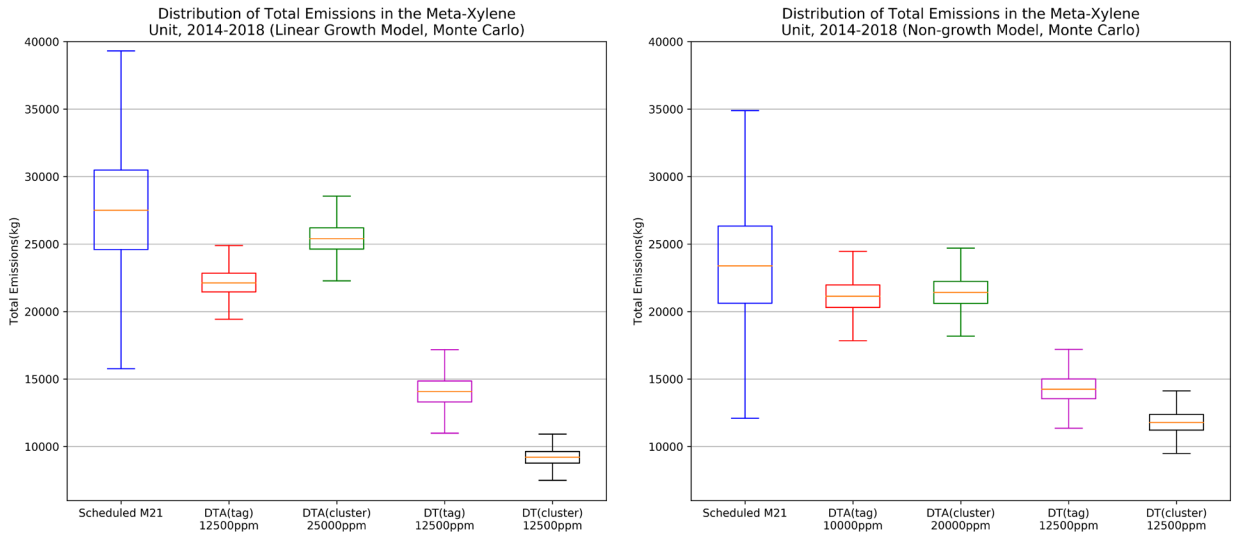

Figure B-16 Distribution of Total Emissions in the Meta-Xylene Unit under the Linear-Growth Model (Left) and The Non-growth Model (Right)

The same comparison was made for the Mid-Crude unit at DTA values with successful Monte Carlo simulations (CLs>67%). As shown in Figure B-17, approximately 36% - 41% reductions in total emissions can be estimated for the DT(tag) and DT(cluster) simulations at 12,500 ppm. These are very similar to the 29 - 37% reduction demonstrated using the randomized historical leak simulations at the same DTA level.

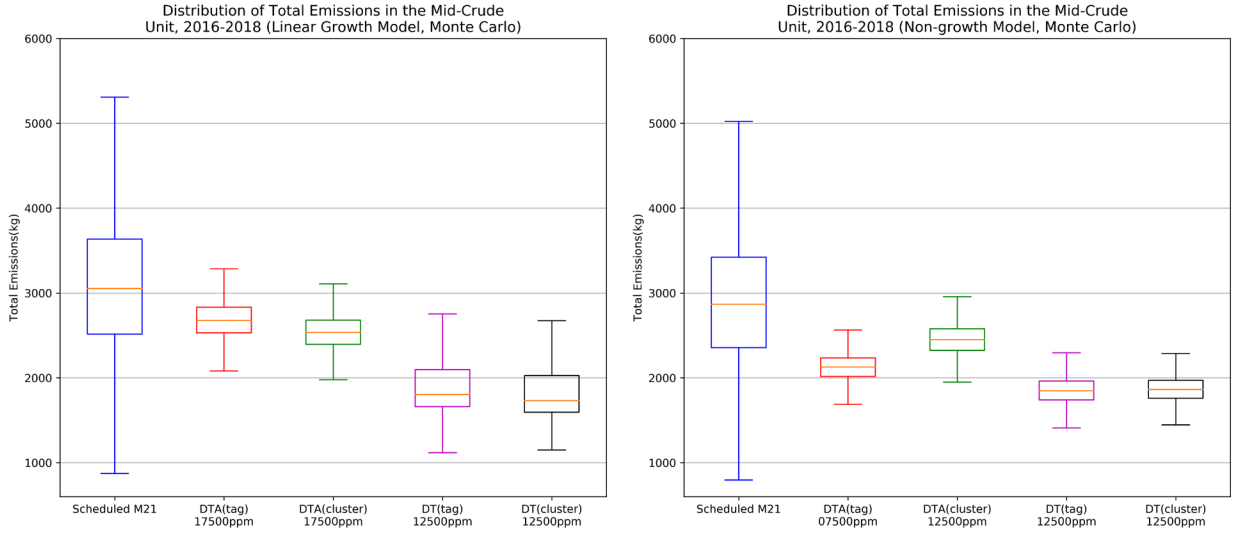

Figure B-17. Distribution of Total Emissions in the Mid-Crude Unit under the Linear-Growth Model (Left) and the Non-growth Model (Right)

DTA simulation results are listed in Table 10 for the Meta-Xylene unit and in Table 11 for the Mid-Crude unit. The Monte Carlo simulation results are very similar to the results obtained from randomized historical simulations in Section 3 of this appendix. Because of a different sampling process for the simulation methods, more components are involved in the randomized historical simulation than in the Monte Carlo simulation. For instance, in the randomized historical simulation, the pegged values will always be included, which is not always the case for Monte Carlo simulation trials. The leak size distribution of the randomized historical simulation should be the same as the historical leak distribution. In contrast, the leak distribution of the Monte Carlo simulation can be different from the historical distribution. If the trial number is large enough however, the overall leak distribution of all Monte Carlo simulation runs should be reasonably similar to the historical leak distribution. In other words, the randomized historical simulation is considered as a unique subset of Monte Carlo simulation, in which all the historical leaks are sampled and simulated.

Table 10 Summary of Simulation Results of the Meta-Xylene Unit

Method	Leak Model	DTA(tag)	DTA(cluster)	DT(tag)	DT(cluster)
Randomized Historical	**Non-Growth**	7500 ppm	17500 ppm	25000 ppm +	25000 ppm +
	Linear-Growth	12500 ppm	25000 ppm +	20000 ppm	25000 ppm +
Monte-Carlo	**Non-Growth**	10000 ppm	20000 ppm	25000 ppm +	25000 ppm +
	Linear-Growth	12500 ppm	25000 ppm +	22500 ppm	25000 ppm +

Table 11 Summary of Simulation Results of the Mid-Crude Unit

Method	Leak Model	DTA(tag)	DTA(cluster)	DT(tag)	DT(cluster)
Randomized Historical	**Non-Growth**	7500 ppm	12500 ppm	22500 ppm +	22500 ppm +
	Linear-Growth	17500 ppm	17500 ppm	22500 ppm +	22500 ppm +
Monte-Carlo	**Non-Growth**	7500 ppm	12500 ppm	22500 ppm +	22500 ppm +
	Linear-Growth	17500 ppm	17500 ppm	22500 ppm +	22500 ppm +

5 Summary

Due to the complexity of leaks from a wide variety of components under varying conditions, two leak rate models and four sensor detection scenarios using the same LDSN-DRF system have been evaluated. Although the non-growth and linear growth models represent both represent valid leak evolution patterns, the average leak rate change for a process unit is likely influenced by both at different times and on varying components. For example, a leak may increase and then stay unchanged or even decrease due to changes in weather conditions, or process conditions such as temperature, pressure, and vibration. A representative eDTA value should be bounded by the simulation results from these two leak models. Likewise, DTA(tag) represents the most conservative detection scenario while DTA(cluster) represents a more realistic scenario. Since the LDSN detects gas plumes at a distance, the sensor detection signals are most likely to be the result of contributions from multiple leaks near each other or within a small area. During the pilot testing, multiple small leaks were

often detected through the DRF activities that had been initiated in response to a single potential source location (PSL) notification. Thus, it is reasonable to assume that eDTA falls in between the DTA(tag) and DTA(cluster) values.

Given the actual locations of the leaks and the locations of the sensors in the plant, DT(tag) and DT(cluster) simulations were added to the analysis at varying DTA values. These additional two scenarios are more site specific. The most conservative approach is to rely solely on the average DTA(tag) results when determining the final eDTA value. Together the two methods support an eDTA of 10,625-12500 ppm, while the Monte-Carlo method alone suggests an eDTA of 11,250 ppm for the Meta-Xylene unit, and a slightly higher eDTA of 12,500 ppm for the Mid-Crude unit. At these eDTA design levels, a substantial reduction potential in total fugitive emissions can be anticipated.

Although the eDTA is useful when estimating the average detection threshold that must be achieved to demonstrate equivalence with M21 CWP, the DTU is better suited for leverageable design specifications and an in-the-field compliance demonstration. DTU represents the smallest leak that is anticipated to be detected by the sensor network at the farthest distance away from a sensor. DTU is at least 1.5 times DTA. So, with an eDTA of 11,250 ppm, the corresponding DTU is conservatively assumed to equal 16,875 ppm. A LDSN-DRF system that detected and located all LDAR leaks above 16,875 ppm for repair would be equivalent to fugitive emissions control provided by M21 CWP.

It should be noted that all the simulations described above utilized historical data from the facility's LeakDAS™ database. AVO leaks were not included in the simulation because of a lack of actual Method 21 measurement data at the time each leak was found. Several non-LDAR component leaks were detected during the in-plant pilot testing but were also not included in the simulations. The ability of the LDSN-DRF system to provide earlier detection of AVOs and leaks from non-LDAR components provides additional emission reductions even beyond those conservatively modeled.

References:

1. *Guiding Principles for Monte Carlo Analysis, EPA/630/R-97/001, March 1997.*

Appendix F2

FHR CC Test Unit Leak Cluster Simulation and Analysis

Appendix F2

FHR Corpus Christi Test Unit Leak Cluster Simulation and Analysis

Leaks with low mass emissions rates (ERs) and/or high leak to node separation distance can be below the detection threshold (DT) of the LDSN system. However, as more leaks occur within a localized area, the signal from these leaks can combine to produce a robust detection event. The set of small leaks within this local area is called a leak cluster. This document analyzes the "cluster" concept using three different approaches:

1. by analyzing and visualizing spatial distribution of historical leak events;
2. by performing computational fluid dynamics (CFD) simulations to demonstrate similar sensor response from a single leak and from a cluster of leaks; and
3. by theoretically predicting the number and distribution of leaks to be detected by Molex LDSN using historical M21 data during 2013-2019.

1. Historical Leak Distribution

Historical M21 leak events on the ground level (2013-2019) are plotted in Figure 1a (Meta-Xylene unit) and Figure 1b (Mid-Crude unit). Larger blue dots (with the number nearby) represent sensor locations, smaller colored dots represent historical leak events, the legend describes the association between dot color and leak size (in ppm, equivalent M21 measurements). Figures1aand 1b, illustrate that the LDAR components are clustered around vessels, pumps, compressors, separation columns, and other large pieces of equipment. The depiction on the map (Figures 1a and1b) corresponding to a piece of equipment often includes a unique identification number shown near the object. An example of a typical cluster (object "54GA4A/B", Meta-Xylene unit) is indicated by a dashed circle in Figure 1a. The radial dashed lines indicate cluster-to-sensor distances (d_1, d_2, d_3 and d_4) for neighboring sensors (S1 to S4) at the same level/elevation.

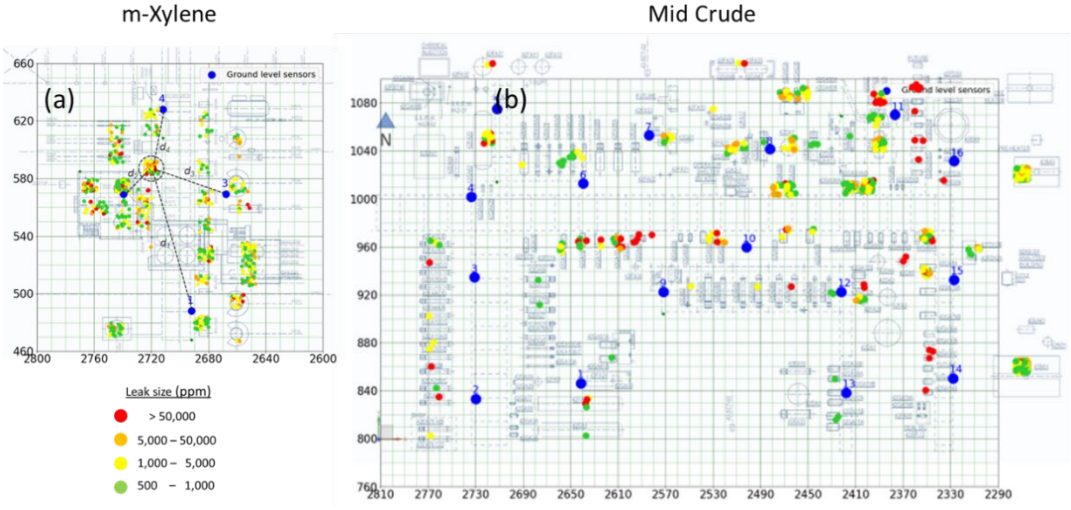

Figure 1. Leak size and location distribution of historical M21 events in Meta-Xylene (a) and Mid-Crude (b) units. Blue circles with an adjacent number represent sensor locations. The green, yellow, orange, and red circles represent leak events.

2. CFD Simulation

In order to gain insight into plume detections, a set of CFD simulations were generated for the Meta-Xylene unit. A single leak of 10^{-5} kg/s (equivalent to 50,000 ppm FID) is compared to a "cluster" of 10 leaks with leak sizes randomized in range from 10^{-7} to 10^{-6} kg/s (500 to 5000 ppm M21 measurements) and leak spatial locations randomized within a 10 ft × 10 ft box centered around the previously defined single 50,000 ppm leak location. Figure 2a illustrates a 3D model of the Meta-Xylene unit used in the simulation. The red circles/balloons represent leak locations within the cluster. Wind (air flow) was modeled utilizing an isothermal k-epsilon (k-ε) turbulence model with standard wall function. Octane (C8H18) was used as a representative leak gas species for both Meta-Xylene and Mid-Crude units. Transient CFD simulations follow a representative 2000 second wind pattern (wind speed and directions) shown in Figure 2b. The calculated gas responses at nearby sensor S1, S2 and S3 locations are shown in Figures 2c and 2d. Each response of a single 50,000 ppm leak (green lines in Figure 2c) is a strong match for the equivalent "cluster" of leaks (blue lines in Figure 2d). During the pilot study, 10 sensors were installed in the Meta-Xylene unit , but only 3 sensors (S1, S2 and S3) at the same elevation (ground level) were close enough to the leak or "cluster" to produce a gas response detectable by Molex LDSN (> ~5 ppb).

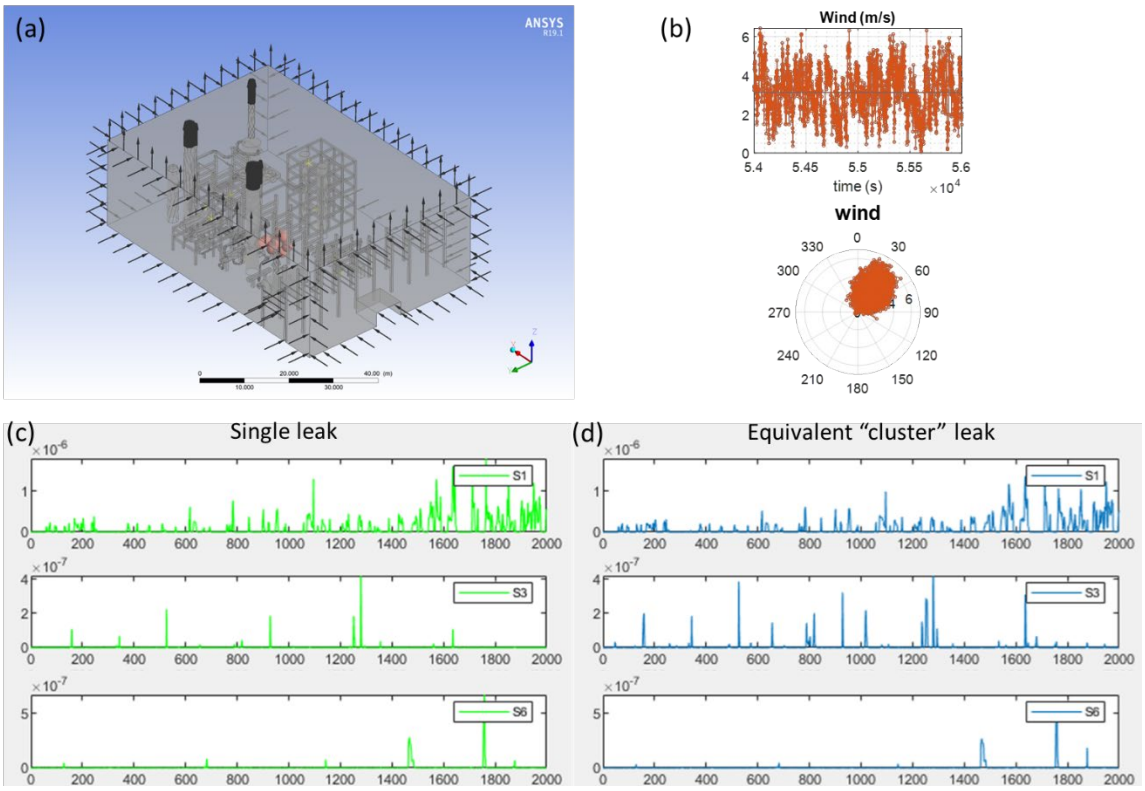

Figure 2. CFD simulation results comparing a single leak (50,000 ppm FID equivalent) to equivalent 10 leak "clusters". Insert (a) is a 3D model used for simulations. Insert (b) illustrates a representative wind-

set used in the transient analysis. Inserts (c) and (d) show mass gas concentrations at sensor locations S1, S2, S3 for a single leak and for cluster scenarios.

3. LDSN Leak Distribution Simulations

The 2013-2019 historical M21 leak events data from the LeakDAS™ database (Meta-Xylene unit) was analyzed to determine the leak distribution and number of leaks that would have been detected by the LDSN/DRF if it were operating during 2013-2019. Each leak event record contains a "location description" field referencing a physical piece of equipment and corresponding to an object on the map. For example, the location description, "G/5 NSD 42DA1 TWR", indicates that leak event occurred for a component located at 5 ft above ground level, and on the north side of tower number 42DA1. The set of leak events near ground level associated with the object 42DA1 is considered in the historical LDSN detects simulation as a cluster object "42DA1 ground".

There are several potential approaches for defining detection event criteria in historical simulations. The simplest approach is to compare the size of the leak against the average fixed detection threshold (DTA) independent of the distance between a sensor and the leak location. The fixed threshold approach is easier to enforce in DRF and implement in historical emissions savings calculations, however it penalizes the emissions calculations because a significant number of smaller leaks near the sensors are detected in real life, but grossly ignored by the LDSN/DRF in the simulation. Therefore, it's necessary to discuss methodology to introduce distance as a variable to the cluster effect.

Three theoretical approaches were utilized to qualify the experimentally observed dependence, ($C \propto 1/D^2$), of sensor peak gas concentration (C) to the distance from the leak (D). These include a source magnitude estimation using short range plume equations at each peak [2], computational fluid dynamics (CFD) calculations, and the analytical Gaussian plume model with dispersion coefficients defined by the Pasquill-Gifford equations [1, 3,4].

A source magnitude estimation using short range plume equations at each peak [2] can be expressed as:

$$S_{ij} = \pi D^2 C_j \sigma_w^2 / u \qquad (1)$$

where:

S_{ij} = source magnitude estimate based on sensor j peak i, g/sec
C_{ij} = peak concentration at sensor j peak I, g/m^3
D = distance to source, m
σ_w = variation of wind velocity over methane peak interval, m/sec
u = average wind velocity over peak internal, m/s

The peak concentration at the sensor can be derived from Equation 1 and is proportional to leak source magnitude S_{ij} but inversely proportional to the square of distance to the sensor (D^2)

$$C_j = S_{ij} \times u / \pi D^2 \sigma_w^2 \qquad (2)$$

CFD simulations were performed using Ansys CFX software. It is a steady state model with a single leak source and wind velocity of u = 1 m/s applied along the long axis (X). Air flow was represented by an isothermal k-epsilon (k-ε) turbulence model with standard wall function. Octane (C_8H_{18}) was utilized as a

representative gas species for the leak. Figure 3 shows a 2D heatmap of downwind and crosswind gas concentrations for the plume.

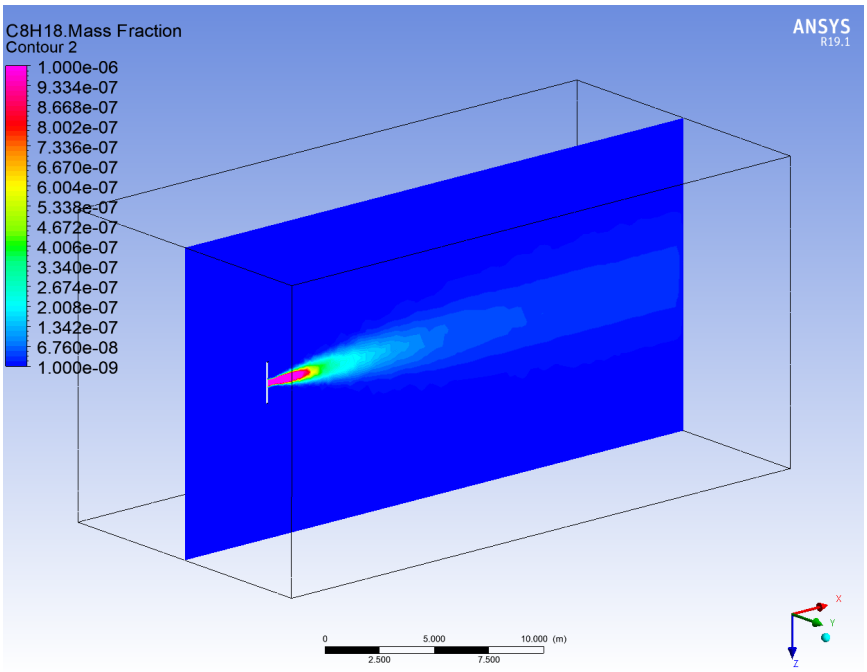

Figure 3. CFD simulation results: 2D heatmap of downwind and crosswind gas concentration of the plume

Figure 4 illustrates calculated gas concentrations along the center of the plume as a function of the distance from leak sources for four leak sizes: 3.6 g/hr, 1.8 g/hr, 0.9 g/hr and 0.45 g/hr. Assuming that the realistic minimal detection level by the sensor is 60 ppb (after background concentration removal), the colored dots illustrate the maximal detection distances for different leak sizes. As anticipated, a 0.45 g/hr leak can be detected only within a 10 ft radius of the sensor. However, a 3.6 g/hr leak can be detected as far as 35.6 ft from the sensor.

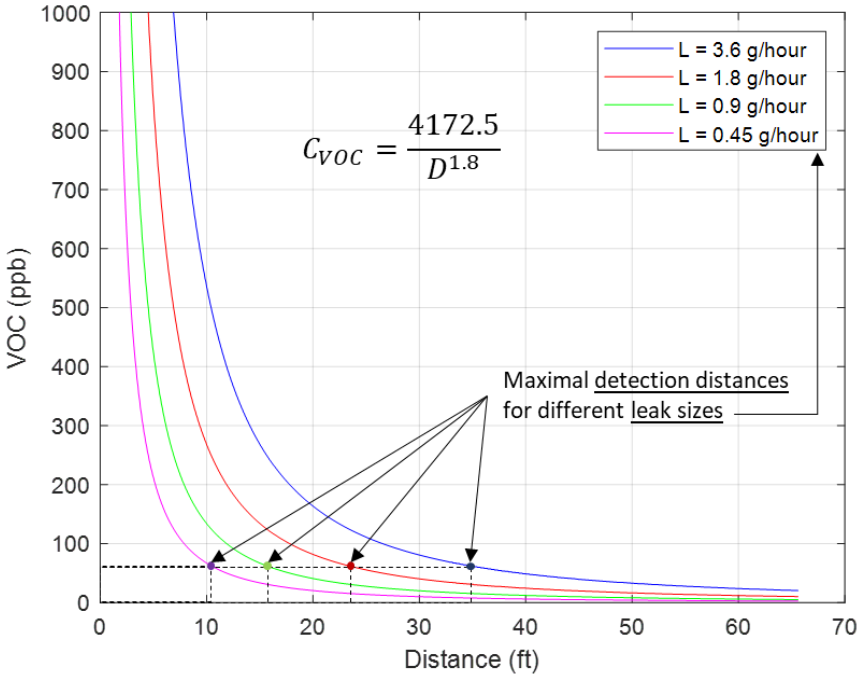

Figure 4. CFD simulation results: VOC gas concentration along the plume for different leak sizes (0.45 to 3.6 g/hr)

For the Gaussian dispersion model, the concentration of gas downwind of a ground level, point leak source at the origin (x, y, z) = (0, 0, 0) is predicted by the following Gaussian Relationship [1].

$$C(x,y,z) = \frac{Q_m}{2\pi\sigma_y\sigma_z u} exp\left[-\frac{1}{2}\left(\frac{y}{\sigma_y}\right)^2\right] \times \left\{exp\left[-\frac{1}{2}\left(\frac{z-Hr}{\sigma_z}\right)^2\right] + exp\left[-\frac{1}{2}\left(\frac{z+Hr}{\sigma_z}\right)^2\right]\right\} \qquad (3)$$

where, C is the concentration in kg/m^3,
Q is the flow rate in kg/s,
σ_y (x) and σ_z (x) are Pasquill-Gifford dispersion coefficients in m,
x, y and z are distances in m,
u is the wind speed in m/s,
H_r is elevation of the source off the ground level in m.

Equation (3) shows that when a sensor is placed at (x, y, z), the sensor reading should be proportional to the gas flow rate Q. The actual exponents of the sensor-to-leak distance (D) dependencies are hidden in distance (x) dependence of Pasquill-Gifford dispersion coefficients σ_y (x) and σ_z (x) for the Gaussian Model and inside the numerical algorithms for the CFD model. To estimate the exponents, the calculated C(x) was plotted vs the leak-to-sensor distance (x) in log-log coordinates (Figure. 5) and fitted with a straight line. The best fit slope resulted in $1/D^{1.9}$ distance dependence for the Gaussian model, and $1/D^{1.8}$ for the CFD model. Both results are similar to the experimentally observed $1/D^2$ dependence.

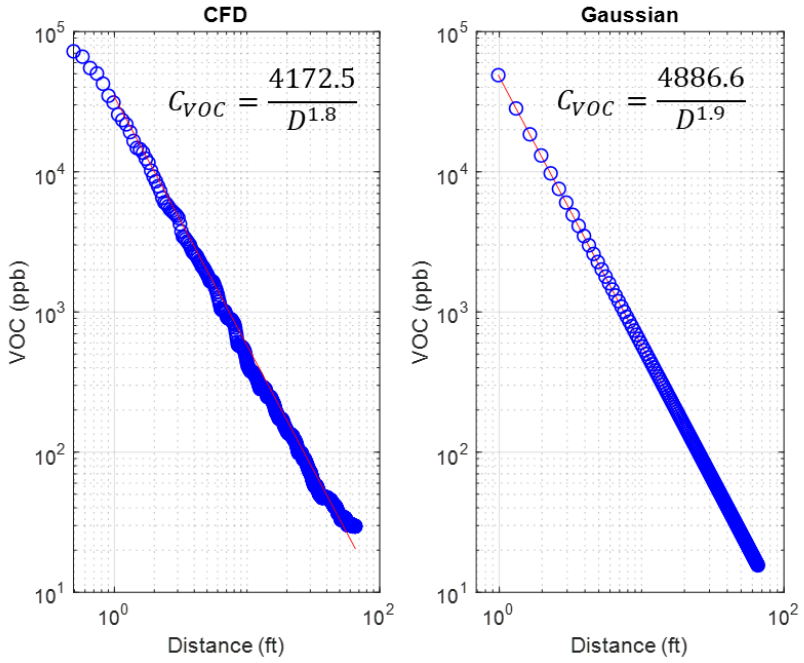

Figure 5. Log-Log plot of VOC concentration as a function of leak-to-sensor distance for the CFD model (left) and the Gaussian model (right)

Detection signal at the sensor S1 location ($S_{(1)}$) is proportional to leak size (L) and inversely proportional to the square of distance ($d_{(1)}^2$) with a proportionality factor (α):

$$S_{(1)} = \frac{1}{\alpha}\frac{L}{d_{(1)}^2} \tag{4}$$

After moving α to the right-hand side of Equation (4), the minimal sensor sensitivity related factor ($\alpha S_{(1)}^{min}$) can be estimated by the equation below:

$$\alpha S_{(1)}^{min} = \frac{L^{min}}{d_{(1)}^2} = \frac{5000\ ppm}{(50ft/\sqrt{2})^2} = 4 \tag{5}$$

where detection threshold average (DTA) is assumed to equal a 5000 ppm M21 reading equivalent at average detection distance ($50ft/\sqrt{2}$)

$$\alpha S_{(1)}^{min} < \frac{L^{min}}{d_{(1)}^2} \quad \rightarrow \quad \frac{5000\ ppm}{(50ft/\sqrt{2})^2} > 4 \tag{6}$$

After $\alpha S_{(1)}^{min}$ is calculated, an individual leak (L^{exp}) at distance ($d_{(1)}$) from S1 sensor location or set of leaks ($L_1^{exp} \ldots L_n^{exp}$) at distances ($d_{(1)1} \ldots d_{(1)n}$) can be compared against $\alpha S_{(1)}^{min} = 4$ from Equation (6) using the equations below:

$$\frac{L^{exp}}{d_{(1)}^2} \geq 4 \quad (7a)$$

$$\frac{L_1^{exp}}{d_{(1)1}^2} + \frac{L_2^{exp}}{d_{(1)2}^2} + \cdots + \frac{L_n^{exp}}{d_{(1)n}^2} \geq 4 \quad (7b)$$

Equations (7a) and (7b) provide the basis for the historical LDSN detection simulation, where the number and distribution of leaks detected by the Molex LDSN is predicted based on historical M21 data from 2013 to 2019.

The simulation was performed for each elevation on a level-by-level basis. For each level, the historical M21 leak events were sorted by "cluster" objects. The distances from each object to all sensors on the same level were calculated and the closest sensor was identified for the analysis. Figure 6 illustrates the scatter of the four closest sensor distances for each "cluster" object in Meta-Xylene unit. The nearest sensor distance is represented by a blue bar. The graphs show that most of the "cluster" objects have a clearly identifiable closest sensor. Although different sensors may respond to the same "cluster" at different times due to geometrically different favorable wind directions, the cluster analysis was limited to a single closest sensor interaction with the "cluster".

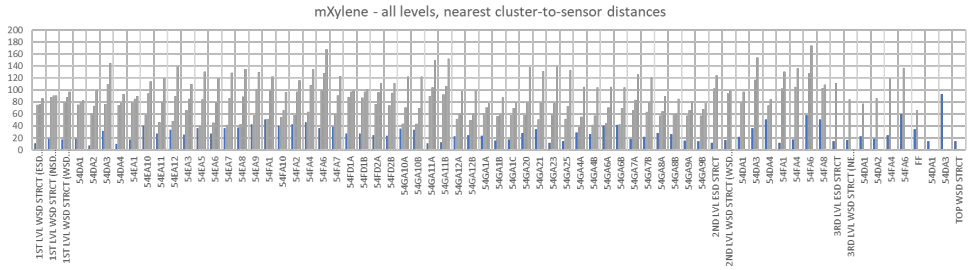

Figure 6. Four closest cluster-to-sensor distances for different clusters (x-axis) in m-Xylene unit. The blue bar represents the distance used in the analysis.

Figure 7a illustrates the time series of historical M21 leak events for the cluster "54DA1 ground". Different colors are used to represent unique LDAR tag numbers within the cluster. Each "x" represents a successful detection prediction by the Molex LDSN system. Figure 7b shows the simulated cluster LDSN detection decision framework. The time series (Figure 7a) indicates that the first two leak events do not meet the Equation 7b criteria to establish a cluster. When the third leak appears, the newly formed three leak cluster meets the detection criteria (Equation 7b) and a detection event is generated. Since none of the leak sizes (ppm, FID equivalent) in the third line [1151, 897, 535 ppm] are greater than the 3000 ppm DRF criteria, the model assumes that only the biggest leak, 1151 ppm, is found. The remaining two leaks continue to be part of the cluster and once a 4th leak appears, the logic repeats until the new three leak cluster meets the Equation 7b criteria and triggers a detection event. When no individual leak is greater than 3000 ppm, the largest leak is assumed to be the one which is detected. Once the 5th leak occurs, a detection event is triggered. In this example, there is a leak > 3000 ppm (4225 ppm) in the cluster and it is the leak that is eliminated from the cluster pool.

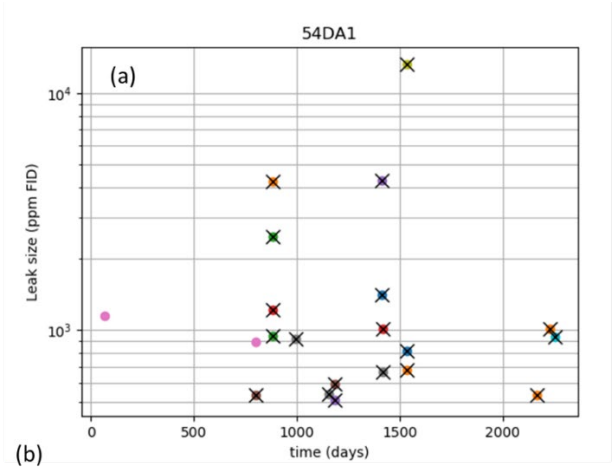

	index	comp	tag	year	date	leak	m21	loc	d_close	DTA	c_detect	c_leaks	c_sum
0	181	VALVE	249488	2013	3/6/2013 15:08	1151	Failed	G/2 CL WSD 54DA1	22.688553	2.235948	False	[1151]	2.235948
1	546	VALVE	250066	2015	3/13/2015 7:53	897	Failed	1/4 1ST LVL WSD STRCT (WSD 54DA1)	23.223656	1.663149	False	[1151, 897]	3.899098
2	180	VALVE	249485	2015	3/13/2015 15:40	535	Failed	G/2 CL WSD 54DA1	16.671317	1.924926	True	[1151, 897, 535]	5.824023
3	107	CONNECT	249467.1	2015	6/3/2015 8:23	2486	Failed	G/1 CL S 54DA1	20.933104	5.673276	True	[897, 535, 2486]	9.261351
4	138	CONNECT	249532.1	2015	6/3/2015 9:13	4225	Failed	G/1 WSD 54DA1	15.703049	17.133999	True	[897, 535, 4225]	20.722074
5	543	CONNECT	250031.1	2015	6/3/2015 11:29	1217	Failed	1/4 1ST LVL WSD STRCT (WSD 54DA1)	19.941820	3.060279	True	[897, 535, 1217]	6.648354
6	542	CONNECT	250028	2015	6/3/2015 11:38	951	Failed	1/4 1ST LVL WSD STRCT (WSD 54DA1)	19.601457	2.475163	True	[897, 535, 951]	6.063238
7	182	VALVE	249505	2015	9/23/2015 11:02	921	Failed	G/2 CL WSD 54DA1 (54FV1)	17.368198	3.053164	True	[897, 535, 921]	6.641239
8	183	VALVE	249505	2016	3/2/2016 14:01	541	Failed	G/2 CL WSD 54DA1 (54FV1)	17.368198	1.793444	True	[897, 535, 541]	5.381519
9	544	CONNECT	250034	2016	3/28/2016 14:26	510	Failed	1/4 1ST LVL WSD STRCT (WSD 54DA1)	18.007950	1.572685	True	[535, 541, 510]	5.291054
10	545	CONNECT	250041	2016	3/28/2016 14:48	592	Failed	1/4 1ST LVL WSD STRCT (WSD 54DA1)	16.859330	2.082769	True	[535, 510, 592]	5.580379
11	389	CONNECT	249475	2016	11/16/2016 14:20	4285	Failed	G/5 SW 54DA1 (FT4)	23.397373	7.827383	True	[535, 510, 4285]	11.324994
12	372	CONNECT	249520	2016	11/16/2016 14:52	1412	Failed	G/4 WSD 54DA1 (PDT8)	20.598328	3.327904	True	[535, 510, 1412]	6.825514

Figure 7. Typical time series of M21 leak events for a representative cluster "54DA1-ground" in the Meta-Xylene unit (a) and an illustration of the model decision process (b).

The process described above covers the most realistic scenario (A) where both the distance dependence detection threshold and the leak clustering effect were considered. The other simulated scenarios were: (B) distance dependent detection without clustering effect, and (C) fixed value detection. For scenario B, the individual leak detection criteria (Equation 7a) was used. For scenario C (fixed threshold), Equation 7a was simplified to an individual leak detection criterion: $L^{exp} > 5000$. These three scenarios illustrate historical progression of approaches for emissions equivalency calculations. The calculations started from scenarios B and C, but it was determined that the emission reductions that could be achieved using the Molex LDSN were underestimated. The analysis of the size and location distribution of the leaks found during the pilot study both process units indicated that several small leaks were detected further away from the sensors than predicted by scenarios B and C. This led to the development and evaluation of scenario A.

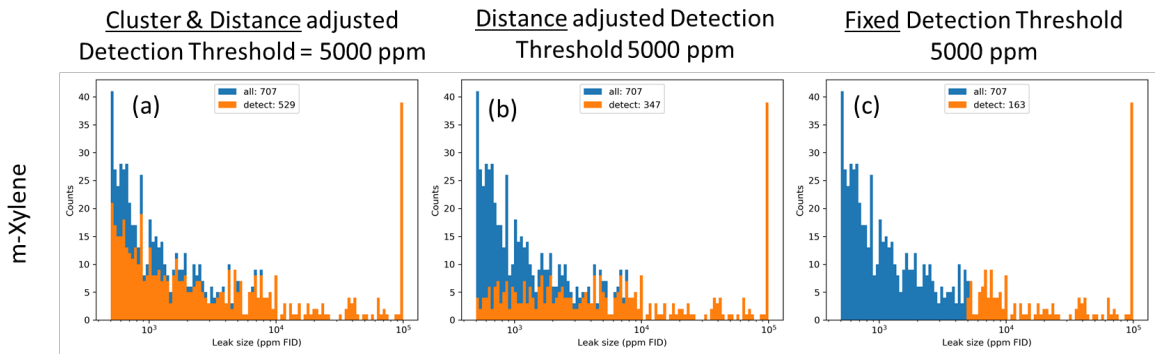

Figure 8. Leak size distribution of all M21 leak events in 2013-2019 in the Meta-Xylene unit (blue bars) compared to simulated leak size distribution of M21 events "to be detected" by LDSN (orange bars) for scenarios A, B and C (inserts (a), (b) and (c) respectively).

The three scenarios for the Meta-Xylene unit are shown in Figure 8. The two histograms in Fig. 8a (scenario A) illustrate leak size distributions of all M21 leak events (blue bars) and leak events simulated "to be detected" by the Molex LDSN system (orange bars) when utilizing the assumptions of distance variable detection threshold and leak clustering. Although the nominal leak average detection threshold (DTA) is 5000 ppm, substantial number of smaller leaks (500-5000 ppm) are predicted to be detected by the Molex LDSN due to peculiarities of leak-to-sensor distance distribution in an operating plant environment. All those "to be detected" leaks have significant impact on emission equivalency calculations. Comparing Figures 8a and 8b (Scenarios A and B, respectively) visualizes the effect of small leak clustering. As shown in figure 8b, after clustering effect is removed from the model, approximately half of "to be detected" smaller leaks (500-5000ppm) from scenario A (Figure 8a) would not "be detected" by scenario B (Figure 8b). Therefore, these would not be included in emissions equivalency calculations. The impact of disregarding the distance dependence of the detection threshold (scenario C) is illustrated in Figure 8c. In this scenario, all the leaks in the 500-5000 ppm range would not be included in the emission equivalency calculations.

Figure 9 shows the year-to-year accumulation of all M21 leak events side-by-side with leak events "to be detected" by the LDSN system. The graphs compare the leak size distributions of all M21 leak events in 2013 vs. leak events predicted as "to be detected" by the LDSN in 2013. Figure 9b provides similar information for two years (2013-2014), Fig. 9c is for 2013-2015, etc. The information from Figures. 9a-9g is compiled in Figure 9h. The total number of leak events "not to be detected" by the LDSN on a year-to-year basis is compared to the yearly accumulated number of all M21 leak events. The area under the blue curve represents the integrated number of leak events "not to be detected" by LDSN. The area between the orange and blue curves represents the integrated number of leak events "to be detected" by LDSN. The LDSN detection simulation from Figure 9h demonstrates that the total number of small leaks "not to be detected" by LDSN does not continuously increase each year. Instead, the number of small undetected leaks reaches steady state. The is a reasonably predictable result since smaller leaks, even if not originally detected by LDSN will aggregate. A detection event will be generated based on the

aggregation of several small leaks within the cluster or upon the growth of one of existing small leaks . Once the detection event is generated, the DRF process is followed and an LDAR technician is dispatched to the cluster area to identify actionable leaks. Experience from DRF implementation in the pilot test units shows the LDAR technician conducting the DRF response in a cluster area, often identifies either a large leak or several smaller contributory leaks.

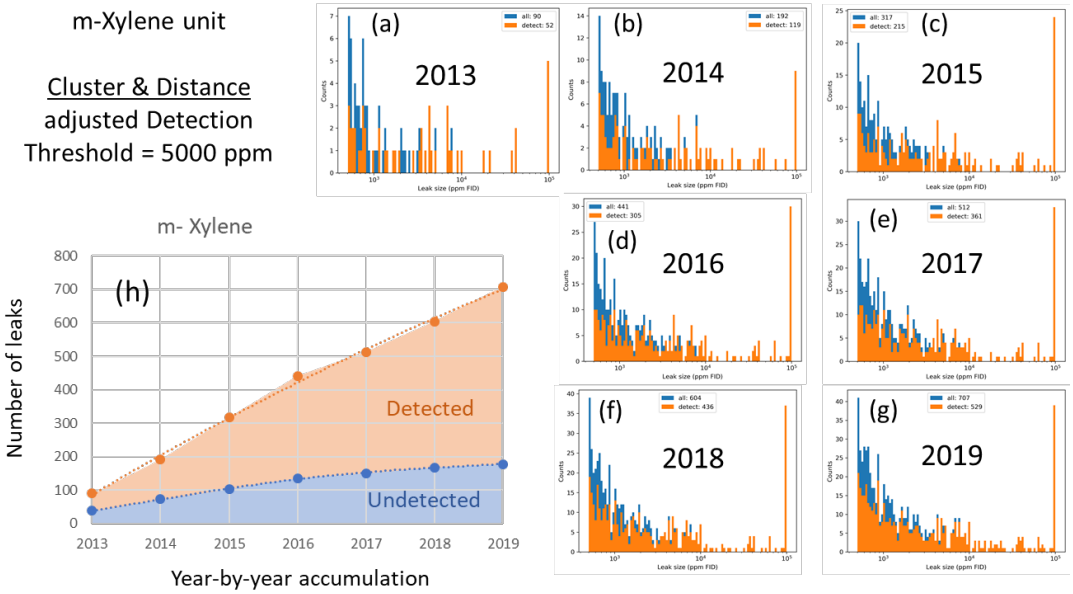

Figure 9. Year-to-year accumulation of all M21 leak events and simulated "to be detected" by LDSN leak events in the Meta-Xylene unit for 2013-2019 period. Inserts (a -g) compare leak size distributions for subsequent years. Insert (h) is the year-by-year accumulation of total number of leak and the area under the blue curve represent leak events "not to be detected" by LDSN. The area between the orange and the blue curves represents leak events "to be detected" by LDSN.

REFERENCES

1. J Hodgkinson et al, Detection of a simulated gas leak in a wind tunnel, Measurement Science and Technology, Vol 17, 2006, P1586-1593

2. Levente J Klein, et al, Distributed wireless sensing for fugitive methane leak detection, IEEE Intl. conf. on Big Data, 2017Ve

3. Robert W. McMullen (1975) The Change of Concentration Standard

Deviations with Distance, Journal of the Air Pollution Control Association, 25:10, 1057-1058

4. D. B. Turner, Workbook of Atmospheric Dispersion Estimates, U.S. Environmental Protection Agency, 1970.